INFORMATION TO USERS

This manuscript has been reproduced from the microfilm master. UMI films the text directly from the original or copy submitted. Thus, some thesis and dissertation copies are in typewriter face, while others may be from any type of computer printer.

The quality of this reproduction is dependent upon the quality of the copy submitted. Broken or indistinct print, colored or poor quality illustrations and photographs, print bleedthrough, substandard margins, and improper alignment can adversely affect reproduction.

In the unlikely event that the author did not send UMI a complete manuscript and there are missing pages, these will be noted. Also, if unauthorized copyright material had to be removed, a note will indicate the deletion.

Oversize materials (e.g., maps, drawings, charts) are reproduced by sectioning the original, beginning at the upper left-hand corner and continuing from left to right in equal sections with small overlaps.

Photographs included in the original manuscript have been reproduced xerographically in this copy. Higher quality 6" x 9" black and white photographic prints are available for any photographs or illustrations appearing in this copy for an additional charge. Contact UMI directly to order.

ProQuest Information and Learning
300 North Zeeb Road, Ann Arbor, MI 48106-1346 USA
800-521-0600

TAPHONOMY AND PALEOSYNECOLOGY OF THE LOWER SILURIAN GRAPTOLOID FAUNA, CAPE PHILLIPS FORMATION, NUNAVUT, CANADA.

by

Jennifer C. Russel-Houston

Submitted in partial fulfillment of the requirements for the degree of Doctor of Philosophy at Dalhousie University

September, 2001

DALHOUSIE UNIVERSITY

FACULTY OF GRADUATE STUDIES

The undersigned hereby certify that they have read and recommend to the Faculty of Graduate Studies for acceptance a thesis entitled "Taphofacies and Paleosynecology of the Cape Phillips Formation Graptoloid Fauna, Nunavut, Canada" by Jennifer C. Russel-Houston in partial fulfillment of the requirements for the degree of Doctor of Philosophy.

Dated: August 22, 2001

External Examiner: [redacted]

Research Supervisor: [redacted]

Examining Committee: [redacted]

DALHOUSIE UNIVERSITY

DATE: September 11, 2001

AUTHOR: Jennifer C. Russel-Houston

TITLE: "Taphonomy and Paleosynecology of the Lower Silurian Graptoloid Fauna, Cape Phillips Formation, Nunavut, Canada"

DEPARTMENT OR SCHOOL: Department of Earth Sciences

DEGREE: Ph.D. CONVOCATION: Fall YEAR: 2001

Permission is herewith granted to Dalhousie University to circulate and to have copied for non-commercial purposes, at its discretion, the above title upon the request of individuals or institutions.

[redacted]
Signature of Author

I started with a dream, but came to a decision.
I started with a dream, but now I have a mission.
I have a goal to see beyond my vision.

With imagination, I'll get there.

- Harry Connick Jr.

This thesis is dedicated to my grandmothers
who showed me what one can achieve with imagination and determination.

Lois Molden Russel, Alice Kincheloe, and Nora Elliott.

Table of Contents

List of figures

List of tables

List of equations

List of plates

List of appendices

ABSTRACT

Uncompressed graptoloids from carbonate concretions of the Late Ordovician to Early Devonian Cape Phillips Formation, Arctic, Canada, yield valuable biostratinomic information unavailable in the study of flattened specimens. The concretions lithified during shallow burial before extensive physical compaction, preserving the three-dimensional nature of the graptoloids and the fine-grained sediment prior to dewatering (Melchin and Coniglio, 1995). Fifty-two concretions and two pieces of limestone beds from two sections on Cornwallis Island were dissolved layer-by-layer in acid, enabling the examination of the graptoloid preservational condition and distribution within single bedding planes and through successive strata at a high level of resolution.

Eleven microlithofacies within the deep-water carbonate slope-to-apron facies in the Lower Silurian of the Cape Phillips Embayment are identified. I describe a process-based graptoloid taphofacies model and define seven distinct taphofacies that can be identified by comparing the microlithofacies with the graptoloid taphonomic characteristics including fragmentation, alignment, size sorting, species composition, and bedding plane concentration (assessed with chi-square). Four taphofacies describe graptoloid concentration beds and three taphofacies have a statistically random vertical distribution of graptoloids. The graptoloid concentration beds were the product of: increased input and concentration of graptoloid rhabdosomes by physical transport; increased input of graptoloids by a paleoecological bloom; cessation or reduction of sediment supply producing a heavily time-averaged graptoloid assemblage; or physical concentration by winnowing of sediment producing a sediment lag accumulation. Three taphofacies describe the non-concentrated graptoloid distribution: constant graptoloid - constant sediment input; sediment event but low graptoloid abundance; or bioturbation. All taphofacies with the exception of the bioturbation taphofacies were recorded from the concretionary material collected from the Cape Phillips Formation. The distribution of taphofacies may be useful, together with other information, in the reconstruction of sedimentary and sea-level history of the Cape Phillips Embayment.

Identification of background and episodic processes, together with measures of overall sediment thickness and estimates of section duration and stratigraphic completeness, permit the calculation of a range of possible, small-scale sedimentation rates for the concretionary strata. The time resolution of a 5 mm thick lamina of concretionary material (average sample size used in this thesis) is approximated to be between 25 and 114 years. The graptolites within that layer are time-averaged because the accumulation time is longer than the probable life span of a graptoloid colony. However, graptoloid assemblages were relatively stable and a cluster analysis identified graptolite assemblages to have an average stratigraphic thickness of 6.5 cm in the concretionary material, or 1.3 cm of shale (corrected for compaction).

Recurrent graptoloid species associations, identified by cluster analysis, are considered to represent graptoloid communities. Whereas some of these community changes are the result of evolutionary changes, others appear to be caused by local environmental changes, ecological blooms, or physical mixing through sediment transport. The concomitant distributions of rhabdosomes and siculae and observations of sicular orientation within the concretions were used as evidence to support the hypothesis that the mode of life of siculae was planktonic, like the mature rhabdosomes.

ACKNOWLEDGEMENTS

When Christopher Melchin was taking his first steps, I was exploring the Arctic for graptoloid-bearing concretions. When Christopher was speaking his first words, I was in Spain presenting my first paper at an international conference. This fall Christopher will begin kindergarten and I will defend this thesis. Christopher can count to 999, spell words like "pig" and "comb", and he knows all the words to the Pokemon theme song. He is well prepared for the classroom and the playground. In the last five years Christopher and I have learned a great deal about ourselves by exploring the world around us and I think we both face the next phase in our lives with fear and excitement as we discover the applications of our knowledge and what is beyond 999.

I thank my advisor, Dr. Michael Melchin (Christopher's father), for teaching me his science and sharing his enthusiasm. His influence and ideas are evident on every page of this thesis. I thank Rosemary, Greg, Brendan, Paul, and Christopher Melchin for welcoming me into their home and always setting a place for me at their dinner table.

I thank my committee members, Dr. Graham Williams and Dr. Martin Gibling for their thoughtful reading of earlier drafts of this thesis. Their comments were formative in the direction this thesis has taken.

I thank my mother and father for encouraging my sense of curiosity and not tiring from all my questions. I thank Kristin for daring me to do this and pushing me to succeed. I thank my colleagues at Dalhousie and St. Francis Xavier Universities who have participated in solving the riddles of the Silurian over many beers at the Grad House or at Pipers. In particular, the following people provided me with needed information, helpful advice, beautiful thin-sections or sometimes just a cup of tea; Gordon Brown, Joyia Chakungal, Dr. Barrie Clarke, Tony Evans, Dr. Rebecca Jamieson, Eugene MacDonald, Craig Powers, Jo Price, Trecia Schell, Dr. David Scott, Charu Sharma, Dr. Paul Schenk, and Dr. Nick Wilson. I thank Gerald, Norma, Darlene, and CBC Radio One for keeping me in touch with "the Recent".

I thank the organizations that supported this research through student grants-in-aide: GSA, AAPG, and SEPM. This thesis work was also supported by a NSERC research grant awarded to M. J. Melchin. I was supported by a NSERC PGSB Scholarship, a Dalhousie University Graduate Scholarship, and a Graduate Scholarship from CSPG. The Polar Continental Shelf Project provided field support as part of two research grants awarded to M. J. Melchin.

And I thank Todd for being my best friend and most loyal supporter, LYLC

1 INTRODUCTION

The Upper Ordovician to Lower Devonian Cape Phillips Formation of the Canadian Arctic has been known for its exquisitely preserved, uncompressed graptolites since Thorsteinsson first reported them in 1958. Graptoloid-bearing concretions of the Cape Phillips Formation were lithified during shallow burial, preserving the three-dimensional shape of the graptoloid rhabdosomes and the character of the sediment before physical compaction (Coniglio and Melchin, 1995). The graptoloids and the sediments captured by this unique preservation give insight into questions unsolved in the studies of flattened graptoloids preserved in shale. In this thesis the exceptional samples were used to address questions regarding graptoloid occurrence. Although graptoloids have been used as a biostratigraphic tool for over 100 years, graptoloid occurrence, the basis of graptoloid biostratigraphy, is poorly understood. How did graptoloids reach the sediment surface and what is their sedimentary history? How much time does one layer of graptoloid-bearing sediment represent? What processes caused the concentration of graptoloids? How does the preservational history (taphonomy) of graptoloids affect biostratigraphical and paleoecological interpretations?

Graptoloids (the planktonic graptolites) were colonial marine animals that were the most commonly preserved faunal group of the Lower Paleozoic plankton. Studies of functional morphology (e.g., Rigby and Rickards, 1989; Underwood, 1993a) and graptoloid distribution (e.g., Finney and Berry, 1997; Cooper, 1999) suggest that graptoloids lived as zooplankton do today, in large planktonic clouds in the warm, tropical to sub-tropical waters near zones of upwelling at the edges of continental shelves and platforms. Every graptoloid sample is a record of the original planktonic community and the taphonomic events that altered that original graptoloid population. The purpose of this thesis is to understand some of the taphonomic processes that acted upon the graptoloids of the Cape Phillips Formation and to use these observations to interpret the composition of the original graptoloid communities.

Taphonomy is the study of "the principles governing the transition (in all its details) of animal remains from the biosphere to the lithosphere" (Efremov, 1940, p. 85). Early taphonomic studies examined the preservational biases in the fossil

record and the extent of biological information lost due to the "taphonomic filter" (e.g., Fagerstrom, 1964; R. G. Johnson, 1960; Schopf, 1978). The last two decades have witnessed a rebirth of the science and an explosion of research that has aimed at understanding how the fossil preservation process, both negatively and positively, affects our ability to interpret past environments (Behrensmeyer *et al.*, 2000). Brett and Baird (1986) recognized that organisms, upon their death, may become sedimentary particles and, like the inorganic grains, can record information about the depositional environment. By comparing taphonomic characteristics, information about the depositional environment and the life, post-mortem, and burial histories of the preserved remains can be gained. Brett and Baird (1986) defined this process as comparative taphonomy, the study of differential fossil preservation.

Speyer and Brett (1986) examined the distribution of various trilobite taphonomic characteristics to create taphofacies that are "facies defined on the basis of diagnostic taphonomic traits" (Speyer and Brett, 1986, p. 312). The creation of a taphofacies model involves the taphonomic characterization of a unit of rock that distinguishes the unit from another with a different preservational history. Taphonomic attributes reflect particular paleoenvironmental conditions and can be used to interpret the depositional environment of the fossil assemblage (Speyer, 1991).

The graptoloid taphofacies model presented in this thesis relates the biostratinomy of the graptoloids to the lithology of the laminae in which they occur in an attempt to identify graptoloid taphofacies that indicate particular combinations of paleoecologic and depositional conditions. Biostratinomy is the study of the sedimentary history of an fossil after death and before final burial (Cadée, 1991). A graptoloid taphofacies model can aid us in understanding the sedimentary dynamics of the graptoloid depositional environment. A taphonomic analysis and a measure of the time that is averaged in a typical graptoloid sample is a prerequisite for a test of ecological fidelity.

This information is then used to identify times of low taphonomic alteration that would be suitable for community analysis. Recurrent species associations are identified by cluster analysis and analysed with regard to graptoloid community structure and

paleosynecology. Paleosynecology: the interaction of ancient communities with their environment and with other organisms in that environment (Prothero, 1998).

This study focuses on graptoloids collected from two sections on Cornwallis Island in the Canadian Arctic Archipelago (Figure 1.1). The two sections were located with in similar proximity to the ancient facies transition with the coeval shallower-water carbonates of the Allen Bay Formation. The two sedimentary units were deposited below wave base in water depths greater than 200 m within the slope-apron facies of the ancient Cape Phillips Embayment (Chapter Five). Therefore, the spatial variation between sections is limited and changes in graptoloid taphonomy or community structure reflect the passage of time. The two sections span most of the Llandovery (Early Silurian). The Cape Manning section is Late Rhuddanian (latest Ordovician) to Early Telychian in age and the Cape Phillips is Mid Telychian to Early Sheinwoodian (Early Wenlock). Although this sampling procedure limits the spatial scope of the taphofacies model and community analysis, the temporal understanding of the distribution of graptoloid taphofacies and communities was greatly enhanced by the detailed vertical sampling at the two sections (in particular Cape Manning). This focus on a short stratigraphic interval that contains the graptoloid-bearing concretions (Figure 1.2) was designed to address the objectives of this study.

Objectives

1. To qualitatively define microlithofacies based upon observations of composition, texture, and sedimentary structures preserved in the concretions.
2. To use the facies classification as a tool for interpreting the depositional environment in the Cape Phillips Embayment, near the shelf-basin transition during the late Rhuddanian to late Telychian.
3. To record associations between the lithology of the lamina, graptoloid distribution, orientation, and preservational condition; horizontally and vertically through the concretions.
4. To infer the paleoecological and taphonomic processes that acted on the fossils.
5. To use the combined lithofacies and graptoloid distribution data to define and describe graptoloid taphofacies.

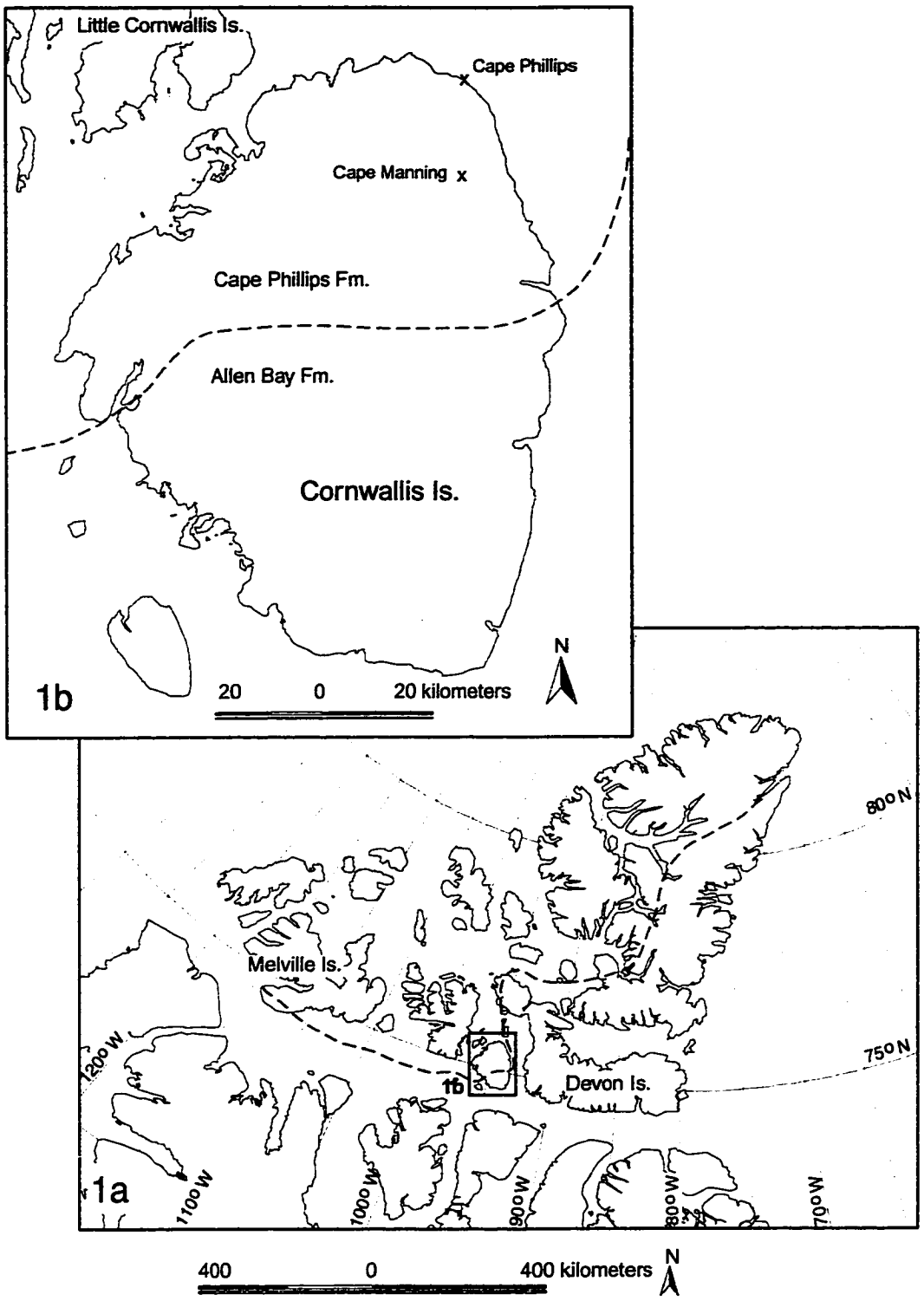

Figure 1.1. Location map of study area. A. Canadian Arctic Archipelago. B. Field localities on Cornwallis Island. 1. Cape Phillips (75° 37'N, 94°30'W), and Cape Manning (75° 26.8'N, 94° 20'W) along an unnamed stream 10 km west of Cape Manning. Dashed line represents the approximate location of the Allen Bay Formation - Cape Phillips Formation facies transistion.

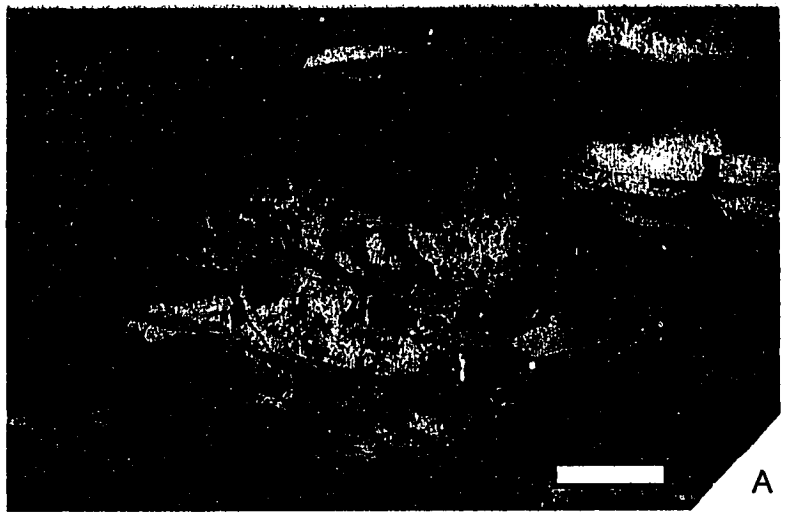

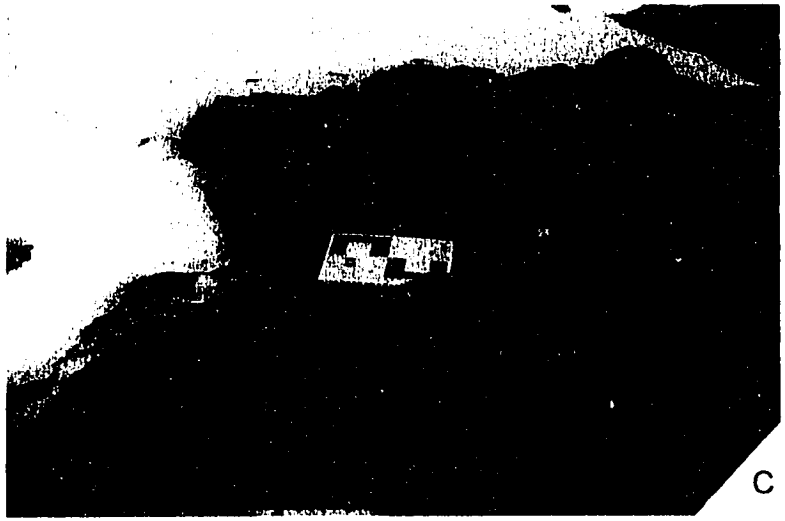

Figure 1.2. Field photographs from the Cape Manning section. A. Weathered concretion *in situ* at approximately CM 48.4 showing compression of surrounding shale. The thickness ratio between the concretion and the stratum that can be traced into the concretion is 5:1. Compression measured from this concretion is estimated as 80%. Scale bar is 10 cm long. B. Abundant concretions in the *R.orbitus* Zone range from small centimeter-scale nodules to large concretions of almost 1 meter diameter. The coarse carbonate bed that is approximately 40 cm thick is the marker bed with the base at CM 51.4. C. Bedding plane view of CM 56.4. Book for scale is 18 cm. long.

6. To record changes in faunal composition within concretions and between concretions in stratigraphic succession in an attempt to understand the modes and degree of time-averaging in the Cape Phillips Formation.
7. To record faunal associations and faunal turnovers in an attempt to identify paleocommunities within the graptoloids of the Cape Phillips Formation.

Organization of the thesis

The thesis is presented in 11 chapters and here I describe the contents of each chapter and the overall organization of the thesis. After three introductory chapters, the results of the thesis are presented in Chapter Four as a detailed and integrated study of the lithology, taphonomy, and graptoloid distribution of each concretion. The results are then discussed in Chapters Five to Nine. Chapter Ten comprises an informal description of some of the graptoloid species and Chapter Eleven summarizes the main conclusions of the thesis.

Background, Geological Setting, Biostratigraphy, Materials and Methods (Chapters Two and Three)

Chapter Two contains the background material needed to understand the results of this investigation of graptolite taphonomy and paleosynecology. I describe and define the concepts of taphonomy, time-averaging, temporal resolution, and community analysis and summarize previous studies of graptolite taphonomy and paleoecology. In Chapter Two, I also review the previous work that has been conducted on the Cape Phillips Formation and I place the Cape Phillips Formation in the context of the Lower Paleozoic Franklinian Basin. To be able to relate my conclusions of graptoloid taphonomy and paleosynecology to global events and to geologic time, a complete biostratigraphic evaluation of the two study areas was necessary. A refinement of the previous biostratigraphy of the Cape Manning section (Lukasik, 1994; Lukasik and Melchin, 1997) is presented in this chapter. Species distributions of isolated graptoloids and those flattened in shale defined the biozones.

Chapter Three describes the research methods, including: a description of the layer-by-layer dissolution method, a report of the methods used to prepare and study the

lithology of the concretions, and a description of the statistical and counting methods employed.

Concretion descriptions: graptoloid taphonomy, distribution and lithology of the concretions (Chapter Four).

Chapter Four contains the results of the layer-by-layer dissolution and the micro-stratigraphic and lithologic investigation of the concretions. For the Cape Manning section, vertical species distribution as counted from the dissolution residues is also presented. The concretion descriptions provided in this chapter are the evidence used to define the microlithofacies, create the taphofacies model, determine the extent of time averaging, and identify species associations. The discussions of these follow in chapters five to nine, respectively.

Microlithofacies of the Cape Phillips Formation Slope-Apron Facies (Chapter Five)

Most of the carbonate concretions of the Cape Phillips Formation were lithified before significant compaction and preserved the fine-grained sediment uncompacted and often undistorted. With rock slabs and thin sections cut perpendicular to bedding, original structures, such as laminae and graded beds can be observed. Additional study of pieces of concretionary material with an environmental scanning electron microscope equipped with an energy dispersive system (ESEM/EDS) elucidated the relationship between lamina colour and clay and organic content. The combined sedimentological data were used to define eleven microlithofacies of the Cape Phillips Formation and place the formation in the slope-apron facies spectrum.

Biostratinomic study and graptoloid taphofacies model (Chapter Six)

The uncompressed graptoloids and the surrounding matrix provide valuable biostratinomic information unavailable in the study of the more common flattened graptoloids preserved in shale. The method of layer-by-layer dissolution (Melchin *et al.*, 1994) enables the examination of the orientation, preservational condition, and small-scale lateral and vertical heterogeneity in graptoloid distribution within single bedding planes and through successive strata. The graptoloid taphofacies model, presented

herein, relates the evidence of biostratinomic alteration and the vertical variability in distribution of the graptoloids to the lithology of the laminae in which they occur in an attempt to define the paleoecological and taphonomic processes that acted on the fossils. From these observations distinct graptoloid taphofacies are recognizable.

Temporal distribution of microlithofacies and taphofacies (Chapter Seven)

The temporal distribution of microlithofacies and taphofacies within the slope-apron facies is related to global sea level changes during the Llandovery and a change in basin morphology from ramp conditions to rimmed shelf in the late Llandovery that may have resulted in changes in sedimentation rates and productivity.

Time-averaging and temporal resolution of the Cape Phillips Formation graptoloid fauna (Chapter Eight)

This chapter includes an estimate of stratigraphic completeness, temporal resolution and accumulation rate of the sediments during the Aeronian at the Cape Manning section. This was accomplished by differentiating the background sedimentary sequences from the episodic, rapidly deposited event beds, such as tempestites or turbidites. This chapter also summarizes a statistical comparison (Q-mode cluster analysis) of the graptoloid faunal composition within concretions and between concretions in stratigraphic succession in the Cape Manning section. This is used to estimate the temporal resolution of a lamina of concretion material and the temporal continuity in graptoloid communities. Heavily time-averaged samples are also identified during these processes as those that contain graptoloids from different age cohorts that are temporally mixed. The identification of heavily time-averaged samples is essential in a paleoecological analysis of graptoloid community structure.

Graptoloid species associations in the Aeronian Cape Phillips Formation and paleosynecological implications (Chapter Nine)

The exceptionally preserved graptoloids are used to study the paleosynecology of graptoloids. A fine-resolution sampling of the graptoloid species distribution vertically through a concretion is a quantitative record of the taphocoenosis (death assemblage).

Small shifts in species composition and dominance are used to understand larger-scale basin dynamics by examining several stratigraphically consecutive concretions. Twenty-eight concretions spanned almost 20 meters of continuous strata from the mid-Aeronian (*Coronograptus cyphus*, *Monograptus pectinatus*, *Rastrites orbitus*, and *Lituigraptus convolutus* Zones) portion of the Cape Manning section. The identification of recurrent species associations using cluster analysis allows the reconstruction of graptoloid paleocommunities.

Graptoloid systematics (Chapter Ten)

Chapter Ten includes brief descriptions of 14 graptoloid species that are not previously described. Six previously identified graptoloids are re-described in light of their excellent preservation in this material or to clarify my identification (*Comograptus comatus*, *Metaclimacograptus sculptus*, *Metaclimacograptus rigidus*, *Monograptus* cf. *arciformis*, *Monograptus falcata*, and *Pribylograptus leptotheca*). The other previously described graptoloid species are illustrated, but not described. Images were obtained using infrared video microscopy (IVM) and image capture with a scanning electron microscope (SEM).

Glossary of terms

argillaceous. Descriptive of a clastic (or detrital) sedimentary rock with particles < 4 mm (Keary, 1996).

astogeny. The pattern of growth of a colony (Palmer and Rickards, 1991).

autecology (paleoautecology). "The functions and life styles of individual (ancient) organisms" (Brenchley and Harper, 1998, p.4).

benthic mixing. Biological and, rarely, physical processes that disturb buried sediment and increase time-averaging that do not involve the erosion and redeposition of the sediment surface (Sadler, 1993).

biostratigraphy. Stratigraphy of the fossil content of the sedimentary strata based on concepts of superposition, original horizontality, and original lateral continuity (Palmer and Rickards, 1991).

biostratinomy. The sedimentary history of a fossil until final burial (Cadée, 1991).

biocoenosis. Original life assemblage or living community of organisms (Prothero, 1998)

carbonate. A biochemical or chemical rock composed of minerals that contain the carbonate anion ($(CO3)^{2-}$) (Tucker and Wright, 1990). Common carbonates are limestone and dolostone.

chi-square analysis. A statistical method used in this thesis to assess the random or non-random (concentrated or even) distribution of rhabdosomes vertically through the sediments. The method compares the number of specimens in one sample (observed) with the average number of specimens in a sample (expected) (Bailey, 1995).

clast. A particle of rock or a single crystal that has been derived by weathering and erosion (Keary, 1996).

clastic sediment. A sediment composed of clasts (Keary, 1996). Also described as "detrital sedimentary rock".

community (paleocommunity). A repetitive association of species (or fossilized species) and "a similarity in species dominance between different samples" (Brenchley and Harper, 1998, p. 230).

comparative taphonomy. The study of differential fossil preservation (Brett and Baird, 1986).

completeness. The proportion of the total span of absolute geologic time as compared to the time recorded witin the sediments in a section (Sadler, 1981; Schindel, 1982).

diagenesis. All the processes (chemical, physical, and biological) that affect the sediment and the fossil after deposition prior to metamorphism (Tucker and Wright, 1990).

event bed. Individual beds that record rapid depositional processes that are characterized by one or more of the following: graded beds, scours, truncated bedding, and current aligned rhabdosomes.

fidelity. The fidelity of a fossil assemblage describes "how closely (faithfully, accurately, truthfully) the fossil record captures original biological information, be it spatial patterning or the presence/absence or relative abundances of species" (Behrensmeyer, *et al.*, 2000, p. 114)

hiatus. Herein used as a break in the stratigraphic sequence of rocks as the result of an interval of time during which sediments were not deposited. Other definitions include the non-depositon and erosion of the overlying beds (e.g., Bates and Jackson,

1987). In this thesis erosion-dominated horizons are termed "sediment removal", and hiatus is used to described a *hiatus* in the depostion of sediment or a horizon that is "sediment starved".

necrolysis. The death and decomposition of an organism (Cadée, 1991).

nepheloid layer. A layer of water in deep oceans, 200 m to 1000 m thick that contains significant amounts of suspended sediment (Bates and Jackson, 1987) that remain in suspension because of the existance of some barrier to settling (salinity, temperature). When this barrier is overcome, rapid deposition of fine-grained sediment results (Trettin *et al.,* 1991).

niche. The physical, chemical, and biological requirements (limits) of an organism. An abstract concept that can address the organism's way of life, the habitat, and its role in the ecosystem (Prothero, 1998)

q-mode cluster analysis. Statistical method used herein to identify the relative similarity of the species assemblages within the samples. Involves the computation of a sample unit dissimilarity matrix and then the grouping of samples based on the similarity of the mutual co-occurrence of taxa (Etter, 1999).

r-mode cluster analysis. Statistical method used herein to identify the relative co-occurrence of taxa distributed within the samples. Involves the computation of a species dissimilarity matrix and then the grouping of species based on their dissimilarity values (Etter, 1999).

reworking. Physical and, rarely, biological processes that disturb buried sediment and increase time-averaging that involve a period of erosion and redeposition of the sediment surface (Sadler, 1993).

rhabdosome. Skeleton of the entire graptoloid colony that was composed of collagen secreted by the zooids of the colony. The size of the rhabdosome increases from the sicula by the addition of thecae secreted by the asexually budding zooids (Palmer and Rickards, 1991).

shale. A class name for all fine-grained, argillaceous sediment, consisting predominately of mudsize particles (less than 0.063 mm (4 Φ)) (Potter *et al.*, 1980).

sicula (siculae). Living tube of the first zooid of a graptoloid colony comprising a conical prosicula and a gradually widening, tubular metasicular (Palmer and Rickards, 1991).

synecology. "The operation of associations or communities" of organisms (Brenchley, *et al.*, 2000, p.4).

taphofacies. "Facies defined on the basis of diagnostic taphonomic traits" (Speyer and Brett, 1986, p. 312). Involves the comparison (often quantified) of taphonomic characters from different depositional environments.

taphonomic filter. Paleobiologic or evolutionary information lost as a result of the process of taphonomy, or biases (non-random, uniform) in the fossil record (Behrensmeyer *et al.*, 2000).

taphonomy. The study of "the principles governing the transition (in all its details) of animal remains from the biosphere to the lithosphere" (Efremov, 1940, p. 85). The science of studying the fossilization process includes aspects of necrolysis, biostratinomy, and diagenesis.

taphocoenosis. Fossil assemblage or death assemblage following taphonomic (necrolytic, biostratinomic, and diagenetic) alteration (Parsons and Brett, 1991).

tempestite. A storm deposit as evidenced by the distrubance of pre-existing sedimments followed by their rapid redeposition all in a shallow-water environment (Bates and Jackson, 1987)

theca (plural thecae). Living tube of the zooid (other than the sicula) constructed by the zooid and forming the main structural component of the rhabdosome (Palmer and Rickards, 1991).

time-averaging. The stratigraphic mixing of cohorts that can occur by reworking, benthic mixing, slow sedimentation rates (Walker and Bambach, 1971), or a low-resolution sampling interval.

time resolution. The acuity or sharpness of the fossil record or the finest temporal interval that the fossils can be confidently sampled (Behrensmeyer, *et al.* 2000)

turbidite. A deposit from a turditity current.

turbidity current. A density current caused by different amounts of sediment in suspension. Specifically "a bottom-flowing current laden with suspended sediment, moving swiftly (under influence of gravity) down a subaqueous slope and spreading horizontally of the floor of the body of water, having been set and/or maintained in motion by locally churned- or sitred-up sediment that gives the water density greater than that of the surrounding or overlying clear water" (Bates and Jackson, 1987).

zooid. The soft-bodied individual of the graptoloid colony that lived in a theca or sicula (Palmer and Rickards, 1991).

2 BACKGROUND

Previous taphonomic research

The sedimentary history of organisms after their death and before final burial is termed biostratinomy. Biostratinomy is an aspect of taphonomy, the study of fossil preservation. Two other research fields that comprise the science of taphonomy bracket biostratinomy: necrolysis, the study of the death and decomposition of an organism; and diagenesis, the study of all the changes (biological, physical, and chemical) that take place after final burial (Allison and Briggs, 1991). Graptolite researchers, like other paleontologists have only recently begun to address questions of how fossils are preserved and what information is lost and gained during the fossilization process. When Efremov (1940, p.85) introduced the term "taphonomy" to describe the study of fossilization the purpose was to understand the process of the "taphonomic filter", to evaluate the amount of information that was lost during the fossilization process, and the fidelity of the biological record. Today, this is still an objective of many taphonomic studies and researchers are approaching the problem with diverse methods, including actualistic experiments and integrated paleontological studies. The techniques of taphonomic analysis have been applied to many fossil groups (e.g., Allison and Briggs, 1991; Donovan 1991; and references within) although with an emphasis on benthic marine fauna.

Brett and Baird (1986) discovered that by comparing taphonomic characteristics between fossil sites within a fossil group, information about the depositional environment and the paleoecology of the fossil fauna could be gained. They termed this approach "comparative taphonomy", the study of differential fossil preservation (Brett and Baird, 1986). They realized that organisms, upon their death became sedimentary particles and, like the inorganic grains, could record information about the depositional environment. The methods of comparative taphonomic analysis were first applied to trilobites (Brett and Baird, 1986; Speyer and Brett, 1986) and were successfully used to investigate many shallow-water fossil organisms and assemblages (e.g., Allison and Briggs, 1991; Donovan 1991; and references within).

The interest in taphonomy in the last two decades has lead to many new advances. These are reviewed in detail in Behrensmeyer *et al.* (2000) and the following is a summary of the main points of that review. Research groups have focused on four main questions of taphonomy. 1) Controls on tissue preservation including microbial, and biogeochemical processes. 2) Fossil concentration processes. 3) The resolution (in time and space) and ecological fidelity of species assemblages. 4) The identification of megabiases that are changes in the quality of the fossil record that affect paleobiological analysis on a provincial or global scale and over tens of millions of years. Megabiases are recognized as large-scale shifts in the environment or in the evolution of a taxon that can cause secular or cyclical changes in preservability (Behrensmeyer and Kidwell, 1985). Megabiases introduce a bias of consistency of preservation through geologic time.

Research in taphonomy has demonstrated many of the biases affecting the quality of the fossil record. Kidwell and Brenchley (1996) showed how differential preservation is relevant to paleobiological questions. Diagenetic or metamorphic changes during fossilization and lithification often change the original composition of the organism and reduce the biochemical fidelity of the fossil assemblage. Biostratinomic events can alter a fossil assemblage by mixing organisms of different ages (time-averaging), or communities and alter the temporal resolution or spatial fidelity of the preserved assemblage. Selective destruction can reduce the preserved parts of a species or alter the species composition of an original community. This affects the compositional fidelity of the fossil assemblage. These aspects of the taphonomic filter are well-modeled and understood as the result of extensive experimentation (e.g., Chave, 1964; Briggs, 1990), study of modern communities (e.g., Allison, 1986; Kidwell, 1998), and integrated studies of ancient successions (e.g., Brett, 1995; Speyer, 1991).

Most organisms will never become fossilized. R. G. Johnson (1964), Stanton (1976), and Schopf (1978) calculated that 25-30% of the fauna from a southern Californian shelf is likely to be preserved in the fossil record. Many of the organisms with a low preservational potential are soft-bodied, lacking the more easily fossilized hard parts. Schopf (1978) found that organisms that lived in soft substrates were more easily preserved than those that lived in hard substrates. He also found that sedentary organisms (herbivores and filter feeders) were more easily fossilized than carnivores and

detritus feeders. He suggested this might be the result of the resistance of the heavier protective skeleton of the sedentary organism and the fragility of the lighter skeletons of the mobile organisms.

To estimate the completeness of the fossil record, researchers focus on particular, well-skeletonized groups and count the number of living and fossilized species (Valentine, 1970; Raup, 1976). Added into the calculation of completeness of the fossil record are estimates of speciation turnover rates and counts of the number of co-existing species with time. Durham (1967) calculated that 2.3% of all the well-skeletonized species were fossilized. Valentine used slightly different estimates of turnover rate and coexisting values and arrived at an estimate that ranges from 4.5-13.6%. Many organisms (84-97%) are not recorded in the fossil record.

The chance for preservation depends on many factors. Figure 2.1 summarizes some of these controls and this discussion was reviewed in Behrensmeyer *et al.*, (2000). These authors considered the preservational potential of a fossil by examining four components of fossilization separately: fossil supply, the preburial environment, the burial environment, and the geologic history of the sedimentary unit. The preservation of a fossil is controlled by the quantity, rate of fossil supply and the durability of the taxa in question (Behrensmeyer *et al.*, 2000). Abundant taxa in life will have a better chance of being preserved in the fossil record than rare taxa. More durable taxa with resistance to physical, biological or chemical destruction will have a better chance of surviving taphonomic alteration than fragile taxa or those susceptible to dissolution. Biological, physical and chemical processes in the pre-burial environment can destroy the organism (e.g., scavenging, fragmentation, or dissolution), or enhance preservation (e.g., bioencrustation). These pre-burial processes can be selective or broad in their effects and can occur at different rates or intensities. Some taphonomic features previously thought to be diagnostic of a particular taphonomic process are now recognized as having a different dominant cause or resulting from multiple processes ("equafinality" [Lyman, 1994]). For example, fragmentation of bivalve shells was regarded as being a good indicator of energy of the depositional environment; more fragmented shells representative of a higher energy (Brett and Baird, 1986). Studies of modern shell beds show that fragmentation commonly varies independently of water energy and is more

commonly produced by scavengers (Best and Kidwell, 2000). In many recently published actualistic studies the disarticulation and fragmentation of animal skeletons is found to be biogenic in origin from predation or scavenging and not an index of physical energy. When scavengers or predators are absent, the degree of destruction is dependent upon the state of decay of connective tissues, rather than the energy of the depositional environment or the distance of transport. Edge rounding of hard parts was also thought to be an indicator of transport distance; however, abrasion is more likely to result from repeated reworking within a high-energy environment than long-distance transport. The immediacy and the permanence of burial will determine the time the organism is exposed to the destructive agents at the sediment surface (Behrensmeyer *et al.*, 2000).

The diagenetic conditions at shallow burial can be variable. Bioturbation, meteoric effects, microbial processes, and physical reworking can all be actively altering the organisms in this zone. This zone has been termed the "taphonomically active zone" (TAZ, Davies *et al.*, 1989). Some processes can enhance preservation (e.g., mineral coatings, infillings, replacements) or reduce biological fidelity (e.g., hydrolysis, maceration, dissolution, and recrystallization) (Behrensmeyer *et al.*, 2000). Finally, the metamorphic and erosional history will determine the fate of the sedimentary unit.

Graptoloid taphonomy

Previous graptolite research has mainly focused on the taxonomy, biostratigraphy, and paleobiology of graptolites, whereas little attention has been paid to graptolite taphonomy. The orientations of elongate graptoloid rhabdosomes have been used as paleocurrent indicators for over 100 years (e.g., Ruedemann 1897), but few researchers have attempted to understand the biostratinomic history of such deposits. Bulman (1955) cited many early examples of reports that describe current alignment of graptolites (e.g., Hundt, 1938) and suggested this is an exaggeration of their importance in the fossil record. Instead, Bulman (1955) believed that most graptolites were uniformly and haphazardly distributed on the bedding plane surfaces. Bulman (1955) suggested that graptolite remains were often confined to thin layers separated by thicker sequences of unfossiliferous strata. Although early graptolite workers described these distribution

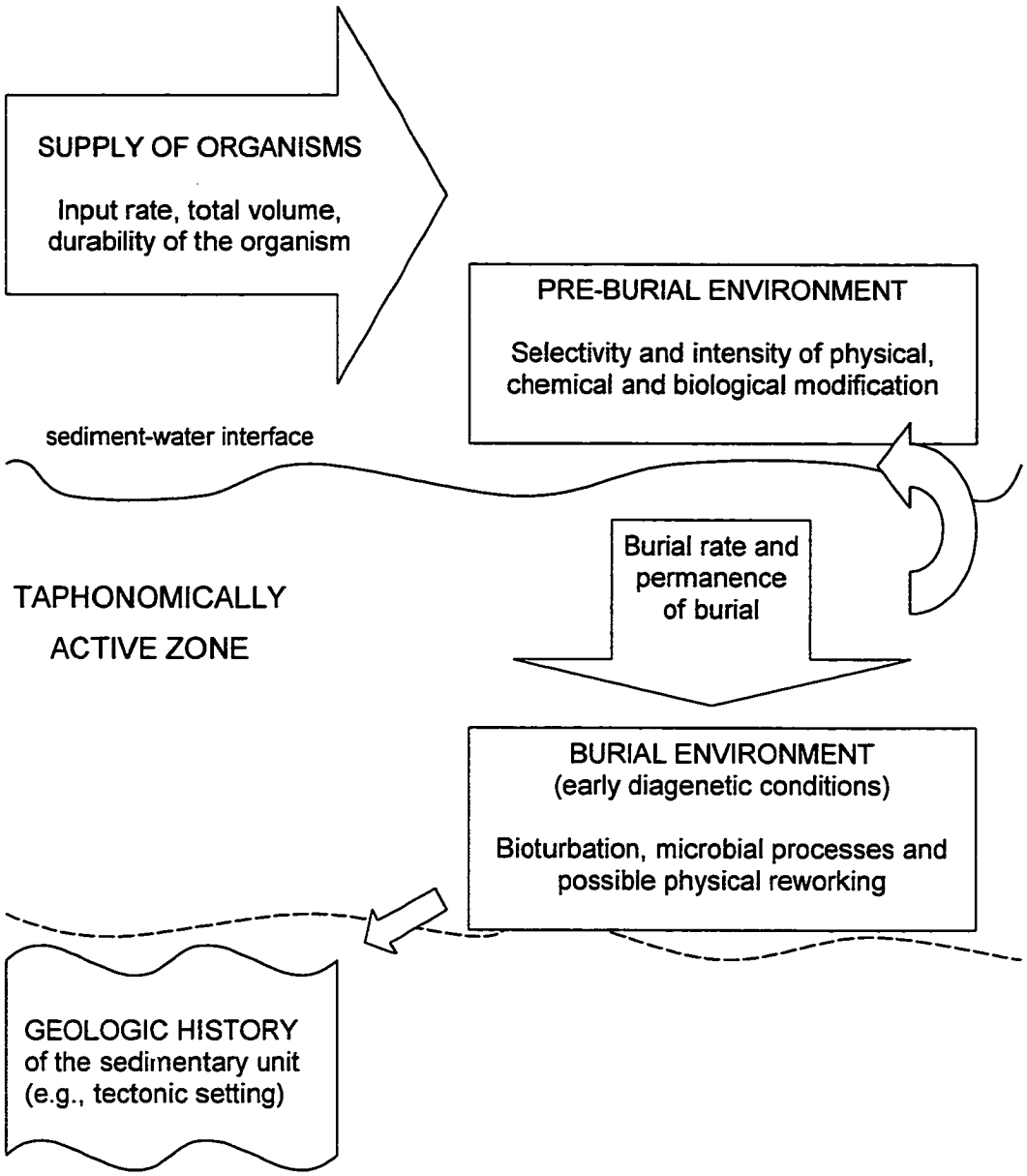

Figure 2.1. Controls on the preservation of biological remains. (Concepts from Behrensmeyer, *et al.*, 2000.)

patterns, little thought was given to the paleoecological or taphonomic significance.

Recent studies of graptolite necrolysis, biostratinomy and diagenesis have enhanced our knowledge of how the graptoloids were fossilized. Briggs *et al.* (1995) considered graptoloid necrolysis in their study of the decay of the modern relative of graptoloids, the benthic hemichordate, *Rhabdopleura*. The researchers observed that the periderm and stolon of the *Rhabdopleura* remained intact for months, whereas the zooids were unrecognizable within days, explaining the extreme rarity of zooid preservation in the graptolite fossil record. Underwood (1992), Underwood and Bottrell (1994) and Bjerreskov (1991, 1994) investigated graptoloid chemical diagenesis and identified graptoloid preservational styles. These reports focused on understanding unique preservation styles, such as pyrite internal molds, pyrite replacement, or silicate overgrowths. Williams *et al.* (1982) investigated the effects of diagenetic flattening of the graptoloid rhabdosome by compressing rhabdosome models in a matrix of plaster.

Attempts to understand the taphonomic filter acting upon graptoloid populations were actively pursued by Underwood (1993b). Underwood's (1993b) dissertation on the topic of graptoloid taphonomy attempted to evaluate the main factors affecting graptoloid preservation. Underwood (1994) addressed aspects of graptoloid biostratinomy in a paper on faunal transport and event beds in which he concluded that storms (tempestites) were the main transport mechanism for bringing the shallow-water fauna to deep-water settings. The graptoloids within the transport horizons were useful for interpreting the paleo-water depth or land proximity based on an assumed depth zonation of graptoloids (Underwood, 1994). Underwood's (1994) study of Ludlow tempestites and turbidites of the Welsh Basin found graptoloids associated with the coarser turbiditic beds and suggested that the fauna was transported and, to some degree, allochthonous. He observed that the smaller forms were absent from these deposits suggesting a preservational bias. The presence of rip-up clasts in the turbidites was considered to be evidence for the reworking and possible autochthonous origin of some of the graptoloid fauna (Underwood, 1994). He summarized that storm-related offshore transport of graptoloids resulted in only minor mixing with autochthonous faunas.

Underwood (1998) made some observations about concentration beds of graptoloids in his population study of graptoloids from the study area of this thesis, the

Cape Phillips Formation. He assumed that graptoloid concentration beds were the result of hiatus horizons and represented times of low sedimentation rates, but continual planktonic input to a quiet sediment surface that was not affected by scavenging. This non-event scenario was important to establish before he could make statements about the original planktonic population. Underwood (1993b) reviewed possible mechanisms of graptoloid concentration other than hiatal accumulation. He described current accumulations including: winnowing of assemblages, storm-generated concentrations, turbidite-generated accumulations, and obrution deposits (deposit in which organisms are killed and buried by rapid sediment influx). From his review of the literature of mostly British graptoloid deposits, Underwood concluded that most graptoloid accumulations are condensed beds from hiatus horizons. He summarized that all graptoloid assemblages show some degree of winnowing, and alignment of elongate rhabdosomes may occur in even light currents. He observed that graptoloid breakage is rare, but buckling of the rhabdosome is common within branching forms and high-energy environments. I will show that some of the graptoloid concentration beds of the Cape Phillips Formation can be described as event beds and current accumulations and can be distinguished from the background, hemipelagic sedimentation.

The method of layer-by-layer dissolution of the graptolite-bearing concretions is used to examine the small-scale vertical distribution of graptolites and taphonomic characters. These observations are the basis for the definition of graptoloid taphofacies that indicate particular combinations of paleoecologic and depositional conditions.

Speyer and Brett (1986) introduced the term taphofacies in the study of trilobites from many depositional environments in a Lower Paleozoic epicontinental sea. They described taphofacies as "facies defined on the basis of diagnostic taphonomic traits" (Speyer and Brett, 1986, p. 312). The creation of a taphofacies model involves the quantification of taphonomic characteristics and provides a background for stratigraphic comparison. Speyer and Brett (1986) attempted to make the taphofacies quantitative by assigning percentage occurrences to the observed taphonomic traits; however, the percentages were estimated and essentially qualitative assessments. For this first attempt at defining graptoloid taphofacies, I will focus on the qualitative aspects of biostratinomy

and will add quantitative measures only when referring to the concentration of graptoloids in strata.

The graptoloids of the Cape Phillips Formation were deposited in deep-water environments below storm wave base. The deep-water facies has been the subject of very few taphonomic investigations and, if included in a taphofacies, is usually grouped into one deep-water facies (e.g., facies IV; Speyer and Brett, 1986). Some of the taphonomic characteristics of shallow-water taphofacies - such as abrasion, bioerosion, and edge rounding (Parsons and Brett, 1991), are unsuitable in the study of fossils from the finer-grained, deep-water environments. In deep-water settings more emphasis is placed on fewer taphonomic traits. In a taphonomic study of shales deposited below storm-wave base, near the lower limits of the photic zone and associated shallower deposits of pyritized fossil beds, Brett and Baird (1986) used lithologic, paleontologic and taphonomic information to create taphofacies and reconstruct paleoenvironments. As a result they created a "pyrite taphofacies model" which is based upon evidence of sedimentation rates and oxygen content of the sediment and the overlying water. This is a diagenetic taphofacies model that can be applied with success to other deposits. The creation of a biostratinomic taphofacies model for deep-water, graptolitic environments that can be generally applicable to other deep-water environments of the Lower Paleozoic is an objective of this thesis.

Graptoloids are preserved in all marine rock types from the Lower Paleozoic, but they are most common in shales from anoxic or dysoxic, deep-water depositional environments (Rickards, 1991). The shales, lime-mudstones and silty limestones of the Cape Phillips Formation are interpreted to be a deep-water (below storm wave base), mostly anoxic sedimentary sequence (Coniglio and Melchin, 1995). Graptoloids of the Cape Phillips Formation were deposited in the deep-water, fine-grained sediments after settling through the water column. Like modern pelagic or planktonic organisms, graptoloids likely died in the water column. Pelagic and planktonic organisms preserved in sedimentary rock can never be considered *in situ* and exploring their taphonomic history offers new challenges as the questions of post-mortem transport and differential settling must be addressed. Decay of the graptolite rhabdosome likely began in suspension and gases released during this process may have caused a period of flotation

("bloat and float" hypothesis of Schäfer, 1972). The duration of flotation is controlled by tissue strength, rate of gas production and hydrostatic pressure (Allison, 1986). Most animals are negatively buoyant and sink upon death, only floating after the generation of sufficient decay gasses (Allison, 1988). Studies of modern fish found the period of flotation to last 3-4 days before final deposition. For a small organism, such as a graptoloid, the flotation period would generally be much less because of the reduced gas generation following death. Therefore, no attempt has been made to understand the extent of necrolytic buoyancy or transport.

This thesis is the first detailed study of graptoloid biostratinomy. Graptoloids of the Cape Phillips Formation are preserved as compressed specimens in shale and as uncompressed specimens in carbonate concretions and carbonate beds. The concretions lithified during shallow burial, reducing the effect of physical compaction experienced by the surrounding shale (Coniglio and Melchin, 1995). This exceptional diagenetic history preserves the graptoloids in semi-compacted or uncompacted form and also records the sedimentary structures before compaction. This unique preservation of deep-water, fine-grained sediments allows the detailed examination of the relationship between the lithology and the distribution and preservational condition of the graptoloid rhabdosomes. In this thesis I will use evidence from a fine-resolution, layer-by-layer sampling through concretions to understand the post-mortem, sedimentary history of planktonic graptolites.

Comparative taphonomy and the construction of taphofacies models are applied to graptoloids to obtain a better understanding of the fossil group in three ways: 1) enhancing paleoecology studies by gaining a better understanding of the "taphonomic filter" that has altered the original life assemblage; 2) increasing our understanding of graptoloid occurrence, the basis of graptoloid biostratigraphy; and, 3) deciphering the taphonomic processes that act upon a fossil and affect sedimentation processes; therefore, describing the taphonomy of graptoloids has implications in understanding the sedimentary dynamics of the Cape Phillips Basin and deep-water facies.

Time-averaging and temporal resolution

How much time does one bed or one lamina represent? Was the bed deposited in an hour, a day, a century, or millennia? The answer to this question is critical for determining rates of sedimentation and in assessing the fidelity of a bed for paleoecological or evolutionary analyses (Brett and Baird, 1993). To resolve the temporal scope of the sedimentary unit in the absence of highly resolved radiometric absolute dating, one must use indirect evidence, such as sedimentary structures, fossil distribution, and differential preservation.

A storm event will leave a characteristic signature in the sedimentary record. Organisms, both dead and alive, on the sediment surface or buried to a shallow depth will be taken up into the water during the high-energy event and redeposited as the energy wanes. The deposit that results is a mixture of the sediments and organisms that were previously laid down, new organisms transported with the event, and those autochthonous to the deposition site. The storm bed may exhibit a concentration of the larger clasts, including the bioclasts in a basal lag and grade the organisms and sediments upwards (Sadler, 1993). The fossils are now temporally mixed and the bed is considered to be "time-averaged". The bed may also be spatially mixed as a result of the fossils carried with the storm currents from another ecological zone becoming incorporated in the new storm layer.

Walker and Bambach (1971) realized that the time needed to bury a fossil community was likely to be greater than the lifetime of an organism of the community. Thus, a sedimentary bed is likely a composite of many generations of organisms and is usually not a record of an instant in time. They used the term "time-averaging" to identify this process. Samples that are not time-averaged record the conditions at the time of final burial with no influence of fossils from an earlier time (Olszewski, 1999). Time-averaged accumulations incorporate material from an interval of time significantly earlier than the moment of final burial (Olszewski, 1999). Any parameter that is being measured, such as taxonomic composition, morphology, or geochemistry will be averaged in the non-contemporaneous population (Olszewski, 1999). This results in the loss of temporal resolution and also produces the "noise-filter" that averages short-term fluctuations related to seasonal or storm events (Wilson, 1988; Fürsich and Aberhan,

1990; Kidwell and Flessa, 1995). In this way time-averaging can help or hinder the paleoecologist (Kowalewski *et al.*, 1998; Olszewski, 1999). Removing the short-term fluctuations helps articulate the larger-scale ecological events; however, extensive time-averaging may alter the resolution needed to observe evolutionary change or subtle ecological shifts. In this thesis "resolution" refers to the acuity or the sharpness of the fossil record, i.e., the finest temporal or spatial bin into which the fossil remains can confidently be assigned" (Behrensmeyer *et al.* 2000, p. 114). In Chapter Eight I estimate the temporal resolution of a 5 mm lamina of concretionary material using an estimated stratigraphic completeness and a calculated sediment accumulation rate.

Studies of various modern marine environments using radiometric techniques and amino acid ratios have attempted to understand the variation in the ages of organisms on the seafloor (Flessa, 1993; Flessa *et al.* 1993; Flessa and Kowalewski, 1994; Martin *et al.* 1996; Meldahl *et al.* 1997; Kowalewski *et al.*, 1998). The results of these studies indicate that in shallow-water, modern environments, the recently dead mollusc shells can be mixed with shells dated to be hundreds or even thousands of years old. In these assemblages the recently dead were far more abundant than the very old – as would be expected. This skewed age distribution was interpreted to be the result of exposure to destructive taphonomic processes (Kidwell and Bosence, 1991). The older fossils that had been on the seafloor for longer periods of time were exposed to taphonomic agents for a longer duration. The rate of shell destruction is exponential (Meldahl *et al.*, 1997) and can be described numerically using the formula for exponential decay:

$$N_t = N_0 e^{-\lambda t} \qquad (2.1)$$

where N_t is the number of shells of age t and N_0 is the number of shells added in each unit time. The decay coefficient, λ, is related to the biological, physical, and chemical taphonomic processes that destroy the fossil assemblage. These models assume that the shell input (N_0) and the chance of destruction or removal (the product following = Nt) are constant. The taphonomic decay constant, λ, can vary between environments (Parsons and Brett, 1991; Meldahl *et al.*, 1997), between taxonomic groups (Cummins *et al.*, 1986), or even between age classes within the same species.

The degree of time-averaging or the decay coefficient, λ, is dependant upon many factors including: 1) the type of tissue, 2) the depositional environment and the rate of

burial, and 3) the depth of bioturbation relative to net sedimentation rate (Fürsich and Aberhan, 1990; Kidwell and Bosence, 1991; Behrensmeyer and Hook, 1992; Cutler, 1993; Martin, 1993; Kowalewski, 1997, Behrensmeyer *et al.*, 2000). Highly time-averaged fossil accumulations are associated with depositional environments dominated by erosion, such as modern coastlines that erode Pleistocene or Tertiary sedimentary rocks (Wehmeiller *et al.*, 1995). Highly time-averaged fossil beds are also associated with low sedimentation rates, such as modern marine transgression, sediment-starved continental shelves, where the age range of shells is 20,000 years (Kidwell and Bosence, 1991; Flessa and Kowalewski, 1994; Flessa, 1998).

Fossils can become time-averaged in many ways and in this thesis I will group the processes in four broad categories: sediment starvation, reworking, benthic mixing, and collection methods. "Sediment starvation", as discussed above, describes an environment where a sedimentation rate is very low compared with the rate of fossil input. The fossils that accumulate on the sediment surface are time-averaged because the fossil assemblages are not diluted by sediment. The hiatus horizons can represent major disconformity surfaces and sequence boundaries (Holland, 2000), or they can be small-scale, non-deposition events between laminae (Kidwell, 1993). "Reworking" and "benthic mixing" both can be the result of biologic or physical processes. However, reworking is the term used to represent the processes that occur at the sediment surface and incorporate a period, however brief, of erosion and redeposition (Sadler, 1993). Benthic mixing differs in that it occurs at or below the sediment water interface and does not involve a period of erosion (Sadler, 1993). Physical processes, such as storm events or turbidity currents are largely responsible for the erosion and redeposition (reworking) of a stratum, however, biological agents, such as marine birds or large marine animals, such as rays, can also stir-up the shallow sediment causing erosion followed by redepostion. In the Silurian, the biological reworking of sediments was not a major factor, because of the absence of marine birds and large marine animals that did not evolve until the Mesozoic. Benthic mixing is largely produced biologically from infaunal organisms although rare examples, such as liquifaction by earthquakes show that benthic mixing can occur also by physcial mechanisms. These processes of benthic mixing and reworking occur in the "taphonomically active zone" (TAZ, Davies *et al.*, 1989). The

longer a fossil stays in the TAZ the greater the chance for destruction. The more quickly the fossil can move through this zone to the underlying sediments that are isolated from the biostratinomic affects, the greater the chance that the fossil will be preserved.

Fossils can also be time-averaged during the processes of collection by the paleontologist. Graptoloid researchers, collecting specimens flattened in shale, normally find it impossible to collect fossils lamina-by-lamina, unless the shale is perfectly fissile and splits on the millimeter scale, which is a rare occurrence. Often, a representative or bulk sample of specimens is collected from a 5 or 10 cm interval. How representative is this sample of life populations or communities and how is the temporal resolution affected by this collection method? Is there information that can be gained by a higher-resolution sampling, or are the natural processes of time-averaging operating on a similar stratigraphic scale to the sampling interval?

In this thesis, I will attempt to understand the dègree of time-averaging and the temporal resolution of the sediments in the Aeronian Cape Manning section of the Cape Phillips Formation to understand what biases may be entering my study of graptoloid communities. I use information gained from the taphofacies analysis to define background and episodic processes and use these in an estimate of accumulation rates and stratigraphic completeness. I use this information to estimate the temporal resolution of graptolite-bearing strata. I also present a statistical comparison of the graptolite faunal distribution within concretions and between concretions to make some observations about the duration of graptolite communities and sample resolution in graptolite studies. I use the approach that moderately time-averaged samples can aide the description of long-term graptoloid communities by averaging the small-scale fluctuations in community composition.

Graptoloid paleoecology

Graptoloids are an extinct group of colonial, marine invertebrates that were an extremely prolific biota, forming the main component of the preserved Lower Paleozoic zooplankton (Palmer and Rickards, 1991). The graptoloids belong to the Order Graptoloidea of the Class Graptolithina, referred to informally as "graptolites". Of the

eight orders of Graptolithina, seven lived a benthic life and one, the Graptoloidea, lived in the planktonic realm (Bulman, 1955, 1970). The Graptoloidea of are of major interest because of their use as index fossils in Lower Paleozoic sedimentary sequences. Graptoloids are commonly fossilized as carbon films on shale and are found in Lower Ordovician to Lower Devonian rocks all over the world (Bulman, 1955, 1970).

Of prime importance to biostratigraphy is an understanding of graptoloid distribution and occurrence in the Paleozoic seas and rocks. An understanding of how graptolites may have lived in the water column and can have significant impact in studies of graptolite occurrence. Can we recognize graptoloid "communities" in the taphocoenosis (death assemblage) and can we relate these to the biocoeonsis (life assemblage)?

An ecological community is an association of species living in a particular habitat (Brenchley and Harper, 1998, p. 218). These species may be highly interactive with complex webs of relationship such that many species are strongly interdependent. In this sense, Southwood (1987) considered communities to be "superorganisms". An alternative viewpoint perceives that communities are the product of the convergence of organisms that share the similar niche requirements, such as light, nutrients, salinity, etc. Most ecological researchers see communities as being somewhere between these two perspectives (Buzas and Culver, 1994). A community is more complex than a "population" in that it involves the interactions of several species and not just the dynamics of population structure of one species. Previous studies of graptoloid communities involved the identification of graptoloid biofacies (Finney, 1986) or the plotting of graptoloid occurrence (Berry, 1962). Berry (1962) used the global occurrence of cosmopolitan and endemic species to describe graptoloid provincialism and discuss modes of locomotion and dispersal of specific species. Finney (1986) used the co-occurrence of key index species to understand sea level and tectonic history though the Middle to Upper Ordovician of North America. The biofacies of Finney (1986) were spatially distinct to the extent that a two distinct biozonations for North America were proposed.

Rickards (1991) considered graptolite communities when he defined two types of graptoloid death assemblages based upon general observations of graptolite distribution.

He described dark shales of "condensed deposition" in which species diversity is high and abundance is great on single bedding planes. For this type he gave the examples of Hartfell and Glenkin shales of Southern Uplands, the Skelgill Beds of the Lake District, and the Abereiddi Bay black shales. The second type of distribution he termed "turbiditic-type" sequences in which the sedimentation was non-condensed and diversity is low and age variation great on single bedding planes. Rickards (1991) suggested this second type might be the result of mass-mortality of monospecific plankton clouds from a particular niche. This question of mass-mortality I will address in Chapter Nine when I estimate sedimentation rates of the Cape Phillips Formation.

The finely resolved and exceptionally preserved graptoloids are used to study the ecology of ancient graptoloid communities (graptoloid paleosynecology). A fine-resolution sampling of the graptoloid species distribution vertically through a concretion is a quantitative record of the taphocoenosis (death assemblage). Small shifts in species composition and dominance are used to understand larger-scale basin dynamics by examining several stratigraphically consecutive concretions. Twenty concretions span almost 20 meters of continuous strata from the upper Rhuddanian to upper Aeronian portion of the Cape Manning section. In addition, eight concretions were sampled from an approximately 5 m thick section in the early Telychian. To avoid problems of major faunal changeovers that accompany some zonal boundaries, the analyses were conducted within concretions all from the same biozone. Five biozones were examined: *Coronograptus cyphus, Monograptus pectinatus, Rastrites orbitus, Lituigraptus convolutus*, and *Spirograptus guerichi* zones. The recognition of recurrent species associations was based on a cluster analysis of the counts of thecae from the layer-by-layer dissolution residues. The identification of species that consistently co-occur and also have similar abundance profiles allows the reconstruction of graptoloid paleocommunities.

The study of ancient ecosystems (paleoecology) is hierarchical. One can focus her research on the individual within a niche or a habitat, the population of individuals, a community of different populations, or an entire ecosystem that summarizes all the biological and physical characteristics of a broad area (Brenchley and Harper, 1998). However, it is difficult to address one aspect of ecology without at least being cognisant

of the others. To understand graptoloid distribution and graptoloid communities it is necessary to first understand how individual graptoloids lived. How did they move through the water? What did they eat? How did they reproduce? Study of behaviour of individual organisms and how they relate to their environment is autecology; whereas, synecology, is the ecology of communities of organisms (Prothero, 1998, pp.117, 118). I will review what is understood from previous investigations regarding graptoloid paleoecology and introduce some of the controversies that are inherent in studying an ancient organism with few modern analogues. To organize this discussion I have focused on three areas of graptoloid paleoecology: biological affinities, autecology, and synecology.

Biological Affinities

The affinity of graptolites with modern hemichordates, based on the similarity of skeletal structure between graptolites and modern hemichordates, is the criterion used to classify the graptoloids in the Phylum Hemichordata (Bulman, 1970). Kozlowski (1948) first noted the similarities in structure between the extinct graptoloids and the modern *Rhabdopleura*: a small colonial marine animal of the Phylum Hemichordata, Subphylum Pterobranchia. This organism is a small, benthic colony of individual tubes, each housing a zooid. The zooids are all connected to each other by means of a stolon system, but are able to leave their tubes to feed or repair the skeleton. The zooid secretes the collagen skeleton of irregular fuselli with its pre-oral lobe and strengthens the structure by applying cortical bandages (Dilly, 1986). Like modern rhabdopleurans, the graptoloids were colonial. Unlike these organisms most graptoloids had a higher degree of colonial integration and symmetry (Urbanek, 1990).

The other living genus of pterobranch is *Celphalodiscus*, but *Rhabdopleura* is generally assumed to be a closer relative to graptoloids for the following reasons; *Rhabdopleura* is a more regular and integrated colonial organism than *Cephalodiscus*, *Rhabdopleura* displays bilateral symmetry which is not apparent in *Cephalodiscus*, but is a characteristic of graptoloids, and the *Cephalodiscus* zooid ranges in size from 2-7mm, much larger than the *Rhabdopleura* (less than 1mm), and too large for most graptoloid thecae (Rigby and Sudbury, 1995). Most researchers support the affinity between

graptoloids and the modern *Rhabdopleura*; however, some see the association as posing problems as they are unable to reconcile their hypothesized graptoloid modes of life with that of the *Rhabdopleura* (e.g., Bates 1989).

Graptoloid autecology

This section of the chapter is an examination of how the graptoloids related to their paleoenvironment as individuals with regards to locomotion, feeding strategies, diet, ontogeny and reproduction. The graptoloids were unique, planktonic, colonial organisms because of their assumed zooidal coordination via the common canal. Based on cortical bandage patterns (collagen-like material applied by the zooids to the exterior of the rhabdosome) it is suggested that the zooids (individuals of the colony) had some degree of freedom from the constraints of colonial behaviour and could divide the labour between the zooids of the colony (Crowther, 1981). In this sense the "individual" is both the zooid and the "supra-individual" of the graptoloid colony, able to act as one, integrated, colonial unit (Underwood, 1993a).

Locomotion

In 1897 Charles Lapworth suggested that the graptoloids were epiplanktonic, suspended by the nema from floating seaweed, relying on chance currents to bring nutrient-rich waters. Bulman (1964, 1970) and Kirk (1969) criticized the attachment model, observing that nema orientation was not suitable for attachment in some scandent forms and finding no evidence for floating algae buoyant enough to support the larger rhabdosomes. Instead, Bulman (1964) described the graptoloids as being truly planktonic with adaptations, such as vanes or floats that allowed them to float passively with water currents. The almost worldwide distribution of graptoloids, their preservation in a variety of rock-types, and their association with other zooplankton led researchers to believe that these animals lived in the planktonic realm (Rickards 1975).

As a planktonic, filter-feeding organism, the graptoloid would have had to travel at a different velocity than the water current to reach fresh food sources and avoid starvation (Melchin and Demont, 1995). Rigby and Rickards (1989) recognized the necessity of directional motion for the rotation of graptoloid rhabdosomes in their feeding strategy

models. Two contrasting hypotheses attempt to explain graptoloid movement. One describes graptoloids as being passive or active floaters, using gas chambers or fat storage to regulate buoyancy (e.g., Bulman 1964, 1970; Rickards, 1975; Finney, 1979). The other hypothesis is that the graptoloid colony was able to coordinate zooid activity to achieve locomotion (e.g., Kirk, 1972, 1978, 1990a,b; Melchin and Demont, 1995).

Rickards (1975) observed that 0.008 cc of oxygen, at standard temperature and pressure, was enough to support a rhabdosome of *Rhabdinopora.* He hypothesized that gas bubbles within the nema, vane structures or vacuolated extrathecal tissue would generate rhabdosome buoyancy. Finney and Jacobson (1985) added to the buoyancy model by describing various flotation devices and rhabdosome structures that increase drag in the passive graptoloids. Rigby and Rickards (1989) and Rigby (1991b, 1992) model the passive filter-feeding descent of the graptoloids through the water column, but do not propose a hypothesis of how they rise again to begin a new feeding descent.

A comparison with the pterobranch affinities provides evidence that cortical bandages were applied from the outside and negates the hypothesis of extrathecal tissue. Long spines of the *Cephalodiscus graptolitoides* were considered "identical" in morphology to the graptoloid nema (Dilly, 1993). Although not necessarily homologous, the presence of these spines also suggests that graptoloids lacked an external membrane. If the gas or fat had been stored within the small space of the rhabdosome or in a nemal vacuolated vein, the upward force generated was likely not enough to create buoyancy (Underwood, 1993a). The complicated pressure changes experienced with changes in depth would require a sophisticated gas chamber to permit the graptoloid to control the degree of buoyancy. Perhaps for this reason, no modern zooplankton in the size range of graptolites use gas bubbles as a method of buoyancy control (Melchin and Demont, 1995).

As planktonic, colonial organisms, the graptoloids have few modern analogues. The physonectid siphonophores and the free-swimming tunicate salps are modern colonial animals that live in the planktonic realm. The physonectid siphonophore is able to coordinate the individual zooids to actively propel the colony by ciliated extrathecal tissue that covers the entire organism (Bates, 1989). Colonial salps, similar in size to a graptolite rhabdosome, use coordinated jet propulsion to move through the water (Madin,

1990). Melchin and Demont (1995) considered all of the modes of locomotion used by living zooplankton, including the siphonophores and the salps, and concluded that all but one would have been ineffective in graptoloid locomotion based on considerations of colony design and hydrodynamics. Melchin and Demont (1995) suggest, based on biomechanical grounds, that modification of one pair of the feeding appendages or cephalic shield of a rhabdopleuran-like zooid to form "wings" would efficiently propel the colony and coordinate of the direction of movement.

Feeding strategies and diet

The zooids were filter feeders, most likely extending ciliated lophophores from the thecal apertures of the graptoloid rhabdosome (Bulman, 1955). Minute phytoplankton and possibly zooplankton were the assumed foods of the graptoloids and whereas there exists an association with graptoloids and organic-rich shales, the source of organic material has not been traced to plant or animal origins (Rickards, 1975), although most is assumed to be of algal or biogenic origin.

Rigby and Rickards (1989) built physical models of graptoloid rhabdosomes to investigate their gravitational descent through the water column. The rotation of the graptoloid rhabdosome model as it descended through the water was caused by a variety of modifications in the form, such as, changes in thecal and stipe orientation, alterations of the colony shape and the addition of vanes and spines. This passive rotation of the rhabdosome, rather than a straight descent, would have allowed each zooid access to unharvested water, a definite advantage to the zooid and the colony. The rhabdosome form also provided an efficient feeding array for the available food. Fortey and Bell (1987) used computer modeling to synthesize patterns of branch formation of multiramous graptoloids that would maximize the effiency in extracting food from the water column and found that many were similar to forms found in the fossil record. Rigby (1991; 1992) related graptoloid morphologies to feeding strategies and Underwood (1993a) classified these feeding strategies into five groups based on graptoloid functional morphology. In this model, Underwood assumed that the "monograptids" descended through the water column horizontally, which opposes the traditionally held view that these rhabdosome had a vertical orientation (e.g., Rickards and Crowther, 1979; Rigby,

1991). Underwood (1993a) argued that the horizontal position allowed each zooid along the rhabdosome access to unharvested water, which is not possible in the vertical orientation.

Ontogeny of the zooid and astongeny (growth pattern) of the colony

Rigby and Sudbury (1995) speculated that the graptoloid zooid underwent three stages of development during its life, similar to those observed in the modern pterobranch: skeletal stage, feeding stage, and reproductive stage. There is little evidence to support this hypothesis and I will only address the aspects of graptolite ontogeny that are considered in this thesis. Controversy exists in the question of how the embryo or zygote metamorphs to the larva and early sicular stage of development. Two hypotheses exist. The first is that the mobile zygote matures to a mobile larva, which, upon attaining a certain weight or size, settles to the sea floor and the secreted prosicula becomes attached to the substrate, later rising into the water column as the rhabdosome matures (Kirk, 1969, 1990a, b). This hypothesis is based upon the development of sessile dendroid graptoloids from which planktonic graptoloids are believed to have evolved. The second hypothesis does not involve the settling of the larva but instead describes all developmental stages as having occurred in the planktonic environment (e.g., Fortey, 1982; and Erdtmann, 1982). These hypotheses can be tested using the observations of sicular and thecal distribution through the samples examined for this thesis (Chapter Nine).

The first stages of the graptoloid reproductive cycle are not clearly understood. Koslowski (1948) reported finding graptoloid "eggs" within encysted thecae of encrusting colonies. Kirk (1990a) proposed the idea that sperm and eggs were liberated into the sea to be fertilized before larval formation. Kirk (1990a) described this mixing as happening in the sea, whereas Koslowski (1948) believed fertilization of the graptoloid "egg" must occur in the colony and found hatched graptoloid embryos in the encysted thecae cavity. The uncertainty of where the fertilization occurred does not overshadow the attempt that both studies make to explain how the graptoloids achieved genetic diversity. The necessity of asexually budding animals to occasionally mix their genetic material with others of their species is the basis of creating a "fit" population as

heterozygotes are more stable than homozygotes (Urbanek, 1990). The graptoloids experienced explosive radiation that could only be produced by a community of heterozygote animals that were able to mix their genetic material (Urbanek, 1990).

Subsequent colony growth from the sicular zooid was the result of asexual budding. Modern pterobranchs exhibit this asexual and sexual reproduction with only some of the zooids maturing to the stage of sexual reproduction (Urbanek, 1990). Underwood (1993a) defined two main strategies in graptoloid reproduction. The building of large, long-lived rhabdosomes represents a partitioning of graptoloid energy towards growth and asexual reproduction and away from sexual reproduction (Underwood, 1993a). The other strategy observed in the preserved graptoloid specimens is to grow small, short-lived colonies that attain maturity rapidly and devote much of their energy to sexual or asexual reproduction (Underwood, 1993a). These graptoloids were likely taking advantage of a plentiful food supply with this rapid growth in their population size (Underwood, 1993a).

Graptoloid population studies (Palmer, 1986; Rigby, 1993; Underwood, 1998) have added to our understanding of population structure and their significance with regards to graptoloid reproductive phases. An assumed relationship between graptoloid length, number of zooids, and graptolite age is essential in credible graptoloid population studies (Rigby and Dilly, 1993). Rigby (1993) used the growth rates obtained from observing modern hemichordates in the interpretation of the population structure of a graptoloid bedding plane. *Rhabdopleura* adds growth rings, analogous to two half-rings ("fuselli") of the graptoloids, every eight hours (Rigby and Dilly, 1993). Rigby and Dilly (1993) estimated that the average graptoloid sicula would take 10.9 to 33.5 days to secrete (95% probability) and the average graptolite colony lived between two to five years. Although the validity of defining exact ages of graptoloid rhabdosomes has been questioned based on evidence of variable fuselli formation rates within at least one genus (Russel *et al.*, 2000), I believe the general concept of longer rhabdosomes being equated with longer-lived, more mature graptoloid colonies. Rigby (1993) used survivorship curves to show that some graptoloids died from constant environmental stress whereas others lived long enough to die from handicap because of increasing length or age.

Synrhabdosomes are clusters of graptolites that some researchers have speculated were for the purpose of reproduction. Synrhabdosomes are preserved in the fossil record as clusters of graptoloids with the nemata overlapping (e.g., Ruedeman, 1947) and less commonly with the virgella overlapping (e.g., Bjerreskov, 1976). It has been suggested that synrhabdosomes served some purpose, such as bringing together graptoloid colonies for sexual reproduction (Hutt, 1991; Gutiérrez-Marco and Lenz, 1998), increasing drag (Kirk, 1972), as a feeding strategy (Underwood, 1993a) or they are the result of a asexual budding from one colony (Zalasiewicz, 1984). Rigby (1993) suggested that marine snow, an aggregate of organic, detritus and living organisms, bound by an organic mucus, could have collected the graptoloids together as they descended in the water column. The marine snow would have had very little preservational potential, but the graptoloids, kept together by the mucus would be preserved as synrhabdosomes and are therefore a product of taphonomy. Gutiérrez-Marco and Lenz (1998) surveyed 200 synrhabdosomes (90 from one locality in Northwest Spain) and found that they shared many features in common. The often straight or weakly curved rhabdosomes with simple or straight thecae were joined at the distal end of their virgulae. The synrhabdosomes were composed of a finite number of rhabdosomes and most were monospecific. Their evidence does seem to dispute the interpretation of synrhabdosomes as taphonomic structures. Gutiérrez -Marco and Lenz (1998) conclude that they were temporary feeding structures that were formed during times of low nutrient supply in relatively restricted water masses. The origin or purpose of the synrhabdosome remains a mystery, but reports of multi-species synrhabdosomes (Goldman and Mitchell, 1994) suggest that reproduction is not the only possible cause of their formation. No synrhabdosomes were found in any of the concretions or shales examined in this thesis.

Graptoloid Synecology

This section of the paper is a review of previous investigations of how the graptoloids related to their paleoenvironment in the faunal communities in which they occurred. Synecological analyses involves the study of organisms and their interactions, interdependencies and co-evolution with other organisms in the common environment (Dodd and Stanton, 1981). In paleoecological analyses this usually involves the

identification of co-occurring organisms, the *community*. At best, this work is speculative due to the planktonic nature of the graptoloids and the overprinting of taphonomy. The work of this thesis attempts to understand the process of the taphonomic filter on these sediments and decipher the paleoecological history of graptolite communities.

Predation and parasitism on graptoloids

As an abundant member of the plankton, graptoloids represented a reservoir of food energy for pelagic or necktonic predators (Underwood, 1993a). The graptoloids are often preserved with the remains of nektonic animals, such as arthropods, cephalopods and eurypterids and other planktonic animals (Palmer, 1991). It is unknown if any of these organisms were predators of the graptoloids. It is possible that potential predators of the graptoloids were not preserved in the fossil record because they lacked hard parts similar to the many Cambrian predators that were uniquely preserved in Konservat-Lagerstatten (Underwood, 1993a). Underwood (1993a) investigated predation on graptoloids by examining rhabdosome and thecal morphology that might be interpreted as defense and by observing the damage of graptoloid periderms. He described three types of predation on graptoloids: 1) "absorption" of the whole rhabdosome, 2) "crunching" (breakage) of the rhabdosome, and 3) "plucking" when zooids are removed individually. Loydell *et al.* 1998 reported ovoid masses of two species of Silurian "monograptids" that were interpreted to be fecal pellets and other forms of damage resulting from predation. Fragmented rhabdosomes not associated with high-energy events and not resulting from the dissolution process were identified on only a few dissolution surfaces examined in this thesis. Damage to the rhabdosome as a result of necrolytic processes is considered to be rare in the samples from the Cape Phillips Formation.

It is possible to see evidence of parasitism in the fossil record if the parasite infestation leaves a recognizable trace on the fossil skeleton. Small rings of cortical tissue are recorded from observations of isolated specimens of "diplograptids" (Jackson, 1971; Loydell 1991). The broken edges of the circles may be evidence that a cyst or flask was anchored at these circle sites. A connection to the interior of the skeleton is not observed. It is possible that the graptoloid was not parasitised but that a small organism

used the cortical secreting behaviour of the graptoloid to create a protected dwelling on the outside of the rhabdosome (Underwood, 1993a). These structures related to parasitism are found on a few isolated rhabdosomes examined in this thesis. A broken cyst-like structure that is not connected with the internal chamber of the rhabdosome is observed on a specimen of *Normalograptus laciniosis* (Plate 7k). A non-fragmented cyst-like structure is observed on a specimen of *Normalograptus nikolayevi* (Plate 4j). Of the thousands of isolated specimens examined in this thesis, cyst-like structures on the exterior of the rhabdosomes numbered less than ten.

Habitat

Graptoloids are most commonly preserved in organic-rich shales deposited in deep, quiet water environments, although they are also found in other marine sediments, such as carbonates, sandstones, siltstones and cherts (Berry, 1962). Planktonic graptoloids are rare in rocks from shallow sediments (Lenz and Chen, 1985). It is uncertain whether this is an indication that their presence was rare in the shallow shelf communities or their rarity in the shallow shelf rocks is due to a preservational bias (Palmer, 1991). Graptoloids preserved in black shales are associated with fossilized land plant debris (Jaeger, 1970) leading some researchers to conclude that the anoxic, deep-water basins were nothing more than graveyards for the drifting dead (Kirk, 1990a). Other researchers believe that graptolites were laterally and vertically separated into communities or species assemblages based upon niche requirements and their distribution can be used to track eustatic change (e.g., Finney and Berry, 1997; Cooper, 1999).

During the Silurian graptoloid faunas were globally distributed, a factor in their use as index fossils, whereas through most of the Ordovician they showed marked provincialism. To explain this variable distribution researchers have proposed models of faunal segregation by water-mass specificity (Skevington, 1974; Watkins and Berry, 1977; Finney, 1984, 1986), vertical segregation by depth zonation (Erdtmann, 1976), or both (Cooper *et al.*, 1991; Lenz *et al.*, 1993; Goldman *et al.*, 1995; Cooper, 1999). Skevington (1974) described two graptoloid faunal provinces of the Ordovician (Pacific and Atlantic provinces) in terms of latitudinal belts defined by steepening thermal gradients between the paleoequator and the paleopoles. The provincialism was likely the

result of differing temperatures that result from current systems in the ocean (Skevington, 1974).

Oceans of the lower Paleozoic were likely intensely stratified with anoxic deep-waters (Kemp, 1991) that allowed the fine preservation of graptoloid fauna (Berry *et al.*, 1978). Modern oceans are not stratified to the same extent as a result of intense vertical and horizontal circulation powered by a strong thermohaline circulation and the configuration of the contents (Bearman, 1989). Phytoplankton, the likely food source of the graptoloids, are restricted to the photic zone at depths between 3-5 m and 150-200 m (Duxbury and Duxbury, 1994). The phytoplankton are often concentrated in areas of upwelling where limiting nutrients are in excess. These upwelling currents often occur at the edges of the continental platforms (Duxbury and Duxbury, 1994). Phytoplankton abundance has been mapped, using satellite data of sea-surface chlorophyll abundance, as thin belts that overlie continental shelves (Duxbury and Duxbury, 1994, Box figure 14.1). Raymont (1983) found that most taxa occur in the waters above the outer shelf and the upper part of the continental slope where upwelling nutrients are likely most concentrated. The inner shelf fauna was composed of a few taxa endemic to the local waters and specialized to the niche (Raymont, 1983). Finney and Berry (1997) and (Cooper, 1998, 1999) suggested that graptoloids had a similar distribution with the greatest abundance and diversity in the waters above the outer shelf and along the continental slope. This lateral variability in graptoloid distribution was probably matched by a vertical (water depth) zonation in graptoloid distribution. An analysis of early Ordovician (Cooper *et al.*, 1991) and Early Tremadoc graptolite distribution (Cooper, 1999) identified three depth-realted biofacies; one found only in deep-water sediments, one found in only shallow-water sediments, and the third group was found in both and was not restricted to a facies.

In studies of modern zooplankton taxa are limited laterally and vertically in their distribution (Bougis, 1976). Euphasiacea are crustaceans that live their adult stage in the plankton realm (Bougis, 1976). In the Northern Atlantic Ocean six species of Euphausiacea are present; two live at a shallow depth, one lives at 200 m, and three are found at great depths, two of which are only found below 1500 m (Bougis, 1976). Each depth is a different niche with particular environmental parameters that vary with

increased or decreased depth, such as light, temperature, food source, salinity, and less importantly, pressure. The reasons for depth zonation may also be a factor of organism-organism interactions and the zooplankton may be following the zonation of a food source or avoiding the zone of a predator. The depth zonation of organisms may show seasonal variations and most zooplankton exhibit some form of vertical migration (Bougis, 1983). Berry *et al.*, (1987) believed that planktonic graptoloids likely lived near the denitrification oxygen minimum zone, located a few hundred to a few thousand meters below the ocean surface, where maximum oxidation of organic matter occurs and productivity was high. The graptoloids would have had a good food source just above this oxygen minimum zone and, due to the low oxygen levels, their preservation potential would be high upon death with the reduction in the amount of scavengers and bioturbation (Berry *et al.*, 1987).

Many researchers examining well-preserved graptoloids report rhythmic dark and light banding from siculae and thecae that alternate every six to nine fuselli (Strachan, 1974; William and Stevens, 1988; Williams *et al.*, 1997). Mitchell (1987) found condensed fuselli intervals that had relief within the structure of metasiculae of *Pseudoclimacograptus sharenbergi*. Williams *et al.* (1997) found the dark bands varied from the rest of the fusellar material in having a very thick fusellar wall. Non-banded siculae were more uniform in wall thickness (Williams *et al.*, 1997). Williams and his co-authors (1997) concluded that the differences in fusellar wall width are the result of variation in the availability of skeletal material during secretion. The rhythmic nature of this banding was interpreted by this group to be a cyclical fluctuation on the scale of a day. Williams *et al.* suggested that this banding pattern was produced by diurnal migration through the water column from oxygen-poor denitrification, nutrient-poor waters to nutrient-rich waters.

There appears to be an association between certain graptoloid forms and deep-marine deposits (Rickards *et al.*, 1990). Kirk (1990) described how depth zonation of graptoloid species would have evolved as a result of niche competition. Graptoloids would evolve to occupy a certain feeding niche within the photic zone, preying upon specific phytoplankton. Kirk (1990) also hypothesized that feeding niches would have

changed with the age of the graptoloid, thus zoning the age cohorts of graptoloid species with regards to depth, although no evidence has been found to support this.

Geological setting of the Cape Phillips Formation

The Cape Phillips Formation is an organic-rich, carbonate/shale sequence of Late Ordovician to Early Devonian age, in the Innuitian Tectonic Province of the Canadian Arctic Archipelago. The Cape Phillips Formation extends from Melville Island to Devon Island in the east and Ellesmere Island in the north (Melchin 1987b, 1989, Melchin *et al.*, 1991). In the 1996 and 1998 field seasons, 52 concretions averaging 15 cm in diameter were collected from two localities of the Cape Phillips Formation on Cornwallis Island: the first along an unnamed stream 10 km west of Cape Manning; and the second, the type section at Cape Phillips (Figure 1.1).

Lithostratigraphy of the Cape Phillips Formation

The Cape Phillips Formation is the distal facies-equivalent of the Allen Bay Formation, a carbonate shelf deposit to the south. The Cape Manning section and the Cape Phillips section were both similarly located with respect to the basin-shelf facies transition with the Allen Bay Formation carbonates (Figure 2.2). Northwestward, the Cape Phillips Formation grades into the deeper-water sediments of the Hazen Trough. The Cape Phillips Formation was first described by Thorsteinsson (1958) and divided into three informal members (members A, B, and C). The sampled portion of the Cape Manning section exposes members A and B and strata range in age from Early Llandovery (Rhuddanian) to Late Llandovery (Telychian) (Figure 2.3). At the type locality, the Cape Phillips section, members B and C are represented and the section ranges in age from Late Llandovery (Telychian) to Ludlow although this thesis studied the strata from the Late Llandovery to the Lower Wenlock (Sheinwoodian) (Figure 2.4).

Throughout the Cape Phillips Formation member A ranges is Ashgill to Mid Llandovery and member B is Late Llandovery. Where member B is present, member C ranges from uppermost Llandovery to upper Silurian or Lower Devonian. Where member

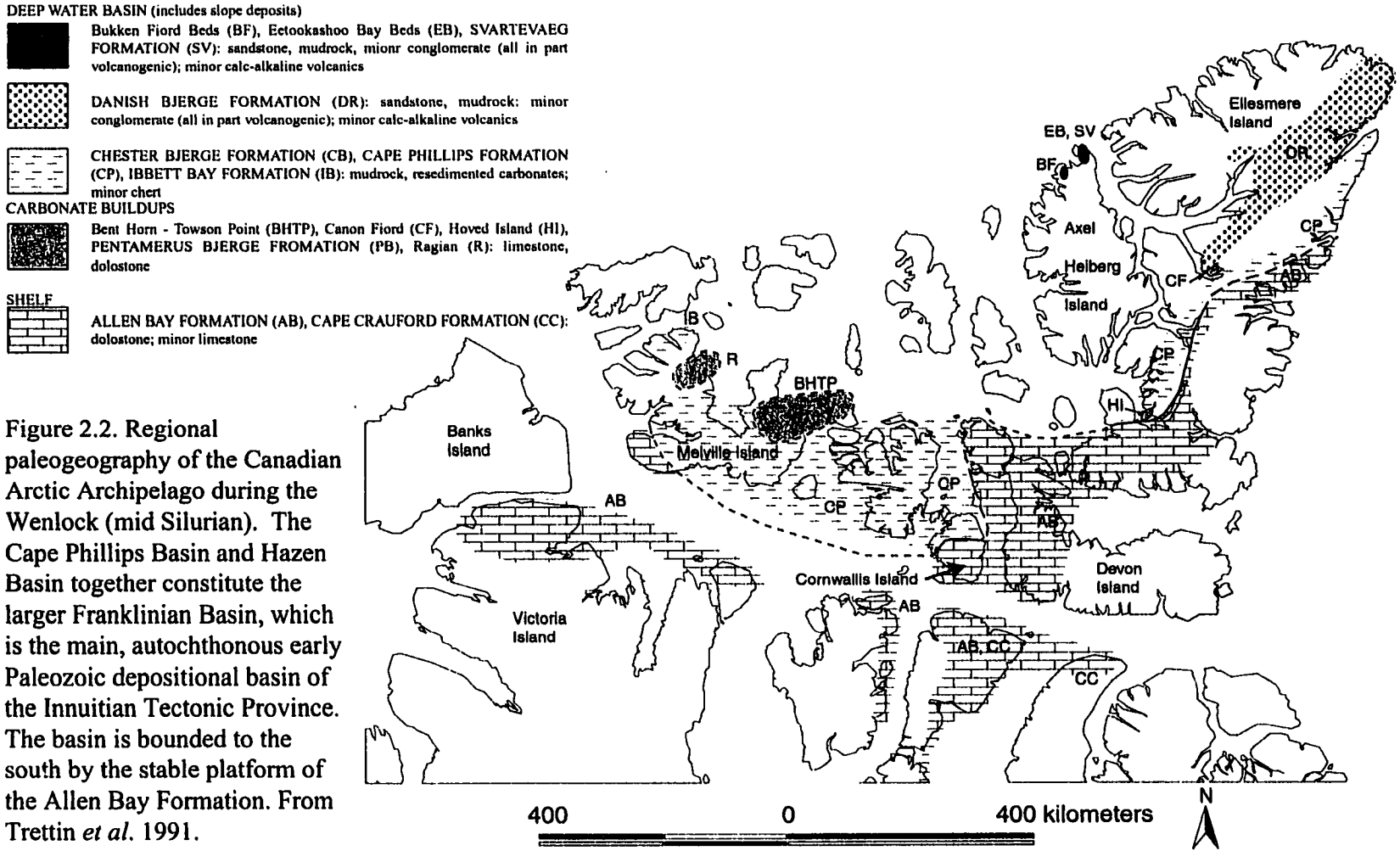

Figure 2.2. Regional paleogeography of the Canadian Arctic Archipelago during the Wenlock (mid Silurian). The Cape Phillips Basin and Hazen Basin together constitute the larger Franklinian Basin, which is the main, autochthonous early Paleozoic depositional basin of the Innuitian Tectonic Province. The basin is bounded to the south by the stable platform of the Allen Bay Formation. From Trettin *et al.* 1991.

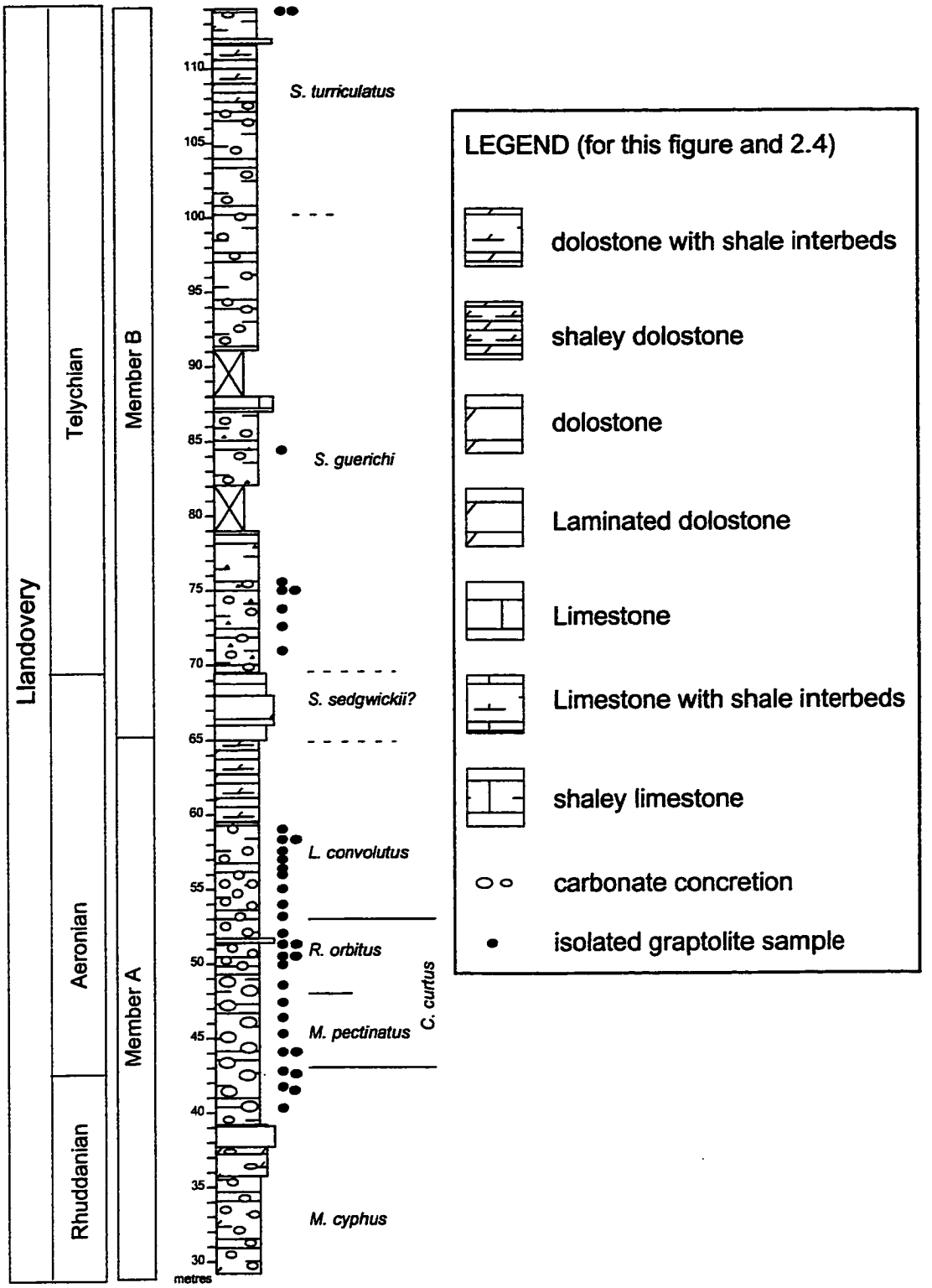

Figure 2.3. Stratigraphy of the Cape Manning section. Closed circles (•) mark sample locations. Note, the sample name is the meterage within this stratigraphy. Graptolite biozones are given.

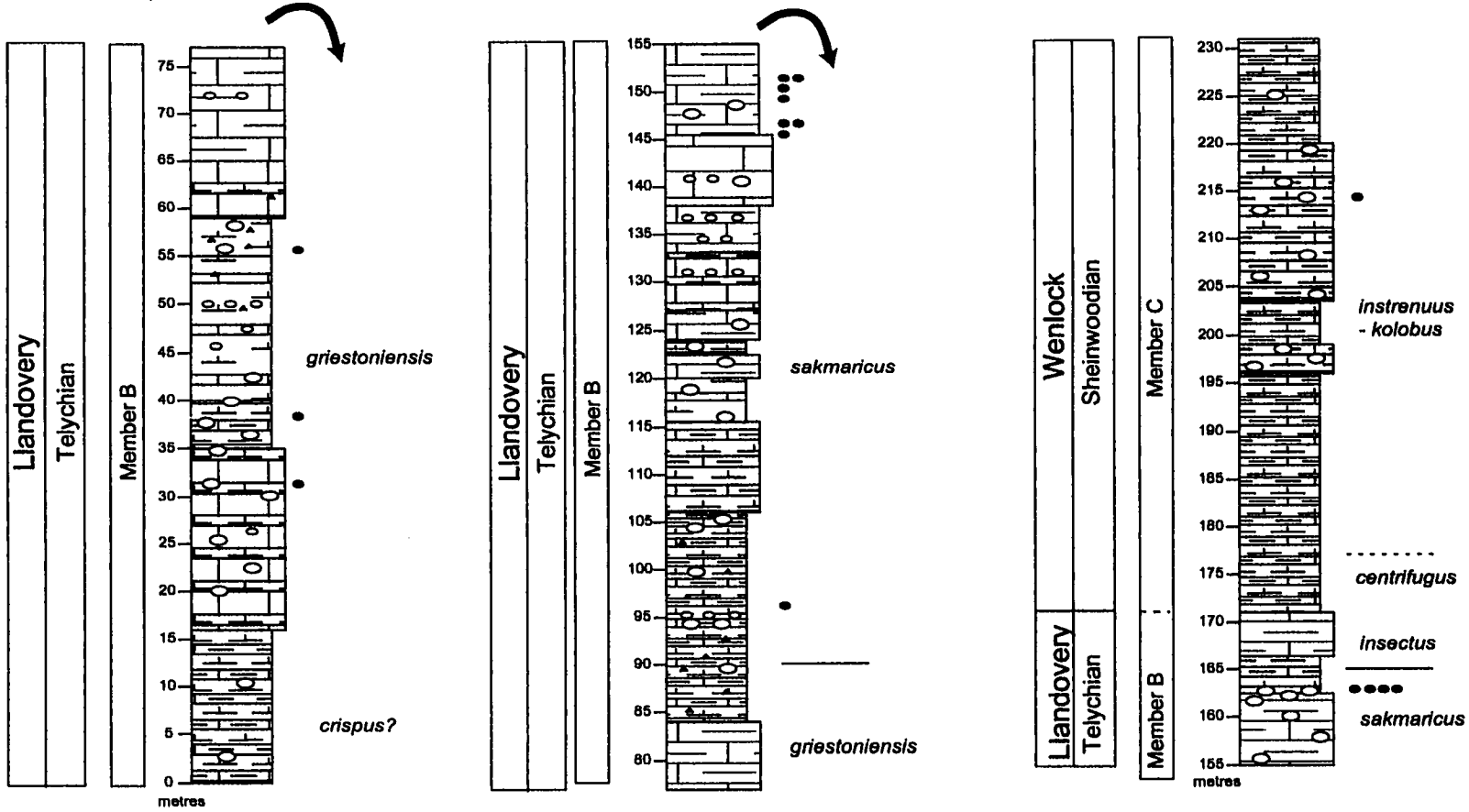

Figure 2.4. Stratigraphy of the Cape Phillips section. Open circles (•) mark sample locations. Note, the sample name is the meterage within this stratigraphy. Graptolite biozones are given. Legend shown in figure 2.4.

B is absent and member A is in direct contact with member C, the latter begins in the lower Upper Llandovery (Lenz 1995, Lenz and Melchin, 1990; Melchin 1989).

Member A is composed of interbedded argillaceous carbonates and calcareous and dolomitic shales (Melchin, 1989). A 10-15 m thickly bedded carbonate (limestone or dolostone) marks the base of the member (Melchin 1989). The lithology of this massive carbonate is regionally uniform, consisting of sparsely fossiliferous lime-muds with no defined shelf-margin facies (de Freitas, *et al.*, 1999). Up-section the member becomes more argillaceous, wavy and planar lamination becomes more common, and the degree of bioturbation decreases (Melchin, 1989).

Member B is differentiated from member A by an increase in the amount of nodular and bedded chert and a decrease in the abundance of shaly beds (Melchin, 1989). Member B is restricted to Cornwallis Island, southern Bathurst Island, Grinnell Peninsula, and central Melville Island (Melchin, 1989).

Member C is composed of calcareous shales and shales with minor siltstones, and thickly bedded argillaceous limestones (Melchin, 1989). Calcite concretions occur in all three members but are most common in member B (Melchin, 1989). At the base of member B is a thickly bedded, light to medium grey limestone with wavy and planar lamination and small ripple marks that indicate resedimentation of the limestone or current reworking of the sediments at depth (Melchin, 1989). Where member B is absent a limestone unit separates member A and member C (Melchin, 1989). This carbonate unit is regionally uniform and a useful marker. Stratigraphically it is bound by the *Lituigraptus convolutus* Zone or *Rastrites orbitus* Zone (*Campograptus curtus* Zone in Melchin, 1989) fauna below and *Spirograptus guerichi* Zone (*Spirograptus minor* Zone in Melchin, 1989) fauna above and is thought to represent the *Stimulograptus sedgwickii* Zone at this interval (Melchin, 1989). Melchin (1989) concluded that the absence of the *S. sedgwickii* Zone graptoloid fauna is the result of sedimentological or preservational factors or both. This carbonate unit is found in the Cape Manning section at 65.0 to 69.5 m.

Resedimented carbonates are most common in member C, less common in member B and member A. Conglomerates and carbonate grainstones, interpreted to be of possible turbiditic origin are less common than the finely laminated mudstones (Melchin, 1989).

The coarse-grained, resedimented carbonates are most abundant near the Cape Philips-Allen Bay facies transition beginning in the Late Llandovery (Melchin, 1989). Detailed lithostratigraphy of the concretionary sediments contributes to the understanding of the depositional processes of the Cape Phillips Formation. Many of the concretions examined from member A of the Cape Manning section or member B of the Cape Phillips section were composed of clay, organic matter and shelf-derived, resedimented carbonate (Chapter Five). The carbonate source for most of the calcareous shales of the Cape Phillips Embayment is interpreted to have come from the shallower carbonate sediments of the Allen Bay Formation. Evidence for coarser carbonate resedimented deposits, which result in thickly (10 to 40 cm) bedded limestones or dolostones, are found rarely in member A of the Cape Manning section and more commonly in member B of the Cape Phillips section. The sediments from the shelf-slope transition were derived from a line source, not a channel or delta source as is common in siliciclastic sedimentation. The deposition in the apron-slope facies, as a result, is unorganized and the strata rarely display Bouma-type sequences (Chapter Five).

Paleogeography and Depositional Environment

The study area was located in a warm, tropical climatic zone during the Early Silurian. The paleolatitude of the Cape Phillips Embayment is estimated to be approximately 15° North as determined from the paleogeographic map (Figure 2.5) of Scotese and McKerrow (1990). Together with the underlying Late Ordovician Irene Bay Formation, members A and B of the Cape Phillips Formation record a gradual change from open-shelf to drowned shelf conditions to a more distal, deep slope environment (Melchin 1987a, 1989). A Late Ordovician (*A. fastigata* Zone) transgression moved the shelf-edge landward (south and east) throughout most of the Canadian Arctic Archipelago, excluding North Greenland and northeastern Ellesmere Island (de Freitas *et al.*, 1999). This shelf-retreat created the "Cape Phillips Embayment" with a shoreline tens to hundreds of kilometres inland of the Ordovician shelf (de Freitas *et al.* 1999, termed Cape Phillips Basin by Melchin, 1989). Following the Late Ordovician marine transgression and the formation of the Cape Phillips Embayment, organic carbon-rich, graptolitic mudrocks, carbonates, and chert were deposited in deep, anoxic conditions

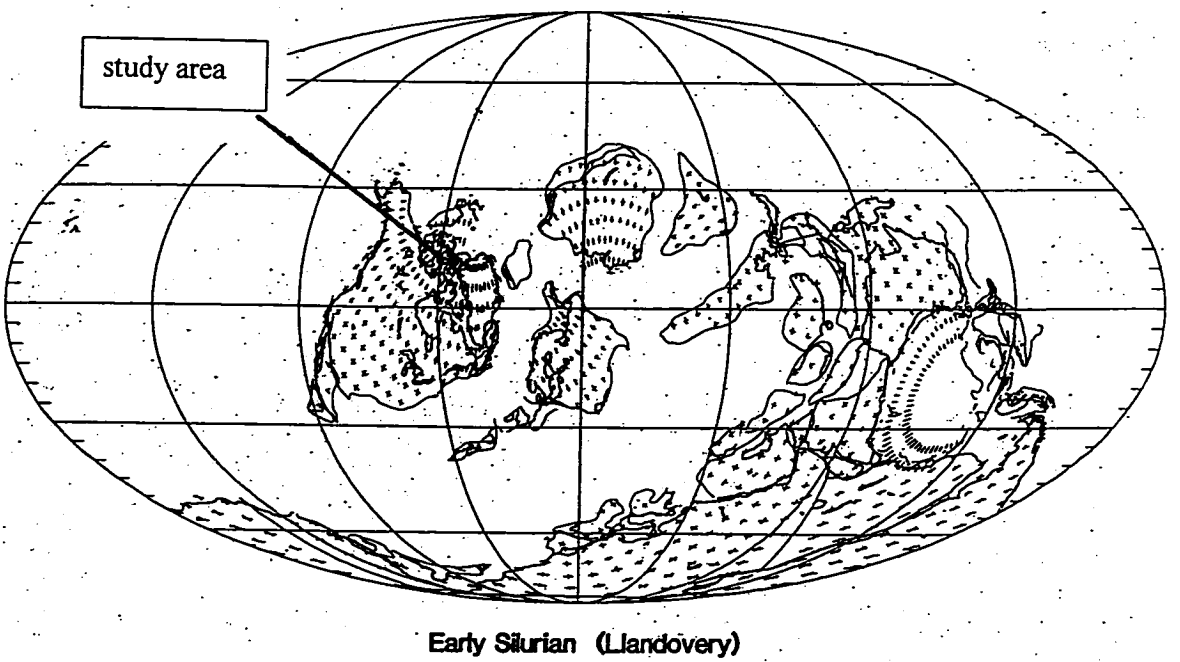

Figure 2.5. Early Silurian (Llandovery) paleogeographic map. The Cape Phillips Embayment is located on the northwest margin of the paleocontinent Laurentia at approximately 15° North. From Scotese and McKerrow, 1990.

with possibly short intervals of oxygenation (Melchin, 1989; Melchin *et al.* 1991). I have found supporting evidence for the anoxia. Finely laminated sediments were common and I found no evidence of traces or burrows in the unlaminated or "structureless" facies. Pyrite coatings on some of the rhabdosomes and disseminated pyrite observed in thin section were further evidence of an oxygen-starved sedimentary environment. Total organic carbon measurements from the shales of the Cape Phillips are as high as 24.6 percent and average 3.9 at the Cape Manning section (Melchin pers. comm., 2001) and 1.75 percent at the Cape Phillips section (Heath, 1998).

The Cape Phillips Embayment is bordered by the stable Arctic Platform to the south and east, and the deeper and more tectonically active Hazen Basin or Foredeep to the north and west (Melchin, 1989; deFreitas et al., 1999). All three units are components of the sedimentary-igneous succession termed the "Franklinian Succession" deposited on a passive continental margin (de Freitas *et al.* 1999). The lateral transition from the shallow carbonates of the Allen Bay Formation to deep-water strata indicate deposition in a carbonate ramp facies from the Ashgill to the early to mid Llandovery (Melchin, 1989). Stepped transgressions from the latest Rhuddanian to the latest Telychian moved the shelf margin inland. At the eastern and southern margin of the Cape Phillips Embayment, cherty mudrock, dolostone and bedded chert directly overlying the shallow water carbonates of the Allen Bay Formation is evidence of this latest Rhuddanian transgression (de Freitas, *et al.*, 1999). The shelf edge retreat stopped and the location of the shelf edge remained constant through the rest of the Silurian as observed in the distinct shelf-edge facies (Sodero and Hobson, 1979; Melchin, 1989). The ramp-like shelf to basin morphology that lacked a distinct platform edge facies, changed in the late Aeronian to early Telychian as reefs and grainstones developed in drowned shelf, shelf interior and shelf margin settings (de Freitas *et al.*, 1999; Melchin, 1989, Sodero and Hobson 1979). During this time, the shelf margin of the Cape Phillips Embayment developed a distinct platform-edge facies and the rimmed shelf morphology characteristic of the Silurian shelf margin in the Arctic islands (Trettin *et al.*, 1991). The steeper, rimmed morphology may have caused the resedimentation of carbonates and the massive carbonate marker observed in the upper Middle Llandovery (*S. sedgwickii* Zone?)

(Melchin, 1989). Syntectonic clastic sedimentation during the early Ludfordian (Late Ludlow) is the product of the Boothia Uplift that is associated with the Caledonia "Orogen" (de Freitas, *et al.*, 1999). The increased sedimentation rate resulting from the uplift effectively "filled" the Cape Phillips Embayment, in which the youngest sediments are Early Devonian.

Carbonate diagenesis of the lower Cape Phillips Formation

The graptoloids are preserved in carbonate concretions, carbonate beds, and as flattened carbon films on shale. Many of the carbonate concretions within carbonate-rich shale of the Cape Phillips Formation lithified early in diagenesis prior to major compaction (Coniglio and Melchin, 1995). Concretionary carbonate is usually precipitated in sediment pore spaces (Raiswell, 1976) preserving structures, such as burrows and fecal pellets, evidence that mineral precipitation did not force sediment particles apart (Allison, 1990). Coniglio and Melchin (1995) estimated shale compaction to range from 73% to 84% based on assessing shale drape and tracing the laminae in the adjacent shale to the concretion interiors. Calcite, and rarely dolomite, precipitated in zones of bacterial-sulphate reduction within the sediment pore waters (Coniglio and Melchin, 1995) and, in most examples, the concretion growth did not disturb the original sedimentary structures of the sediment.

Zones of concretion growth are identified in the lithology of the stratigraphic section for the Cape Manning section (Figure 2.4) and Cape Phillip section (Figure 2.5). Concretions within the *C. cyphus* Zone and lower *M. pectinatus* Zone of the Cape Manning section between 40.5 and 44.1 m contain compressed graptoloids. These concretions were lithified later in diagenesis following some compaction and dewatering of the muds. Compressed graptoloids are also found in two concretions (CP 38.4 and CP 56.9) of the *M. griestoniensis* Zone of the Cape Phillips section. Thecal apertures and proximal portions of the rhabdosomes, strengthened with apertural processes or extra cortical tissue, were not compressed whereas the rest of the rhabdosome was. In the lower Aeronian strata the whole rhabdosomes were flattened with only rare exceptions.

Graptolite biostratigraphy of the Cape Phillips Formation in this study

The graptoloid biostratigraphy of the Cape Phillips section by Melchin (1989) and Melchin *et al.* (1991) for the Llandovery and Lenz and Melchin (1990, 1991) and Lenz (1995) for the Wenlock has been slightly modified in this study. Stratigraphic measurements recorded in the previous publications are reassigned based on the measurements obtained by M. Melchin during the 1998 field season (Figure 2.4). Lukasik (1994) described the graptoloid biostratigraphy of the Cape Manning section from the latest Ordovician to the Aeronian. A more detailed study of a portion of the latest Rhuddanian, Aeronian, and earliest Telychian graptoloid distribution through an interval of the Cape Manning section is presented herein (Figure 2.3, Appendix B). Graptoloids flattened in shale and three-dimensional graptoloids isolated from carbonate concretions provided the basis for the re-description. Of the eleven sections included in the biostratigraphic study conducted by Melchin (1989), all but Cape Manning were collected in stratigraphic detail (to the nearest 0.5 m).

Five graptoloid zones are recognized in the sampled interval of the Cape Manning section: *Coronograptus cyphus* Zone, *Monograptus pectinatus* Zone, *Rastrites orbitus* Zone, *Lituigraptus convolutus* Zone, and *Spirograptus guerichi* Zone. There are difficulties in correlation with the well-described zonal scheme for the Lower Silurian established in Britain because of the absence of some key index fossils. There are more similarities between the Lower Silurian Canadian Arctic graptoloid assemblage and those of Kazakhstan, China, and Bornholm (Melchin, 1987). The correlation of world-wide graptoloid zonal schemes for the Lower Silurian is presented in Figure 2.6.

In previous publications describing the Llandovery graptolite biostratigraphy of Arctic Canada (Melchin, 1989; Lukasik and Melchin, 1997), the *M. pectinatus* Zone and the *R. orbitus* Zone were considered subzones of the *Campograptus curtus* Zone. Improved sampling through this interval allows the recognition of these as distinct zones: *R. orbitus* and *M. pectinatus*.

SERIES and Stages		Generalized zonation	British Isles Composite	British Isles Wales	Bohemia	Poland & Bornholm	Arctic Canada
WENLOCK	Homerian	*"M". ludensis*	*"M". ludensis*		*"M". ludensis*	*"P. vulgaris"*	*"M". ludensis*
		"M". deubeli U / *"M". praedeubeli-* L	*G. nassa*		*"M". deubeli* / *"M". praedeubeli-*		*"M". deubeli* / *"M". praedeubeli-*
		P. parvus-G. nassa			*P. parvus-G. nassa*	*G. nassa*	*P. dubius-G. nassa*
		Cy. lundgreni U / L	*Cy. lundgreni*		*Cy. lundgreni*	*Cy. lundgreni*	*Te. testis* / *Cy. lundgreni-*
	Sheinwoodian	*Cy. perneri* U / *Cy. rigidus-* L	*Cy. ellesae* / *M. flexilis* / *Cy. rigidus*		*Cy. ramosus* / *Cy. perneri-* / *Cy. rigidus*	*Cy. radians* / *Cy. ellesae-* / *M. flexilis* / *Cy. rigidus*	*M. opimus* / *Cy. perneri-*
		M. belophorus U / *M. riccartonensis-* L	*M. riccartonensis*	*M. riccartonensis* / *M. firmus*	*M. belophorus* / *P. dubius* / *M. riccartonensis*	*M. riccartonensis*	*Cy. kolobus* / *M. instrenuus-*
		Cy. murchisoni U / *Cy. centrifugus-* L	*Cy. murchisoni* / *Cy. centrifugus*	*Cy. murchisoni* / *Cy. centrifugus*	*Cy. murchisoni* / *Cy. centrifugus*	*Cy. murchisoni* / *Cy. centrifugus*	*Cy. centrifugus*
LLANDOVERY	Telychian	*Cy. insectus* U / *Cy. lapworthi-* L		*Cy. insectus* / *Cy. lapworthi*	*Cy. insectus* / *Sto. grandis*	*Cy. lapworthi*	*Cy. insectus* / *Cy. sakmaricus*
		O. spiralis		*O. spiralis*	*O. spiralis*	*O. spiralis*	*Mcl. griestoniensis* U / M / L
		Mcl. crenulata U / *Mcl. griestoniensis-* L	*Mcl. crenulata* / *Mcl.griestoniensis*	*Mcl. crenulata* / *Mcl.griestoniensis*	*To. tullbergi* / *Mcl.griestoniensis*	*Mcl.griestoniensis*	
		M. crispus U / *Sp. turriculatus-* L	*M. crispus* / *Sp. turriculatus*	*M. crispus** / *Sp. turriculatus**	*M. crispus* / *Sp. turriculatus*	*M. crispus* / *Sp. turriculatus*	*M. crispus* / *Sp. turriculatus*
		Sp. guerichi U / L	*Ra. maximus*	*Sp. guerichi**	*Pp. hispanicus* / *Ra. linnaei* / *Pp. palmeus*	*Sp. turriculatus*	*Sp. guerichi* U / L
	Aeronian	*St. sedgwickii* U / L	*St. sedgwickii*	*St. halli* / *St. sedgwickii*	*St. sedgwickii*	?	?
		Dm. convolutus U / L	*Dm. convolutus*	*Dm. convolutus*	*Dm. convolutus*	*Ce. cometa* / *Dm. convolutus*	*Dm. convolutus*
		M. argenteus	*Pb. leptotheca*	*Pb. leptotheca*	*Dm. simulans*	*Co. gregarius* ?	*Cam. curtus* *Ra. orbitus*
		Dm. pectinatus U / *Dm. triangulatus-* L	*Ndp. magnus* / *Dm. triangulatus*	*Ndp. magnus* / *Dm. triangulatus*	*Dm. pectinatus* / *Dm. triangulatus-*	*Dm. pectinatus* / *Dm. triangulatus*	*Dem. pectinatus* U / L
	Rhuddanian	*Co. cyphus* U / L	*Co. cyphus* / *"Lg." acinaces*	*Co. cyphus* / *"Lg." acinaces*	*Co. cyphus*	*M. revolutus*	*Co. cyphus*
		Cys. vesiculosus U / L	*At. atavus*	*At. atavus*	*Cys. vesiculosus*	*Cys. vesiculosus*	*"Lg." acinaces* / *At. atavus*
		Pk.acuminatus U / L	*Pk.acuminatus*	*Pk.acuminatus*	*Pk.acuminatus* / *Ak.ascensus-*	*Pk.acuminatus* / *Ak.ascensus-*	*Pk.acum* *H. sinitzini* / *N. mademi-* / *N. lubricus*

Figure 2.6. Early Silurian correlations between the British Isles, Bohemia, Poland and Bornholm and the study area, Arctic Canada. The asterisks indicate Welsh zones that have subzones. From Melchin *et al.* 1998, Fig. 2.

Coronograptus cyphus Zone (Plates 1-4)

The *C. cyphus* Zone is recognized by the presence of species of *Coronograptus*, including *Coronograptus cyphus* (Lapworth, 1876), and *Coronograptus gregarius* (Lapworth, 1876). The base of this zone is not observed in the section of strata sampled at Cape Manning, but from previous work (Lukasik, 1994) it is clear that the zone is defined by the first appearance of *C. cyphus*. Also appearing at this time are species of *Agetograptus*, of which I observe *Agetograptus hubeiensis* (Ni, 1978) in the Cape Manning section. This biozone also records the first appearance of *Metaclimacograptus minimus* (Paškevičius, 1976), *Pribylograptus angustus* (Rickards, 1970), *Comograptus comatus* (Obut and Soblevskaya, 1968), and *Pseudorthograptus inopinatus* (Bouček, 1944).

Monograptus pectinatus Zone (Plates 5-7)

The *M. pectinatus* Zone is recognized by the first appearance of triangulate "monograptids", (isolate theca with a broad metatheca) including *Monograptus pectinatus pectinatus* Richter, 1853. Graptoloid diversity greatly increases in the *M. pectinatus* Zone (Figure 2.7) with much of the earlier fauna persisting and new taxa appearing. This pattern is similar to what was recorded from this interval from around the world (Rickards, 1975; Melchin *et al.*, 1998). The *M. pectinatus* Zone, together with the overlying *R. orbitus* and *L. convolutus* zones, is the acme of the Llandovery radiation (Melchin *et al.*, 1998). This zone records the first appearance of *Campograptus communis* (Lapworth, 1876), *Agetograptus secundus*, Obut and Sobolevskaya, 1968, *Coronograptus arcuatus* Obut and Sobolevskaya, 1968, *Metaclimacograptus orientalis* (Obut and Sobolevskaya, 1968), *Glyptograptus* n. sp., *Metaclimacograptus rigidus* (Chen and Lin, 1978), New Genus A n. sp. A Lukasik, 1994, *Pribylograptus* cf. *imprimus* Lukasik and Melchin, 1997, *Pseudoglyptograptus barriei* Zalasiewicz and Tunnicliff, 1994, and *Normalograptus laciniosis* (Churkin and Carter, 1970).

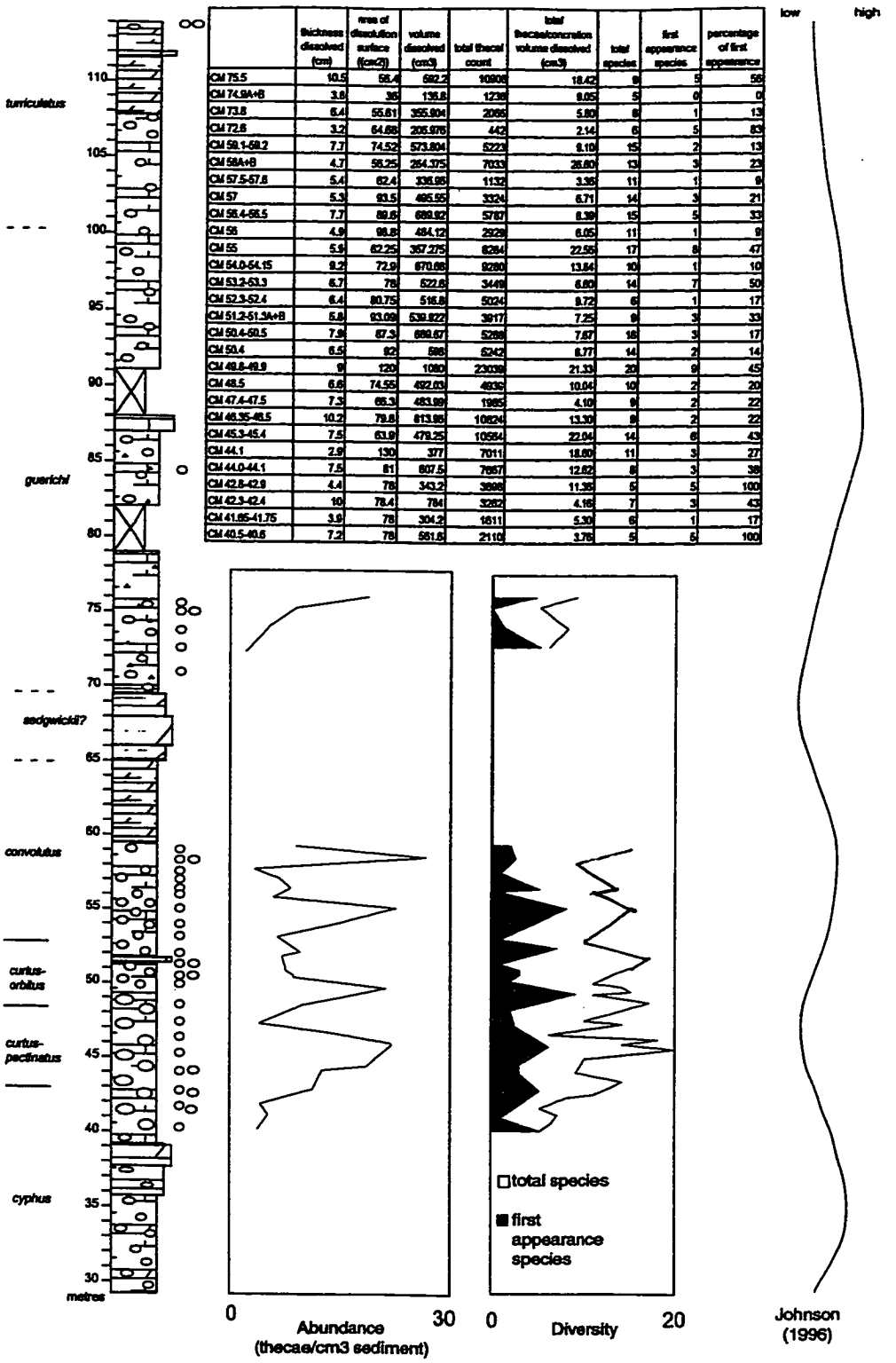

	Thickness dissolved (cm)	Area of dissolution surface (cm2)	Volume dissolved (cm3)	Total thecal count	Total thecae/concretion volume dissolved (cm3)	Total species	First appearance species	Percentage of first appearance
CM 75.5	10.5	58.4	682.2	10906	18.42	9	5	56
CM 74.9A+B	3.8	35	136.8	1236	9.05	5	0	0
CM 73.8	6.4	55.61	355.904	2095	5.89	8	1	13
CM 72.6	3.2	64.69	205.976	442	2.14	6	5	83
CM 59.1-59.2	7.7	74.52	573.804	5223	9.10	15	2	13
CM 58A+B	4.7	56.25	264.375	7033	26.60	13	3	23
CM 57.5-57.8	5.4	62.4	336.96	1132	3.36	11	1	9
CM 57	5.3	93.5	495.55	3324	6.71	14	3	21
CM 56.4-56.5	7.7	89.5	689.92	5787	8.39	15	5	33
CM 56	4.9	98.8	484.12	2929	6.05	11	1	9
CM 55	5.9	62.25	367.275	8284	22.55	17	8	47
CM 54.0-54.15	9.2	72.9	670.68	9280	13.84	10	1	10
CM 53.3-53.3	6.7	78	522.6	3449	6.60	14	7	50
CM 52.3-52.4	6.4	80.75	516.8	5024	9.72	6	1	17
CM 51.2-51.3A+B	5.8	93.09	539.922	3917	7.25	9	3	33
CM 50.4-50.5	7.9	87.3	689.67	5288	7.67	18	3	17
CM 50.4	6.5	92	598	5242	8.77	14	2	14
CM 49.8-49.9	9	120	1080	23039	21.33	20	9	45
CM 48.5	6.6	74.55	492.03	4935	10.04	10	2	20
CM 47.4-47.5	7.3	66.3	483.99	1985	4.10	9	2	22
CM 46.35-46.5	10.2	79.8	813.96	10824	13.30	9	2	22
CM 45.3-45.4	7.5	63.9	479.25	10584	22.04	14	6	43
CM 44.1	2.9	130	377	7011	18.60	11	3	27
CM 44.0-44.1	7.5	81	607.5	7667	12.62	8	3	38
CM 42.8-42.9	4.4	78	343.2	3898	11.35	5	5	100
CM 42.3-42.4	10	78.4	784	3262	4.16	7	3	43
CM 41.85-41.75	3.9	78	304.2	1611	5.30	6	1	17
CM 40.5-40.6	7.2	78	561.6	2110	3.76	5	5	100

Figure 2.7. Diversity and abundance of graptoloid species as recorded from the thecal counts of graptoloids from the dissolution residues of concretions through the Cape Manning section. Abundance is measured by calculating the thecae counted per cubic centimeter of concretion. The raw data are tabulated.

Rastrites orbitus Zone (Plates 8-10)

Triangulate "monograptids", such as *Monograptus involutus* Lapworth 1876, *Monograptus decipiens decipiens* Törnquist, 1899; *Monograptus paradenticulatus* Zalasiewicz, 1996, and species of *Campograptus* including *Campograptus curtus* (Obut and Sobolevskaya, 1968) are found in strata of the *R. orbitus* Zone of the Cape Manning section. This zone is defined by the first appearance of *Rastrites orbitus* Churkin and Carter, 1970. Other important graptoloids appearing for the first time are *Glyptograptus tamariscus distans* Packham, 1962, *Monograptus calamistratus* Churkin and Carter, 1970, *Monograptus falcata* Chen and Lin, 1978, *Neodiplograptus tcherskyi*, (Obut and Sobolevskaya, 1967), *Monograptus* cf. *triangulatus* (Harkness, 1851), *Monograptus involutus* (Lapworth, 1876), *Neodiplograptus* n. sp. A Melchin, 1987b, *Petalolithus intermedius* (Bjerreskov, 1981), *Pristiograptus fragilis pristinus* Hutt, 1975.

Melchin (1989) noted the absence of several key British index fossils in the *C. curtus* Zone of the Arctic Islands. One was identified in this study, *Pribylograptus leptotheca* Lapworth. *Pribylograptus leptotheca* was found in abundance in the *C. cyphus* Zone, *M. pectinatus* Zone and *R. orbitus* Zone, which correlates well with its temporal distribution in Bornholm and the British Isles. The *P. leptotheca* Zone of the British Isles is not named for the first appearance of *P. leptotheca* but is an assemblage zone named for the peak abundance of this species (Rickards, 1976). The *P. leptotheca* Zone of Britain correlates with the *R. orbitus* Zone of the Canadian Arctic (Figure 2.6).

Lituigraptus convolutus Zone (Plates 11, 12)

The base of the *L. convolutus* Zone is placed at the first appearance of *Lituigraptus convolutus* (Hisinger, 1837). This is a common zonal index fossil around the world (Figure 2.6) and is accompanied by a diverse assemblage of graptoloids. Many of the graptoloid species recorded from the *M. pectinatus* Zone and *R. orbitus* Zone of the Cape Manning section continue into the *L. convolutus* Zone. The new species include some that appear to have been endemic to the Cape Phillips Embayment and are not previously described. Making their first appearance are *Campograptus obtusus* (Rickards, 1970),

Campograptus lobiferus lobiferus (M'Coy, 1850), *Monograptus dracocephalus* Štorch, 1998, *Neodicellograptus siluricus* (Mu et al., 1974), *Petalolithus ankyratus* (Mu *et al.*, 1974), *Rivagraptus bellulus* (Törnquist, 1890), and *Rivagraptus kayi* (Churkin and Carter, 1970). The "paramonoclimacids", graptoloids with proximal hooked thecae and distal monoclimacid type thecae, such as *Monograptus sidjachenkoi* Obut and Sobolevskaya, 1965 and *Monograptus falcata* Chen and Lin, 1978 (extends into underlying zone), are common in the *L. convolutus* Zone. Also representative of the zone is the first appearance of the true pristiograptids such as *Pristiograptus* n. sp. A Lukasik, 1994, *Pristiograptus* n. sp. B Lukasik, 1994, and *Pristiograptus* n sp. C Lukasik, 1994.

Spirograptus guerichi Zone (Plate 13)

In the Cape Manning section the *S. guerichi* Zone is separated from the *L. convolutus* Zone by a 4.5 m thick dolostone that is thought to occupy the *Stimulograptus sedgwickii* Zone, although no graptoloids have yet been found to confirm this interpretation (Melchin, 1989). Many graptoloids from the four concretions examined for this interval could not be assigned to described species and are therefore not useful for global correlation. The first three concretions were sparsely fossiliferous and record a low abundance and diversity of graptoloid species. The eponymous species, *Spirograptus guerichi* (Loydell *et al.*, 1993), is easily identified but is not used as the basal marker of the biozone. The specimens of *S. guerichi* were found in the highest concretion (CM 75.5). However, *S. guerichi* was previously identified in a sample at 73.0 m, just above the dolostone marker bed. Also present are *Stimulograptus halli* (Barrande, 1850), *Pristiograptus regularis regularis* (Törnquist, 1899), and *Petalolithus palmeus* (Barrande, 1850), which are found in similar deposits around the world.

3 METHODS AND MATERIALS

The methods described in this chapter show how I generated the three data sets that were the basis of the taphofacies model and the description of graptoloid communities (Figure 3.1). The three data sets include: a description of lithology of the concretions with an emphasis on lamination style from thin section and polished slab; a count of graptoloid rhabdosomes on the dissolution surfaces and a description of the taphonomic features of those graptoloids; and a species identification and a count of graptoloid thecae and siculae from the dissolution residues of each layer. These last two data sets were generated during the process of layer-by-layer dissolution of graptoloid-bearing carbonate concretions in acid. The time-consuming thecal counts of the isolated graptoloids were conducted for most of the samples from the Cape Manning section where a detailed sampling was required for the community analysis. I did not count the thecae from the residues of the Cape Phillips section concretions because of time constraints. The same scale of measure was used for each data set so that I could correlate laminae between them. For example, a unique lithologic feature of a lamina could be traced to taphonomic characters on the dissolution surface and distinct species distributions in the dissolution residues. This ability to relate the three data sets was integral to the creation of the graptoloid taphofacies model and the clear identification of graptoloid communities.

Field methods and materials

Graptoloid-bearing carbonate concretions and graptoloid specimens flattened in shale were collected from two localities of the Cape Phillips Formation on northeastern Cornwallis Island: Cape Phillips (CP) and Cape Manning (CM) (Figure 2.1). Fifty-two concretions averaging 20 cm in diameter and two limestone beds were sampled and oriented as to the "way up". The name used for each concretion throughout this thesis refers to the location (in meters) in the stratigraphy as shown in Figures 2.3 and 2.4. Fieldwork was conducted by the author and by M. J. Melchin in the 1996 field season and additional concretion collection was carried out by E.W. MacDonald and M. J.

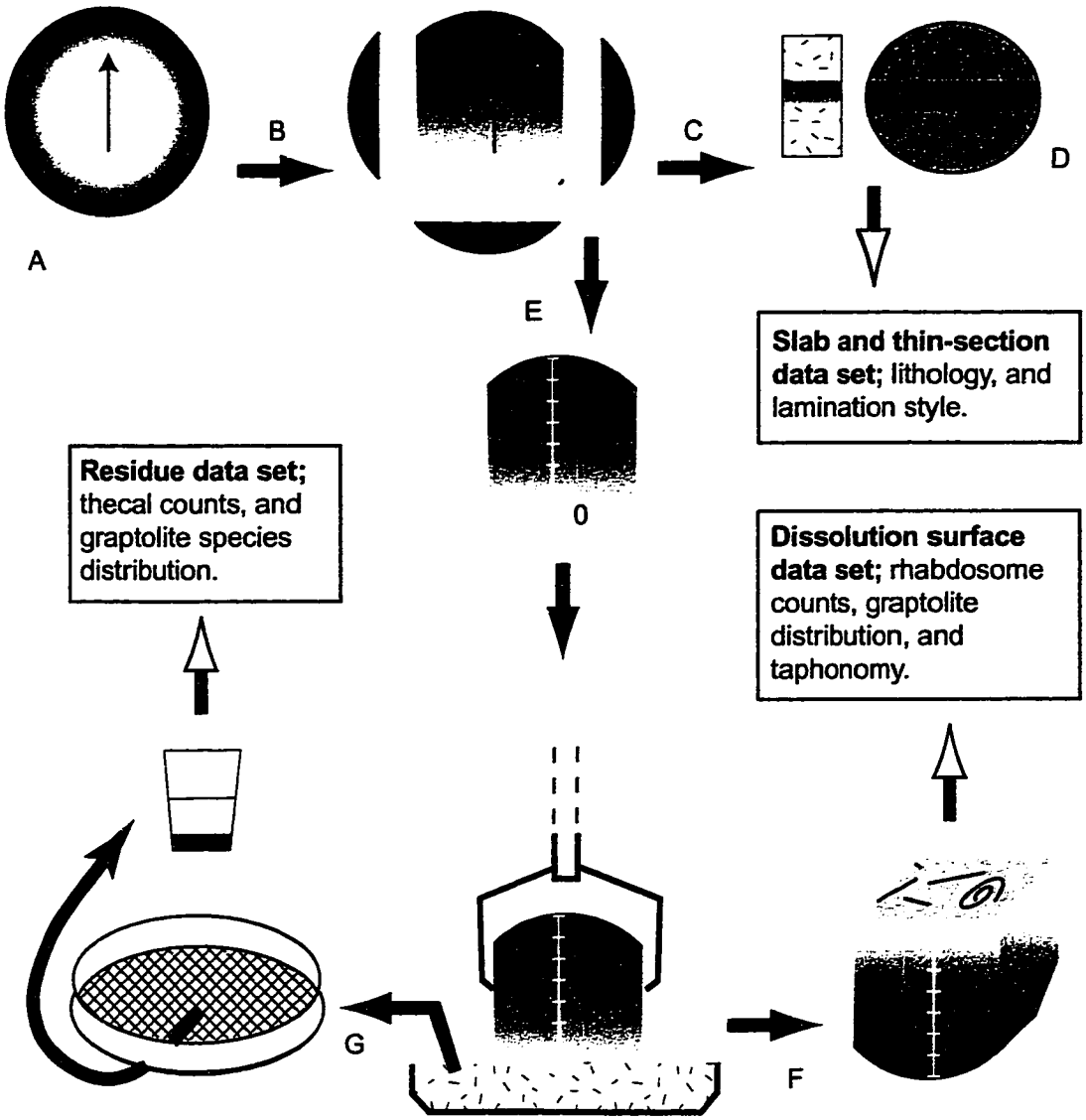

Figure 3.1. Methods used in the examination of graptolite taphonomy and paleoecology of one concretion and the generation of three separate data sets. A. Samples collected from shale sequences and oriented in the field as to the "way-up". B. Concretion is cut with the first dissolution surface parallel to bedding. C. Off-cuts are used for lithologic investigation by thin section (C) and by polished slab (D). The cut concretion is varnished on the non-dissoution surfaces and marked with a scale bar. E. The prepared concretion is suspended in dilute HCl(aq) using a clamp and retort stand. F. After about 5 mm of stratigraphic thickness was dissolved the dissolution surface was examined, the rhabdosomes were counted and taphonomic observations were recorded. G. The residue from the dissolution was collected in a 177 μm sieve and the species were identified and the thecae and siculae were counted

Melchin in the 1998 field season. Reference beds maintained consistency in stratigraphic measurements. The stratigraphic locations of the concretion sampling horizons are marked on the stratigraphic columns (Figure. 2.3, 2.4). For many of the concretions, a sample of the surrounding shale with flattened graptoloids was collected for taphonomic and taxonomic comparison. Stratigraphy of the Cape Manning section is described in previous works (Lukasik, 1994; Lukasik and Melchin, 1997) and most measurements of strata were based on marker horizons published in these reports. This a new description of the Cape Phillips section, based in part on previous observations (Lenz and Melchin, 1990, 1991; Melchin 1987b; Melchin, 1989). Field measurements were conducted using a Jacob staff and a clinometer and by pacing. The sedimentology of the beds from which concretions were studied are based, in part, on 1996 filed notes by the author (Appendix A).

Cape Phillips (CP; 75 37'N, 94 30'W), the type section of the Cape Phillips Formation, is a coastal cliff exposure of gently dipping, interbedded, calcareous shales, shales and bedded limestones (Thorsteinsson, 1958). In the 1996 field season a section of the Cape Phillips Formation exposed in a stream that cuts inland from the cliff was sampled (CPa). This section exposes carbonate shales with minor carbonate concretions and more common chert nodules than in the stream-cut cliffs. Two concretions from this locality were used in the taphofacies analysis. Based on biostratigraphy, the CP 96a section is Wenlock in age. We collected 18 concretions bearing uncompressed graptoloids from the CP site; 15 from the Llandovery portion of the cliff section (*M. griestoniensis* and *C. sakmaricus* Zones), one carbonate concretion from the Wenlock of the cliff section (*M. instrennuus - C. kolobus* Zone), and two from the Wenlock stream section (CPa).

The Cape Manning locality (CM; 75 26.8'N, 94 20'W) is exposed in stream-cut cliffs along an unnamed stream 10 km west (inland) of Cape Manning. Multiple reference beds were used for correlation across the stream and between the field seasons. Concretions were abundant in the MCM section -- 28 were collected in 1996 and an additional 10 in 1998.

The primary criteria for the selection of the concretions was concretionary size. A concretionary diameter of 20 to 30 cm was ideal for the method of layer-by-layer

dissolution. Larger concretions often contained many fractures or they would have been too heavy for the clamp and retort stand used during dissolution. Smaller concretions did not provide a large enough dissolution surface area to make observations of graptolite occurrence and taphonomy. Concretions were collected at least every metre through the Lower to Mid Llandovery, twenty-metre, concretion-rich interval of the Cape Manning section (Figure 2.3). Concretions through this interval were not locallized to a specific lithology and many different microlithofacies could be identified in the sediments preserved in the concretions. This interval is organic-rich and the total organic carbon (TOC) averages 5.7% (Melchin pers. comm., 2001). Concretions from this interval record both graptolite rich and graptolite poor samples and the precipitation of the concretions does not appear to have been localized to the graptolite-rich strata.

Through other intervals of the two study sections that record lower TOC (Melchin pers. comm., 2001; Heath, 1998), the concretions were found more sporadically (Figure 2.3, Figure 2.4). In these intervals it is likely that the concretions are localizing on carbonate-rich or organic-rich horizons.

Concretion processing and dissolution

The method of layer-by-layer dissolution enables the examination of the orientation, preservational condition, and small-scale lateral and vertical heterogeneity in graptoloid distribution within single bedding planes and through successive strata. Melchin *et al.* (1994) first described the method of layer-by-layer dissolution I used and present herein (Figure 3.1).

Each concretion was cut to an approximately cube shape with one side parallel to bedding. The sides of the cube not parallel to bedding were coated with shellac and labeled with a rule bar that could be used to measure dissolution increments. The concretion was then suspended by a clamp and retort stand over a shallow HCl_{aq} bath (5-10% HCl_{aq}), with the bottom bedding surface slightly submerged in the acid (Figure 3.2). The concretion remained undisturbed in this position until approximately 3-5 mm of rock thickness was dissolved. The dissolution of one layer took approximately 8 to 24 hours. This variation in dissolution times may have been the result of variable amounts of

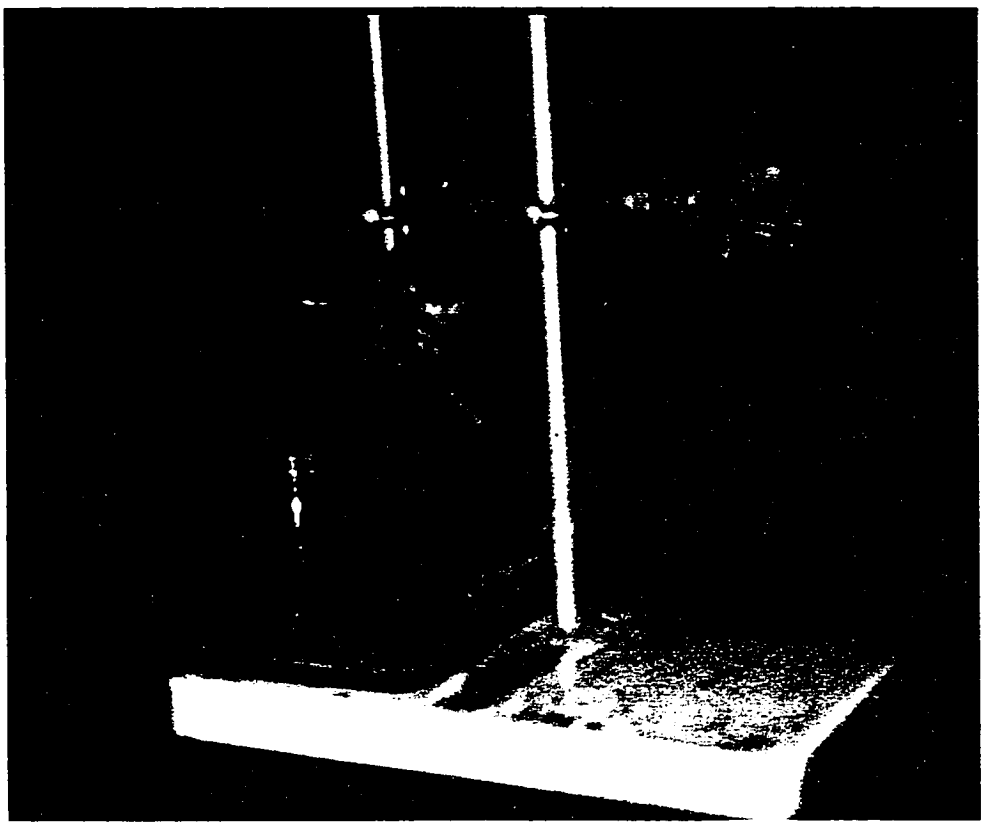

Figure 3.2. Layer-by-layer dissolution apparatus. Concretion cut with the bottom surface parallel to bedding is marked with a scale that zeros at the first dissolution surface. The concretion is suspended in a dilute hydrochloric bath using a clamp and retort stand. Approximately 0.5 cm of concretion thickness is submerged in the acid. This is left undisturbed until the rock submerged in the acid has dissolved.

dolomite, clay and/or organic matter in the limestone-dominated concretions. It was found that small additions of acid to the bath over an eight hour period was less destructive than an initial acid bath of higher concentration. The concretion was then removed from the acid bath and the sides of the concretion were gently rinsed to ensure all insoluble residue from the dissolution was collected in the bath. The graptoloid periderm is insoluble in the dilute acid, and the graptoloids were therefore revealed on the surface of the bedding plane.

There are some limitations to this method. Some of the concretions contained cores that were insoluble in the dilute acid and impeded the rhabdosome counts. If the diameter was less than the width or length of the square dissolution surface, than dissolution continued and the results of data taken from the surface were later corrected for the presence of the core. If the core occupied a large portion (80% or greater) of the surface than the concretion was cut parallel to bedding above the height of the greatest diameter of the core and dissolution commenced again. The cut portion of the concretion was archived.

When the graptoloid is released from the rock matrix it is easily susceptible to fragmentation even when every attempt is made to make the dissolution process gentle. Distinguishing fragmentation that resulted from the dissolution process and fragmentation that was prior to dissolution and of taphonomic importance was extremely difficult. When I was not sure of the mechanism of fragmentation I cautiously decided to not include the observation. In rare occasions when both ends of the fragmented rhabdosome could be identified on the bedding surface, I record the graptolites as being taphonomically fragmented.

One concretion, CM 48.5, was inadvertently cut oblique to bedding. As a result of the dark colour of the concretion and the poorly defined bedding, this was not discovered until thin-section analysis revealed the error. I decided to keep the concretion in the study for two reasons. 1) The concretion records a graptolite concentration horizon that can be identified even with the dissolution layer oblique to bedding and this supports the hypothesis that the *R. orbitus* Zone was a time of transport and physical reworking. 2) The isolated thecae supported a graptoloid species association even with the temporal mixing created by the oblique sampling. As a result of the angle of obliqueness (20° as

measured from Figure 4.26C), each dissolution surface crosses approximately 22 mm of stratigraphic thickness within the concretion. The average dissolution residue for this concretion records 27 mm of stratigraphic thickness.

Data collection: graptoloid occurrence and preservation

Each dissolution surface was examined under binocular microscope and a record was kept of the graptoloid preservational condition, orientation, size distribution, and abundance of the two major graptoloid groups ("monograptid" and "diplograptid") for each dissolution layer. The chart information was stored and manipulated in Microsoft Excel 97/2000. For each concretion the information from the dissolution surfaces (approximately 10 per concretion) was summarized in a chart and total rhabdosome distribution through the concretion was plotted. Statistical analysis (chi-square test) revealed the layers that had concentrated graptoloid rhabdosomes. Many of the revealed surfaces were photographed or the image was recorded digitally with a video capture program. These images recorded the positioning of graptoloids and the layer characteristics: i.e. colour, insoluble cores or rims, and other fauna. Textural analysis of isolated graptoloids displaying some degree of diagenetic encrustation was performed using a scanning electron microscope (JEOL-5300).

Data collection: thecal counts of isolated graptoloids and biometrics

The residue collected from the dissolution of each layer was sieved through two mesh sizes (177 μm, 63 μm) to collect the graptoloids and insoluble material. The graptoloids were picked from the residues using a small brush and preserved in ethanol. The isolated graptoloids were identified to the species or subspecies level through the dissolution residues of 29 concretions of the Cape Manning section. This was a time-consuming procedure that was originally intended to be of primary importance in the community analysis presented in Chapter Ten. However, the thecal counts of species distributions through the residues became an important component of the taphofacies analysis. The species abundance profiles enhanced my ability to interpret and define certain taphofacies such as graptolite blooms. The absence of species abundance profiles

for the Cape Phillips section may have reduced the range of possible graptoloid taphofacies I was able to see through that interval.

Biometrical analysis of the isolated fragments and graptoloids flattened in shale from equivalent strata aided in species identification. Descriptions of new graptoloid species and some new insights into some previously described graptoloids are presented in Chapter Eleven. Measurements used to describe the species are based upon isolated, uncompressed material, unless otherwise stated. Figure 3.3 illustrates the biometrics of the graptoloid rhabdosome and the morphologic terms used in this study. With the often-fragmented isolated specimens the two thecae repeat distance (2TRD; Howe, 1982) was a better measure of thecal spacing than the traditional counts to thecae per 5 mm or 10 mm.

Graptoloids were observed with a transmitted light stereomicroscope (Nikon, SMZ-10) and drawn with a camera lucida. Images of graptoloid rhabdosomes for this thesis were captured digitally from an infrared video microscope (IVM) and a scanning electron microscope (SEM). The organic-walled graptoloids, mostly opaque in visible light, appear transparent when viewed in infrared light (Melchin and Anderson, 1998). The specimens were placed in an optical liquid with a refractive index of 1.63, mounted in the well of a glass slide, and covered with a loose cover slip. The specimens were viewed with an Olympus BH-2IR transmitted infrared microscope with a Micronviewer Model 7290A Infrared Video Camera by Electrophysics Corp. attached to the trinocular head. Visible light was filtered with a 1000 nm longpass filter. The images were captured and digitized by the Snappy video capture system by Play Inc. and printed in hard copy form by an inkjet printer. A detailed explanation of the IVM method can be found in Melchin and Anderson (1998). The SEM used for this study was the JEOL 5300.

Species distribution was quantified by counting the number of thecae per layer thickness for each species group. The decision to count thecae and not rhabdosomes as had been done on the dissolution surface, was one of practicality and purpose. Other analyses of graptolite paleoecology have counted the rhabdosome as an individual (e.g., Rigby, 1993; Underwood, 1998). Isolated from the rock matrix, many of the rhabdosomes became fragmented and reconstruction of the number of rhabdosomes would be an act of imagination or statistics (Underwood, 1998), with varying degrees of reliability for different species. Thecal counts provide a more accurate assessment of the

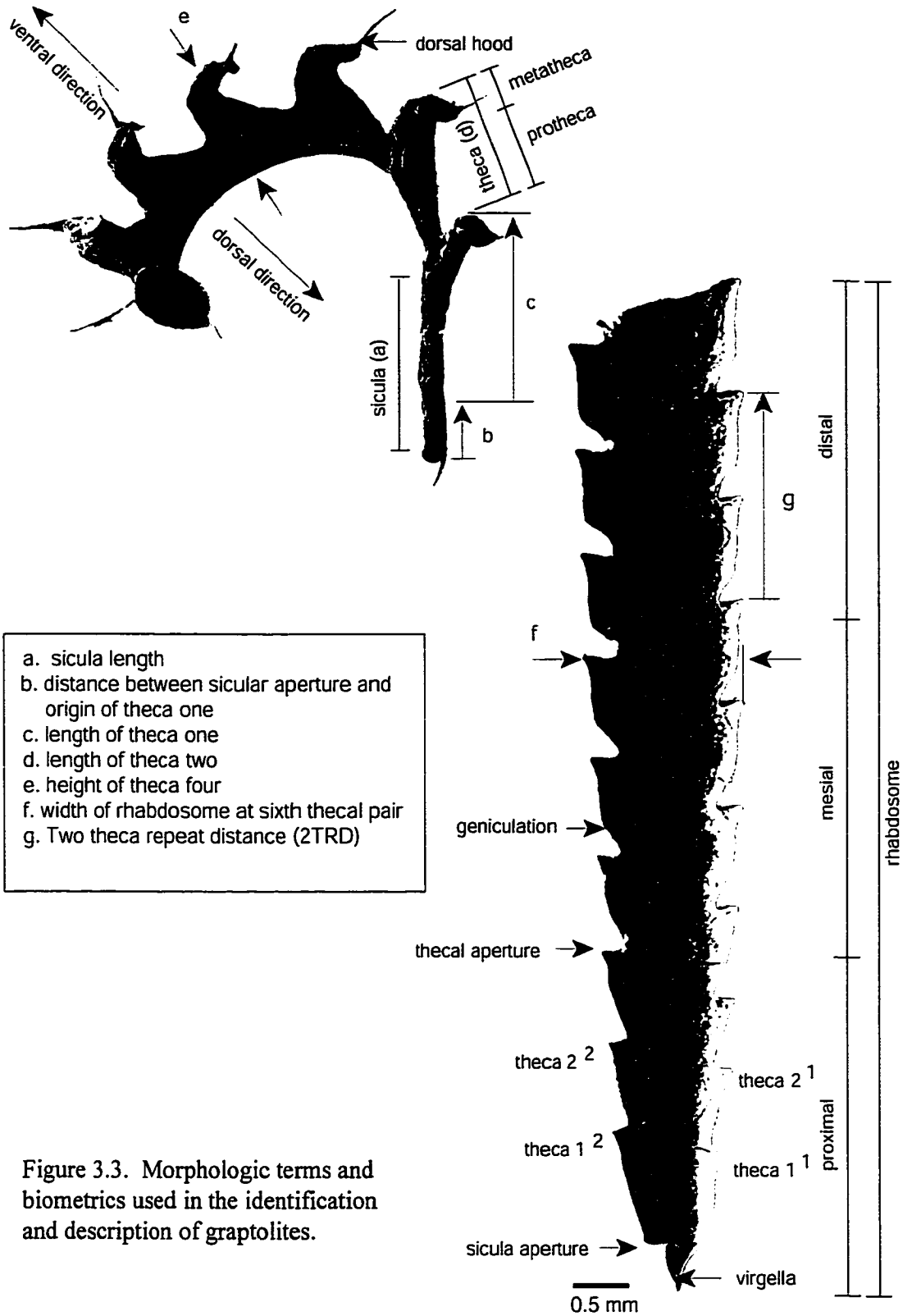

Figure 3.3. Morphologic terms and biometrics used in the identification and description of graptolites.

population. As a colonial organism, the zooids of the graptoloid are the true individuals and an evaluation of the number of individuals in a population must therefore include a count of the number of thecae. The number of thecae was divided by the thickness of the concretion interval that was dissolved to obtain the sampled residue. This count (thecae per millimeter thickness of concretion) for a species was then represented as a percentage of the total thecae of that residue and plotted with depth through the concretion. The number of rhabdosomes can be estimated from the number of proximal ends.

Siculae that had no thecae attached were counted semi-quantitatively. To obtain an accurate estimate of the number of siculae for any given residue, one-third of the sample was counted and this number was multiplied by three. The residue, preserved in ethanol, was washed into a tray that was evenly divided into 36 sections. The siculae were counted in every third section (12 total sections). This number was then multiplied by three to obtain the total siculae per residue. To obtain the value of one-third, I conducted a study of three residues in which I counted all the siculae and then compared this with the sectional counts. An accumulated average graph is produced by plotting the number of the section (1-36) versus the accumulated average. After one sample the accumulated average is just the count of the first section; after two samples it is the average of the first and second sections; after three sections it is the average of the first, second, and third; etc. Using this method one can identify the point at which the graph plateaus and delineate how many sections are required to estimate the average for the total sample. The thirty six sections (Table 3.1) for a residue were reordered randomly and plotted again. A third rearrangement was produced and this too was plotted. These three trials of show the variability in the accumulated average that occurs when only a few sections are counted. The result of this study showed that the accumulated average of siculae counted remained relatively constant after a third of the sample was counted (Figure 3.4).

These sicular counts were important for identifying periods of reworking. During high energy events the small rhabdosomes were more likely to be winnowed from the graptoloid assemblage at the sediment surface. For this reason the siculae that were a part of a colony (i.e. siculae with theca(e) attached) were not included in the sicular counts so as not to bias this biostratinomic measure. Instead, the siculae that had theca(e) were included in the total thecal counts for each species. This is recorded in

Table 3.1. Sicular counts from 36 sections of 3 different residues of concretion CM 75.5

	sicular counts per section		
section	Residue 0 5	Residue 5 10	Residue 10-16
1	9	8	5
2	8	7	11
3	15	11	6
4	11	14	18
5	17	12	8
6	5	0	6
7	15	8	6
8	13	19	11
9	7	16	6
10	14	7	13
11	28	7	11
12	14	8	15
13	25	6	7
14	20	16	9
15	15	10	8
16	19	9	7
17	24	12	15
18	11	13	17
19	22	15	14
20	24	15	11
21	21	3	8
22	29	4	11
23	20	14	10
24	10	8	14
25	34	19	12
26	27	9	15
27	17	12	9
28	17	3	9
29	18	8	11
30	21	13	11
31	26	14	2
32	17	8	7
33	26	16	13
34	32	10	19
35	16	6	11
36	10	6	8

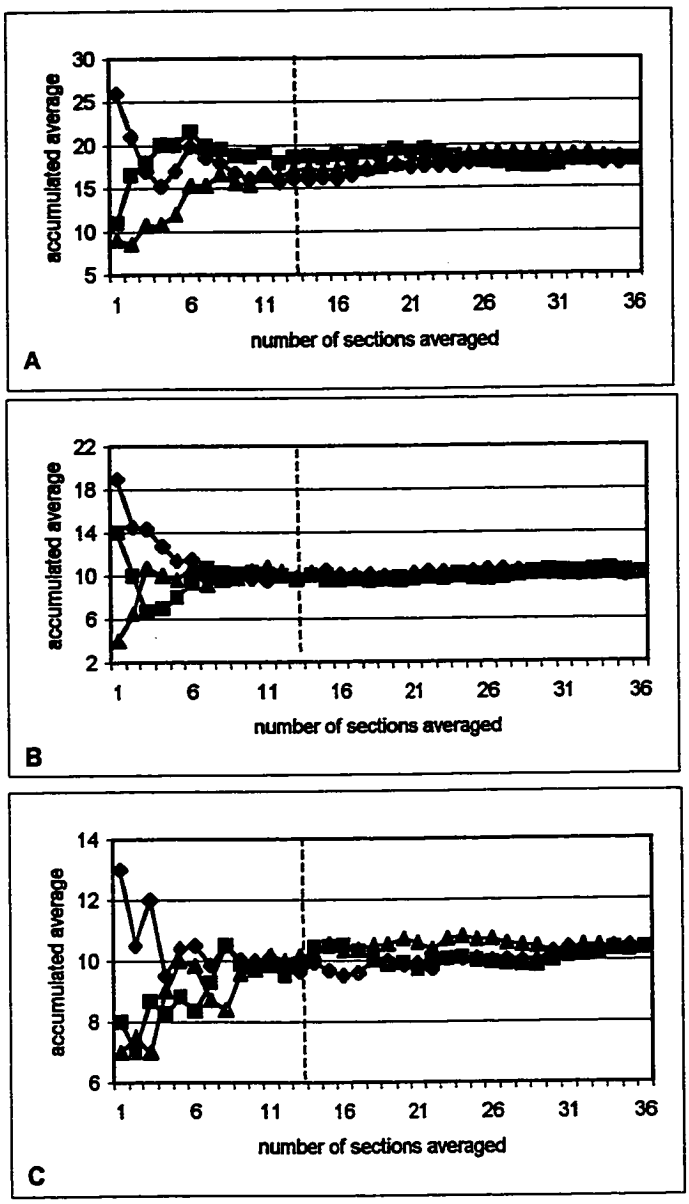

Figure 3.4. Graphs of accumulated average of siculae counted from three residues of concretion CM 75.5. Three trials (sections plotted three times in random order) for each residue are graphed to show that the accumulated average plateaus. Dashed line on each graph represents the average after 12 counted sections (one-third of the sample). A. Residue 0-5. B. Residue 5-10 C. Residue 10-16.

Appendix E. In addition, identification of isolated siculae to the species level is fraught with difficulties and it was more accurate to count all non-theca-bearing siculae as one group.

Data collection: lithology of the laminae

Microscopic study of thin sections allowed the comparison of lamina colour and carbonate crystal size in the assessment of original carbonate and clay content and the observation of small-scale current indicators. Forty-three thin sections from additional off-cuts of the concretions (cut perpendicular to bedding) were examined in plane polarized and cross-polarized light using a Leitz, Laborux 11 Pol and Nikon SMZ-10. Each thin section was marked with a way-up arrow. The variation in concretionary carbonate crystal size from bottom to top of each thin section was measured. Also recorded was the variation in colour (clear to dark brown) up-concretion. The relative amounts and the location in the thin section of any visible grains (biogenic and/or inorganic) were recorded. Relative homogeneity or heterogeneity of the clasts was noted. Additional information about diagenetic fabrics, cements, and features (stylolites, veins, infills) was also recorded for each thin section.

Polished slabs of each concretion cut perpendicular to bedding were used to examine the lithology of the laminae and the presence of sedimentary structures. Slabs from 53 concretions were cut perpendicular to bedding. Collection methods for the 53 concretions are described in Chapter Two. The slabs were polished by hand in 200, 400, 600 grit and then placed in on a vibrating polisher for a lapidary polish with aluminum, zircon or tin oxide. The slabs were examined with a binocular microscope (Nikon, SMZ-10) and with the naked eye. Recorded observations included: lamination style and thickness, continuity of lamination, presence of cores or rims, presence of veins, stylolites or other diagenetic features, and the colour of the different laminae. Colour variation within concretions was the best indicator of lamination style as grain-size was cryptic in the polished slabs. Colour was also an important indicator of relative organic content (darker colour related to higher organic content) between concretions. These observations were recorded relative to concretion thickness on a scale similar to that

constructed for the layer-by-layer dissolution (results from dissolution presented in Chapter Six). In this way layers from the dissolution could be matched with their corresponding lithology.

To understand the relationship between concretionary carbonate and the original distribution of clay and resedimented carbonate, two pieces of concretionary material from MCM2-98 44.0-44.1 and MCM2-98 59.1-59.2 were etched in dilute HClaq for 5 minutes and mounted on stubs. These carbonate pieces were examined with the ElectroScan E3 Environmental Scanning Electron Microscope (ESEM) equipped with an energy dispersive system (EDS) and Noran Voyager analytical software. Original texture (grain size and grain sorting) and original sediment composition are difficult to discern as a result of diagenetic alteration during concretion precipitation. This study led to an association between diagenetic crystal size and assumed original sediment composition (clay/organic dominated vs. carbonate dominated). I was unable to completely resolve the original texture of the sediment within the mud-sized fraction.

Data manipulation: statistical methods

The qualitative and quantitative (chi square analysis and cluster analysis) examination of species distribution vertically through the concretions allowed for the identification of faunal changes that may be associated with taphonomic alteration or population dynamics. The vertical distribution of rhabdosomes as recorded from the dissolution surfaces within a concretion was statistically analysed. Concentration of graptoloids among bedding planes can be quantitatively measured and represented statistically by a chi-square analysis.

$$\chi^2 = \sum_{j=1}^{k} \frac{(O_j - E_j)^2}{E_j} \qquad (3.1)$$

where k = the number of layers measured, O_j = the number of graptoloids observed in the jth layer and E_j = the number of graptoloids expected in the jth layer. E_j can be calculated as the total number of graptoloids from all layers divided by the number of layers (k) (Bailey, 1995). Degrees of freedom = k-1. The null hypothesis is that the graptoloids have a random distribution and are not concentrated in layers. The χ^2 distribution table

required for significance tests is presented in Appendix G. The null hypothesis was tested at 0.001 probility (99.9% significance). If the total χ^2 for a concretion was greater than the tabulated value of χ^2 at 0.001 probilitiy for a given degrees of freedom then the data did not support the null hypothesis and the graptoloids were considered to be non-randomly distributed and concentrated on one or more bedding planes. If the total χ^2 for a concretion was less than the tabulated value of χ^2 at a probabilitiy of 0.999 for a given degrees of freedom then the data did not support the null hypothesis and the graptoloids were considered to be evenly distributed amoung the bedding planes. Even distribution amoung the dissolution surfaces was not observed in any of the concretions studied in this thesis.

To semi-quantitatively describe the temporal resolution of relatively uniform graptolite assemblages (Chapter Eight) and to identify recurrent species associations (Chapter Nine), five separate R-mode and Q-mode cluster analyses were conducted on five groups of concretions divided by the biozone boundaries (*C. cyphus* Zone, *M. pectinatus* Zone, *R. orbitus* Zone, *L. convolutus* Zone, and *S. guerichi* Zone). Cluster analysis involves the calculation of similarities between sampling units and is useful for grouping recurrent species assemblages (Etter, 1999). In a Q-mode cluster analysis, sampling unit dissimilarities are computed and these are used in the identification of species associations (Etter, 1999). This was used as a statistical tool to identify and describe the average thickness of vertically distributed species clusters in the isolated thecal counts. From this information I can then make inferences about the vertical continuity of the graptolite assemblages and the ideal sampling interval that is required to capture a consistent assemblage. The R-mode cluster analysis involves the computation of a species dissimilarity matrix where different species are grouped according to their dissimilarity values (Etter, 1999). This statistical method was employed to identify species that had a similar distribution through the residues of a biozone. These recurrent and persistent species associations were important for interpreting the paleoecology of graptolite communities.

The rough species counts from the residues were standardized so that the species were expressed as proportions and the sum of all the species (and the unknown fragments) equaled 100 (Krebs, 1989). The data were then transformed by recalculating

the standardized data to a logarithmic scale (Krebs, 1989). The standardized data values were recalculated using the formula:

$$x_{tr} = \log (1+x) \tag{3.2}$$

where x_{tr} is the transformed species value and x is the species value before transformation. This transformation reduced the differences in abundances between the species (Etter, 1999) and worked well for these graptoloid counts that were often dominated by one or a few species.

A rectangular matrix with sampling units tabulated against relative species abundance in a Microsoft Excel format was imported into SPSS 8.0 and run through the Euclidean cluster analysis. The sampling units for the cluster analysis are the residues from multiple concretions (4 to 5) in stratigraphic succession. Many measures of dissimilarity can be used in a cluster analysis. I have chosen to use a distance coefficient (Average Euclidean distance) that works well with large sample sizes and high species diversities (Etter, 1999). The Average Euclidean Distance (AED) is measured geometrically as the distance between two points in the sampling units dissimilarity matrix (Etter, 1999). In this study AED is preferred over Euclidean distance, which emphasizes the larger differences in abundance between species. The AED between two sampling units, *j* and *k*, is:

$$\text{AED} = \sqrt{\frac{\sum_{i=1}^{s} (x_{ij} - x_{ik})^2}{S}} \tag{3.3}$$

where *s* is the number of species; x_{ij} is the abundance of the *i*th species in the *j*th sampling unit; x_{ik} is the abundance of the *i*th species in the *k*th sampling unit (Etter, 1999). Once the dissimilarity matrix has been computed this can then be run through a cluster analysis to produce a hierarchical agglomerative classification (Etter, 1999). For this analysis the Ward's method (error sum of squares) clustering strategy was employed. The Ward's method of deriving clusters from similarity matrices was recommended as the best for paleoecological analysis by Jones (1999). For community analysis, Etter (1999)

suggested Ward's method and two other types of distance clustering techniques; average linkage and Lance and Williams flexible beta. I used all three methods and found that Ward's method gave me the clustering patterns that seemed to be most clearly representing the data. Ward's method forms the clusters such that each clustering step should have the minimum increase in "information loss" (Etter, 1999). The results of the hierarchical Q-mode and R-mode cluster analyses are displayed in dendrograms with a rescaled distance of similarity scale bar that rates residues (Q-mode) or species (R-mode) as being more (low number) or less (high number) similar.

The results of these R-mode cluster analysis were compared with the Q-mode cluster analyses in a set of crossplots (Tables 8.3 to 8.8). The crossplots were organized with the residues along the y-axis in the order they were grouped by the cluster analyses and the species along the x-axis in the order they were grouped by the cluster analyses. The crossplots show the species that are present in each residue and the species that is most abundant. These crossplots were very useful for interpreting and understanding the cluster dendrograms.

4 CONCRETION DESCRIPTIONS

This chapter contains the results of the layer-by-layer dissolution and the sedimentologic study for each concretion. These results are described for 18 concretions from the Cape Phillips section and 33 concretions and 2 limestone beds from Cape Manning section. Additionally, 30 of the Cape Manning section concretions and 2 of the limestone beds include quantitative descriptions of the distribution of species through the residues from the layer-by-layer dissolution. Each concretion is placed in one of eleven microlithofacies and one or sometimes two of the seven possible taphofacies. A description of the microlithofacies and taphofacies and a discussion of the criteria used in classification of each facies can be found in Chapter Five and Chapter Six, respectively. A concretion was placed into two taphofacies when elements of the two separate taphofacies were equally dominant. Most concretions showed some degree of "background" sedimentation of the taphofacies "random flux of graptoloids and sediment"; however, only those concretions that lacked evidence of an event and uniformly recorded a random rate of graptoloid and sediment input were placed in that taphofacies.

For each sample, a quantitative determination of randomness of graptoloid vertical distribution is assessed with a chi-square (χ^2) (Chapter Three). The sum of chi-square for each concretion is listed in Table 4.1 and Table 4.2 and can be compared with the χ^2 distributions in Appendix G to assess whether the distribution of graptoloids supports the null hypothesis of random vertical distribution with 99.9% significance). Corrected for Bonferroni inequality (Rice, 1989), the total significance of all of the chi-square calculations in table 4.1 and 4.2 is approximately 95%. The degree of freedom is n-1, where n is the number of dissolution layers. For a rough calculation of randomness I have given the χ^2/n as an estimate. Generally, a χ^2/n less than two will support the null hypothesis of random distribution (99.9% confidence) and greater than two is indicating that graptoloid distribution was non-random with one or more graptoloid concentration layers.

Table 4.1. Concretion summary of the Cape Manning section. Statistical significance of table, corrected for Bonferroni is 95%.

Concretion name and meterage (m)	Biostrati-graphic zone	graptoloids per layer	Chi square (χ^2) and distribution quality		χ^2/n	micro-lithofacies	thecal count		sicular count		number of species	first appear-ance species	Dominant species	Taphofacies
							total	total/ cm^3	total	% of total (th + sic.)				
96-6 loose	*guerichi*	2.1	13.8	random	0.9	7	Not studied							sediment event – low graptolite abundance
114.4a		2.8	15.0	random	1.7	6								random flux of graptoloids and sediment
114.4b		2.4	13.4	random	0.7	6								
84.5		2.7	13.1	random	1.9	5								
75.5		46.0	176.5	non-random	8.8	5	10788	18.42	14172	55	9	5	*P. regularis regularis*	graptolite boom
74.9a		21.7	21.8	non-random	5.4	5	1238	9.05	2639	68	5	0	*Monograptus* n. sp. G	sediment starved
74.9b		52.3	35.5	non-random	5.9	5	Not studied							
73.8		11.9	123.2	non-random	9.5	5	2066	5.80	3975	64	8	1	*Metaclimacograptus* n. sp.	
72.6		4	2	random	0.5	5	442	2.14	312	43	6	5	*P. cf. variabilis*	random flux of graptoloids and sediment
59.1-59.2	*convolutus*	12.3	51.2	non-random	4.3	11	5223	9.10	9513	66	15	2	*C. communis*	physical addition of graptolites
58 a		32.7	23.1	non-random	2.3	3	7043	26.60	4557	39	13	3	*M. sidjachenkoi*	random flux of graptoloids and sediment
58 b		16.1	7.1	random	1.0	3	Not studied							
57.5-57.6		1.6	8.4	random	0.9	11	1132	3.36	2271	64	11	1	*M. falcata* forma C	
57.0		10.1	8.8	random	1.1	3	3324	6.71	4510	57	14	3	*M. crenularis?*	physical addition of graptolites
56.4-56.5		20.1	17.6	random	1.2	1	3111	8.39	17661	78	15	5	*M. sidjachenkoi*	random flux of graptoloids and sediment
56.0		11.5	83.2	non-random	8.3	1	2929	6.05	6456	70	11	1	*M. falcata* forma B	
55.0		23.4	50.9	non-random	5.1	3	8284	22.56	14397	64	17	8	*M. falcata* forma B	sediment starved
54.0-54.1		7.1	22.6	random	1.5	1	9279	13.84	13200	58	10	1	*Monograptus* n. sp. B forma A	graptolite boom
53.2-53.3		10.4	29.4	non-random	2.1	1	3449	6.60	6111	63	14	7	*M. falcata* forma A	
52.1-52.2		5.6	40.4	non-random	3.11	5	5024	9.72	3886	46	6	1	*M. orientalis*	
51.2-51.3a	*orbitus*	29.8	36.7	non-random	3.7	4	3917	9.10	2579	40	8	2	*N. nikolayevi*	physical addition of graptolites
51.2-51.3b		13	14	random	1.4	4	1493	5.25	2962	67	8	2	*C. gregarius*	random flux of graptoloids and sediment
50.4-50.5		6.7	13.9	random	1.0	3	5288	7.67	9715	66	18	3	*R. sinicus*	
50.4		2.8	29.9	non-random	2.98	1	5241	8.77	4740	51	14	2	*M. tenuissimus*	physical addition of graptolites
49.8-49.9		29.5	45.9	non-random	2.5	1	23041	21.33	31716	58	20	9	*Pribylograptus?* n. sp. A	sediment starved
48.5		13.1	35.8	non-random	3.6	3	4939	10.04	9707	66	10	2	*C. comatus*	physical addition of graptolites
47.4-47.5	*pectinatus*	6.8	49.0	non-random	3.8	10	1985	4.10	1773	50	9	2	*N. nikolayevi*	
46.35-46.5		31.5	568.6	non-random	33.4	1	10824	13.30	13110	67	9	2	*Monograptus* n. sp. B Melchin	
45.3-45.4		9.6	146.1	non-random	12.2	1	10564	22.04	23779	69	14	6	*N. magnus*	
44.1		12.4	62.9	non-random	3.7	7	7156	18.60	14616	66	11	3	*M. cf. arciformis*	graptolite boom
44.0-44.1		22.1	101.3	non-random	7.2	7	7634	12.62	23647	74	8	3	*A. praestrachani*	sediment starved
42.8	*cyphus*	15.0	74.9	non-random	10.7	7	3447	11.36	6280	61	5	5	*M. cf. arciformis*	
42.342.4		2.2	10	random	0.7	7	3262	4.16	7518	66	7	3	*A. hubeiensis*	sediment event – low graptolite abundance
41.65-41.75		8.6	4.6	random	0.8	7	1611	5.30	4569	74	6	1	*M. minimus*	random flux of graptoloids and sediment
40.5-40.6		2.3	10.25	random	1.5	7	2110	3.76	5087	69	5	5	*A. hubeiensis*	sediment event – low graptolite abundance

Table 4.2. Concretion summary of the Cape Phillips section. Statistical significance of table, corrected for Bonferroni is 95%.

Concretion name and meterage (m)	Biostrati-graphic age	Dissolution layers (=n)	Rhabdosomes/ dissolution layer	Chi square (χ^2) and distribution quality (random, non-random)		χ^2/n	micro-lithofacies	Taphofacies
CP 96a 7.5	*instrenuus – kolobus ?*	9	10	6	random	0.7	2	random flux of graptoloids and sediment
CP 96a 6.0		8	3.1	9.2	random	1.2	8	
214.5	*instrenuus-kolobus*	21	132	4196	non-random	200	9	physical addition of graptolites
163.1	*sakmaricus*	10	3.6	11.8	random	1.2	9	sediment event – low graptolite abundance
163a		9	3.6	18.1	non-random	2.0	9	
163b		5	1.8	2.7	random	0.5	9	
162.8		6	2.0	7.0	random	1.2	9	
152a		8	8.3	42.8	non-random	5.4	6	physical addition of graptolites
152b		7	4.14	6.7	random	1.0	6	random flux of graptoloids and sediment
150.6		9	2.6	15.5	random	1.7	9	physical addition of graptolites
148.1		9	15.7	123.9	non-random	13.7	8	
146.5 a		5	0.8	3.5	random	0.7	6	random flux of graptoloids and sediment
146.5 b		5	0.4	3	random	0.6	6	random flux of graptoloids and sediment
145.2		4	0.75	3.7	random	0.9	8	sediment event – low graptolite abundance
96		12	0.5	18	random	1.5	8	
56.9	*griestoniensis*	13	1.2	13.3	random	1.0	8	
38.4		14	1.3	19.9	random	1.4	8	
32		13	1.8	6.9	random	0.5	8	

For each sample the distribution of graptoloid rhabdosomes (not thecae) counted from the dissolution surface is plotted next to the polished slab of the concretion or limestone bed. The species distribution charts are counts of thecae (not total rhabdosomes). Total counts were divided by the layer thickness dissolved and they are shown as percentages of the total count for each residue. Thecal counts include all thecae greater than th1^{I} and all siculae with attached th1^{I}. Thecal counts do not include siculae without the first thecae. These were counted separately. An explanation of the reasoning behind the thecal count versus the rhabdosome count and a description of the counting methods is given in Chapter Three. The residues were collected from the 177 μm mesh size sieve during the layer-by-layer dissolution and therefore can be related to the distribution of rhabdosomes observed on the dissolution surfaces and to the polished slab by the same measured labels. For example, in concretion CM 40.5-40.6 the dissolution surface 22 is related to residue 22-30 that is plotted as the mid-value 26 on the species distribution chart. For an explanation of why the bottom two residues of this concretion are not matched with dissolution layers read the concretion description that follows.

Sicular counts include all siculae without the first theca. Because of the abundance of this growth stage and the inability to accurately classify most siculae to the species level, the siculae were counted together and total abundance was estimated based on counting one-third of the residue and multiplying by three (Chapter Three). The total siculae count was divided by the thickness of the layer dissolved. The "percentage siculae" was calculated by adding the total siculae and total thecal count and dividing by the total of siculae.

The polished slabs are represented as actual size with the graptoloid distribution plot arranged with the correlated dissolution layer aligned with the respective laminae in slab. In this way comparisons between the distribution of graptoloids vertically through the concretion can be directly compared with the lithology of the laminae in which the graptoloids are found. Descriptions of lamination style and lithology are grouped into like units and labeled with the measure of basal and top boundaries of the unit in milimeters (e.g. lamina 0-17). The lithologic criteria used in the classification of the microlithofacies are more fully expanded in Chapter Five. For the purpose of this introduction to the concretion descriptions I will preview some of the lithologic

characters encountered in the examination of thin sections and polished slabs of the concretionary material.

Grain size?

Carbonate crystal size was identified in plane polarized light by a dark rim of clay that was either "pushed aside" during concretionary carbonate growth or represent original carbonate texture. Often more than one of the outlined crystals shows a nucleus and margin in optical continuity in cross-polarized light. The crystal-sizes given in the following concretion descriptions describe the crystals in plane-polarized light unless otherwise noted.

A relationship between an increase in the darkness of a lamina (organic matter and clays) and a decrease in carbonate crystal size was established in the thin section analysis. An SEM/EDS study of CM 44.0-44.1 revealed that laminae are defined by clay content and graded beds show an upward increase in clay. Unfortunately, the SEM/EDS examination does not elucidate the grain size of the original carbonate sediments. I was unable to confidently assign grain size measurements to the sedimentary rocks because of their recrystallization during diagenetic growth of the concretion. Although these detailed case concretions show the problem of diagenetic alteration of carbonate grains, my general observations show that graded beds show an abrupt base of light material of to a dark top. I consider this to be a grading of a "coarser" carbonate to a "finer" carbonate and clay – a normally graded bed. I believe it is reasonable that coarser carbonate sediment with less clay would have a higher initial porosity and thus diagenetic crystals would grow larger. I feel that I can reasonably speculate that this is a prominent (if not invariable) tendency.

Graptolite rhabdosomes: dark brown circular or ovoid shapes

Dark brown circular, ovoid shapes (e.g., Figure 4.21) or dark circular shapes that have been flattened or crushed (e.g., Figure 4.10G) are preserved cross-sections of graptolite rhabdosomes. They can be identified in polished slab but are more easily

identified in thin section analysis as a result of the colour contrast with the concretionary material in normal transmitted light.

Radiolarian molds: small white spheres

Small, rounded, white objects with distinct boundaries and measuring 10 to 100 μm in diameter are observed in thin section (e.g., Figure 4.10A, B, E, F) and polished slab (e.g., Figure 4.7). SEM/EDS analysis of a piece of concretionary material from CM 49.8-49.9 identified the composition of the rounded grains interpreted to be internal molds of radiolaria (Figure 4.59A). The sphere is 10 μm in diameter with dolomite-type rhombahedral cleavage. The diameter of the grain suggests that these rounded grains are internal molds of radiolarians (E. W. MacDonald, pers. comm.). The predominant elements identified from the EDS were those of C, O, Mg, Cl, Ca, and Si (Figure 4.60). The composition as measured from the EDS, the rhombohedric cleavage on the surface of the mold in Figure 4.59A, and the fact that this grain resisted dissolution in dilute hydrochloric acid suggests that this is dolomite $CaMg(CO_3)_2$. Based upon this evidence, I have identified white spheres of similar size in polished slab and thin section of other concretions as radiolarian molds. These others are similarly assumed to be dolomitic, although it is quite possible that some are silica. The radiolarian test of original silica composition has been dissolved from the fossil record in this particular example. Many of the concretions from the Cape Phillips Formation are rich in radiolarians, some with silica tests and internal precipitates.

Organic-rich clasts: dark flattened grains

Some dark brown or black fragments of material had a platy appearance (Figure 4.11C, Figure 4.59B). These plates are too large and uncharacteristic of the platy minerals to be clay species. They could be rip-up clasts from a surface that was partially lithified at the sediment-water interface, fragments of bacterial mats that survived at the sediment-water interface, or aggregates of flocculated grains or peoloids deposited from suspension.. The EDS/SEM chemical signature of a platy grain from CM 59.1-59.2 shows an abundance of silica, oxygen, aluminum, carbon, chlorine, and calcium

suggesting an aluminum silicate type clay mineral in a carbonate matrix (Figure 4.61). These platy grains are most likely the "dark flattened grains" observed in polished slab. To identify the unique composition of these flattened grains (Figure 4.59B), the SEM/EDS signatures (4.61) were compared with the "background" SEM/EDS chemical signature for this concretion material (Figure 4.62). This signal was enriched in carbon, oxygen, chlorine and calcium, suggesting a carbonate matrix.

Cape Manning section concretion descriptions

Concretion: CM 40.5-40.6

Lithofacies: 7, graded laminae, clay/organic-rich, compressed graptoloids
Graptoloid distribution: random ($\chi^2/n= 1.46$)
Taphofacies: sediment event – low graptoloid abundance.

Laminae of grey, medium brown, and light brown characterize this very fine-grained carbonate concretion (Figure 4.1B). Three graded beds are identified in the polished slab based upon colour variation and relative heterogeneity. Heterogeneous laminae have a light to medium brown matrix that contains brown grains and clasts in a range of shades and sizes, as well as radiolaria. Many of the grains are elongate and parallel to bedding. Lamina 0-17 grades from a light heterogeneous base to a dark heterogeneous top. Lamina 17-40 grades from a medium brown base of heterogeneous composition to a medium brown homogeneous top. This same lamina shows a grading of radiolarian molds (abundant basally and rare at the top). Laminae 45-60 and 66-77 grade from a medium brown base of heterogeneous composition to a light brown homogeneous top.

Thin section analysis shows that the concretion is dominated by a carbonate matrix of indistinguishable grain size (Figure 4.1C-F). Visible carbonate grains within this matrix range in size from 5 to 40 μm. Dark grains (20 – 100 μm) are flattened in the plane of bedding. Faint laminae are defined by an increase or decrease in the amount of

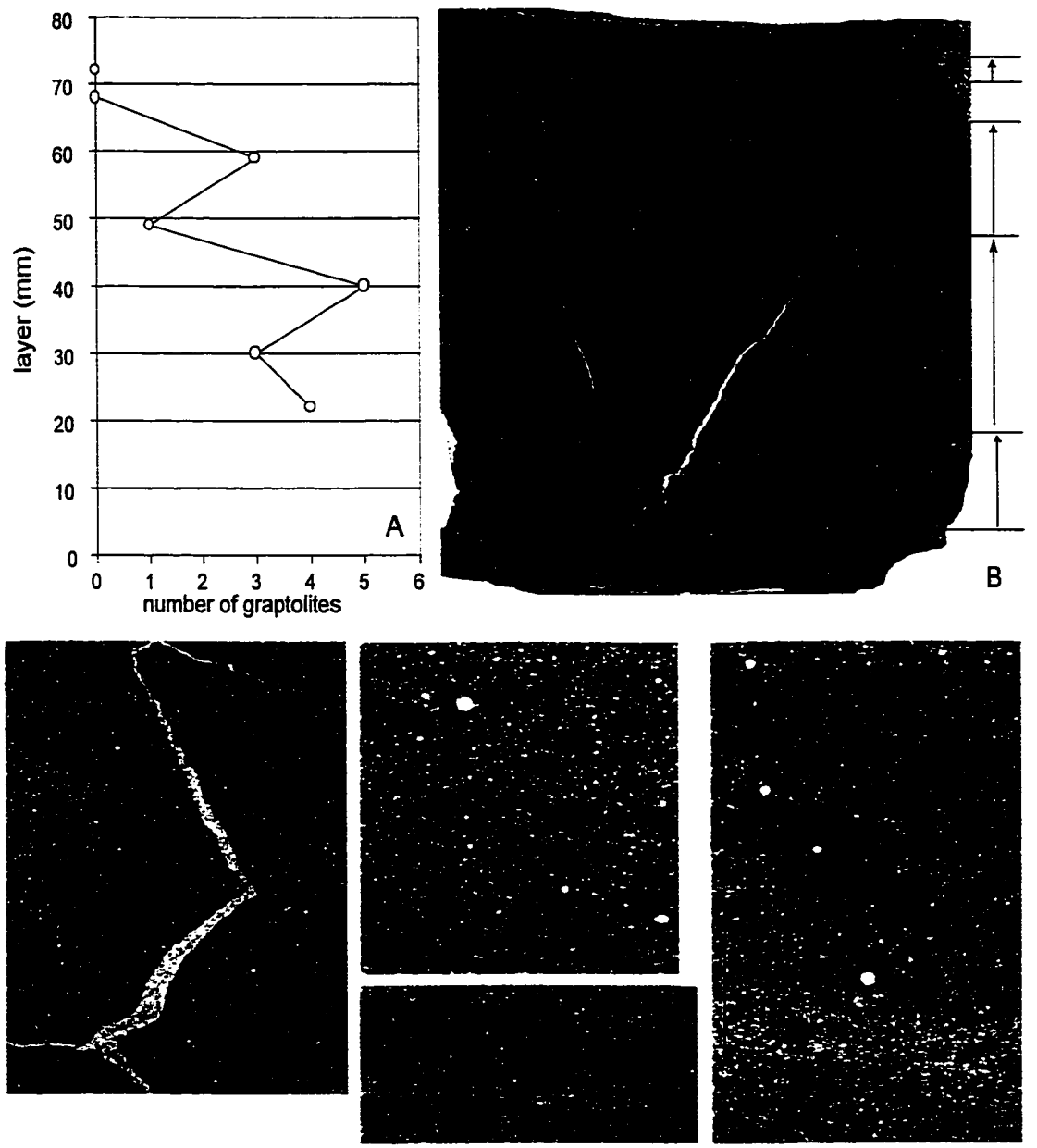

Figure 4.1. Concretion CM 40.5-40.6. A. Graptolite rhabdosome distribution vertically through the concretion as recorded from the dissolution surfaces. B. Digital scan of polished slab aligned with dissolution surfaces. Actual size. Arrows indicate graded beds. C-F. Digital scans of thin-sections. C. Thin-section from the base of the concretion showing laminae defined by organics. Square is shown in D. Magnification x1.5. D. From thin-section imaged in C. showing brown organics flattened in the plane of bedding (some likely graptolites) and radiolarian molds. Magnification X4. E. Thin-section from the top of the concretion showing a bed that grades from light to dark (indicated by arrow). Square is shown in F. Actual size. F. Graded bed is a grading of organics and possibly grain size. Basal portion of graded bed lacks flattened organics and radiolarian molds. Magnification x4.

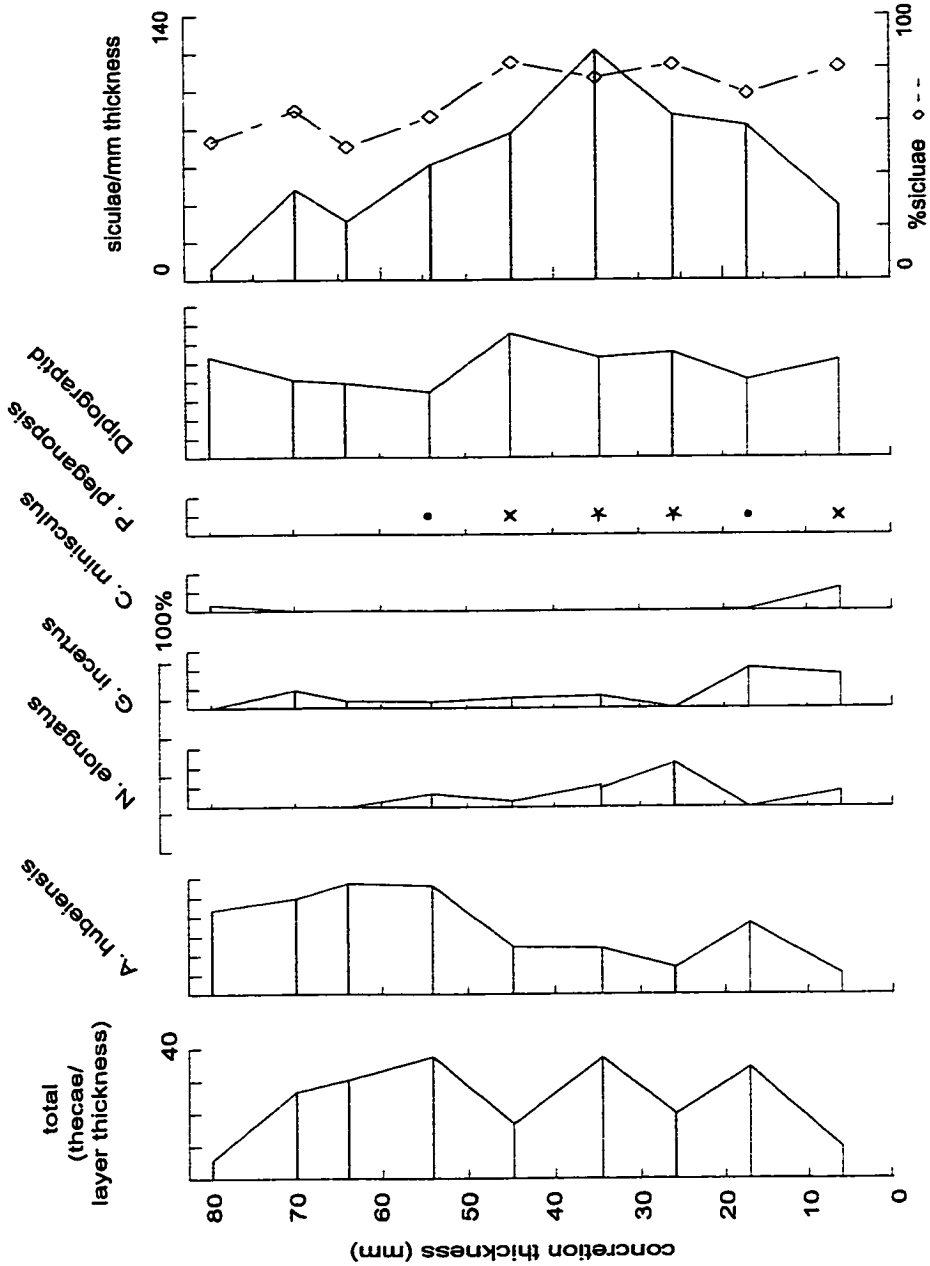

Figure 4.2. Percentage distribution of graptolite species from the dissolution residues of concretion CM 40.5-40.6; ⋆ 5-10%, × 1-5%, • < 1%

dark grains. In one graded bed an increase in matrix was observed in the darker portion at the top of the graded bed (Figure 4.1E, F). This is perhaps related to original grain size and identifies the graded-bed as a fining-upward, normally graded lamina. Observations of laminae in polished slab that grade from dark to light (66-77, 45-60) are not thought to represent inversely graded-beds because of the associated observation of the up-lamina decrease in heterogeneity. In these two beds the darker base is recording more of the larger grains, including the dark grains. Only 18 graptoloid rhabdosomes were recorded from the layer-by-layer dissolution of this concretion (Figure 4.1A). The 18 graptoloid rhabdosomes were distributed randomly on the 7 surfaces examined (chi-square analysis). Two layers were barren (layers 68, 72). Overall, there was a decrease in rhabdosome abundance on the dissolution surfaces up-concretion.

Total rhabdosome count from the layer-by-layer dissolution was low, but almost 2000 graptoloid thecae were counted from the residues (Figure 4.2). Qualitative assessment of the thecal counts do not reveal an up-concretion trend in total abundance similar to that observed from the dissolution surfaces. Three moderate peaks of abundance are observed at 12-22, 30-40, and 49-59. These correspond to the tops of three separate graded laminae (0-17, 17-40, 45-60). *Agetograptus hubeiensis*, the predominant species in the concretion, increases slightly in dominance up-concretion.

The sicular count is roughly similar to the total thecal count with the most abundant residue (30-40) the same in both counts. They differ in overall distribution. The percentage of siculae decreases up-concretion from a maximum of 80% in the basal residue to a low of 52% in the top residue. This could be a hydrodynamic sorting that is winnowing away the siculae. The repeated graded-beds suggest that currents or flows are sorting the sediments. The graded beds are thinner up-concretion and may represent an increase in the rate of reworking or sediment event bed deposition. The result is an increase in the rate of winnowing up-concretion. Alternatively, the decrease in the percentage of siculae up-concretion may be a signature of a paleoecological event. If graptoloids lived in age-segregated clouds, then the change in siculae percentage up-concretion accompanied by the change in appearance of graded beds (0-17 and 17-40 are different in appearance than 45-60 and 66-77) may represent two sets of event beds with two different source areas. The two different sources incorporate graptoloids from

different, age-segregated populations. Previous research does not support this, because age-mixed bedding plane assemblages are far more common than age segregated assemblages (Rickards, 1991). The winnowing hypothesis seems more likely, with the evidence of multiple graded beds thinning up-concretion.

The two basal residues below layer 22 are not related to measurements from the dissolution surface. No observations could be made from the first dissolution surface because of the presence of an insoluble rim. This rim is visible at the base of the polished slab (Figure 4.1B). This rim was cut away to enable the layer-by-layer dissolution process to continue. Whereas no records were obtained from the dissolution surface the residues were still examined for the species distribution study.

Concretion: CM 41.65-41.75

Lithofacies: 7, graded laminae, clay/organic-poor, compressed graptoloids
Graptoloid distribution: random ($\chi^2/n= 0.77$)
Taphofacies:random flux of graptoloids and sediment

Laminae are defined by colour variation and distribution of radiolarian molds in this very fine-grained carbonate concretion (Figure 4.3B). Three main laminae are observed on the slab surface. Lamina 0-11 is a medium to dark brown with radiolarian molds. The top contact grades over 1 mm into the layer above. Lamina 11-19 is light brown in colour at the base and grades to medium to dark brown. The radiolarian molds are observed throughout this layer but they are concentrated at 14 mm. The contact between this lamina and the one above is gradational over 2-3 mm. Lamina 19-54 grades from a light brown base to a medium to dark brown top. Radiolarian molds are constant throughout but concentrated at 37-40 mm.

In thin section, the distribution of radiolarian molds and the size and abundance of the dark brown grains define the laminae (Figure 4.3C). The very fine-grained matrix contains dark brown grains (20 to 50 μm) and radiolarian molds with an average diameter of 0.3 mm. The carbonate crystals within the molds range from 10 to 100 μm. The dark grains represent 2% of the thin section and the radiolarian molds are 10% of the sample.

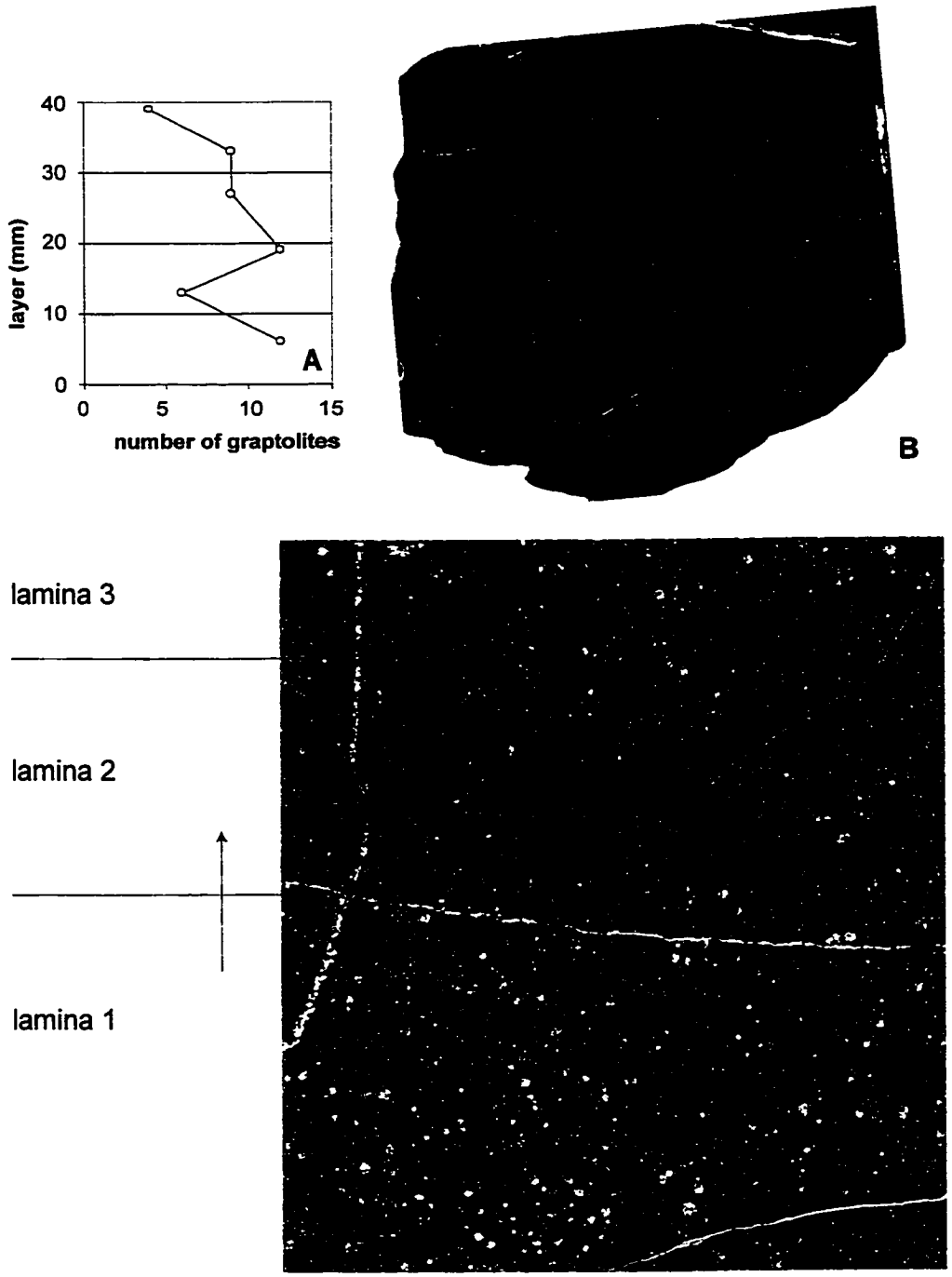

Figure 4.3. Concretion CM 41.65-41.75. A. Distribution of graptolite rhabdosomes vertically through the concretion. B. Digital scan of polished slab. Actual size. C. Digital scan of thin section. Laminae are defined by the distribution of radiolarian molds (white spheres) and the size and abundance of the dark brown grains. Laminae 1 and 3 contain abundant radiolarian molds and common organic grains (brown). Lamina 2 contains rare radiolarian molds and abundant organic grains that are smaller than those of Laminae 1 and 3. Lamina 1 grades into lamina 2 and on polished slab this was interpreted as a graded lamination. Magnification x4.

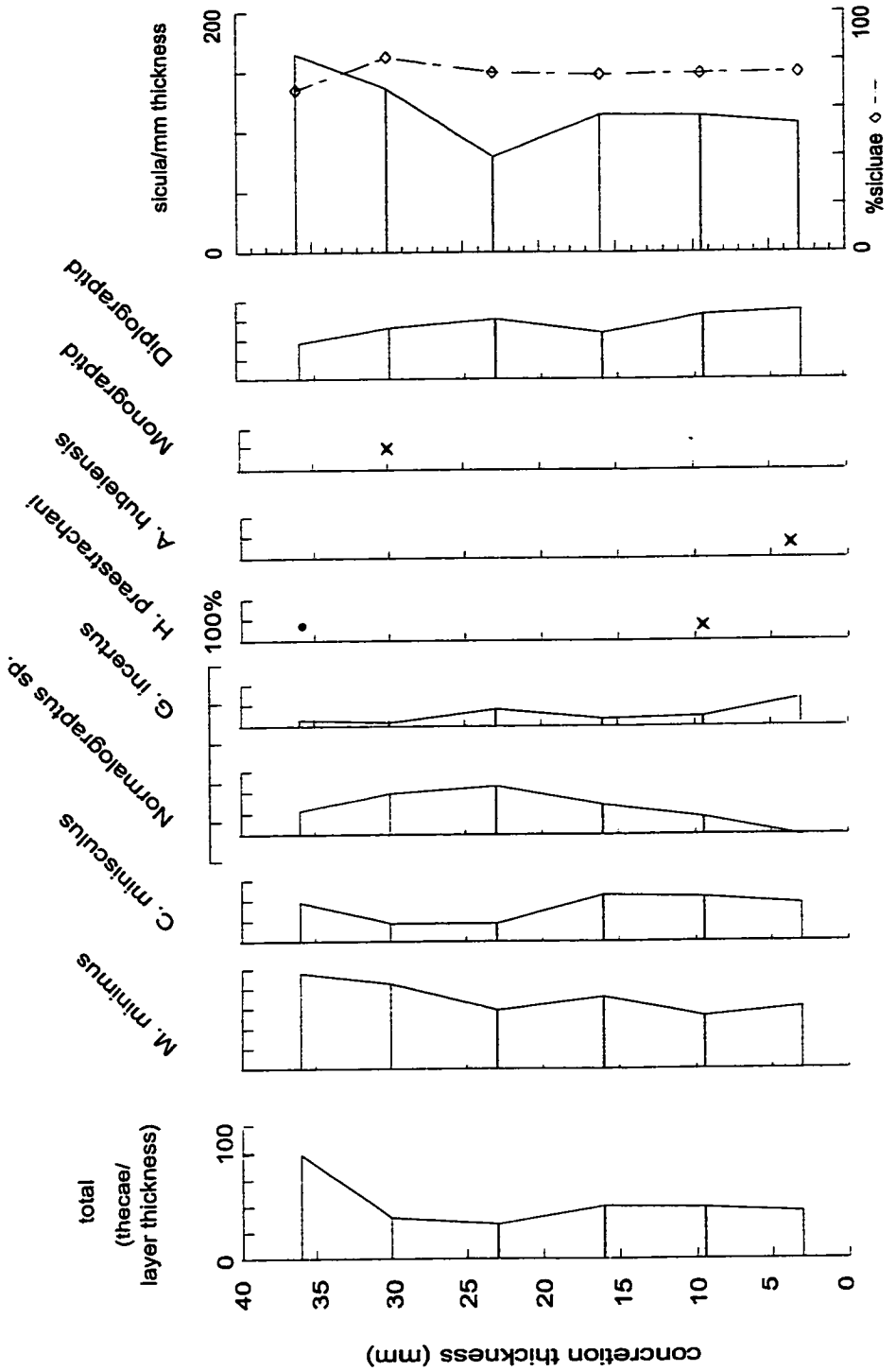

Figure 4.4. Percentage distribution of graptolite species from the dissolution residues of concretion CM 41.65-41.75;* 5-10%,× 1-5%,• < 1%

Graptoloids are randomly distributed among the 6 layers (Figure 4.3A). Layer 19 contained many fragmented graptoloid rhabdosomes, but it could not be determined if the fragmentation was taphonomic or a result of the dissolution process. Qualitative analysis of the thecal counts shows an increase in the top residue (33-39) of total thecae and siculae (Figure 4.4). The percentage of siculae remains constant throughout the residues. Of minor note is an up-concretion increase in the predominant species, *Metaclimacograptus minimus*. *Normalograptus* sp. and *Coronograptus minisculus* are secondarily dominant.

Concretion: CM 42.3-42.4

Lithofacies: 7, graded laminae, clay/organic-rich, compressed graptoloids
Graptoloid distribution: random ($\chi^2/n= 0.71$)
Taphofacies: sediment event – low graptoloid abundance.
Paleoecological event: siculae bloom

This very fine-grained carbonate concretion displays continuous and discontinuous laminae of dark and medium brown (Figure 4.5B). The overall appearance is of a finely laminated concretion with laminae defined by colour differences, relative heterogeneity, and distribution of radiolarian molds. Lamina 0-10 was possibly silicified and dissolution in HClaq was not possible. The lamina grades from dark brown base to a medium brown top. Four graded laminae within the soluble portion of the concretion are identified. Laminae 26-38, 72-88, 88-98, and 98-110 all have sharp bases of light brown that graded into a medium brown top. Many also showed a grading of radiolarian molds from abundant at the base to moderate at the top.

Carbonate crystals range in size from 5 to 30 μm and average 10 μm. More than one crystal is usually in common extinction in cross-polarized light. Radiolarian molds 0.3 mm in diameter composed of coarser carbonate crystals (10 to 100 μm) represent approximately 10 % of the sample. Faint laminae are identified by an increase in dark, flattened, and irregular shaped, poorly defined patches that average 0.2 mm long. Laminae are not defined by a change in the size of carbonate crystals. Radiolarian molds are more abundant in the basal units of graded laminae, as observed in polished slab.

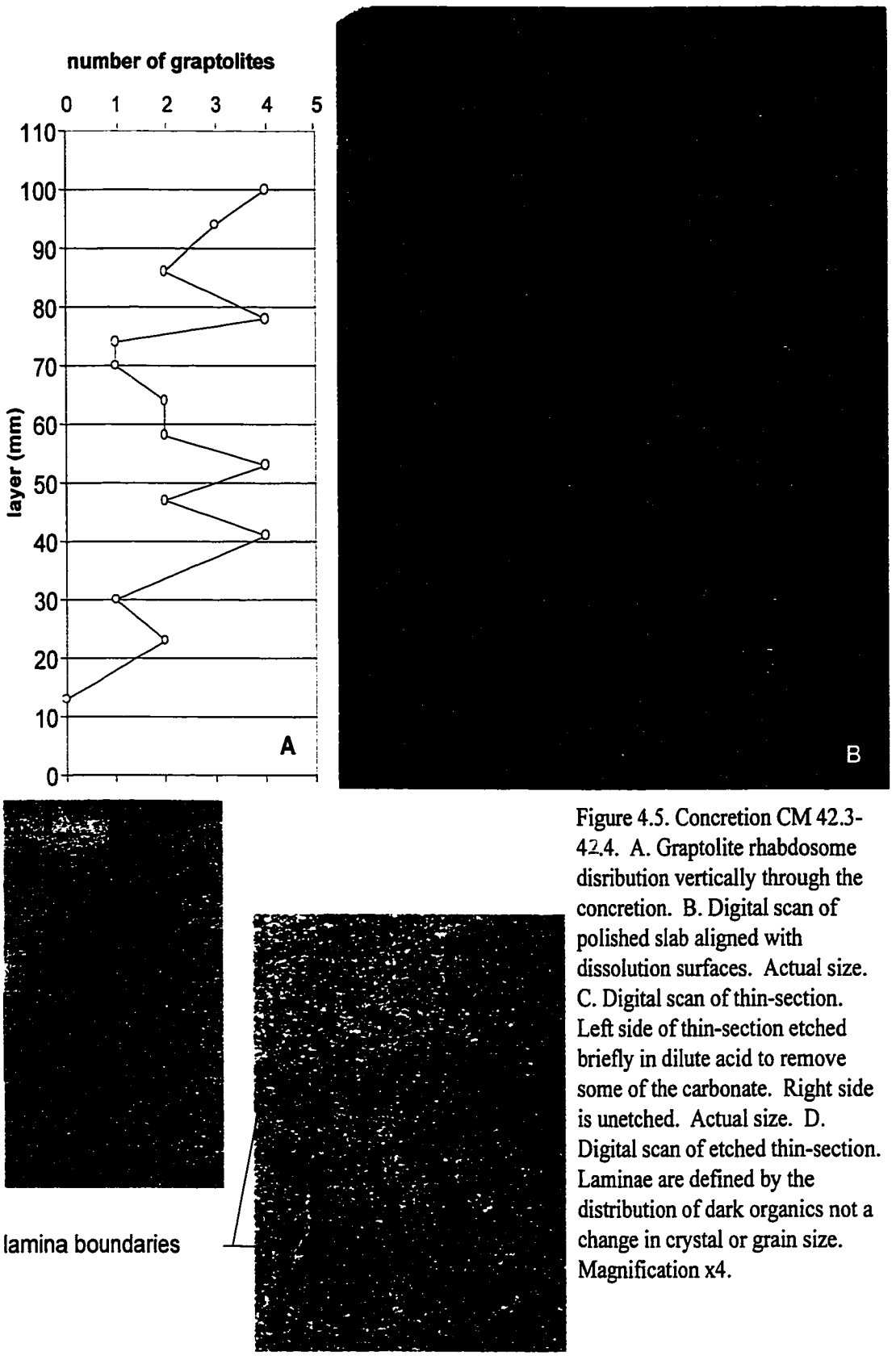

Figure 4.5. Concretion CM 42.3-42.4. A. Graptolite rhabdosome disribution vertically through the concretion. B. Digital scan of polished slab aligned with dissolution surfaces. Actual size. C. Digital scan of thin-section. Left side of thin-section etched briefly in dilute acid to remove some of the carbonate. Right side is unetched. Actual size. D. Digital scan of etched thin-section. Laminae are defined by the distribution of dark organics not a change in crystal or grain size. Magnification x4.

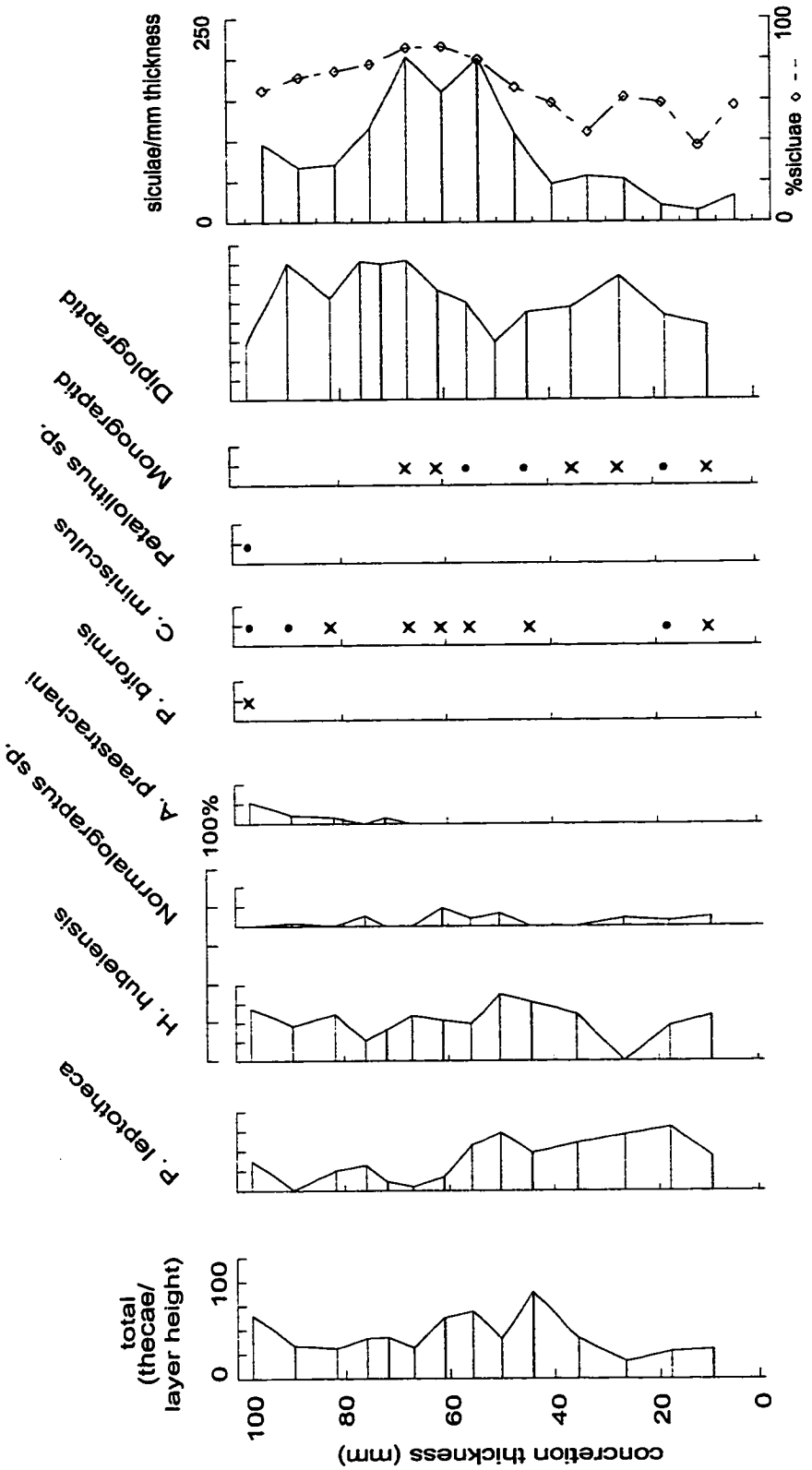

Figure 4.6. Percentage distribution of graptolite species from the dissolution residues of concretion CM 42.3-42.4; *5-10%, × 1-5%, • < 1%

Thirty-one graptoloid rhabdosomes were distributed randomly on the 14 dissolution surfaces examined (Figure 4.5A). All graptoloids were flattened. Even though the abundance was low on the dissolution surfaces, there were 4390 thecae counted from the residues (Figure 4.6).

The thecal counts revealed a slight increase in thecae counted per layer height in residue 41-47. Siculae are abundant in residues from layer 47 to layer 74. This increase is not related to a graded lamina or taphonomic observations of reworking/winnowing. The increase is thought to represent a paleoecologic event. Two species dominate the samples from this concretion: *Pribylograptus leptotheca,* and *Agetograptus hubeiensis*. *Pribylograptus leptotheca* is more predominant in the bottom-half of the concretion. *Agetograptus hubeiensis* is randomly distributed through the concretion with an absence in residue 23-30. There were many unidentifiable "diplograptid" early growth forms throughout the concretion. Most are assumed to be of *Normalograptus* sp., although without more thecae, this classification cannot be confirmed.

Concretion: CM 42.8-42.9

Lithofacies: 7, graded laminae, clay/organic-rich, compressed graptoloids
Graptoloid distribution: non-random ($\chi^2/n= 10.70$)
Taphofacies: sediment-starved

This very fine-grained carbonate concretion comprises laminae that are defined by colour variation, relative heterogeneity, and the distribution of radiolarian molds (Figure 4.7B). Lamina 0-5 is medium brown with radiolarian molds and minor bedding parallel rip-up clasts. Lamina 5-8 has a sharp irregular (erosive?) base. A light brown/buff-coloured base (2 mm thick) grades into a medium brown with radiolarian molds and rip-up clasts constant throughout. Lamina 8-20 is a graded lamina that has a light brown base that grades to a medium brown top. This lamina has a slightly gradational basal contact (over 1 mm thick grade) and a gradational top. Radiolarian molds and rip-up clasts are common throughout and define discontinuous internal laminae. Lamina 20-27 has a base that is in gradational contact with the medium brown lamina below. Lamina 20-27 is light brown with the radiolarian molds less common higher in the lamina to

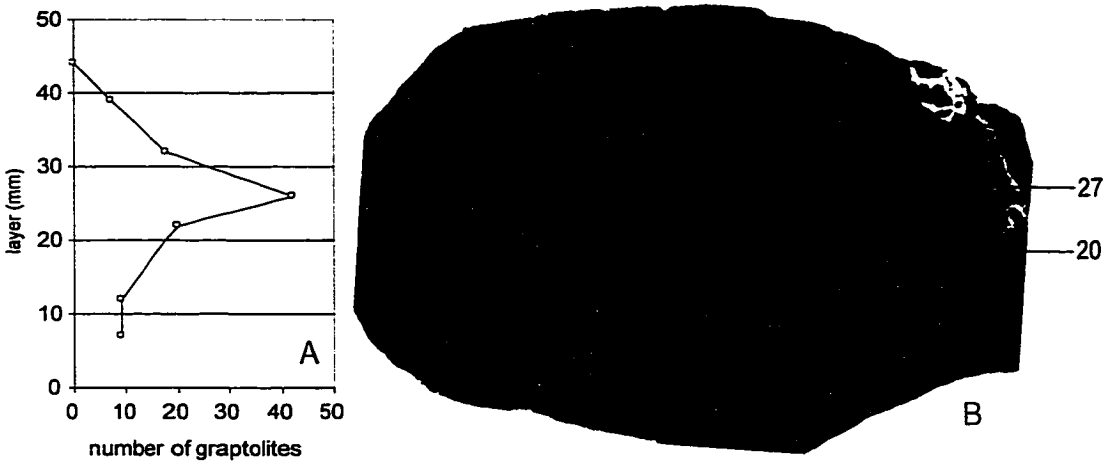

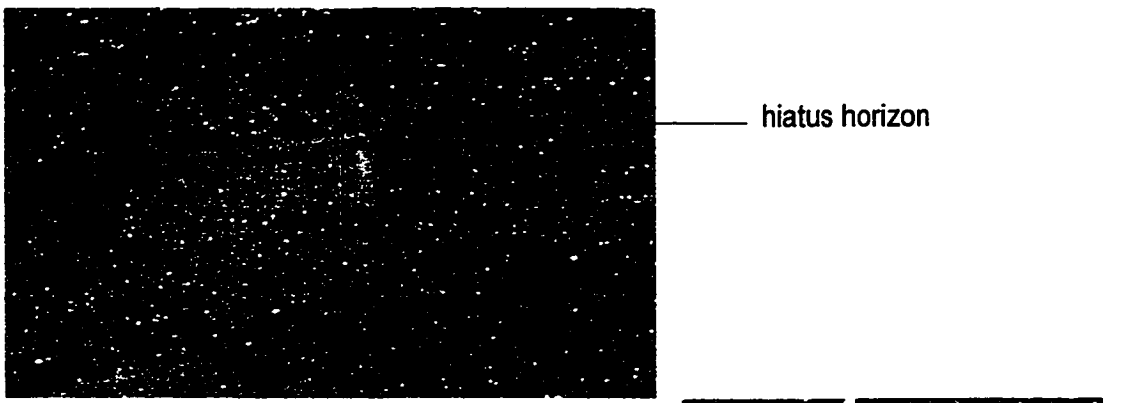

Figure 4.7. Concretion CM 42.8-42.9. A. Graptolite rhabdosome distribution vertically through the concretion as recorded during the dissolution. B. Digital image of polished slab aligned with the correlating dissolution layer. Note the top of the light coloured homogeneous layer correlates to the abundance of rhabdosomes at layer 26. C. Digital scan of thin-section showing the thickness and continuity of the light layer. Magnification x1.5. D. Light layer shows an up-concretion decrease in dark organics and radiolarian molds. The top boundary of the lamina is marked by a thin, dense organic layer. Concretionary carbonate crystal size in this light lamina is larger than throughout the rest of the concretion. Magnification x5.

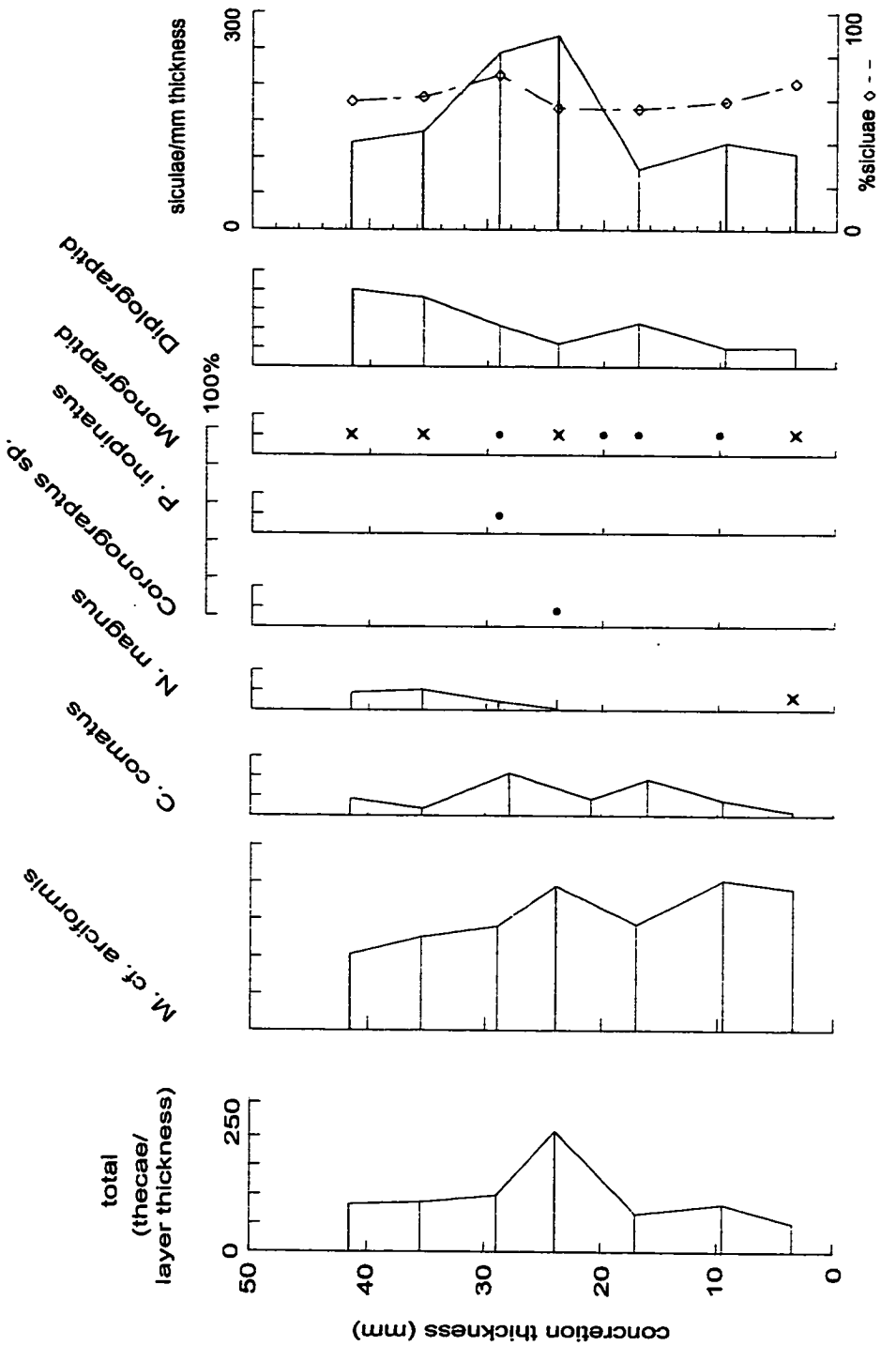

Figure 4.8. Percentage distribution of graptolite species from the dissolution residues of concretion CM 42.8-42.9; * 5-10%, × 1-5%, • < 1%

absent at the top. The top contact is sharp. Lamina 27-54 has a sharp base. At the base of the unit is a double light brown/buff laminae separated by 2 mm thick lamina of medium brown with rip-up clasts. The radiolarian molds increase in abundance up through the lamina.

Visible crystals in thin section ranged in size from 5 to 40 μm and averaged 15 μm in the darker laminae in the lower half of the thin section. A light lamina correlated with lamina 20-27 of the polished slab has a more finely crystalline texture. In this lamina the crystals are 2 to 20 μm in diameter and average 5 μm. There are no radiolarian moldsin this light lamina.

Dissolution surface layer 26 contained 42 graptoloid rhabdosomes (Figure 4.7A), almost half of all of the rhabdosomes counted for this concretion (105). Of the 42 rhabdosomes, 30 were siculae, and 10 were "monograptids" 1-2 thecae in size. This abundance of small-sized graptoloid rhabdosomes is similar to the size distribution revealed on the other dissolution surfaces and does not represent a size-sorted deposit. It is within the range of error that this enriched graptoloid layer corresponds to the dark layer between the light lamina 20-27 and the graded bed 27-54. The dark organic material in this thin layer is characteristic of the sediment-starved taphofacies. The condensed graptoloid deposit was created from the lack of sediment supply between two event beds. During this hiatus in sediment deposition, graptoloids were still being deposited. This is supported by observations made in the residues.

An abundance of graptoloid thecae per layer height was counted in residue 22-26 (Figure 4.8). This was matched by an abundance of siculae resulting in a relatively constant percentage of siculae through this interval. This residue, like the others in this concretion, was dominated by one species, *Monograptus* cf. *arciformis*. Minor (< 1%) *Coronograptus* sp. was counted only from this residue. Rare (< 1%) *Petalolithus inopinatus* was only recorded from the dissolution residue above. Other than this rare occurrence, no major change in species composition is recorded at this interval. This suggests that the source of graptoloids was constant, as would be expected in sediment-starved condensed horizon.

Concretion: CM 44.0-44.1

Lithofacies: 7, graded laminae, clay/organic-rich, compressed graptoloids
Graptoloid distribution: non-random ($\chi^2/n= 7.23$)
Taphofacies: sediment-starved, hiatus horizon
Paleoecological event: subtle changes in species dominance

Laminae of alternating dark and medium brown are observed on the polished slab surface of this very fine-grained carbonate concretion (Figure 4.9B). The distribution of the radiolarian molds and the colour variation from light to dark brown define the laminae. Four laminae show some degree of grading. Lamina 15 to 31 grades from a light-medium brown at the base to a medium brown top. Medium-dark brown discontinuous laminae increase upwards. The basal and top contacts are sharp to gradational over 1 mm. Lamina 31-36 grades from a light brown base to a dark brown top with sharp contacts at both the top and base of the lamina. Radiolarian molds are common in this lamina. Lamina 42-47 and lamina 47-52 each grade from a light brown base to a medium brown top. Radiolarian molds are rare in the basal unit of the graded lamina. Lamina 52-60 displays a decrease in abundance of radiolarian molds upwards through the light brown matrix. Lamina 60-67 is dark brown with a sharp basal and top contact and rare radiolaria. Lamina 67-73 has a dark top with numerous radiolarian molds and a pale orange-brown patchiness that tends to increase at the outer edge of the concretion. The base of this lamina is light-medium brown with numerous radiolarian molds.

In thin section the light portion of the lamina differed from the dark in the decreased amount of clay-size, brown matrix, a decrease in the abundance of rip-up clasts, and importantly, an increase in carbonate crystal size (Figure 4.9C, D). Concretionary carbonate crystals in the darker laminae ranged in size from 5 to 20 μm and averaged 10 μm (Figure 4.10A, B, D). In the lighter laminae these crystals were 10 to 50 μm in size and averaged 20 μm (Figure 4.10A, B, C). The radiolarian molds seen in the polished slab were observed in thin section to be composed of coarsely crystalline carbonate (Figure 4.10 E, F). Graptoloids are flattened in the bedding plane (Figure 4.10G). It is likely that the radiolaria were filled with carbonate prior to the physical compaction that

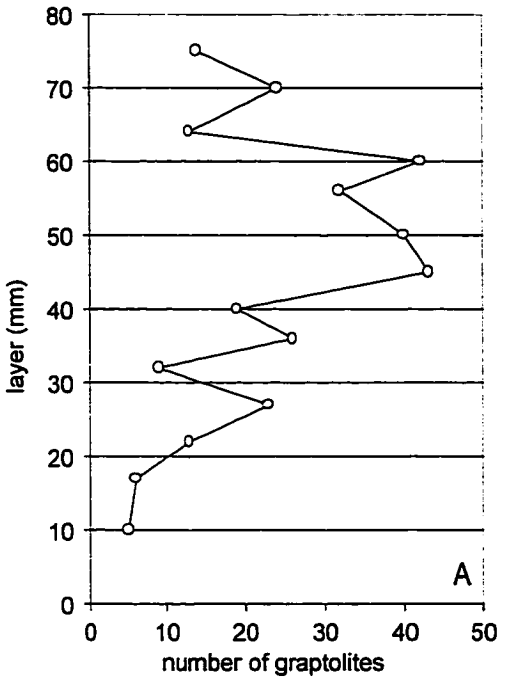

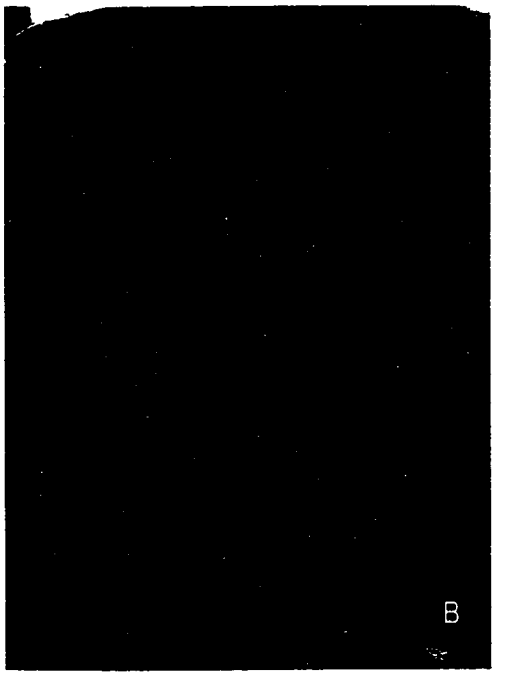

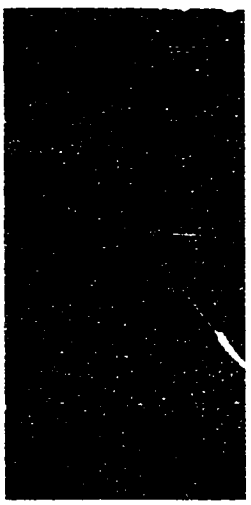

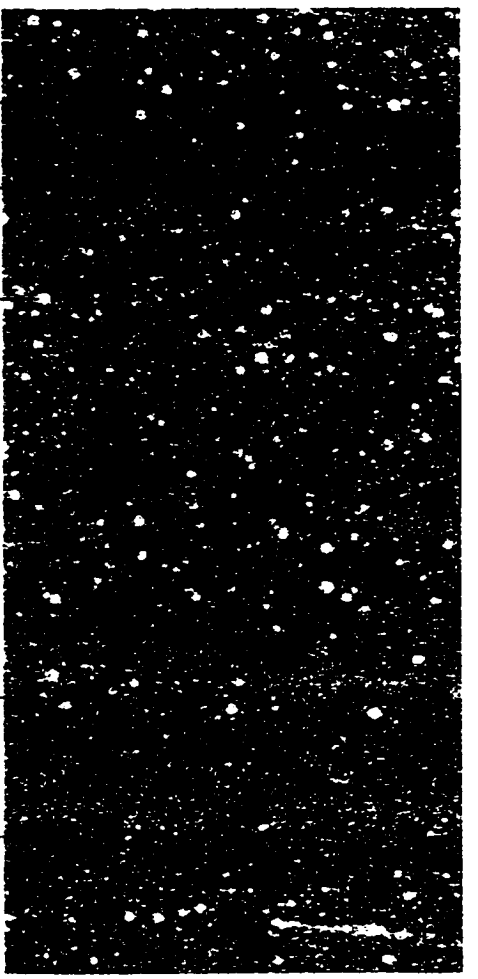

Figure 4.9. Concretion CM 44.0-44.1. A. Distribution of graptolite rhabdosomes vertically through the concretion as revealed during the dissolution. B. Digital scan of polished slab aligned with dissolution layers. Note the abundant graptolite surfaces are correlated to two graded beds and a dark lamina. C. Digital scan of thin section. Acutal size. D. The two graded beds and the dark lamina defined by the distribution of radiolarian molds, organics, and carbonate crystal size. Magnification x4.

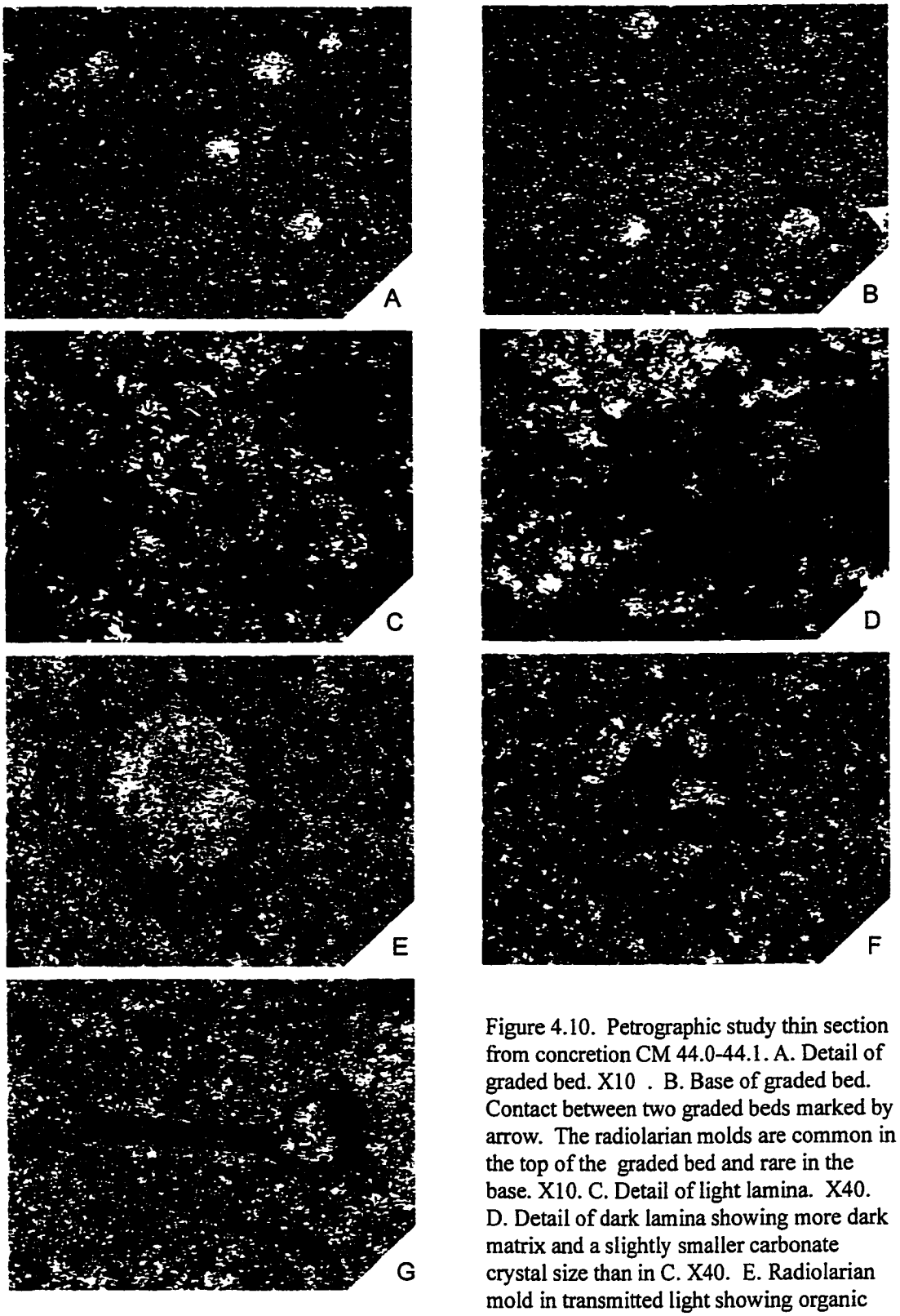

Figure 4.10. Petrographic study thin section from concretion CM 44.0-44.1. A. Detail of graded bed. X10 . B. Base of graded bed. Contact between two graded beds marked by arrow. The radiolarian molds are common in the top of the graded bed and rare in the base. X10. C. Detail of light lamina. X40. D. Detail of dark lamina showing more dark matrix and a slightly smaller carbonate crystal size than in C. X40. E. Radiolarian mold in transmitted light showing organic rim. X40. F. The same radiolarian mold imaged in E shown in cross-polarized light. Note the coarse crystal size that composes the mold. G. Flattened graptolite. x10.

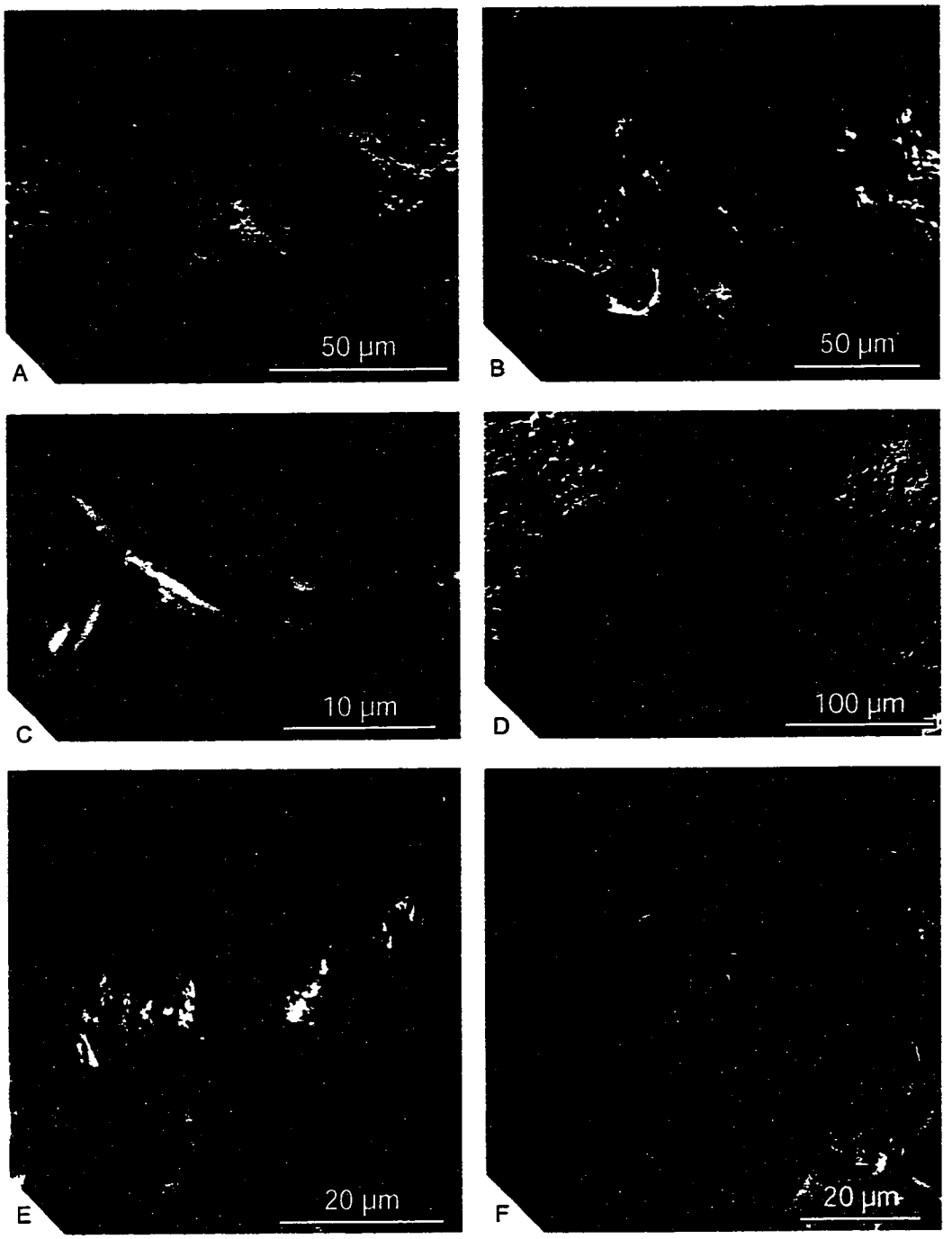

Figure 4.11. SEM study of MCM2-98 44.0-44.1. A. The darker portion from the top of the graded bed. B. Graptolite rhabdosome from the top of the graded bed. C. platy or flattened "grain" from the top of the graded bed. D. Intermediate area between the light base and the dark top showing thin discontinuous clay laminations (high relief) interbedded with carbonate. This concretion fragment surface is perpendicular to bedding and the fragment is oriented with the original top towards the top of the page. E. Detail of clay material with cubic pyrite at center. F. Top of the graded bed showing no relief and an absence of fine-grained material. Grooved pattern is a product of etching and may reflect carbonate grain size.

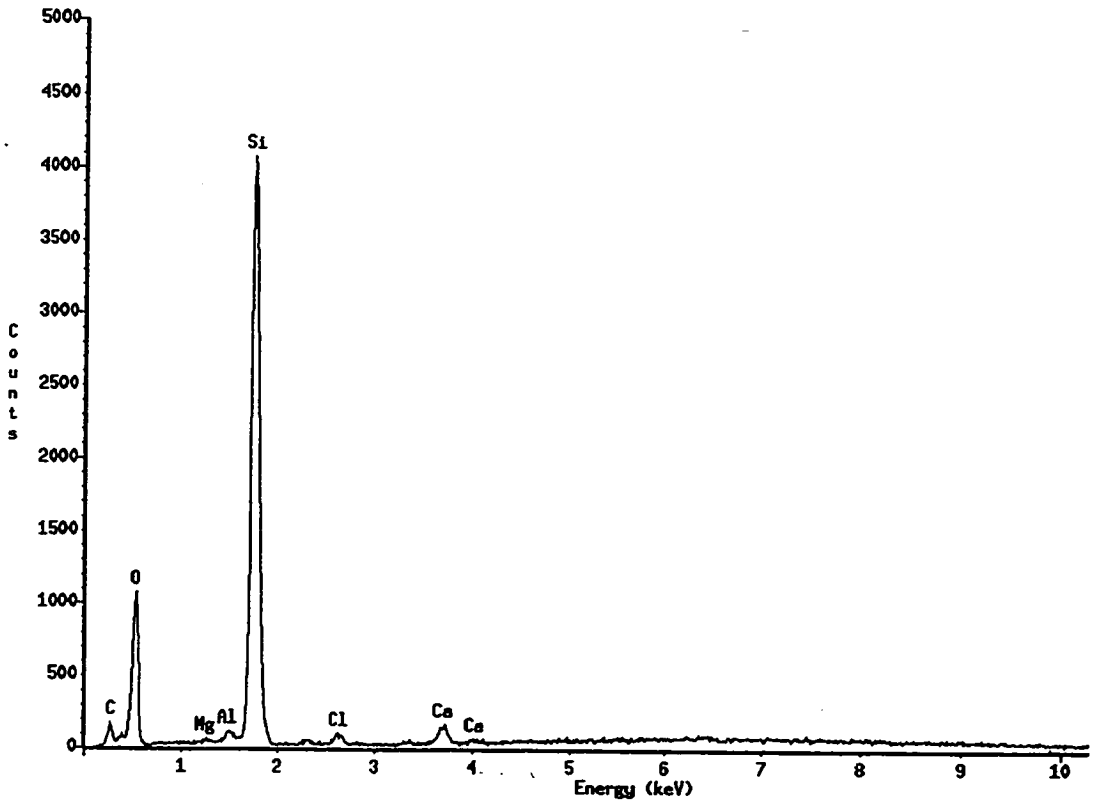

Figure 4.12. Spectral analysis from the darker base of a graded bed from MCM2-98 44.0-44.1. The analysis was conducted on a spot focused on the area with relief (darker portion of lamina) that is shown in Figure 4.11D. The spectral analysis indicates concentrations of silica (Si), oxygen (O), and slight carbon (C), magnesium (Mg), aluminum (Al), and chloride (Cl), and calcium (Ca). This is consistent with a clay (aluminum silicate) in a carbonate matrix.

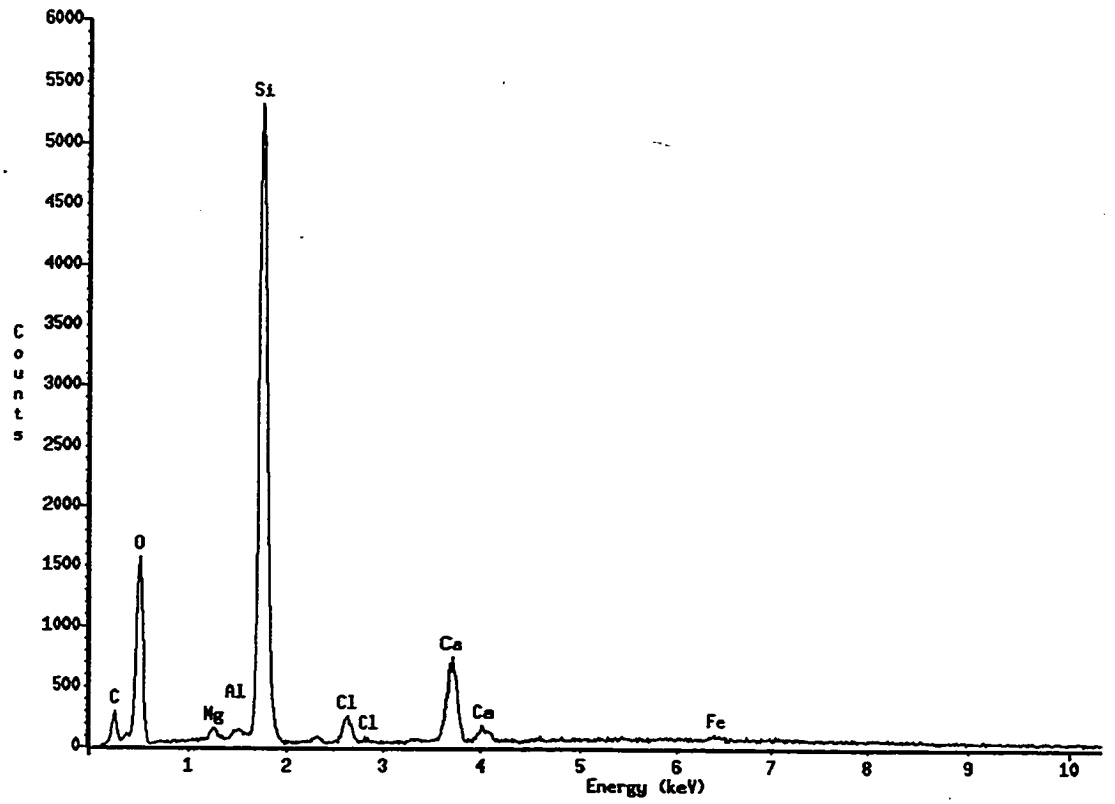

Figure 4.13. Spectral analysis of a platy grain from MCM2-98 44.0-44.1. The analysis was conducted on a spot focused on the centre of the platy grain shown in Figure 4.11C. Silica (Si) and Oxygen (O) dominate, consistent with a quartz (SiO2) composition.

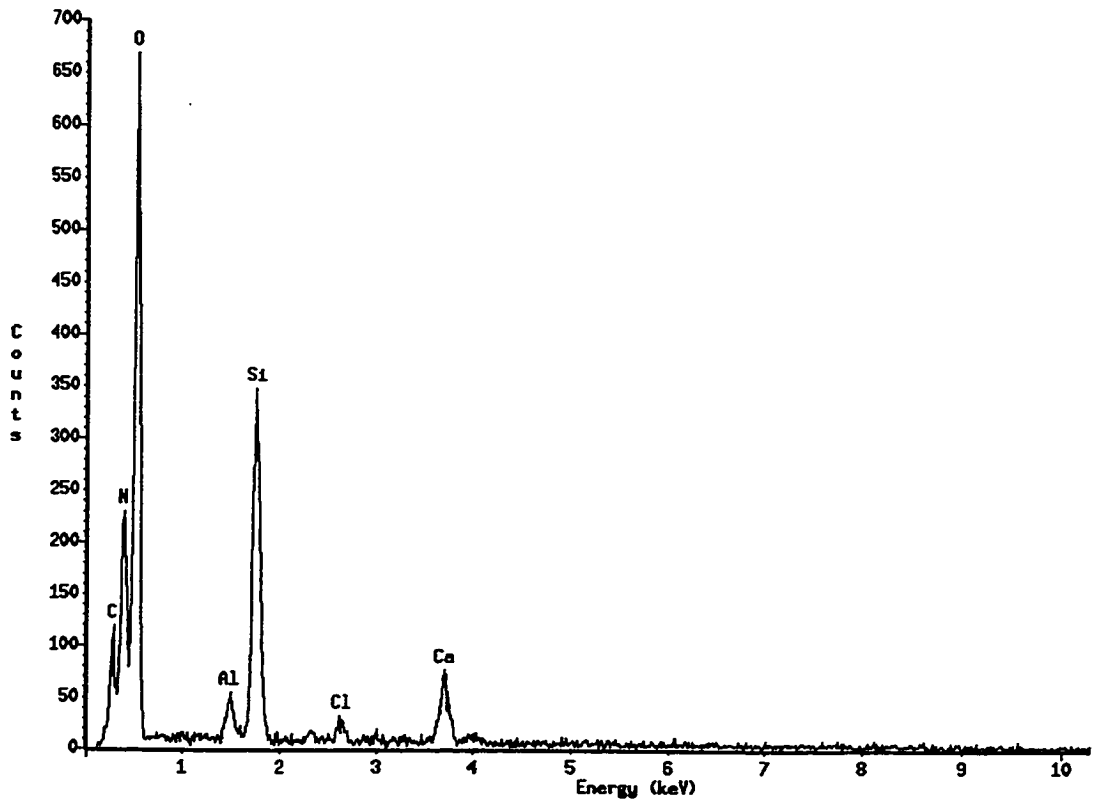

Figure 4.14. Spectral analysis of the lighter portion of from the top of a graded bed from MCM2-98 44.0-44.1. The analysis was performed on a spot within Figure 4.11F. The peaks of calcium (Ca), carbon (C), and oxygen (O) are consistent with a calcium carbonate (CaCO3) composition. Also present are clays (aluminum silicate) and organic matter (C, N).

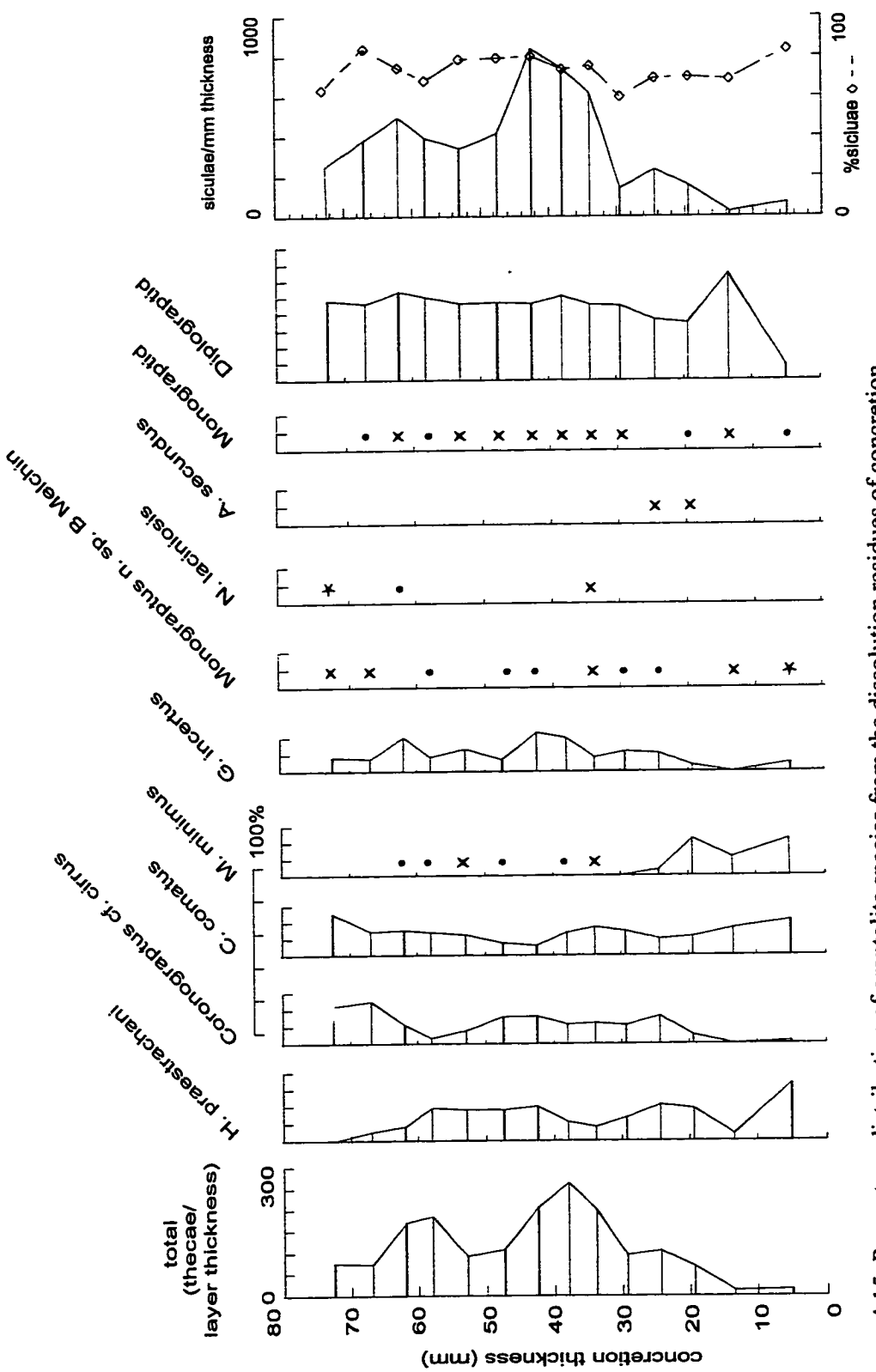

Figure 4.15. Percentage distribution of graptolite species from the dissolution residues of concretion CM 44.0-44.1;* 5-10%,× 1-5%,• < 1%

flattened the graptoloids. The internal mold maintained the three-dimensional sphere during compaction.

An SEM/EDS analysis of a graded bed etched in dilute hydrochloric acid was carried out in an attempt to relate the colour variation to a grain size variation. The concretionary piece of CM 44.0-44.1 sampled a bed that in polished slab graded from a light brown base to a medium brown top (lamina 40-42). I found that the dark brown portion of the graded lamina contained an abundance of clay-sized particles (Figure 4.11A) with a chemical signature recorded by the EDS of silica and oxygen suggesting quartz or silicate (Figure 4.12). Within this half of the graded bed were small, euhedral cubic, crystals of probable pyrite (Figure 4.11E) and a graptoloid fragment (Figure 4.11B). Some fragments of material within the dark layers had a platy appearance (Figure 4.11C). These plates are too large and uncharacteristic to be of the platy minerals of clay (e.g., kaolinite). They could be rip-up clasts from a surface that was partially lithified at the sediment-water interface, fragments of bacterial mats that survived at the sediment-water interface, or aggregates of flocculated grains or peloids deposited from suspension. The EDS/SEM chemical signature shows an abundance of silica and oxygen suggesting a quartz or silicate composition (Figure 4.13). These platy grains are most likely the "dark flattened grains" observed in polished slab and thin section.

The silicate, clay-sized material was less abundant to absent in the lighter portion of the graded bed (Figure 4.11F). This basal unit of the graded bed was either pure carbonate or the lamina was composed of a grain-size fraction that did not adhere to the surface after etching. The polygonal pattern of Figure 4.11F is likely a record of the carbonate fabric and grain size. The etching in acid would have attacked the crystal edge first producing the reusltant pattern. The average size of these polygons is comparable with the grain size range (10 to 50 μm) recorded from thin section. If the layer was carbonate-dominated then etching would plane the surface leaving no topography. In fact, the limited texture observed on the concretion surface in Figure 4.11F is the result of etching. Suspiciously, very few "grains" are observed in this portion of the graded bed. The chemical signature from these lighter layers was of calcium, carbon and oxygen with silica, nitrogen, aluminum and chlorine. The composition of the basal layer is carbonate with minor clay (Figure 4.14). It seems likely that this light-coloured basal unit of the

graded bed records the sedimentation of carbonate grains (carbonate mud) derived from the carbonate platform. This grades up into the clay- and organic-dominated top. Intermediate between the light carbonate base and the dark top are regions that show thin discontinuous microlaminae of clay interbedded with carbonate (Figure 4.11D).

This study reveals that laminae of CM 44.0-44.1 are defined by organic and clay-sized silicate content and that in this concretion the graded beds show an upward increase in the organic matter and silicate. Unfortunately, the SEM/EDS examination does not elucidate the grain size of the original carbonate sediments. The dark laminae are primarily clay-sized although grain size is difficult to determine in the very fine-grained material. I determined that the light-coloured laminae of this concretion were most likely originally carbonate sediments. The diagenetic overprint of the carbonate concretion growth has removed any information about the original carbonate texture. The larger crystal sizes observed in thin section within these layers may be the result of a greater carbonate source for reprecipitation or the lack of clays to impede crystal growth.

Three layers were considered abundant in graptoloid rhabdosomes: layer 45, 43 rhabdosomes; layer 50, 40 rhabdosomes; and layer 60, 42 rhabdosomes (Figure 4.10A: average per layer = 22, n = 14). The rhabdosomes on the dissolution surfaces includes many siculae (layer 45, 84% siculae; layer 50, 70% siculae; layer 60, 64% siculae). However, this is within the range of variation seen on all the dissolution surfaces of this concretion and is not believed to be an artifact of size-sorting. These abundant layers can be correlated to the dark brown tops of two graded beds (layer 42-47, 47-52) and to the dark lamina 60-67. The three abundant layers are likely the product of sediment starvation. The result is an increased amount of organic carbon; radiolaria and graptoloids accumulating on the seafloor without dilution by carbonate sediment.

Analysis of the thecal counts revealed an abundance of thecae per layer thickness in residue 36-40, with secondary abundance in the residues directly above and below. This distribution pattern was also observed in the counts of siculae. From this evidence size-sorting is not occurring. The thecal counts of the concretion showed some trends. Basal residues contained *Metaclimacograptus minimus* that was absent in the residues from the top of the concretion. *Coronograptus arcuatus* was predominant in residue 64-70 (second from top) and rare in the basal residues. *Huttagraptus praestrachani* was

predominant in the basal residue and rare in the top residues. Both *C. arcuatus* and *A. praestrachani* were moderately dominant in the mid-concretion residues. Residue 36-40 was not unique in its species composition and this suggests that the source of graptoloids (from a particular niche) was relatively constant during the sediment deposition that formed this concretion.

Concretion: CM 44.1

Lithofacies: 7, graded laminae, clay/organic-rich, compressed graptoloids
Graptoloid distribution: non-random ($\chi^2/n= 3.70$)
Taphofacies: graptoloid bloom
Paleoecological event: bloom of *Monograptus* cf. *arciformis*

A sequence of six graded beds is observed on the surface of the polished slab of this very-fine-grained carbonate concretion (Figure 4.16B). Basal laminae contacts are at 4, 7, 29, 35, 42, and 50 mm. All laminae grade from a light brown base to a medium brown top that contains lenses or discontinuous lamina of dark brown. All six layers have sharp bases and tops with layer 29-35 displaying an irregular (erosive?) base. This same lamina also has a thicker basal light unit (4 mm thick, average for the rest of the lamina was 2 mm). Radiolarian molds are more abundant in the medium brown laminae and predominant in certain layers (33-43). The radiolarian molds were less abundant from 18-24 in the medium brown unit of layer 7-29.

The lighter laminae were observed in thin section to have a finer carbonate crystal texture than the darker laminae (Figure 4.16C, D). The crystals in the darker laminae were 5 to 30 μm and average 10 μm. In the lighter laminae the crystals ranged from 3 to 20 μm with the average 5 μm. Circular pockets of more coarsely crystalline carbonate interpreted to be radiolarian molds were observed in the darker laminae but not in the lighter laminae. If crystalline texture of the concretion is related to original grain size then the graded beds identified in both thin section and polished slab are inversely graded. If this relationship can be trusted then we have a preserved contourite-type deposit in which inversely graded beds are common (Stow, 1979). However, it is also

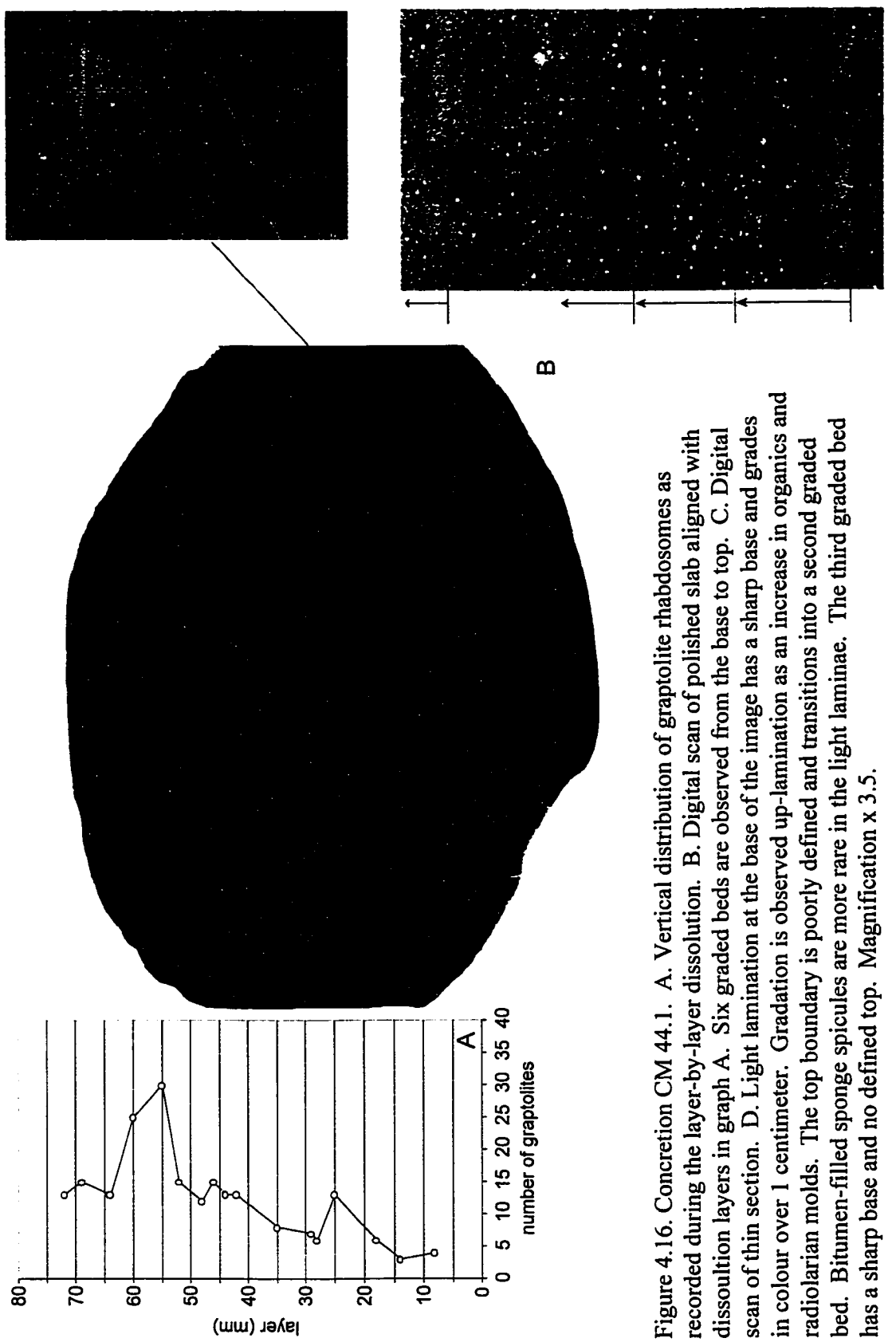

Figure 4.16. Concretion CM 44.1. A. Vertical distribution of graptolite rhabdosomes as recorded during the layer-by-layer dissolution. B. Digital scan of polished slab aligned with dissoultion layers in graph A. Six graded beds are observed from the base to top. C. Digital scan of thin section. D. Light lamination at the base of the image has a sharp base and grades in colour over 1 centimeter. Gradation is observed up-lamination as an increase in organics and radiolarian molds. The top boundary is poorly defined and transitions into a second graded bed. Bitumen-filled sponge spicules are more rare in the light laminae. The third graded bed has a sharp base and no defined top. Magnification x 3.5.

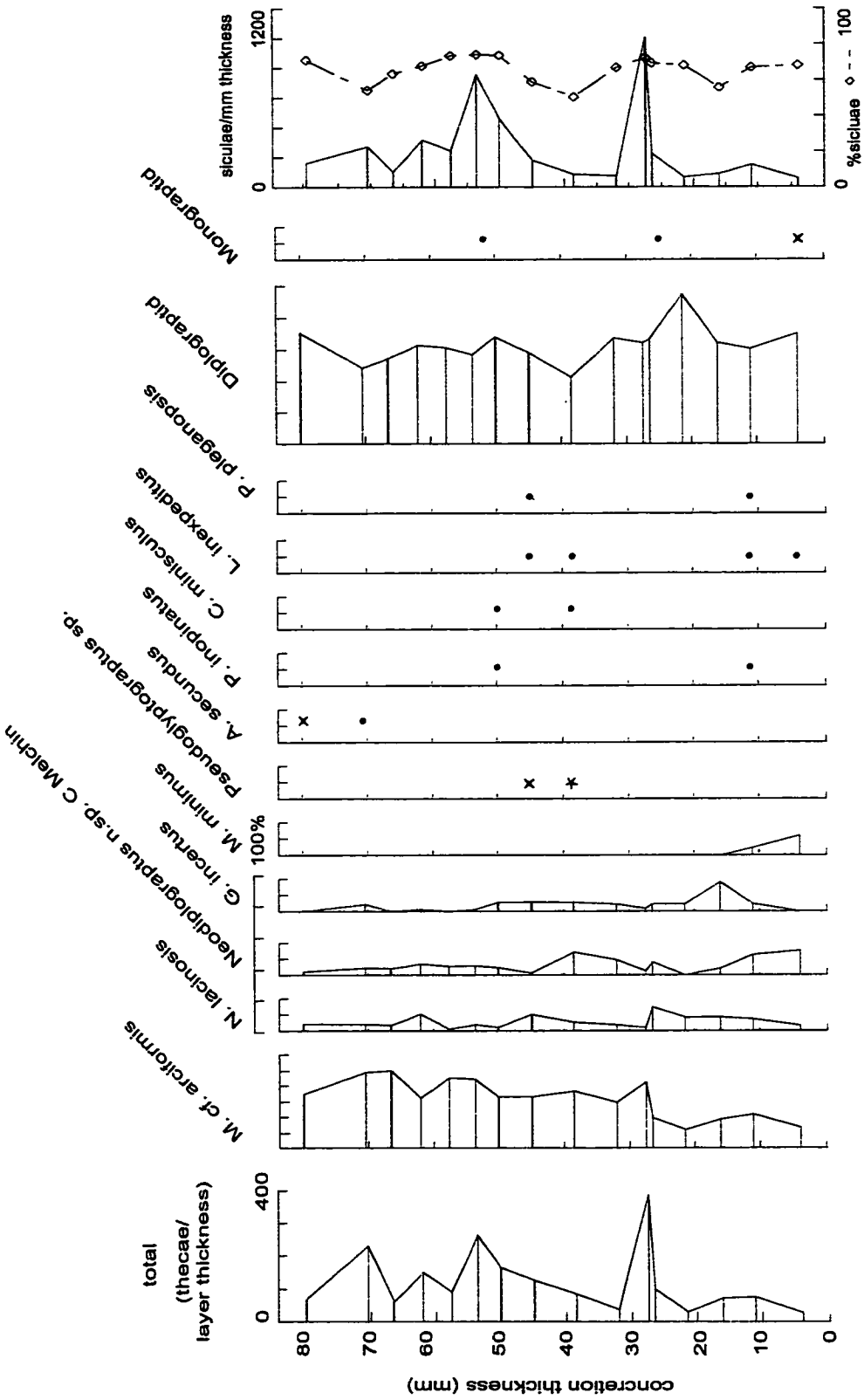

Figure 4.17. Percentage distribution of graptolite species from the dissolution residues of concretion CM 44.1;* 5-10%,× 1-5%,• < 1%

possible that the "tool" of relating original fabric to the concretionary texture does not work in this concretion. Perhaps the grading of carbonate sediment grain-size was not preserved during lithification (recrystallization) of the concretion.

Two dissolution surfaces (layer 55 and layer 60) are enriched in graptoloid rhabdosomes (Figure 4.16B). These layers correspond to the last graded bed that begins at layer 50. Thirty rhabdosomes including 21 siculae were counted on layer 55. A mature "monograptid" and two mature "diplograptids" were recorded on layer 55. Layer 60 contains 25 rhabdosomes of which 11 are siculae, and 10 are mature "monograptids". These rhabdosome size profiles are characteristic of the rest of the concretion and are not unique to these two layers. There is no evidence for size-sorting.

Thecal counts reveal a subtle up-concretion increase in *Monograptus* cf. *arciformis*, the most abundant graptoloid of the concretion (Figure 4.17). The pattern recorded in the residues is most likely the same occurrence that was revealed as the increase in mature "monograptids" on the dissolution surfaces higher in the concretion. Thecal counts show a slight increase in graptoloid thecae per layer thickness near the abundant layers 55 and 60. Peak abundance of thecae per layer height however, is found in residue 28-29. A similar distribution pattern was observed in the sicular counts. This thin layer contained a similar number of thecae as layers 3 to 7 times as thick. When corrected for concretion thickness the thecae appear to be more concentrated. This could represent an error in the dissolution process. A layer of 1 mm height is unlikely given the time for dissolution and the strength of the acid. I do not doubt that 1 mm was the measurement read from the scale that was etched on the side of the squared concretion. I question whether the dissolution surface was perfectly parallel to the previous dissolution surface and perpendicular to the scale. If not, more concretionary material was dissolved the thecal count for this layer would not appear as concentrated. The difference of 1 mm caused the concentration to drop by ½ and made the abundance of this residue comparable of that of the others. If this error is corrected then residues 52-55 and 69-72 are revealed as the residues with the most thecae per layer height. Both are dominated by *M.* cf. *arciformis* and unidentified "diplograptids".

With no evidence of size-sorting, fragmentation, orientation or a species assemblage shift, I can not relate the two graptoloid-abundant layers to the grading of

sediments observed from layer 50 to the top. To be accurate the grading of sediments happens in the basal unit of layer 50 – 55 with constant sediment composition above this. It appears that the abundance of *M.* cf *arciformis* in the residues 52-55 and 69-72 is an increase in the life community (biocoenosis) that is led by one species.

Limestone bed: CM 45.3-45.4

Lithofacies: 1, structureless, clay/organic-rich
Graptoloid distribution: non-random (χ^2/n= 12.18)
Taphofacies: physical addition of graptoloids and sediment removal – resedimented bed.

There is no evidence of lamina or bioturbation in the polished slab of this dark grey, very fine-grained carbonate bed (Figure 4.18B). In the field this bed was laterally continuous through the several meters exposure. The 10 cm thick limestone bed from base to top is shown in the polished slab illustrated in Figure 4.18B. Graptoloid rhabdosomes were visible at the base of the polished slab and on the basal bedding plane surface. Mature graptoloid rhabdosomes are very abundant at the base of this bed (Figure 4.18A; 42 rhabdosomes, all mature, no siculae). Elongate rhabdosomes show some degree of current alignment on dissolution surface layer 10 (Figure 4.18C). The top dissolution layers show a slight increase in rhabdosomes, but statistically these counts do not represent a concentration of graptoloids.

The residues from layers 0-10 and 10-16 show a large increase in most of the species represented in the concretion (Figure 4.19). Species of significance are: *Pribylograptus leptotheca*, *Normalograptus magnus*, *Glyptograptus incertus*, and *Monograptus* n. sp. B Melchin. Some species appear in the bottom two residues but are absent throughout the rest of the concretion (*Pristiograptus* n. sp. A, and *Pribylograptus imprimus*). Two patterns can be described from the sicular counts. 1) The first two residues are not enriched in siculae and thus the percentage siculae of the total count is low (33 and 39 % compared with the concretion average of 69%). 2) The top few residues contain abundant siculae, but the percentage siculae remains constant at approximately 80%, a result of a concomitant increase in thecae counted from the top residues. The top event shows an increase in all sizes (ages) of rhabdosomes whereas the

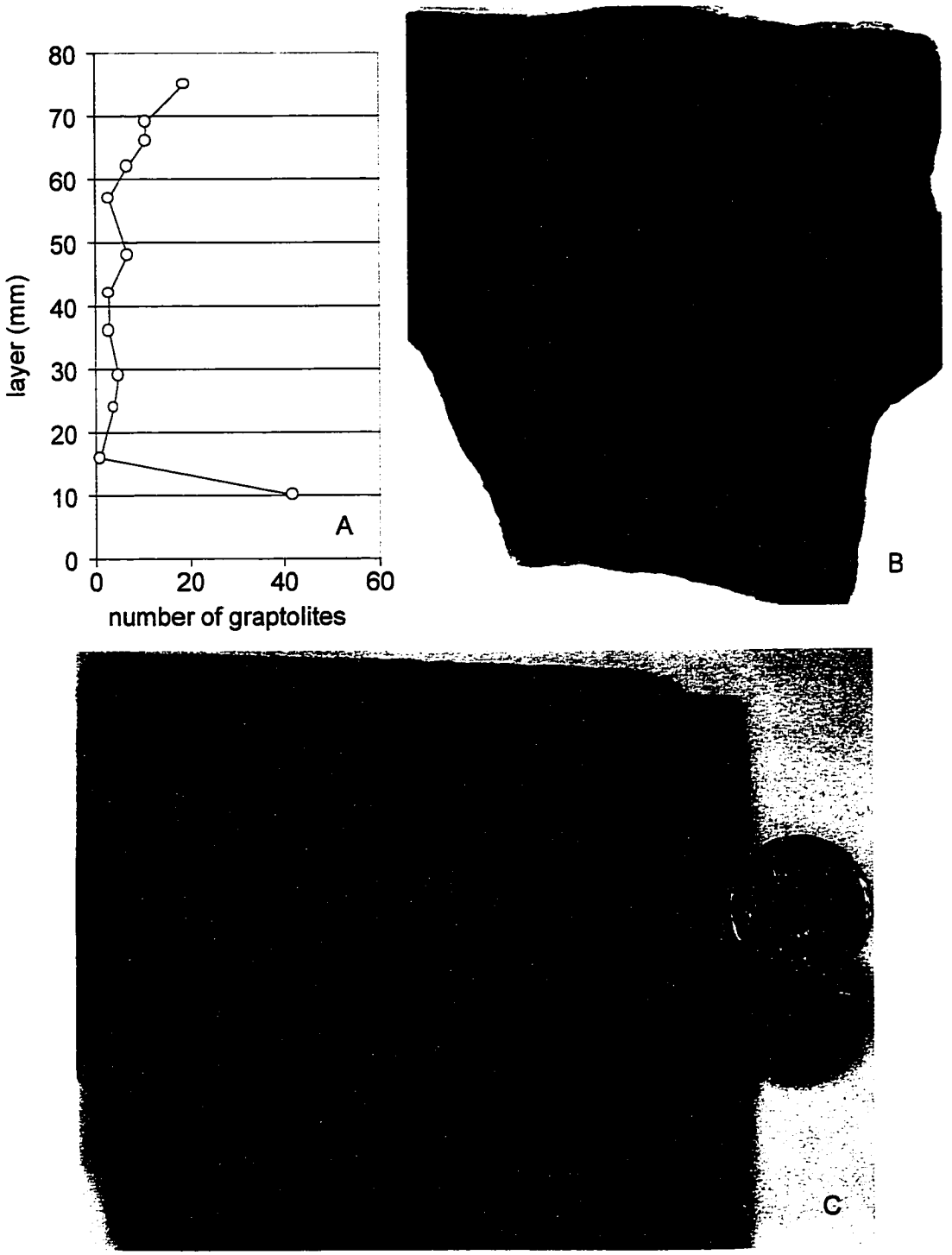

Figure 4.18. Limestone bed CM 45.3-45.4. A. Vertical distribution of graptolite rhabdosomes as revealed on the dissolution layers. The base of the limestone bed is abundant with rhabdosomes. B. Digital scan of polished slab showing no laminae. C. Dissolution surface of layer 10. Rhabdosomes showing some current alignment. Diameter of coin is 20 mm.

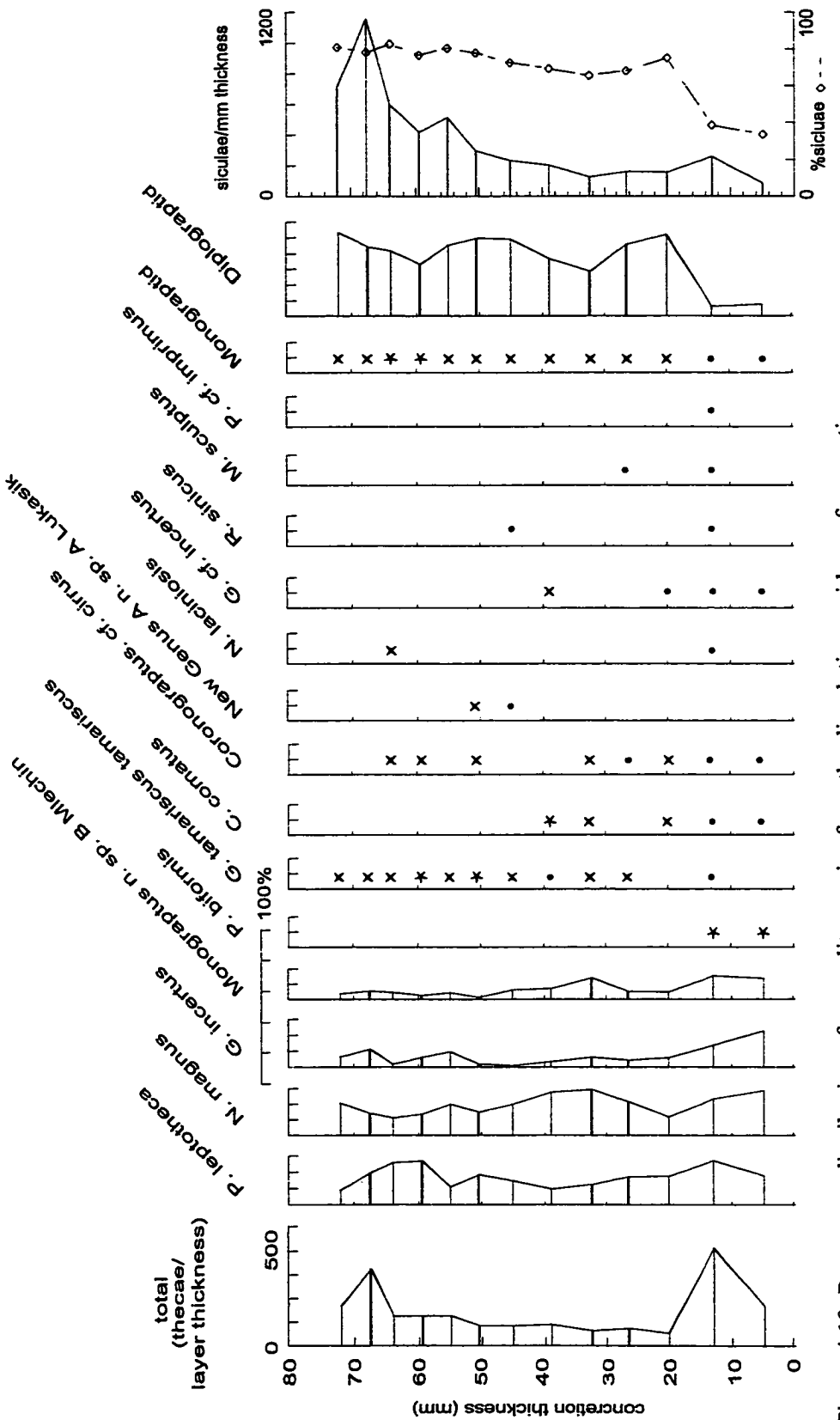

Figure 4.19. Percentage distribution of graptolite species from the dissolution residues of concretion CM 45.3-45.4; * 5-10%, × 1-5%, • < 1%

bottom event shows only an increase in the large (mature) rhabdosomes. The top event is not marked by the increase of one dominant species nor a lithologic variation. This basal event could be the result of taphonomic alteration, such as a winnowing event or the result of a paleoecological event, such as a bloom and subsequent mass-death of the mature rhabdosomes. Current evidence from alignment of rhabdosomes on the bedding plane surface and the absence of small rhabdosomes indicates that this basal unit is an event horizon recording the biostratinomic alteration of the assemblage. This event brought in new species but also concentrated the mature individuals from the surrounding waters/sediments. This limestone bed appears to be a resedimented limestone with a basal lag and an upward decrease in sediment input that results in the subtle concentration of graptoloids in the top residues.

Concretion: CM 46.35 - 46.5

Lithofacies: 1, structureless, clay/organic-rich
Graptoloid distribution: non-random ($\chi^2/n= 33.45$)
Taphofacies: physical addition of graptoloids

This very fine-grained carbonate concretion has an abundant graptoloid layer (Figure 4.20A) that is observed in polished slab (Figure 4.20B, C; layer 52-58). The concretion is weakly laminated with slight colour variations of medium brown to light brown defining discontinuous laminae that are in gradational contact. Radiolarian molds with 1 mm diameter show some variation in distribution with an increase at the base of layer 0-25, and an increase at the top of 31-52. Although rare laminae are weakly defined in thin section, the overall appearance is one of un-laminated, fine-grained carbonate, and therefore this concretion has been classified as structureless.

The concretionary carbonate has a very fine texture with "grains" averaging 10 to 50 μm (Figure 4.21B). The brown matrix material is present between these carbonate crystals/grains. Laminae of varying organic carbon content or grain size were not identified in thin section. Irregular shaped "pockets" (some circular) of more coarsely crystalline carbonate are 0.5 to 2 mm in diameter. Some of these are possibly diagenetically altered radiolarian molds. The interlocking crystals of these pockets

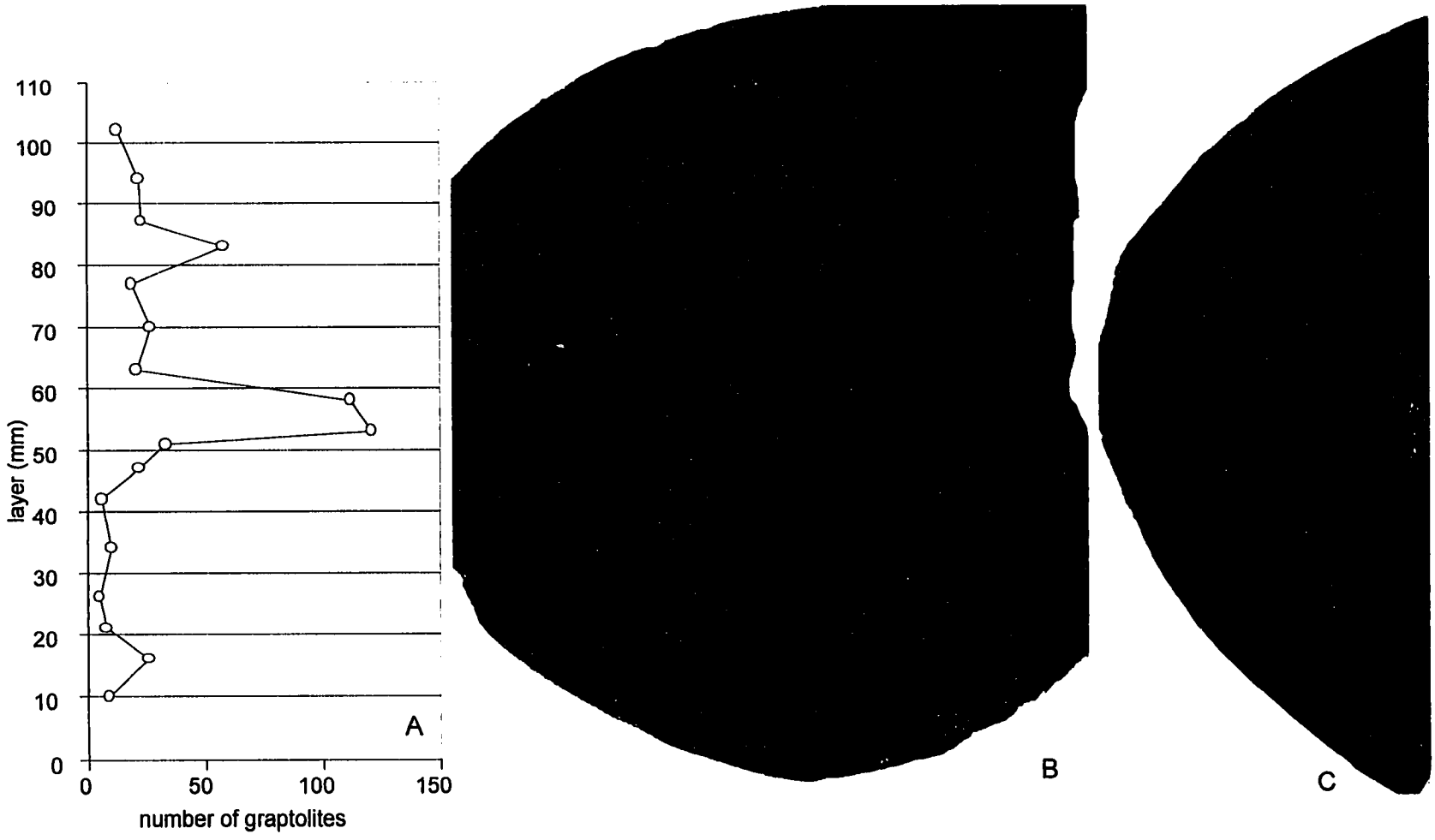

Figure 4.20. Concretion CM 46.35-36.5. A. Distribution of graptolite rhabdosomes upconcretion as recorded during dissolution. B, C. Digital scans of polished slabs aligned with correlated dissolution surfaces. Actual size. B. Cut perpendicular to graptolite alignment. C, Cut parallel to graptolite alignment.

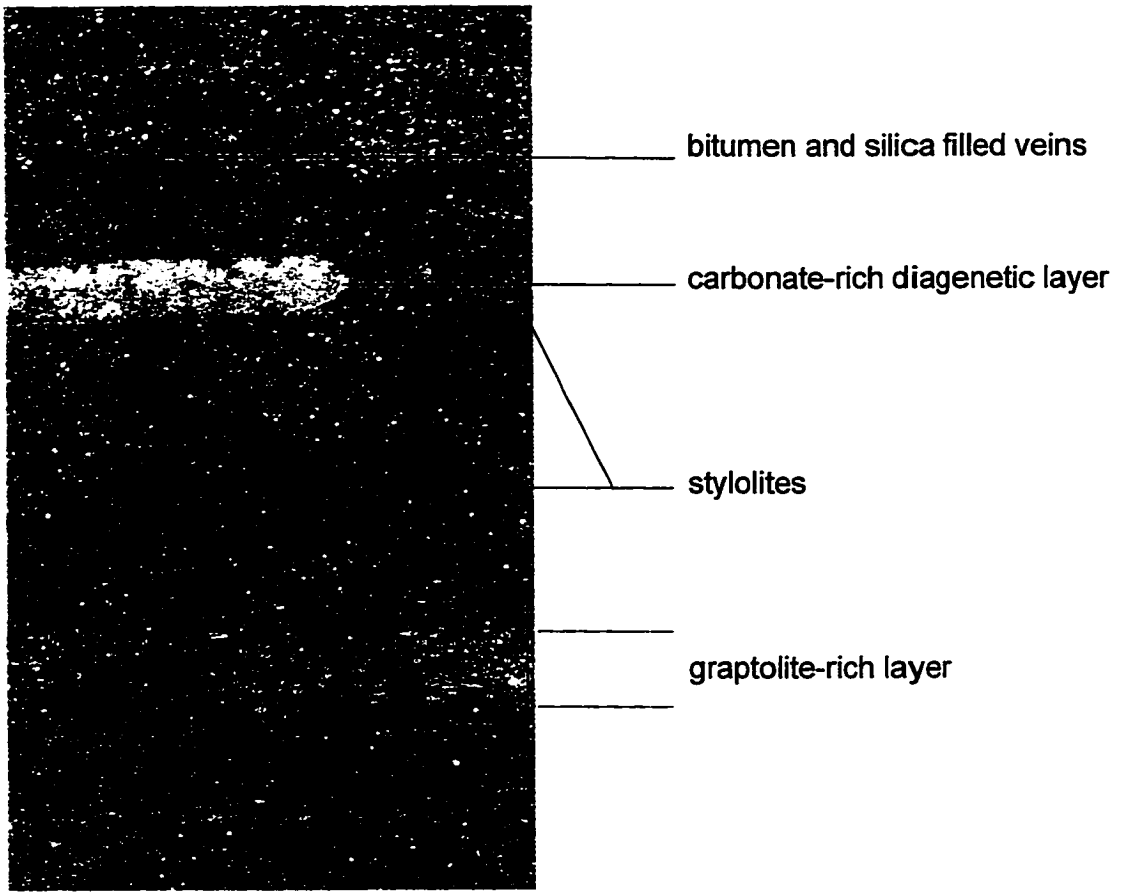

Figure 4.21. Concretion CM 46.35-46.5. Digital scans of thin section. A. A brown matrix with a grain-size too fine to distinguish is disseminated throughout. The grain size of the identifiable concretionary carbonate crystals ranges from 10 to 50 μm. Radiolarian molds or voids of other origin range in diameter from 0.5-2 mm and are filled with crystals that average 0.1 mm in size. Magnification x1.5. B. The base and top of the graptolite-rich layer are gradational and the crystal size between the rhabdosomes is constant with some coarser crystal growth in possible sediment voids. The sediment of this graptolite layer contains less brown matrix and fewer brown "grains". Magnification x6.

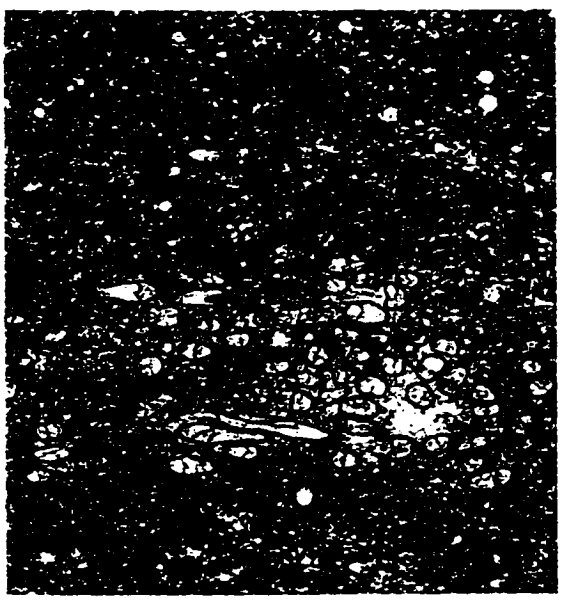

A

B

C

Figure 4.22. Three dissolution surfaces from Concretion CM 46.35-46.5. Up-concretion is into the page. Coin is 20 mm. in diameter. A. Layer 53. Monograptids (102 rhabdosomes) are more abundant than diplograptids (10 rhabdosomes) in this layer. Nine siculae were counted from this layer. Diplograptids were more abundant than monograptids on dissolution layer 51 (2 mm below layer 53). Monograptids from layer 53 are orientedapproximately perpendicular to the diplograptids in layer 51.

B. Layer 58. Abundant monograptids (112 rhabdosomes) with a similar orientation in the horizontal plane as in layer 53. No siculae or diplograptids were counted from this layer.

C. Layer 63. Graptolites are rare on this dissolution surface. Of the 21 rhabdosomes counted, 14 were siculae. This is similar to the appearance of the other dissolution surfaces below and above the abundant layers.

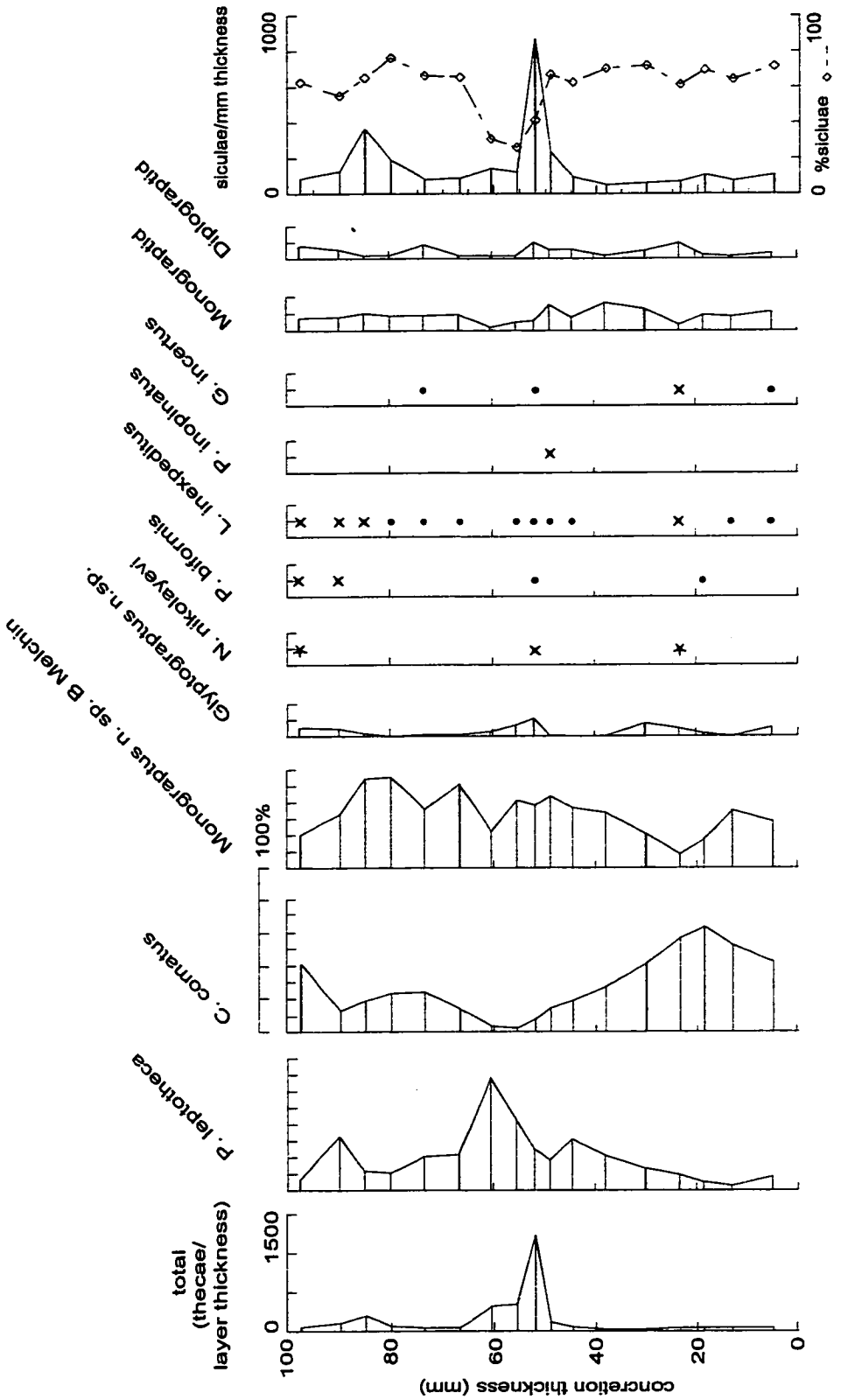

Figure 4.23 . Percentage distribution of graptolite species from the dissolution residues of concretion CM 46.35-46.5: * 5-10%, × 1-5%, • < 1%

average 0.1 mm in size. More of these coarsely crystalline pockets occur at the graptoloid-rich layer (52-58). The internal cavities of the graptoloid rhabdosomes are filled with the coarse carbonate crystals, whereas the rhabdosome is organic in its optical properties.

The abundant graptoloid layer (52-58) was observed during layer-by-layer dissolution (Figure 4.22A, layer 53, 121 rhabdosomes; Figure 4.22B, layer 58, 112 rhabdosomes; average number per layer, 31 rhabdosomes). The graptoloid rhabdosomes of this rich layer are oriented in the horizontal plane. Siculae and smaller growth stages were counted on layer 53 but the mature rhabdosomes dominated the assemblage. No siculae or smaller growth stages were recorded from layer 58. On layer 53 I observed that the "monograptids" (almost monospecific) were in one general orientation and the "diplograptids" (again, almost monospecific) were oriented almost perpendicular to the "monograptids". This might record two monospecific kills arriving to the sediment surface in two different flow events (Rigby, 1993). Above and below this abundant layer, graptoloids were randomly oriented with all size ranges present (e.g., Figure 4.22C)

The thecal counts through the residues revealed a slightly different distribution. Residues 51-53 and 53-58 were dominated by the two species *Pribylograptus leptotheca* and *Monograptus* n. sp. B Melchin (Figure 4.23). These large "monograptids" could easily have been mistaken for the same species upon quick examination of the dissolution surface. The co-occurrence (and co-dominance) of these two species has been identified in other concretions in this thesis (Chapter Nine). Notably rare from this diverse graptoloid-rich layer is *Comograptus comatus*, a predominant species throughout the concretion. The "diplograptids" identified from the dissolution surface study layer 53 can be ascribed to *Glyptograptus* n. sp. B, the most abundant "diplograptid" in the two residues.

The observed rarity of siculae from the abundant graptoloid dissolution layers is also seen in the counts of siculae from the residues. Residue 51-53 contained 2104 siculae (807 siculae/mm), residue 53-58 contained 465 siculae (121.8 siculae/mm), and residue 58-62 contained 460 (144 siculae/mm). When compared with the average count for the concretion of 169 siculae/mm, residue 51-53 could be considered enriched in

siculae, and residues 53-58 and 58-62 slightly depleted. When compared to the thecal counts from the same residues, residue 51-53 represented only 41% of the total count even though there was an abundance of siculae, the residue 53-58 sicular count was 26% of the total, and the residue 58-62 was 31% of the total. Residue 51-53 displays an increase in both siculae and mature rhabdosomes with the mature rhabdosomes proportionately more abundant when compared with the non-event layers (average = siculae 66.5% of total count). Residues 53-58 and 58-62 record an abundance of mature rhabdosomes but the sicular count is similar to the other non-event layers. Given the evidence of current alignment of the rhabdosomes, it seems likely that the siculae were deposited in numbers similar to the non-event layers (66.5% of the total) and were winnowed from the event horizon to produce the assemblage of depleted siculae (41%, 26%, 31% of the total).

There is little evidence in the sedimentology for describing layer 52-58 as a hydrodynamic event. In polished slab and in thin section there are no sedimentary structures, such as graded beds, scours, or cross-bed sets that would aid in the interpretation of depositional energy. The evidence for a hydrodynamic event is in the biostratinomic information recorded in the graptoloid assemblage. Horizontal alignment of the elongate rhabdosomes on the dissolution surfaces and winnowing of the small rhabdosome sizes (siculae and early growth stages) is evidence of a moderate energy current or flow. This was not high energy as there was no clear evidence of biostratinomic fragmentation. The graptoloid source for this event was slightly different than for the non-event beds, bringing in more *P. leptotheca* and fewer *C. comatus*.

Concretion: CM 47.4 - 47.5

Lithofacies: 10, graded-stratified, clay/organic and carbonate
Graptoloid distribution: non-random ($\chi^2/n = 3.77$)
Taphofacies: physical addition of graptoloids

This very fine-grained carbonate concretion comprises thin laminae of buff, light brown, and medium brown with gradational tops and bases. Overall there seem to be more light coloured laminae at the base (Figure 4.24B). Light brown laminae are slightly

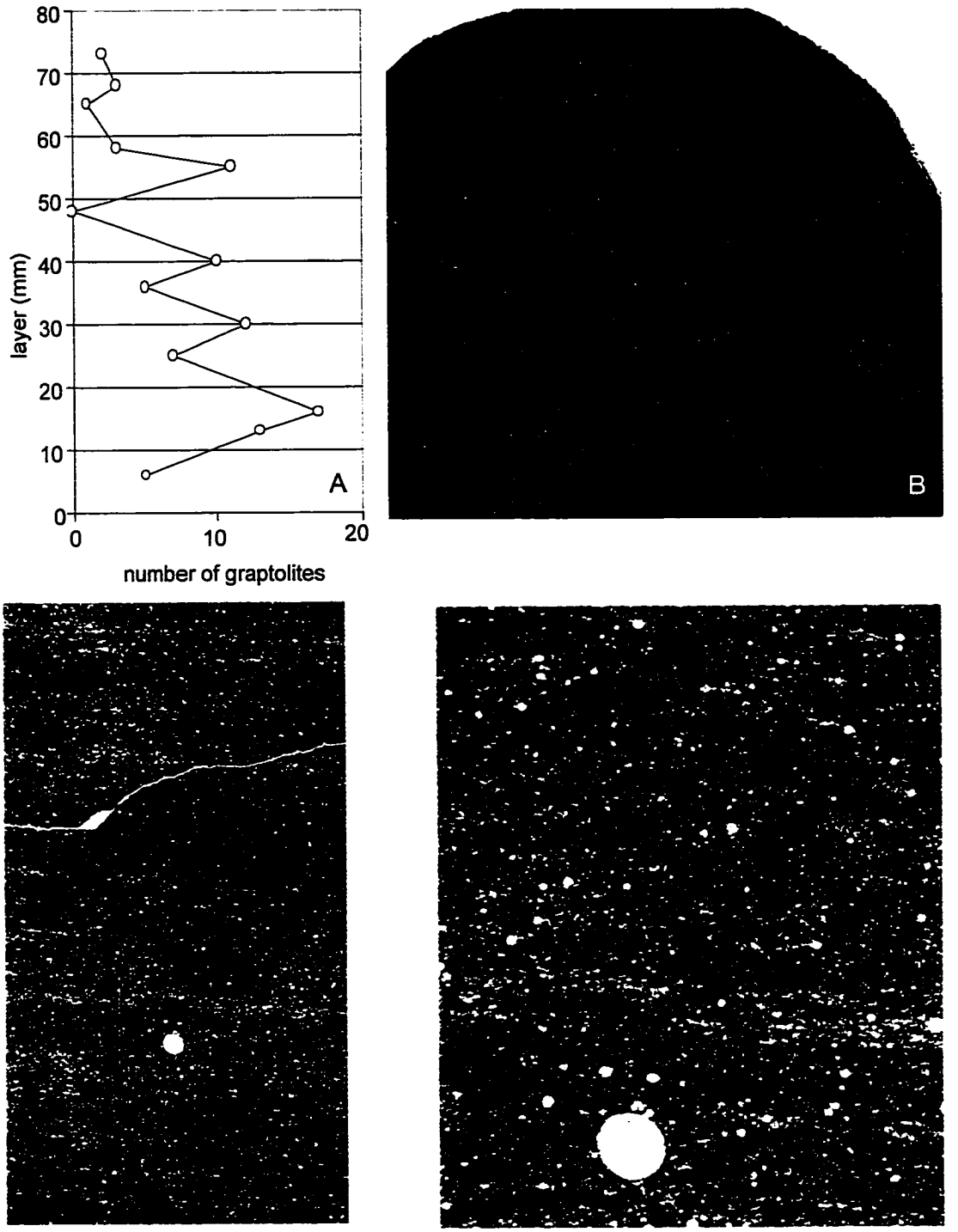

Figure 4.24. Concretion CM 47.4-47.5. A. Distribution of rhabdosomes vertically through the concretion. B. Digital scan of polished slab aligned with dissolution surfaces in figure A. Actual size. C. Digital scan of thin section showing an up-concretion increase in organics. Magnifcation x1.5. D. Laminae are defined by the organic content. Magnification x5.

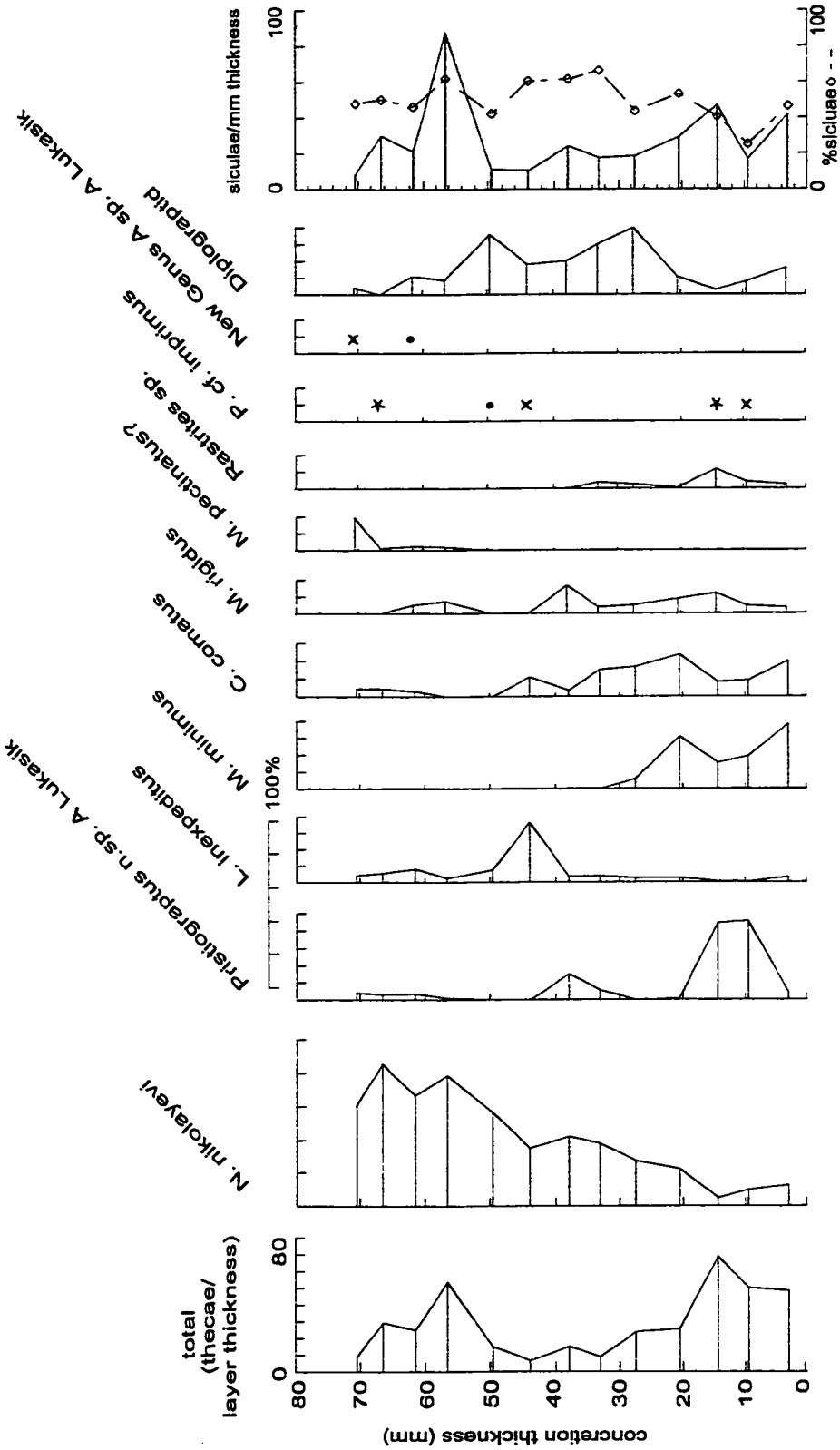

Figure 4.25. Percentage distribution of graptolite species from the dissolution residues of concretion CM 47.4-47.5; * 5-10%, x 1-5%, • < 1%

thicker than dark brown laminae. Dark stylolites are parallel to bedding at layer 47 and 65. These stylolites correspond to a lower rhabdosome count from dissolution surfaces 48 and 65. Layer 48 was barren and layer 65 contained 1 graptoloid (average count was 7 rhabdosomes per layer, n=13). It is possible that the lack of graptoloids is the result of obliteration by pressure solution. If these two layers are removed from the chi-square test, the result still shows that vertical distribution of the graptoloids is non-random. Graptoloids are concentrated on layer 16 (17 rhabdosomes) and show a slight increase at layer 13 (13 rhabdosomes) (Figure 4.24A). Graptoloids are more common on the basal dissolution surfaces, than dissolution surfaces up-concretion.

Thin section examination reveals numerous circular radiolarian molds (0.1 – 0.5 mm diameter) of more coarsely crystalline carbonate (Figure 4.24C, D). The crystal size within these circles ranges from 20 to 40 μm. Some radiolarian molds are clearly defined from the matrix and others are poorly defined, suggesting they have undergone further diagenetic alteration. The concretionary carbonate crystals range from indistinguishable grain sizes to a maximum of 40 μm, the average being 10 μm. There is no grading of crystal size from top to bottom of the thin section. The laminae are defined by the presence or absence of the very fine brown matrix. Pale laminae were more common at the base of the thin section than at the top. The thin section displays an overall normal grading of crystal size. This concretion is the only concretion that is placed within the microlithofacies termed graded-stratified, clay/organic and carbonate.

The relative decrease in grain-size up-concretion co-occurs with a variation in species distribution (Figure 4.25). The residues for this concretion show an up-concretion increase in *Normalograptus nikolayevi*. Whereas, *Pristiograptus* n. sp. A, *Metaclimacograptus minimus*, and *Comograptus comatus* are more predominant basally and decrease in abundance up-concretion. *Lagarograptus inexpeditus* does not show a graded distribution but instead peaks in abundance in residue 40-48.

Total thecal counts are high in the basal residues. At the top of the concretion an abundance of total thecae is secondary to the basal peak. This double abundance peak distribution is observed in the sicular counts; however, the top peak is more significant than the basal peak in the sicular counts. This could be associated with the observed up-concretion fining of sediments.

The bottom half of the concretion appears to host a slightly different graptoloid assemblage. This information along with the lithologic observation of an overall grading of colour from a lighter base to a darker top may be used to infer a grading of two populations of graptoloids from different sources. The basal residues of abundant *Pristiograptus* n. sp. A, *M. minimus*, *C. comatus*, and common siculae were deposited with a resedimented carbonate (coarse grained?) in a low energy event. This was gradually replaced with a more hemipelagic source of clays, organic carbon, siculae and a graptoloid assemblage dominated by *N. nikolayevi*.

Concretion: CM 48.5

Lithofacies: 3, coarsely laminated, clay/organic-rich
Graptoloid distribution: non-random ($\chi^2/n= 3.58$)
Taphofacies: physical addition of graptoloids

This concretion was inadvertently cut oblique to bedding. As a result of the dark colour of the concretion and the poorly defined bedding, this was not discovered until thin-section analysis revealed the error. I decided to keep the concretion in the study for two reasons. 1) The concretion records a graptolite concentration horizon that can be identified even with the dissolution layer oblique to bedding and this supports the hypothesis that the *R. orbitus* Zone was a time of transport and physical reworking. 2) The isolated thecae supported a graptoloid species association even with the temporal mixing created by the oblique sampling. As a result of the angle of obliqueness (20% as measured from Figure 4.26C) each dissolution surface spans approximately 22 mm of stratigraphic thickness within the concretion. The average dissolution residue records 27 mm of stratigraphic thickness.

This very fine-grained carbonate concretion records three major laminae that contain discontinuous finer laminae of light to medium brown (Figure 4.26A). The major laminae are defined by the distribution of white to pale brown patches that are possibly of diagenetic origin. Lamina 37-70 and lamina 0-22 contain this patchy texture. The middle lamina (22-37) has fewer white patches. This lamina displays white crystalline calcite lenses 4 mm to 30 mm in length and thin black partings 1 mm to 12 mm in length

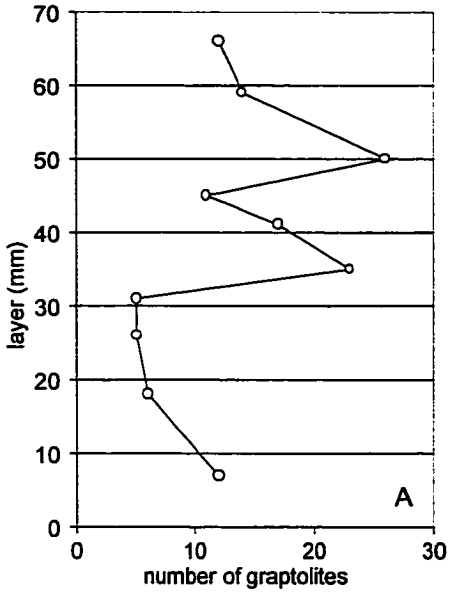

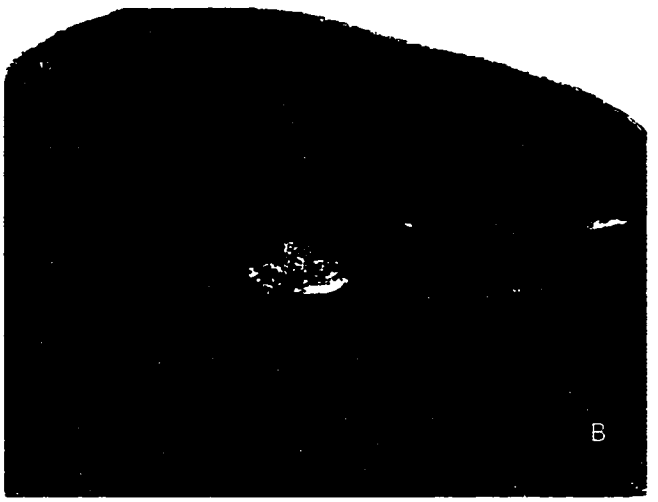

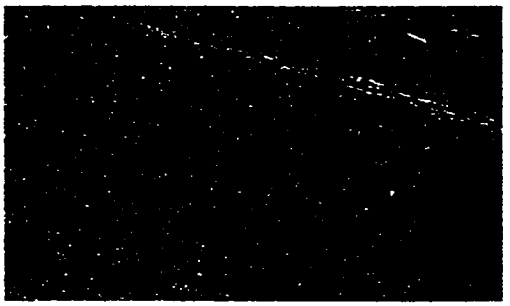

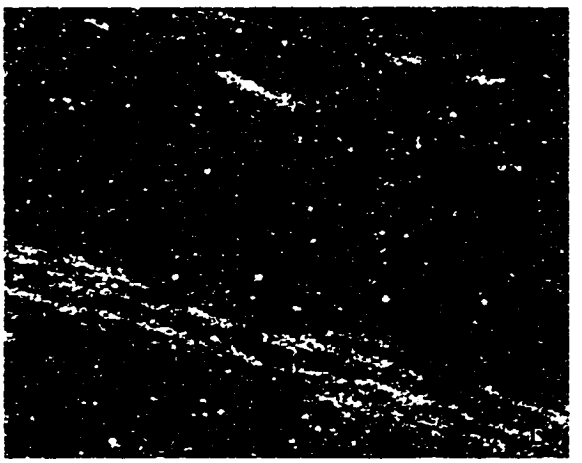

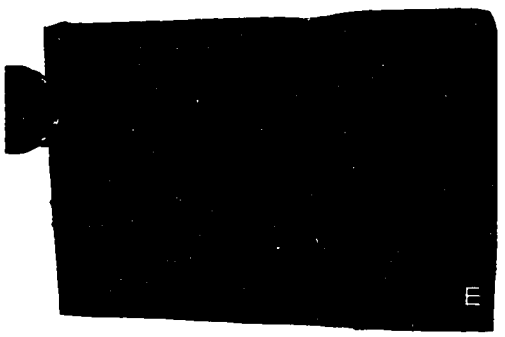

Figure 4.26. Concretion CM 48.5. A. Vertical distribution of graptoltie rhabdosomes as recorded during the layer-by-layer dissolution. B. Digital scan of polished slab aligned with layers in A. Infilled bivalve or brachipod at centre. Actual size. C. Digital scan of thin-section. Laminae are oblique to upconcretion arrow. Actual size. D. Light laminae lack organics and have a slightly larger carbonate concretion crystal texture than the darker laminae. Magnification x4. E, F. Dissolution surfaces. Coin diameter is 20 mm. E. Layer 45. Graptolites are not parallel to dissolution surface and likely represent a concretion cut oblique to bedding. F. Layer 50. The same graptolite rich layer non-parallel to bedding. Organic (?) object at centre.

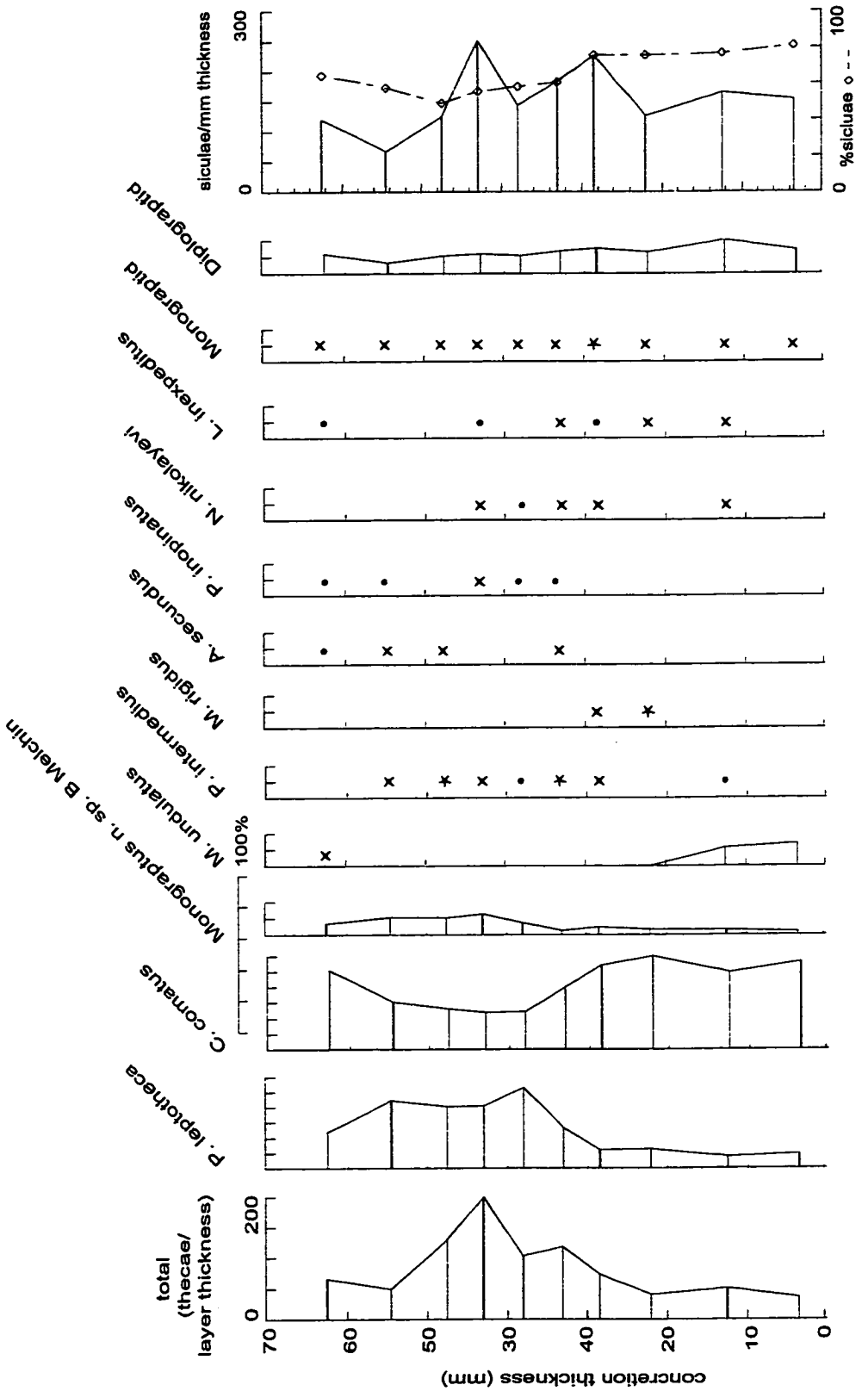

Figure 4.27. Percentage distribution of species through concretion CM 48.5: * 5-10%, x 1-5%, • < 1%

parallel to bedding. This lamina also contains a spar-filled cavity of a possible bivalve or brachiopod 8 by 18 mm. A second spar-filled object was observed during the dissolution on layers 35, 41, 45, and 50. This organic object was most likely the locus for concretion formation.

The matrix was observed in thin section as a brown material that was disseminated throughout with very few well-defined concretionary carbonate crystals. This fine texture had grains that ranged in size from the immeasurable to 20 μm in diameter. The thin and infrequent lighter laminae had less matrix and more clearly defined crystals that measured 10 – 50 μm. It should be noted that during dissolution the sieves (both 63 μm and 177μm) were relatively clean, agreeing with the determination of grain size observed in thin section.

Two of the ten layers examined during dissolution showed a concentration of graptoloid rhabdosomes (Figure 4.26A: layer 35, 23 rhabdosomes; layer 50, 26 rhabdosomes; average number of rhabdosomes per layer = 13, n=10). Layer 41 contained many fragmented graptoloids and some were not included in the count of 17 recorded for the layer. It is possible that some fragmentation occurred prior to burial. Fifty-six percent of the total 104 rhabdosomes (excluding siculae) were observed to be oriented non-parallel to bedding as a result of the oblique sampling of this concretion (Appendix B; Figure 4.26E, F). This caused the rhabdosomes counts to be shared between many dissolution surfaces (35, 41, 45, and 50) when in truth they represent only one graptoloid-rich lamina. Assuming an oblique sampling, the abundant graptoloid layer can be recreated from dissolution photos (e.g., Figure 4.26E, F). The organic object was stratigraphically lower than the graptoloid layer. The orientation of the graptoloids in three-dimensions suggests that the rhabdosomes were aligned on the bedding plane of this graptoloid-rich layer.

Thecal counts of the residues defined an increase of graptoloid thecae in residue 41-45 (Figure 4.27), the residue that sampled the largest portion of the obliquely oriented graptoloid-rich layer. The predominant species in the residue is *Pribylograptus leptotheca* with lesser amounts of *Comograptus comatus*, *Monograptus* n. sp. B Melchin, and other graptoloid species in minor abundance. *Pribylograptus leptotheca* is less common in the basal residues where *C. comatus* dominates instead. *Monograptus* n. sp.

B Melchin, although low in abundance, has the same profile of occurrence as *P. leptotheca*. *Metaclimacograptus undulatus* only occurs in the basal residues that are dominated by *C. comatus*. The dominance of *P. leptotheca* and *Monograptus* n. sp. B Melchin through the top residues is likely a product of the oblique sampling. During dissolution the abundant graptoloid layer was recorded to be dominated by mature "monograptids". The abundant graptoloid layer was likely dominated by the two species *P. leptotheca* and *Monograptus* n. sp. B Melchin.

Siculae counted from the residues are comparatively less dominant in the top half of the concretion. The percentage siculae of the total count drops from an average of 77% in the bottom four residues to an average of 57% in the top six residues. This is a product of an increase in mature rhabdosomes in the top residues that is unmatched by a relative increase in the numbers of siculae. This is likely a size-sorting process related to the event bed. The effect of the size-sorting has been diluted among all the top residues as a product of the oblique sampling of the event horizon.

Although sampling errors confuse the observations, this event bed records a current-aligned transport of a graptoloid assemblage dominated by *P. leptotheca* and *Monograptus* n. sp. B Melchin. Other organic clasts are concentrated within or near this graptoloid event.

Concretion: CM 49.8-49.9

Lithofacies: 1, structureless, clay/organic-rich
Graptoloid distribution: non-random ($\chi^2/n= 2.42$)
Taphofacies: Sediment-starved, hiatus horizon.

Coarse laminae were faintly visible as variations in the darkness of the carbonate in the polished slab (Figure 4.28B). In thin section faint laminae were observed as lighter carbonate material with a slightly coarser texture (Figure 4.28C). Carbonate crystals were 20 to 100 μm in diameter and averaged 30 μm in the dark concretionary material. Darker brown grains comprise approximately 1-3 % of the sample and average 15 to 300 um in size. Some of these grains are cubic, opaque and are identified as disseminated pyrite. Dark stylolites are oriented non-parallel to assumed bedding.

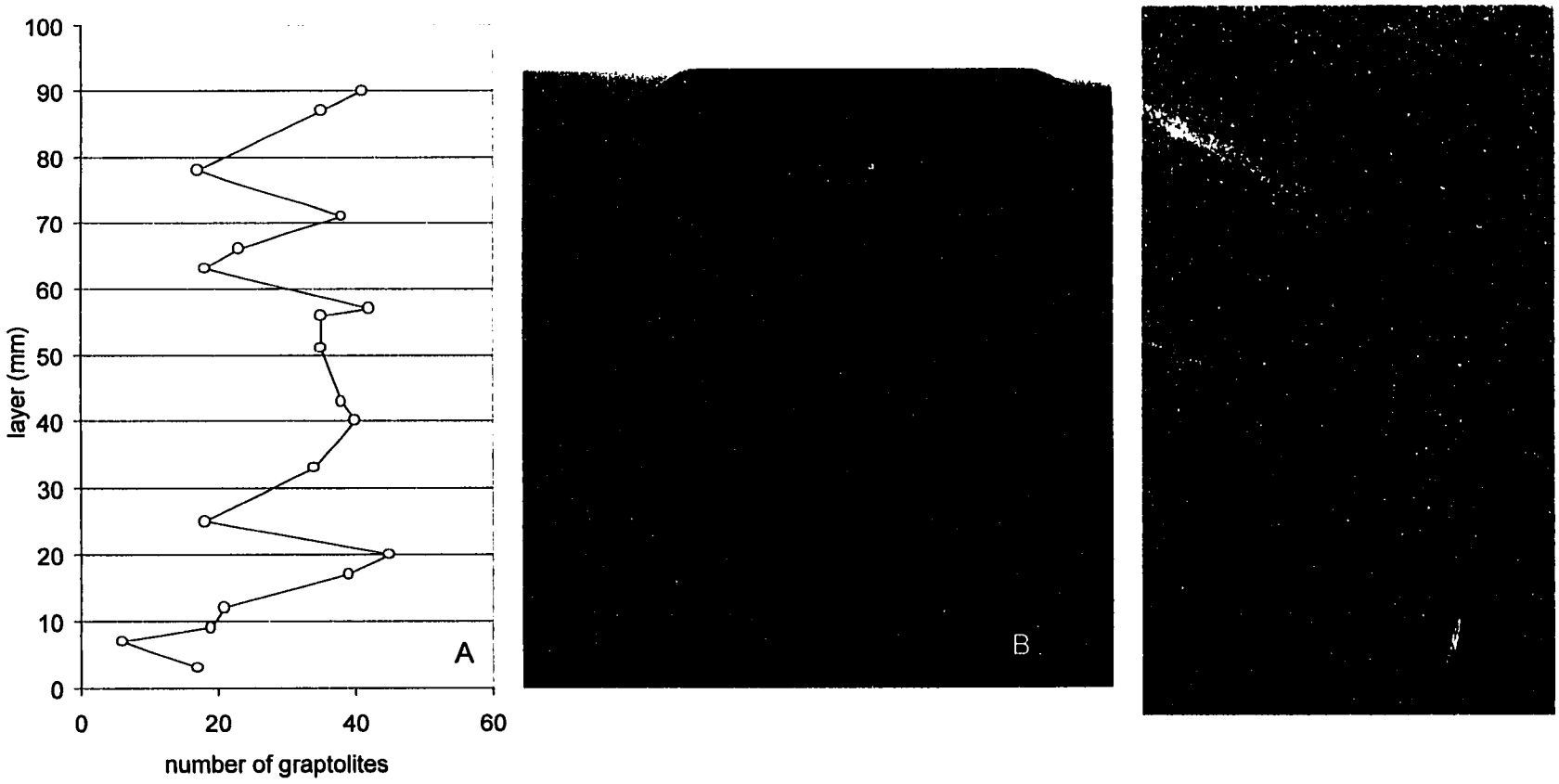

Figure 4.28. Concretion CM 49.8-49.9. A. Vertical distribution of graptolite rhabdosomes as observed during the layer-by-layer dissolution of the concretion. Most dissolution surfaces were abundant with rhabdosomes. B. Digital scan of polished slab. No visible bedding or sedimentary structures. Actual size. C. Digital scan of thin-section cut oblique to bedding. Some laminae lack brown organic materal and define bedding. Dark brown stylolites and silica internal molds of nautaloids cut bedding. Magnification x1.5.

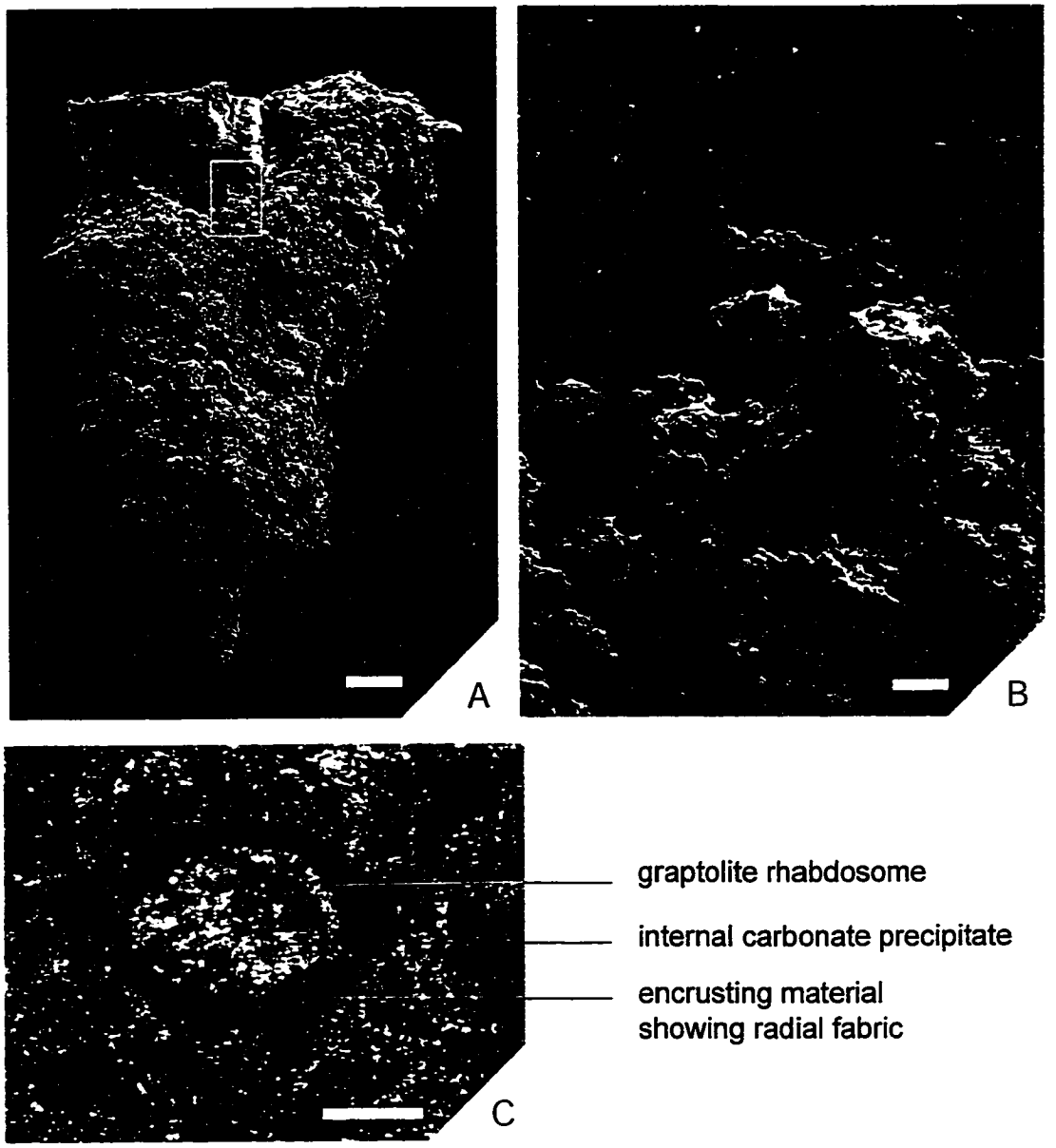

Figure 4.29. A-B SEM of encrusted *Normalograptus nikolayevi* from CM 49.8-49.9 residue 33-40. A. Fine-grained light brown material thickly encrusts three-quarters of the rhabdosome. Square at centre is shown in figure 4.29B. Scale bar is 100 μm. B. Image of unaltered rhabdosome (top half of image) and encrusting material (bottom half of image). The encrusting material forms in clusters or spheres and does not penetrate the rhabdosome. No obvious organic sturctures such as bacteria strings are observed. All spheres and clusters can be formed by diagenetic mineral precipitation. The hole in the rhabdosome at the top-centre is a puncture in the rhabdosome, not a boring. The edges of the hole are not clean, but fractured and a portion of the rhabdosome has caved into the puncture hole. Scale bar is 10 μm. C. Digital image of encrusted graptolite as seen in thin-section from CM 49.8-49.9. Scale bar is 50 μm.

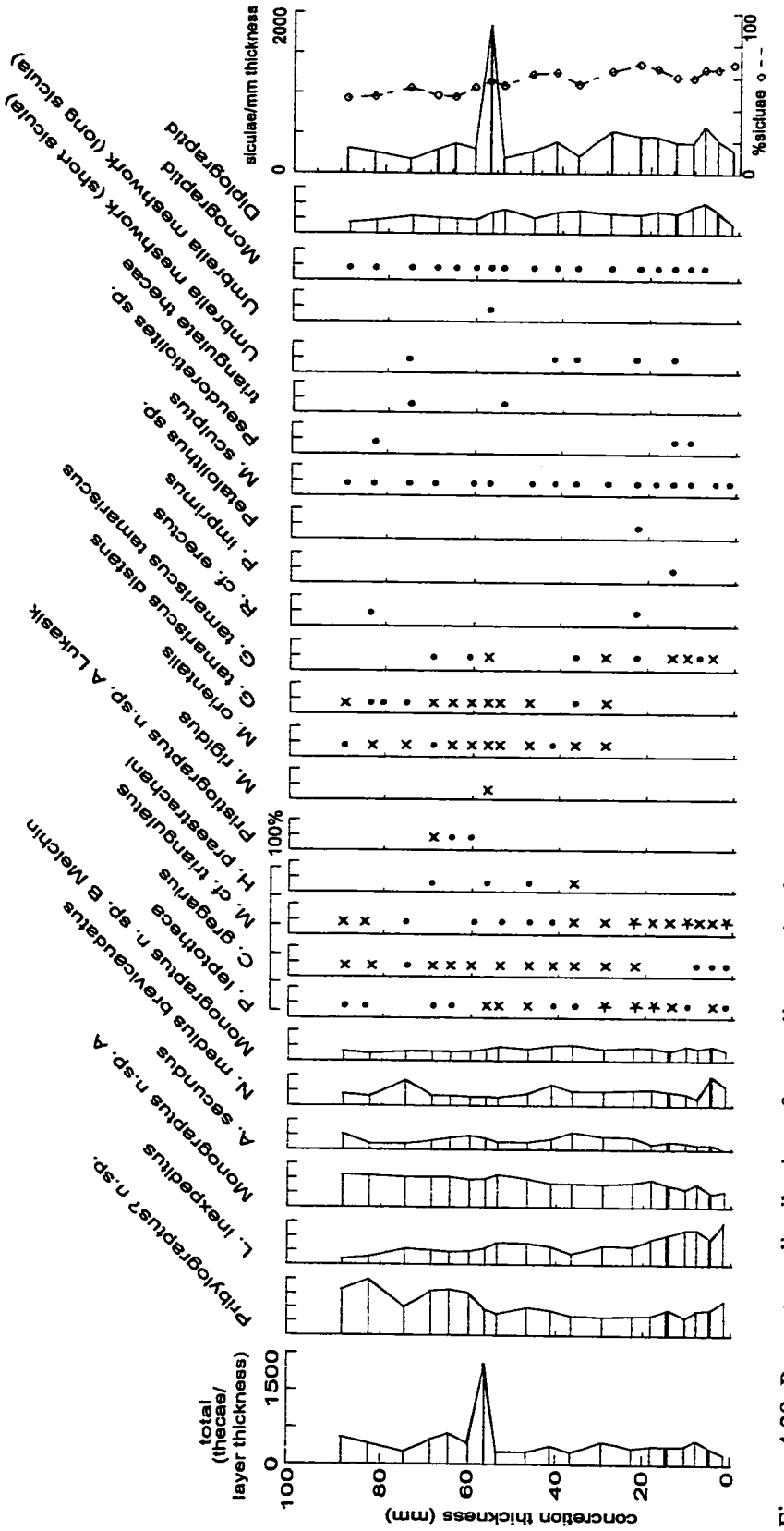

Figure 4.29. Percentage distribution of graptolite species from the dissolution residues of concretion CM 49.8-49.9: * 5-10%, × 1-5%, • < 1%

Graptoloids were very abundant on most of the 19 layers recorded during the dissolution of this very fine-grained concretion (Figure 4.28A). Only 6 rhabdosomes were counted from layer 7, well below the average of 30 rhabdosomes per layer for the concretion. Even if this one layer is removed, the graptoloid distribution does not support the null hypothesis of random distribution. Whereas the number of rhabdosomes on each surface is variable, there does not seem to be one layer that is more concentrated than others. The average number of graptoloid rhabdosomes that were counted for each layer was 30, n = 19. There appear to be four layers that are well above this average (layer 20, 45 rhabdosomes; layer 40, 40 rhabdosomes; layer 57, 42 rhabdosomes; and layer 90, 41 rhabdosomes). There are six layers that are well below this average (layer 3, 17 rhabdosomes; layer 9, 19 rhabdosomes; layer 25, 18 rhabdosomes; layer 63, 18 rhabdosomes; layer 78, 17 rhabdosomes; and layer 7 with 6 rhabdosomes). There does not appear to be any relationship between the abundance measured on the dissolution surface and the vertical position in the concretion. The graptoloids were randomly oriented in the horizontal plane on all dissolution surfaces.

Some of the rhabdosomes on layers 43, 51, 71, and 78 were encrusted with a brown, opaque, fine-grained, insoluble material. To understand the nature of this encrustation and whether it was the product of biological organisms or later diagenetic alteration I examined a few of the encrusted graptoloids in SEM (Figure 4.29A, B). No characteristic algae or organic shapes could be distinguished from the fine-grained light brown material that thickly encrusted the rhabdosome. The encrusting material formed in clusters or spheres and did not penetrate the rhabdosome. In thin section the encrusting material was observed to radiate out from the organic rhabdosome (Figure 4.29C). In these ways the encrusting material had the appearance of diagenetic cement, not biologic encrustation. Holes in the rhabdosome were observed to be puncture holes probably resulting from processing methods, not biological borings. Further evidence for the diagenetic origin of the encrusting material is found on the dissolution surface. Layers 43, 51, 71, and 78 contained a fine brown insoluble material that was concentrated at the centre of the concretion – a poorly formed core. The graptoloids at the centre of the concretion were preferentially covered with this material.

The graptoloid assemblage of this concretion is the most diverse of the 29 concretions examined (Figure 4.30). Twenty-three species are recognized, of which six are first appearance species in the stratigraphy. Peak abundance for the concretion is reached in residue 56-57 (1364 thecae/mm thickness, compared with an average of 308 thecae/mm thickness, n = 19). This concentrated abundance in residue 56-57 was also observed in the siculae (1848 siculae/mm compared with an average of 433 siculae/mm, n=19).

Qualitative analysis of the thecal counts reveals some trends. *Pribylograptus? n. sp.* and *Monograptus* n. sp. C increase slightly up through the concretion as *Lagarograptus inexpeditus* decreases. These three species comprise the predominant graptoloid fauna of this concretion. Interestingly, they are all thin "monograptids" that fragment easily in the residues. It is possible that their presence was missed in the rhabdosome counts from the dissolution surface. It is also possible that the rhabdosome count of one mature "monograptid" in the dissolution surface is expanded in significance in the residues where thecae were the basis of measure. Both scenarios explain the lack of a significant abundance peak at the 56 or the 57 dissolution surfaces as compared with the obvious increase in residue 56-57.

The graptoloid assemblage of residue 56-57 is not unique in species composition. One species or one group of species does not show a dominance in this residue that is unique to the concretion. If this increase in graptoloids in this layer represents a paleoecological bloom in the biocoenosis then all species were affected. This is rare in modern zooplankton (Bougis, 1976) and in well-studied micropaleontology examples (e.g., dinocysts; G. L. Williams, pers. comm., 2001). It is more common for one species or one species association to dominate during a bloom at the cost of the other zooplankton not able to take advantage of the change in environmental conditions (Bougis, 1976).

The concentration of graptoloids in residue 56-57 is not the result of physical transport as the assemblage showed no signs of biostratinomic alteration, such as size-sorting or current alignment. It is not interpreted as a graptoloid bloom. The layer most likely contains concentrated graptoloids because of a decreased rate of sedimentation of carbonate and clay. Typically, sediment-starved deposits are identified by an increase in

dark organic matter or clays resulting from the steady "rain" of suspended organic matter and clay without the dilution by more coarse grained carbonates or silicates. In this concretion, laminae are not well defined and the whole concretion is very dark with organic carbon abundant in most laminae. If the sediment input decreased or ceased, the effect would not have been as clearly distinct a break in the sediment record. For these reasons I classify this concretion in the taphofacies "sediment-starved".

Limestone bed: CM 50.4

Lithofacies: 1, structureless, clay/organic-rich
Graptoloid distribution: non-random (χ^2/n= 2.99)
Taphofacies: physical addition of graptoloids – resedimented bed.

This very fine-grained, dark grey, structureless carbonate bed contains some randomly distributed, white diagenetic patches and minor bioclasts (Figure 4.31B). This was sampled from a limestone bed that is approximately 8 cm thick and laterally continuous through the approximately 3 m exposed outcrop. The polished slab samples the bed from base to top. In thin section, carbonate crystals were 10 – 50 μm in size. No laminae were observed in either thin section or polished slab(Figure 4.31C). This thin section appeared to have less of the inter-crystalline matrix/mictire than CM 49.8-49.9 or CM 50.4-50.5. Brown grains, 10-30 μm in diameter represent approximately 1% of the thin section. Randomly oriented brown stylolites are common.

More than half (57%) of all of the rhabdosomes are concentrated on two (layers 13 and 46) of the ten dissolution surfaces (Figure 4.31A). Two layers were barren. Abundance for the whole concretion was low with the total number of rhabdosomes observed during dissolution being 28. Examination of the species distribution (Figure 4.32) shows an abundance in total thecae counted per layer thickness in residue 10-13. This corresponds to the increase observed on layer 13 during dissolution. Overall, total thecal abundance decreases up-concretion with a minor increase observed in the residue 40-46 matching the abundant dissolution layer 46. Both residues are dominated by *Monograptus tenussimus* (53% residue 10-13, 52% residue 40-46). Residue 10-13 also contains a high percentage of *Pristiograptus fragilis pristinus* (29%), whereas residue 40-

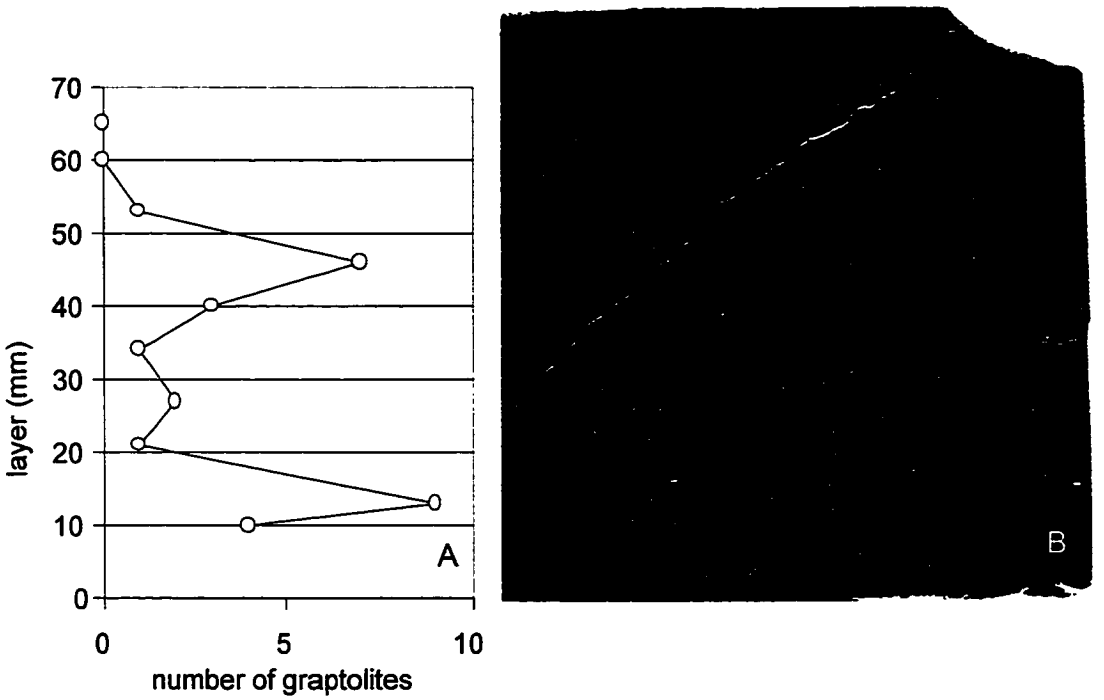

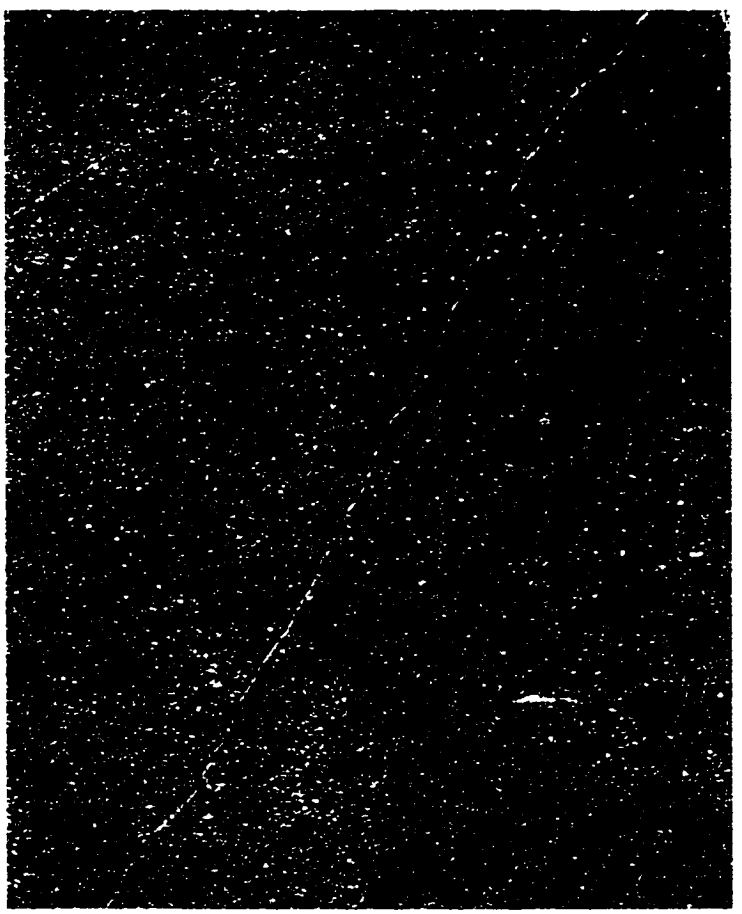

Figure 4.31. Limestone bed CM 50.4. A. Vertical graptolite rhabdosome distribution from the layer-by-layer dissolution. Two concentrated layers (13, 46) are observed although overall abundance is low. Two layers are barren. B. Digital scan of polished slab of struceless dark grey-brown concretion. C. No sedimentary structures are observed in thin-section. Carbonate crystal size ranges from 10 to 50 μm with brown grains representing about 1% of the sample. Inter-crystalline brown matrix is common throughout. Stylolites common. Magnification x2.5.

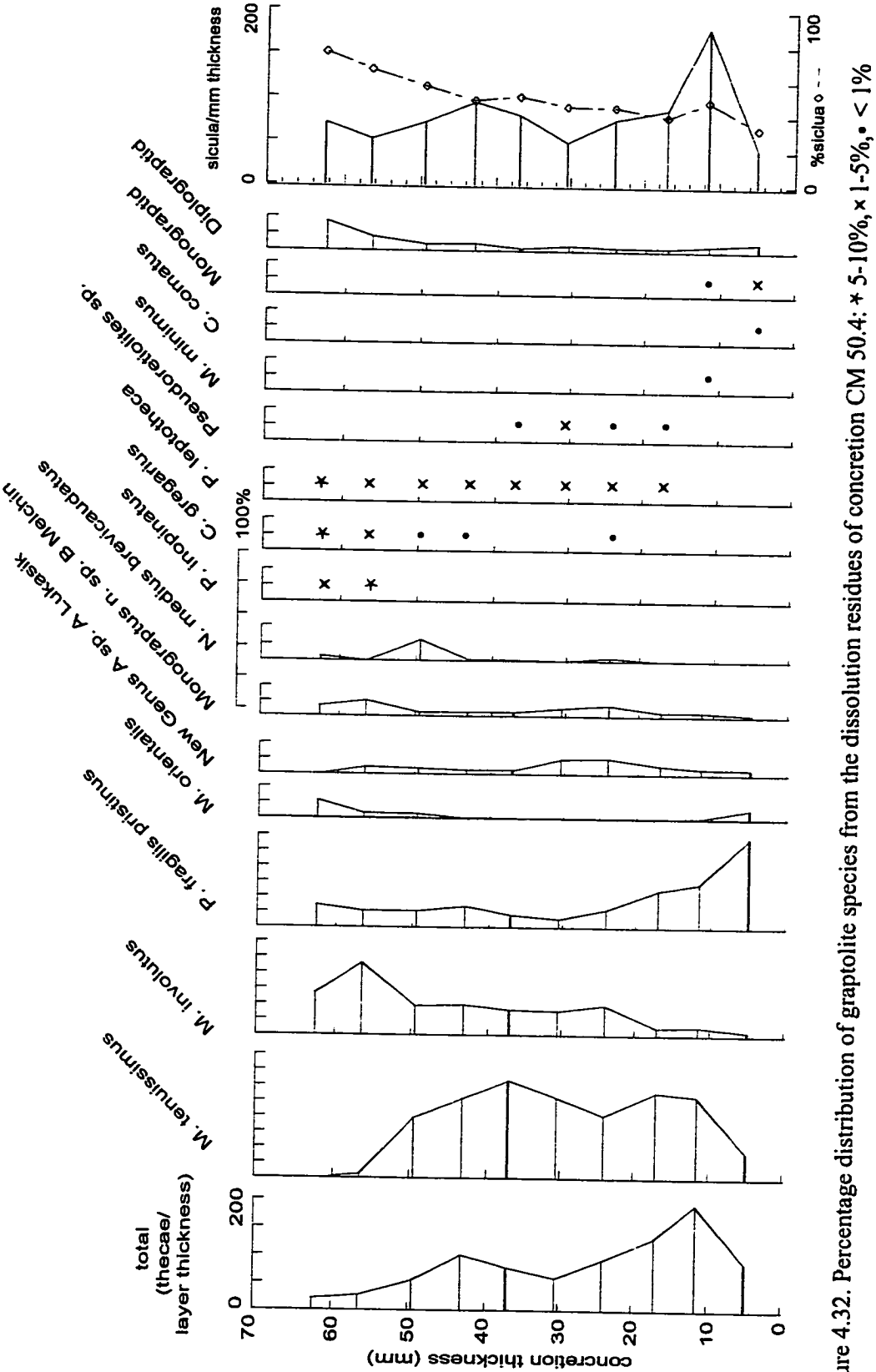

Figure 4.32. Percentage distribution of graptolite species from the dissolution residues of concretion CM 50.4: * 5-10%, × 1-5%, • < 1%

46 does not appear to have a secondarily dominant species. *Pristiograptus fragilis pristinus* decreases in relative abundance upwards as *Monograptus involutus* increases. The sicular counts are concomitant with the thecal counts; however, the percentage siculae of the total thecal count increases upward.

The vertical variation in the graptoloid assemblage is likely the result of biostratinomic processes. The distribution of graptoloids within the residues is similar to the distribution recorded from a lower limestone bed CM 45.3-45.4. In that bed an abundance of rhabdosomes was recorded from the first dissolution surface and from the basal residues. The species assemblage shifted in composition vertically through the bed. Both beds are structureless and dark greyish brown in colour. Both show an upward increase in siculae. The limestone bed CM 45.3-45.4 contains clear evidence of current alignment and winnowing in an interpreted basal lag. These observations were not recorded from CM 50.4; however, many of the rhabdosomes in this bed were not elongate but coiled, and as such would not record current alignment. Total rhabdosome counts from the dissolution surfaces were low, making the identification of current aligned rhabdosomes difficult. Both limestone beds are interpreted to be resedimented limestone with an upward variation in graptoloid assemblage suggesting deposition from two slightly different sources: a transported basal assemblage that also incorporates graptoloids in the existing sediment, and a hemipelagic source from the waters above.

Concretion: CM 50.4-50.5

Lithofacies: 3, coarsely laminated, clay/organic-rich
Graptoloid distribution: random ($\chi^2/n= 0.99$)
Taphofacies: random flux of graptoloids and sediment

This very-fine-grained carbonate concretion contains three coarse laminae (Figure 4.33B). Lamina 0-20 is greyish black with scattered bioclasts (bivalve/brachiopod, and nautiloids) and radiolarian molds. The bioclasts are more abundant between layers 55 and 70 with a radiolarian-rich lamina at layer 70. Other than this bedding-parallel feature, there is little evidence of internal laminae within this unit. Lamina 20-30 is grey

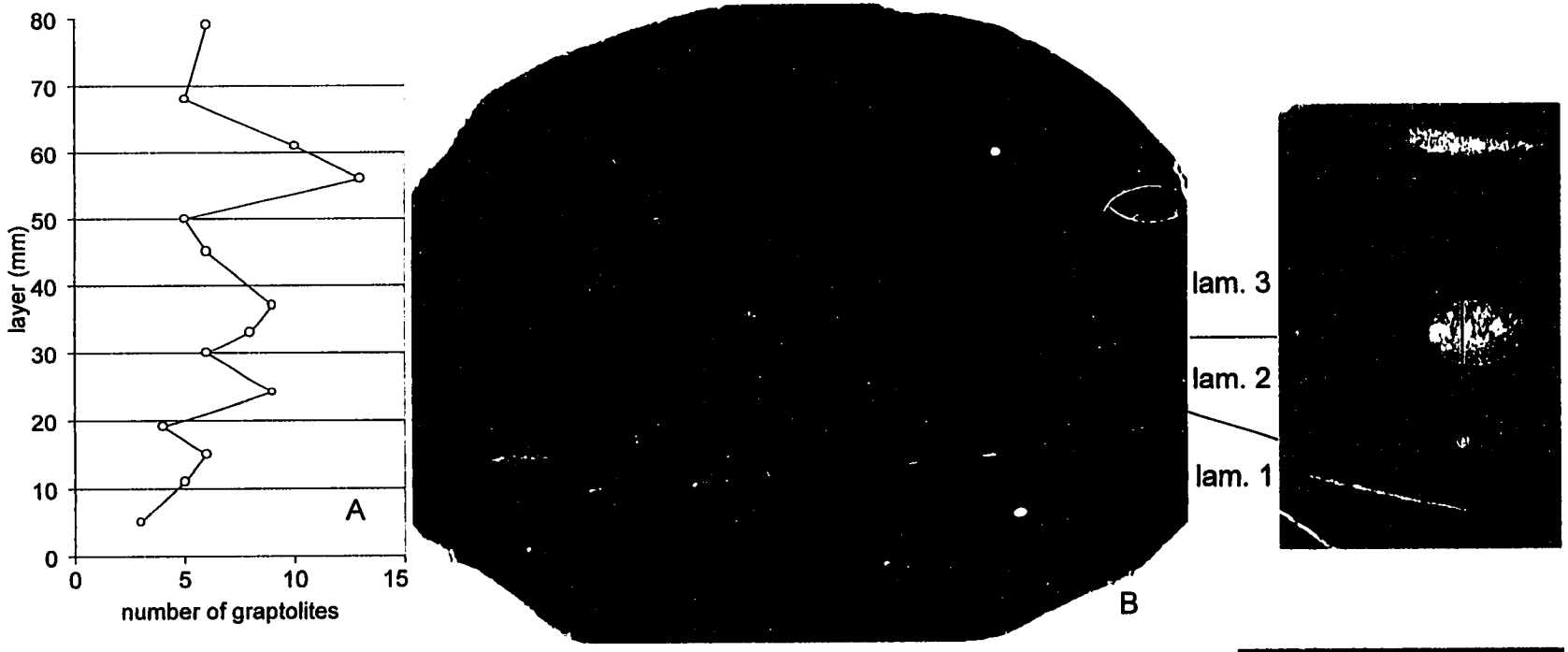

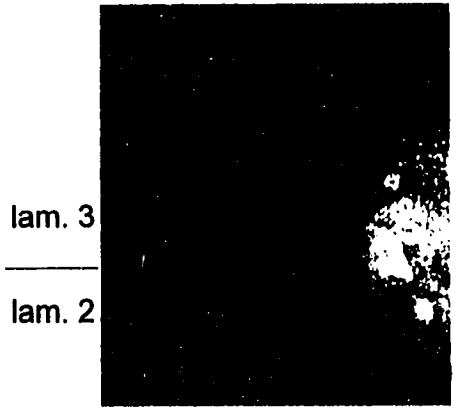

Figure 4.33. Concretion CM 50.4-50.5. A. Distribution of graptolites vertically through the concretion based upon dissolution results. B. Digital scan of polished slab. Dark limestone with calcitic nautaloid infills and clacitic brachiopod and bivavles. Concretion is comprised of three coarse laminae. Laminae 1 and 3 are rich with organic matter and shelly fauna. Lamina 2 is grey with abundant radiolarian molds but few other organics. Actual size. C. Digital scan of thin-section showing the same three laminae. Lamina 2 contains less brown organic material in the matrix and a larger carbonate crystal size. Actual size. D. Enlargement of lamina 2 and 3 boundary. Cross-section of large nautaloid at right is infilled with a coarsely crystalline calcite. Stylolites and viens are deflected around the nautaloid. Magnification x4.

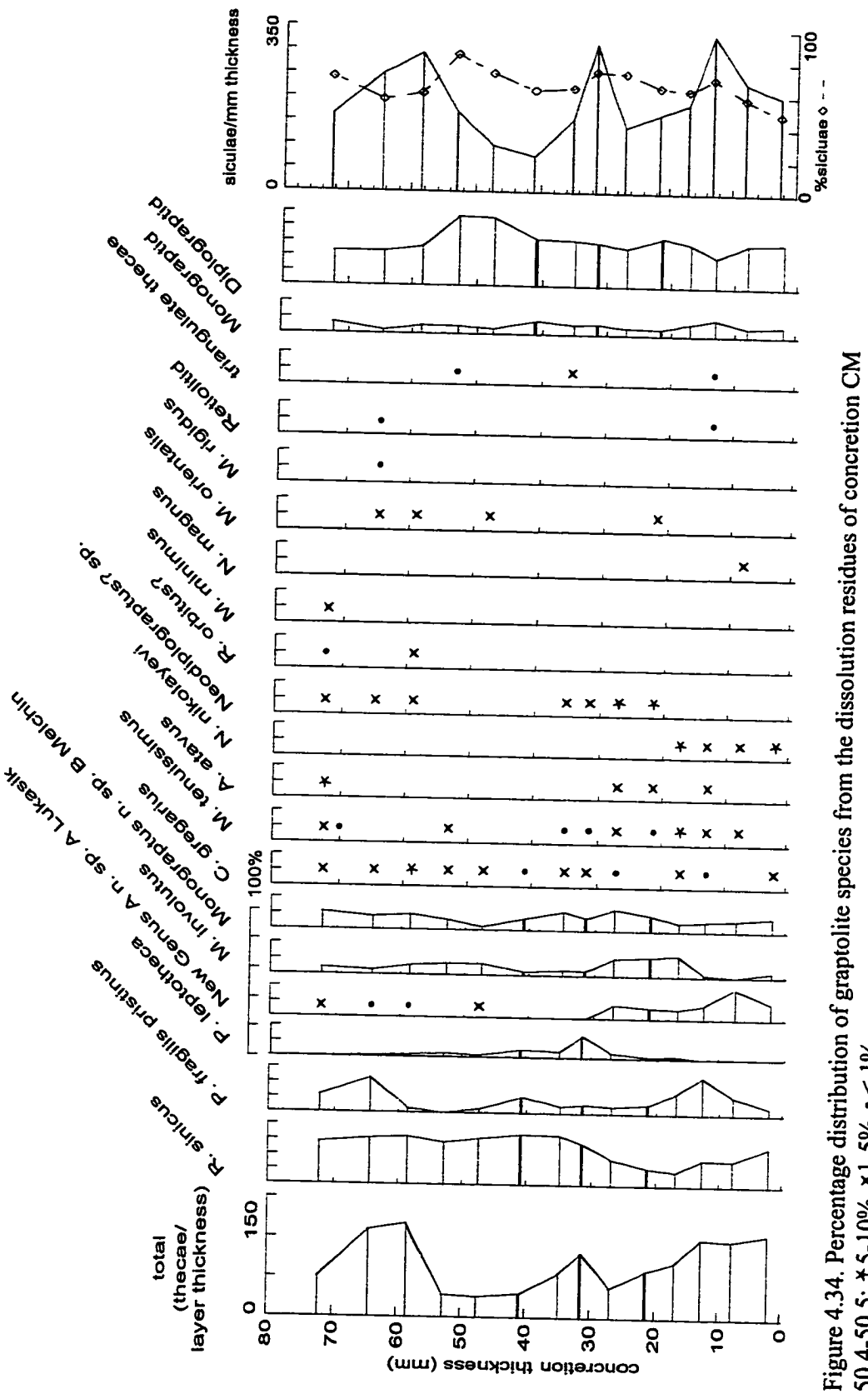

Figure 4.34. Percentage distribution of graptolite species from the dissolution residues of concretion CM 50.4-50.5: * 5-10%, × 1-5%, • < 1%

buff with many small radiolarian molds. The top and basal contacts of this lamina are gradational. Lamina 30-79 is similar to 0-22.

These three laminae are also identified in thin section (Figure 4.33C, D). Lamina 30-79 has a crystal size of 10 to 80 μm with an average diameter of 30 μm. Lamina 20-30 has a coarser texture (20 to 100 μm) and contains less matrix. Lamina 0-20 is similar in character to lamina 30-79. Stylolites are common and do not follow bedding. Thin veins of bitumen and calcite are also observed to cut bedding.

Graptoloids are randomly distributed among the 14 dissolution surfaces and support the null hypothesis (Figure 4.33A). A slight increase (no statistical significance) is seen at layer 56 and 61, but there is no corresponding lithological evidence to support an event bed at this location in the concretion. The thecal counts revealed a variation in total thecal counted per layer thickness in the dissolution residues (Figure 4.34). Mid-concretion residues were less concentrated with graptoloid thecal fragments than those from the top and base of the concretion. This abundance trend was mirrored by the distribution of *P. fragilis pristinus*, which was more abundant in the top and basal residues. *Pribylograptus leptotheca* was more abundant in the mid-concretion residues. The predominant species of the concretion, *Rhaphidograptus sinicus* was consistently dominant in the top two-thirds of the concretion and of secondary importance to two thin "monograptids", *P. fragilis pristinus* and New Genus A n. sp. A Lukasik, in some of the basal residues.

Counts of siculae from the residue have a distribution similar to that of the total thecal counts. The siculae are abundant in residues 11-15, 30-33, and 56-61, the same residues identified as enriched with thecae. The percentage siculae of the total count varies between 48% and 83%. The top and basal peaks are not as great in the siculae as in the total thecal counts resulting in a lower percentage of siculae. Residue 30-33 had a greater peak in the sicular counts than in the rhabdosome counts and is represented by a higher percentage of siculae. The overall distribution of siculae suggests that they were not subject to a different sorting process than the graptoloid rhabdosomes.

The changes in species composition identified by the thecal counts are thought to be subtle changes within the biocoenosis and not a biostratinomic alteration of the taphocoenosis. The statistically insignificant increase of rhabdosomes on dissolution

layers 56 and 61 is observed as an abundance of graptoloid thecae and to a lesser extent siculae, in the residues 56-61 and 61-68. This is accompanied by an increase in bioclasts from layer 55-70, some of which may be shelf-derived. This is thought to be related to a change in the rate or composition of sediment supply and not a major biostratinomic event. The change in lithology at layer 20-30 may be related to a decrease in the total thecal count and sicular count. The graptoloids were possibly diluted by an increased sediment supply, represented by a coarser carbonate texture and less matrix. These subtle variations in lithology and graptoloid distribution fit within the taphofacies of random flux of graptoloids and sediment. This concretion is thought to represent a hemipelagic depositional environment.

Concretion: CM 51.2-51.3a

Lithofacies: 4, coarsely laminated, clay/organic-poor
Graptoloid distribution: non-random ($\chi^2/n= 3.67$)
Taphofacies: physical addition of graptoloids

This concretion was sampled 1.2 m from 51.2-51.2b at the same stratigraphic level and shows a similar internal stratigraphy. Three layers comprise this fine-grained carbonate concretion (Figure 4.35B). The basal layer 0-25 is medium greyish-brown with some faint lighter laminae just visible on the polished slab. Radiolarian molds are common. This basal layer is in gradational contact with a medium to dark brown lamina (25-33). This lamina contains radiolaria that grade in abundance from common at the base to rare/absent at the top. Layer 25-33 is in sharp contact with the layer above. Layer 33-80 is medium brown with lighter patches (1-2 mm in length) and common radiolarian molds. A buff-coloured wedge, parallel to bedding extends across one half of the slab. The base of the wedge is at 50 mm and it obtains a maximum thickness of 4 mm. This was revealed to be a sponge spicule mass during dissolution (Figure 4.35E). White to buff-coloured, thin, discontinuous internal laminae are present in layers 0-25 and 33-80. Two nautiloids are seen in cross section.

The crystals in layer 0-25 range in size from 20 to 60 μm and contain more of the brown matrix than the lamina 33-80. Within layer 0-25 are two laminae (0.5 cm and

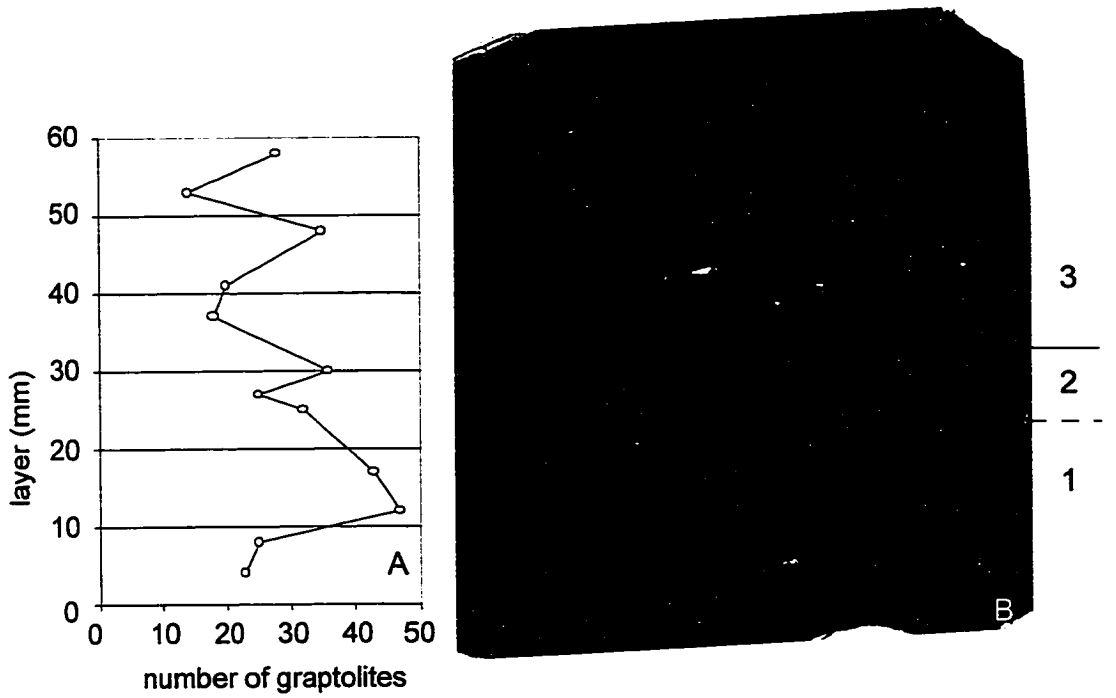

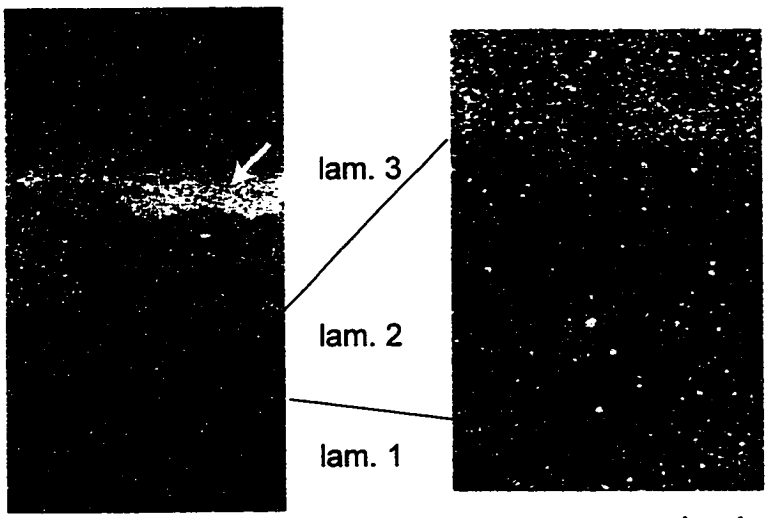

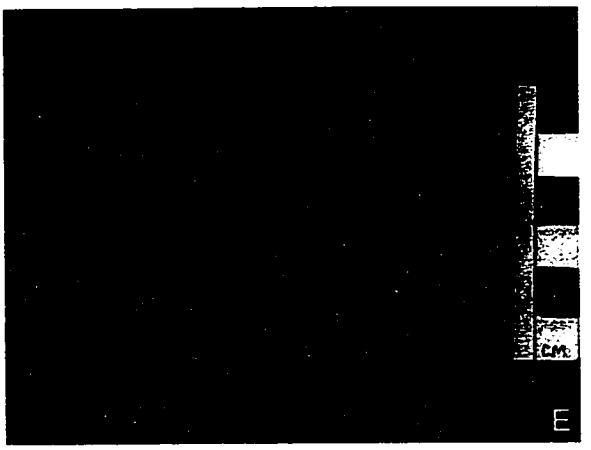

Figure 4.35. Concretion CM 51.2-51.3A. A. Distribution of graptolite rhabdosomes vertically through the concretion as revealed in the layer-by-layer dissolution. B. Digital scan of polished slab aligned with the dissolution layers. C. Digital scan of thin section showing three major layers. White arrow points to sponge spicule mass. Actual size. D. Detail of the two contacts between the 3 layers. Lamina 2 has a gradational base and a sharp top contact. Lamina 2 has a smaller carbonate crystal size (20-70 μm) than lamina 1 and 3 (40-180 μm). Magnification x3. E. Dissolution surface of layer 53 revealing a mass of sponge spicules that have formed a silica-rich insoluble mass.

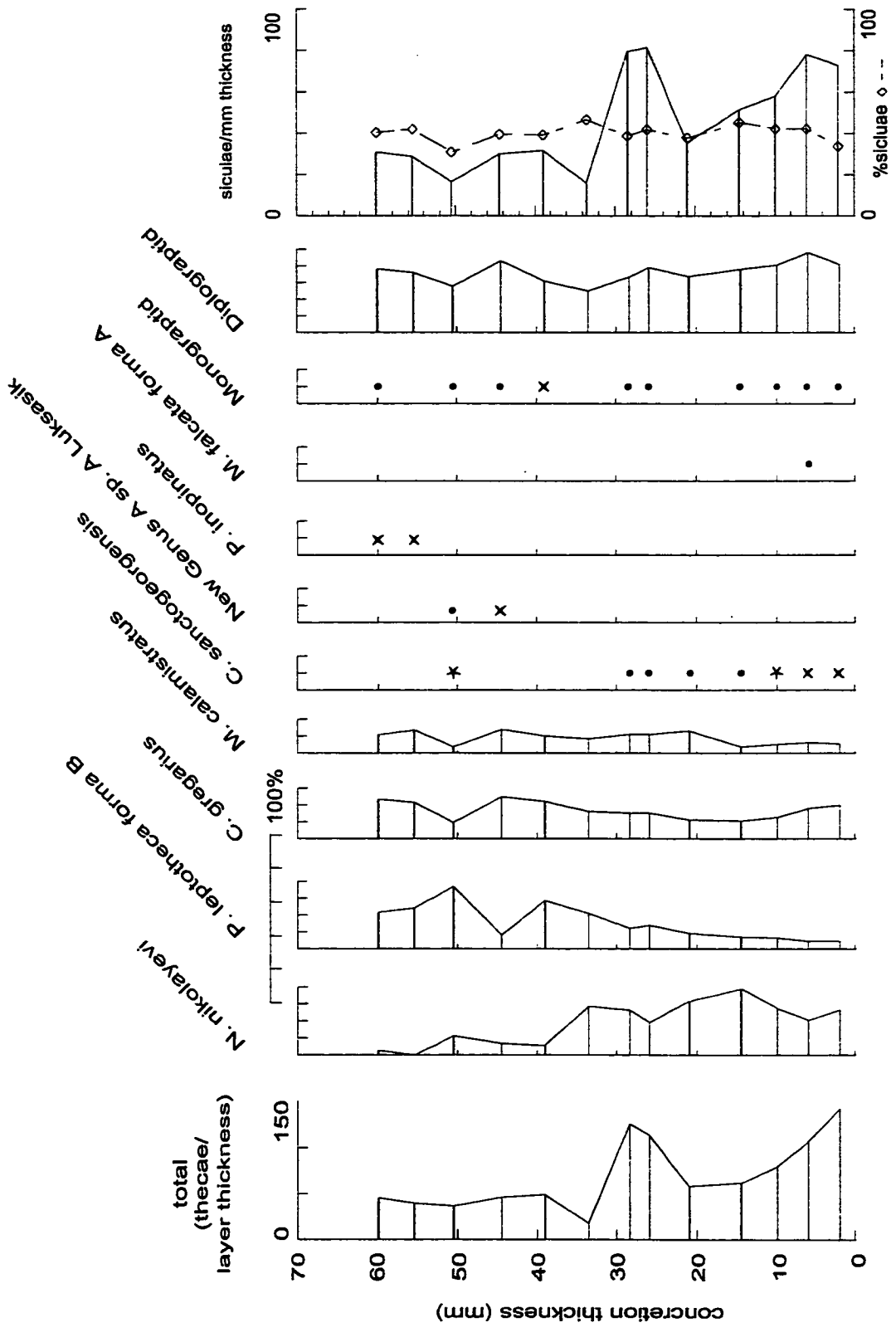

Figure 4.36. Percentage distribution of graptolite species from the dissolution residues of concretion CM 51.2-51.3A * 5-10%, × 1-5%, • < 1%

greater than 0.9 cm) with less brown matrix and a coarser carbonate texture. These internal laminae have a character similar to the layer 33-80. The layer 33-80 has a crystal size that ranges from 40 to 150 μm and contains less of the brown matrix. Within this layer is a buff-coloured sponge spicule mass with indistinguishable grain size, an irregular base (0.6 cm relief) and a bedding-parallel top.

Graptoloids are concentrated in two layers (layer 12, 47 rhabdosomes; layer 17, 43 rhabdosomes; average rhabdosomes per layer = 30). These enriched graptoloid layers are associated with a sponge spicule mass with the spicules oriented in the lattice and a large gastropod. Many of the rhabdosomes have siculae oriented perpendicular to the bedding surface near the sponge spicule mass. Layer 48 showed a slight increase in graptoloid rhabdosomes and also had an abundance of other fossil fauna. Abundant small gastropods, bivalves, nautiloids, sponge spicules and a hemispherical bryozoan were found on layer 48. Similar fossil fauna, although less abundant, were also reported from layer 53 (Figure 4.35E) and 58. Many of the mature graptoloids from layer 27, 30, and 37 are encrusted with a brown, fine-grained material that does not dissolve in acid. Like the encrusted graptoloids from CM 49.8-49.9 these are thought to be diagenetic in origin.

Vertical variation in the abundance of graptoloids in the residues is related to subtle variations in the composition of the assemblage (Figure 4.36). Graptoloid thecae and siculae are more abundant in the basal residues (0-27). Abundance drops sharply above this in both the thecal and the sicular counts. The average count of thecae/mm in the basal residues is 99, compared with an average of 39 thecae/mm in the top residues. Counts of siculae/mm are 65 and 26, respectively. *Normalograptus nikolayevi* is the predominant species in the basal residues. Two "monograptid" species dominate the top residues; *Pribylograptus leptotheca* and *Coronograptus gregarius*. Two species are found only in the top residues; New Genus A sp. A Lukasik, and *Petalolithus inopinatus*. *Monograptus falcata* forma A is only found in one residue in the basal unit and *Campograptus sanctogeorgensis* is common in the basal residues and rare in the top residues (only in residue 48-53). *Monograptus calamistratus* and *Coronograptus gregarius* maintain a constant relative abundance throughout the concretion.

The change in lithology and the sharp contact at the base of layer 30 is associated with a change in graptoloid abundance, a shift in the graptoloid assemblage composition,

and an increase in shelly fauna. This sediment and the graptoloid species composition has been altered by physical transport. Two transport events are recorded (0-25 and 25-33). The first is a thick graded bed with abundant graptoloids dominated by *Normalograptus nikolayevi* and common shelf-derived shelly fauna. The second is a structureless, coarse-grained carbonate resedimented bed that contains abundant shelf-derived organisms and a graptoloid fauna dominated by *P. leptotheca* and *C. gregarius*.

Concretion: CM 51.2-51.3b

Lithofacies: 4, coarsely laminated, clay/organic-poor
Graptoloid distribution: random (χ^2/n= 1.40)
Taphofacies: random flux of graptoloids and sediment

This concretion was collected 1.2 m away from CM 51.2-51.3a at the same stratigraphic level. This very fine-grained carbonate concretion comprises three thick laminae (Figure 4.37B). Lamina 0-44 is medium brown with irregular shaped light brown patches (1-2 mm) and radiolarian molds (circular in cross-section). A buff-coloured wedge, parallel to bedding that is 4 mm thick at its greatest height extends across ½ of the slab surface at layer 35. Six nautiloids and 2 bivalves are seen in cross-section in layer 0-44. Layer 44-54 is brown with rare radiolarian molds. The top and basal contact is gradational. Layer 54-80 is similar to layer 0-44. Crystal size of layers 0-44 and 54-80 (Figure 4.37C, D; lamina 1 and 3) ranges in size from 40 to 180 μm. Layer 44-54 (lamina 2 in Figure 4.37 C, D) has a smaller crystal size (20 to 70 μm) and more matrix. Nautiloids are observed in cross-section in all three laminae of the thin section.

Graptoloid rhabdosomes on the 10 dissolution surfaces are randomly distributed (Figure 4.37A). Similar to CM 51.2-51.3A, there is a decrease in graptoloid abundance following the centimeter thick fine-grained carbonate lamina at layer 44-54. This was not statistically significant in CM 51.2-51.3b. Qualitative analysis of the species distribution through the dissolution residues does not support an up-concretion decrease in graptoloids. Total counts of thecae/mm and siculae/mm were relatively uniform throughout the concretion. Similar to CM 51.2-51.3A, the basal residues were dominated by *Normalograptus nikolayevi*.

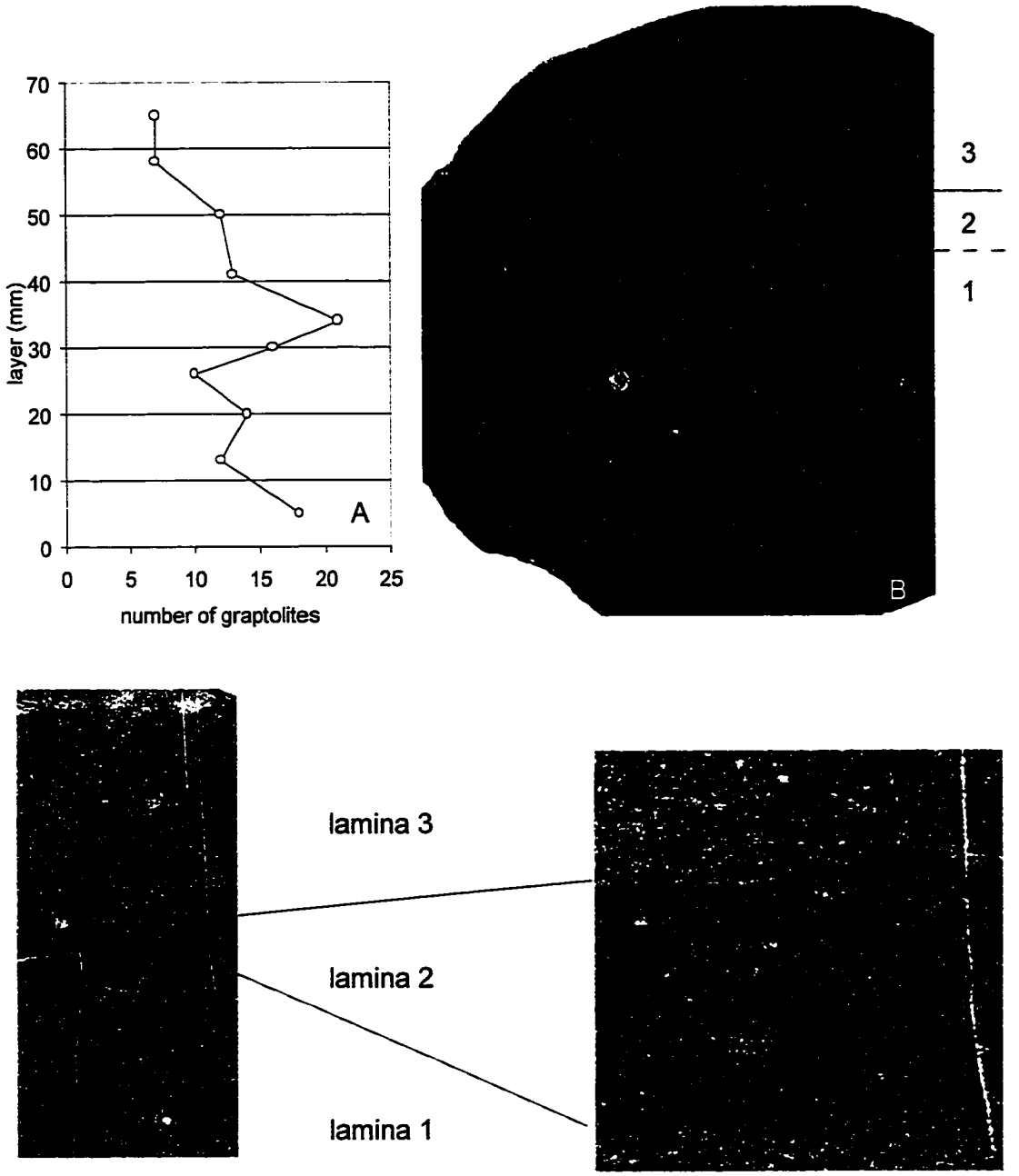

Figure 4.37. Concretion CM 51.2-51.3B. This concretion was sampled 1.2 m. from 51.2-51.2A and shows a similar internal stratigraphy. A. Distribution of graptolite rhabdosomes vertically through the concretion as revealed during the layer-by-layer dissolution. B. Digital scan of polished slab aligned with dissolution layers. Actual size. C. Digital scan of thin section showing three defined laminae and a cross-section of some nautiloids. Actual size. D. Laminae are defined by the size of the carbonate crystal and percentage of matrix/micrite. Magnification x4.

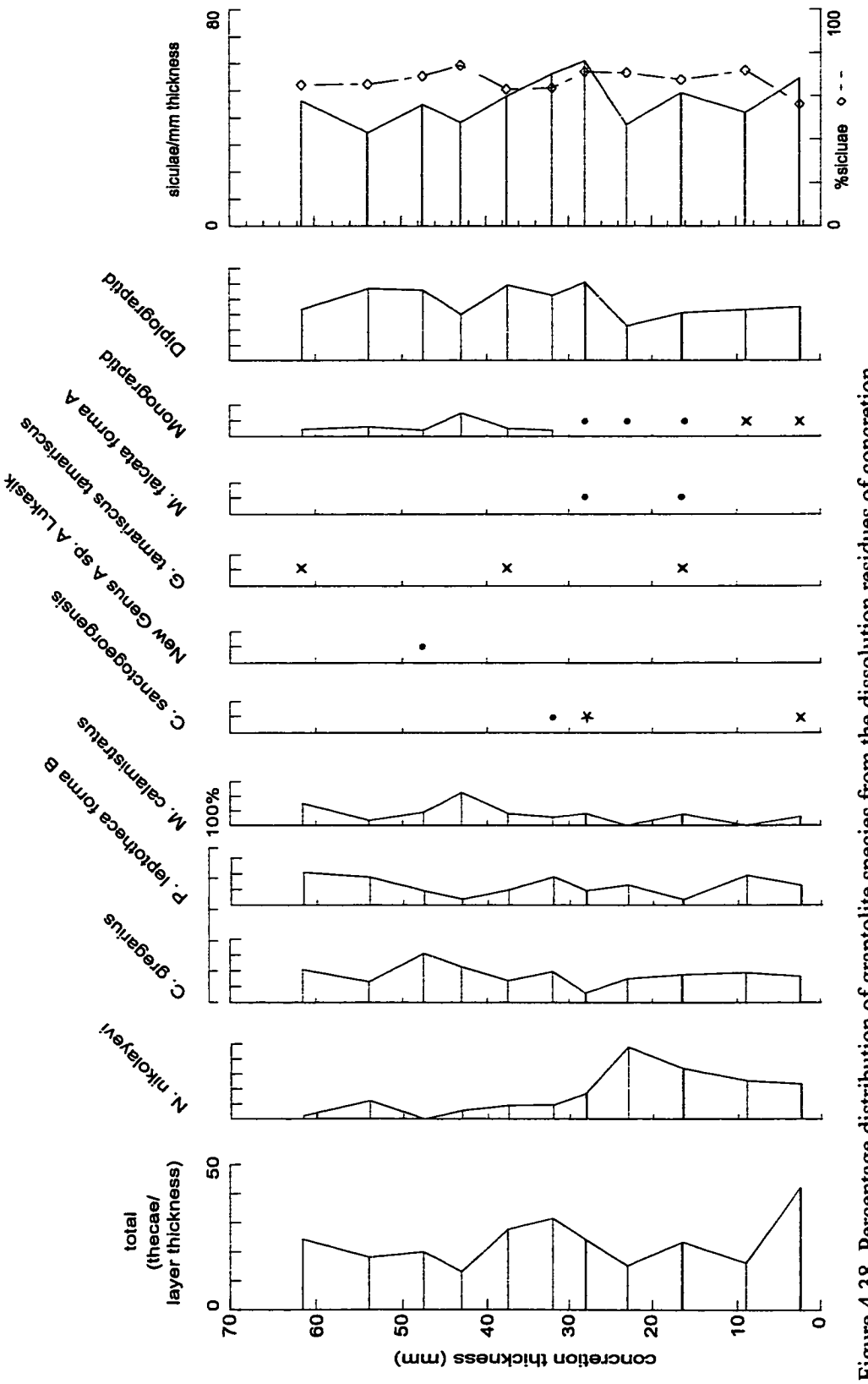

Figure 4.38. Percentage distribution of graptolite species from the dissolution residues of concretion CM 51.2-51.3B * 5-10%, × 1-5%, • < 1%

This concretion samples most of "lamina 1" from CM 51.2-51.3A and CM 51.2-51.3B. Although a subtle shift in the graptoloid assemblage is recognized by the decreasing *N. nikolayevi*, a change in graptoloid abundance or preservation is not observed. This concretion is therefore considered to be an example of the random flux of graptoloids and sediment taphofacies. If more of the "lamina 3" had been included in the concretion and sampled during dissolution we may have seen the change in graptoloid concentration that aided in the determination of the taphofacies classification of CM 51.2-51.3 A of physical transport/addition of graptoloids.

Concretion: CM 52.1-52.2

Lithofacies: 5, finely laminated, clay/organic-rich
Graptoloid distribution: non-random (χ^2/n= 1.82)
Taphofacies: graptoloid bloom
Paleoecological event: dominance of *Metaclimacograptus orientalis*

The polished slab of this carbonate concretion shows faint bedding, visible as lighter and darker brown, irregular and discontinuous, thick laminae. Light brown layers that average 0.8 cm in thickness are in gradational contact with greyish-brown layers that average 1.5 cm in thickness. A bitumen-rich diagenetic core was observed during dissolution on layers 32-42 and can also be observed in the polished slab. Prior to this diagenetic alteration the laminae were most likely clearly defined with sharp contacts, and the laminae were most probably continuous across a 15 cm bedding plane (the width of the concretion). For this reason the microlithofacies classification is considered finely laminated, clay/organic-rich. No thin section was cut for this sample.

Unlike most of the concretions in the dissolution study, CM 52.1-52.2 was dissolved from the top down. The layer numbers, therefore decrease up stratigraphy. The null hypothesis of random distribution is not supported with the data from the 13 dissolution layers. There is a slight abundance of graptoloid rhabdosomes at the centre of the concretion (layers 35, 39) and at the top (layers 2 and 5). After correction for the core the mid-concretion abundance of graptoloids is further emphasized. It appears as if these two enriched zones correspond to the darker laminae observed on the polished slab.

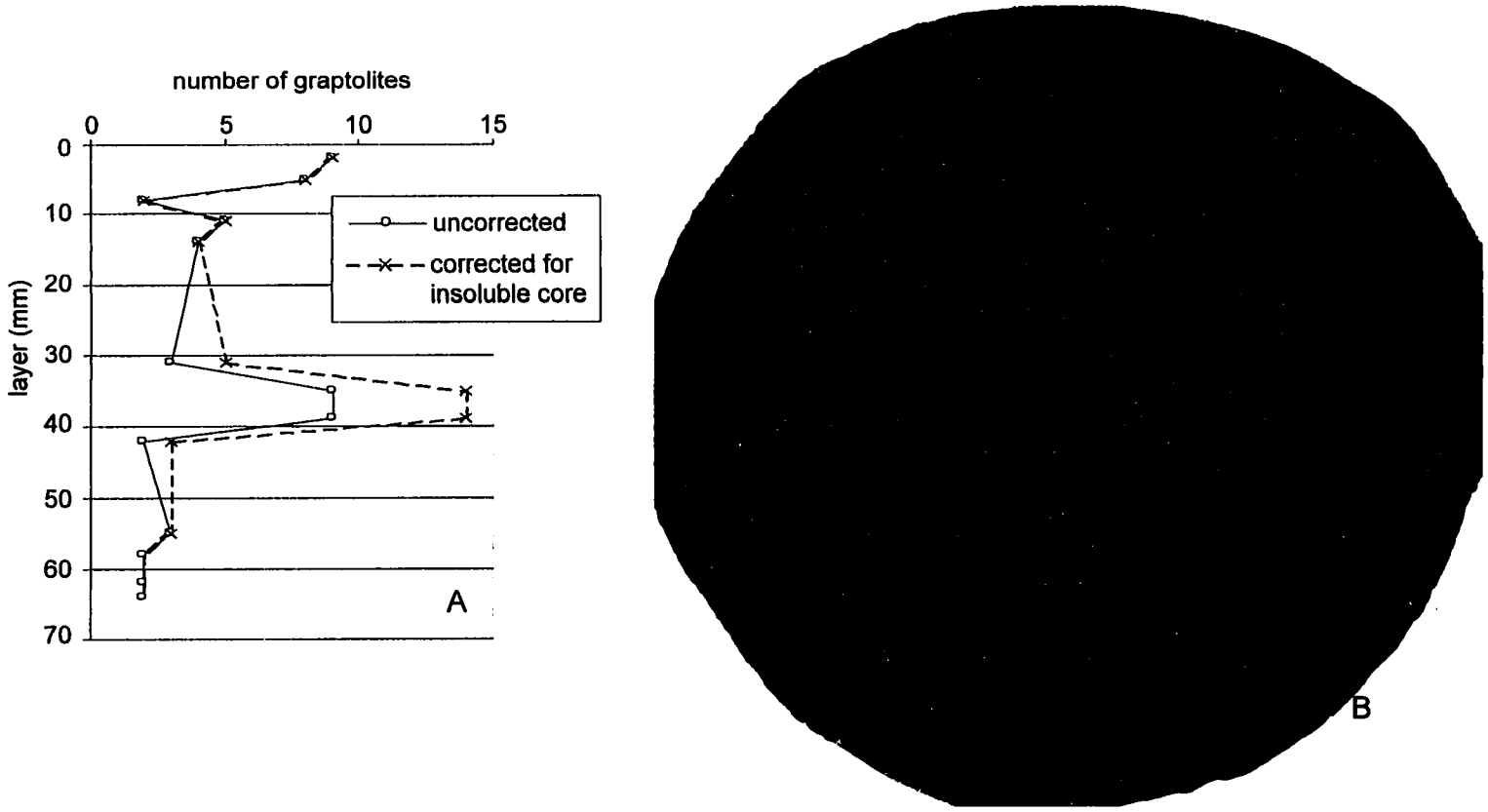

Figure 4.39. Concretion CM 52.1-52.2. A. Vertical distribution of graptolite rhabdosomes as recorded during the layer-by layer dissolution of the concretion and corrected for the presence of an insoluble core. With or without correction graptolties were observed to be concentrated on layers 42 and 46. B. This increase in graptolites corresponds to a portion of a dark brown lamina observed in the digital scan of the polished slab. Actual size.

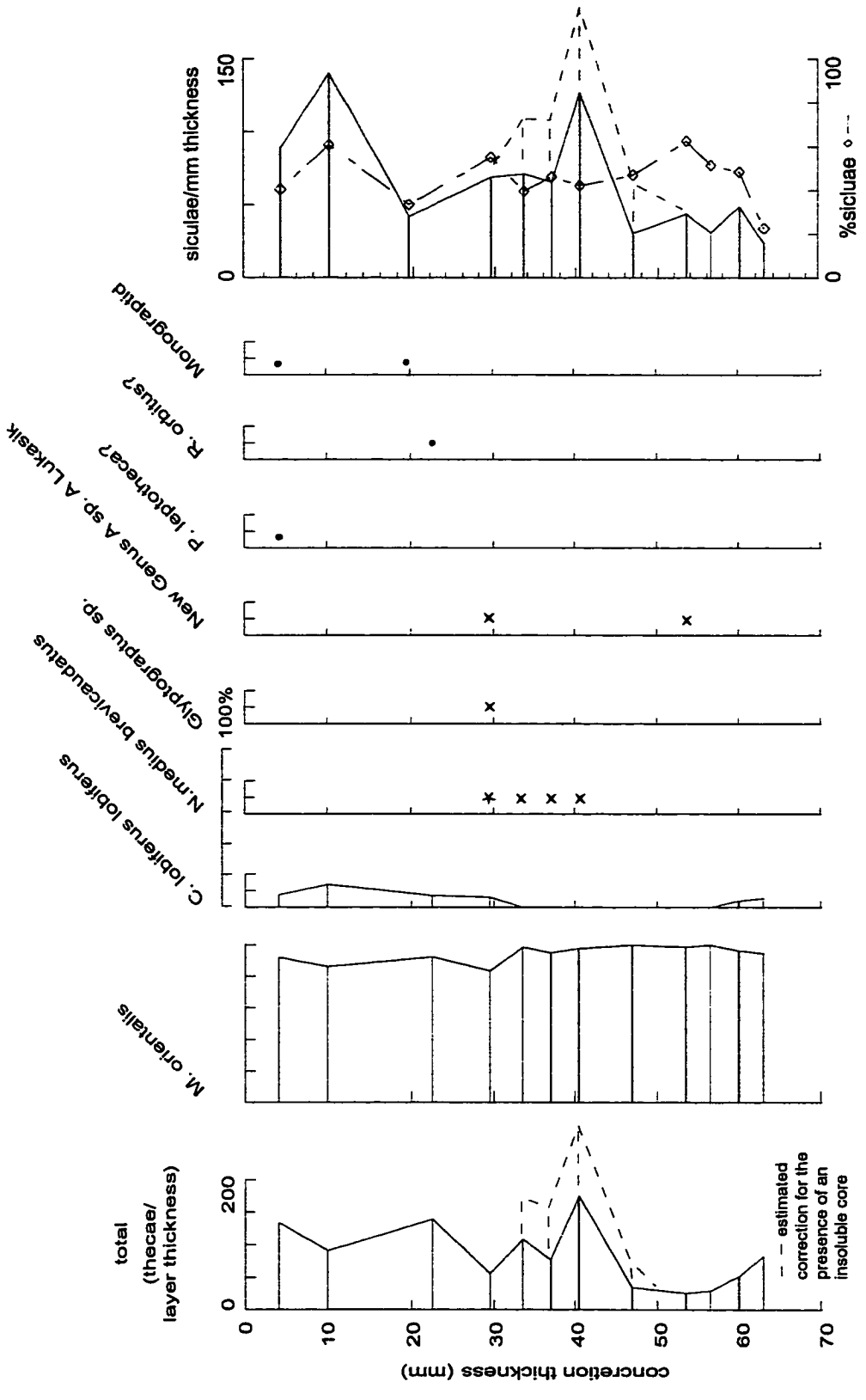

Figure 4.40. Percentage distribution of graptolite species from the dissolution residues of concretion CM 52.1-52.2; * 5-10%, x 1-5%, • < 1%

Nautiloids were found on dissolution layers 2, 5, 11, 62, and 64. Layer 31 contained a brachiopod and layer 35 contained the imprint of a brachiopod. Layer 62 contained a mid-conispiral gastropod and a sponge spicule mass was found on layer 64.

The graptoloid assemblage as assessed from the residues is dominated by *Metaclimacograptus orientalis* (Figure 4.40; average relative abundance = 94.6%). *Campograptus lobiferus lobiferus* is secondarily predominant in the top residues. *Normalograptus medius brevicaudatus* is of secondary dominance in the mid-concretion residues 27-42 and barren throughout the rest of the concretion. These two species may represent events of deposition that vary from the normal background deposition of *M. orientalis*. The total thecal count per layer thickness shows a slight increase in the 39–42 residue. This abundance is also observed in the counts of siculae. Sicular counts track the total thecal counts but diverge from the thecal pattern at the top and base of the concretion. Percentage of siculae was high (60%) in residue 8-12 and low (23%) in the basal residue 62-64. With the cryptic sedimentology of this concretion and no evidence of graptoloid orientation or fragmentation it is difficult to determine the process of siculae dilution or concentration. These two residues could be the result of paleoecological or biostratinomic processes.

With no evidence of biostratinomic alteration of this graptoloid assemblage I classify the concentration of graptoloids on layers 35 and 39 as a graptoloid bloom. *Metaclimacograptus orientalis* dominates the assemblage from all residues including the mid-concretion abundance. The whole 65-millimeter sample from concretion CM 52.1-52.2 could be considered a bloom of *M. orientalis*, which in the other concretions is not dominant.

Concretion: CM 53.2-53.3

Lithofacies: 1, structureless, clay/organic-rich

Graptoloid distribution: non-random ($\chi^2/n = 2.11$)

Taphofacies: graptoloid blooms

Paleoecological events: two graptoloid blooms; *Monograptus falcata* forma A followed by *Monograptus* n. sp. C

This grey-brown, very fine-grained, carbonate concretion contains light brown oval grains (less than 1 mm), dark brown discontinuous stylolites, and one continuous, buff-coloured lamina at layer 8-10 mm (Figure 4.41B). A continuous dark stylolite is visible at layer 35. The dark concretion contains a few faint, thin (2 mm thickness) continuous laminae that are light brown. Light laminae less than 1 mm in thickness are discontinuous. These light brown continuous and discontinuous laminae are difficult to see in polished slab and rare in thin section.

In thin section, the concretionary carbonate crystal size range is 10 – 40 μm and the average is 20 μm (Figure 4.41C-E). The dark greyish-brown laminae contain dark brown grains that are 10 to 20 μm in size, dark brown intercrystalline patches that are 10 to 50 μm in diameter, and a greyish-brown very-fine-grained matrix. The brown grains and patches represent 2 % of the lamina. Light laminae are differentiated from the dark laminae by containing fewer of the dark patches or grains (< 1%) and a grey coloured matrix. Carbonate concretion crystal size is constant through the concretion.

Even with the rhabdosome dissolution counts corrected for the presence of an insoluble core, the null hypothesis of random distribution of graptoloid rhabdosomes cannot be supported. Graptoloids are concentrated on two layers: layer 47; 20 graptoloid rhabdosomes, 14 siculae; and layer 18, 15 counted graptoloid rhabdosomes, 12 siculae (Figure 4.41A). A large sponge spicule mass with the spicules oriented in the lattice was observed on layer 18. A second spicule mass was observed on layers 43 and 47. A bivalve with both valves present was observed in the core on layer 24. One fragmented mature "diplograptid" was observed on layer 43.

The association between the increase in the graptoloid rhabdosomes on layers 18 and 47 and the increase in sponge spicules may indicate a proximal shelf origin for both. The observations of sedimentary structures and lithology cannot support this hypothesis. Current indicators, such as graded bedding or cross bedding were absent from these graptoloid concentration beds. No change in lithology is recorded at these intervals. The association between the sponge spicules in lattice orientation and the graptoloid-rich layers may be coincidental. Spicules were observed on all layers of this concretion, and in other concretions lattice-oriented spicules are not associated with graptoloid concentrations.

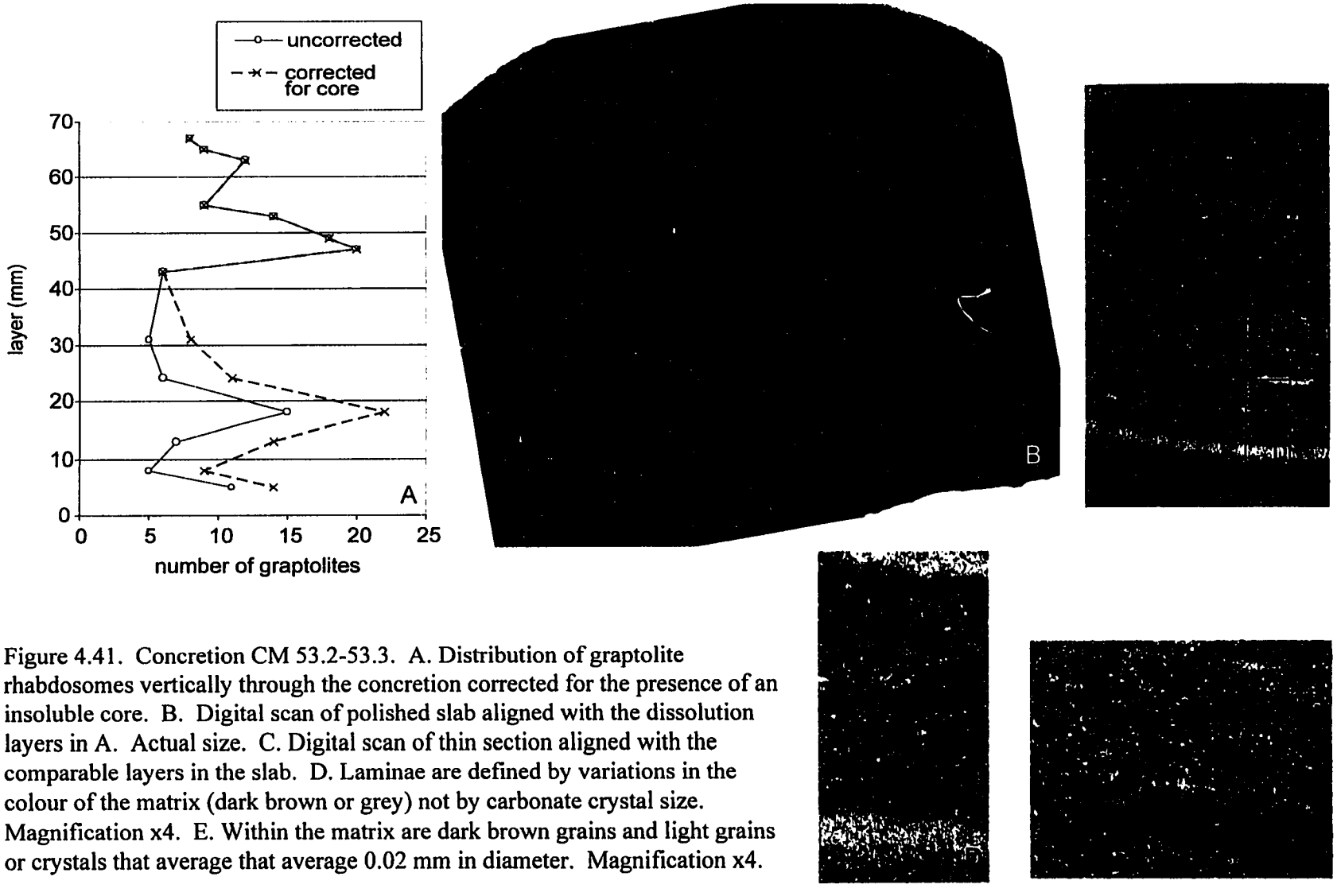

Figure 4.41. Concretion CM 53.2-53.3. A. Distribution of graptolite rhabdosomes vertically through the concretion corrected for the presence of an insoluble core. B. Digital scan of polished slab aligned with the dissolution layers in A. Actual size. C. Digital scan of thin section aligned with the comparable layers in the slab. D. Laminae are defined by variations in the colour of the matrix (dark brown or grey) not by carbonate crystal size. Magnification x4. E. Within the matrix are dark brown grains and light grains or crystals that average that average 0.02 mm in diameter. Magnification x4.

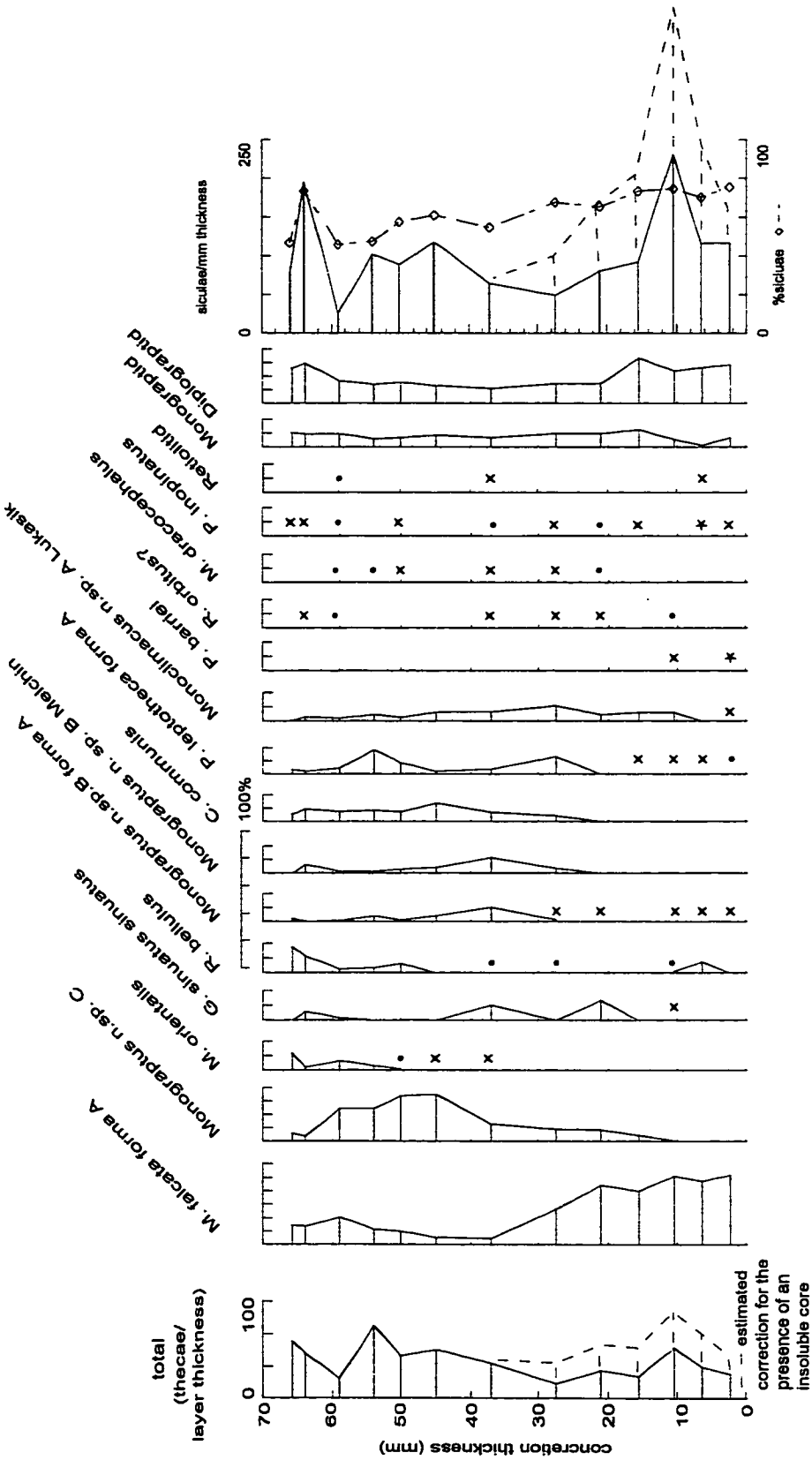

Figure 4.42. Percentage distribution of graptolite species from the dissolution residues of concretion CM 53.2-53.3: 5-10%, 1-5%, < 1%

The thecal counts identified a subtle faunal change at mid-concretion with the basal residues dominated by *Monograptus falcata* forma A and the top residues dominated by *Monograptus* n. sp. C. Therefore, the two layers identified as abundant in the layer-by-layer dissolution are composed of slightly different graptoloids; layer 18 is dominated by *M. falcata* forma A and layer 47 is dominated by *Monograptus* n. sp. C. Total thecal counts do not show a significant abundance in any one residue. This change in species composition is likely reflecting a change that occurred in the biocoenosis. A shift in dominance resulted in a brief (duration unknown) pulse of abundance for each of the two species.

The percentage of siculae/mm of the total thecae/mm counted from the residues decreases up-concretion from a maximum of 76% in the basal residue to 46% in the top residue. An exception to the general decrease is the abundance of siculae (195 siculae/mm; 74% of the total count) counted from residue 63-65. No unique sicular distributions match the two abundant dissolution surfaces 18 and 42. This supports the hypothesis that the concentrations are paleoecological and not the result of biostratinomic processes. I cannot confidently account for the general trend of up-concretion decrease in siculae counted per millimeter. I can suggest that it may also be the result of paleoecological processes. Perhaps *Monograptus* n.sp. C., which dominates the top half of the concretion, did not produce as many siculae during life.

Concretion: CM 54.0-54.15

Lithofacies: 1, structureless, clay/organic-rich
Graptoloid distribution: non-random (χ^2/n= 1.63)
Taphofacies: paleoecological bloom
Paleoecological event: bloom in *Metaclimacograptus orientalis*

This very fine-grained carbonate concretion is light to medium brown with thin, grey, continuous laminae 1-2 mm thick at 39 and 52 mm (Figure 4.43B). A white to buff-coloured lamina at 37 mm corresponds to a sponge spicule mass on the 37 mm dissolution surface. It is possible that the light grey colour of layers 39 and 52 are also reflecting an increase in the spicules and possibly resedimented proximal shelf material.

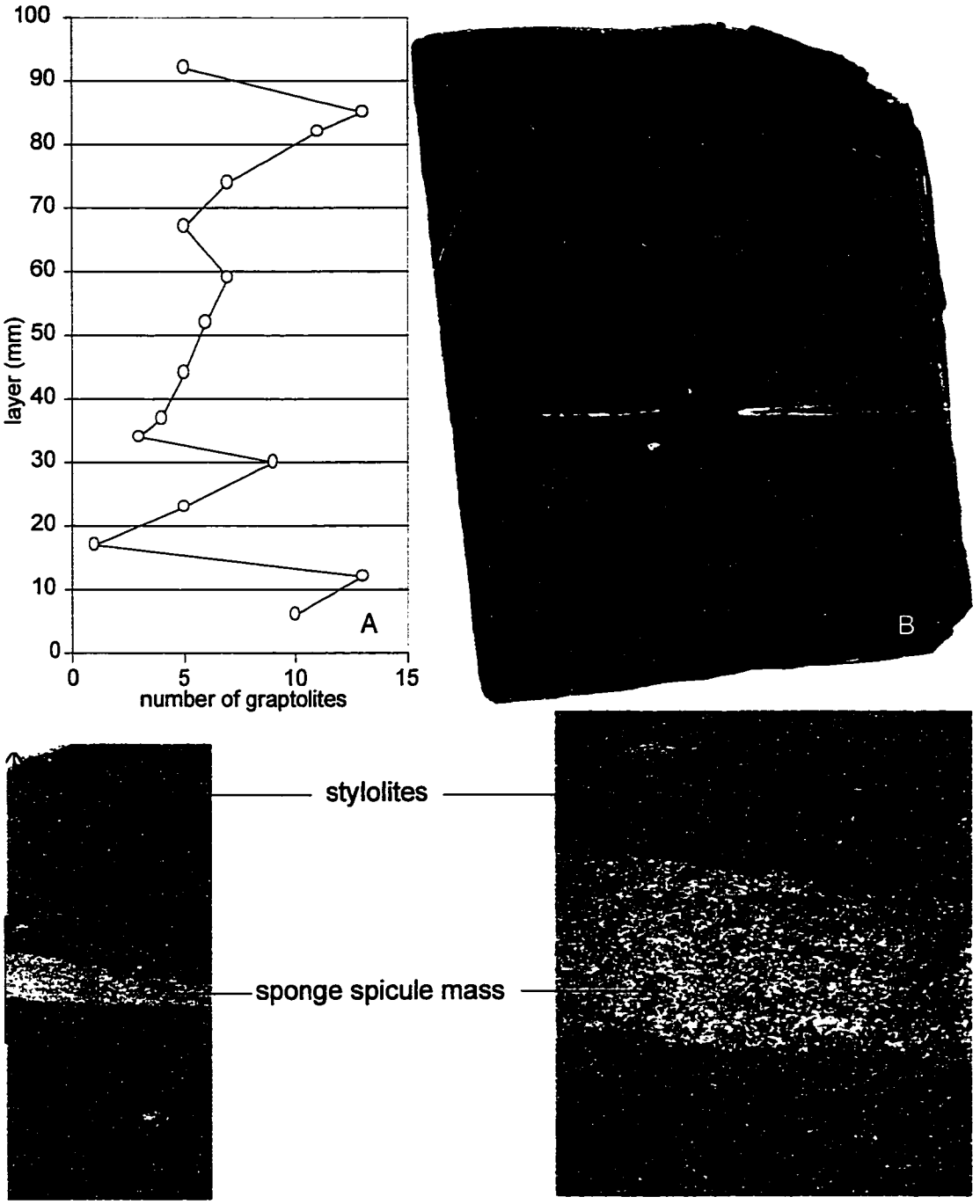

Figure 4.43. Concretion CM 54.0-54.15. A. Vertical distribution of graptolite rhabdosomes as observed on the dissolution layers. B. Digital scan of polished slab aligned with dissolution layers of A. A light discontinuous lamina near layer 40 is related to a sponge spicule mass that was revealed on this layer during dissolution. Actual size. C. Sponge spicule mass in thin-section. Actual size. D. Sponge spiclues are in-filled with bitumen/carbon and silica and surrounded by silica (remobilized?) and calcite cement. The sponge layer is in sharp contact with the layers above and below. Magnification x4.

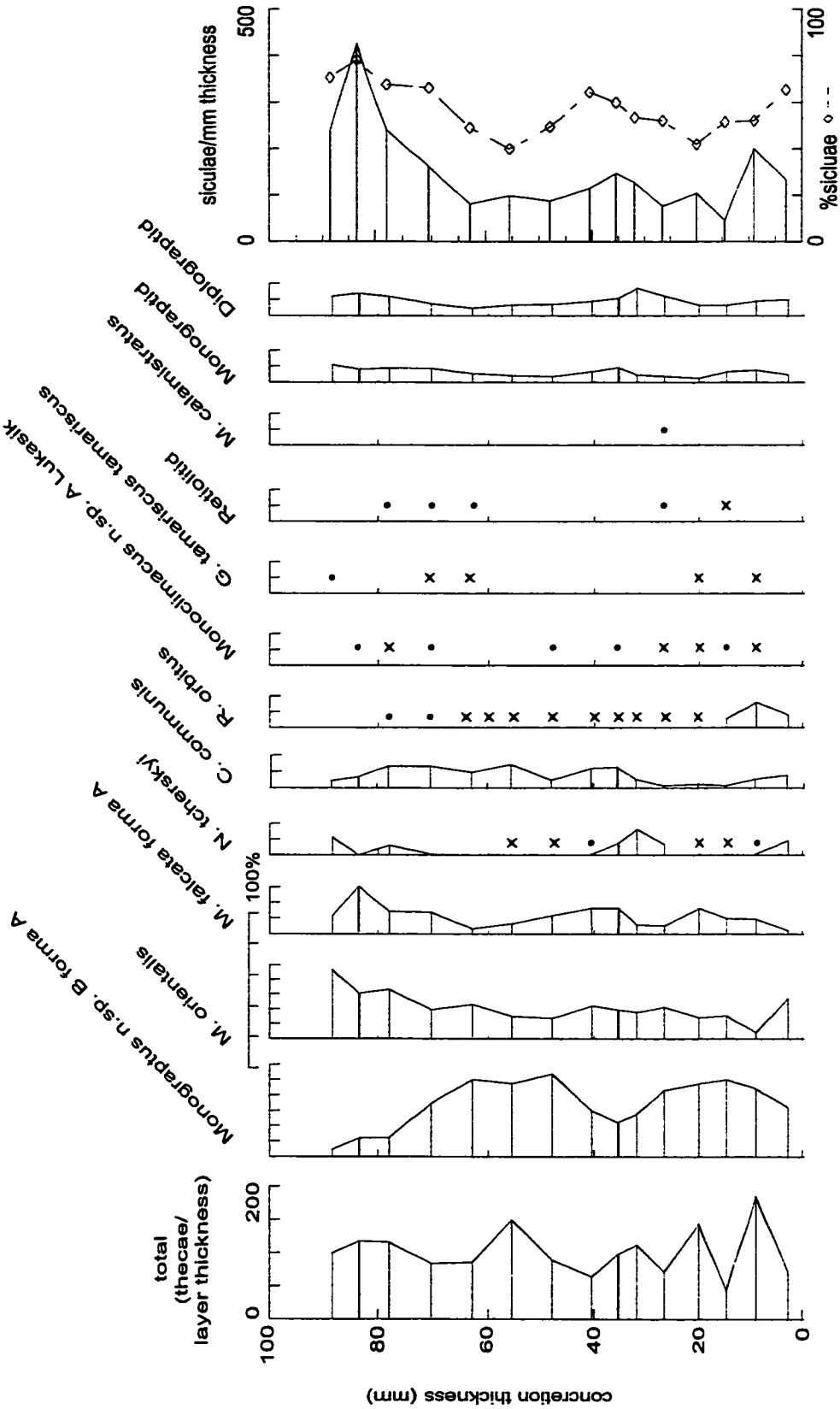

Figure 4.44. Percentage distribution of graptolite species from the dissolution residues of concretion CM 54.0-54.15: * 5-10%, × 1-5%, • < 1%

During dissolution, a large mass of spicules at layer 40 to layer 52 impeded dissolution and was cut away (and archived).

Within the sponge spicule mass, crystal sizes range from 40 to 300 μm and average 80 μm (Figure 4.43C, D). The basal contact of the sponge layer is sharp and possibly erosive although no clear scours were observed. The layers above and below this sponge layer consist of crystals that range in size from 20 to 80 μm with an average size of 40 μm. Two bedding-parallel stylolites are visible, but other than these and the sponge spicule mass there is little to define bedding. For this reason this concretion is placed in the structureless microlithofacies. The sponge spicule layer is a predominant feature of the concretion, but the overall character of this concretion is that of a structureless, fine-grained, organic/clay-rich carbonate.

The hypothesis of random distribution was supported at the 5% significance level, but not at the 10% significance level. Dissolution layers 12 and 85 had 13 graptoloids each. Layer 12 had 11 siculae. Layer 85 contained a fragmented mature "diplograptid" and 6 siculae. Fragmentation was not a result of the dissolution process. No corresponding lithologic evidence was observed to support bioturbation or transport as a mechanism of fragmentation.

The graptolite assemblage does not record a significant faunal change from base to top nor significant changes in total abundance. *Monograptus* n.sp. B forma A is the predominant graptoloid through most of the concretion but shows a decrease in dominance in the top four residues. *Metaclimcaograptus orientalis* and *Monograptus falcata* forma A are in greater abundance in these top samples. *Rastrites orbitus*, although in low abundance, decreases up-concretion. At the sponge spicule level (37 mm) the predominant species, *Monograptus* n.sp. B. forma A, slightly decreases and *Neodiplograptus tcherskyi*, and *Metaclimacograptus orientalis* slightly increase in abundance. Both of these species are present throughout the concretion and are not unique to this spicule layer. Therefore, the thecal counts do not identify layer 37 as an event horizon, even though the increase in sponge spicules at this layer suggests that this layer may have been transported. It is possible that these sponges settled out of the water column as debris and are not necessarily indicative of an event.

The counts of siculae reveal a distribution pattern different than the plot of total thecae/mm through the concretion. Siculae/mm counts increase in the top three residues. Residue 81-84 has a total of 427 siculae/mm, which represents 78% of the total thecae and sicular count, compared with the average for the concretion of 57%. This is associated with the shift in the graptolite assemblage from a predominance of *Monograptus* n. sp. B forma A to a predominance of *M. orientalis* and *M. falcata* forma A. At the lamina level of this change in the residues, an observed abundance of rhabdosomes was recorded on the dissolution surface layer 85 along with the fragmented rhabdosome. This abundance seems to be the result of a paleoecological bloom in *M. orientalis*, siculae of unknown taxonomy, and to a lesser extent in *M. falcata*. This is at the expense of *Monograptus* n.sp.B forma A. The fragmentation cannot be attributed to a biostratinomic process and may be necrolytic.

Concretion: CM 55

Lithofacies: 3, coarsely laminated, clay/organic-rich
Graptoloid distribution: non-random (χ^2/n= 5.68)
Taphofacies: sediment-starved, hiatus horizon

This very fine-grained, medium brownish grey, carbonate concretion does not appear to be laminated when examining only the polished slab (Figure 4.45B). However, three coarse laminae bounded by stylolites are observed in the thin section (Figure 4.45C). Thin section laminae can be accurately correlated to layers of the slab and dissolution layers. The three coarse laminae are labeled; Lamina 1 (layer 2-30 mm), 2 (layer 30-46 mm), and 3 (layer 46-70), with Lamina 1 the stratigraphically lowest. Lamina 1 and 3 are composed of carbonate crystals 20 to 100 μm in diameter (average = 50 μm), with rare bedding parallel rip-up clasts, all within a greyish brown matrix of indistinguishable grain-size. Approximately 5% of these two laminae are composed of white to light brown patches of more coarsely crystalline carbonate. The patches are elongate in the plane of bedding, and rarely circular, with an average length/diameter of 1mm. Dissolution reveals the "patches" to be nodules of insoluble material. These are possibly diagenetically altered radiolarian molds. Lamina 2 has a smaller carbonate

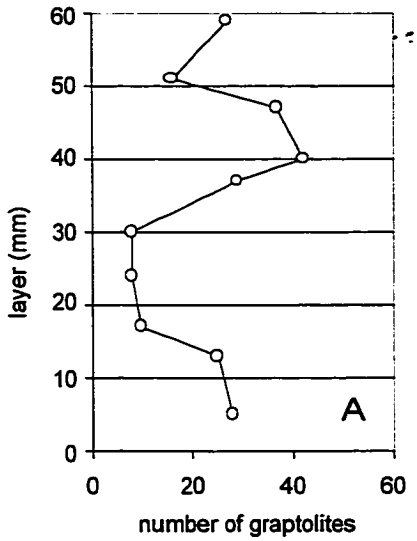

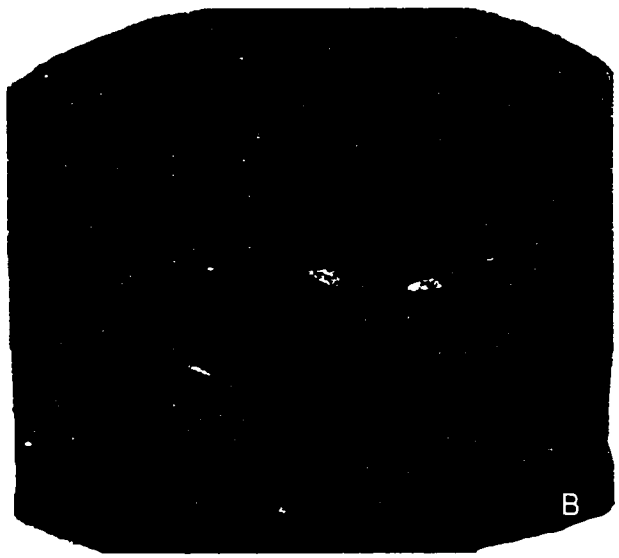

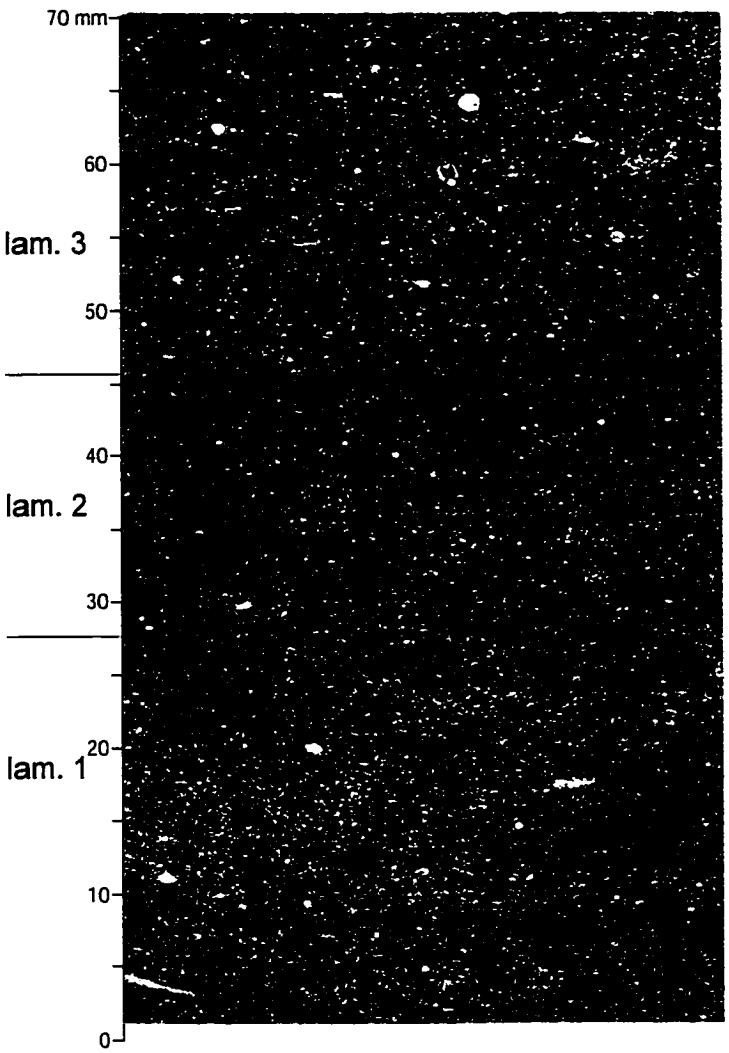

Figure 4.45 . Concretion CM 55. A. Distribution of graptolite rhabdosomes vertically through the concretion based on counts from the dissolution surfaces. B. Digital scan of polished slab. Coarse laminations are weakly present. Black bedding parallel stylolites, with calcite veins, and nautiloids in cross-section are observed on the slab. Actual size. C. Faint laminae are bounded by stylolites and defined by carbonate crystal size which is possibly reflecting original texture. Lamina 2 has an average crystal size of 0.03 mm and laminae 1 and 3 have an average crystal size of 0.05 mm and a more heterogeneous grain composition. Magnification x2.

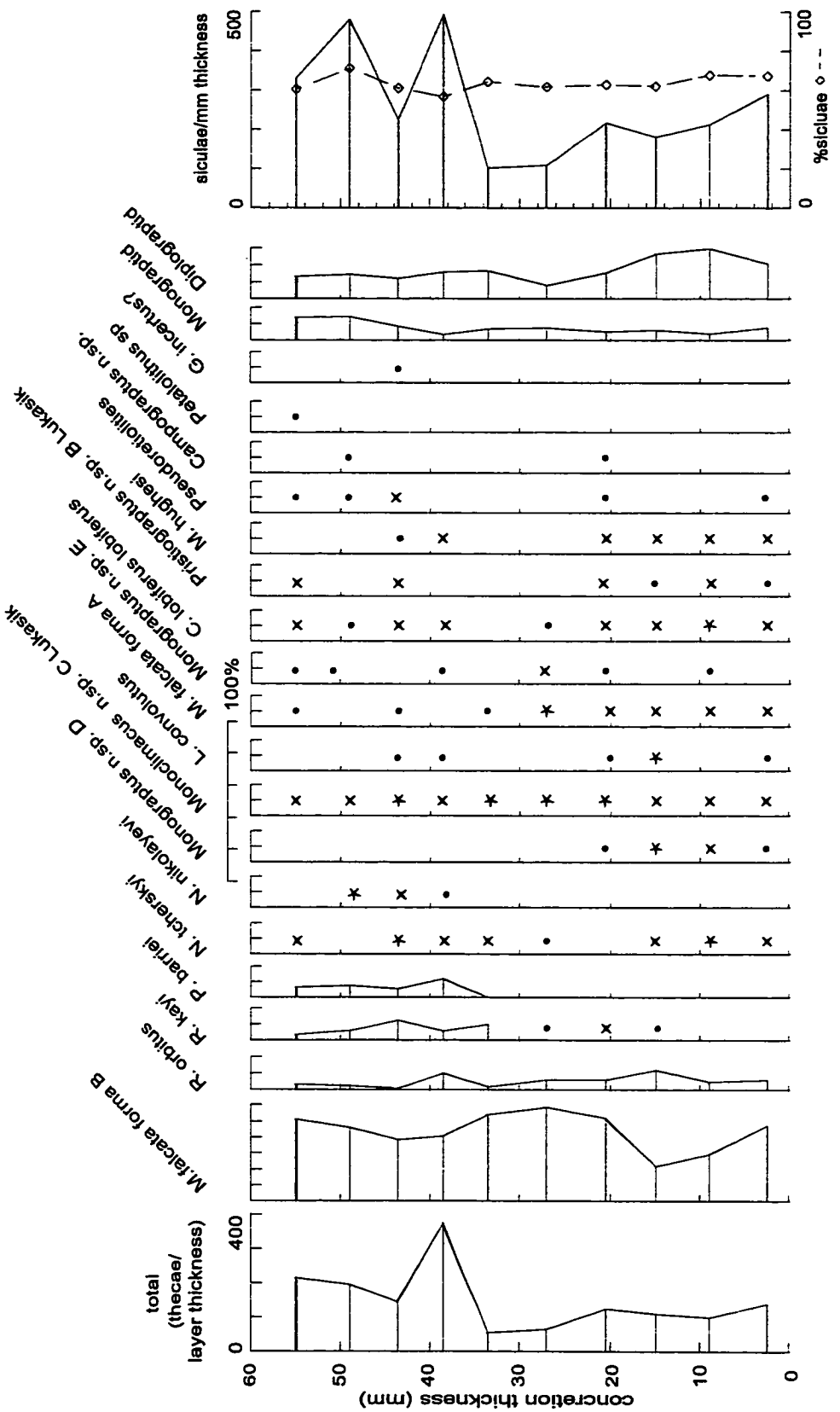

Figure 4.46. Percentage distribution of graptolite species from the dissolution residues of concretion CM 55: * 5-10%, × 1-5%, • < 1%

crystal size (10 to 80 μm; average = 30 μm) and perhaps because of the finer crystal size appears to contain more matrix. The light brown patches of coarser carbonate are rare in this lamina. The top of lamina 2 is bounded by bedding-parallel stylolite and the top is bounded by a discontinuous bedding-parallel stylolite. Where the stylolite is absent the basal contact of lamina 2 is gradational (over 3 mm) with lamina 1. Lamina 2 is correlated to an abundance of graptoloid rhabdosomes counted during layer-by-layer dissolution.

Graptoloid rhabdosomes are abundant throughout the concretion (total count of rhabdosomes from dissolution layers = 230, 10 layers) with two layers having a greater abundance than most (Figure 4.45A; layer 40; 42 rhabdosomes, and layer 47; 37 rhabdosomes). The increase in rhabdosome abundance at these two dissolution layers is characterized by an increase in all rhabdosome sizes.

The thecal counts reveal an increase in thecae/mm in residue 37-40. The assemblage in this residue as with the others in the concretion is dominated by *Monograptus falcata* forma B (Figure 4.46). The assemblage of residue 37-40 is diverse and comprises most of the species present through the rest of the concretion. It does not seem that this abundance in residue 37-40 can be attributed to the dominance and increased importance of a single species or group. The sicular counts are concomitant with the total thecal distribution through the residues. The siculae/mm counts are high in residues 37-40, 47-51,and 51-59; however, the percentage siculae of the total count is constant throughout the concretion at approximately 64%. Siculae were not biostratinomically winnowed, nor did biostratinomic or paleoecologic processes concentrate them.

This concretion is a good example of a sediment-starved graptoloid concentration. The sediment is more fine-grained with slightly increased matrix and organic carbon. The graptoloid taphocoenosis is unchanged in composition from the non-event layers through the concretion but is found to be statistically concentrated in a chi-square analysis.

Concretion: CM 56

Lithofacies: 1, structureless, clay/organic-rich

Graptoloid distribution: non-random ($\chi^2/n= 2.49$)

Taphofacies: random flux of graptoloids and sediment ?

This medium greyish-brown, very fine-grained, carbonate concretion contains small patches of lighter brown and thin pale brown, discontinuous laminae (Figure 4.47D). A dark brown to black rim 1 cm from the edge of the concretion is seen in the polished slab. Concretionary carbonate crystals range in size from 20 to 80 μm. Within the matrix are darker brown grains of possible biogenic origin and black cubic grains identified as disseminated pyrite (Figure 4.47A). The top of the concretion contains more of the inter-crystal/grain matrix although the crystal size remains constant. This is sampling the dark rim that was observed on the polished slab and during dissolution (Figure 4.47B).

Graptoloids were concentrated on layer 45 (Figure 4.47C; 18 rhabdosomes, average per layer is 8). A large insoluble core decreased the amount of surface area that was examined for graptoloid rhabdosomes by almost one half. If a correction is made for this (doubling the original count) layer 45 and layer 49 are seen to show a concentration of graptoloids (layer 45, 36 rhabdosomes; layer 49, 22 rhabdosomes; corrected average per layer, 12 rhabdosomes). No apparent relationship is observed between the increase in graptoloid rhabdosomes in the top layers examined and a change in lithology in the polished slab or thin section.

The residue counts display an opposite trend in abundance. The mid-basal residues contain more thecae/mm and more siculae/mm. An abundance of total thecae is observed in residue 12-16. Residues above layer 27 have a low thecal and sicular abundance. Peak abundance is not recognized from residues that include layer 45 or 49, the abundant layers from the dissolution process. Distributions of siculae and total thecae counts have a similar profile with siculae increasing slightly up-concretion relative to total thecae.

The graptoloid assemblage records a subtle change in composition from the base of the concretion to the top. The basal residues are dominated by *Monograptus falcata* forma C, whereas this species is rare in the top residues. The opposite profile of

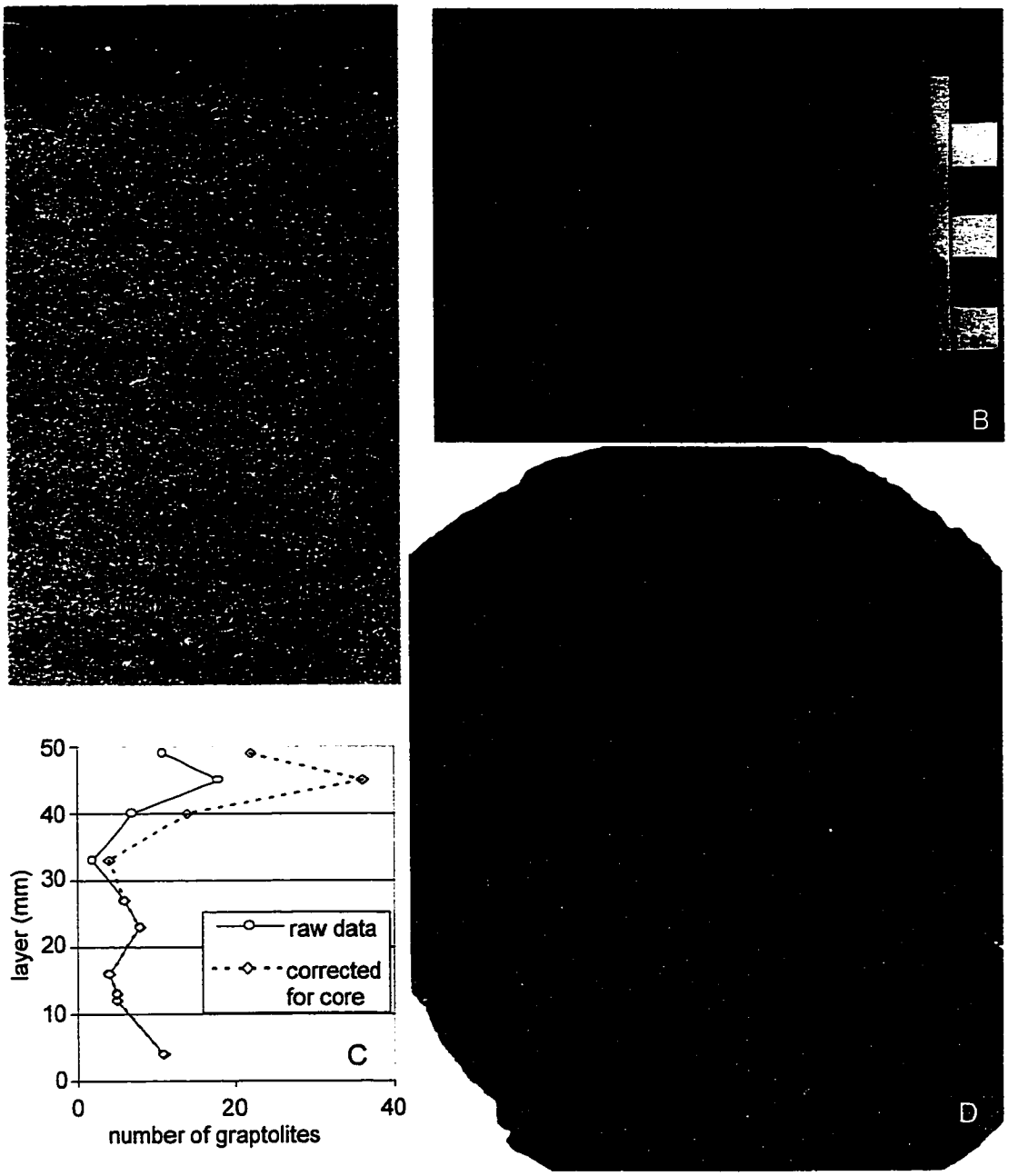

Figure 4.47. Concretion CM 56. A. Digital scan of thin section that samples the rim (top of thin section). Laminae are poorly defined. There is no evidence of bioturbation that may have disrupted a previous lamination. Bedding is defined by the brown grains flattened in the plane of bedding. Magnification x1.5. B. Photo of dissolution surface 33. The core is lighter brown in colour than the concretionary material and displays a zonation in colour and texture. C. Distribution of graptolite rhabdosomes vertically through the concretion corrected for the presence of an insolulble core. D. Digital scan of polished slab aligned with dissolution layers. Laminae are vague and discontinuous. A diagenetic rim is visible as a dark brown ring around the slab. Actual size.

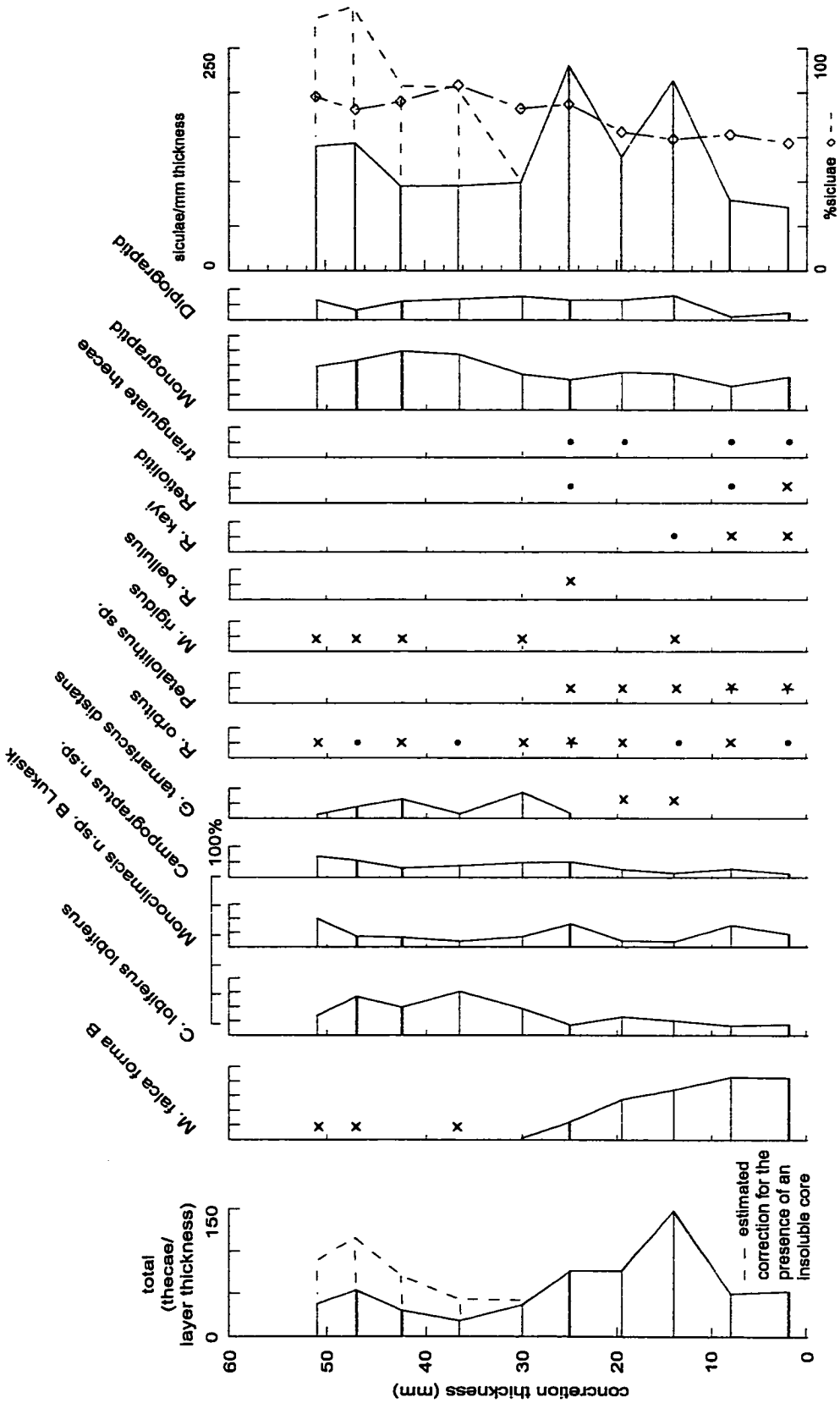

Figure 4.48. Percentage distribution of graptolite species from the dissolution residues of concretion CM 56; * 5-10%, x 1-5%, • < 1%

abundance is seen with *Campograptus lobiferus lobiferus*, which is the predominant species at the top of the concretion.

The poor preservation of the sedimentary structures, the difficulty of observing graptoloid rhabdosomes on the dissolution surfaces with insoluble cores and rims, and the discrepancy between the dissolution surface counts and the residue counts make it difficult to assign a taphofacies to this concretion. For now it is placed in the "catch-all" taphofacies of random flux of graptoloids and sediment.

Concretion: CM 56.4 - 56.5

Lithofacies: 1, structureless, clay/organic-rich
Graptoloid distribution: random ($\chi^2/n= 1.2$)
Taphofacies: random flux of graptoloids and sediment
Paleoecological event: Inter-grading of two graptoloid faunas.

This very fine-grained, medium greyish-brown carbonate concretion is weakly laminated (Figure 4.49B). Laminae are discontinuous and basal and top contacts are gradational. Diagenetic precipitates appear as lighter patches approximately 1 mm in diameter. In thin section, the texture is seen in cross-polarized light as interlocking carbonate crystals ranging in size from 20 to 100 μm and averaging 40 μm in diameter. Laminae are poorly defined in the thin section. One light brown discontinuous layer less than 0.3 cm thick, contains less of the brown matrix but the carbonate "grain" size is the same as the texture throughout the thin section.

The distribution of graptoloids among the 14 layers does not support the null hypothesis of random distribution (Figure 4.49C). Corrected for the presence of an insoluble rim, which on surface 54 covers approximately 40% of the surface and impedes the rhabdosome counts, the null hypothesis of random distribution is accepted. I believe this is a more accurate representation of the vertical graptoloid distribution. This correction de-emphasizes the weight a chi-square test places on less abundant layers, such as layer 54. Graptoloid rhabdosomes were slightly concentrated on layer 77 (36 graptoloids; average number per layer prior to correction was 19; average number of graptoloids per layer with following correction was 21). This layer has 81% siculae,

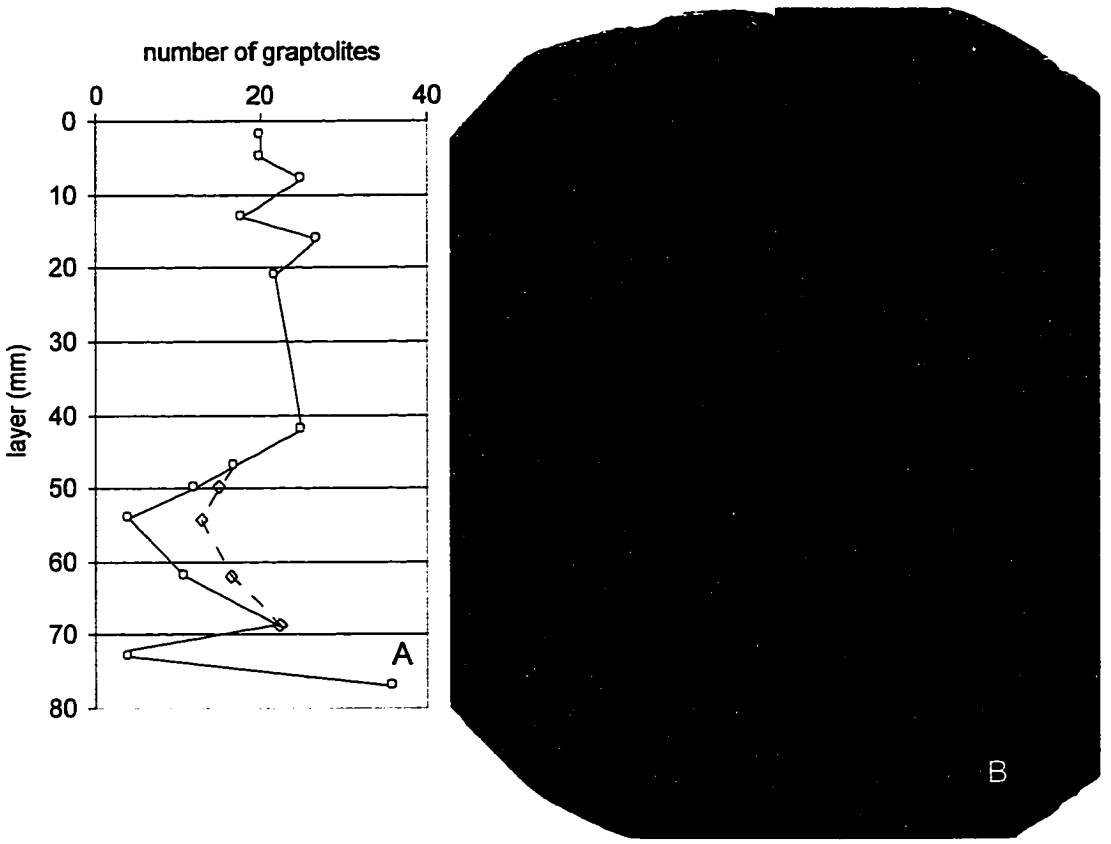

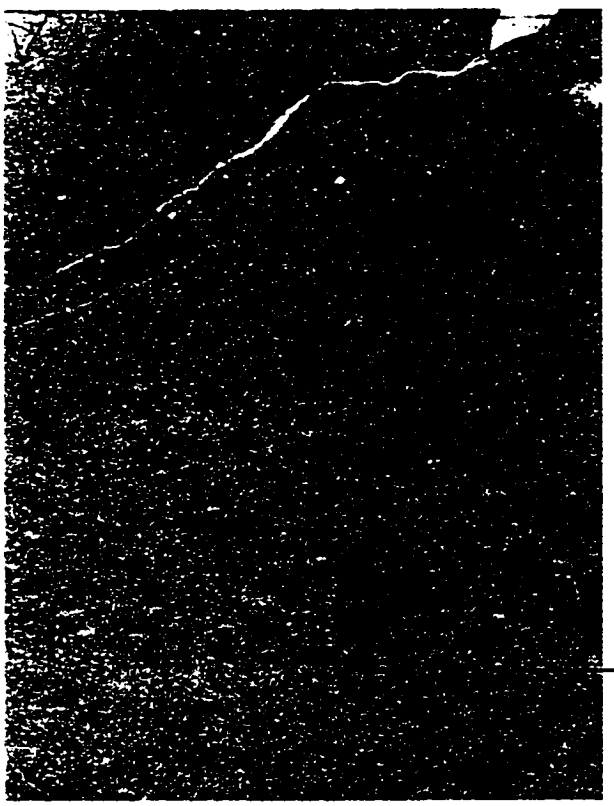

Figure 4.49. Concretion CM 56.4-56.5. A. Vertical distribution of graptolite rhabdosomes as counted from the dissolution surfaces. B. Digital scan of polished slab. Faint laminae are discontinuous and in gradational contact. A dark brown diagenetic rim is visible at the edge of the slab. Actual size. C. Digital scan of thin section. The interlocking carbonate fabric is composed of crystals that average 40 μm. One subtle lamina is visible as a layer with less brown matrix/micrite. Magnification x2.

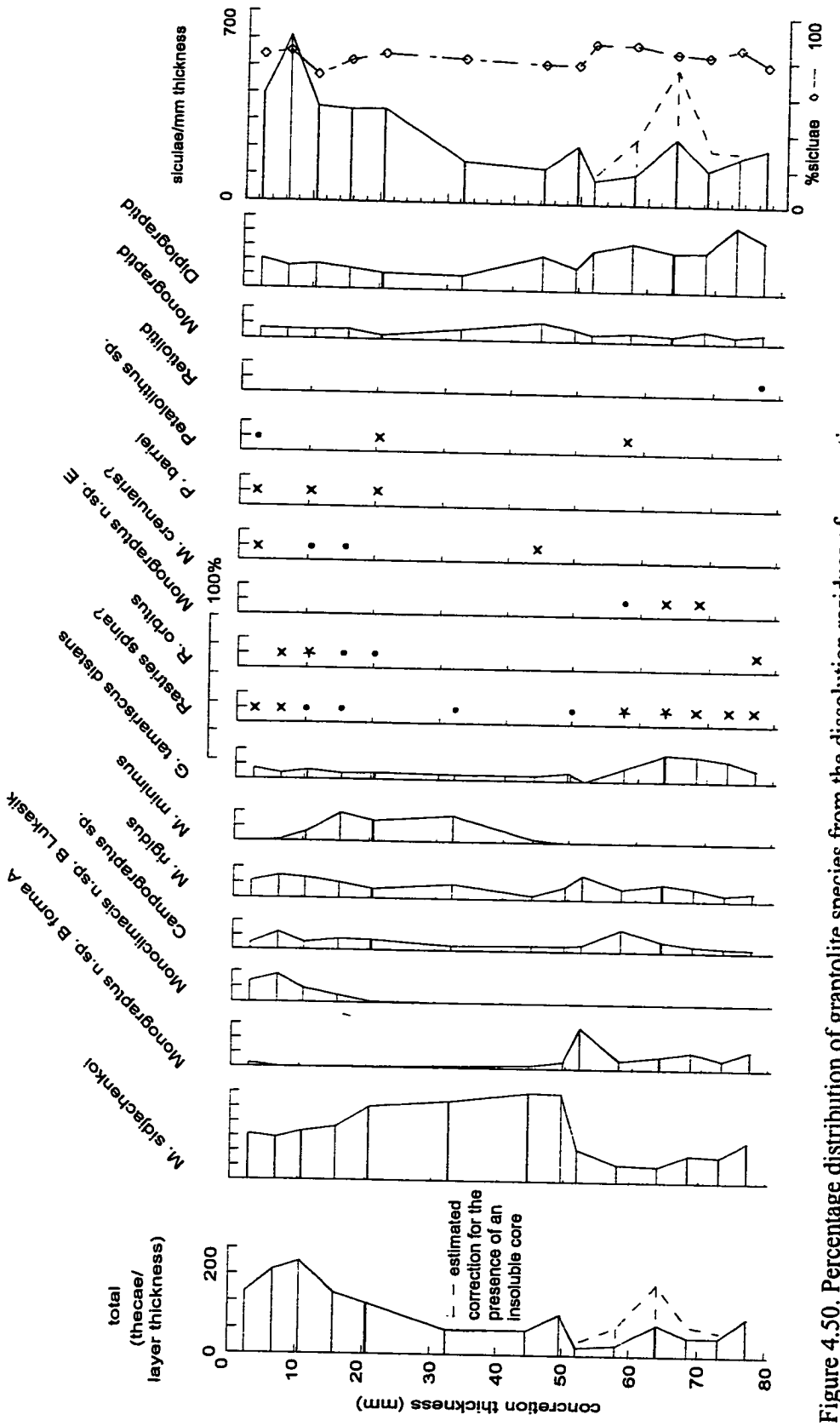

Figure 4.50. Percentage distribution of graptolite species from the dissolution residues of concretion CM 56.4-56.5: * 5-10%, x 1-5%, • < 1%

similar to the average percentage of siculae for the concretion of 77%. In the same layer two mature graptoloids are too fragmented to identify. It is likely that this fragmentation was the result of disturbances during the dissolution process, and not taphonomic. Layer 47 shows a subtle orientation of the elongate rhabdosomes.

Total thecal count is higher in the basal residues of the concretion (Figure 4.50). The sicular counts are concomitant with the thecal counts. The counts of siculae/mm in the residues are consistently approximately 77% of the total counts (siculae/mm and thecae/mm). This suggests that the siculae and thecae were arriving at the sediment in equal proportions through time without biostratinomic winnowing or concentration altering that proportion. The average percentage of siculae/mm among the total count and the average percentage of siculae of the rhabdosomes on the dissolution surface was the same (77%) even though one count is based on thecae and the other is based on total rhabdosomes.

The abundance of rhabdosomes at dissolution layer 77 is reflected in the residues as a minor increase in unidentifiable early growth stage "diplograptids". The residues before and after layer 77 are diverse without a major predominant species. Three graptoloid faunas seem to be represented in this concretion. A diverse basal fauna has some species not found in the middle or top residues such as *Pristiograptus* n. sp. B Lukasik and *Pseudoglyptograptus barriei.* The mid-residues are dominated by *Monograptus sidjachenkoi*, with rare *Metaclimacograptus minimus*. The top residues contain a fauna dominated by *M. sidjachenkoi, Monograptus* n. sp. B forma A, *Glyptograptus tamariscus distans*, and minor *Monograptus* n. sp. C, and *Monoclimacis* n. sp. C Lukasik. Two species are randomly distributed through the concretion: *Metaclimacograptus rigidus* and *Campograptus* sp. No lithologic change accompanies this shift in the graptoloid assemblage. These three faunas may represent three graptoloid communities that are intergrading in time or space or both.

Concretion: CM 57

Lithofacies: 3, coarsely laminated, clay/organic-rich
Graptoloid distribution: random ($\chi^2/n= 1.09$) – non-random in residues.
Taphofacies: physical addition of graptoloids – low energy event

There are two coarse laminae observed on the polished slab of this very fine-grained carbonate concretion (Figure 4.51B). Lamina 0-22 is greyish brown with small, buff-coloured patches 0.2- 0.5 mm in diameter and rare radiolarian molds that have solid boundaries as compared to the patches. There is a faint grading of colour from a lighter base to a darker top (less buff-coloured patches at the top). Above this layer is a light orange-brown coloured, discontinuous wedge up to 3 mm thick. The wedge extends most of the way across the slab. This bed has a sharp base and top and has been included in the basal unit of layer 22-68. During dissolution, this wedge was insoluble in the weak acid and was recorded as an insoluble core. Where this wedge layer is not present, layer 22 is still in sharp contact with the layer below. The boundary between layer 0-22 and 22-68 is sharp and irregular. Three nautiloids are visible in lamina 22-68, whereas only one nautiloid was visible in the basal lamina.

Thin section analysis of the concretion suggested an original texture of sub-rounded to angular (mostly angular) "grains" or crystals that range in size from 20 to 40 μm and are tightly packed together in a brown matrix (Figure 4.51 C-E). These are overprinted by a coarser texture (40 to 80 μm) of interlocking carbonate crystals that are identified in cross-polarized light. Dark brown to black stylolites that are parallel to bedding and branch across bedding are common. Internal, continuous microlaminae, not identified in the polished slab, were defined in thin section based on variations in the grain size. A darker lamina was defined by a finer grain size (Figure 4.51D). The light lamina that is identified in the polished slab as the 3 mm thick, light orange-brown wedge is also observed in the thin section (Figure 4.51E). The crystal size is similar to that described for the overprinted texture. This bed lacks the brown matrix and for this reason the identification of "grains" is not possible. Composition of this layer is an intergrowth of dolomite/carbonate and silica. The basal unit wedge is possibly a deposit of

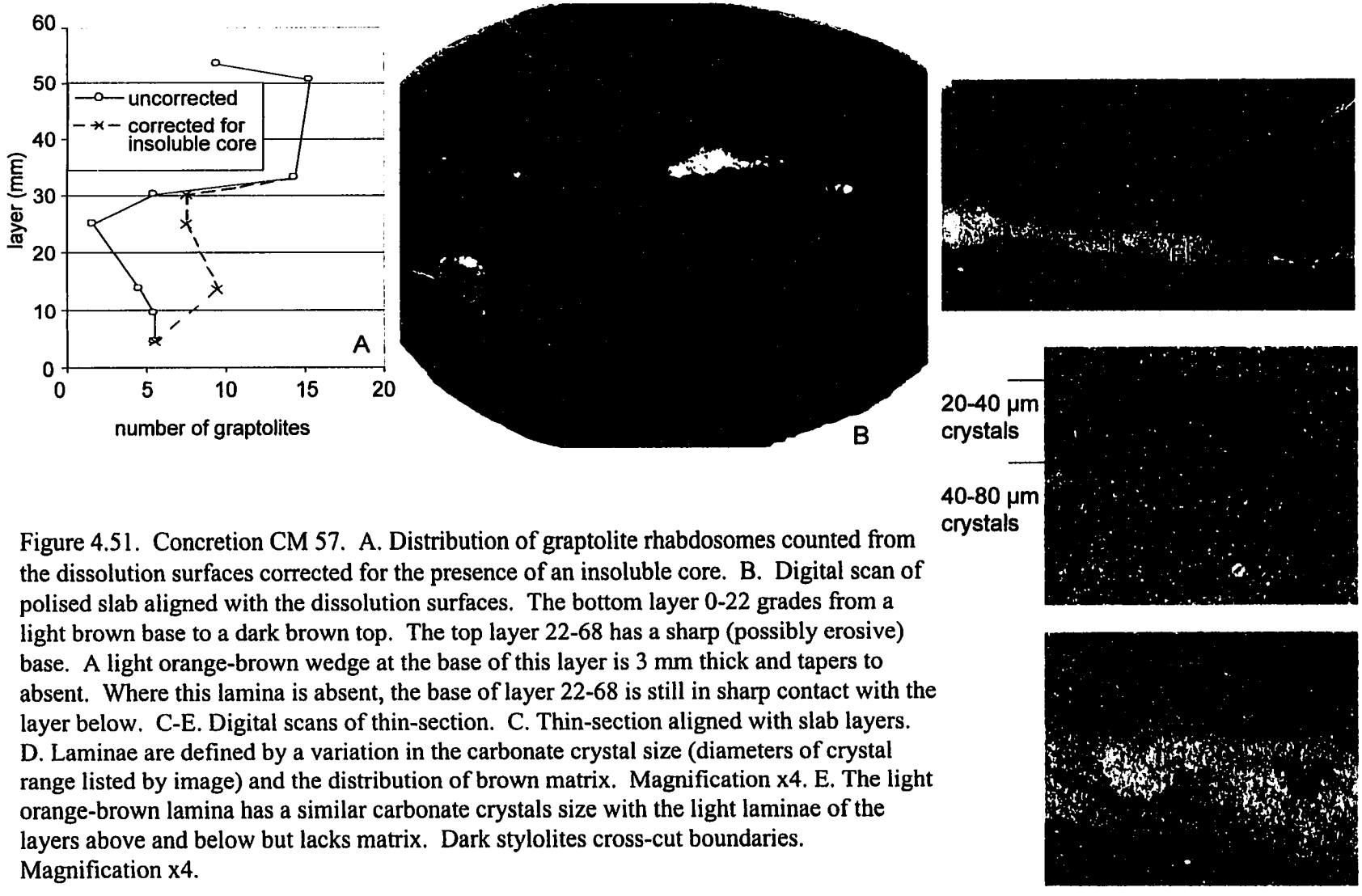

Figure 4.51. Concretion CM 57. A. Distribution of graptolite rhabdosomes counted from the dissolution surfaces corrected for the presence of an insoluble core. B. Digital scan of polised slab aligned with the dissolution surfaces. The bottom layer 0-22 grades from a light brown base to a dark brown top. The top layer 22-68 has a sharp (possibly erosive) base. A light orange-brown wedge at the base of this layer is 3 mm thick and tapers to absent. Where this lamina is absent, the base of layer 22-68 is still in sharp contact with the layer below. C-E. Digital scans of thin-section. C. Thin-section aligned with slab layers. D. Laminae are defined by a variation in the carbonate crystal size (diameters of crystal range listed by image) and the distribution of brown matrix. Magnification x4. E. The light orange-brown lamina has a similar carbonate crystals size with the light laminae of the layers above and below but lacks matrix. Dark stylolites cross-cut boundaries. Magnification x4.

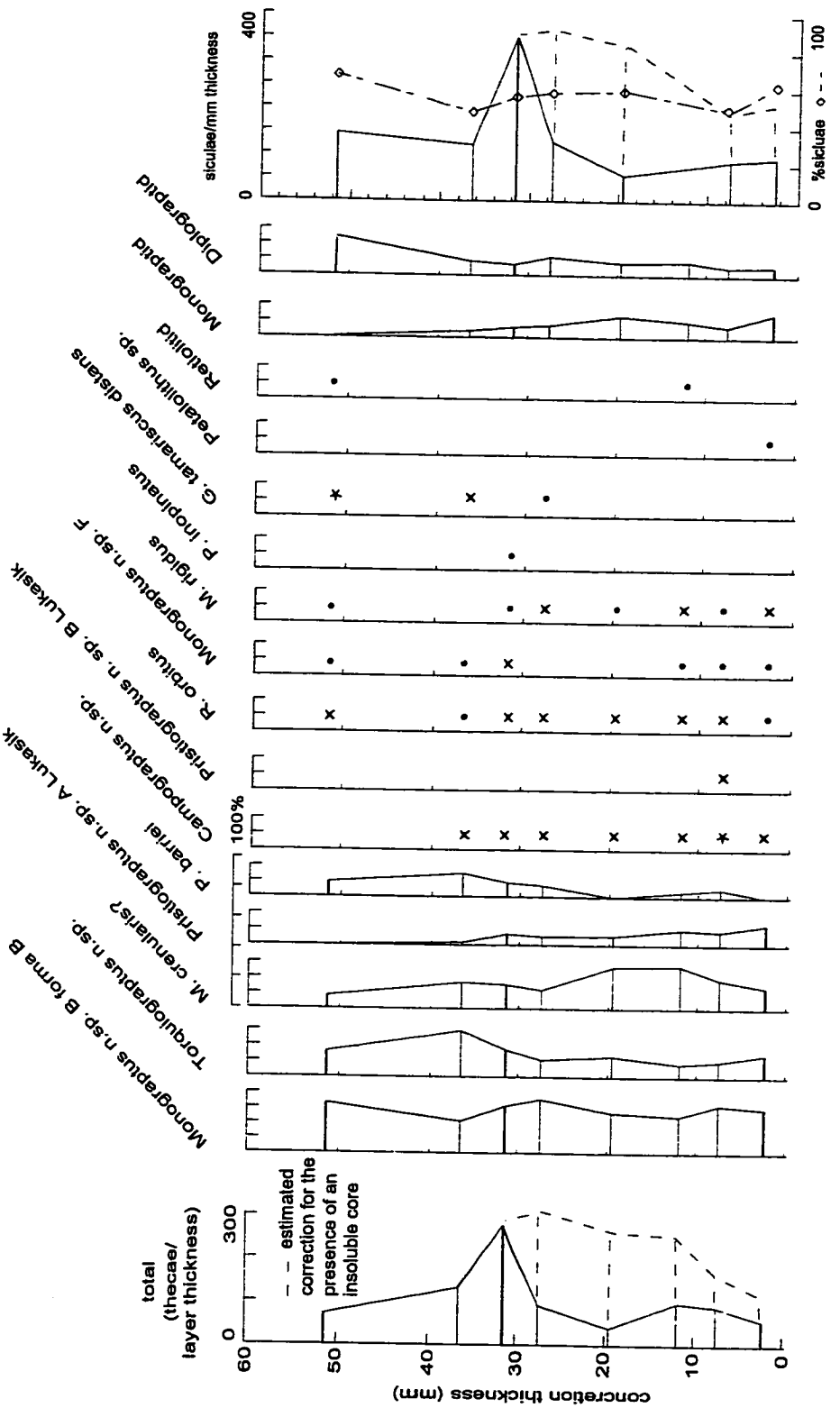

Figure 4.52. Percentage distribution of graptolite species from the dissolution residues of concretion CM 57; * 5-10%, × 1-5%, • < 1%

diagenetically altered sponge spicules, a biogenic source for the silica. A similar deposit with recognizable spicules is reported from concretion CM 54.0-54.15.

Graptoloids were found to be randomly distributed among the dissolution surfaces once the data had been corrected for the presence of the core (Figure 4.51A). The core obstructed the view of the dissolution surface and lowered the count possible from the surfaces in which it was present. The graph of distribution of rhabdosomes among the dissolution surface plots both data sets; corrected and uncorrected (Figure 4.51A).

Arandom distribution of graptoloid thecae was not observed in the dissolution residues (Figure 4.52). Peak abundance was found in residue 30-33. Like the other residues of this concretion, this sample was dominated by *Monograptus* n.sp. B forma B, *Torquigraptus* n.sp. A, and *Monograptus crenularis*?. There appear to be no trends in species distribution vertically through the concretion. Only a subtle faunal shift was observed between the two coarse layers identified on the polished slab. The basal layer (0-23) contains more *M. crenularis*? and *Pristiograptus* n.sp. A Lukasik than the top layer, whichcontains more *Torquigraptus* n.sp. A and *Pseudoglyptograptus barriei*. The predominant species *Monograptus* n.sp.B forma B is consistently abundant in both units.

Sicular counts show an abundance distribution similar to the distribution of thecae. Siculae are most abundant in residue 30-33. Note that residue 10-14 was not included in the sicular counts because of a spillage of the residue following the thecal counts. The basal layer 0-22 and top layer 22-68 are both abundant with siculae. The abundance of thecae and siculae from residue 30-33 is at the base of a thick layer and near the graptoloid faunal shift. Although not seen as concentrated on the dissolution surface following corrections for the core, this abundance in the residues is interpreted as a graptoloid concentration. There were no observations of graptoloid alignment or fragmentation on the dissolution surfaces. The sicular distribution matches total thecal distributions and does not therefore indicate a biostratinomic event. However, the interpreted sponge-spicule layer, the shift in graptoloid assemblage and the associated lithologic change at layer 22 suggest that there has been a subtle shift in the sedimentary dynamics. This was a very low energy event as there is no evidence of winnowing, alignment or fragmentation of the graptoloid assemblage and no current indicators in the sediment.

Concretion: CM 57.5-57.6

Lithofacies: 11, wavy-bedded

Graptoloid distribution: random (χ^2/n= 0.93)

Taphofacies: random flux of graptoloids and sediment – subtle shifts in sediment source.

This very fine- to fine-grained carbonate concretion revealed a silty-sand texture between layers 14 and 42 mm during dissolution. It is uncertain whether these sandy particles are of a sedimentary or diagenetic origin. Wavy laminae defined by light brown/buff and dark grey brown colour changes characterize the concretion (Figure 4.53B). In thin section the "wavy" beds are observed to be stylolite-bound laminae (Figure 4.53C, D).

Light laminae average 3 mm in thickness and are characterized by a grey matrix with carbonate crystals in grain/crystal contact and a few brown (organic?) patches. The crystals range in size from 20 – 100 μm. The dark laminae average 4 mm in thickness and contain more clearly defined crystal boundaries and more common brown patches. In these laminae the carbonate crystals are smaller than in the light laminae (20 – 40 μm). The silt laminae are possible grouped into graded units.

The bottom of the concretion (layers 0-30) contains more abundant light laminae thanthe top (layers 30-65). Because of the stylolitic alteration of the sediments, it is difficult to say if there is a stratified grading of light to dark laminae. If concretionary carbonate crystal size can be related to original texture then this concretion records a change in sedimentological conditions from coarse to finer grain size with time (light to darker laminae). There appears to be a sharp and irregular base to bed 30-65. The irregular nature of the basal contact is a product of a bedding-parallel stylolite and cannot be assumed to be recording an erosive base.

Graptoloids were rare in this concretion with a total rhabdosomes count during dissolution of 15 (Figure 4.53A). Two layers were barren (layers 46, and 48). The 15 rhabdosomes were randomly distributed among the 9 layers counted. The dissolution residues also show low abundances and a random distribution (Figure 4.54). The samples are dominated by *Monograptus falcata* forma D and show an up-concretion increase in *Monograptus crenularis*?. The presence of *M. crenularis*? in the top three

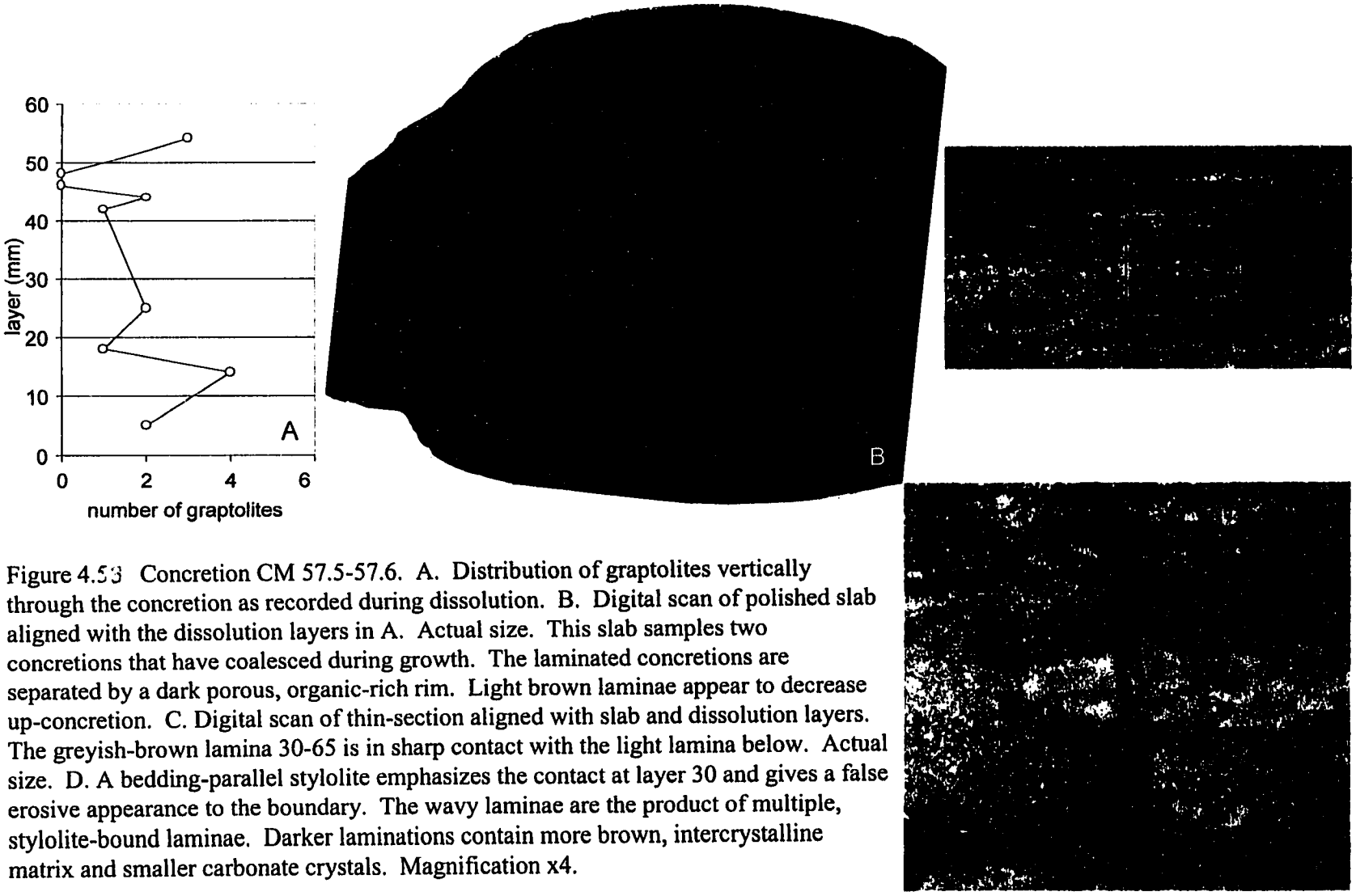

Figure 4.53 Concretion CM 57.5-57.6. A. Distribution of graptolites vertically through the concretion as recorded during dissolution. B. Digital scan of polished slab aligned with the dissolution layers in A. Actual size. This slab samples two concretions that have coalesced during growth. The laminated concretions are separated by a dark porous, organic-rich rim. Light brown laminae appear to decrease up-concretion. C. Digital scan of thin-section aligned with slab and dissolution layers. The greyish-brown lamina 30-65 is in sharp contact with the light lamina below. Actual size. D. A bedding-parallel stylolite emphasizes the contact at layer 30 and gives a false erosive appearance to the boundary. The wavy laminae are the product of multiple, stylolite-bound laminae. Darker laminations contain more brown, intercrystalline matrix and smaller carbonate crystals. Magnification x4.

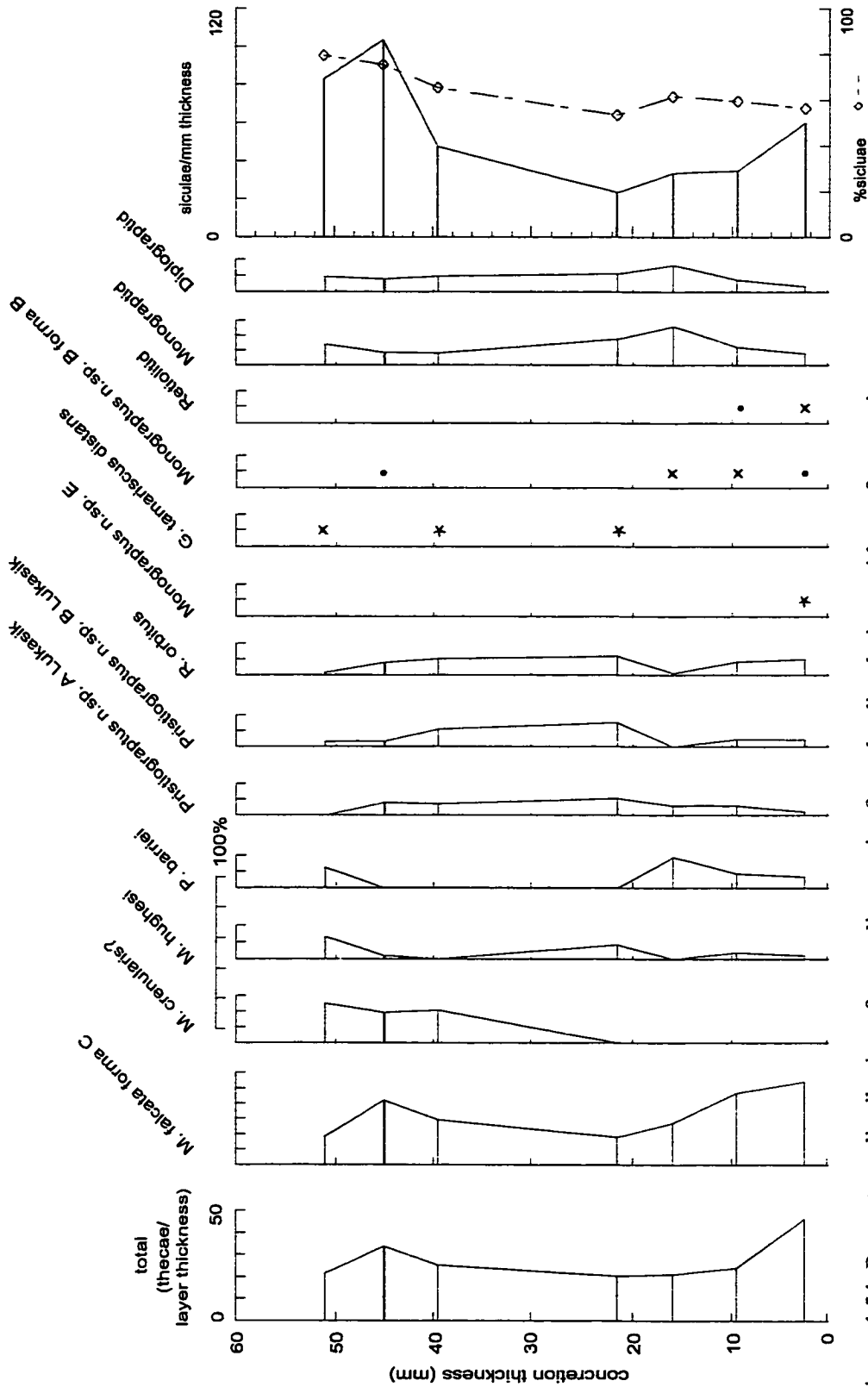

Figure 4.54. Percentage distribution of graptolite species from the dissolution residues of concretion CM 57.5-57.6: * 5-10%, × 1-5%, • < 1%

residues (37-54) could be related to the change in lithology (layer 30-65 with darker laminae). This could represent a shift in the source of the sediment that brings with it the new species and the muddier sediments. However, only a minor increase in total thecae is observed in these top residues. Sicular counts reveal a more major increase in the top residues. Percentage siculae calculations of the total count average 58% in the four basal residues and 73% in the top three residues. The change in lithology, accompanied by the shift in the taphocoenosis with the addition of *M. crenularis*? and the increased abundance of siculae, suggest that there is slight change in sediment source. This is interpreted to be a minor event in the background sedimentation.

Concretion: CM 58a

Lithofacies: 3, coarsely laminated, clay/organic-rich
Graptoloid distribution: random (χ^2/n= 2.31)
Taphofacies: random flux of graptoloids and sediment
Paleoecological event: shift from *Monograptus falcata* forma D and *Campograptus communis* co-dominance to single dominance of *Monograptus sidjachenkoi*.

Concretion CM 58a was collected 2.3 meters from CM 58b at the same stratigraphic level and displays a similar concretionary fabric. Colour variations from light pinkish-brown to grey brown define four coarse laminae of this very fine-grained concretion (Figure 4.55B). The layers are also defined by the distribution of radiolarian molds. and the relative abundance of bedding-parallel rip-up clasts averaging 0.5 cm in length. Layer 50-30 contains a greyish-brown matrix with common radiolarian molds and rare black grains. Layer 30-0 contains a brown matrix with rare radiolarian molds and rare black grains. Within this layer is the preserved dark core. Above this, is a 27 mm thick lamina composed of a brown matrix with common radiolarian molds and rare black grains. This layer is in gradational contact with the bed below except where this layer is in sharp irregular contact with the dark core..

Thin section examination reveals a possible peloidal fabric. The peloids are brown to dark brown circles or ovals in cross-section and range in size from 10 to 50 μm. They are in grain contact or suspended in a very fine-grained grey matrix. The style of the

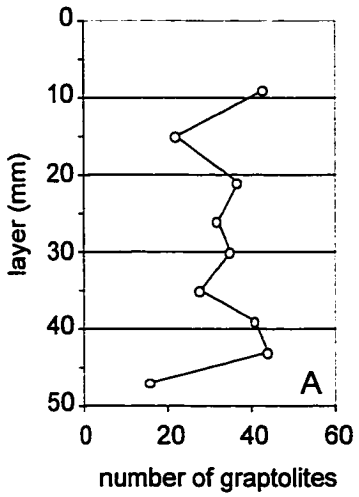

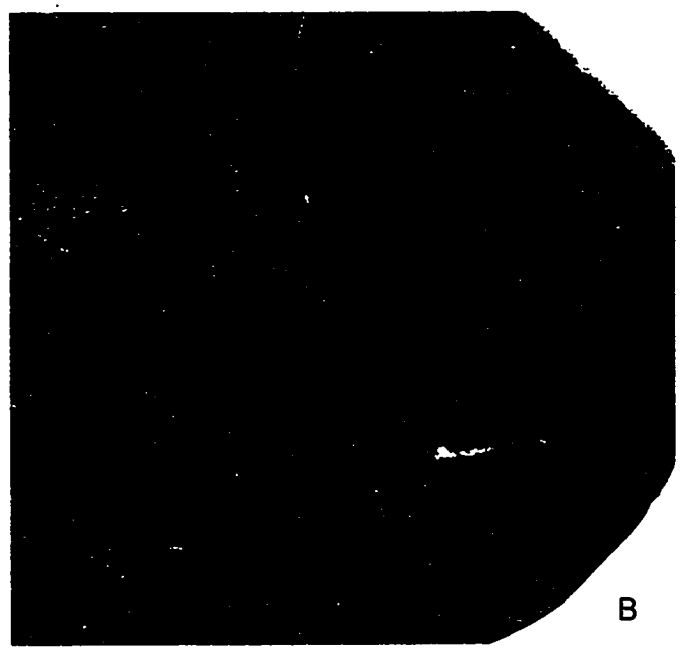

Figure 4.55. Concretion CM 58a. A. Vertical distribution of graptolite rhabdosomes through the concretion as revealed during dissolution. No correction was made for the core. B. Digital scan of polished slab. Showing 3 of the 4 coarse laminae: -5-22, 22-48, 48-75. Just the basal portion of layer 75-100 is included in the slab image. Actual size. C. Digital scan of thin-section containing a peloidal type fabric. Medium brown "peloids" are oval to circular in shape with diameters that range from 10 to 50 μm. Magnification x2.

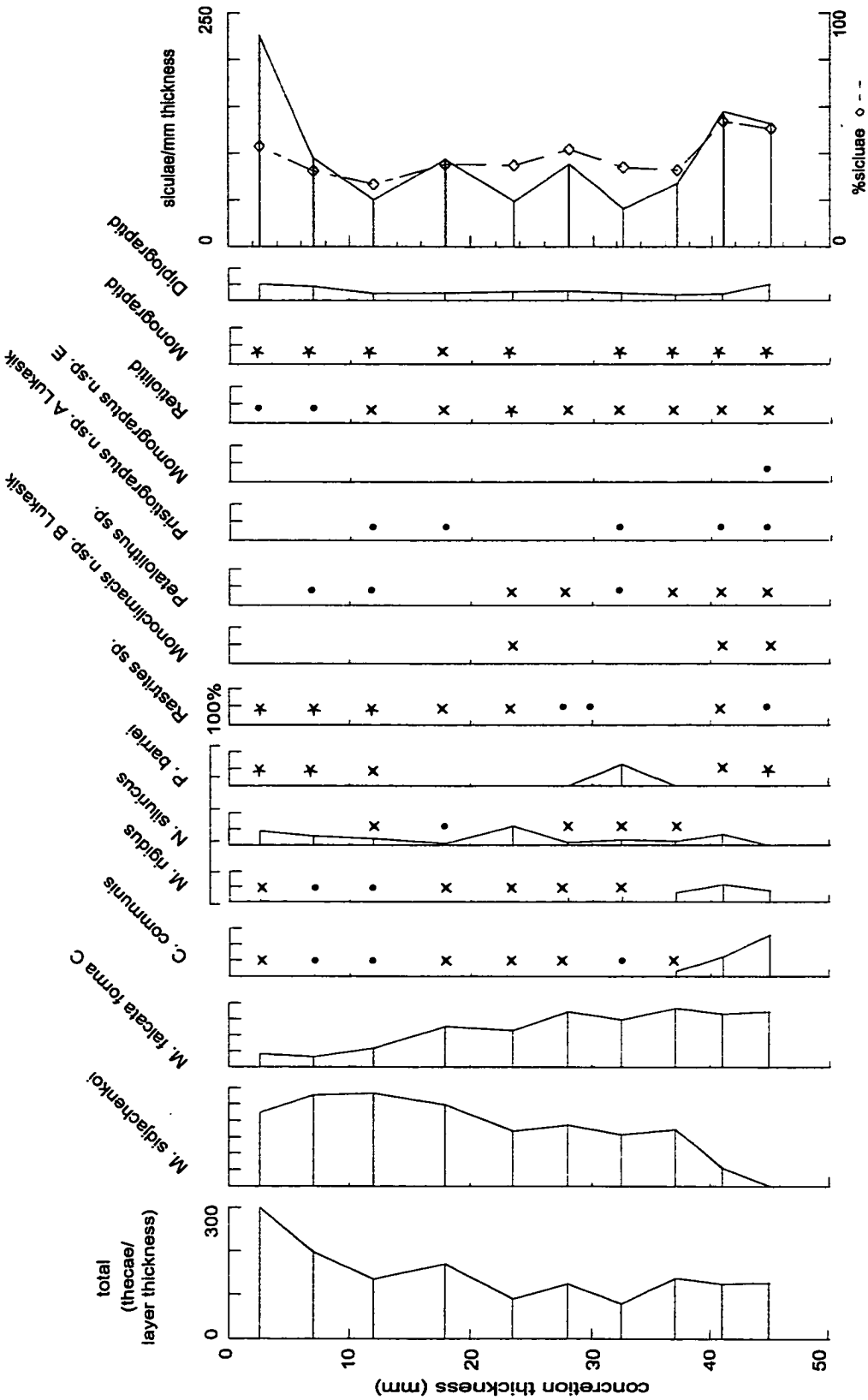

Figure 4.56. Percentage distribution of graptolite species from the dissolution residues of concretion CM 58A: * 5-10%, × 1-5%, • < 1%

peloidal packing defines the laminae. The four layers present in the slab and identified in the thin section are most likely depositional laminae preserved in anoxic conditions and not the product of currents.

Concretion CM 58a was dissolved from the top down, reverse to the normal dissolution direction described in the methods. Graptoloids were abundant (327 rhabdosomes) on the 10 surfaces examined during the layer-by-layer dissolution (Figure 4.55A). No correction was made for the presence of a core, since graptoloids were still found within the core and therefore the core did not hinder the count. When a chi-square test was performed on the dissolution counts, the null hypothesis of random distribution was not supported; however, one layer was skewing the results. Layer 47 contained 16 graptoloids, less than half of the average 33 rhabdosomes per layer. If that layer is removed from the counts, the remaining 9 layers display a random distribution of rhabdosomes. In my opinion this is a better representation of the sample as no one layer or layers can be said to be enriched in graptoloids. A "monograptid" on layer 30 showed evidence of fragmentation prior to burial.

The thecal counts reveal a gradual (inconsistent) increase in thecae and in siculae up through the concretion (Figure 4.56). Siculae and thecae from rhabdosomes vary proportionately through the residues, maintaining a constant siculae percentage of 39%. This increase in total thecae was matched by an increase in the most dominant species, *Monograptus sidjachenkoi* and a decrease in *Monograptus falcata* forma D and *Campograptus communis*. This distribution pattern of the graptoloid taphocoenosis is identifying a shift in species dominance in the assemblage. This is most likely connected to a shift in the life assemblage and a change in the paleocommunity. It is not likely that this is a taphonomic concentration as no lithologic or biostratinomic evidence supports a biostratinomic process.

Concretion: CM 58b

Lithofacies: 3, coarsely laminated, clay/organic-rich
Graptoloid distribution: random (χ^2/n= 1.01)
Taphofacies: random flux of graptoloids and sediment

Concretion CM 58b was collected 2.3 meters laterally from CM 58a and displays a very similar concretionary fabric. At least four coarse laminae that average greater than 2 cm in thickness are displayed in the polished slab (Figure 4.57B). These are defined by dark boundaries, representing an increase in clay and organic content. A coarse concretionary carbonate texture can be seen in low magnification. Lamina 26-55 contains a concretion core that is lighter in colour than the surrounding material. Variations within the coarse laminae are subtle in polished slab and more easily defined in thin section. No thecal or sicular count data were obtained from the residues of this concretion

A peloidal texture similar to CM 58a was identified in thin section (Figure 4.57C). The concretionary material is similar to CM58a in concretionary carbonate size and appearance, although CM 58b contains a higher amount of medium brown matrix between the carbonate grains and more of the dark brown grains with in the matrix. The distribution of this organic material defines the laminae. Similar to the observations of the polished slab, the laminae are bounded by an increase in organic matter. However, in thin section it is also observed that the organic matter is dispersed throughout the lamina. Some laminae are defined not by organic-rich or organic-poor boundaries but by a slight increase in organic matter throughout the lamina.

Graptoloid rhabdosomes are randomly distributed among the seven layers once corrected for the presence of a large insoluble core (Figure 4.57A). At layer 37, the core occupies almost 95% of the surface and impedes accurate counts of graptoloid rhabdosomes. The corrections made for this core are based upon the percentage of the surface occupied by the core, the count from the surface and the abundance of rhabdosomes on the surfaces where the core is not present. Therefore the result of the correction is to dilute and remove any significant abundance peaks and produce a

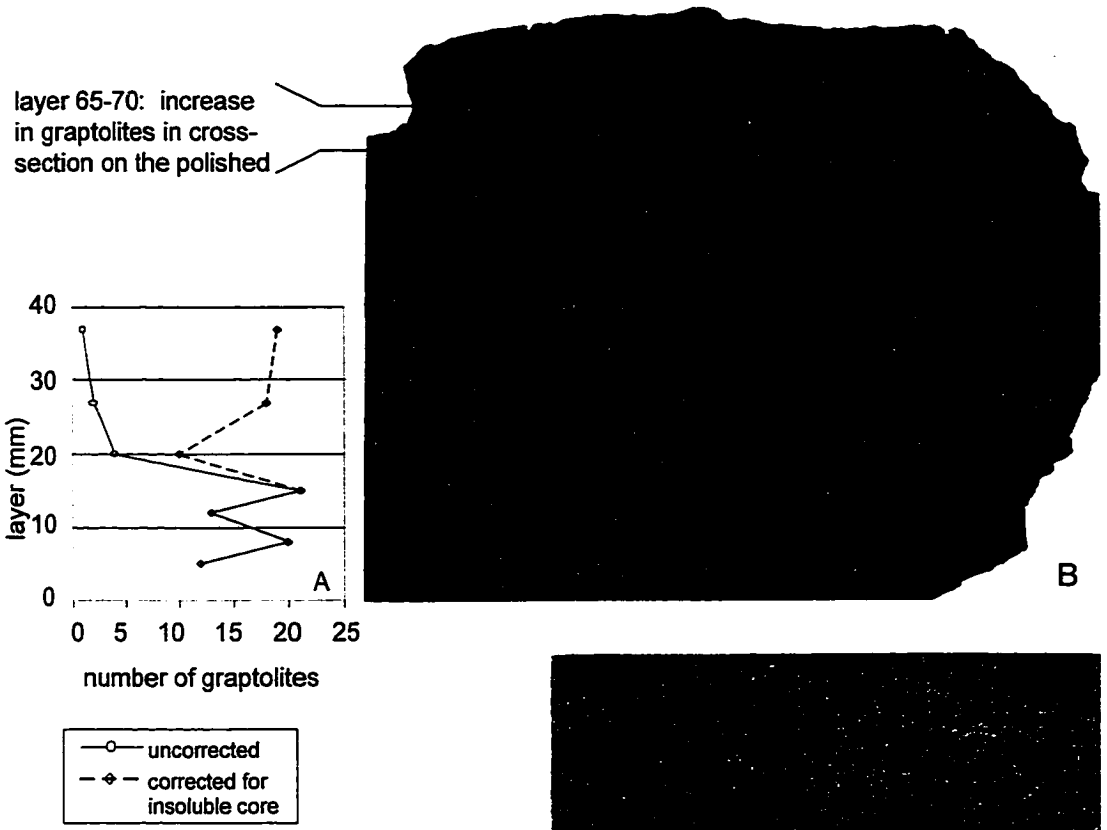

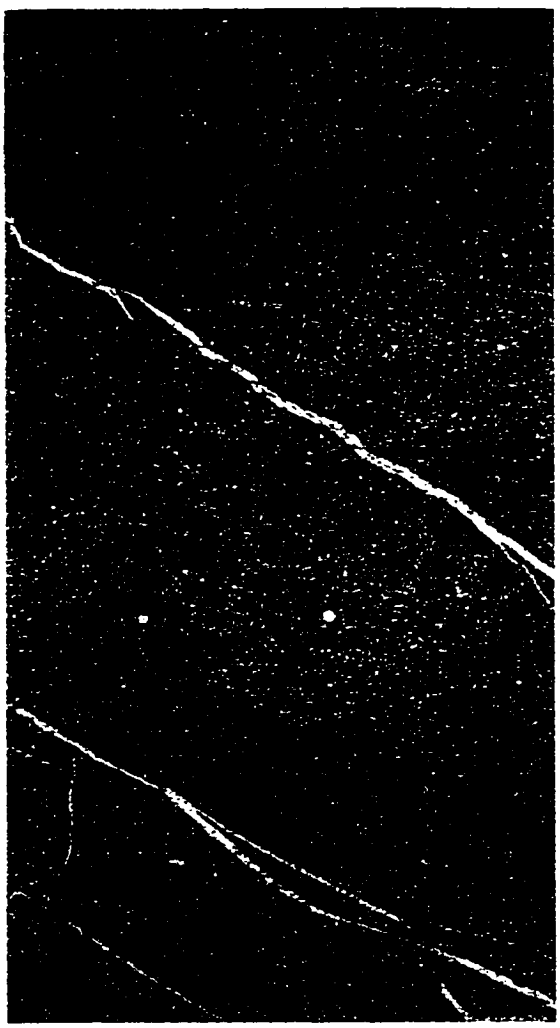

Figure 4.57. Concretion CM 58b. This concretion was collected 2.3 meters away from CM 58a in the same stratum. A. Distribution of graptolite rhabdosomes vertically through the concretion as recorded during the layer-by-layer dissolution. Corrected for the presence of an insoluble core. B. Digital scan of polished slab showing coarse laminae that are poorly defined. The slab cross-cuts the core at centre. White viens are off-set by mirco-fractures and faults. Actual size. C. Digital scan of thin section. Similar peloidal-type fabric to CM 58a. Brown organics are observed in the intercrystalline texture and as whole grains. Magnification x2.

statistically random distribution. The interpretation of this concretion will be greatly affected.

Layer 65-70 is a dark to medium brown lamina with nine visible graptoloid rhabdosomes in cross-section representing approximately 80% of the rhabdosomes seen in the polished slab. This layer was not dissolved and if included in the study would have most likely resulted in the statistical conclusion that the graptoloids were not randomly distributed vertically through the strata. These nine graptoloids had diameters greater than 1 mm and for this reason were thought to be mature rhabdosomes. This is in contrast to the layers that were recorded during the dissolution process that contained many siculae and early growth stage graptoloids, but few mature rhabdosomes. However, this unique layer cannot be included in the chi-square analysis and the conclusion of this concretion having a random vertical graptoloid distribution remains.

Concretion: CM 59.1-59.2

Lithofacies: 11, wavy-bedded
Graptoloid distribution: non-random ($\chi^2/n= 4.27$)
Taphofacies: physical addition of graptoloids

Wavy laminae of buff and brown characterize this very fine-grained carbonate concretion (Figure 4.58B). Laminae average 2 mm thick and are defined by matrix colour variation and the distribution of rip-up clasts that average less than 1 mm in length. Layer 35-47 is a medium to dark brown layer with few internal laminae. Layer 47-60 grades from a light brown base to a medium brown to dark brown top. The many internal laminae within Layer 47-60 make the grading of colour difficult to identify. Layer 78-84 has a sharp, irregular base of buff-coloured carbonate that grades to medium brown to dark brown and then back to buff. The top contact is also sharp and irregular. Lamina 84-87 has a sharp, irregular base that is dark brown and grades to a medium brown at the top. The "irregular" quality of the contacts may be a result of the wavy lamination that may be diagenetic in origin. No thin section was prepared from this concretion for examination. I described wavy bedding from the polished slab of concretion CM 57.5-57.6 and found in thin section that the wavy character was a

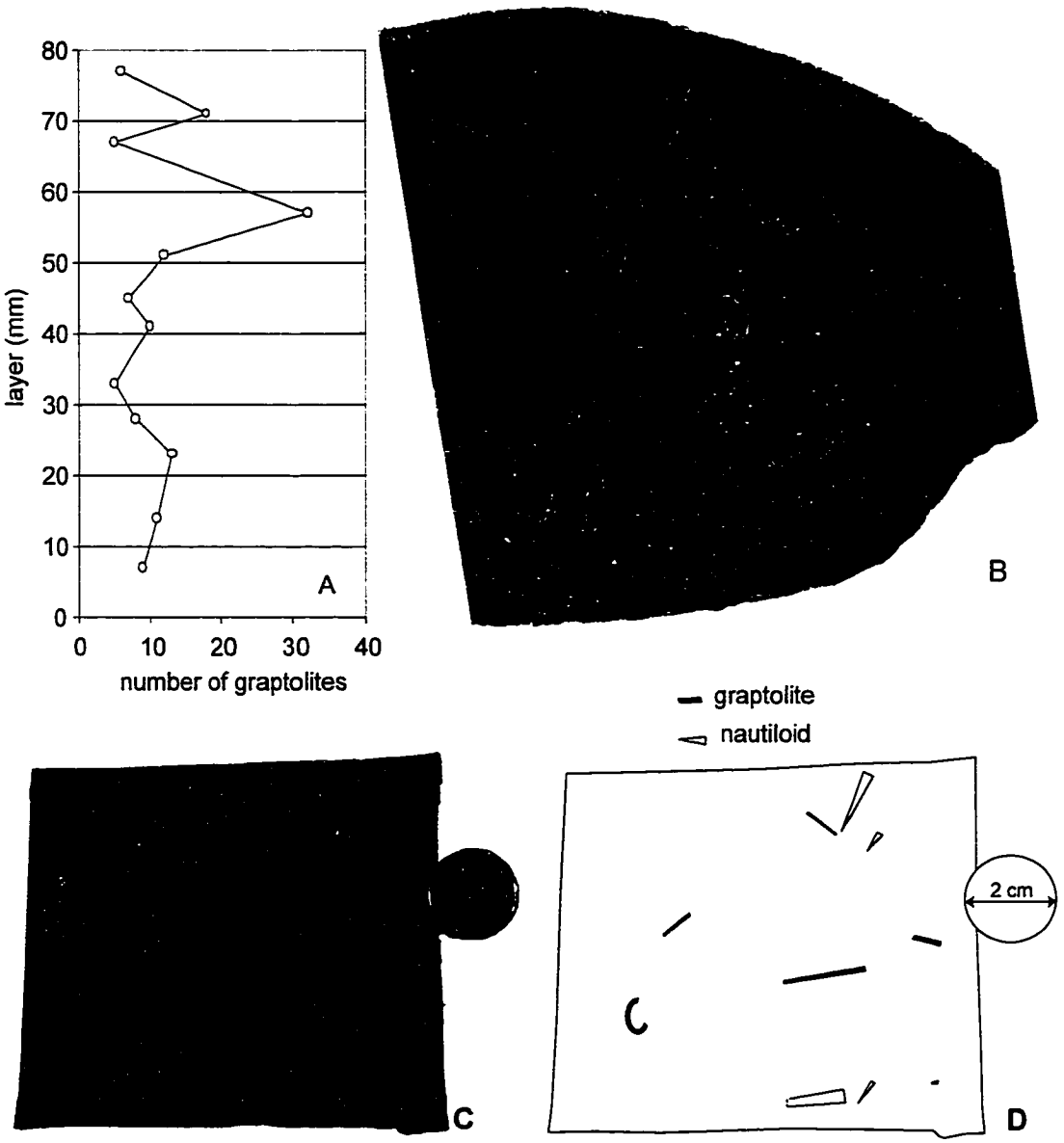

Figure 4.58. Concretion CM 59.1-59.2. A. Vertical distribution of graptolite rhabdosomes showing a statistically significant increase at layer 57. B. Digital scan of polished slab. Laminae defined by colour variation are wavy and discontinuous. The wavy character may be diagenetic as the CM 57.4-57.5 and not representative of sedimentologic conditions. Layer 0-35 contains more of the light laminae. Layer 35-47 contains few internal laminae and is medium to dark brown in colour. Layer 78-84 and 84-87 grade from light to dark and have sharp basal contacts. No unique features distinguish layer 57. C. Dissolution surface layer 57. D. Line drawing of graptolite distribution on dissolution surface revealing weak orientation of the elongate rhabdosomes.

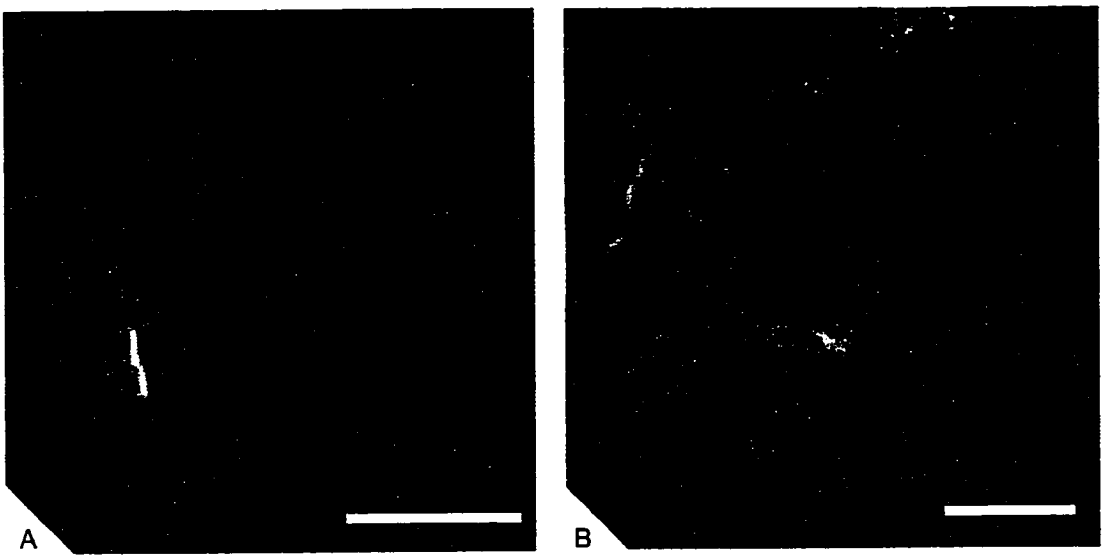

Figure 4.59. SEM of CM 59.1-59.2. A. A rounded grain with rhombohedral cleavage suggestive of carbonate. This grain with a diamter of 10 μm is interpreted to be an internal mold of a radiolarian test that has since been dissolved leaving only the mold. SEM/EDS chemical signature of grain is given in Figure 4.60. Scale bar is 5 μm. B. A platy grain oriented parallel to bedding. This 30 to 40 μm wide grain is considered to be a rip-up of a partially lithified sediment and is correlated to the dark grains observed in the polished slab. Scale bar is 10 μm.

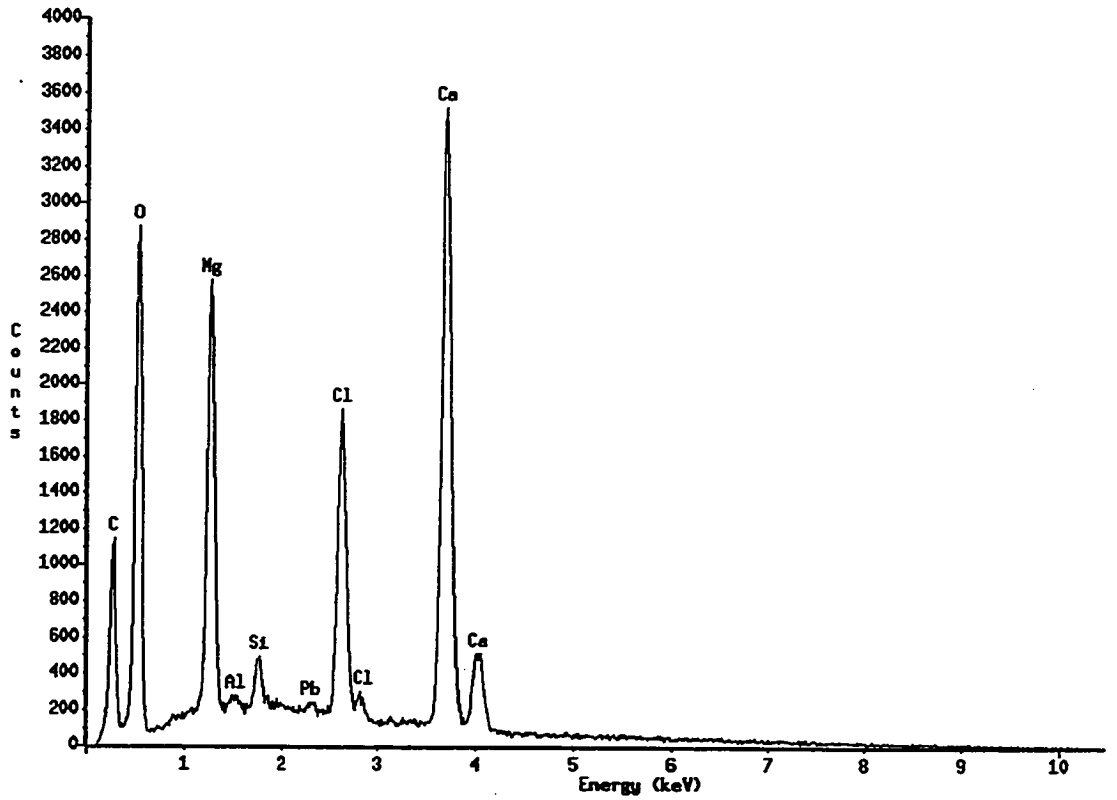

Figure 4.60. Spectral analysis of the rounded grain from CM 59.1-59.2 shown in Figure 4.59A. The predominant elements of carbon (C), oxygen (O), magnesium (Mg), chlorine (Cl), calcium (Ca), and silica (Si) are characteristic of dolomite CaMg(CO3)2. Silica (Si) and chlorine (Cl) are likely picked up by the EDS from the minor clay in the vicinity.

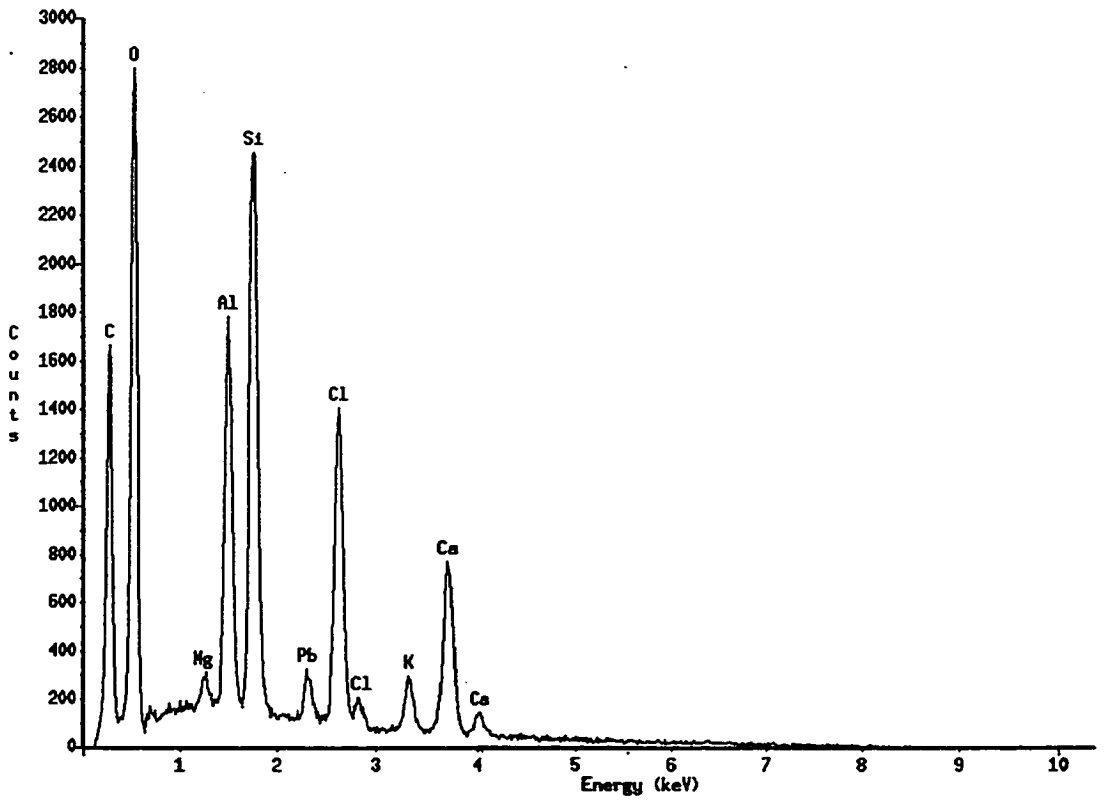

Figure 4.61. Spectral analysis of the flattened grain from CM 59.1-59.2 shown in Figure 4.59B. The predominant elements of carbon (C), oxygen (O), aluminum (Al), chlorine (Cl), calcium (Ca), and silica (Si) are characteristic of an aluminum rich clay in a carbonate matrix.

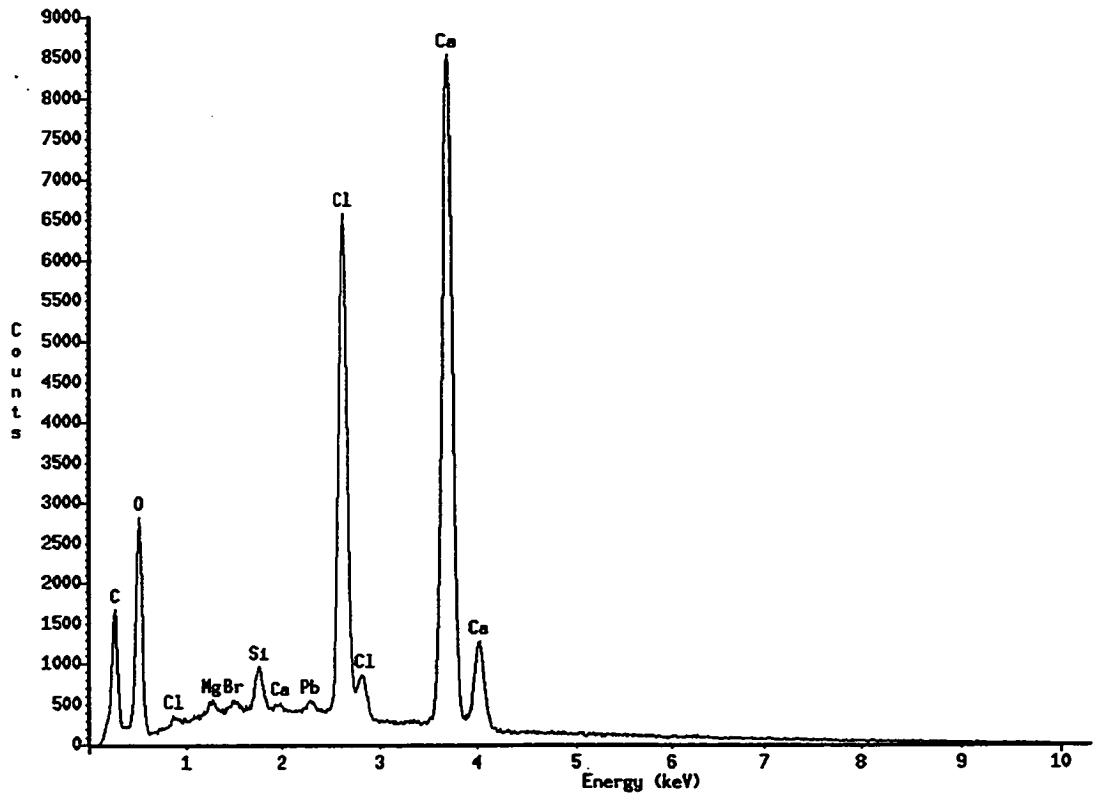

Figure 4.62. Spectral analysis of the background carbonate from CM 59.1-59.2. The predominant elements of carbon (C), oxygen (O), chlorite (Cl), and calcium (Ca) are characteristic of chorine-enriched carbonate (CaCO3).

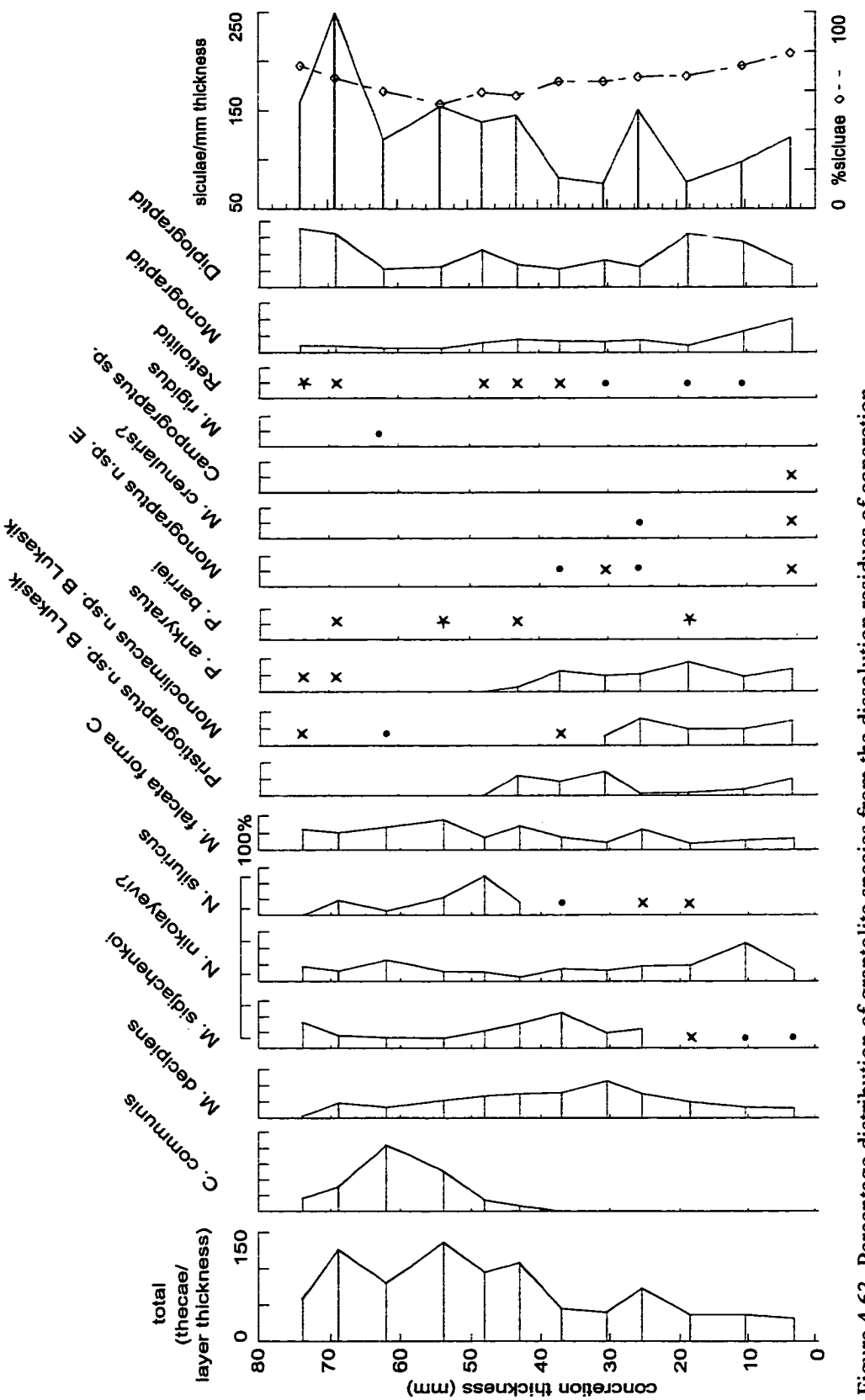

Figure 4.63. Percentage distribution of graptolite species from the dissolution residues of concretion CM 59.1-59.2: * 5-10%, × 1-5%, • < 1%

representation of multiple bedding-parallel stylolites (Figure 4.53). This diagenetic alteration is possibly affecting this concretion too.

SEM/EDS analysis of a piece of concretionary material identified the composition of the rounded grains interpreted to be internal molds of radiolaria (Figure 4.59A). The sphere is 10 μm in diameter with dolomite-type rhombahedral cleavage. The diameter of the grain suggests that these rounded grains could be internal molds of radiolarians (E. W. MacDonald, pers. comm.). The predominant elements identified from the EDS were those of C, O, Mg, Cl, Ca, and Si (Figure 4.60). The fact that this grain resisted dissolution in dilute hydrochloric acid also suggests that this is dolomite $CaMg(CO_3)_2$. Based upon this evidence I have identified white spheres of similar size observed in polished slab and thin section of other concretions as radiolarian molds. These others are similarly assumed to be dolomitic. The radiolarian test of original silica composition has been dissolved from the fossil record in this particular example. Many of the concretions from the Cape Phillips Formation are rich in radiolarians, some with silica tests and internal precipitates. In this concretion the radiolarian molds are common in the light laminae and rare in the dark laminae. The radiolarian molds seem to be randomly distributed within the lamina.

Some fragments of material had a platy appearance (Figure 4.59B). These plates are too large and uncharacteristic of the platy minerals of clay (e.g., kaolinite). They could be rip-up clasts from a surface that was partially lithified at the sediment-water interface, or fragments of bacterial mats that survived at the sediment-water interface. The EDS/SEM chemical signature shows an abundance of silica, oxygen, aluminum, carbon, chlorine, and calcium suggesting an aluminum silicate type clay mineral in a carbonate matrix (Figure 4.61). These platy grains are most likely the "dark flattened grains" observed in polished slab. To identify the unique composition of this flattened grain (Figure 4.59B) and the rounded grain (Figure 4.59A) these SEM/EDS signatures (4.60, 4.61) were compared with the "background" SEM/EDS chemical signature for this concretion material (Figure 4.62). This signal was enriched in carbon, oxygen, chlorine and calcium, suggesting a carbonate matrix.

Graptoloid rhabdosomes are not randomly distributed among the 12 dissolution layers (Figure 4.58A). There is an abundance of graptoloids on dissolution layer 57 (32

rhabdosomes; 17 mature "monograptids"), with some orientation in the horizontal plane (Figure 4.58C, D) indicating alignment by flow. This abundance corresponds to the darker portion of the graded lamina layer 47-60.

A greater number of thecae and siculae were counted from the residues in the top half of the concretion than from the bottom half (Figure 4.63). Sicular and thecal counts were relatively concomitant with residue 45-71 slightly depleted in siculae. The greatest abundance of thecae per layer height was counted from residue 51-57, with secondary abundance peaks in residues 41-45 and 67-71. The top half was dominated by *Campograptus communis* and *Neodicellograptus siluricus*, which were absent (*C. communis*) or rare (*N. siluricus*) in the bottom half. The residues from the bottom half of the concretion record a more diverse assemblage of graptoloids. Six species are present in the basal residues and are rare or absent in the top of the concretion. Although many species are present throughout, there does seem to be a significant faunal change in the thecal counts at layers 41 to 51. Based upon evidence from the lithology, the distribution of graptoloid species on the dissolution surfaces and in the residues, and the taphonomy of the graptoloids, this concretion is interpreted to preserve a low energy transport event. This event was strong enough to winnow some of the smaller rhabdosomes (depleted of siculae in residues 45-71), orient the elongate graptoloids in layer 57, concentrate the mature rhabdosomes, change the composition of the assemblage by bringing graptoloids from a different niche, and sorting the sediment (graded beds).

Concretion: CM 72.6

Lithofacies: 5, finely laminated, clay/organic-rich
Graptoloid distribution: random ($\chi^2/n= 1.1$)
Taphofacies: random flux of graptoloids and sediment

This weakly laminated carbonate concretion is medium to dark brown and very fine-grained (Figure 4.64 B). A dark brown core is visible on the polished slab. Four major layers are weakly distinguishable. Layer 0-5 is medium brown with darker brown partings. Faint internal discontinuous laminae are defined by these partings. Layer 5-14 contains more of the darker partings than the layer below and overall appears darker in

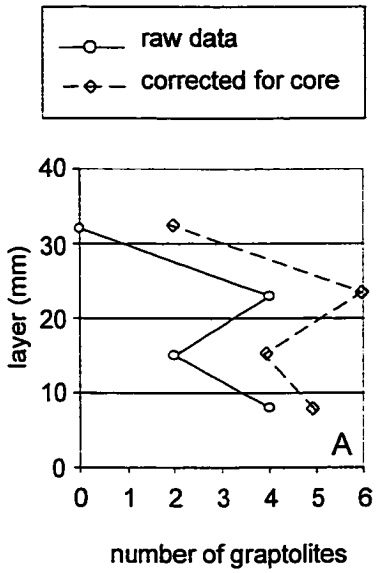

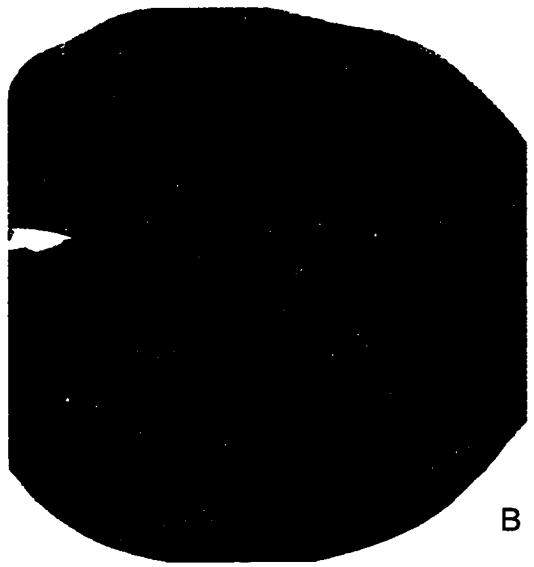

Figure 4.64. Concretion CM 72.6. A. Distribution of graptolite rhabdosomes vertically through the concretion corrected for the presence of a core. Very few graptolites were present on the dissolution surfaces. The large insoluble core was present on each surface and the simple correction should be interpreted with caution. B. Digital scan of polished slab. Laminae are defined by the concentration of dark brown flattened grains or partings. Layer 14-30 and layer 30-50 contain fewer dark grains at their base and therefore display an overall grading of colour from medium brown to dark brown up-lamina. Actual size. C. A light brown, insoluble core composed of sand-sized insoluble grains, dominated the concretion as shown on dissolution layer 15.

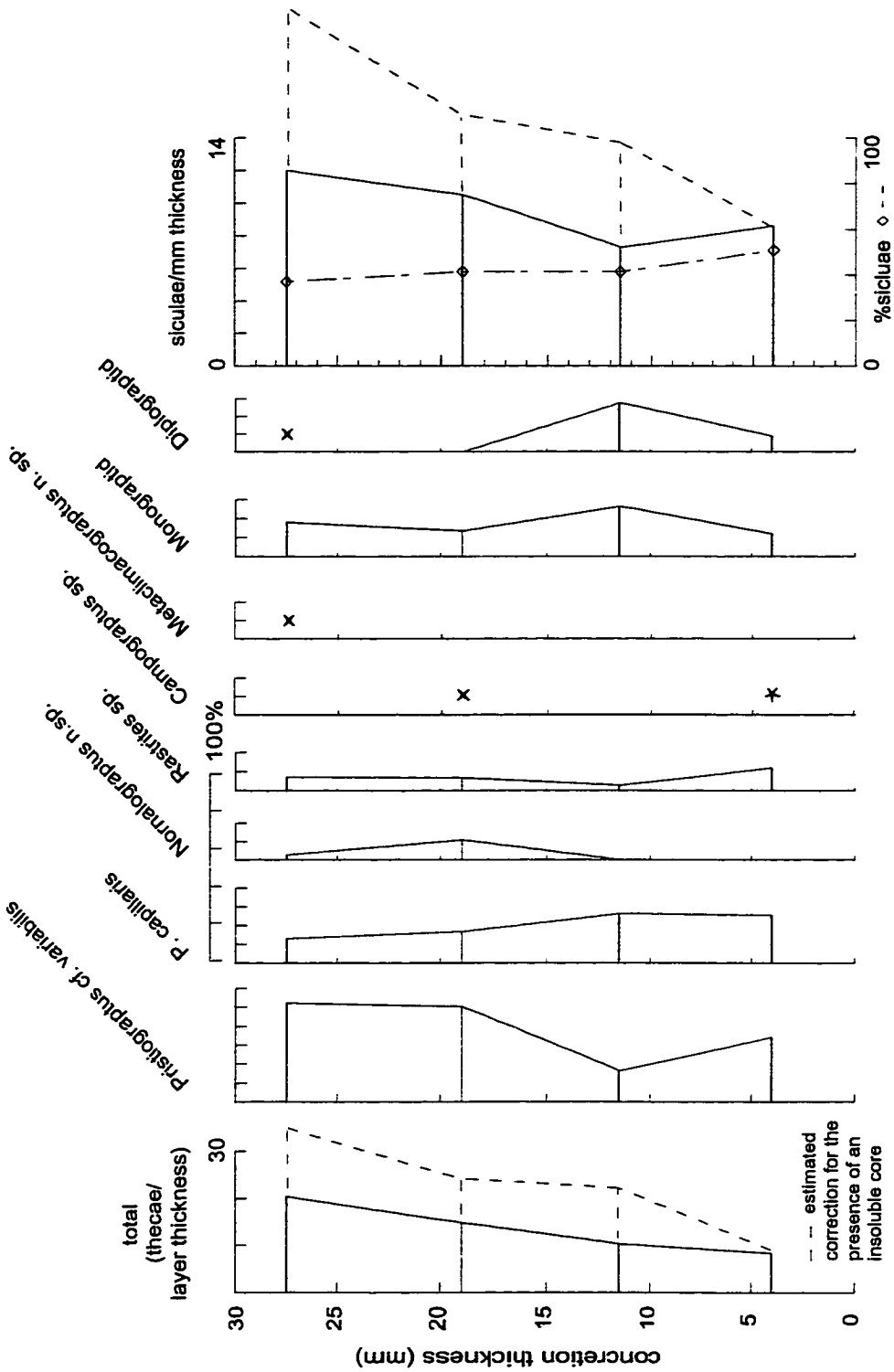

Figure 4.65. Percentage distribution of graptolite species from the dissolution residues of concretion CM 72.6: * 5-10%, × 1-5%, • < 1%

colour. Layer 14-30 and 30-50 are both medium brown with dark partings. The basal few millimeters of both laminae contain no dark partings. These observations are from the polished slab and no thin section analysis was conducted.

Overall graptoloid abundance is low in this small concretion (total count = 10). The graptoloids were randomly distributed among the 4 dissolution surfaces examined even though one surface was barren. The correction for the core did not change the result of the chi-square analysis. The core was equally dominant on all of the four surfaces. The distribution of thecae and siculae through the concretion residues shows a slight increase in abundance up-concretion with the siculae increase greater than the increase in thecae. With only four residues and low total abundance, trends in the faunal composition are difficult to identify with certainty and this concretion is hesitantly placed in the taphofacies of random flux of graptoloids and sediment.

Concretion: CM 73.8

Lithofacies: 5, finely laminated, clay/organic-rich
Graptoloid distribution: non-random (χ^2/n= 6.07)
Taphofacies: sediment-starved. – not a true hiatus.

This light to medium brown carbonate concretion is finely laminated (Figure 4.66B). A lamina of lighter brown (patches of white/buff) occurs at 10 mm to 13 mm. A solid and discontinuous lamina of white/buff appears at layer 21 mm to 24 mm. Thin, medium brown laminae occur at 64 mm and 72 mm.

In thin section, the very fine-grained texture was determined to be crystals of concretionary carbonate that ranged in size from 10 to 60 μm, average = 20 μm (Figure 4.66C). Bedding-parallel rip-up clasts are abundant. These grains are 2 – 3 mm in length and less than 0.5 mm in height. Laminae are defined by the relative amounts of matrix, brown grains, and the size of the carbonate "grains".

The rhabdosome data from the dissolution layers of this concretion do not support the null hypothesis of random distribution. Two surfaces appeared to be rich in graptoloid rhabdosomes (layer 10, 10 rhabdosomes; layer 25, 15 rhabdosomes; average per layer = 6, n = 13). After correction for the insoluble core that appears in many of the

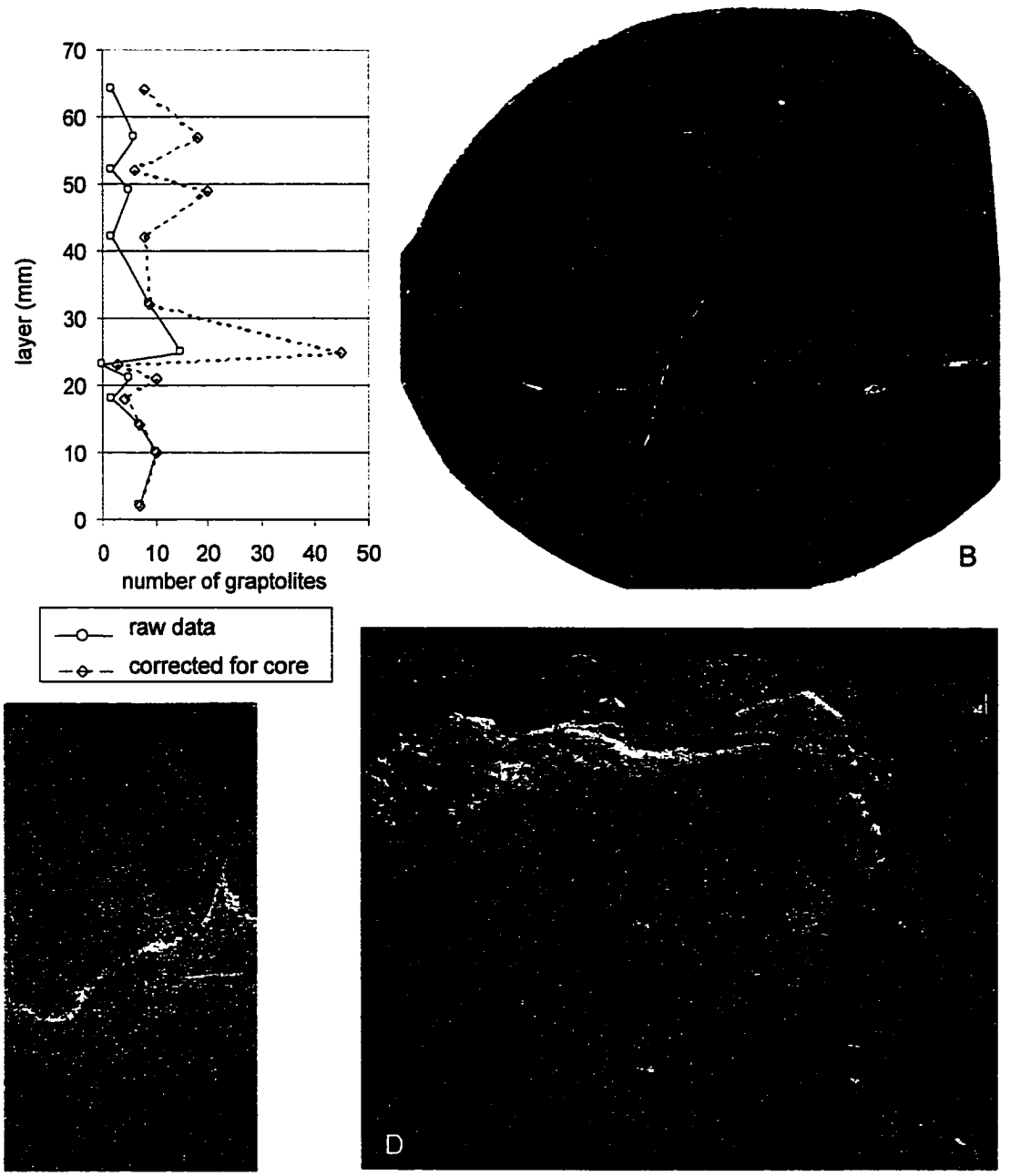

Figure 4.66. Concretion CM 73.8. A. Vertical distribution of graptolite rhabdosomes through the strata corrected for the presence of a core. B. Digital scan of polished slab. Laminae average 8 mm in thickness and are defined at this scale by overall colour variation and the distribution of white to light brown grains or diagentic patches. Contacts between laminae are gradational. Actual size. C. Digital scan of thin section. Laminae are defined by the distribution of lenses (2-3 mm in length 0.5 mm in thickness) of carbonate material that are finer in grain-size and contain a darker matirx than the rest of the concretion. D. Dissolution surface layer 57. The light brown core was cut between layers 32-42. The large core obstructs accurate rhabdosome counts. Magnification x1.5.

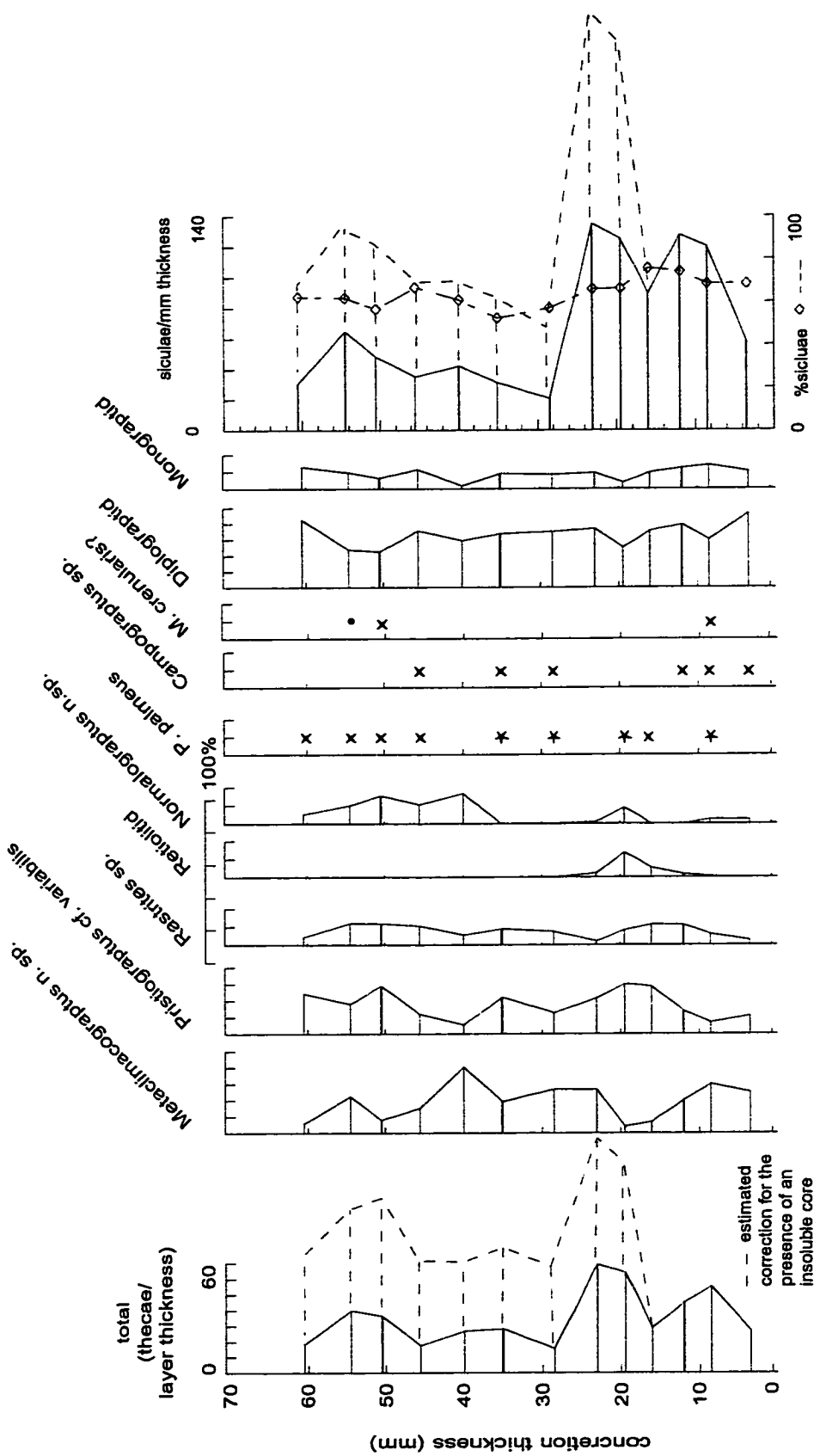

Figure 4.67. Percentage distribution of graptolite species from the dissolution residues of concretion CM 73.8: * 5-10%, x 1-5%, • < 1%

dissolution surfaces the abundance at layer 25 is enhanced. Of the 15 rhabdosomes on layer 25, 14 were siculae. An abundance of silica nodules were observed on this surface. The source of the silica is likely biogenic, originating with the radiolaria. It is possible that this layer records a size sorting of the smallest bioclasts, the early growth stages of the graptoloids and the radiolaria. The dissolution surface assemblage of layer 10 is composed of 5 siculae and 3 early growth stage "monograptids".

Thecal counts are concomitant with the sicular counts in the basal residues 0-25. Sicular and thecal abundances are proportionate in each residue with siculae approximately 64% of the total count. The residues related to layer 25 (21-25, 25-32) are dominated by *Metaclimacograptus* n. sp., lesser amounts of *Pristiograptus* cf. *variabilis* and early growth stages of unidentified "diplograptids". This is similar to the other residues. Residue 21-25 records a maximum abundance for the concretion. Residues 0-7 and 7-10 (related to layer 10) are dominated by *Metaclimacograptus n. sp.* and early growth stages of unidentified "diplograptids". Layer 25 and layer 10 do not appear to have a graptoloid composition (other than total abundance) that differs greatly from other residues in the concretion. There is no evidence for a single species or assemblage bloom.

This is an example of a slight change in the relative rates of sediment and graptoloid input concentrating the graptoloid rhabdosomes. It is likely that a subtle decrease in the sediment supply (perhaps accompanied by a slight increase in abundance of the biocoenosis) has caused the graptoloids in the lower strata to become concentrated. This reduction in sediment supply did not likely result in a true hiatus horizon. There was no taphonomic or lithologic evidence of a sediment-starved horizon.

Concretion: CM 74.9a

Lithofacies: 5, finely laminated, clay/organic-rich
Graptoloid distribution: non-random ($\chi^2/n= 5.44$)
Taphofacies: sediment-starved

This very fine-grained, medium greyish-brown, carbonate concretion has weak laminae with gradational boundaries that are defined by colour variation (Figure 4.68B). A light layer exists at 20 mm to 23 mm. Bioclasts of graptoloids and spar filled cavities

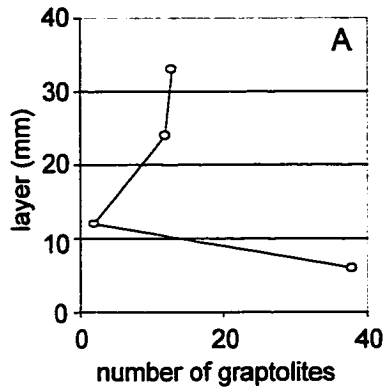

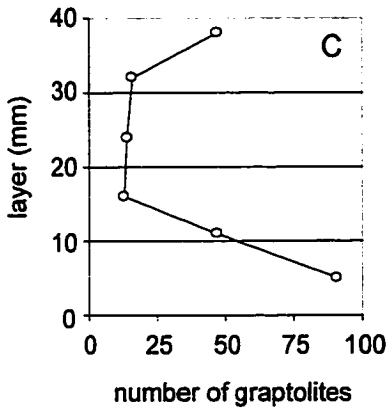

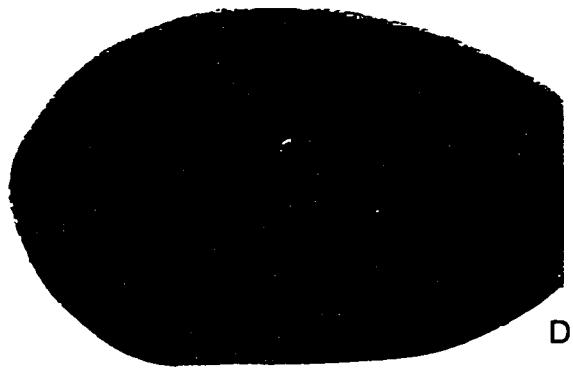

Figure 4.68. A, B. Concretion CM 74.9a. C-E Concretion CM 74.9b. originally conjoined to CM 74.9a. A, C. Vertical distribution of graptolite rhabdosomes as recorded during dissolution. B, D. Digital scans of polished slabs aligned with the respective dissolution layers . Actual size. Both concretions are dark greyish brown with visible bioclasts and spar-filled cavities of likely organic orign. Both contain a lighter brown lamina that in 74.9b is recorded at layer 20-23 and in 74.9b at 23-25. Other laminae are only faintly visible. E. Digital scan of thin section. Average crystal size is 20-80 μm. Lighter laminae show an increase in the average crystal size and contain less brown matrix between the crystals. Arrow points to bed that may be correlated to graptolite concentrated layer. Magnification x1.5.

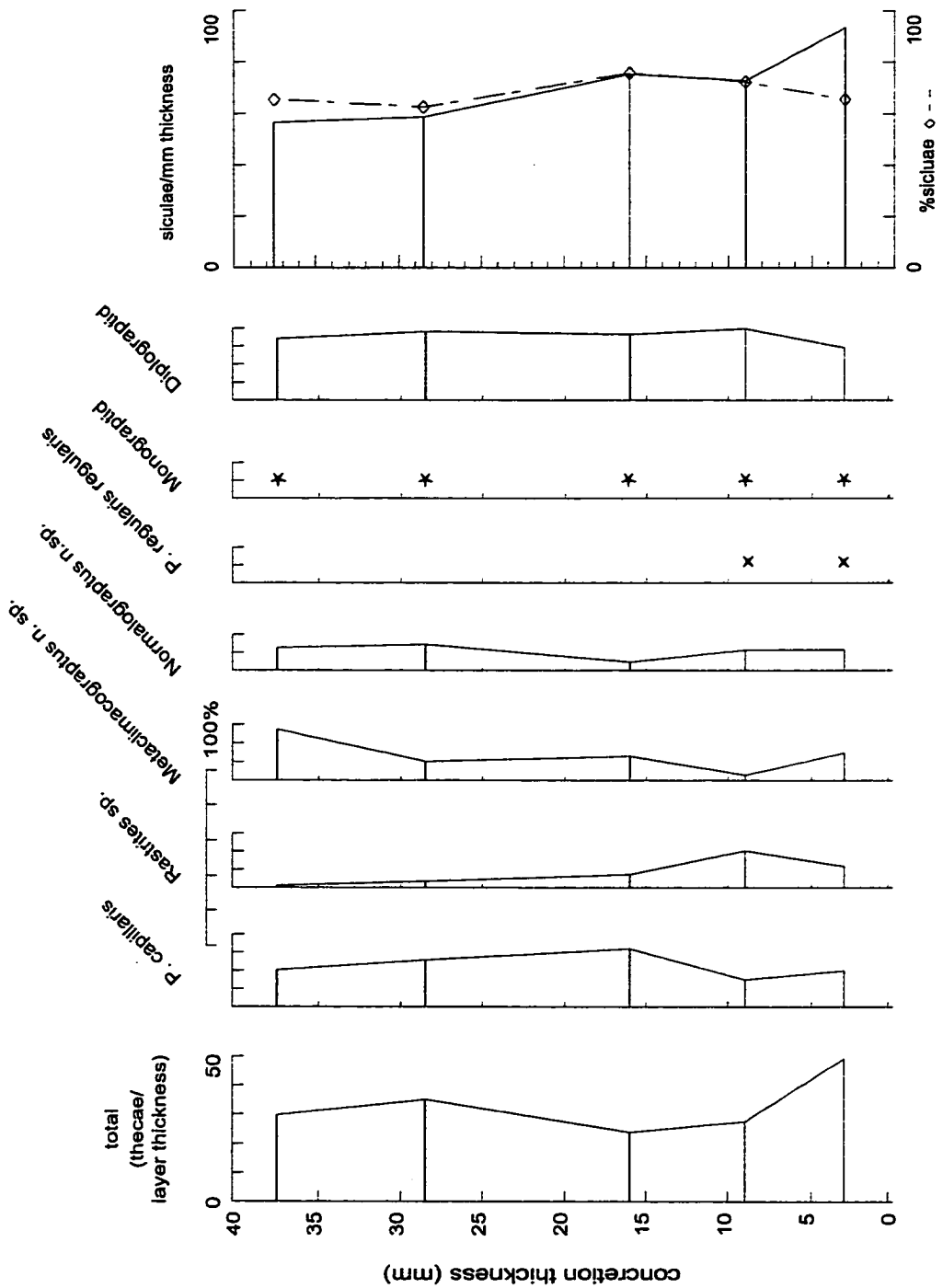

Figure 4.69. Percentage distribution of graptolite species from the dissolution residues of concretion CM 74.9A: * 5-10%, × 1-5%, • < 1%

of possible shelly fauna are visible on the polished surface. Thin section examination was carried out on the conjoined concretion CM 74.9b (Figure 4.68E). Both concretions are classified in lithofacies 3 and contain a similar graptoloid distribution and microstratigraphy. It is assumed that the observations could be used to assess the texture of concretion CM 74.9a.

Only 4 surfaces were examined during the dissolution of this small concretion. Graptoloids were abundant on layer 6 (Figure 4.68A; 38 rhabdosomes; average per layer = 16, n = 4). Thirty one of the 38 rhabdosomes (81%) were siculae and two of the mature graptoloids were fragmented. The high percentage of siculae on the surface is within range of the average percentage of siculae for the dissolution surfaces of 76%. No change in lithology was observed at or near layer 6, although more graptoloids could be seen in cross-section on the polished slab.

The thecal counts did not identify a significant change in the fauna in the residues that succeed or preceded layer 6 (Figure 4.69). A slightly higher total thecal and sicular count was observed in residue 0-6. This residue and the one above (6-12) differed slightly from the others in species diversity with the only occurrence of *Pristiograptus* cf. *variabilis* in this concretion. The anomalously high number of rhabdosomes on the basal dissolution surface (layer 6) is not associated with a major variation in graptoloid species distribution, or with a sedimentological event. A discussion of the taphofacies definition is provided in the description of CM 74.9b.

Concretion: CM 74.9b

Lithofacies: 5, finely laminated, clay/organic-rich
Graptoloid distribution: non-random ($\chi^2/n = 5.44$)
Taphofacies: sediment-starved

This concretion was joined to CM 74.9a and it was evident that these two concretions grew together, originating from two different, closely spaced nuclei. The lithology of the two is very similar. This concretion is medium greyish-brown with weak laminae defined by colour variations (Figure 4.68D). There is a light brown layer at 23 mm to 25 mm that is possibly contiguous with layer 20-23 of CM 74.9a. The

concretionary carbonate grain size ranged from 20 to 80 μm as observed in thin section (Figure 4.68E). These grains were in grain-to-grain contact in a grey matrix. Commonly more than one grain was in optical continuity suggesting a concretionary overprint on the original fabric. The lighter laminae display an interlocking more coarsely crystalline texture and are thought to represent a larger grain size in the original fabric and/or a less proportion of the clay matrix.

Like the sister concretion, an abundance of graptoloids is found on the basal dissolution surface (Figure 4.68A). Ninety-one rhabdosomes were counted on layer 5 (average per layer = 38, n = 6). Of these, 79 were siculae representing 80% of the count. This is similar to the average calculation of siculae percentage from the dissolution surface 75%. This layer may correspond to a dark lamina that is identified more easily in thin section (Figure 4.68E). No major sedimentological or taphonomic observations aid in the interpretation of the taphofacies or depositional environment. This concentration of graptoloids at the base of the two conjoined concretions CM 74.9a and CM 74.9b is likely a subtle change in the relative rate of sediment and graptoloid rhabdosome supply. The dark lamina is suggestive of a decrease in the rate of sediment input that concentrated the graptoloids and other dark organic matter. Evidence of fragmentation of two mature rhabdosomes from CM 74.9a, layer 6, may be related to prolonged exposure at the sediment water-interface. This may also be related to the occurrence of the rare species, *Pristiograptus* cf. *variabilis* that is unique to the two basal residues. The combined effects of a slight decrease in sediment supply and a slight increase in graptoloid supply concentrated the graptoloid rhabdosomes.

Concretion: CM 75.5

Lithofacies: 5, finely laminated, clay/organic-rich
Graptoloid distribution: non-random ($\chi^2/n= 8.82$)
Taphofacies: graptoloid bloom
Paleoecological event: bloom in *Pristiograptus regularis regularis*

Medium greyish-brown laminae that are gradationally in contact with light orange-brown laminae characterize this very fine-grained carbonate concretion (Figure 4.70B).

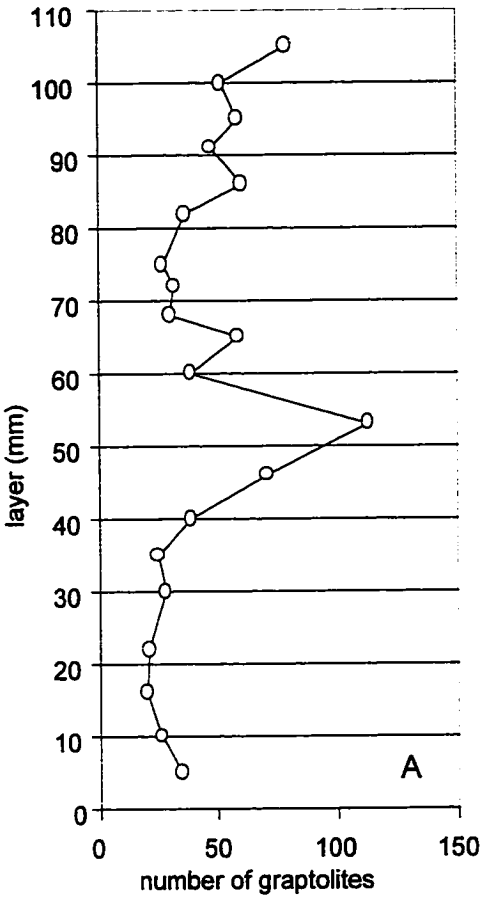

Figure 4.70. Concretion CM 75.5. A. Distribution of graptolite rhabdosomes vertically through the concretion. The increase in graptolites at layers 46 and 53 is accommodated by all graptolite sizes (siculae and mature). B. Digital scan of polished slab aligned with dissolution layers. The thin laminae are often in gradational contact. The light laminae at layer 52 and 40 are in sharp, irregular(?) contact with medium brown beds below. Sharp contacts also exist at 70 and 94 mm. Graptolites seen in cross section are more common between layers 40-80. C. Digital scan of thin-section. Average crystal size is 20 μm (range 10-60 μm) with a coarser crystal size in the lighter laminae. A possible original fabric was visible and grains were measured to have an average diameter of 5 -10 μm. These grains visible in normal and polarized light were in grain-to-grain contact and overprinted with the coarser carbonate fabric. Magnification x1.5.

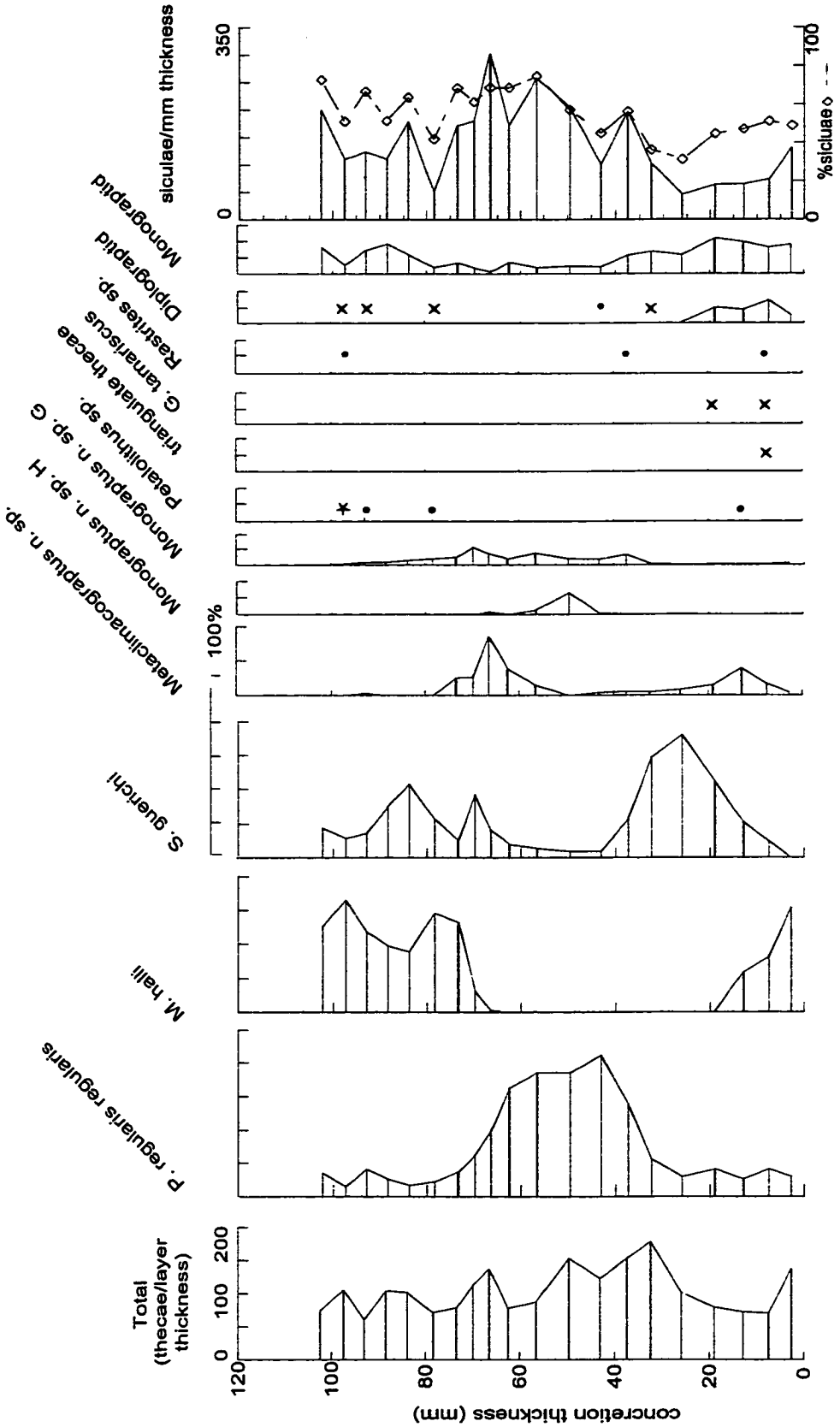

Figure 4.71. Percentage distribution of graptolite species from the dissolution residues of concretion CM 75.5: * 5-10%, × 1-5%, • < 1%

Laminae average 4 mm in thickness. Graptoloids observed in cross-section on the polished slab are common in both the dark and light brown laminae and are more abundant from layers 40 to 80. At layer 52 a light brown bed is in sharp, irregular contact with the darker bed below. This contact becomes gradational towards the centre of the concretion. At layer 70, a dark bed grades up to a light bed over 1 mm. At layer 94, a very light bed 1mm thick is in sharp contact with the bed below and in gradational to sharp contact with the bed above. This layer is discontinuous.

In thin section, the concretionary carbonate crystals range in size from 10-60 μm with an average crystal size of 20 μm (Figure 4.70C). The crystals are interlocking and visible in plane-polarized light. Smaller silica grains (5 – 10 μm) comprise less than 1 percent of the sample. These silica grains are in contact with grains of a similar size that are over-printed with the coarser grained, carbonate crystal texture. The lighter laminae contain larger carbonate crystals and larger grains. This is most likely recording a variation in the original grain size.

An abundance of graptoloids was observed on all 20 layers during the dissolution (Figure 4.70A) with a total of 901 rhabdosomes (426 "monograptids", 18 "diplograptids", 457 siculae). Three layers had a statistically greater number of rhabdosomes (layer 46, 71 rhabdosomes; layer 53, 113 rhabdosomes; layer 105, 79 rhabdosomes; average number of rhabdosomes per layer for concretion = 45, n=20). Evidence of fragmentation prior to burial is seen on layer 86. All mature "monograptid" rhabdosomes on layers 72 and 91 are fragmented; however, timing and cause of the fragmentation is uncertain.

The thecal counts identify three dominant species: *Monograptus halli*, *Spirograptus guerichi, and Pristiograptus regularis regularis.* *Pristiograptus regularis regularis* dominates the mid-concretion residues (layers 37-62). *Monograptus* n. sp. I and *Monograptus* n. sp. H are minor components of this mid-concretion assemblage and they are rare (*Monograptus* n. sp. H) or absent (*Monograptus* n. sp. I) from the basal and top residues. *Monograptus halli*, and *S. guerichi* follow a similar pattern of occurrence, although not identical. Together, they comprise most of the thecae at the top and base of the concretion. *Metaclimacograptus* n. sp. A, *Petalolithus* sp. and *Rastrites* sp. are minor components of this assemblage. *Monograptus halli* is predominant in the basal residues and *S. guerichi* succeeds in dominance in the mid-basal residues. *Glyptograptus*

tamariscus is found only in the near-basal residue 5-10. Total abundance although variable through the concretion does not identify one residue or one section of the concretion as having a peak abundance. These residues between 22 and 60 plot as slightly more abundant. These residues sample the graptoloid concentration layer observed during the dissolution of layer 46 and layer 53. The siculae show an even greater increase in the mid-concretion residues. Sicular abundance from layer 53-68 has an average count of 345 siculae/mm thickness and represents 71% of the total count. This compares with the average siculae percentage of 55%. Relative to the distribution of siculae through the rest of the concretion and relative to the thecal counts, siculae are very abundant in these strata. This abundance could be the result of taphonomic concentration or an abundance in the biocoenosis.

The two graptoloid assemblages described above are not seen to be related to a particular lithology or to the presence of unique sedimentary features. The concretion displays an even layering of fine-grained sediments characteristic of hemipelagic-type environments. The shifting dominance of the two graptoloid assemblages is possibly related to changes in the paleocommunity. The abundance of the assemblage dominated by *P. regularis regularis* in the residues and on the dissolution surfaces is interpreted to be a bloom in the biocoenosis. *P. regularis regularis*, present in minor abundance in the basal and top residues, "bloomed" during the time represented by the mid-concretion strata at the ecological cost of the other graptoloids in the assemblage. The duration of this dominance is unknown but can be estimated to be on the order thousands of years (Chapter Eight). A shift in environmental conditions or ecological relationships within the graptoloid community caused a collapse of this dominance and returned the biocoenosis to an assemblage similar to, but slightly altered from the pre-bloom assemblage.

Concretion: CM 84.5

Lithofacies: 5, finely laminated, clay/organic-rich
Graptoloid distribution: random ($\chi^2/n= 1.86$)
Taphofacies: random flux of graptoloids and sediment

Lamination is weakly present in this concretion (Figure 4.72B). Laminae are defined by the distribution and orientation of the patches of darker material and the variation in crystal size. In the polished slab these darker patches average 1 mm in length. A core is visible in the cut and polished slab and the dark patches are observed to be more common in the vicinity of the core. It is assumed, therefore, that these patches are not primary textures but diagenetic in origin. Concretionary carbonate crystals range in size from 10 – 30 μm (Figure 4.72C). Crystals cannot be distinguished from the very fine grey matrix in some laminae. Pore-filling organic matter occurs at the centre of the thin section and assumed to be a part of the core of the concretion. Grains of biogenic origin (bivalves, nautiloids, graptoloids) occur throughout the thin section.

Graptoloids were rare on the dissolution surfaces with 15 rhabdosomes counted from 7 layers (Figure 4.72A). Two layers were barren and two layers contained the maximum of 5 rhabdosomes (layers 18 and 50). The low abundance of graptoloid rhabdosomes places more emphasis on smaller differences in the graptolite distribution and skews the chi-square results. Graptoloid distribution in this concretion is considered to be random, although the data did not support the chi-square null hypothesis. No thecal or sicular count data was obtained from the residues.

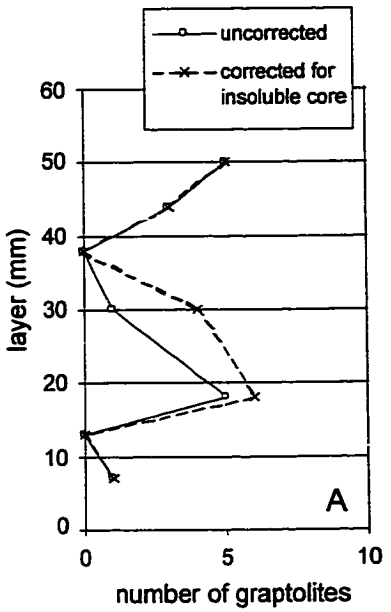

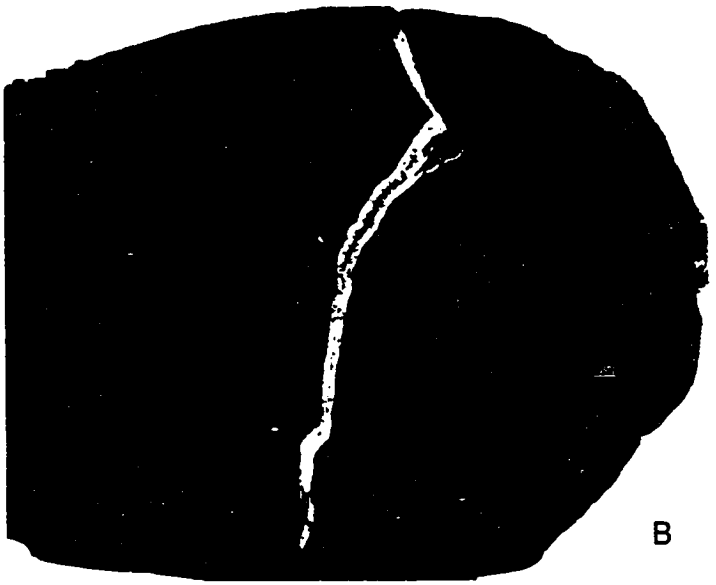

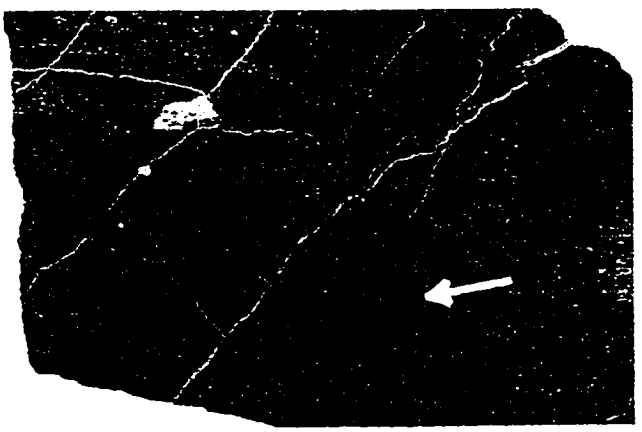

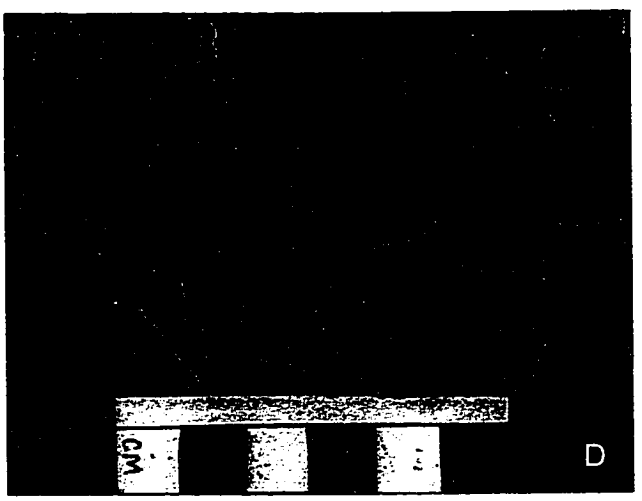

Figure 4.72. Concretion CM 84.5. A. Vertical distribution of graptolite rhabdosomes corrected for the presence of an insoluble core. B. Digital scan of polished slab showing a dark core and a calcite -filled vein. Laminae are weakly present and the bedding is defined by the orientation of flattened/elongate dark grains. Actual size. C. Digital scan of thin section. Carbonate crystals when visible are 10-30 μm. The grey-brown matrix has an indistinguishable grain size. The dark material marked by the white arrow is observed in higher magnification to be a pore-filling organic/bitumen and is likely part of the core. Magnification x1.5. D. Dissolution surface 30 revealing the oblong core.

Concretion: CM 114.4a

Lithofacies: 6, finely laminated, clay/organic-poor
Graptoloid distribution: random (χ^2/n= 1.66)
Taphofacies: random flux of graptoloids and sediment

This concretion was collected 1 m from CM 114.4b at the same stratigraphic level. The coarse laminae of this very fine-grained carbonate concretion are defined by the presence of a light orange-brown patchiness of probable diagenetic origin (Figure 4.73B). Layer 0-10 is greyish-brown with light orange-brown irregular patches that average 1 mm in length. Layer 10-15 is a homogeneous, greyish-brown with sharp basal and top contacts. Layer 15-30, and layer 50-67 are greyish-brown with light orangey brown patches that are not individual masses but one interconnected network. In layer 30-50, orange-brown laminae averaging 4 mm thick are interbedded with thin (1-3 mm) greyishbrown laminae.

Concretionary carbonate crystal size ranges from 10 to 100 μm and averages 30 μm in diameter. Laminae observed in the thin section are differentiated by crystal size and the relative amount of brown matrix (Figure 4.73C). Disseminated, dark brown organic matter represents approximately 5% of the thin section. The dark brown organic material is a bitumen infill of sponge spicules and fine-grained material disseminated through the matrix.

Data were corrected for the presence of an insoluble rim that interfered with the observation of rhabdosomes on the dissolution surfaces on three layers (Figure 4.73D). With or without, this correction the data did not support the null hypothesis of random distribution at the 10% confidence level. However, the null hypothesis was accepted at the 5% confidence level. A random distribution of the few graptoloid rhabdosomes counted seems to more accurately describe what was observed. Graptoloids were slightly more abundant on layer 53. This correlates to the base of the orange-brown layer 50-67. No thecal or sicular count data was obtained from the residues of this concretion

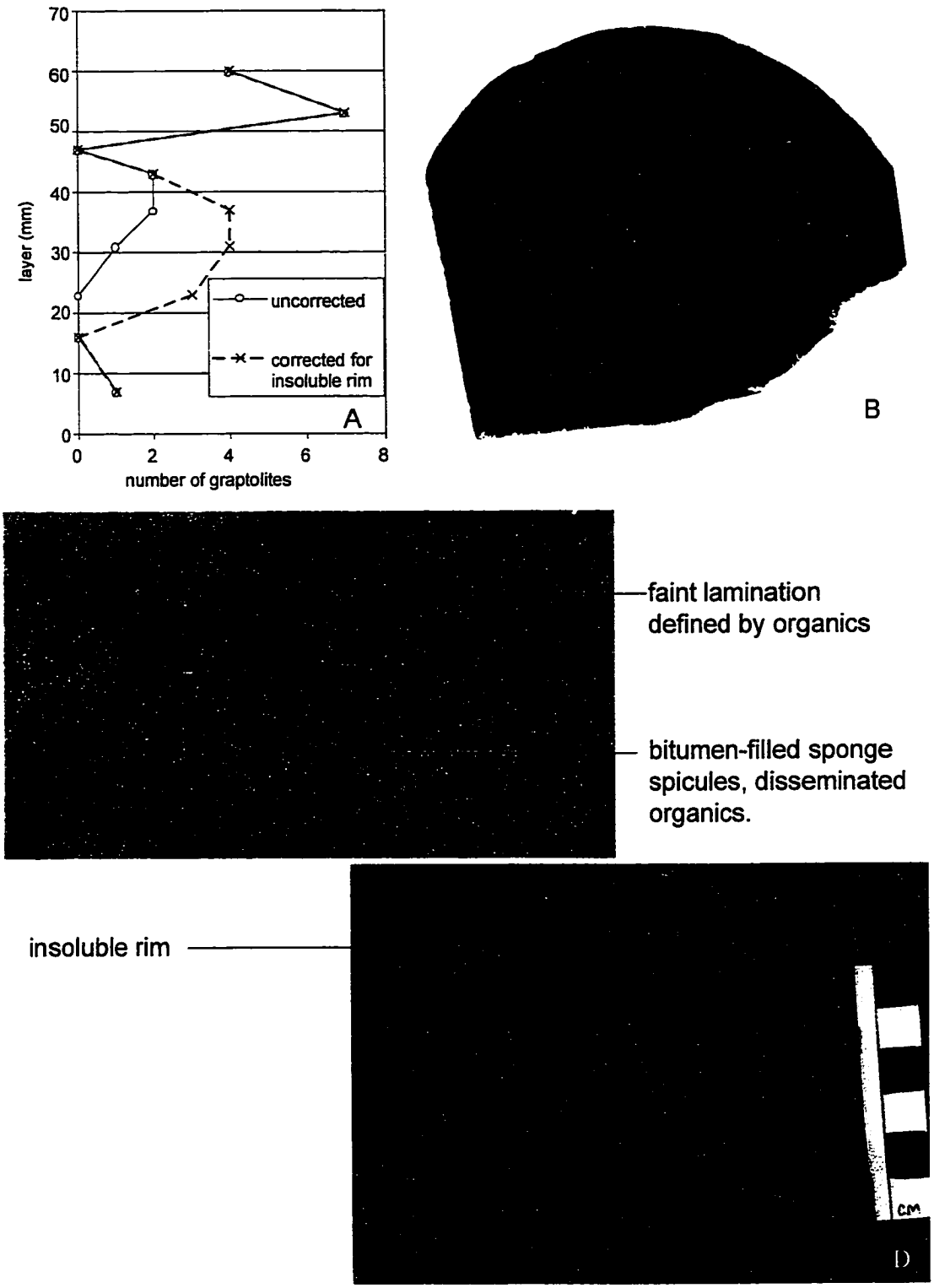

Figure 4.73. Concretion CM 114.4a. A. Distribution of rhabdosomes as recorded during the layer-by-layer dissolution. B. Polished slab aligned with the correlated dissolution layers. Actual size. C. Digital scan of unstained thin section. Magnification x1.5. D. Photo of dissolution layer 8.

Concretion: CM 114.4b

Lithofacies: 6, finely laminated, clay/organic-poor
Graptoloid distribution: random (χ^2/n= 0.71)
Taphofacies: random flux of graptoloids and sediment

This very fine-grained concretion has laminae that are greyish-brown to light orange-brown. The light orange-brown appears as irregular patches that are interpreted to be diagenetic in origin. Interlocking, concretionary carbonate crystals are 40 to 100 μm in size (Figure 4.74 C, D). The grey matrix is very fine-grained and the crystal size cannot be measured. In thin section, the laminae are defined by slight variations in the size of the carbonate crystals and the amount of the matrix material. It is assumed that the diagenetic carbonate is patterned after the original texture.

The graptoloids are not abundant on the dissolution surfaces (40 rhabdosomes total, counted on 19 layers; average of 2 rhabdosomes per layer). The graptoloid rhabdosomes counted were distributed randomly among the 19 layers before and after the correction for the presence of the core at layers 37 – 46 (Figure 4.74A). One layer associated with the core was barren of graptoloids (layer 40). Three additional layers not related to the core are also barren. Layer 67 and 70 contained many radiolarians, small gastropods and small bivalves. Minor radiolarians were found on layer 73 and 77. These more diverse faunal assemblages are associated with a homogeneous greyish-brown lamina that is 32 mm thick. No thecal or sicular count data were obtained from the residues of this concretion

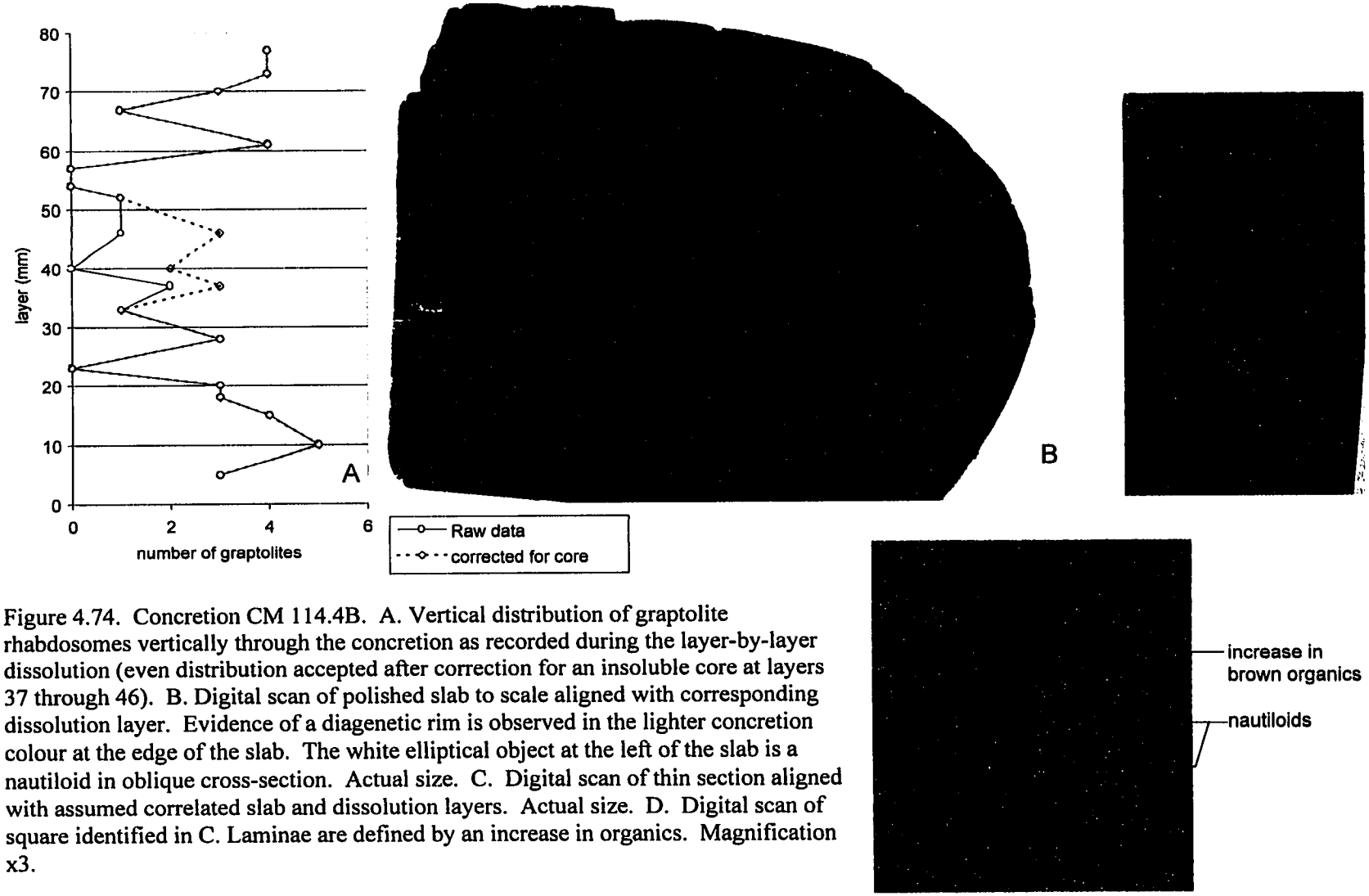

Figure 4.74. Concretion CM 114.4B. A. Vertical distribution of graptolite rhabdosomes vertically through the concretion as recorded during the layer-by-layer dissolution (even distribution accepted after correction for an insoluble core at layers 37 through 46). B. Digital scan of polished slab to scale aligned with corresponding dissolution layer. Evidence of a diagenetic rim is observed in the lighter concretion colour at the edge of the slab. The white elliptical object at the left of the slab is a nautiloid in oblique cross-section. Actual size. C. Digital scan of thin section aligned with assumed correlated slab and dissolution layers. Actual size. D. Digital scan of square identified in C. Laminae are defined by an increase in organics. Magnification x3.

Concretion: CM 96-6 loose

Lithofacies: 7, graded laminae, clay/organic-rich, compressed graptoloids
Graptoloid distribution: random (χ^2/n= 1.2)
Taphofacies: sedimentologic event – low graptoloid abundance

This very fine-grained carbonate concretion comprises well-defined, dark and light brown, continuous laminae (Figure 4.75B). Buff-coloured spheres and elongate dark brown patches in a matrix of light brown is the predominant pattern. Seventeen distinct laminae averaging 3 mm in height are defined by the distributions of the brown and buff patches. The contacts between the laminae are most often sharp and some show irregular (erosional?) bases. Evidence for current activity is preserved in three layers. Lamina 42-38 is a pale layer with darker brown patches defining faint cross-bedding (wave length 4 mm, amplitude 0.75 mm). Lamina 75-65 has a sharp irregular base that grades from a pale brown to a darker brown top. A second graded lamina 82-75 has a similar colour pattern. Both are assumed to represent normally graded beds. In thin section the carbonate crystals range from 50 to 100 μm (Figure 4.74C, D). The cross-bedding observed in lamina 38-42 is weakly visible in the thin section.

Although the chi-square analysis statistically demonstrates that the graptoloids are randomly distributed among the layers examined, the three layers with the most rhabdosomes are also associated with the darker bands and the graded beds identified in the polished slab analysis. Fragmented graptoloids were identified on layers 17, 22, 32, and 53. None was clearly fragmented prior to burial or processing. A bitumen-rich core was revealed on layers 40 to 53. Nautiloids and a small brachiopod were also discovered on dissolution surfaces (layer 22 and 45). No thecal or sicular count data were obtained from the residues of this concretion

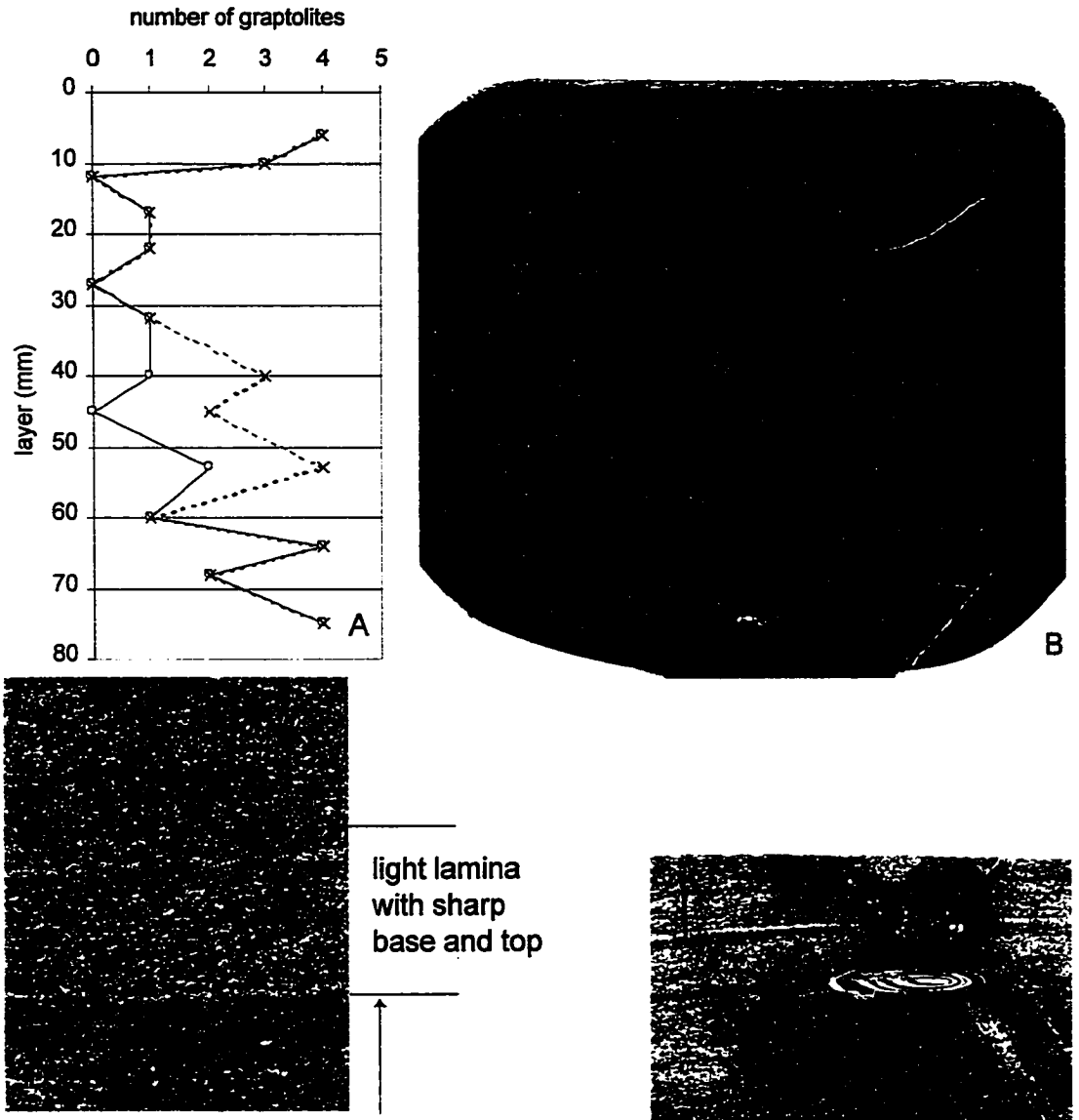

Figure 4.75. Concretion CM 96-6 loose. A. Distribution of graptolites vertically through the strata recorded from the dissolution surfaces corrected for an insoluble core. B. Digital scan of polished slab aligned with dissolution surfaces. The dark laminae correlate to statistically insignificant graptolite increases. Some of the laminae grade from a light brown base to a dark brown top. C. Digital scan of acid etched thin-section showing a basal graded lamina. Magnification x1.5. D. Graded lamina with a light lamina above in sharp contact. Magnification x3.

Cape Phillips section concretion descriptions

Concretions from the Cape Phillips section with low graptoloid abundance

Most of the concretions sampled from the Cape Phillips section contained less than three graptoloids on a dissolution surface, and thus the frequency of taphonomic observations was greatly reduced. Also, most of these concretions showed a random vertical distribution of the few graptolites that were counted from the dissolution surfaces. The concretions were considered to be members of the "sedimentologic event, low graptoloid abundance" taphofacies if the sediment recorded graded laminae (microlithofacies 8); or members of the " random flux of graptoloids and sediment" if the sediments were finely laminated (microlithofacies 6).

Concretions of microlithofacies 8 and taphofacies " sedimentologic event, graptolite dilutioninclude: CP 32 (Appendix F, Figure F1), CP 38.4 (Appendix F, Figure F2), CP 96 (Appendix F, Figure F3), and CP 145.2 (Appendix F, Figure F3). A brief description of each concretion is included in the figure caption of the Appendix F figures. Although each concretion is unique and there are some interesting diagenetic features preserved in the concretions such as the compressed graptolites in CP 38.4 and CP 56.9 and the septarian cracks of CP 38.4, I have decided to describe them as one group. To do this, Concretion CP 56.9 (Figure 4.76) will be described as a representative sample of this group of concretions.

Concretions of microlithofacies 6 and taphofacies "random flux of graptoloids and sediment" include: CP 146.5a (Appendix F, Figure F4), CP 146.5b (Appendix F, Figure F4), CP 152a (Appendix F, Figure F6), and CP 152b (Appendix F, Figure F6). These concretions are similar to the group classified as "sedimentologic event, low graptoloid abundance" with the exception that the sediments of these concretions do not record features indicative of a sedimentary event such as graded beds. Because of the similarity between these two groups they will be described together.

Concretion: CP 56.9 (representative)

Lithofacies: 8, graded laminae, clay/organic-poor, (compressed graptoloids)
Graptoloid distribution: random (χ^2/n= 1.02)
Taphofacies: sedimentologic event, low graptoloid abundance

Thin light brown and medium brown laminae (average 0.5 mm thick) characterize this very fine-grained carbonate concretion (Figure 4.76B). The laminae are both continuous and discontinuous. Layer 66-75 displays a faint grading in colour from a light base to a darker top. Relative heterogeneity of clast type defines the laminations. This lamination style is a characteristic of all of the concretions of this group. Bedding parallel rip-up clasts and radiolarian molds are observed in both polished slab and thin section. In the other concretions of this group fossil fauna other than graptolites and radiolarian were found, including nautiloids, hectinae sponge spicules, spicule masses with spicules in lattice arrangement, and small brachiopods. A darker core is dissected by the slab surface. The core has a light brown nucleus and shows a deflection of the internal layering and perhaps identifies the lithification of a primary concretion prior to some compaction. A core is also observed in CP 32.

In thin section, the darker brown grains are honey-brown in plane-polarized light and opaque in cross-polarized light (Figure 4.76C). The grains are oval in cross-section and flattened in the plane of bedding. They range in size from 0.05 to 0.7 mm, average 0.1 mm and comprise approximately 5 % of the thin section. Some of the larger grains may be preserved fecal pellets or peloids. This is the only concretion of this group with these fecal pellets or peloids. The darker grains are more concentrated at the base of the graded beds (seen in thin section and slab). The matrix of the concretion is grey in colour with a grain size too small to be discerned. Within this matrix are darker grey grains approximately 0.1 mm in diameter. The carbonate crystals are 50 to 150 μm. Larger carbonate crystals are observed in the cross-section of a partially compressed nautiloid preserved at the base of the thin section.

Graptoloid rhabdosomes occur randomly through the concretion (Figure 4.76A). Chi-square analysis identifies a random distribution among the 13 layers. This low abundance and random distribution of graptoloids is characteristic of this group. The

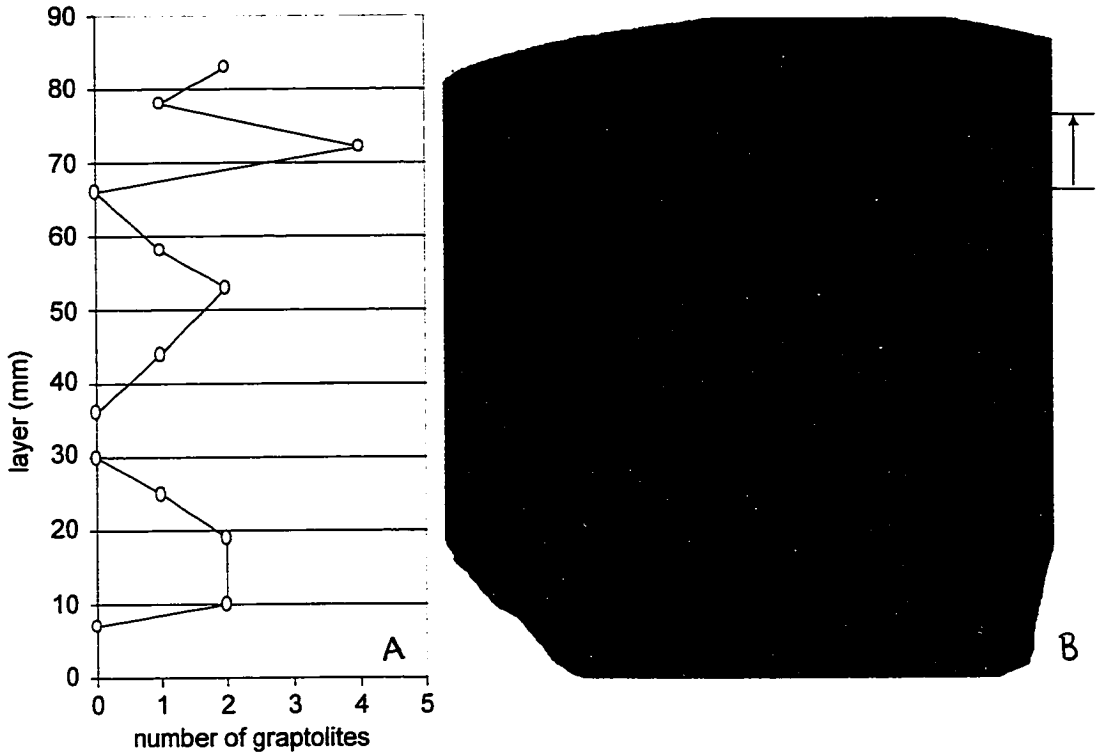

Figure 4.76. Concretion CP 56.9. A. Vertical distribution of graptolite rhabdosomes as recorded during dissolution. B. Digital scan of polished slab. Minor dark brown grains and light brown grains flattened in the plane of bedding are visible in the medium brown matrix. Thin light brown laminae are both continuous and discontinuous. The variation in preservation of the laminae at the center of the slab is probably related to diagenesis although an insoluble core was not observed during dissolution. Layer 66-75 displays a grading in colour from a light base to a medium brown top. C. The dark "grains" range in size from 50-70 μm (average 10 μm.) and represent approximately 5% of the sample. In normal light they are golden brown and in cross-polarized light they are opaque. Often they are flattened in the plane of bedding and help define laminations. The grey-brown matrix is very fine-grained. Carbonate crystals range in size from 50-150 μm. Compressed nautaloid at the base is composed of 100-300 μm size silica crystals. Magnification x1.5

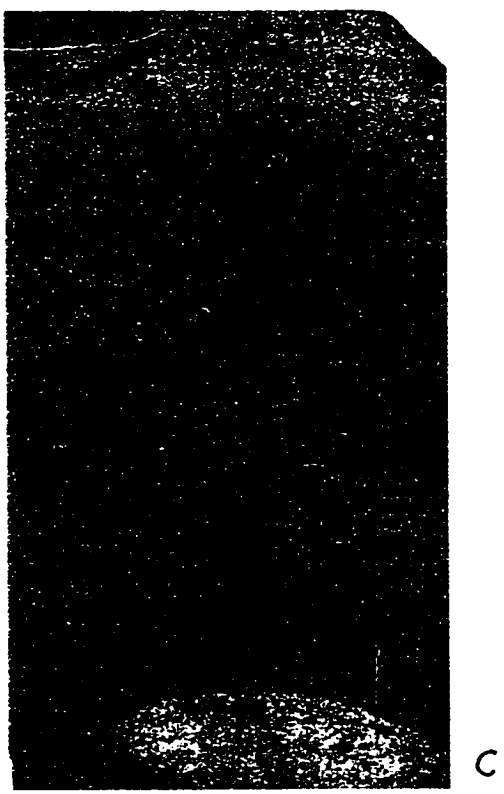

lack of graptoloids may be the result of taphonomic bias and encrustation. The only clear graptoloid rhabdosome was a large "monograptid" on layer 40 that had been pyritized during diagenesis. I observed cylindrical masses of lighter material the size of elongate graptoloid rhabdosomes on most dissolution surfaces. Perhaps the graptoloids are severely encrusted, beyond recognition. The pyritized graptoloid, for some reason, was perhaps not susceptible to the same diagenetic fate as the others and was not encrusted.

Concretions of the "physical addition of graptoloids" taphofacies from the late Telychian

Three concretions of three different taphofacies display graptoloid concentration beds that appear to be the result of physical transport of the rhabdosomes. Concretions CP 148.1 (Figure 4.77), CP 150.6 (Appendix F, Figure F5), and CP 152a (Appendix F, Figure F6) were all classified in the same taphofacies, physical addition of graptoloids. However each of these concretions is of a different microlithofacies: CP 148.1, microlithofacies 8; CP 150.6, microlithofacies 9; CP 152a, microlithofacies 6. Concretion CP 148.1 is described as a representative from this group. CP 152b (Appendix F, Figure F5) collected from the same stratigraphic interval as CP 152a does not contain a graptolite concentration bed. The concretion CP 152b is of microlithofacies 6 and the taphofacies "random flux of graptoloids and sediment".

Concretion: CP 148.1 (representative)

Lithofacies: 8, graded laminae, clay/organic-poor.
Graptoloid distribution: non-random ($\chi^2/n= 13.75$)
Taphofacies: physical addition of graptoloids - low energy

Thin, well-defined continuous laminae of light brown and medium greyish-brown characterize this very-fine-grained carbonate concretion (Figure 4.77B). The laminae are deflected around the core of the concretion. It is assumed that this records the early lithification of the centre of the concretion that preserved the sediment in a more uncompacted nature than the rest of the concretion. It is not thought to be evidence of sediment deposition around an object that created an uneven topography on the seafloor

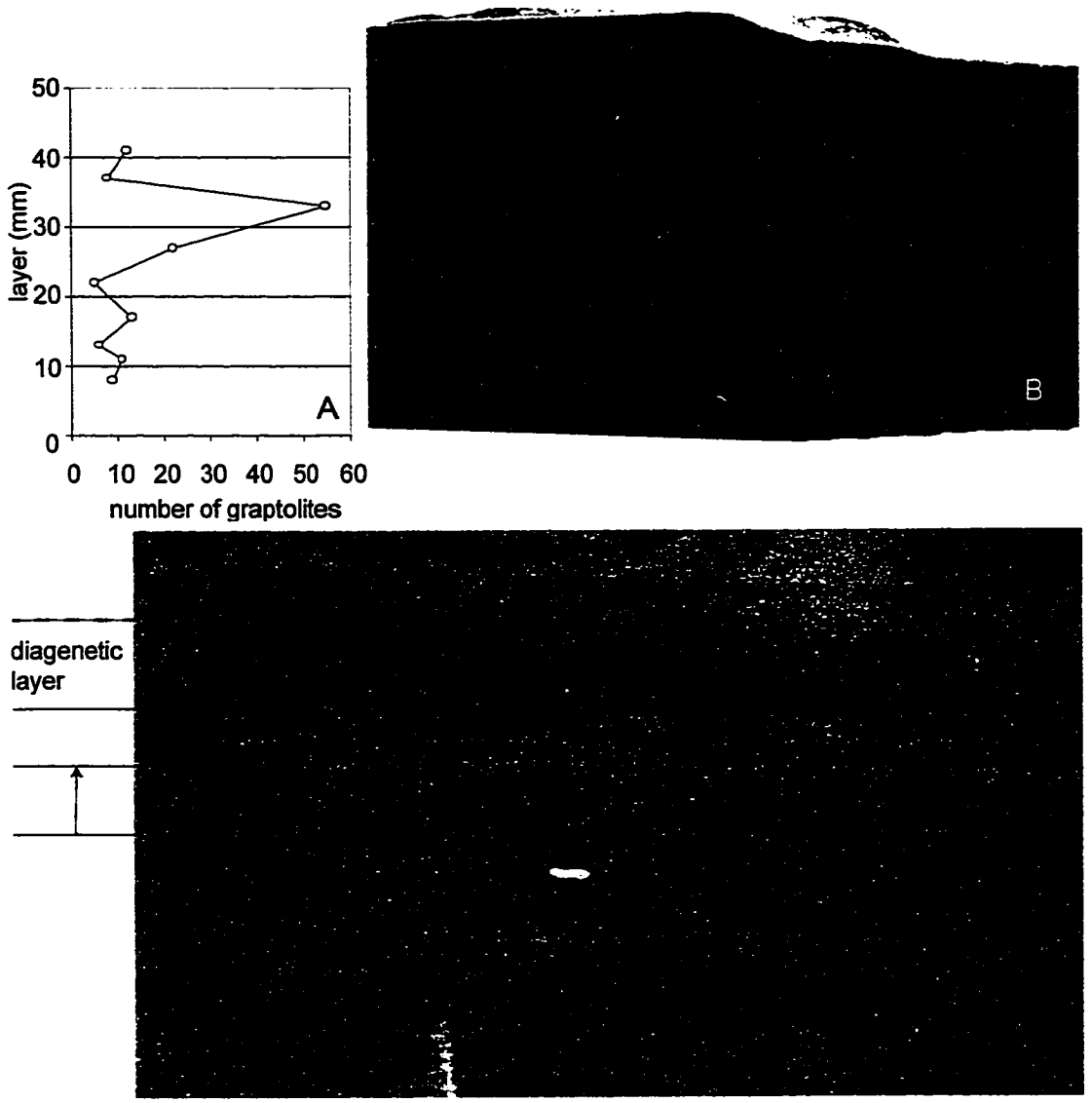

Figure 4.77. Concretion CP148.1. A. Distribution of graptolite rhabdosomes vertically through the concretion. The abundance of rhabdosomes at layer 33 is accommodated by a large increase in siculae. B. Digital scan of polished slab of alternating thin laminae of light and medium brown. Laminae are deflected around and continue within an object at layer 35-45 that is possibly a nodule formed prior to main concretion formation. No core was observed during dissolution. Lamina at layer 29-34 grades from a light brown to a medium brown and this corresponds to the increase in rhabdosomes at layer 33. C. Digital scan of thin section. Diagenetic layer that corresponds to the nodule at layer 35 appears as a reversely graded bed (dark to light brown upconcretion). At the base a grey-brown, very fine-grained matrix dominates. Up-concretion the grey masses become more distinct and the top is more heterogeneous with shell fragments and darker brown grains. The graded bed in slab is not so clear in thin-section (dashed arrow). Magnification x2.

since the laminae can be traced into the core. Layer 38-43 is a light orangey-brown with thin, continuous medium brown laminae. The base is sharp and the top is a gradational contact (over 1 mm) with the layer above. The width of layer 38-43 changes from 5 mm to 13 mm (layer 33-46) as the laminae are deflected around and continue within the core. Layer 41-55 is medium brown with thin laminae of light orange-brown..

Layer 0-38 is medium brown with thin laminae (0.5-2 mm) of light orange-brown. All contacts are sharp. Within this unit is layer 29-34 that grades from a pale peachy-brown base to a medium brown top. This graded bed corresponds to the increase in graptoloid rhabdosomes on the dissolution surface of layer 33 (Figure 4.77A). Fifty-one siculae on layer 33 account for all but 4 of the rhabdosomes of that layer. The mature "monograptid" that is found on this layer is fragmented. No clues are revealed as to the cause of fragmentation (taphonomic or processing). There are two nautiloids on this surface (1.5 and 2.5 cm long). It is likely that the nautiloids are from a deposition event previous to, or following this layer, but because of their relief they are revealed on this layer as well.

A very fine carbonate matrix texture dominates the thin section from this concretion (Figure 4.77C). The grain size of this grey-brown "matrix" was indistinguishable. Dark brown grains with well-defined boundaries range in size from 30 to 60 μm and represent 1-3 % of the thin section. Some of these grains are spheroidal (circular in cross-section). A graded bed almost 1 cm in height is composed of closely packed, homogeneous, grey matrix at the base. The top of the layer is composed of larger, more distinct grey masses, and a more heterogeneous mix of shell fragments and darker brown grains. This matches the description of the graded bed from layer 29-34 that grades from a light base to a medium brown top. It is possible that the base has been recrystallized to form what appears as a massive carbonate layer. It is uncertain whether this is a normally or reversely graded bed. If this is a fining-upwards, graded bed the graptoloids may be at the top because of their ability to stay in suspension as a result of the rhabdosome structure.

Concretions of microlithofacies 9, low graptolite abundance, random distribution

Four concretions from the upper Telychian will be described together because of the similarity of lithology, lamination style and graptolite distribution and abundance. Concretions CP 162.8 (Figure 4.78), CP 163a (Appendix F, Figure F7), CP 163b (Appendix F, Figure F7), and CP 163.1 (Appendix F, Figure F8) were all classified in the taphofacies "sedimentological event, low graptoloid abundance". The clast type was heterogeneous with all of these concretions containing shelf-derived shelly fauna, including crinoid ossicles and a hemispherical coral or bryozoan.

Concretion: CP 162.8 (representative)

Lithofacies: 9, graded laminae, heterogeneous clasts.
Graptoloid distribution: random ($\chi^2/n= 1.17$)
Taphofacies: sedimentologic event, low graptoloid abundance

This very fine-grained carbonate concretion contains laminae that are defined by colour variation on the polished slab. Variation in the distribution of diagenetic patches may reflect original variation in grain size or grain sorting. The light patches are white to buff and have a sharp boundary with the surrounding medium-brown matrix. During dissolution, these light-coloured patches appear as spherical and elongate insoluble (silica?) nodules. Radiolaria are associated with the nodule layers and may be the biogenic source for the silica. The dark patches have a gradational boundary with the same matrix.

In thin section, it is observed that concretionary carbonate crystals average 30 to 60 μm. Silica-filled voids are composed of larger crystals. These are most likely the thin section representation of the nodules identified in polished slab and during dissolution. The silica was precipitated in voids, possibly created by organic decay of radiolarians or other microfossils. The dark laminae have smaller concretionary carbonate crystals and a greater amount of very fine-grained brown matrix. Light laminae are associated with coarser concretionary carbonate crystals and less matrix. This most likely reflects a coarser grain size of the original fabric. Cross-bedding is evident in a 4-6 mm thick layer

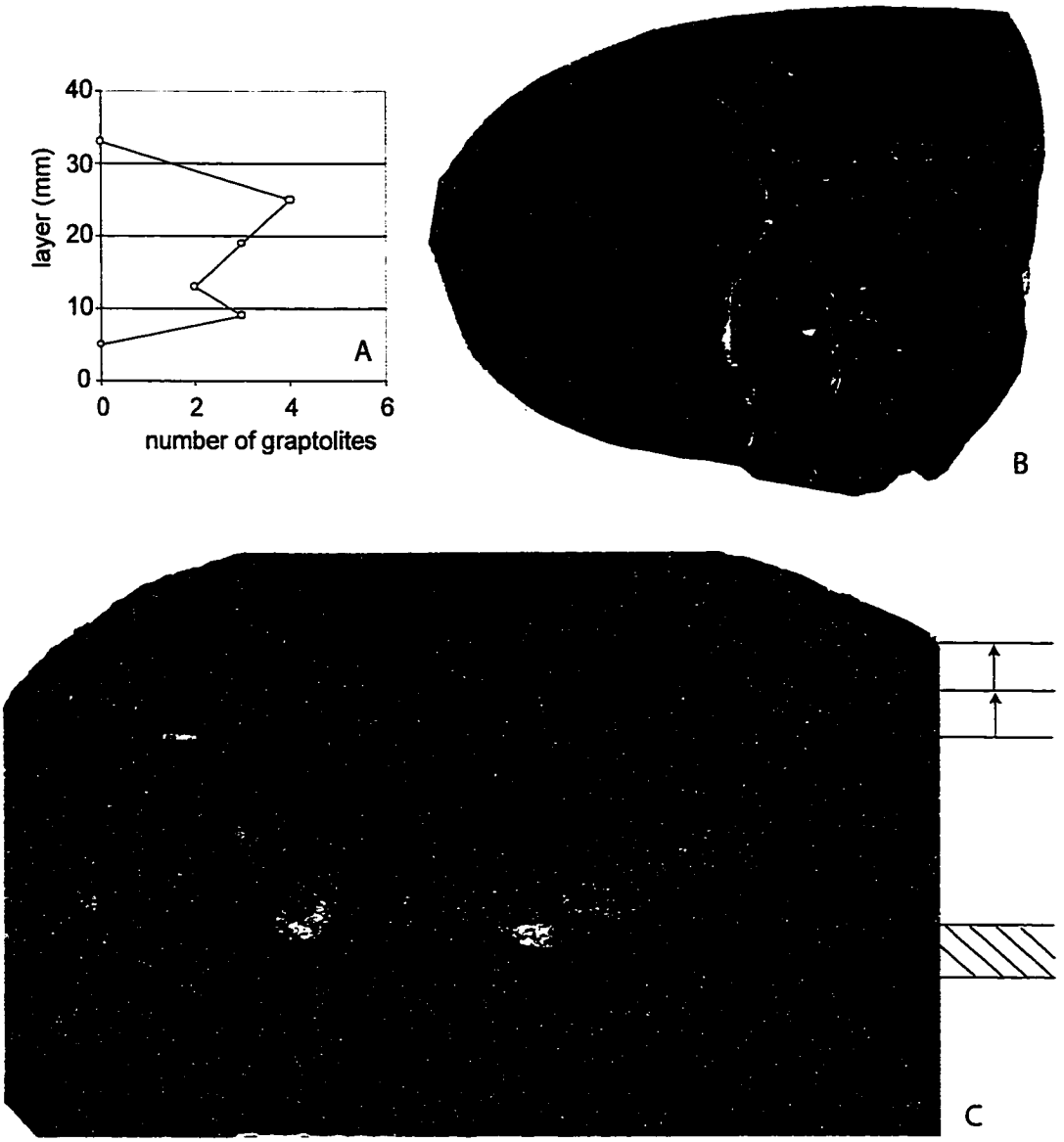

Figure 4.78. Concretion CP 162.8. A. Vertical distribution of graptolite rhabdosomes as recorded during dissolution. B. Digital scan of polished slab aligned with corresponding dissolution layers. The white irregular shaped patches are diagenetic silica that is preferentially precipitating in some layers perhaps indicating a higher original porosity/permeability in those layers. C. Digital scan of thin section. The diagenetic silica is visible throughout the concretion and forms larger crystals than the concretionary carbonate that ranges 30-60 μm. in size. The dark laminae lack the silica crystals and contain more of the matrix. Within the dark laminae some oval masses may be peloidal. Brown matrix delineates the cross-sets of the crossbedded lamina identified. Two graded laminae are defined by sharp basal and top contacts and a grading of colour from medium to light brown. Up orientation arrow is correct. Magnification x2.

that begins 12 mm from the base of the dissolution. This cross-bedding was only visible in thin section and was defined by darker laminae that lap down onto the 12mm surface. The base of the cross-bedded layer consists of a dark lamina, 1 to 2 mm thick. Cephalopods and other fauna are preferentially found in this cross-bedded layer. The cross-bedding and the associated increase in other fossil fauna (no increase in graptoloid rhabdosomes) at this interval suggest an event of higher energy.

Two graded beds are identified in thin section. They are both defined by a sharp basal contact and a grading of colour from medium to light brown. Like the cross-bedded lamina these contain a dark base and a lighter top. If these are normally graded beds than this colour gradation is the reverse of what has been identified in concretions from lower strata (e.g., CM 44.0-44.1). It is possible that the extensive silica precipitation has altered the pattern established for the lower strata. Otherwise, these are reversely graded beds and would have a different mode of formation (e.g., contourite; Stow, 1979). Without further evidence the assumption of normal grading is maintained. The cross-bedded layer, together with the graded beds is a record of a higher energy, multiple sedimentary event. Unfortunately, the two graded beds were not dissolved layer-by-layer and therefore no relationship can be established between the graded beds and the distribution of graptoloids. On the 6 layers examined, the graptoloid abundance was low (Figure 4.78A - total for concretion was 12, maximum of 4 on layer 25). This maximum abundance corresponds to the cross-bedded, nautiloid-rich layer.

Pelmatozoan ossicles are the main components of a bioclastic layer at 0-3 mm. A light brown, more homogeneous layer exists at layer 18-23 along with two large, irregular shaped objects that appear to be filled with a precipitate. Layer 30 –34 and 35 – 40 are also paler and less heterogeneous in colour.

Crystal size was difficult to discern in thin section. The concretionary carbonate matrix was medium brown with a grain size too fine to measure. Within the matrix some visible crystals averaging 30 μm in diameter filled the voids (Appendix F, Figure F7E). These filled voids are roughly circular with undefined boundaries and they appear white in plane polarized light. They are interpreted to be radiolarian molds that were altered through the process of diagenesis. The voids average 0.25 mm in diameter and represent 3-5 % of the sample. Similar sized brown patches, also with undefined boundaries

represent 1-3% of the sample. A hemispherical bryozoan or coral was sampled in cross-section at the base of the thin section. Within the voids of the bryozoan/coral and graptoloid structures, the crystal sizes are larger with a 50 – 300 μm range. The other half of this bryozoan/coral was observed during the dissolution process on layers 6 and 12 and the three-dimensional hemispherical shape determined. Layer 21-26 is composed of objects of suspected organic origin. Bedding-parallel lamination is disrupted and the layer has a coarser crystalline texture. A 5 mm long insoluble cylindrical object, not a nautiloid, was found on dissolution surface 25. This object of possible organic origin is related to the layer 21-25 observed in thin section.

Concretion: CP 214.5

Lithofacies: 9, graded laminae, heterogeneous clasts
Graptoloid distribution: non-random (χ^2/n= 199.79)
Taphofacies: physical addition of graptoloids – high energy

Concretion CP 214.5 records two depositional events that are identified in a 40 - 58 mm thick graptoloid-rich layer. The events are defined by distinct graptoloid assemblages, size-sorting, rhabdosome fracture and bending, and current aligned elongate graptoloids. Two slabs, were prepared from two off-cuts that were oriented perpedicular to one another. (Figure 4.79, 4.80). The basal lamina comprises 0.01-0.3 mm long bedding-parallel rip-up clasts (5%), and white irregular-shaped grains 0.5-0.2 mm (10%), in a matrix of light brown with immeasurable grain size. Radiolarian molds with pyrite and silica or calcite infill average 0.3 mm in diameter and comprise approximately 1% of the sample. The laminae are defined by a variation in the percentage of white and brown grains. Internal laminae are 1-3 mm thick and continuous across the slab. This first unit has a topography of at least 15 mm (Figure 4.79). The 16 mm thick lamina above is rich with graptoloids with an average diameter of 1.2 mm (taphocoenosis 1 of Figure 4.80, 4.81). These graptoloids are aligned., filled with cement (calcite or silica), and are in a light brown matrix. The base of this layer truncates the laminae below and has the morphology of a scour (Figure 4.81A, B). Rhabdosomes are more common in the deepest part of the scour where they are in contact. Elsewhere in this unit the

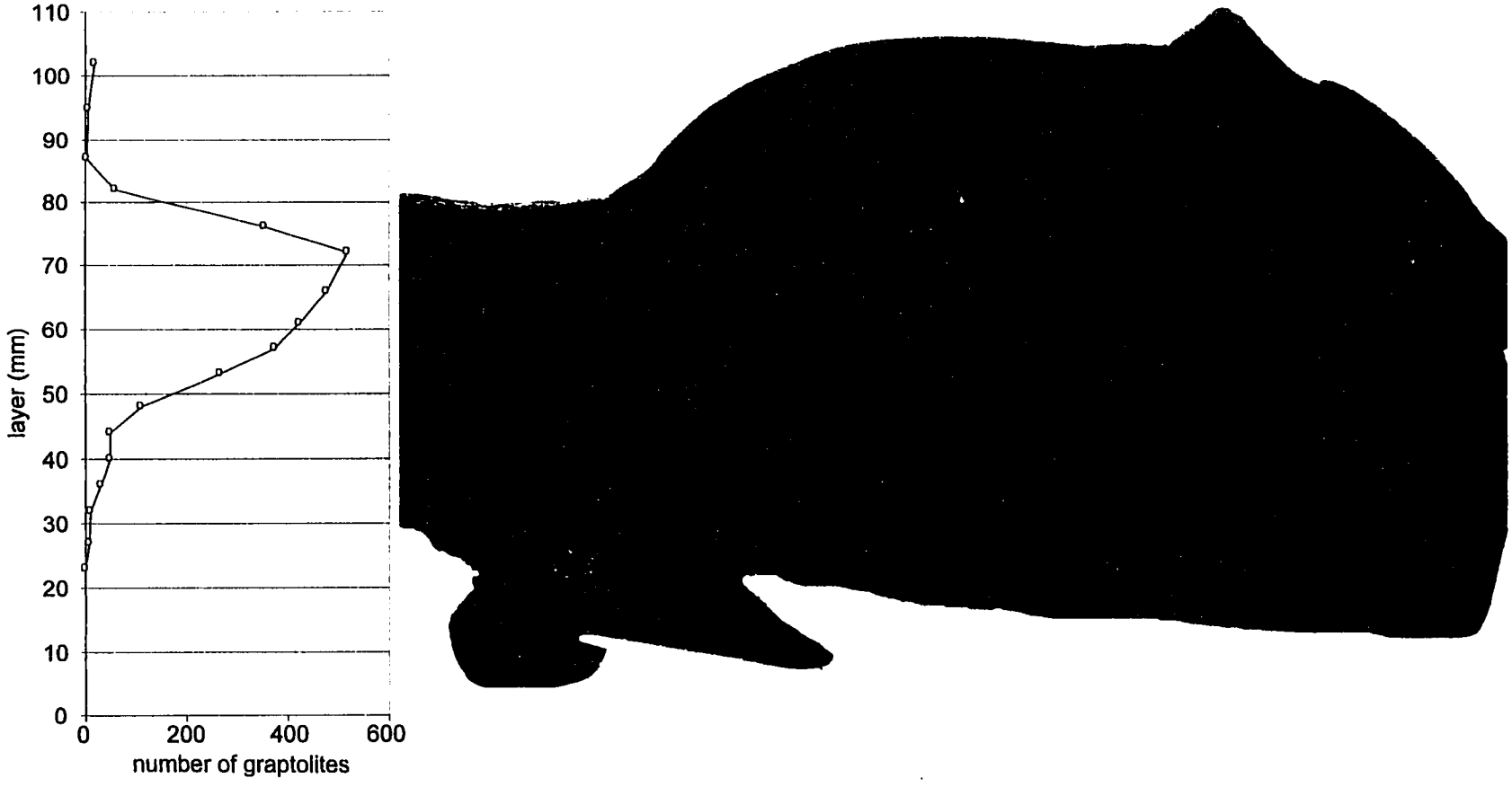

Figure 4.79. Concretion CP 214.5. A. Distribution of graptolite rhabdosomes vertically through the concretion as recorded during the dissolution process. Two taphocoenosis groups were revealed during dissolution. The group between 30 and 60 mm. was dominated by *M. instrenuus* and the second group from 60 to 80 mm. was dominated by distal fragments of a cyrtograptid. In slab these have different cross-sectional diameters. B. Digital scan of polished slab aligned with dissolution layers. The graptolite-rich layer that begins at layer 30 truncates basal laminae (closer examination in Figure 4.81). The fine laminae of alternating light and medium brown resume following the graptolite event. Actual size.

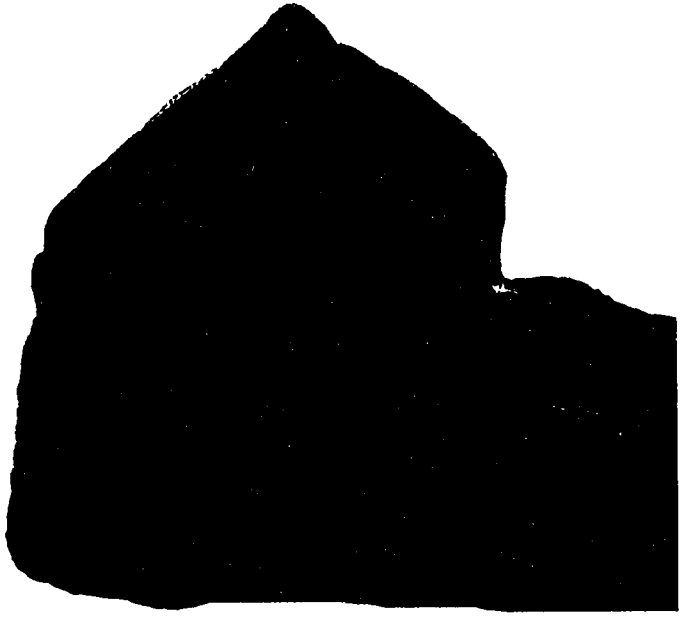

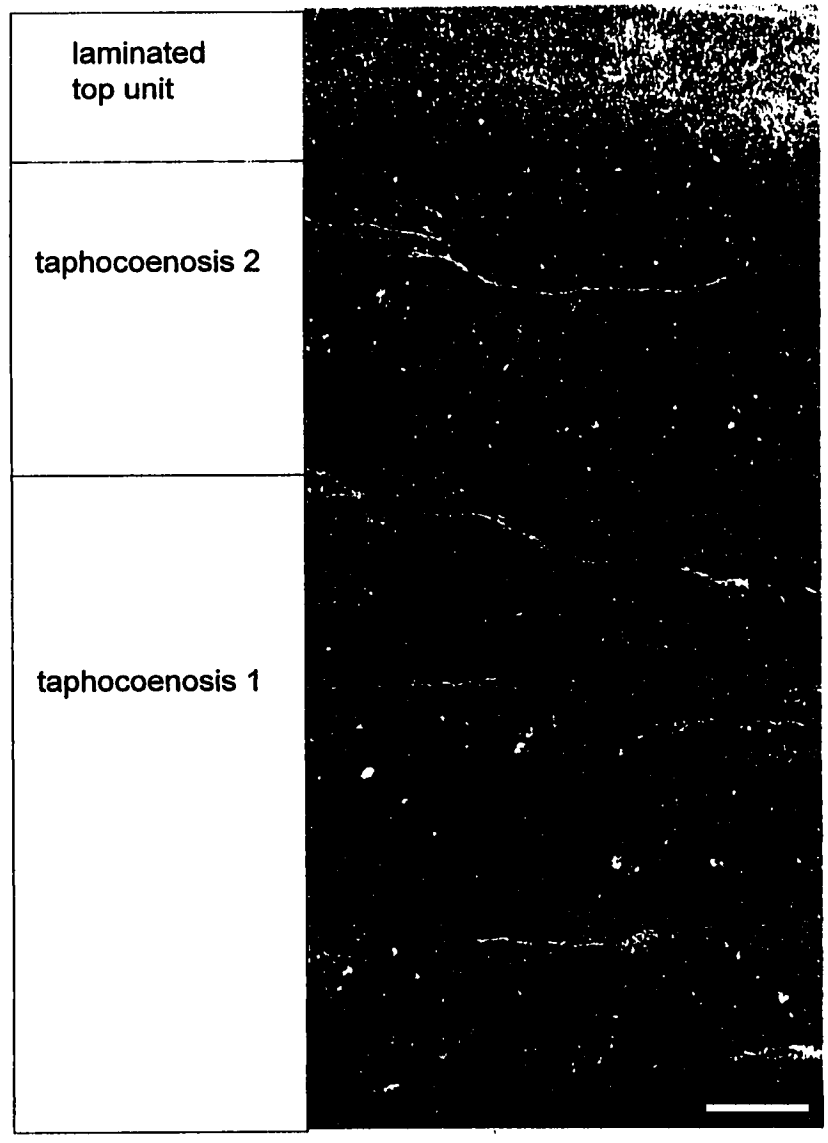

Figure 4.80. Concretion CP 214.5. A. Digital scan of polished slab (oriented perpendicular to slab shown in Figure 4.79) showing differential alignment of graptolites from taphocoenosis 1 and taphocoenosis 2.. Actual size. B. Photo of polished slab showing the graptolites in longitudinal cross-section in taphocoenosis 1 and the graptolites in rhabdosome cross-section in taphocoenosis 2. The rhabdosome diameter of the graptolites in taphocoenosis 1 is a larger than the diameter of the cyrtograptids of taphocoenosis 2. This difference helps differentiate the two groups. Scale bar = 5 mm.

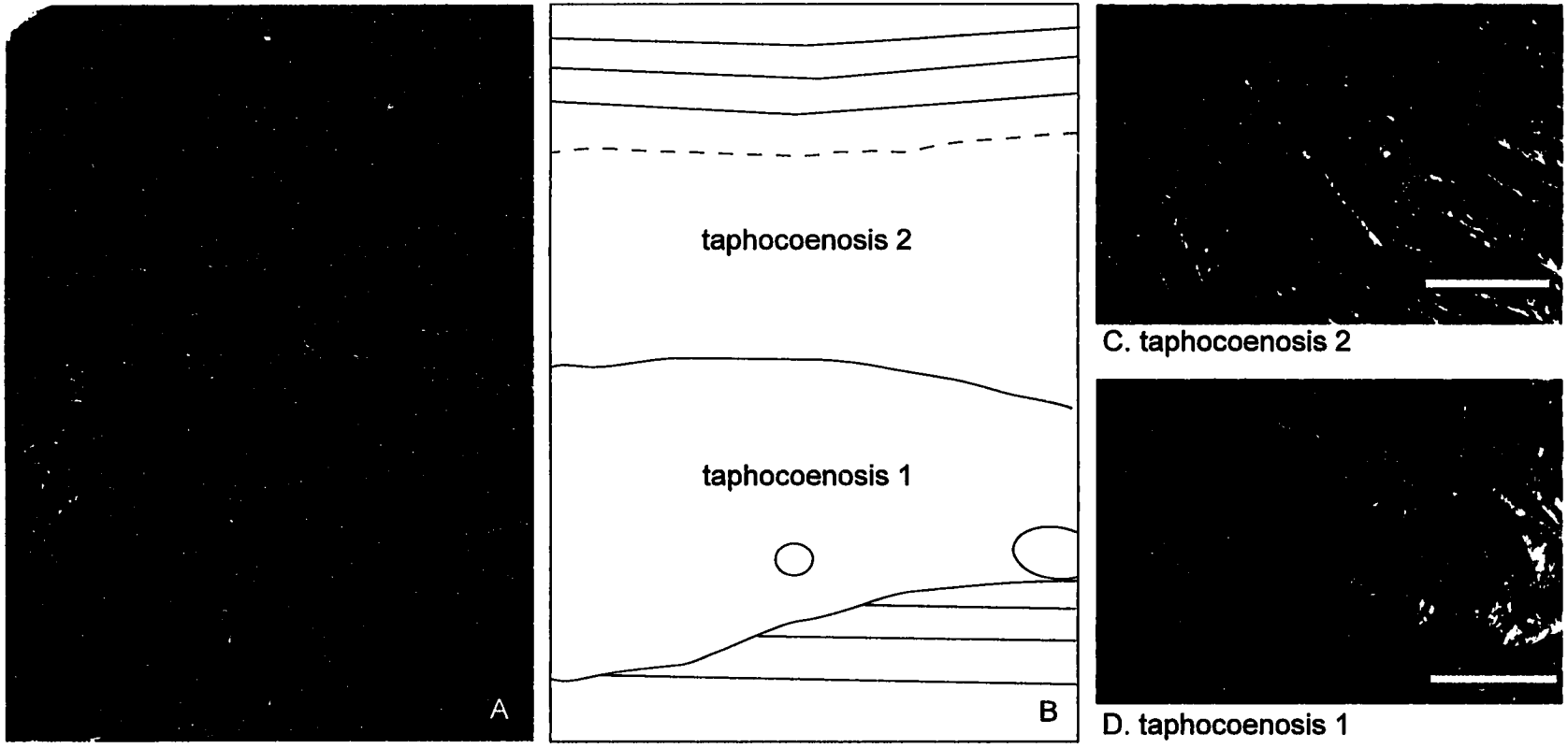

Figure 4.81. Concretion CP 214.5. A. Detail of polished slab from Figure 4.79. Magnification x1.5. B. Line drawing of polished slab detail showing truncation of bottom laminated unit by taphocoenosis 1. Taphocoenosis 2 is in sharp contact with taphocoenosis 1 and grades into the laminated unit at the top of the slab. Nautaloids are identified by ovals. C, D. Photos from layer 61 dissolution surface. Scale bar = 4 mm. C. Taphocoenosis 2 dominates the dissolution surface. The distal cyrtograptid fragments are in horizontal alignment. Many are fragmented and rhabdosome at centre is bent. D. Dissolution surface 61 also samples part of taphocoenosis 1, mature *M. instrenuus* fragments in alignment. The contact between taphoceonosis 1 and 2 has extreme topography and allows for this view of taphocoenosis 1 at layer 61. Scale bar = 4 mm.

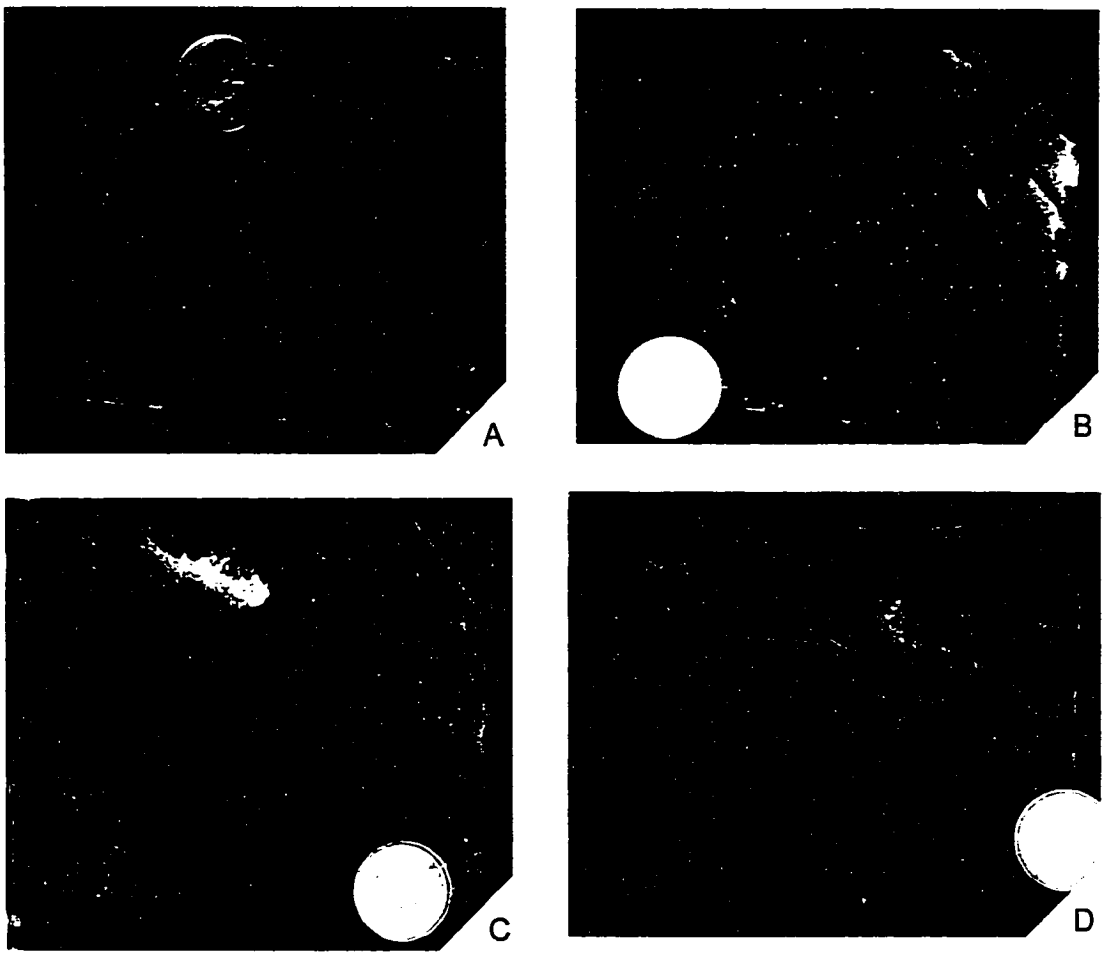

Figure 4.82. Concretion CP 214.5 dissolution surfaces. Penny for scale is 1.9 cm in diameter. A. Layer 32. Many radiolaria but few graptolites. Includes sicula, early growth stages and mature rhabdosomes. B. Layer 36. Evidence of fragmentation. Radiolaria are abundant. C. Layer 48. *M. instrenuus* in the top-right corner and cyrtograptid fragments in the bottom-left corner. Cyrtograptids display a weak alignment similar to *M. instrenuus*. D. Layer 53. Graptolites display preferred alignment. Graptolites in the bottom-left corner are more chaotic in their orientation and many are flattened, fragmented and bent. *M. instrenuus* shows evidence of fragmentation and alignment. Radiolaria and graptolite early growth stages are rare. E. Layer 57. Graptolites on the bottom-half are oriented almost perpendicular to those at the top of the image that maintain the orientation observed on earlier dissolution surfaces or are chaotically arranged. Radiolaria are absent.

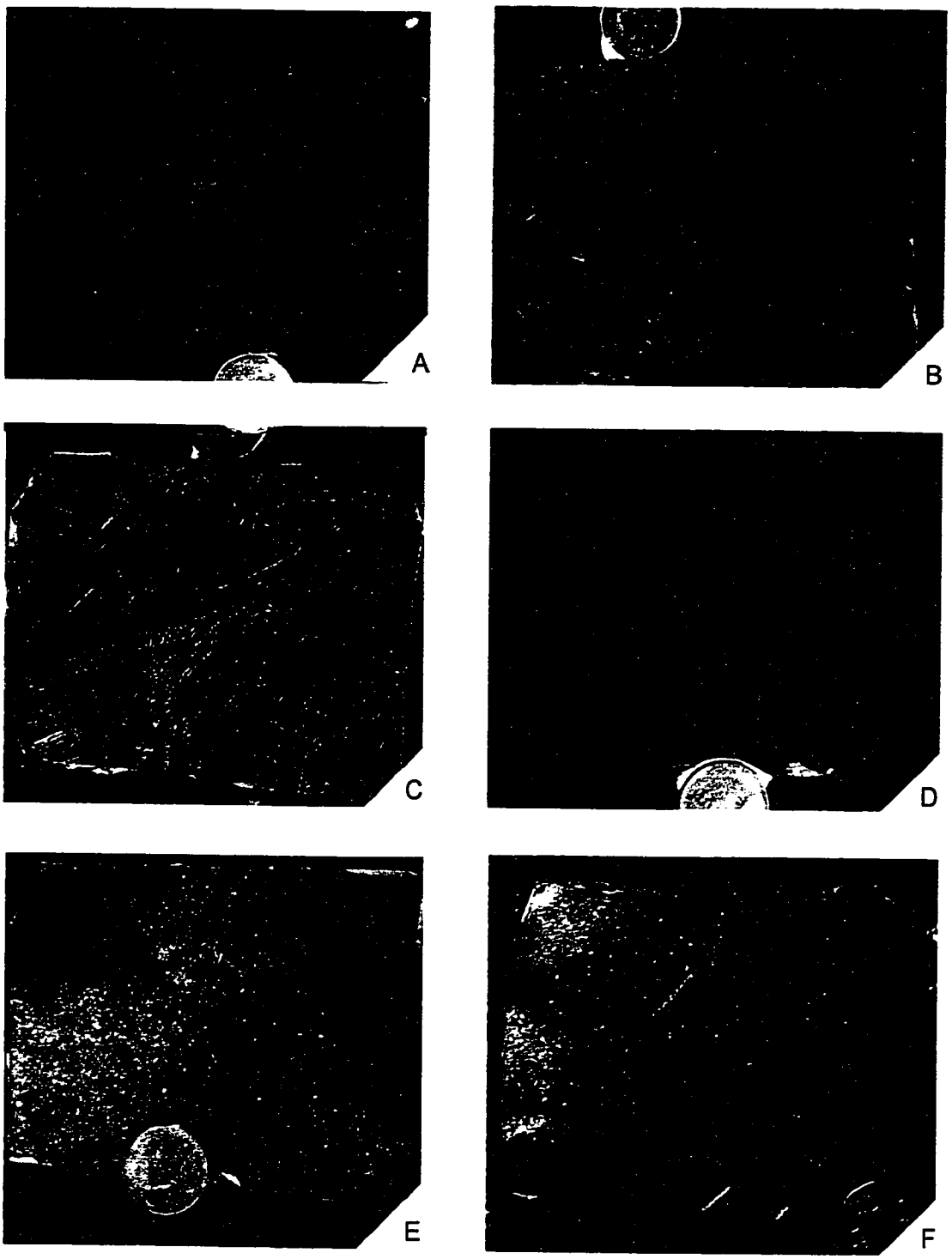

Figure 4.83. Concretion CP 214.5 dissolution surfaces. Penny for scale is 1.9 cm. in diameter. A. Layer 61. No early growth stage graptolites observed. Graptolites aligned, fragmented and bent. B. Layer 66. C. Layer 72. D. Layer 76. No alignment. E. Layer 82. F. Layer 92. Radiolaria abundant, graptolites rare.

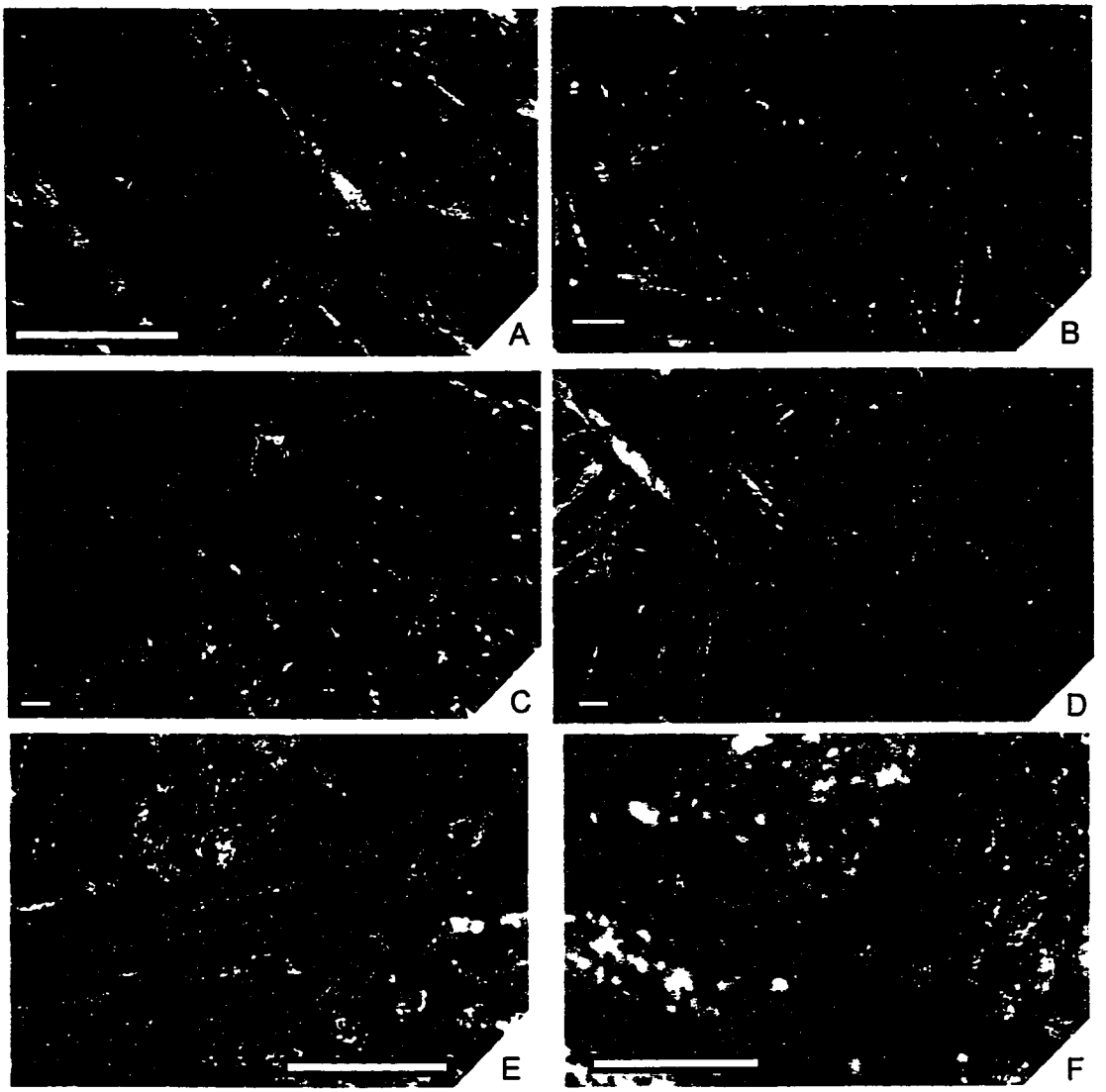

Figure 4.84. Concretion CP 214.5. All scale bars = 2 mm. A-C Photos from dissolution surface at 61 mm. A. Magnification of figure showing bent cyrtograptid within a cluster of cyrtograptids that show prefered alignment. B. *M. instrenuus* curved over a second *M. instrenuus* rhabdosome. There is a tendancy for the cyrtograptids to bend drastically and for the *M. instrenuus* to curve gently perhaps indicating a difference in the original strength of the rhabdosomes. Smaller cyrtograptid distal fragments are chaotically arranged. This may be related to the branching structure of the rhabdosome that would have not been conducive to easy alignment in a current/flow. C. Some physical compaction was accommodated by the cyrtogratids on dissolution surface 61. D. A rare bent and fractured *M. instrenuus* overlying (up is into the page) a rare flattened *M. instrenuus* that along its length is uncompacted. Photo of layer 72. E. Fractured and bent cyrtograptid fragments from layer 82. F. Branching cyrtograptid from layer 82.

rhabdosomes are floating in the brown matrix. At the top of this layer the graptoloids are in bioclast contact across the slab with minor matrix. A second graptoloid horizon is comprosed of rhabdosomes that are 8 mm in diameter (taphocoenosis 2 of Figure 4.80, 4.81). The elongate rhabdosomes are aligned with and oriented approximately perpedicular to those of taphocoenosis 1. Rhabdosomes of this unit are in contact.. The layer has an average thickness of 35 mm and a basal topography of 16 mm. The top unit (layer 83/80 to 110) contains more radiolarian molds (5%), but otherwise is similar to the basal unit of finely laminated sediment. The graptoloid rhabdosomes are rare in this layer and the basal unit.

The rhabdosome counts from the layer-by-layer dissolution do not support the null hypothesis of random distribution and show a gradual increase in rhabdosomes from layer 40 to a maximum of 519 rhabdosomes at layer 72. The number of rhabdosomes decreases quickly after this layer to values resembling the basal unit. This is directly correlated to the first and second graptoloid layers observed in the polished slab.

The first graptoloid layer was dominated by *Monograptus instrenuus*, a robust and long graptoloid (Figure 4.81D). Few proximal ends were observed on the dissolution surface or in the dissolution residues. This may be the result of the unusually long nature of this graptoloid. *Monograptus instrenuus* is rarely found with a proximal end in studies of flattened material and it reaches unknown lengths at maturity (M. Melchin pers. comm.). The majority of the specimens are oriented (Figure 4.92B-E, Figure 4.83A).

The second graptoloid layer was dominated by distal fragments of an unidentified cyrtograptid (Figure 4.81C). The rhabdosome of this species contains cladia that branch away from the main stipe at an angle of 90° (Figure. 4.94F). In the basal portion of this layer, distal fragments that are not branched are aligned in an orientation that is almost perpendicular to the orientation of the *M. instrenuus* of taphocoenosis 1 (Figure 4.82D,E, 4.83A, B). Up-concretion, this layer becomes more chaotic in orientation perhaps resulting from the branches interfering with the ability to align with a current (Figure 4.83B-D, Figure 4.84B, C). Many bent and fragmented cyrtograptids are observed in this chaotic layer (Figure 4.84A, E). A few specimens of *M. instrenuus* are present in this mixture and show evidence of bending (Figure 4.84B) and fracture (Figure 4.84D). Up-

concretion the rhabdosomes show slight alignment in an orientation that is similar to that of taphocoenosis 1.(Figure 4.84D).

Siculae and radiolarians are not recorded from the dissolution layers 61-72, although they are both recorded from layers above and below. A qualitative examination of the dissolution residues supports the results of the layer studies. Siculae and proximal fragments are present in the residues that preceed and follow the depositional event, and rare to absent in the residues of the event bed. This is most likely the result of winnowing. Shelly fauna and other fossils (bivalves, nautiloids, sponge spicules and radiolarian observed on layers 40, 44 and 48 were observed in sediments, which were not a part of the scour-filled, graptoloid-rich portions of the dissolution surface. These shelly fauna were from the basal unit and were revealed at these dissolution layers as a result of the uneven basal topography of the graptoloid-rich layer (Figure 4.92C).

Concretion: CP 96a 6.0

Lithofacies: 8, graded laminae, clay/organic-poor, uncompressed graptoloids
Graptoloid distribution: random (χ^2/n= 1.16)
Taphofacies: random flux of graptoloids and sediment.

Graptoloids are randomly distributed among the layers examined during the dissolution of this very fine-grained, laminated concretion. The four main layers are defined by colour variations of light to medium brown and the presence and style of minor, thin, light brown laminae (Figure 4.85B). Layer 21-29 is a homogeneous, medium brown with no internal laminae and in sharp contact with the layers above and below. Layer 29 to 36 mm shows a slight gradation, with fewer light patches at the top of the bed and a sharp basal and top contact. The rest of the concretion comprises thin laminae of light and medium brown. In thin section, the homogeneous layer 21-29 lacks visible grains other than diagenetic carbonate crystals visible in previous voids (Figure 4.85C). This layer is in sharp contact with the layers above and below that are heterogeneous in their grain size, composition and colour (Figure 4.85D). This

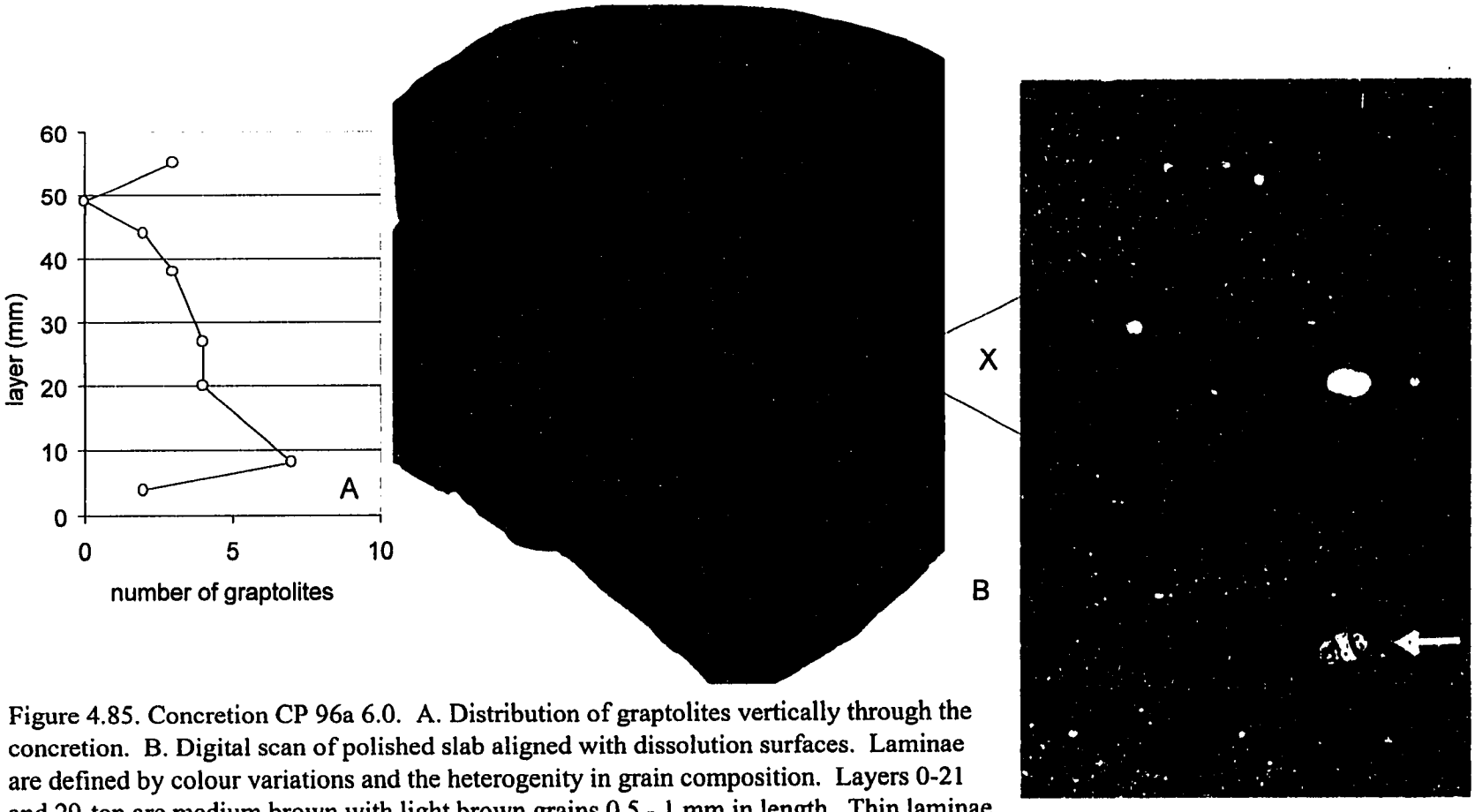

Figure 4.85. Concretion CP 96a 6.0. A. Distribution of graptolites vertically through the concretion. B. Digital scan of polished slab aligned with dissolution surfaces. Laminae are defined by colour variations and the heterogenity in grain composition. Layers 0-21 and 29-top are medium brown with light brown grains 0.5 - 1 mm in length. Thin laminae of light brown at 10, 17, 19, 41, 52, 66, 69, 79 mm are in sharp contact with medium brown interlamiations. Layer 21-29 is medium brown with no light brown grains and a more homogeneous texture. Actual size. C. Digital scan of thin section. The homogeneous layer, labeled "X", contains carbonate-filled voids, but lacks other visible grains. Laminae below and above are heterogenous in grain composition/colour. Graptolite identified by the white arrow. Magnification x4.

concretion is classified as lithofacies 8 and aside from the normally graded bed is very similar to lithofacies 4, the finely laminated, clay/organic-poor lithofacies.

Graptoloids are low in abundance (25 rhabdosomes counted) with one layer (layer 49) barren (Figure 4.85A). Statistically, this graptolite distribution supports the null hypothesis of random distribution. This concretion is placed in the random flux of graptoloids and sediment taphofacies.

Concretion: CP 96a 7.5

Lithofacies: 2, structureless, clay/organic-poor
Graptoloid distribution: random ($\chi^2/n = 0.67$)
Taphofacies:random flux of graptoloids and sediment.

This very fine-grained carbonate concretion contains no laminae and no clear evidence of bioturbation. In polished slab, the grain size of the matrix could not be measured with magnification (Figure 4.86B). Radiolarian molds and tests, rounded, brown silt-sized grains, and graptoloids in cross-section were randomly distributed throughout the concretion. The only identification of bedding was from a slight elongation of the concretion shape that was likely the result of compaction.

There are many mature graptoloids in this concretion with a slight abundance at layer 6 (6 mature "monograptids"). However, with siculae included in the count (Figure 4.86A), this layer is not identified by the chi-square analysis as being concentrated. There are no distinctive sedimentary structures at the 6 mm layer. A fragmented mature "monograptid" was found on layer 51. The cause or timing of fragmentation could not be determined.

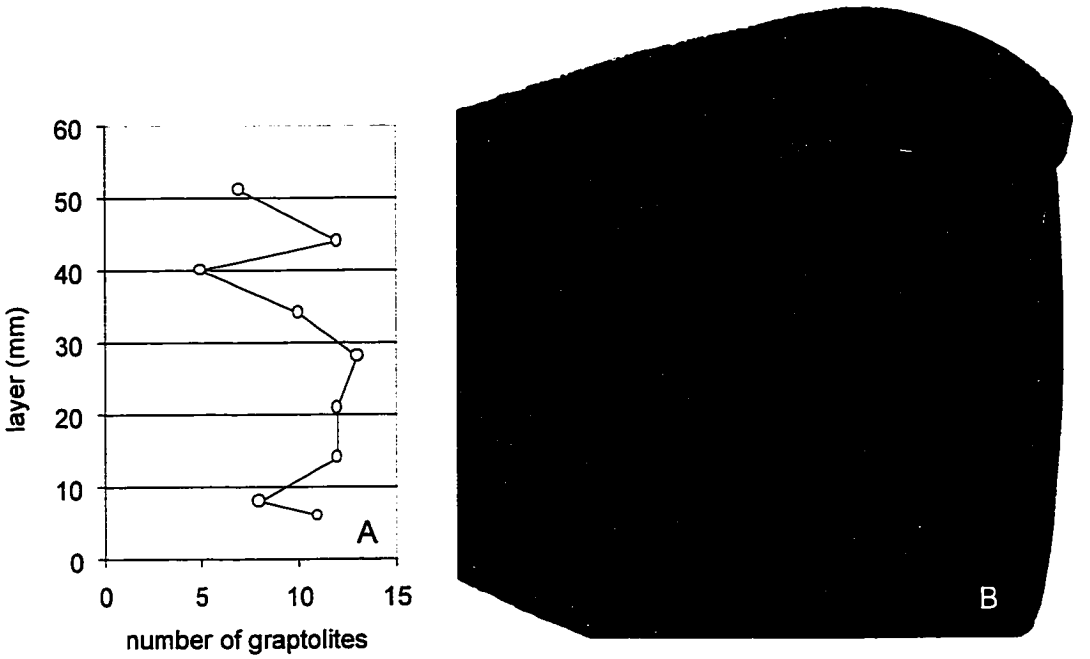

Figure 4.86. Concretion CP 96a 7.5. A. Distribution of graptolites vertically through the concretion as recorded during the layer-by-layer dissolution. B. Digital scan of polished slab. The concretion is a greyish-brown matrix of indistinguishable grain size with light brown, silt-sized rounded grains (possible radiolarian molds), angular to rounded, silt-sized brown grains, radiolaria tests, and graptolites in cross-section. No laminae are visible. Actual size.

Concretion description summary

The concretions described in this chapter are summarized in Tables 4.1 and 4.2. The describtions and definitions of the microlithofacies and taphofacies are presented in Chapters Five and Six, respectively. In Chapter Seven, I interpret the distribution of microlithofacies and taphofacies and suggest that this distribution records some of the history of sea-level change and basin dynamics of the Early Silurian in the Cape Phillips Embayment.

5 MICROLITHOFACIES OF THE CAPE PHILLIPS FORMATION SLOPE-APRON FACIES

The study of fine-grained, deep-water deposits in the ancient record is hindered by the fissile nature of fine-grained rocks and the compaction of muds during the process of lithification (Potter *et al.*, 1980). Many of the carbonate concretions within carbonate-rich shale of the Cape Phillips Formation lithified early in diagenesis, prior to major compaction (Coniglio and Melchin, 1995). Concretionary carbonate is usually precipitated in sediment pore spaces (Raiswell, 1976), preserving structures such as burrows and fecal pellets - evidence that mineral precipitation did not force sediment particles apart (Allison, 1990). These concretions preserve the uncompacted nature of the fine-grained sediments and record small-scale lithologic variations that are difficult to observe in the surrounding shale. The lithification of the carbonate concretions of the Cape Phillips Formation also produced a strong diagenetic overprint and this chapter focuses on the problem of interpreting the often-cryptic original fabric of the Cape Phillips Formation concretions. The objective of this chapter is a definition and description of the microlithofacies present in the concretions of the study area (Figure 2.1).

Deep-water siliciclastic facies were described from modern (e.g.,, Piper and Stow, 1991; Stow and Piper, 1984; Piper, 1972a, 1978) and ancient (e.g., Pickering *et al.*, 1986, 1989; Piper, 1972b) systems. The alpha-numeric code developed by Mutti and Ricci-Lucci (1978) is often used because it easily identifies facies associations and sequences and many of the later facies models are based upon this classification. Pickering *et al.* (1989) modify this scheme into seven classes based on grain size, divided into 15 facies groups based on internal organization of structures, bed thickness and composition. Aspects of these facies schemes can be applied to deep-water carbonates; however carbonates are resedimented by slightly different processes and modification is needed at the individual facies level where resedimented carbonates show deviations from the siliciclastic norms.

In this thesis I use the term "microlithofacies" to represent the collective observations of lithology and small-scale sedimentary structures as defined in the

polished slab, thin section, and related to the field observations. Each lithofacies is labeled as a number (1 – 11) and described (e.g., finely laminated, carbonate-rich mudstone). These lithofacies are then given a paleoenvironmental interpretation and processes of deposition are discussed.

In this chapter, I will show how the microlithofacies can be placed in the context of a slope-apron facies model and related to global sea level history. Mullins and Cook (1986) created the slope-apron facies model to describe many ancient, deep-water carbonate deposits. Unlike many siliciclastic, deep-water deposits (e.g., submarine fans), the sediment source is not localized to a channel but generalized to the whole platform margin. Much of the sediment bypasses the upper slope or is temporarily deposited with interbeds of pelagic sediments, before resedimentation by sediment gravity flows to the lower slope apron. The resulting apron is a broad wedge of shallow-water sediments and pelagic sediments with little vertical organization and only local channeling. Although this facies is not well described from modern settings the most similar analogues are parts of the Florida Reef Tract where reef debris is being deposited along a gradual slope to a platform tens of metres below the shelf break (Tucker and Wright, 1990).

The Cape Phillips Formation of Arctic Canada is composed of fine-grained calcareous shale and silty carbonates that were deposited in distal, ramp-like conditions (Melchin *et al.*, 1991). A full description of the paleogeography of the Cape Phillips Formation is found in Chapter Two. Deposition within the Cape Phillips Embayment began in the Late Ordovician and continued until the Early Devonian, when accommodation space in the basin was limited (de Freitas *et al.*, 1999). This study focuses on a Llandovery section, which outcrops along an unnamed stream west of Cape Manning and the Llandovery to mid-Wenlock portion of a section, which is exposed in the coastal cliffs and along a stream at Cape Phillips. Both sites are located on Cornwallis Island in Arctic Canada.

The Cape Phillips Formation is the distal shelf facies equivalent of the shallow shelf carbonates of the Allan Bay Formation that outcrops to the south of the Cape Phillips Formation. The source of sediment was most likely from the shallow-water carbonates of the Allen Bay Formation with a land-derived source for the minor siliceous sediments. In this thesis, "mud" is the term used to describe sediment of clay-sized and silt-sized

siliceous and organic particles and carbonate particles (carbonate mud). Melchin (1987b, 1989) identified a thickly bedded, fine-grained, resedimented limestone that occupied the *S. sedgwickii* zone and possibly represented a change in platform-margin morphology in the late Middle Llandovery. During the Late Llandovery there was a retreat in the location of the platform margin as indicated by the Cape Phillips Formation sediments overlying the carbonates of the Allen Bay Formation. After this time the platform margin became more abrupt, with a distinct, platform-edge facies (Sodero and Hobson, 1979), and the proximal Cape Phillips Formation sections begin to show an increase in frequency of coarser, resedimented carbonates (Melchin, 1989). The investigation of the lithology of concretions may provide further evidence for this change in basin morphology.

The graptoloids of the Cape Phillips Formation are preserved in carbonate concretions, carbonate beds, and as flattened carbon films on shale. Coniglio and Melchin (1995) estimate the shale compaction is 73% to 84% that of the sediment within the concretions. Estimates were based on tracing laminae within the shale into the concretion that developed in the same bedding plane (Figure 1.2). Calcite, and rarely dolomite, precipitated in zones of bacterial-sulphate reduction within the sediment pore waters (Coniglio and Melchin, 1995) and in most examples the concretion growth did not disturb the original sedimentary structures of the sediment. With rock slabs and thin sections cut perpendicular to bedding, original structures, such as laminae and graded beds can be observed. However, original texture (grain size and grain sorting) is difficult to discern in the diagenetically altered concretions. Patterns of concretionary carbonate crystal fabric observed in thin section were related to the study of etched stubs of concretionary material with a scanning electron microscope (SEM) equipped with an energy dispersive system (EDS) in an attempt to define original texture. Unfortunately, these studies failed to establish a reliable association between diagenetic crystal size and assumed original sediment texture. In this chapter, a simplified lithofacies classification is based on sedimentologic characteristics that were observable in the concretionary material, such as, lamination style, graded beds, and relative homogeneity.

Eleven lithofacies were observed in 53 of the Cape Phillips Formation concretions using classification criteria unique for the concretionary material. Following each

lithofacies description is a discussion of how the lithofacies can be related to processes of deposition. Finally, a temporal and spatial analysis of the distribution of these lithofacies within the Cape Phillips Embayment will define sedimentary dynamics and basin characteristics.

Establishing lithofacies criteria

Classifications of fine-grained, deep-water deposits are difficult to apply to the diagenetically altered sediments examined in this study. Many previously developed classifications were based on the detailed study of modern environments and are difficult to apply to the study of lithified sediments. Important in many lithofacies classifications is the determination of grain-size distribution and the assessment of the grain character (roundness and sphericity) (Prothero and Schwab, 1996). For fine-grained sedimentary rock, such as the clay to silt sized sediments within the carbonate concretions of the Cape Phillips Formation, the measure of grain character is not often observable. The concretionary carbonate cement overprints the original carbonate sediment texture and makes grain size determination of the carbonate grains difficult, if not impossible. In many classifications, the thickness of the bed on the outcrop scale is a diagnostic trait (e.g., Pickering *et al.*, 1989) and this was difficult to accurately assess in the physically uncompressed concretionary material. In the following section I assess the lithologic criteria that may be used in a lithofacies model for the Cape Phillips Formation.

Grain-size

Quantitative assessment of grain-size is of primary importance in most lithologic classifications. Understanding the texture (grain size and grain sorting) provides information about the mechanism of transport and deposition, so it is a useful tool in paleoenvironmental interpretations. I was not able to consistently and confidently observe grain size in the polished slabs. Larger biogenic grains and some other grains of questionable origin were measurable, but usually represent only a small portion (1-10%) of the total material. Laminae were defined by colour variations and by differences in the relative heterogeneity of the layers. Some concretions show evidence of graded bedding.

A thin section analysis of concretions was conducted to understand the character of the graded beds (normally or inversely graded) and to determine the extent to which grain size was defining the laminae.

A relationship between an increase in the darkness of a lamina (organic matter and clays) and a decrease in carbonate crystal size was established in the thin section analysis. Two questions arise from this observation. 1) Does the carbonate crystal texture reflect the original grain size of the sediment? 2) Can we use the relationship between colour (organic and clay content) as an indicator of grain size? This correlation between darker colour and smaller carbonate crystals was consistent in most of the laminated concretions, but one showed the opposite relationship - an increase in carbonate crystal size in the darker layers (e.g., CM 44.1). Does this represent an inversely graded bed? To understand this relationship I undertook a detailed study of two laminated concretions CM 44.0-44.1 and CM 59.1-59.2 using the SEM/EDS (see Chapter 4).

The SEM/EDS study revealed that laminae are defined by clay content and that in concretion CM 44.0-44.1 the graded beds show an upward increase in clay. Unfortunately, the SEM/EDS examination does not elucidate the original grain size of the carbonate sediments. I was unable to confidently assign grain size measurements to the sedimentary rocks, because of their recrystallization during diagenetic growth of the concretion. Although these detailed case concretions show the problem of diagenetic alteration of carbonate grains, my general observations show that graded beds have an abrupt base of light material of to a dark top. This is a grading of a "coarser" carbonate to a "finer" carbonate and clay – a normally graded bed. I believe it is reasonable that coarser carbonate sediment with less clay would have a higher initial porosity and thus diagenetic crystals would grow larger. I feel that I can reasonably speculate that this is a prominent (if not invariable) tendency.

Colour – carbonate, clay content

The concretions and the laminae within the concretions range in colour from buff to grey to orange-brown to dark brown or black. Graded bedding, and locally, cross-bedding are identified by the colour variations observed in polished slab and thin section. As described above, I have interpreted the lighter colours (buff, orange-brown, light

brown) to represent higher original carbonate content as opposed to clay or organic content. The darker layers (medium brown, dark brown, black) are recording an increase in the clay and organic content. The increase in clays is partially accommodated by a relative decrease in the original carbonate sediment. The black layers usually appear as thin, discontinuous laminae or partings that may represent organic bacterial fragments, clay clasts, hiatus horizons, or stylolites.

Lamination style

Forty-five of the concretions display some form of lamination defined by the colour variation. Those that were not laminated were classified as structureless. The laminated concretions were divided into four categories: finely laminated, coarsely laminated, graded laminae, and graded-stratified laminae. These categories are not mutually exclusive; one could find a finely laminated sediment that is also graded-stratified. In this thesis; however, a concretion described as "finely laminated" without any other observations of lamination style, suggests that most of the laminae do not show any signs of gradation. Finely laminated concretions display laminae that are 1 to 5 mm in thickness with rare thicker laminae 5 – 10 mm. Coarsely laminated concretions have laminae that are 5 mm to 40 mm thick. Concretions with graded laminae are those that contain one, or more than one lamina that grades in colour from base to top over a lamina thickness of less than one centimeter on average. Concretions that contain graded-stratified laminae differ in that the laminae within the graded interval show an overall grading of colour from base to top over the thickness of the concretion, approximately 10 cm.

Heterogeneity of grain type and colour

Heterogeneous laminae or concretions contain an assortment of grains of various colours and a variety of sizes. Homogeneous laminae or concretions are uniformly the same colour sediment with minor clasts of other colours. Some graded beds record a grading of relative heterogeneity – with a more consistent colour and clast type at the top of the lamina and a more heterogeneous mix of grains at the base. The heterogeneity

could be a measure of grain size although no direct relationship could be established in this study. It is included as a lithologic character that is possibly indicative of sorting.

Microlithofacies of the Cape Phillips Formation

Eleven microlithofacies are identified in the 51 concretions and two limestone beds using the criteria described above. Each microlithofacies is given a number (1-11) and a short descriptive label. Following a list of the concretions that are including in the microlithofacies is a short description of the distinguishing characters and a brief interpretation of the possible processes that formed the facies. A concretion classified in one microlithofacies may show some characteristics of another. For example, a concretion comprising fine laminations characteristic of microlithofacies 5 or 6 (finely laminated) with one graded laminae will be classified as microlithofacies 7 or 8 (graded laminae). The other finely laminated sediments of the concretion are considered background sedimentation to the event that produced the graded lamination. Distinction of this facies that contains an event bed is important for later interpretations.

Microlithofacies 1: structureless, clay/organic-rich

Concretions:

CM 56.4-56.5
CM 56
CM 54.0-54.15
CM 53.2-53.3
CM 50.4
CM 49.8-49.9
CM 46.35-46.5
CM 45.3-45.4

Description

This lithofacies is characterized by dark brown or dark grey, homogeneous concretions. Planar laminae are absent or very poorly defined. Weak laminae are defined by variations in heterogeneity, percentage of brown matrix (CM 56.4-56.5, CM 53.2-53.3) and texture of the carbonate crystals (CM 49.8-49.9). The weak laminae are

discontinuous with gradational contacts. Bioclastic-rich layers of sponge spicules or graptoloids define some laminae. All grains visible with the naked eye are interpreted to be bioclasts or they are diagenetic in nature. In thin section the carbonate crystals average 30 μm in diameter and can range from 10 to 100 μm in size. Bioclasts include: graptoloid rhabdosomes, radiolaria, sponge spicule, nautiloids, and rare bivalves or brachiopods. Alignment of elongate graptoloids is observed in CM 45.3-45.4 and CM 46.35-46.5

Interpretation

The lack of laminae in these concretions may be the result of three processes: 1) bioturbation, 2) consistent sediment source or, 3) rapid deposition of massive mud layer. Each mechanism is discussed below.

1. No evidence for bioturbation, such as preserved burrows or fragmented bioclasts, were found in these concretions. Although the abundance of fossils may indicate oxygenation of the bottom waters there is no evidence that these were deep-water, autochthonous communities. Most of the fossils are allochthonous pelagic organisms (graptoloids, radiolarians, orthoconic nautiloids), or benthic organisms (sponge spicules and rare shelly fossil fauna) that were likely transported to the deeper, anoxic settings.
2. In a hemipelagic depositional environment where the sediment supply is constant in source and rate, the result is a non-laminated fine-grained, mud. If productivity and supply of organic carbon were high during this time and organic matter preservation was enhanced by anoxic conditions, there would beorganic-rich, non-bioturbated sediment. This is the inferred depositional environment for CM 53.2-53.3, CM 54.0-54.15, CM 56, and CM 56.4-56.5. The structureless concretion CM 49.8-49.9 is interpreted to be the product of a consistent sediment source. Faint laminae and an abundance of graptoloid rhabdosomes at mid-concretion were the result of slight variations in the rate of sediment supply. The graptoloid-rich lamina does not represent a true cessation of sediment and a hiatus horizon, but a decrease in the rate of sediment supply.

3. The structureless mud facies in siliciclastic studies is considered to be the result of rapid deposition of flocculated mud that results from the ponding of mud-rich turbidity currents in confined basins (Pickering and Hiscott, 1985). Rapid deposition of the carbonate mud could explain the evidence of rhabdosome transport within the graptoloid taphocoenosis of some of these samples. Concretion CM 46.35-46.5 contains a graptoloid-rich layer that shows signs of current alignment and size-sorting but the lithology above, below and within this unit does not show major variation in texture or sedimentary structures. This is likely the basal lag, indicating physical addition of graptoloid rhabdosomes at the base of a rapid, carbonate mud deposition event. Both limestone beds examined (CM 45.3-45.4 and CM 50.4) are classified in this microlithofacies. Both show an abundance of graptoloids basally and a shift in the graptoloid assemblage composition and an increase in siculae up-lamina. The limestone bed CM 45.3-45.4 contains clear evidence of current alignment and winnowing in an interpreted basal lag. The limestone beds (CM 45.3-45.4 and CM 50.4) are interpreted to be resedimented limestone with the upward variation in graptoloid assemblage composition suggesting deposition from two slightly different sources: a transported basal assemblage that also incorporates graptoloids in the existing sediment, and a hemipelagic local source from waters above.

For the concretions that show no sedimentary structures and no evidence of transport and were considered to be in a depositional environment with consistent sediment supply and rate (hypothesis #2 above), the sedimentation rates are assumed to be high. These structureless concretions are closely associated in appearance and in stratigraphic position with the concretions that show signs of sediment and fossil transport (hypothesis #3) - CM 46.35-46.5, CM 45.3-45.4 and CM 50.4. Both groups are likely the result of rapid deposition.

<u>Microlithofacies 2: structureless, clay/organic-poor</u>

Concretion:

CP 96a 7.5

Description

Similar to microlithofacies 1, this facies is defined by a lack of sedimentary structures. It differs in the lower percentage of organic material, determined qualitatively from the pale colour. Only one concretion (CP 96a 7.5) has been assigned to this microlithofacies. This very fine-grained carbonate concretion contains no laminae and no clear evidence of bioturbation. In polished slab the grain size of the matrix could not be measured and no thin section was prepared for examination. Radiolarian molds and tests, rounded, brown, silt-sized grains, and graptoloids in cross-section were randomly distributed throughout the concretion. The only identification of bedding was from a slight elongation of the concretion shape that was likely the result of compaction.

Interpretation

With no evidence of bioturbation, this structureless concretion is interpreted to be deposited in a hemipelagic environment where the sediment source was consistent and sedimentation rate was constant. Productivity of organic matter was low or the organic matter was poorly preserved, resulting in the organic-poor carbonate. Low organic matter content could also be produced by an increased carbonate sedimentation rate that dilutes the organic matter with more carbonate. Of course, both a change in productivity and an increased rate of carbonate sedimentation may be lowering the organic content of this microlithofacies.

Microlithofacies 3: coarsely laminated, clay/organic-rich

Concretions:

CM 58a
CM 58b
CM 57
CM 55
CM 50.4-50.5
CM 48.5

Description

This microlithofacies is very similar to microlithofacies 1, structureless clay/organic-rich with perhaps the only difference being a clear distinction of one or more lamina contacts. In microlithofacies 1, the "coarse laminae" or beds are greater than the thickness of the concretions. The concretions of microlithofacies 3 are characterized by laminae that are greater than 5 mm and average 30 mm in thickness. Contacts between the laminae are often sharp (some with evidence of scoured bases). The laminae are defined by variations in carbonate crystal size, percentage of fine-grained matrix, or both. Medium to light brown laminae have an average carbonate crystal size of 50 μm and range of 20 to 100 μm. This is slightly larger than the dark brown laminae that have an average carbonate crystal size of 30 μm and range of 10 to 80 μm. Rare laminae contain internal microlaminae (e.g., CM 48.5). One coarse lamina (CM 57, 0-22) displays a faint grading of colour from a lighter base to a darker top. However, laminae that are internally structureless, are most common. Some laminae are bounded by organic-rich horizons (e.g., CM 58b). Concretions CM 58a and CM 58b have a possible peloidal fabric. The lithologic change between two coarse laminae is often accompanied by a change in the composition or quantity of bioclasts. Size-sorted, aligned graptoloids are found with a large bivalve or brachiopod at the base of a coarse lamina in CM 48.5.

Interpretation

All the concretions with this microlithofacies record a change (subtle or distinct) in the sedimentary dynamics. CM 50.4-50.5, CM 51.2-51.3b, CM 58a, and CM 58b record subtle changes in the sediment source and supply rate in the laminae. The change in supply rate is more pronounced in CM 55 with the organic-rich, fine-grained layer interpreted from faunal evidence to represent a sediment-starved horizon. CM 51.2-51.3a, CM 48.5 and CM 57 record a change in the sedimentary dynamics represented by a shift in the graptoloid taphocoenosis and a change in the abundance of other bioclastic material associated with a sharp lithologic change. The sharper, scoured base; size sorting and alignment of fossils; and varied laminae types are indicative of a reasonably active environment.

Microlithofacies 4: coarsely laminated, clay/organic-poor

Concretions:

CM 51.2-51.3a
CM 51.2-51.3b

Description

This microlithofacies differs from microlithofacies 3 in the decreased clay and organic content. This is reflected in the lighter overall colour, a decrease in the content of grey/brown matrix of undetermined grain size and the larger concretionary carbonate crystals. The carbonate crystals range in size from 10 to 80 μm in the darker laminae to 40 to 150 μm in the lighter laminae. Contacts between the laminae are sharp. There is no evidence of bioturbation. Concretions CM 51.2-51.3a and CM 51.2-51.3b sampled one meter away from each other in the same stratum both contain small brachiopods and bivalves, large and small gastropods, sponge spicules in lattice orientation, and rare hemispherical bryozoans. These concretions also contain the pelagic fossil fauna of graptoloids, orthoconic nautiloids and radiolaria. The fossils are concentrated within certain laminae and are more abundant in CM 51.2-51.3a. Therefore, these fossil-rich strata are laterally continuous with variable abundance over the one-meter interval that separates the two samples of this microlithofacies.

Interpretation

The more coarsely crystalline, more carbonate-rich layers with sponge spicules, bryozoans, and gastropods indicate sediment transport from the carbonate shelf. The energy of these events was dissipated as a result of the assumed distance from the carbonate source and there is only minor evidence of sediment sorting by currents in the sharp contacts between laminae. The small brachiopods, bivalves and gastropods are typical of a deep-water benthos that lives in nutrient-poor or oxygen-limited environments. The abundance of these fossils in the CM 51.2-51.3 strata may indicate an oxygenation of the bottom waters at the sediment-water interface, if not in the sediments. However, the absence of trace fossils (even of a restricted ichnofacies) and the preservation of lamination are evidence of the anoxia of the sediments and suggest

Microlithofacies 4: coarsely laminated, clay/organic-poor

Concretions:

CM 51.2-51.3a
CM 51.2-51.3b

Description

This microlithofacies differs from microlithofacies 3 in the decreased clay and organic content. This is reflected in the lighter overall colour, a decrease in the content of grey/brown matrix of undetermined grain size and the larger concretionary carbonate crystals. The carbonate crystals range in size from 10 to 80 μm in the darker laminae to 40 to 150 μm in the lighter laminae. Contacts between the laminae are sharp. There is no evidence of bioturbation. Concretions CM 51.2-51.3a and CM 51.2-51.3b sampled one meter away from each other in the same stratum both contain small brachiopods and bivalves, large and small gastropods, sponge spicules in lattice orientation, and rare hemispherical bryozoans. These concretions also contain the pelagic fossil fauna of graptoloids, orthoconic nautiloids and radiolaria. The fossils are concentrated within certain laminae and are more abundant in CM 51.2-51.3a. Therefore, these fossil-rich strata are laterally continuous with variable abundance over the one-meter interval that separates the two samples of this microlithofacies.

Interpretation

The more coarsely crystalline, more carbonate-rich layers with sponge spicules, bryozoans, and gastropods indicate sediment transport from the carbonate shelf. The energy of these events was dissipated as a result of the assumed distance from the carbonate source and there is only minor evidence of sediment sorting by currents in the sharp contacts between laminae. The small brachiopods, bivalves and gastropods are typical of a deep-water benthos that lives in nutrient-poor or oxygen-limited environments. The abundance of these fossils in the CM 51.2-51.3 strata may indicate an oxygenation of the bottom waters at the sediment-water interface, if not in the sediments. However, the absence of trace fossils (even of a restricted ichnofacies) and the preservation of lamination are evidence of the anoxia of the sediments and suggest

that the small shelly fossils were transported from more proximal depositional environments.

Microlithofacies 5: finely laminated, clay/organic-rich.

Concretions:

CM 84.5
CM 75.5
CM 74.9a
CM 74.9b
CM 73.8
CM 72.6
CM 52.1-52.2

Description

The concretions of this lithofacies comprise thin, medium to dark brown laminae with rare, light brown or light grey laminae. The laminae often have relatively sharp bases and tops and internal, discontinuous microlaminae of a darker colour. Rare laminae, often those lighter in colour are homogeneous and contain no internal laminae. In all concretions the carbonate texture was coarser in the lighter than in the darker laminae. Concretionary carbonate crystals range in size from 10-60 μm and average 20 μm. The darker laminae showed an increase in the clay content and probably organic content. Silicate grains (5 – 10 μm) comprise less than 1% of the sample. These silicate grains are in grain-to-grain contact with carbonate crystals with dark (clay/organic) outlines of a similar size that were over-printed with the coarser-grained carbonate crystal texture. The laminae of this microlithofacies show no apparent grading either within single lamina or overall grading from the base of the concretion to the top.

Interpretation

Concretions of the microlithofacies 5 record variations in the sediment source or rate of supply that is typical of deep-water, non-bioturbated sediments (Potter *et al.* 1980). The absence of an infaunal benthos is interpreted to be the result of anoxic conditions within the sediment and above the sediment-water interface. The finely

laminated organic-rich concretions of microlithofacies 5 were likely deposited a hemipelagic depositional environment.

Microlithofacies 6: finely laminated, clay/organic-poor

Concretions:

CP 152a
CP 152b
CP 146.5a
CP 146.5b
CM 114.4a
CM 114.4b

Description

The difference between lithofacies 5 and lithofacies 6 is in the relative heterogeneity and the inferred original carbonate content. The concretions of microlithofacies 6 are finely laminated (less than 5 mm thickness, average 2 mm) with most laminae continuous and in gradational contact. They are lighter overall in colour and contain a coarser carbonate concretionary crystal texture (range 20-110 μm; average 50 μm) than concretions of lithofacies 5. The laminae of these concretions are more heterogeneous in composition than the laminae of lithofacies 5. The laminae are commonly defined by the size of the concretionary carbonate crystals. Like lithofacies 5, the darker laminae were composed of a finer crystal-size and contain less organic matter and clay than the lighter laminae.

Interpretation

Finely laminated sediments of microlithofacies 6 suggest a hemipelagic depositional environment similar to that proposed for microlithofacies 5. Concretions of lithofacies 6 were perhaps more affected by diagenetic alteration (white patches in slab, coarse carbonate or silica in thin section). It is possible that the difference between lithofacies 5 and 6 is only diagenetic, but the lighter overall colour suggests less organic matter and clay and a dominance of carbonate in the original sediment. This could be reflecting a decrease in productivity of organic matter or a reduction in its preservation.

Another possible explanation is that the organic-poor sediments are the result of dilution from the increased sedimentation of carbonate material. Of course, the organic-poor deposits could be the result of a combination of these factors. Graptoloid abundance is low on the dissolution surfaces of the concretions of microlithofacies 6, which suggests decreased productivity and increased sedimentation rate.

Microlithofacies 7: graded laminae, clay/organic-rich, compressed graptoloids

Concretions:

CM 44.1
CM 44.0-44.1
CM 42.8-42.9
CM 42.3-42.4
CM 41.65-41.75
CM 40.5-40.6
CM 96-6 loose ?

Description

Laminae of this lithofacies are defined by the organic/clay content. Two concretions (CM 44.1, CM 42.8-42.9) show a reverse in the relationship displayed in other concretions between crystal size and lamina colour. In these two concretions, the light laminae are seen to have a finer concretionary carbonate texture, not coarser as observed in other microlithofacies. This may indicate a recrystallization texture and be unrelated to original grain-size. Alternatively, reverse graded beds are common in deep-water depositional environments (Stow, 1979; Stow and Lovell, 1979; Stow and Piper, 1984; Pickering et al. 1989), and these textural patterns may correspond to reverse grading. The other concretions of this microlithofacies show little or no variation in carbonate crystal size with lamina colour. Each concretion displays one or more graded bed(s). These graded beds are usually less than 1 cm in thickness and grade from a light base to a dark top. Commonly, the light–graded base is capped by a sequence (2-3 cm) of thinly laminated, non-graded laminae. Bases of all graded beds are sharp. The laminae of microlithofacies 7 are also defined by the distribution of radiolarian molds

(Figure 4.10E, F, 4.59A, 4.60). The radiolaria are more common in the clay-dominated laminae and in the clay portion of the top of the graded beds (Figure 4.10A, B).

Interpretation

The thin, graded beds of these fine-grained sediments are not accompanied by an abundance of shelf-derived sediments or fossil fauna. It seems likely that these graded beds are the products of currents that were either very distal to a discrete flow event, such as a tempestite or turbidite, or they are the result of a local current that reworked the hemipelagic sediments. The latter seems more likely because of the very fine-grained nature of the sediments and the pelagic in origin of the fossils. It is speculative to assign a depositional regime to the event beds; however, without an idea of the lateral extent of these events and the spatial variability within the Cape Phillips Embayment. The same currents that created the graded beds sorted rare graptoloids and abundant radiolaria. The pelagic organisms were concentrated in the tops of the graded laminae along with the dark organic matter. In studies of modern, fine-grained turbidites, planktonic organisms settle-out following an influx of sediment during a transport event and the deposition of a graded bed (Piper and Deptuck, 1997). The smaller organisms are suspended by the increased water energy and fall from suspension as the energy wanes.

Bottom currents in carbonate-rich, deep-water sediments arise from thermohaline circulation or internal waves and tides, and result in deposition of contourite deposits, a break in the stratigraphic record, and cementation and *in situ* mineralization of sediments (Tucker and Wright, 1990). The result is a sorting of pelagic fossils and reworked tops that show some alignment of fossils with the paleocontour, parallel to the strike of the slope (Stow and Lovell, 1979; Tucker and Wright, 1990). The samples for this study were not collected with azimuthal orientation, making the distinction between contourite and turbidite deposits difficult. In addition, most of the graded laminae are not associated with oriented pelagic organisms or large-scale sedimentary breaks. These graded beds record minor events and gentle currents at depth that were not persistent as would be expected in contourite-type deposits.

Microlithofacies 8: graded laminae, clay/organic-poor,

Concretions:

CP 96a 6.0
CP 148.1
CP 145.2
CP 96
CP 56.9
CP 38.4
CP 32

Description

Similar to microlithofacies 7, this microlithofacies is composed of finely laminated sediments of clay and carbonate. The lighter colour of the concretions of this microlithofacies may be the result of a different diagenetic history than the more organic-rich concretions. The graptoloids of these concretions are compressed (Figure 4.10F), suggesting that precipitation of the concretions followed some dewatering and compaction of the sediment. In lithofacies 8, most of the graptoloids are uncompressed and suggest an early lithification of theconcretions during shallow burial prior to compaction. The compaction of the graptoloids and the sediment matrix of microlithofacies 7 concretions may have also condensed the clay and created a darker resultant concretion. Alternatively, the organic content may be greater in microlithofacies 7. This is supported by the exceptional concretions CP 38.4 and CP 56.9 of microlithofacies 8 that contain flattened graptoloids and have a lighter overall colour (Appendix F). The organic-rich microlithofacies 7 is found only in the Aeronian *C. cyphus* Zone and *C. pectinatus* Zone (Figure 5.3). The organic-poor microlithofacies 8 is found only in the middle Telychian *M. crispus?*, *M. griestoniensis*, and lower *C. sakmaricus* Zones. This distribution is likely recording a difference in the productivity of organic matter, in organic matter preservation, in sedimentation rates, or a combination of these factors.

One or several graded lamina(e) are seen in each concretion of this microlithofacies. Finely laminated, non-graded laminae (background sedimentation) predominate with graded laminae (event beds) representing a small percentage of the

total sediments. A typical graded lamina is thin (less than 5 mm) with a sharp base that grades from light brown to a medium brown top. Two thicker graded laminae (20 mm, 25 mm) from CP 32 show a different style of gradation. These grade from a heterogeneous brown base to a homogeneous grey top. It is assumed that both the grading of light and dark or heterogeneous to homogeneous record a normal grading pattern of coarse to fine.

Pelagic fossils, such as radiolaria, orthoconic nautiloids and graptoloids dominate the fossil assemblage. Other fossil elements were only observed on the dissolution surfaces of CM 96. In this concretion, a brachiopod and a parabola-shaped sponge spicule mass with the hectinae spicules in lattice orientation were observed on two different dissolution surfaces. These dissolution surfaces were not correlated to the graded beds observed on the polished slab that were stratigraphically above and below, implying that the transport of the shelf-derived fossils was not directly related to the events recorded in the sediments.

Interpretation

The concretions of lithofacies 8 appear to be dominated by background sedimentation (hemipelagic) process with small-scale, minor event beds. These finely laminated and graded sediments are interpreted in a similar way to the organic–rich graded sediments of microlithofacies 7. The graded sediments of microlithofacies 8 are either the far-distal equivalents of tempestite or turbidite events on the shelf or the product of a current-reworking of the deep-slope sediments. Carbonate sediments were transported from proximal sources to deeper depositional environments in slow and constant sedimentation rates and in events. Rare shelf-derived fossils from an assumed proximal source were not associated with the sedimentation events. This suggests that the graded beds were not associated with major events with a proximal origin. The events may be triggered by proximal storms or sediment events such as slumps, but the distal events appear to be low energy current reworking of the sediments already at depth. Graptoloid rhabdosomes and radiolaria are rare in these strata. No association was found between the distribution of the planktonic organisms and the sorting of sediments within the graded beds. The lack of planktonic fossils and the pale colour of the organic-poor

sediments suggest that productivity was low during this time or carbonate sedimentation was high, or both.

Microlithofacies 9: graded laminae, heterogeneous clasts

Concretions:

CP 214.5
CP 163.1
CP 163a
CP 163b
CP 162.8
CP 150.6

Description

The concretions of lithofacies 9 comprise a variety of grain types and grain sizes and record more or larger scale events than those of microlithofacies 8. Radiolarian molds are seen in two concretions (CP 150.6, CP 162.8). Like those of microlithofacies 7, the spheres are more common at the top of the graded beds. Although CP 150.6 and CP 162.8 show a heterogeneous, coarse clastic composition and sedimentary structures that indicate sediment sorting (cross-bedding and graded-beds), the graptoloids are not concentrated in the event beds. Graptoloids are rare in these two concretions and display a random vertical distribution. In sharp contrast to CP 150.6 and CP 162.8, concretion CP 214.5 contains a graptoloid-rich layer that is more than 4 cm thick. The background sedimentation to this graptoloid transport event in CP 214.5 is similar to that of CP 162.8 and CP 150.6.

Interpretation

The sparsity of the graptoloid rhabdosomes in CP 150.6 and CP 162.8 probably relfects the sparsity of graptoloids in the overlying water. This low abundance of graptoloids is probably related to the low organic carbon content in the sediments observed throughout the Cape Phillips section and a lower overall productivity as compared to the Cape Manning section. The graptoloids are not concentrated by the sediment-sorting events, because of the rarity of fossils. The event bed in CP 214.5 is

early Wenlock, when graptoloids in the Cape Phillips Embayment were abundant but of low diversity. The transport event concentrated the graptoloids from the water column and the sediment into a complex deposit composed of two different taphocoenosis assemblages. The two different assemblages - each complete with scour bases, orientation and grading of sediment - are interpreted to represent two different high-energy transport events from a waning flow. The sedimentary structures in CP 150.6 and CP 162.8 and the graptoloid concentration bed of CP 214.5 record distal transport events initiated by a shallower tempestite or turbidite or by rapid deposition from nepheloid layers.

Microlithofacies 10: graded-stratified, clay and carbonate

Concretion:

CM 47.4-47.5

Description

The finely laminated concretion CM 47.4-47.5 displays an overall grading of colour from a light base to a dark top, represented by an upward increase in darker laminae. Light brown laminae are slightly thicker than dark brown laminae. Without the overall grading this concretion would be classified as microlithofacies 5 (finely laminated, clay/organic-rich). Carbonate crystal size ranges from indistinguishable matrix to 40 μm with an average diameter of 10 μm. The crystals are of this range throughout the concretion, with neither an overall grading in size nor an association between size and lamina colour. Dark brown organic material in the matrix defines the laminae.

Interpretation

In studies of siliciclastic sediments, the graded-stratified silt facies is a characteristic deposit of a low concentration turbidity current (Piper, 1978; Piper and Stow, 1991) and can be described using the Bouma (1962) turbidite model. The stratified silts are produced by grain-by-grain deposition from suspension followed by traction transport (Pickering *et al.* 1989). The silts grade into clays that were deposited from suspension as flocculated masses with no subsequent traction transport (Pickering *et al.*,

1989). In this carbonate-dominated deposit, the graded stratified microlithofacies is given a similar interpretation. Instead of a silt to clay gradation, the finely laminated sediments record a carbonate to clay gradation with an assumed decrease in grain-size up-concretion. The sediments of CM 47.4-47.5 are assumed to be the result of a carbonate turbidite that distally was limited in energy and sediment supply and produced this parallel-laminated stratified sediment.

Microlithofacies 11: wavy-bedded

Concretions:

CM 59.1-59.2
CM 57.5- 57.6

Description

The two concretions that share the characteristic wavy-bedding are classified as microlithofacies 11. In thin section, the wavy character of the lamina was a representation of multiple, bedding-parallel stylolites. Light laminae average 2 - 3 mm in thickness and dark laminae 2-4 mm. In thin section, a grey matrix characterizes the light laminae with carbonate crystals in grain/crystal contact and few brown (organic?) patches. The crystals range in size from 20 – 100 μm. The dark laminae contain more clearly defined crystal boundaries and common brown patches. In these dark laminae, the carbonate crystals are smaller than in the light laminae (20 – 40 μm). The lower part of CM 57.5-57.6 contains more abundant light laminae than the upper part. It is difficult to say if there is a grading of light laminae to dark, because of the stylolitic alteration of the sediments. Similarly, CM 59.1-59.2 contains a 6 mm graded lamina, which is difficult to interpret as a result of the stylolites that bound the top and base of the lamina. Sharp, and irregular contacts recorded from this lithofacies are likely a product of bedding-parallel stylolites and cannot be assumed to be recording an erosive base.

Interpretation

I determined this lithofacies to be a diagenetic alteration of a finely laminated sediment. The wavy beds are the product of bedding-parallel stylolites. The bedding-

parallel stylolites are relics of a directed pressure that was likely perpendicular to bedding. The pressure was accommodated by pressure solution at weak boundaries (bedding contacts). It is not clear how much of the sediment has been lost due to pressure solution. Interpretations of the depositional environment are impeded by this diagenetic overprint. Evidence of graded beds or overall grading and the dominance of coarsely crystalline carbonate laminae suggest a depositional environment similar to lithofacies 10 (CM 57.4-57.5) or lithofacies 4 (CM 59.1-59.2)

Summary of the microlithofacies of the Cape Phillips Formation

The resedimented facies model of the slope-apron is most useful for the study of ancient deep-water carbonates. In this model developed by Mullins and Cook (1986) the shallow-water debris is shed into the embayment from a line source, the whole platform margin. The apron is therefore a wedge of shallow water and pelagic sediment with little vertical organization. This is characteristic of the Cape Phillips Embayment sediments. Shelf-derived sediments and fauna are interbedded with hemipelagic sediments and fossils from the pelagic realm. Microlithofacies dominated by shelf-derived sediments (1, 3, 9) are interpreted to be deposited in a more proximal slope setting. Microlithofacies dominated by hemipelagic sedimentation (5, 6, 7, 8) are interpreted to be more distal to the slope-shelf transition.

Table 5.1 summarizes the eleven microlithofacies identified from the concretions of the Cape Phillips Formation, using the criteria outlined in this chapter. These microlithofacies and the lamination styles are an important component of the taphofacies model presented in the following chapter. A discussion of the temporal distribution of these lithofacies within the Cape Phillips Formation is presented in Chapter Seven and used in an interpretation of the history of sea level, sedimentation, and productivity in the Cape Phillips Embayment.

Table 5.1. Microlithofacies of the Cape Phillips Formation

microlithofacies		number of concretions	crystal size (μm)		colour	lamination style	clast type
			range	ave.			
1	structureless, clay/organic-rich	8	10-100	30	dark brown or grey-brown	weak or absent	bioclasts, mud clasts and homogeneous mud
2	structureless, clay/organic-poor	1	indistinguishable		medium brown	absent	
3	coarsely laminated, clay/organic-rich	6	20-100	50	medium to light brown laminae	laminae greater than 5 mm (ave. =30 mm) in thickness	
			10-80	30	dark brown laminae		
4	coarsely laminated, clay/organic-poor	2	40-150	80	light to medium brown laminae		
			10-80	30	medium to dark brown laminae		
5	finely laminated, clay/organic-rich	7	10-60	20	medium to dark brown laminae, rare light brown laminae	fine laminae, average less than 5 mm in thickness	
6	finely laminated, clay/organic-poor	6	20-110	50	light to medium brown laminae, rare dark brown laminae		bioclasts, mud clasts and heterogeneous mud
7	graded laminae, clay/organic-rich	7	10-60	20	medium to dark brown laminae, rare light brown laminae	finely laminated with graded laminae less than 1 cm in thickness; most commonly grades from light to dark.	bioclasts, mud clasts and homogeneous mud
8	graded laminae, clay/organic-poor	7	20-110	50	light to medium brown laminae, rare dark brown laminae	finely laminated with graded laminae less than 5 mm in thickness; most commonly grades from light to dark; or from homogeneous to heterogeneous	bioclasts, mud clasts and heterogeneous mud
9	graded laminae, heterogeneous clasts	6	20-110	50	light to dark brown laminae	finely laminated with multiple or thickly laminated graded beds that grade from homogeneous to heterogeneous	
10	graded-stratified, clay and carbonate	1	?-40	10	light to dark brown laminae	finely laminated with an overall grading from more light laminae at the base to more dark laminae at the top.	bioclasts, mud clasts and homogeneous mud
11	wavy-bedded	2	20-100		light brown laminae	wavy laminae are bound by bedding - parallel stylolites	
			20-40		dark brown laminae		

6 GRAPTOLOID BIOSTRATINOMIC TAPHOFACIES

In this chapter I will use the evidence from a fine-resolution sampling vertically through concretions to understand the post-mortem sedimentary history of graptoloids. The method of layer-by-layer dissolution enables the examination of the orientation, preservational condition and small-scale lateral and vertical heterogeneity in graptoloid distribution within single bedding planes and through successive strata. The lithology and sedimentary history can be deciphered by examining polished slabs and thin sections of the concretions cut perpendicular to bedding, and by studying etched fragments of concretion in a ESEM/EDS. Also valuable in this study are the residues from the dissolution that contain the isolated graptoloids and the insoluble portion of the sediment. It is then possible from the above information to identify graptoloid taphofacies that indicate particular combinations of paleoecologic and depositional conditions.

The taphofacies model I propose relates the evidence of biostratinomic alteration and the vertical variability in graptoloid distribution to the lithology of the laminae in which they occur, to define the paleoecological and taphonomic processes that acted on the fossils. Comparative taphonomy and the construction of taphofacies models have proved to be useful tools in previous paleontological investigations (Chapter two). When applied to graptoloids we obtain a better understanding of the fossil group in three ways: 1) influencing paleoecology studies by understanding the "taphonomic filter" that has altered the original life assemblage, 2) enhancing our understanding of graptoloid occurrence, the basis of graptoloid biostratigraphy, and 3) understanding the sedimentary dynamics of the Cape Phillips Embayment and deep-water facies.

Measuring graptoloid taphonomic characters

Graptoloids are commonly preserved in organic-rich shales that were deposited in deep-water environments. The deep-water facies is rarely the subject of taphonomic investigations. Many taphonomic attributes examined in the creation of benthic, relatively shallow-water taphofacies models, such as abrasion, articulation, orientation, bioerosion, edge rounding, and encrustation are not readily applicable to the study of

deep-water taphofacies. Primary sedimentary structures defined for coarser sediments are rarely seen in fine-grained sediments and the sedimentological characteristics of different deep-water regimes are subtle. The interpreted anoxic bottom-water, depositional environment of graptoloid-bearing, black shales precludes the development of benthic macroinfauna, an important requirement of benthic taphofacies models. Benthic taphofacies indices do not accurately measure characteristics of the graptoloid taphonomy and therefore a new model must be created.

Graptoloid taphonomic characteristics examined herein include: pre-dissolution fragmentation of rhabdosomes, misshaped rhabdosomes (bent or flattened), orientation of rhabdosomes in the horizontal and vertical planes, and bedding concentration of rhabdosomes. This examination is a systematic, qualitative assessment of graptoloid taphonomic characteristics and only bedding concentration was quantified and statistically summarized (chi-square analysis).

Encrustation is an important taphonomic characteristic in shallow-water, benthic taphofacies models, because of the information that can be obtained regarding exposure of the organism at the sediment-water interface (Kidwell and Bosence, 1991). In shallow-water, benthic environments, the encrustation is biologically induced and the bioencruster can often be identified. Some graptoloid rhabdosomes isolated from the concretions are encrusted with a brown, opaque, fine-grained, insoluble material. To understand the nature of this encrustation and whether it was the product of biological organisms or diagenetic alteration after burial, I examined a few encrusted graptoloids in SEM from CM 49.8-49.9 (Figure 4.29A, B) and CM 45.3-45.4 (Chapter four). No characteristic algae or organic shapes could be distinguished from the fine-grained, light brown material that thickly encrusted the rhabdosome. The encrusting material formed in clusters or spheres and did not penetrate the rhabdosome. In thin section, the encrusting material was observed to radiate out from the organic rhabdosome (Figure 4.29C). In these ways the encrusting material had the appearance of diagenetic cement, not a bioencrustation. Holes in the rhabdosome were observed to be puncture holes, probably resulting from processing methods, and not biological borings. Further evidence for the diagenetic origin of the encrusting material is found on the dissolution surface. The layers of CM 49.8-49.9 that contained the encrusted graptoloids also contained a fine,

brown, insoluble material, which was concentrated at the centre of the concretion – a poorly formed core. The graptoloids at the centre of the concretion were preferentially covered with this material. The decay of the organic matter in the sediments at this interval initiated precipitation of the cement by bacterial sulphate reduction and methane generation (Coniglio and Melchin, 1995). In some concretions (e.g., CM 49.8-49.9), the initial precipitation of cement resulted in the encrustation of the rhabdosome. Encrustation of graptoloid rhabdosomes may help decipher the diagenetic history of the graptoloid-bearing concretions but it cannot be used as a biostratinomic indicator.

Graptoloid taphonomic characters were described for each layer for each of the 53 concretions or limestone beds dissolved in this study. These were compared with the lithologic evidence for sediment events (Chapter Five) to understand the biostratinomic history of the graptoloid rhabdosomes.

Bedding Plane Concentration

It is assumed that the normal, hemipelagic settling of graptoloids and sediment, resulted in a random distribution of graptoloids vertically through the concretion. The concentration of graptoloids into single horizons is recording an "event" that was the result of paleoecological or taphonomic processes. Concentration of graptoloids onto bedding planes can be quantitatively measured and represented statistically by a chi-square analysis (See Chapter Three, Equation 3.1). The null hypothesis is that the graptoloids have a random distribution and are not concentrated in layers.

Size-sorting

As the current energy at the sediment surface increased, the first biostratinomic alteration would be a winnowing of the finer grains and the smaller graptoloid rhabdosomes. The resultant taphocoenosis would over-represent the larger rhabdosomes of the life population. The size of the graptoloid rhabdosome is thought to represent the age of the graptoloid colony at the time of death (Rigby and Dilly, 1993). It has generally been assumed that graptoloids lived in age-integrated life populations (Rickards, 1991), but some researchers have argued that the younger or siculae

rhabdosomes lived segregated from the plankton cloud and attached on the seafloor (Kirk, 1990a). The correlated thecae and sicular distributions observed in many concretions of this thesis (e.g., CM 55, Cm 56.4-56.5), suggest that the mature and juvenile colonies are both planktonic and settled from the water column at a similar rate. It is possible that the age classes are segregated within the water column or the plankton cloud.

It is difficult to differentiate size-sorted graptoloid horizons that were the result of biostratinomic processes, such as winnowing, from those due to an ecological separation of age-classes during life. However, when size-sorting is associated with other observations of current alignment or a sorting of the lithic fraction of the sediment, then an argument for biostratinomic removal of the smaller rhabdosomes can be made. A size-sorted deposit of the finer rhabdosome sizes may also be the result of biostratinomic concentration. A few examples, showed an increase in siculae and smaller rhabdosomes at the tops of graded beds. In studies of modern fine-grained turbidites, planktonic organisms settle-out following an influx of sediment during a transport event and the deposition of a graded bed (Piper and Deptuck, 1997). The smaller organisms are suspended by the increased water energy and fall from suspension as the energy wanes.

Underwood (1993b) interpreted the necrolytic history of the planktonic graptoloids to be a great source of bias. Differential settling based on rhabdosome density, size, and drag would alter the thanatocoenosis and the fossil assemblage. He suggested this would alter the final assemblage in two ways: 1) slower settling rhabdosomes would be more susceptible to physical or biological destruction resulting in an under-representation in the fossil record, and 2) slower settling rhabdosomes were more susceptible to transportation resulting in mixed ecological deposits.

I see the bias introduced by differential settling rates to be a minor taphonomic alteration in the fossil preservation process. A modern, small, planktonic invertebrate called a copepod, is similar in size to a graptolite colony and can be used as a modern analogue to study settling rates. The settling rate for anaesthetized copepods (*Calanus*) with a length of 2 mm is 5 meters/hour (Marshall, 1979). Assuming that the organism is near the surface and is sinking through approximately 200 meters of water, that depth could be reached by the small copepod in 40 hours. A larger copepod (*Calanus*) with a

length of 4 mm sinks at a rate of 30 meters/hour (Marshall, 1979) and would reach the sediment surface in 6.7 hours. These settling rates are geologically instantaneous. Transportation distances during this time would be limited, even if flotation was prolonged as a result of decay. Finally, the destruction experienced during settling is may be minimal compared with the taphonomic alteration that might take place on the sediment surface if the conditions favour biological or physical destruction.

For each rhabdosome on a dissolution layer the size-class was recorded (Appendix D): sicula, theca 1-2, theca 3-4 and theca 5 or greater. Rhabdosome sicular distribution was measured through the residues of the Cape Manning section. The method of counting the siculae is described in Chapter Three. The comparison between the distribution of the thecae and the smaller siculae was an important measure of the presence or absence of size-sorting.

Orientation: alignment of elongate rhabdosomes

As the current energy at the sediment surface increased the elongate rhabdosomes favoured an orientation parallel to the current energy. Orientation of the rhabdosomes is evidence of biostratinomic processes acting upon the fauna at the sediment surface and was not the result of paleoecologic interactions. Orientation is easily measured on shale bedding planes and represented by rose diagrams. Graptoloid orientation is more difficult to observe on the concretion dissolution layers because of the small surface area. Low rhabdosome abundance makes observations of orientation difficult. Orientated graptoloids were recorded from dissolution surfaces with as few as seven mature specimens (e.g., CM 59.1-59.2; Figure 4.58C, D). In this thesis graptoloid orientation is associated with two depositional regimes: mass transport, and *in situ* sediment lag.

Fragmentation

Fragmentation is a taphonomic indicator that can occur during necrolysis, or during biostratinomic processes in the water-column, at the sediment surface, or after burial as a result of bioturbation. Most of the Cape Phillips Formation fauna is assumed to have been deposited in anoxic sediments and possibly anaerobic overlying waters. These low

oxygen conditions limited the extent of bioturbation and scavenging. Most biostratinomic fragmentation is usually accompanied by the orientation of elongate rhabdosomes and is therefore related to higher energy deposition (e.g., CM 214.5). Rhabdosomal resistance to fracture varies taxonomically and the observations of fragmentation are relative to the species. Processing methods of the concretions in acid may account for some fracturing, but the acid concentration was dilute and the dissolution was gentle and only fragmentation that clearly took place prior to processing was recorded.

Species distribution

The isolated graptoloids from the insoluble residues collected during the dissolution process were identified to the species level and counted in concretions from the Cape Manning section. The rhabdosomes were usually fragmented in the residues and it seemed inappropriate to reconstruct colonies for the population count, as Underwood attempted to do in his graptoloid population study (Underwood, 1998). Underwood (1998) differentiated the fractured end versus the true distal ends and proximal ends, and used a random generation program to recreate full colonies from the fragments. The result was a very smooth distribution of sizes in which growth stages were averaged-out of the population. Instead, I counted the number of thecae in defined size categories for each species. This results in an accurate representation of the number of individuals (zooids of the colony) in the taphocoenosis and a quantitative measure of diversity and abundance.

Sudden shifts in the taphocoenosis may represent events that can be related to a change in the source of the organisms (e.g., deposition from another planktonic niche), a change in the paleoecology (e.g.,. a bloom of one or more species), or a change in preservational conditions (e.g., different rhabdosomes are preserved, increasing or decreasing diversity).

Graptoloid biostratinomic taphofacies model

The graptoloid taphofacies model is designed to be a tool for understanding how graptoloids accumulate on the sediment surface. The model is based upon hypothetical biostratinomic processes that may have acted upon graptoloids in the Early Silurian. The ideas generated from this model are then tested against the concretionary material of the Cape Phillips Formation. One taphofacies, "bioturbation" is proposed as possible, but is not observed in the material examined in this thesis. It is the purpose of this model to relate the evidence of biostratinomic reworking and the vertical variability in distribution of the graptoloids to the lithology of the laminae in which they occur in an attempt to define the paleoecological and taphonomic processes that acted on the fossils. From these observations, distinct graptoloid taphofacies are recognizable (Figure 6.1). The model involves the quantification of graptoloid vertical distribution and the qualitative assessment of biostratinomic alteration.

Graptoloid rhabdosomes can be randomly distributed through the sediment or concentrated on one or more bedding planes. Random vertical distribution, as measured by a chi-square analysis, can be the product of a random influx of graptoloids and sediment. Low graptoloid abundance in the life assemblage in the waters over the slope can also result in a random distribution even if event beds are recorded in the sediment. Bioturbation can dilute and distribute graptoloid concentration beds, creating a random distribution of rhabdosomes vertically through the sediment. These three conditions (random flux of graptoloids and sediment; sediment events, low graptoloid abundance; and bioturbation) are three taphofacies that describe sediments with a random vertical distribution of graptoloids.

Graptoloid concentration beds can be produced by many mechanisms. Graptoloids will appear concentrated if the rate or quantity of sediment input or graptoloid input is not consistent during the time of deposition. The quantity or rate of graptoloids reaching the sediment surface can increase as a result of paleoecological changes in the life assemblage (blooms) or as a result of hydrodynamics (transportation of graptoloids in a turbidite or tempestite and concentration or winnowing in the flow). The graptoloids could also be concentrated into bedding surfaces by the removal (lag) or non-deposition of sediment (hiatus). All four types of graptoloid concentration events can be found in

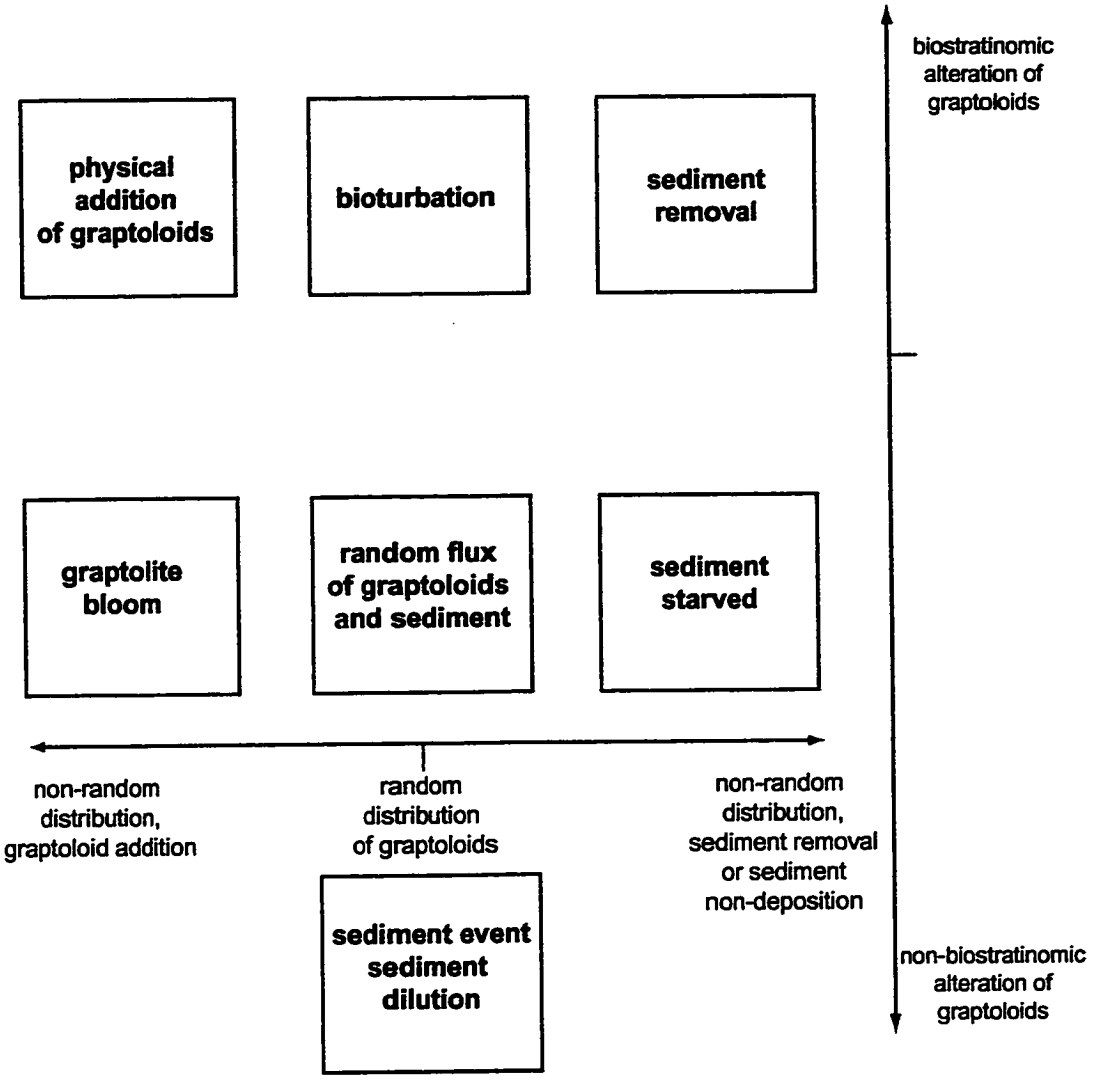

Figure 6.1. The graptoloid biostratinomic taphofacies model based upon quantitative measurement of graptoloid vertical distribution and qualitative information regarding graptoloid taphonomic features, distribution of species assemblages and the lithology and lamination style of the sediment.

the Cape Phillips Formation concretions and in the following section all will be described and distinguished from the others. The taphofacies are given names that are interpretive. The details of this interpretation will be expanded upon following each taphofacies diagnosis.

Random flux of graptoloids and sediment – (Table 6.1)

Description

The graptoloids are randomly distributed through the dissolution surfaces as revealed from the chi-square analysis (Table 6.1). The sediments are commonly laminated (microlithofacies 5, 6) and rarely record sedimentary events, such as graded beds (microlithofacies 7, 8, 9). Unlaminated (microlithofacies 1,2) or coarsely laminated (microlithofacies 3) sediments are also present in this taphofacies. Orientation and fragmentation of graptoloid rhabdosomes are not observed on the dissolution surfaces. The thecal counts from the dissolution residues may vary in species dominance or composition, but not significantly in total abundance.

Interpretation

This taphofacies is considered to represent the "background sedimentation" in the Cape Phillips Formation with which the "event sedimentation" is compared. The finely laminated sediments with random vertical graptoloid distribution are interpreted to be deposited in a hemipelagic depositional environment. The alternate dark and light laminae represent subtle variations in the source sediment or rate of sedimentation. The absence of an infaunal benthos is interpreted to be the result of anoxic conditions within the sediment and above the sediment-water interface. Small-scale, minor sedimentary events that resulted in graded beds were not great enough to alter the biostratinomy of the graptoloids and concentrate them. Bottom currents are common in modern deep waters (McCave, 1984) and reworking of the sediments with no effect on graptoloid distribution could have occurred if the energy of the current was low. Coarse laminae with random graptoloid distribution are also considered to be hemipelagic. They differ from the finely

laminated sediments in that they are the product of a more consistent sediment source, with little variation in grain characteristics or rate of deposition.

Table 6.1 Concretions of the "random flux of graptoloids and sediment" taphofacies

Concretion name and meterage (m)	zone	microlithofacies	χ^2/n	taphonomic observations
CP 96a 7.5	*instrenuus-kolobus?*	2; structureless, clay/organic-poor	0.7	random orientation, random vertical distribution, no evidence of size-sorting, rare evidence of biostratinomic or necrolytic fragmentation,
CP 96a 6.0		8; graded laminations, clay/organic-poor	1.2	
CP 152b	*sakmaricus*	6; finely laminated, clay/organic-poor	1.0	
CP 146.5a			0.7	
CP 146.5b			0.6	
CM 114.4a	*turriculatus*	6; finely laminated, clay/organic-poor	1.7	
CM 114.4b			0.7	
CM 84.5	*guerichi*	5; finely laminated, clay/organic-rich	1.9	
CM 72.6			0.5	
CM 58b	*convolutus*	3; coarsely laminated, clay/organic-rich	1.0	
CM 58a			2.3	
CM 57.5-57.6			0.9	
CM 56.4-56.5		1; structureless, clay/organic-rich	1.2	
CM 56			8.3	
CM 50.4-50.5	*orbitus*	3; coarsely laminated, clay/organic-rich	1.0	
CM 41.65-41.75	*cyphus*	7; graded laminations clay/organic-rich	4.6	

Sediment event – graptoloid dilution (Table 6.2)

Description

Concretions that represent this taphofacies are very similar to those of the taphofacies random flux of graptoloids and sediment. They differ in that the concretions

record a sedimentary event, identified by one or more graded lamina(e), and the overall graptoloid abundance is low. The events that produced the graded beds are not associated with graptoloid biostratinomic alteration and this appears to be the result of the rarity of the graptoloid rhabdosomes in these concretions (average of 1.6 graptoloids per dissolution surface, Appendix E). Statistically, the graptoloid distributions within these concretions supports the null hypothesis of random distribution. The rarity of graptoloids could be the result of a reduced input of graptoloids, or, more likely, a high sedimentation rate. Most of the concretions of this taphofacies are from the Cape Phillips section. The evidence for a high sedimentation rate in the Cape Phillips section, as compared with the Cape Manning section discussed in Chapter seven. A high sedimentation rate may have diluted the graptoloids in the sediment. The rare graptolids were not concentrated during the small-scale sedimentary events that sorted the sediments. So that this lack of a graptoloid concentration does not detract from the significance of these sediment events, these concretions are placed in a taphofacies other than random flux of graptoloids and sediment. Concretions of this taphofacies that were collected from the Cape Phillips section also contain common shelly fauna that are possibly from more proximal, shallow-shelf settings.

Interpretation

Currents or distal flows at depth can rework the sediments and create graded sedimentary beds (McCave, 1984). The scarcity of graptoloids in the sedimentsdetermined that graptoloid concentration beds were rare. The sediments record episodic, rapid deposition of graded laminae, even though this is not recorded by the graptolites. This may be the result of two inter-related factors: the scarcity of graptolites, and the increased rate of sediment supply coming from the shelf (as indicated by the common shelly fauna). The flows were likely rich in fine-grained, carbonate sediments and shelf-derived fauna and upon reaching deeper waters lost energy and deposited this sediment without physically reworking the sediments previously laid down. This would be possible if the environment and basin morphology was such that the flow energy was above the sediment-water interface or that these sediment accumulations were distal to the higher-energy flows.

Table 6.2 Concretions of the "sediment event-low graptoloid abundance" taphofacies

Concretion name and meterage (m)	zone	microlithofacies	χ^2/n	taphonomic observations
CP 163.1	*sakmaricus*	9; graded laminations, heterogeneous clasts	1.2	random orientation, random vertical distribution, no evidence of size-sorting, no evidence of biostratinomic or necrolytic fragmentation,
CP 163a			2.0	
CP 163b		5; finely laminated, clay/organic-rich	0.5	
CP 162.8		9; graded laminations, heterogeneous clasts	1.2	
CP 145.2		8; graded laminations, clay/organic-poor	0.9	
CP 96			1.5	
CP 56.9	*grieston-iensis*		1.0	
CP 38.4		7; graded laminations clay/organic-rich	1.4	
CP 32		8; graded laminations, clay/organic-poor	0.5	
CM 96-6	*guerichi*	7; graded laminations clay/organic-rich	0.9	
CM 42.3-42.4	*cyphus*		0.7	
CM 40.5-40.6			1.5	

Bioturbation

Description and interpretation.

This graptoloid taphofacies is presented herein although no representatives were found in the concretions examined from the Cape Phillips Formation. Although brief periods of bottom-water oxygenation may have existed during the Early Silurian, a benthic infauna, even of a restricted ichnofacies, did not appear to develop. To positively identify this taphofacies, evidence of bioturbation or a mottled texture was necessary and this was not observed in the 52 concretions I examined. Fragmentation of the rhabdosome or orientation of a majority of the rhabdosomes oblique to bedding are graptoloid taphonomic characters I associate with this hypothetical bioturbation taphofacies. Clear evidence of major taphonomic fragmentation by metazoan recyclers was not observed. Although rare fragmented rhabdosomes were recorded, most often the

fragmented graptolites were associated with evidence for physical reworking such as orientation or size-sorting of the graptoloid assemblage. In addition, most rhabdosomes recorded from the dissolution surfaces of the 52 concretions were oriented parallel to bedding (Appendix E). The absence of lamination was not considered convincing. Most of the concretions classified in the structureless microlithofacies were organic-rich (microlithofacies 1), and did not seem to be depleted in organic mater when compared to the laminated facies. Often the reverse was true, and these beds were darker in colour and from intervals in which the organic matter content from the shales was high (Figure 7.1). In addition some of the concretions classified in the structureless microlithofacies showed taphonomic evidence of physical reworking, suggesting that the lack of lamination was the result of rapid deposition rather than benthic mixing. The absence of this taphofacies from the Cape Phillips Formation supports the previously stated interpretation that the sediments of the Cape Phillips Embayment were deposited under anoxic conditions.

Graptoloid Bloom (Table 6.3)

Description

The distribution of graptoloids through the consecutive dissolution surfaces is inconsistent with the null hypothesis of random distribution. The graptoloid concretion layers are not associated with graded beds or organic-rich horizons. Concretion CM 44.1 is classified as microlithofacies 7, graded laminae; however, the graded laminae are not correlated with the graptoloid concentration beds. The graptoloids of these layers do not display distinctive taphonomic characters, such as fragmentation or orientation. These taphofacies were identified based on the detailed analysis of the species distribution through the residues of the layer-by-layer dissolution of the concretions. Each of the concretions records an abundance in one species or species assemblage.

Interpretation

A bloom in the biocoenosis that is caused by a paleoenvironmental change, such as an increase in a limiting nutrient, a bloom in the phytoplankton, or the reduction of competition or predation, will result in an increase in the number of individuals of the beneficent species or assemblage in the taphocoenosis. It is most common for one species or a species association to dominate during a bloom at the cost of the other zooplankton not able to take advantage of the change in environmental conditions (Bougis, 1976). The record of a paleoecological graptoloid bloom, therefore, is an increase in the relative abundance of one species or a species association through a particular interval of the concretion. Graptoloids commonly occur on single bedding planes, with diversity low and age variation great (Rickards, 1991). Rickards (1991) suggested this was the result of mass-mortality of monospecific plankton clouds from a particular niche. The episodic deposition of graptoloid blooms would result in the concentration of graptoloids on the sediment surface. Graptoloid blooms appear in the strata as an influx of graptoloids with no change in background sedimentology.

Table 6.3. Concretions of the "graptolite bloom" taphofacies

Concretion name and meterage (m)	Zone	microlithofacies	χ^2/n	bloom species
CM 75.5	*guerichi*	5; finely laminated, clay/organic-rich	8.8	*Pristiograptus regularis regularis*
CM 54.0-54.15	*convolutus*	1; structureless, clay/organic-rich	1.5	*Metaclimacograptus orientalis*
CM 53.2-53.3			2.1	*Monograptus falcata* forma A followed by *Monograptus* n. sp. C
CM 52.1-52.2		5; finely laminated, clay/organic-rich	3.1	*Metaclimacograptus orientalis*
CM 44.1	*pectinatus*	7; graded laminations clay/organic-rich	3.7	*Monograptus* cf. *arciformis*

Physical addition of graptoloids (Table 6.4)

Description

Graptoloid distribution is not statistically random but instead graptoloids are concentrated on one or more layers in the concretions of this taphofacies. The concentrated graptoloid horizon has a sedimentological and paleontological signature that is different from the strata above and below. Clear lithologic breaks or sedimentary structures resulting from currents or flows are evidence of hydrodynamic events or a shift in the sediment grain composition and source. Some higher energy transport events (e.g., CP 214.5) resulted in scour marks and truncated bedding. Paleontological evidence of transport is recorded in the graptoloid species distributions. The transport event shows an influx of a taphocoenosis that is distinct in composition from the graptoloids found above and below the event. This is usually accompanied by allochthonous fauna that were derived from shelf environments. Elongate graptoloids often display orientation and even fragmentation and bending. Size-sorting is common with a rarity of siculae (small, juvenile colony) in the graptoloid concentration beds.

Interpretation

Graptoloids that form the concentration beds of this taphofacies can be far-traveled (reworked from elsewhere on the sediment surface or from the water column) or near-traveled (reworked from the original sediments at the depositional site). All graptoloids by the nature of their planktonic lifestyle are allochthonous to their depositional sediment. I employ the terms "far-traveled" and "near-traveled" here to describe relative lateral transport distances. It seems clear from the species distribution plots and the observations of the dissolution surfaces, that the concentration beds of this taphofacies are a mixture of far-traveled fauna that were transported from a different pelagic niche with a near-traveled fauna that lived in the overlying waters. The far-traveled fauna is unique to the event bed and the near-traveled fauna is common throughout the strata above and below.

Table 6.4. Concretions of the "physical addition of graptoloids" taphofacies

Concretion name and meterage (m)	Zone	microlithofacies	χ^2/n	taphonomic observations in the event bed
CP 214.5	*instrenuus-kolobus*	9; graded laminations, heterogeneous clasts	200	alignment, fragmentation, winnowing of small graptoloids, grading of bioclasts, scoured base, two distinct graptolite assemblages.
CP 152a	*sakmaricus*	6; finely laminated, clay/organic- poor	5.4	grading of graptolite size with grading of sediments, increased shelly fauna.
CP 150.6		9; graded laminations, heterogeneous clasts	1.7	
CP 148.1		8; graded laminations, clay/organic- poor	13.7	fragmentation?, increased shelly fauna, heterogeneity of clast-type
CM 59.1-59.2	*convolutus*	11; wavy bedding	4.3	alignment, faunal composition change
CM 57		3; coarsely laminated, clay/organic-rich	1.1	increased shelly fauna, faunal composition change
CM 51.2-51.3a	*orbitus*		3.7	
CM 50.4		1; structureless, clay/organic-rich	3.0	basal abundance; assemblage with distinct composition.
CM 48.5			3.6	alignment, size-sorting, assemblage with distinct composition
CM 47.4-47.5	*pectinatus*	10; graded stratified	3.8	faunal composition change with overall grading of lithology
CM 46.35-46.5		1; structureless, clay/organic-rich	33.4	alignment, size-sorting, faunal composition change
CM 45.3-45.4			9.6	alignment, size-sorting (scarcity of siculae in lag), distinct species assemblage in lag

The transport events are accompanied by higher energy flows that can orient the elongate graptoloids and fragment or bend the rhabdosomes, depending on their durability (see discussion in Chapter Four, CP 214.5). One recorded transport event is associated with a basal lag (CM 45.3-45.4) that resulted from the winnowing of small graptoloids and fine sediment. The winnowing of sediment in these transport events was probably more prevalent than recorded in this thesis, because of infiltration of fine-

grained sediment into the spaces between the bioclasts flowing the winnowing event and prior to lithification. Infiltration fabrics, common in shell layers, are produced by the percolation of finer grained sediment down into the lag, as the energy subsides and material in suspension settles out (Tucker and Wright, 1990).

Sediment-starved (Table 6.5)

Description

Graptoloids are not randomly distributed vertically through the concretion but are concentrated on one or more layers. In condensed horizons, it is possible to find a few fragments of species that are rare in the rest of the concretion (e.g., *Coronograptus* sp. and *P. inopinatus* of CM 42.8-42.9). Rare species have a greater chance of making it into the taphocoenosis of the sediment-starved horizon simply because of exposure time. Therefore, the concentration beds identified as sediment-starved are often higher in diversity than the strata above or below. Unlike a concentration bed of the taphofacies graptolite bloom, one species or a species assemblage does not dominate the assemblage. The relative proportions of the main species of the graptolite assemblage are not unlike those of the strata above or below. The event beds are not enriched or depleted with respect to siculae and do not appear to be size-sorted. They lack other signs of current reworking, such as alignment of the elongate rhabdosomes or biostratinomic fragmentation of delicate rhabdosomes. These event beds are associated with an increase in the dark organic material and a reduction in the carbonate crystal size that may be related to a finer-grained original texture. Concretions CM 73.8, 74.9a and 74.9b contain graptoloid concentration layers with all the characteristics of a sediment-starved depositional environment but do not show a dark, organic layer associated with the condensed horizons.

Interpretation

The stratigraphically condensed beds were interpreted to be deposited in anoxic bottom-waters, where the graptoloid rhabdosomes were free from the effects of scavengers or other metazoan recyclers. Encrustation, although common in one

concretion of this facies (CM 49.8-49.9), was not associated with bioencrusters or exposure time (see discussion in Chapter Four, CM 49.8-49.9). The increase in dark organic matter is interpreted to reflect the "raining down" of hemipelagic organic material from the waters above, without pronounced dilution by a fine-grained carbonate or siliclastic sediment. For the same reason graptoloids accumulate on these hiatus horizons. These condensed horizons represent significant amounts of time. The taphocoenosis assemblages from these horizons are likely significantly time-averaged (Chapter eight) and should be avoided in paleoenvironmental reconstructions or detailed evolutionary studies.

Concretions CM 73.8, 74.9a, and 74.9b are interpreted as sediment-starved deposits, but not true hiatus horizons. Sedimentation of fine-grained carbonate and clay had decreased but not stopped. This variation in sedimentation rate combined with a possible subtle increase in graptoloid input creates the concentrated graptoloid horizons.

Table 6.5. Concretions of the "sediment-starved" taphofacies

Concretion name and meterage (m)	zone	microlithofacies	χ^2/n	taphonomic observations of sediment-starved layer
CM 74.9a	*guerichi*	5; finely laminated, clay/organic-rich	5.4	fragmentation; rare species in horizon, *P.* cf. *variabilis*; no alignment, no size-sorting
CM 74.9b			5.9	
CM 73.8			9.5	rare group in horizon, Retiolitid; no orientation, no size-sorting
CM 55	*convolutus*	3; coarsely laminated, clay/organic- rich	5.1	rare species in horizon, *N. nikolayevi* and *G. incertus?*; no alignment, no size-sorting
CM 49.8-49.9	*orbitus*	1; structureless, clay/organic-rich	2.5	high diversity; no alignment, no size-sorting
CM 44.0-44.1	*pectinatus*	7 graded laminations clay/organic	7.2	associated with the tops of two graded beds, no alignment, no size-sorting
CM 42.8-42.9	*cyphus*		10.7	rare species in horizon, *Coronograptus* sp. and *P. inopinatus*; no alignment, no size-sorting

Sediment Removal (Table 6.6)

Description

Mature graptoloid rhabdosomes are very abundant at the base of this bed as observed on the basal dissolution surfaces (Figure 4.18A; 42 rhabdosomes, all mature, no siculae) and in the dissolution residues (Figure 4.19). Most species observed higher in the concretion are observed in this basal layer; however, two species *Pristiograptus* n. sp. A, and *Pribylograptus imprimus* occur only in the basal residues. The basal residues are not enriched in siculae and thus the percentage siculae of the total count is low (33 and 39 % compared with the concretion average of 69%). Elongate rhabdosomes show some degree of current alignment only on the basal dissolution surface (Figure 4.18C).

Interpretation

The alignment and absence of small rhabdosomes indicates that this basal unit is an event horizon recording the biostratinomic alteration of the assemblage. This event brought in new species but also concentrated the mature individuals from the surrounding water/sediment. This limestone bed appears to be a resedimented limestone with a basal lag. Winnowing of fine-grained sediments from graptoloid-bearing deposits in a current with a velocity great enough to orient the graptoloids can produce a concentrated horizon of oriented graptoloids. Sedimentological and paleontological consistency with adjacent strata is characteristic of *in situ* sediment lag deposits and distinguishes them from mass-transport processes. Winnowing of small-sized graptoloids also produces a skew in the graptoloid assemblage towards larger rhabdosomes in the sediment lag accumulations.

Table 6.6. Concretions of the "sediment removal" taphofacies

Concretion name and meterage (m)	zone	microlithofacies	χ^2/n	taphonomic observations
CM 45.3-45.4	*pectinatus*	1; structureless, clay/organic-rich	12.2	alignment, size-sorting (scarcity of siculae in lag), distinct species assemblage in lag.

The nature of the physical transport events: regional scale.

The transport events identified by the taphofacies "physical addition of graptoloids" could be the product of contour currents, settling from nepheloid layers, storm events, or turbidity currents. Bottom currents and contourites (deposits from bottom currents) in carbonate-rich, deep-water sediments arise from thermohaline circulation, and internal waves and tides (Tucker and Wright, 1990). Contourites record a break in the stratigraphic record, and result in the cementation and *in situ* mineralization of sediments (Tucker and Wright, 1990). Pelagic fossils are sorted by the currents and reworked deposits show some alignment with the paleocontour, parallel to the strike of the slope (Tucker and Wright, 1990). The samples for this study were not collected azimuthal orientation, making the distinction between contourite and turbidite deposits difficult. Rare examples of inverse graded beds found in the concretions of this study are not convincingly of the contourite-type inverse grading described in siliciclastic studies (e.g., Stow, 1979). In addition, regional geologic knowledge does not support the evidence for a constant and persistent geostrophic bottom-water current (Melchin, 1989, de Freitas *et al.*, 1999), and it seems unlikely that a contour current could have created the types of transport events I have recorded.

Nepheloid layers are layers of water with suspended material that is kept in suspension by barriers to settling, such as temperature, salinity or density. When the barrier is overcome, rapid sedimentation can result. This depositional process may explain much of the laminated nature of the hemipelagic facies and some of the smaller scale transport events in the Cape Phillips Formation (Trettin et al. 1991). However, many of the transport events are associated with shelf-derived fauna and this can only be explained with the turbiditic and tempestite process models.

Tempestites are the deposits of storm events. Tempestites usually record complex current information, such as unidirectional currents and waves and paleocurrents markers (Aigner, 1982). Proximal storm beds are thick units of composite beds composed of bioclasts and coarse-grained sediment (Aigner, 1982). Distal equivalents are thin, fine-grained single event beds (Aigner, 1982). The storm events lose their energy and sediment supply as they move oceanward. This scenario is complicated by ocean floor

topography, the source of the storm (shelf or shoreline), and variations in the strength and the frequency of the storms (Tucker and Wright, 1990).

Storm events probably created many of the graptoloid concentrations identified in the taphofacies physical addition of graptoloids. The evidence of physical reworking of the sediment and the graptoloids (fragmentation, orientation, size-sorting) is suggestive of a flow-event. The evidence of mixing of far-traveled and near-traveled fauna and the associated input of shelly fauna from the shelf, suggests that these beds were an accumulation of material from proximal to distal depositional environments, as would be expected in a tempestite. However, a similar concentration bed could also be produced by a turbidity current.

Turbidites are deposits from waning turbidity currents. Turbidity currents are described as the down-slope movement of sediment driven by gravity or density (Piper, 1972b). These are well analyzed in siliciclastic environments, ancient and modern (e.g., Pickering *et al.*, 1989 and references therein). Carbonate turbidites have only recently gained the attention of researchers. Where sediments are less than medium sand in size, as in the Cape Phillips Formation, they can be carried in suspension and the resultant flow is termed a low-density turbidity current (Tucker and Wright, 1990). As the energy wanes the suspended load becomes bed-load and the result in siliciclastic sediments is the Bouma T_{bcde} sequence (Tucker and Wright, 1990). The turbidite from this flow is 0.05 to 0.3 m thick and not all elements of the Bouma sequence may be present (Tucker and Wright, 1990). The carbonate turbidite can be identical to this siliciclastic turbidite but the identification of the sedimentary structures may be difficult, because of the fine grain size (Tucker and Wright, 1990). An example of a possible low-density turbidite is recorded in CP 214.5. A discussion of the internal structures of the event bed and their interpreted depositional regime can be found in the concretion description in Chapter Four. For the other graptoloid concentration beds of the physical addition of graptoloids facies, it is more difficult to differentiate distal tempestites from distal turbidites.

7 TEMPORAL DISTRIBUTION OF THE MICROLITHOFACIES AND TAPHOFACIES OF THE CAPE PHILLIPS FORMATION: PALEOENVIRONMENTAL IMPLICATIONS.

The microlithofacies identified from the concretions of the Cape Phillips Formation are plotted against the stratigraphy for the Cape Manning (Figure 7.1) and Cape Phillips sections (Figure 7.2). In this way, the temporal distribution of the microlithofacies can be established and discussed. All graptoloid biostratinomic taphofacies, with the exception of the bioturbation taphofacies are observed in the concretions and limestone beds of the Cape Phillips Formation. The distribution of graptoloid taphofacies through the Cape Manning (Figure 7.3) and Cape Phillips sections (Figure 7.4) can be related to the microlithofacies. This distribution is discussed with respect to the global sea-level curves of M. E. Johnson (1996) and and Loydell (1998) presented in Figures 7.1 – 7.4).I use this information, in addition to a regional geological understanding based on previous studies, to interpret the history of productivity and sea-level during the Early Silurian in the Cape Phillips Embayment.

The observations are discussed chronologically in eight sections that represent eight intervals of stratigraphy. The time units discussed in each of the eight sections are related to the strata in the following way:

- late Rhuddanian – early Aeronian; *Coronograptus cyphus* Zone and lower *Monograptus pectinatus* Zone.
- early middle Aeronian; middle to upper *Monograptus pectinatus* Zone.
- middle Aeronian; *Rastrites orbitus* and lower *Lituigraptus convolutus* Zone.
- middle late Aeronian; middle to upper *Lituigraptus convolutus* Zone.
- late Aeronian; *Stimulograptus sedwickii?* Zone.
- early Telychian; *Spirograptus guerichi* Zone.
- mid Telychian; *Monograptus crispus*, and *Monoclimacis griestoniensis* zones.
- late Telychian; *Cyrtograptus sakmaricus*, and *Cyrtograptus insectus* zones

Figure 7.1. Distribution of microlithofacies through the Cape Manning section. Each open circle to the right of the stratigraphic column is a studied concretion. Microlithofacies are identified by numbers: 1, structureless, clay/organic-rich; 3, coarsely laminated clay/organic-rich; 4, coarsely laminated, clay/organic-poor; 5, finely laminated, clay/organic-rich; 7, graded laminae, clay/organic-rich; 10, graded-stratified, clay and carbonate; 11, wavy-bedded. Diagonal lines depict stratigraphic intergrading of two microlithofacies. Descriptions of these facies are in Chapter Five. The percentage of total organic content (TOC %) measured from shales collected from the same section is from Melchin (pers. comm., 2001) was not used in microlithofacies classification but is presented here for comparison. Global sea-level curves of of M. E. Johnson 1996. and Loydell (1998) are presented for comparison.

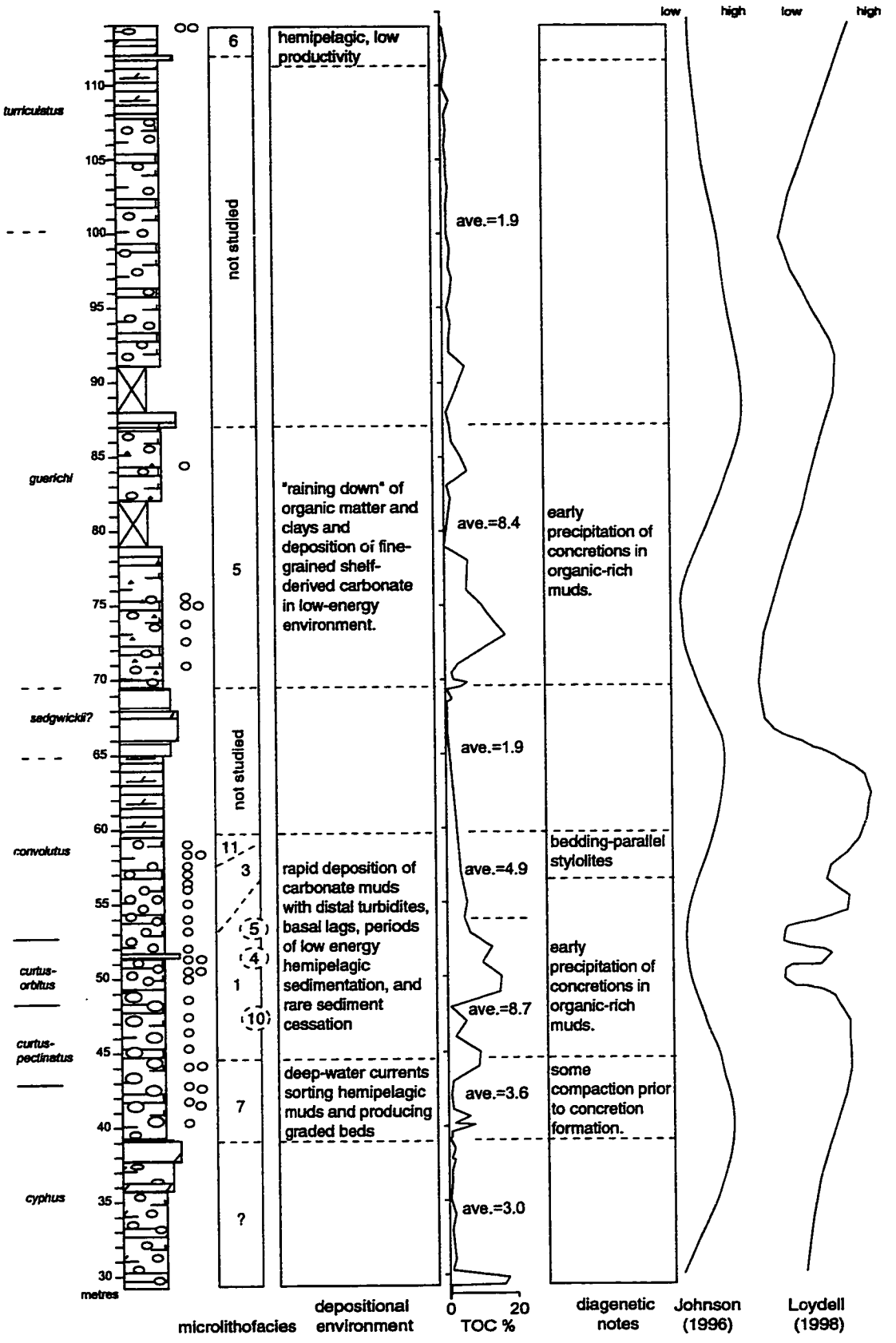
low
high
low
high
turriculatus
guerichi
sedgwickii?
convolutus
curtus-orbitus
curtus-pectinatus
cyphus
110
105
100
95
90
85
80
75
70
65
60
55
50
45
40
35
30
metres
6
not studied
5
not studied
11
3
5
1
4
1
10
7
?
hemipelagic, low productivity
"raining down" of organic matter and clays and deposition of fine-grained shelf-derived carbonate in low-energy environment.
rapid deposition of carbonate muds with distal turbidites, basal lags, periods of low energy hemipelagic sedimentation, and rare sediment cessation
deep-water currents sorting hemipelagic muds and producing graded beds
ave.=1.9
ave.=8.4
ave.=1.9
ave.=4.9
ave.=8.7
ave.=3.6
ave.=3.0
early precipitation of concretions in organic-rich muds.
bedding-parallel stylolites
early precipitation of concretions in organic-rich muds.
some compaction prior to concretion formation.
0
20
TOC %
microlithofacies
depositional environment
diagenetic notes
Johnson (1996)
Loydell (1998)

Figure 7.2. Distribution of microlithofacies through the Cape Phillips section. Each open circle to the right of the stratigraphic column is a studied concretion. Microlithofacies are identified by numbers: 6, finely laminated, clay/organic-poor; 8, graded laminae, clay/organic-poor; 9, graded laminae, heterogeneous clasts. Diagonal lines depict stratigraphic intergrading of microlithofacies. Descriptions of these facies are in Chapter Five. The percentage of total organic content (TOC %) measured from shales collected from the same section is from Heath (1998) was not used in microlithofacies classification, but is presented here for comparison. The sea-level curve of Loydell (1998) is presented for comparison. The rapid marine regression at the end of the *C. sakmaricus* Zone identified by Loydell may also be reflected in the change of microlithofacies from 6/8 to 9 (see text).

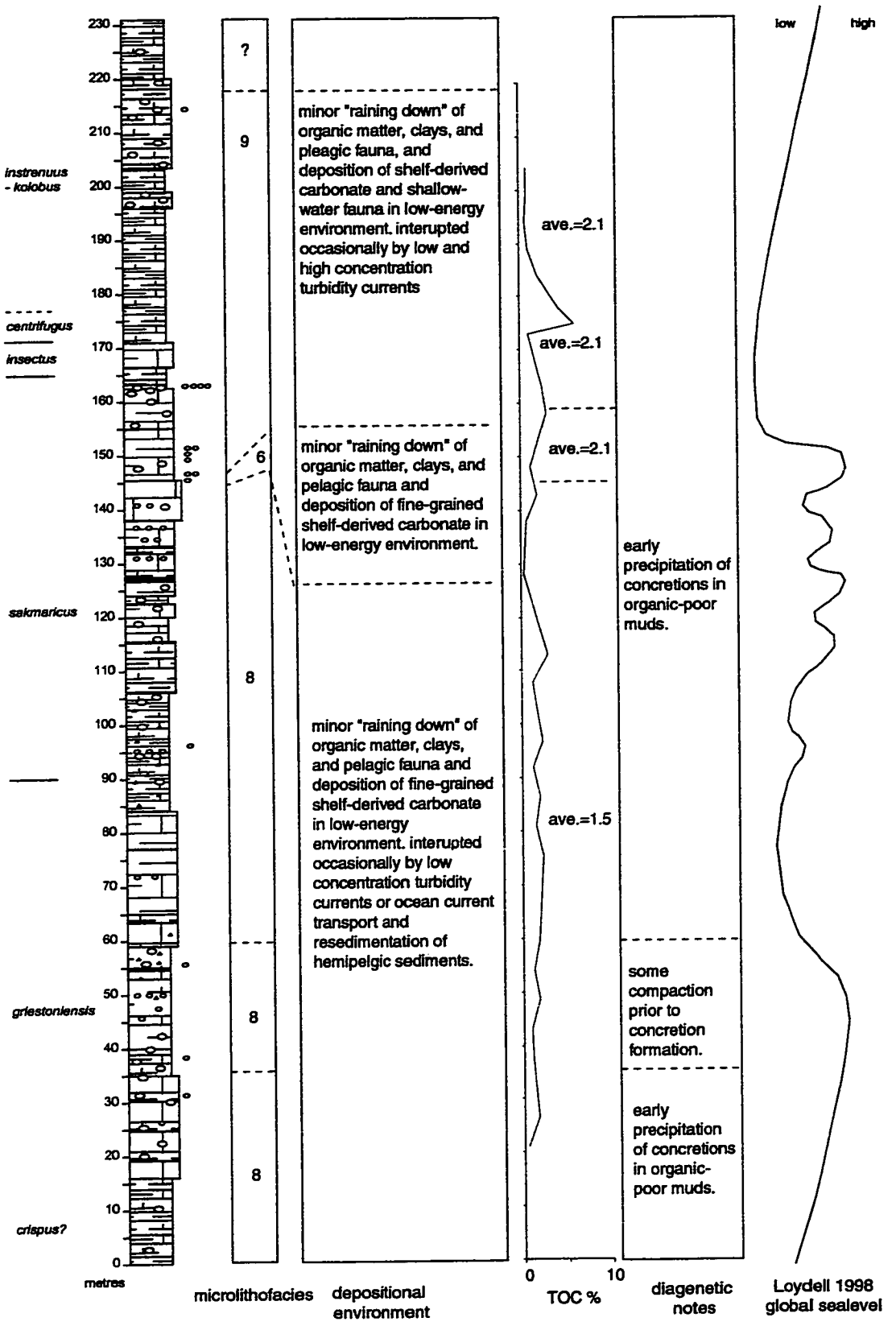
230
220
210
200
190
180
170
160
150
140
130
120
110
100
90
80
70
60
50
40
30
20
10
0
metres
instrenuus - kolobus
centrifugus
insectus
sakmaricus
griestoniensis
crispus?
?
9
6
8
8
8
microlithofacies
minor "raining down" of organic matter, clays, and pleagic fauna, and deposition of shelf-derived carbonate and shallow-water fauna in low-energy environment. interupted occasionally by low and high concentration turbidity currents
minor "raining down" of organic matter, clays, and pelagic fauna and deposition of fine-grained shelf-derived carbonate in low-energy environment.
minor "raining down" of organic matter, clays, and pelagic fauna and deposition of fine-grained shelf-derived carbonate in low-energy environment. interupted occasionally by low concentration turbidity currents or ocean current transport and resedimentation of hemipelgic sediments.
depositional environment
ave.=2.1
ave.=2.1
ave.=2.1
ave.=1.5
0
10
TOC %
early precipitation of concretions in organic-poor muds.
some compaction prior to concretion formation.
early precipitation of concretions in organic-poor muds.
diagenetic notes
low
high
Loydell 1998 global sealevel

Figure 7.3. Distribution of taphofacies through the Cape Manning section. Each open circle to the right of the stratigraphic column is a studied concretion. Descriptions of the taphofacies are in Chapter Five. The microlithofacies are identified by numbers: 1, structureless, clay/organic-rich; 3, coarsely laminated clay/organic-rich; 4, coarsely laminated, clay/organic-poor; 5, finely laminated, clay/organic-rich; 7, graded laminations, clay/organic-rich; 10, graded-stratified, clay and carbonate; 11, wavy-bedded.

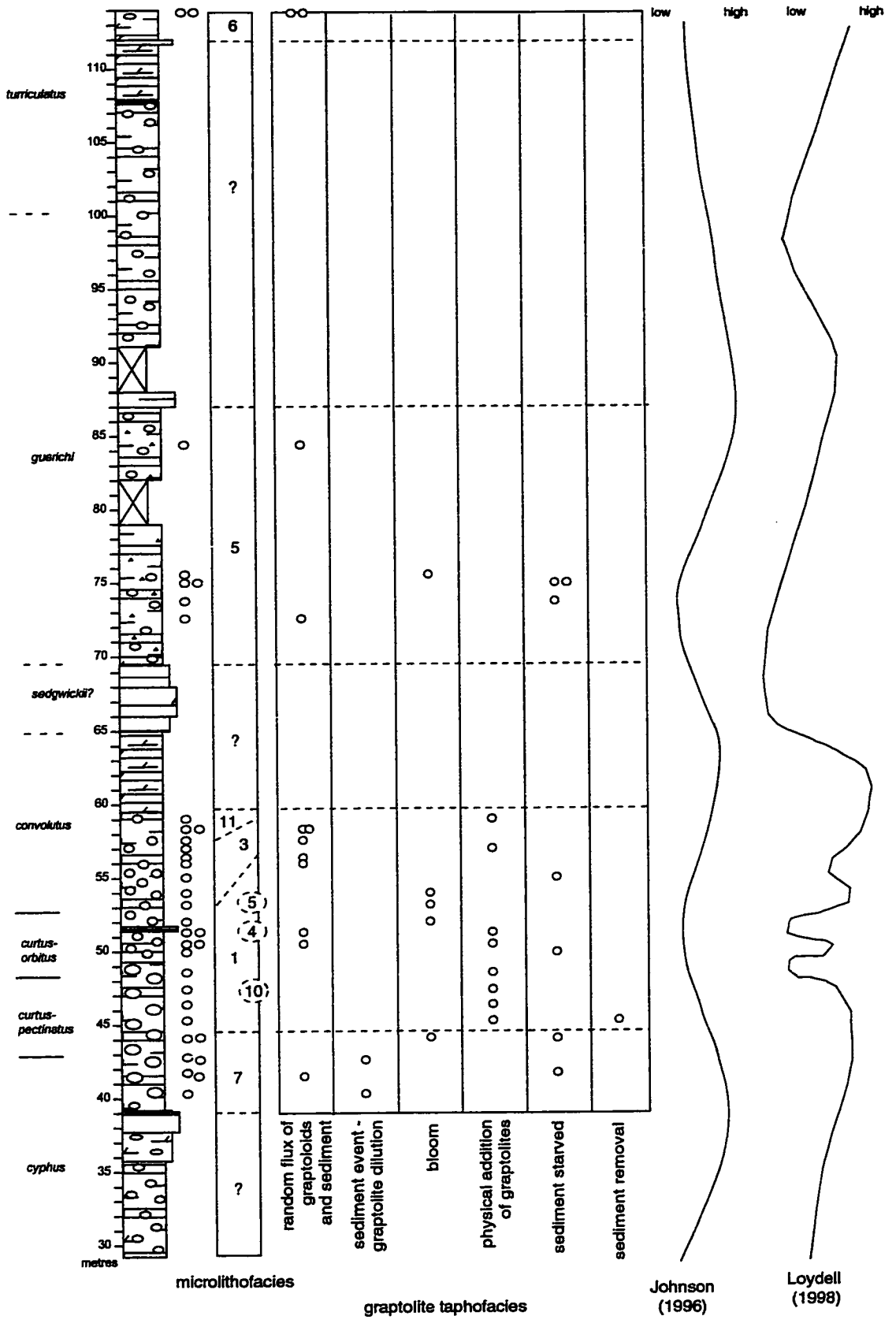
turriculatus
guerichi
sedgwickii?
convolutus
curtus-orbitus
curtus-pectinatus
cyphus
110
105
100
95
90
85
80
75
70
65
60
55
50
45
40
35
30
metres
6
?
5
?
11
3
5
1
4
1
10
7
?
microlithofacies
random flux of graptoloids and sediment
sediment event - graptolite dilution
bloom
physical addition of graptolites
sediment starved
sediment removed
graptolite taphofacies
low
high
low
high
Johnson (1996)
Loydell (1998)

Figure 7.4. Distribution of taphofacies through the Cape Phillips section. Each open circle to the right of the stratigraphic column is a studied concretion. Descriptions of the taphofacies are in Chapter Six. The microlithofacies are identified by numbers: 6, finely laminated, clay/organic-poor; 8, graded laminae, clay/organic-poor; 9, graded laminae, heterogeneous clasts.

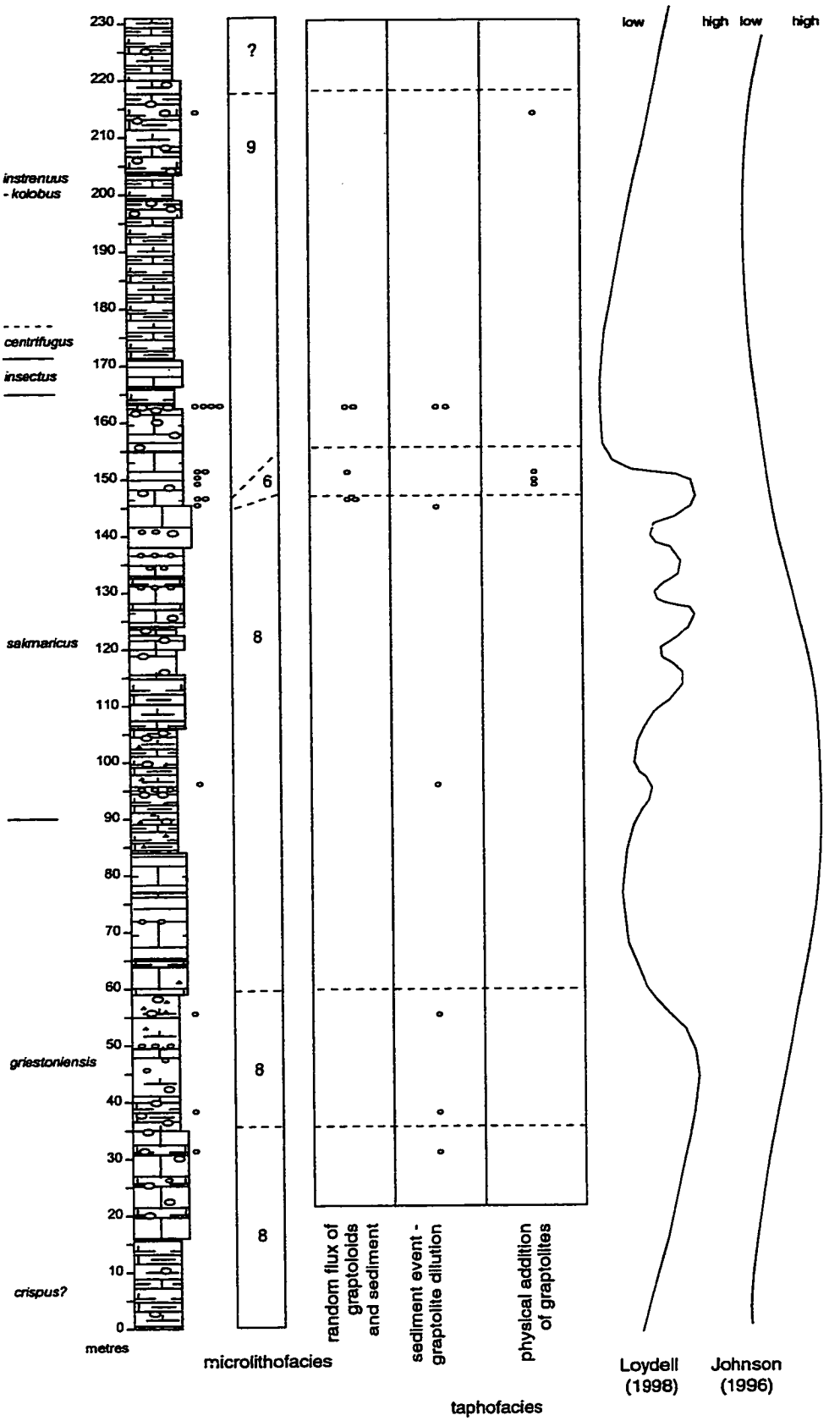
low
high
low
high
instrenuus - kolobus
centrifugus
insectus
sakmaricus
griestoniensis
crispus?
metres
microlithofacies
random flux of graptoloids and sediment
sediment event - graptolite dilution
physical addition of graptolites
taphofacies
Loydell (1998)
Johnson (1996)

Late Rhuddanian – early Aeronian; *Coronograptus cyphus* Zone and lower *Monograptus pectinatus* Zone.

During the late Rhuddanian and early Aeronian when global sea level was high (M. E. Johnson, 1996; Loydell, 1998), four taphofacies are identified in the Cape Phillips Formation concretions: random flux of graptoloids and sediment; sediment event –low graptoloid abundance; graptoloid bloom; and sediment-starved (Chapter Six). Graptoloids are concentrated by paleoecological mechanisms (bloom of *Monograptus* cf. *arciformis* in CM 44.1) or by the reduced input of sediment (CM 42.8-42.9, CM 44.0-44.1). Graded beds that record paleocurrents or flows did not concentrate the graptoloid rhabdosomes, because the rhabdosomes were not common in the sediments (CM 40.5-40.6, CM 42.3-42.4). All of the concretions from this interval are assigned to microlithofacies 7, graded laminae, clay/organic-rich, compressed graptoloids (Chapter Five). The "hemipelagic" sediment that was occasionally reworked by low-energy flows may support the deep-water scenario suggested by the global sea-level curve. This is in disagreement with regional geology studies; however, which place the Cape Manning section in a proximal setting close to the Allen-Bay Facies transition during the Rhuddanian (Melchin, 1989; de Freitas, 1999). The Snowblind Creek section, south of Cape Manning and closer to the Cape Phillips-Allen Bay facies transition reveals Aeronian carbonates of the Allen Bay Formation overlain by Telychian shales of the Cape Phillips Formation (Melchin, 1989). This back-stepping of the facies transition suggests a change in basin morphology from a ramp to a steeper- rimmed shelf (Melchin, 1989; de Freitas, 1999). During the Rhuddanian, the Cape Manning section was likely in a proximal setting. The microlithofacies and taphofacies described during this interval could be the product of sediment by-pass. The sediment-starved taphofacies would support this. Overall graptoloid abundance was low. Blooms of certain taxa (e.g., bloom of *M.* cf. *arciformis*) may be evidence of a group of graptoloids that were "cratonic invaders" (Finney and Berry, 1997), able to exploit rare opportunities inland of the upwelling waters on the continental margin. The high sea level in the Rhuddanian followed by a marine regression in the early Aeronian that is identified globally (M. E. Johnson, 1996; Loydell, 1998), is not observed in the Cape Phillips Embayment. The taphofacies and microlithofacies identified from the concretions of the *C. cyphus* Zone

(Rhuddanian) and *M. pectinatus* Zone (Aeronian) are clearly different, however, and in the next section I suggest some possible reasons for this change.

Early middle Aeronain; middle to upper *Monograptus pectinatus* Zone.

All four samples collected from the middle to upper *M. pectinatus* Zone show the characteristics of the same taphofacies; physical addition of graptoloids (Chapter Six). One limestone bed (CM 45.3-45.4) is placed into two taphofacies as it displays the characteristics of the physical addition of graptoloids and those of a sediment lag. Two concretions are classified as microlithofacies 1, structureless clay/organic-rich and one is microlithofacies 5, coarse laminae, clay/organic-rich. All three are interpreted to be the product of rapid mud deposition (Chapter Five). One concretion is classified as microlithofacies 10, graded stratified. When the lithologic evidence is matched with the taphonomic evidence, such as the biostratinomic reworking, it seems evident that the environment of the late Rhuddanian and early Aeronian dominated by background processes, has been replaced with a more event-rich environment. The increased number of event beds and the abundance of graptoloids could be related to a change in basin morphology, such that sediments and graptolites could accumulate and were not carried past to deeper waters. A slight change in basin morphology could alter the location of upwelling cells, thus changing the graptoloid assemblage from the low diversity "cratonic invaders" to the diverse "margin dwellers" (Finney and Berry, 1997). Alternatively, the abundance of resedimented carbonate beds and graptoloid concentration horizons at this interval may be the products of increased storminess or earthquakes.

Middle Aeronian; *Rastrites orbitus* and lower *Lituigraptus convolutus* Zone.

Global sea level as interpreted by Loydell (1998), was low at the beginning of this time inerval, rises rapidly in the middle, falls towards the top, and then rises through the time represented by the *L. convolutus* Zone (Loydell, 1998). Other sea-level curves (e.g., M. E. Johnson, 1996) show this as an interval of low sea level without the fluctuations identified by Loydell (1998). The detailed lithologic study from concretions sampled from one-meter intervals at the Cape Manning section was not sufficient to identify the

short-term fluctuations of sea level proposed by Loydell (1998); however, the concretions may reflect a low sea-level that does match M. E. Johnson's (1996) sea-level curve in its simplicity.. The evidence for this is in the predominance of non-laminated or coarsely laminated sediments, the increased abundance of shelf-derived sediments and organisms, and the variety of taphofacies that may suggest a more proximal location. The diversity of microlithofacies and taphofacies in this interval may suggest a complex sea-level history; however, they could also be reflecting a complexity of sedimentation, basin dynamics, local tectonics, or environmental variables.

Multiple bloom events in the three concretions from the top of the *R. orbitus* (CM 52.1-52.2) and lower *L. convolutus* zones(CM 53.2-53.3 and CM 54.0-54.15) suggest a relatively stable depositional environment; this is indicative of a change from the high-energy, taphonomically active environment recorded by the sediments of the lower *R. orbitus* Zone. Sea level had probably started to rise at the time of the lower *L. convolutus* Zone. These graptoloid blooms may be indicative of this changing environment and the ability of a few species to dominate the biocoenosis. On the other hand, the graptolite blooms may just be more clearly preserved in these sediments because of the absence of physical reworking, which would otherwise mix the separate assemblages.

Middle late Aeronian; middle to upper *Lituigraptus convolutus* Zone.

Microlithofacies 3 (coarse grained, clay/organic-rich) and the graptoloid taphofacies of random flux of graptoloids and sediment predominate in the concretions collected from the middle *L. convolutus* Zone. Many of these sediments and graptolites suggest deposition in a hemipelagic environment. One concretion that shows characteristics of sediment starvationand two that show taphonomic features of the physical transport of graptoloids, suggest that steady hemipelagic deposition was interrupted periodically by transport events and sedimentation hiatuses.

During the mid-Aeronian, a sea level fall is followed quickly by a sea level rise, with the highest sea levels of the Llandovery recorded in the time of the mid-late *L. convolutus* Zone (Loydell, 1998). In the *L. convolutus* Zone of the Cape Manning section the last of the graptolite-bearing concretions is found at CM 59.1-59.2. Above this, the

lithology changes to a laminated dolostone from which no graptolites have been collected. This is likely recording the beginning of the shallowing event that reaches a maximum at the *L. convolutus - S. sedgwickii* boundary (M. E. Johnson, 1996).

Late Aeronian; *Stimulograptus sedwickii?* Zone.

The massive carbonate marker (CM 65 - 69.5 m) occupying the *S. sedgwickii* Zone is composed of coarse-grained, resedimented carbonate and is found at this stratigraphic interval throughout the region (Melchin, 1989). Although the Cape Phillips Formation lacks graptolites that would positively identify this biozone, the thick, graptolite-barren carbonate is stratigraphically bounded by the *L. convolutus* and *S. guerichi* Zones and is thought to represent the *S. sedgwickii* Zone. The sea level fall and erosion/emerge history during the *S. sedgwickii* Zone is recorded in the stratigraphic record of many paleocontinents (Loydell, 1998). Here in the Cape Phillips Embayment, this zone is also associated with a change from a carbonate ramp to a rimmed-platform (Melchin 1989 de Freitas, 1999).

Early Telychian; *Spirograptus guerichi* Zone.

Global sea level rose during the early Telychian and fell during early middle Telychian (recorded in the upper *S. guerichi* – lower *Spirograptus turriculatus* Zones (M. E. Johnson, 1996; Loydell, 1998). Sea level was high during the upper *S. turriculatus* and remained high with only slight fluctuation until the mid *Cyrtograptus lapworth* Zone of the late Telychian. The concretions sampled from the *S. guerichi* and *S. turriculatus* zones of the Cape Manning section provide an incomplete picture of sea level history. The distance between samples is too great to make any statements about relative depth of deposition with any certainty.

Mid Telychian; *Monograptus crispus*, and *Monoclimacis griestoniensis* zones.

The organic-rich microlithofacies (1, 3, 5, 7, 10) are found in the Aeronian of the Cape Manning section and the organic- poor microlithofacies are found in the Telychian of the Cape Phillips section. It should be noted that this is a relative measure of organic

matter based solely on colour. A study of the total organic content (TOC) of the shales from the Cape Phillips Formation supported these conclusions. The average TOC measured from shale samples from the Cape Manning section was 3.86 (n=107) (Melchin, pers. comm., 2001); whereas, the average TOC measured from shales from the Cape Phillips section was 1.75 (n=27) (Heath, 1998; Figures 7.1, Figure 7.2). The darker, more organic-rich concretions of the Cape Manning section may be related to productivity in the overlying water, preservation of the organic matter in the anoxic sediments, or a slow sedimentation rate. The organic-poor sediments of the Cape Phillips section are associated with fewer graptoloids than the graptoloid-abundant, and organic-rich sediments of the Cape Manning section. This suggests that the difference between the two time periods reflects productivity, increased carbonate sedimentation, or both. Of these, variations in sedimentation rates seem most likely. The *M. griestoniensis* Zone and the *C. sakmaricus* Zone at the Cape Phillips section comprise approximately 150 m of strata; two biozones of the Cape Manning section (e.g., *R. orbitus* and *L. convolutus*) represent approximately 15 m. The biozones may not represent the same amount of time (Melchin and Cooper, in prep.) but they do not differ ten-fold. The two biozones of the Telychian section represent approximately twice the age of the two biozones from the Aeronian. The thick sequence of strata through the Telychian was most probably being deposited at a faster rate, thus diluting the organic matter and the graptolites. The change in sediment dynamics in the basin at this time may have also affected upwelling currents and the diversity and abundance (productivity) of graptoloids, but it would be difficult to extract that information from the two sections examined.

Late Telychian; *Cyrtograptus sakmaricus*, and *Cyrtograptus insectus* zones

At the Cape Phillips section, the interpreted sea level is relatively uniform in the *M. crispus*?, *Monoclimacis griestoniensis* and lower *Cyrtograptus sakmaricus* Zones. All concretions examined from these strata are classified as microlithofacies eight, graded laminae, clay/organic-poor or microlithofacies six, finely laminated, clay/organic-poor. Both are considered to be deposits typical of normal hemipelagic sedimentation in a basin with deep, low-energy currents. The resolution of this investigation was not satisfactory for identifying the fluctuations in sea level identified by Loydell (1998) during this same

time period. A change is identified in sediments of the concretions at the end of the *C. sakmaricus* Zone and the lower *Cyrtograptus insectus* Zone with the appearance of microlithofacies 9, graded laminae, heterogeneous clasts. This is interpreted to represent a shallowing event and correlates to the mid-*C. sakmaricus* Zone global sea level drop (Loydell, 1998).

8 TIME-AVERAGING AND TEMPORAL RESOLUTION IN THE CAPE PHILLIPS FORMATION

Fossils can become time-averaged in four ways: slow sediment accumulation rates, reworking, benthic mixing, and during fossil collection. Slow sediment accumulation rates result in time-averaged samples when the life-span of the individual organism is less than the time it takes to bury the fossil. In this way, organisms from multiple generations accumulate on the sediment surface and are incorporated into one "time-averaged" bed (Walker and Bambach, 1971). "Reworking" and "benthic mixing" are the result of biologic or physical processes and result in the mixing of fossils and their host sediments following initial deposition (Sadler, 1993). Finally, fossils can also be time-averaged during the processes of collection by the paleontologist. Graptoloid researchers collecting specimens flattened in shale normally find it impossible to collect fossils lamina-by-lamina, unless the shale is perfectly fissile and splits on the millimeter scale, which is a rare occurrence. Often, a representative sample of specimens is collected from a 5 or 10 cm interval. How representative is this sample and how do we affect the temporal resolution, if at all, by this collection method? Is there information that can be gained by a higher resolution sampling or are the natural processes of time-averaging operating on a similar stratigraphic scale to the sampling interval?

I shall present two approaches to attempt to understand the temporal resolution of the Cape Phillips Formation graptoloid-bearing strata. 1) The differences between fossils that record background sedimentation processes and those that define episodic sedimentation processes aid in estimates of time-averaging and temporal resolution (Brett and Baird, 1993). The comparative taphonomic study of the graptoloid-bearing concretions presented in Chapter Six will be reviewed, with the objective of understanding background sedimentation processes and episodic sedimentation processes. One estimate of stratigraphic resolution and completeness of a particular interval is to use absolute ages indirectly from the biostratigraphy, and then to attempt to estimate the relative frequency and durations of single event beds versus background sedimentation. This allows for an estimate of the total time represented by the strata. This method was used by Brandt Velbel (1984) to estimate the completeness of a 30-

meter section from the Upper Ordovician. In that study, summing the estimated durations for ten distinct types of beds and dividing by the absolute age for the section, it was estimated that only 40% of the time was recorded by rock. 2) The layer-by-layer sampling of graptoloids from uncompacted carbonate concretions of the Cape Phillips Formation provides us with a window into the fine-resolution distribution of graptoloids. A statistical comparison (R-mode cluster analysis) of the graptoloid faunal composition within and between concretions in stratigraphic succession through the Cape Manning section is presented in the second part of this chapter. The purpose of the cluster analysis is to understand the stratigraphic continuity in graptolite assemblages and assess the average thickness of vertically distributed species assemblages. This will aide in estimating the degree of time-averaging introduced at the time of fossil collection. Finally, I will suggest the ideal sampling interval in concretionary and shale material that is required to accurately capture distinct graptoloid assemblages in the Cape Phillips Formation.

Background and episodic processes: estimates of stratigraphic completeness and temporal resolution.

Six taphofacies are recognized within the Cape Phillips Formation at two localities exposed on Cornwallis Island (Figure 1.1). The classification of taphofacies is based upon the recurrence of diagnostic suites of taphonomic and sedimentologic attributes (Chapter Six). The taphofacies illustrate the combined effects of processes operating at two temporal scales: background processes that took place over relatively long intervals of time, and episodic processes that were effectively instantaneous.

Background taphonomic processes

In shallow-water environments, background taphonomic processes are very destructive (Speyer and Brett, 1991; Davies *et al.*, 1989). Actualistic studies of modern shallow water environments suggest that the main control on the degree of taphonomic alteration is the duration of the fossil in the taphonomically active zone (TAZ; Davies et al., 1989). A slower rate of burial means that the fossil will persist in the TAZ for greater amounts of time, when it will be exposed to the processes of mechanical and biological

destruction (Davies *et al.*, 1989). The TAZ of the slope sediments of the Aeronian Cape Phillips Embayment was very different from the shallow-water environments often studied in taphonomic analyses. The taphonomic alteration by recycling metazoans (scavengers) was reduced or eliminated as a result of the anoxic conditions of the sediments and bottom-waters. Only anaerobic microbial processes of decay operated in the sediments, during which the release of cations and the alteration of alkalinity in the sediment pores allowed the early precipitation of carbonate (Coniglio and Melchin, 1995). The fine-grained sediments that hosted the graptoloid rhabdosomes were not coarse enough to replicate the damaging physical processes, which operate in shallower sediments such as abrasion. The deep shelf environment witnessed some episodic, moderate to high-energy events, but generally the conditions were quiet with gentle reworking by bottom currents. This differs greatly from the TAZ of the shallow shelf where physical reworking by waves and storms can be damaging if the fossil stays in the high-energy environment for long periods of time (Behrensmeyer, *et al.* 2000). The background taphonomic processes of the Cape Phillips Embayment are defined by the absence of event stratigraphy and the rarity or absence of biostratinomic characters such as fragmentation, size sorting, and orientation.

Sixty three percent of the concretions studied for this chapter are considered to record background taphonomic processes (14 concretions, n=22). Four taphofacies represent the background taphonomic processes of the Cape Phillips Formation; 1) random flux of graptoloids and sediment, 2) sediment event – low graptoloid abundance, 3) graptoloid bloom, 4) bioturbation, and 5) sediment-starved. The first three taphofacies listed are interpreted to be from a hemipelagic depositional environment that recorded the constant "raining-down" of the planktonic graptoloid fauna from the over-lying waters. Small-scale current reworking by distal storm events or geostrophic bottom waters may have produced some graded beds but the graptoloid distribution was not affected by these low-energy events. Times of graptoloid blooms in the living population are recorded as an abundance of graptoloids in the sediments with no accompanying biostratinomic or sedimentologic evidence for a taphonomic event. When sedimentation rates were reduced the graptoloids "raining-down" from the overlying waters accumulated on the sediment surface without being buried. The condensed graptoloid beds recorded as

"sediment-starved" are considered to represent processes of the background sedimentation. Graptoloid biozonation of the two study sections (Chapter two) suggests that major disconformities are not present.. All condensed horizons are likely the result of short-term variations in the sediment supply rate. Four concretions in the Aeronian Cape Manning section (the interval assessed for completeness in the following section) are of the sediment-starved taphofacies: CM 42.8-42.9, CM 44.0-44.1, CM 49.8-49.9, and CM 55 (Table 8.1).

Table 8.1. Estimate of temporal scale of sedimentary starved horizons based upon graptoloid distribution.

Concretion	Number of rhabdosomes on the hiatus horizon	Average number of rhabdosomes per dissolution layer from the non-hiatal horizon	Difference in rhabdosome counts from the hiatus vs. non-hiatal layers.
CM 55	two layers, one sediment-starved horizon ~ 7 mm thick, ave = 39.5	19.4	x 2
CM 49.8-49.9	one thick layer (90 mm) approximately x 4 the graptoloids in comparison with concretions below and above		
CM 44.0-44.1	3 horizons, ave. = 42	16.7	x 2.5
CM 42.8-42.9	42	10.5	x 4

If we can assume that the long-term average input of graptoloid rhabdosomes was constant, then by comparing the relative abundance of rhabdosomes from the condensed horizons and non-condensed intervals in the concretions classified as sediment-starved we have a proxy for estimating the relative temporal richness or condensation of these hiatal horizons. The percentage of rhabdosomes in the condensed horizon versus the rhabdosome count from the rest of the concretion is given for each concretion in Table 8.1. The condensed horizons contain two to four times the number of rhabdosomes as the non-condensed horizons within the same concretion. This can be used indirectly to infer that condensed horizons through this interval represent approximately two to four times the amount of time as non-condensed horizons. The sediment-starved taphofacies was found to be 18% (n=22) of the concretions from the Aeronian Cape Manning section.

The sediment-starved layers represented approximately 25% of the concretion thickness in which they were found (including CM 49.8-49.9 in the average, n=4). Approximately 5% of the sediment from the concretions can be considered to be sediment-starved and represent two to four times the amount of time as compared with the other background sediments.

Episodic taphonomic processes

Sedimentary features that were formed during short intervals of time during events that involve the reworking of the sediment surface include: scour bases, truncated bedding, graded bedding and cross-bedding. Graptoloid taphonomic features that accompany these events include: graptoloid concentration, orientation of the elongate rhabdosomes, fragmentation or bending, and size-sorting of the graptoloid assemblage with the winnowing of the smaller rhabdosome fraction. Two taphofacies are considered to be the product of episodic processes: physical addition of graptoloids, and sediment removal (sediment lag). Eight concretions and limestone beds are classified in the taphofacies physical addition of graptoloids. One carbonate bed (CM 45.3-45.4) is cross-categorized as the only sample in the taphofacies sediment removal. This bed displayed clear evidence of a basal lag. The other samples probably experienced some degree of sediment removal or erosion during the high-energy event that quickly deposited the sediment. Taphonomic evidence for episodic deposition is found in 36% (n=22) of the concretions sampled from the Aeronian Cape Manning section (the interval assessed for completeness in the following section). The graptoloid concentration beds in some samples were only a portion of the total concretion or bed examined. They range from approximately 2 cm to 10 cm in thickness. The event beds ranged from 100% of the concretion or carbonate bed thickness to less than 15 % of the thickness of the sample (average approximately 60%). Therefore, approximately 20% of the thickness of the sediment examined from the concretions of the Aeronian was deposited rapidly in episodic events. This relationship is presumed to apply to the shales deposited laterally at the same time.

Estimate of the accumulation rate and completeness of the Aeronian aged Cape Manning section.

Accumulation rates as inferred from a stratigraphic section will include the quickly deposited, event beds, the background sedimentation that includes hiatus horizons, and the effects of compaction (Sadler, 1993). Completeness of a stratigraphic section is the fraction of time that is recorded in the strata (Sadler and Strauss, 1990). Sedimentary records are never 100% complete, because the depositional process in all environments will involve periods, however short, of erosion or non-deposition (Sadler, 1981; Sadler and Strauss, 1990). Completeness is a function of the age of the section, long term net accumulation rates ("drift"), and the fluctuations in accumulation rates ("unsteadiness") (Sadler and Strauss, 1990).

If approximately 20% of the sediment examined from the concretions displayed signs of episodic deposition and concretion samples were selected based on concretion size, rather than inferred fossil content, can we assume that 20% of the Cape Manning section was deposited episodically? Carbonate concretions precipitate in reduction zones created by anaerobic decay of organic matter. However, the abundance of concretions through this interval suggest that they are not preferentially preserving the graptolite-rich beds. No attempt was made to record the number or scale of event beds in the shale sequences. Not included in the estimate episodic deposition as 20%, is a thickly bedded turbidite that occurs at CM 51.4-51.8. Estimated sedimentation rates outlined below will correct for this rapidly deposited turbidite. The episodic processes operated on a scale of hours to days and the deposition of the event beds was likely preceded by a period of erosion.

The accumulation rate (S) for the Aeronian Cape Manning can be calculated by first estimating the age of the section as inferred from the biozones present. From the base of the Aeronian to the mid *L. convolutus* (top of the concretion-rich interval) is 2.1 million years (Melchin and Cooper, in prep.; methods described in Cooper, 1999b). The total thickness of the Aeronian portion of the section up to the base of the top of the *L. convolutus* is 17 m. The shales were compacted since their original sedimentation, but in this procedure Sadler (1981) has already corrected for compaction. The accumulation rate (S) is simply calculated by the following equation:

$$S = T/t \quad (8.1)$$

where T is the section thickness in meters, and t is the absolute time represented by the section inferred from the biostratigraphy. For this section the accumulation rate is calculated to be 0.0081m/1,000 yr.

In modern marine settings, accumulation rates vary on the scale of 11 orders of magnitude (Sadler, 1981). The rates vary with the time span that is being measured and between different environments (Sadler, 1981). The trend of decreasing accumulation rate with increasing time span is interpreted to be the result of unsteady, discontinuous sedimentation (Sadler, 1981). Sadler (1981) emphasizes the importance of the position above or below wave base, which will influence the rate of erosion and the "steadiness" of accumulation. For sediments that accumulate below wave base Sadler (Figure 12, 1981) gives a range of accumulation rates for "siliciclastic mud" (0.007 m/1,000 yr to 0.01 m/1,000 yr), "calcareous mud" (0.01 m/1,000 yr to 0.013 m/1,000 yr), and "mud" (0.013 m/1,000 yr to 0.5 m/1,000 yr). These are the accumulation rates for sections on the order of 10^6 yr time spans. The calculated accumulation rate from the Cape Manning section of 0.0081 m/1,000 yr compares well with these figures. By following the trend of accumulation rates as the time span of the section decreases to 10^2 yr, I can estimate the accumulation rate of a 100-year interval in the Cape Manning section. This accumulation rate for sections on the order of 10^2 yr time span is between 0.1 m/1,000 yr to 0.2 m/1,000 yr.

The expected stratigraphic completeness is related to accumulation rate by the following equation:

$$\text{Expected completeness} = (t_*/t)^{-m} \quad (8.2)$$

where t is the time span of the whole section, t_* is the time unit of the interval of that section of interest and m is the slope of the regression of accumulation rate (S) on t. The gradient m can be estimated using Figure 13 of Sadler (1981). Figure 13 of Sadler (1981) plots the frequency distributions of m values by environment of deposition. Of the five environments he provides for comparison, the Cape Phillips is most similar to the environment below wave base, "abyssal calcareous ooze". For the t_*/t we are considering (100/2,100,000) the value m is –0.2 (Figure 13, Sadler, 1981). This is the m value I will use to estimate the completeness of a 100 year interval in the Aeronian Cape Manning

section (Table 8.2). This results in an expected completeness of 21% (i.e., only 21% of the 100 year interval is recorded by rock). Choosing a slightly higher m value can have a major effect on the completeness. For example, if m is equal to -0.1 (which is within the range of possibilities for this depositional environment), then completeness is 47%. To provide a range of sedimentation rates, I will use this value of completeness as well in my calculations (Table 8.2). In the previous section, I estimated that approximately 5% of the sediment from the concretions could be considered to be sediment-starved or that 95% of the sediment was other background sedimentation or episodic event beds. I will use this as a high estimate of completeness.

Table 8.2. Estimated background sedimentation rates for the Aeronian Cape Manning sections, based on estimated accumulation rate and two estimates of assumed completeness. Age data from Melchin and Cooper (in prep.).

Age of section (m.y.)	2.1		
Total stratigraphic thickness (m)	17.4		
Accumulation rate (m/1,000 yr)	0.0083		
Total episodic bed thickness (m)	3.8		
Total background bed thickness (m)	13.6		
Expected completeness on the scale of 1,000 years (%)	21	47	95
Net accumulation rate (m/1,000 yr)	0.040	0.018	0.0087
Time resolution of a 5 mm shale bed (years)	125	277	574
Time resolution of a 5 mm concretion bed (years)	25	55	114

Estimates of time-averaging and temporal resolution based upon accumulation rates.

The typical sample interval employed in this study has been approximately 5 mm thickness of concretionary material. Using the estimates of accumulation rate and completeness (Table 8.2), I can also estimate the time recorded by a 5 mm lamina of concretionary material. First, I must calculate the temporal resolution of a 5 mm lamina of shale, since these estimates of completeness have incorporated a compaction with time. The temporal resolution for 5 mm of shale can range from 125 to 526 years, based upon using a completeness of 21 and 95%, respectively. By Walker and Bambach's (1971) definition, the graptoloids contained within a 5 mm shale interval are necessarily time-averaged since their life span was perhaps a few years (Rigby, 1993). The shale-to-concretion to shale compaction ratio averages 5:1 (73 – 84%; Coniglio and Melchin, 1995). The time recorded by 5 mm of concretionary material is therefore less than the compacted concretionary material. A 5 mm thickness of concretionary sediment may record 25 to 114 years of accumulation. Although this is significantly less than a 5 mm interval of shale, the residues are still time-averaged. Horizons identified in Chapter Six as sediment-starved were calculated to represent approximately 2 to 4 times the amount of time as the normal background sedimentation. A five-millimeter thick condensed horizon in concretionary carbonate could average graptoloids from a 50 to 456 year time period.

Episodic beds are deposited orders of magnitude more quickly, within hours or days. Beds produced by episodic short duration events were laid down quickly, but may also incorporate a reworking of the time-averaged background sediments. Only when these event beds are accompanied by a distinct turnover in the graptoloid assemblage, can it be assumed that the contained graptoloids are new additions to the sediment and not reworked assemblages from beds previously laid down at this location. In addition, it is possible the graptoloids could be reworked from a different location and transported to the new depositional site. Both types would show signs of fragmentation and biostratinomic alteration and have a graptoloid assemblage distinct from the strata below and above. The way to distinguish between the two might be in the diversity in the fossil assemblage, with the less time-averaged fauna being more homogeneous.

The evidence from this analysis concludes that most graptoloid assemblages of the Cape Phillips Formation are time-averaged. The temporal resolution of a 5 mm lamina in shale from a non-event bed is on the scale of 125 to 574 years and a 5 mm lamina of concretionary material is 25 to 114 years. These calculations ignore other sources of time-averaging such as reworking, benthic mixing, or sampling methods. In the following section, I examine the vertical continuity in graptolite assemblages and suggest a sampling strategy (for shale and concretionary material) for reducing the effects of time-averaging samples during collection.

R-mode cluster analysis: stratigraphic continuity in graptolite assemblages and ideal graptolite sample intervals

To understand the degree of time-averaging induced by sampling procedures, five separate R-mode cluster analyses were conducted on five groups of concretions divided by the biozone boundaries *C. cyphus* Zone, *M. pectinatus* Zone, *R. orbitus* Zone, *L. convolutus* Zone, and *S. guerichi* Zone. R-mode cluster analysis involves the computation of a species dissimilarity matrix where different species are grouped according to their dissimilarity values (Etter, 1999). The methods of this analysis are described in Chapter Three.

The results of the cluster analyses showed that in most samples, the within-concretion difference in taphocoenosis was less than the between-concretion difference. Five separate cluster analyses divided by biozone boundaries produced similar results. The sample residues from the same concretion were generally more similar to each other than to other sample residues from the same biozone. Variation from this observed clustering pattern was seen when two concretions were in close stratigraphic proximity or when biostratinomic mixing or an ecological shift created distinct assemblages within one concretion.

Coronograptus cyphus Zone (Figure 8.1; Table 8.3)

The concretions CM 40.5-40.6 and CM 42.3-42.4 are similar in species composition and cluster together in the dendrogram with a rescaled distance cluster calculated to be less than 10. One residue of CM 40.4-40.5 (80) is more similar to CM

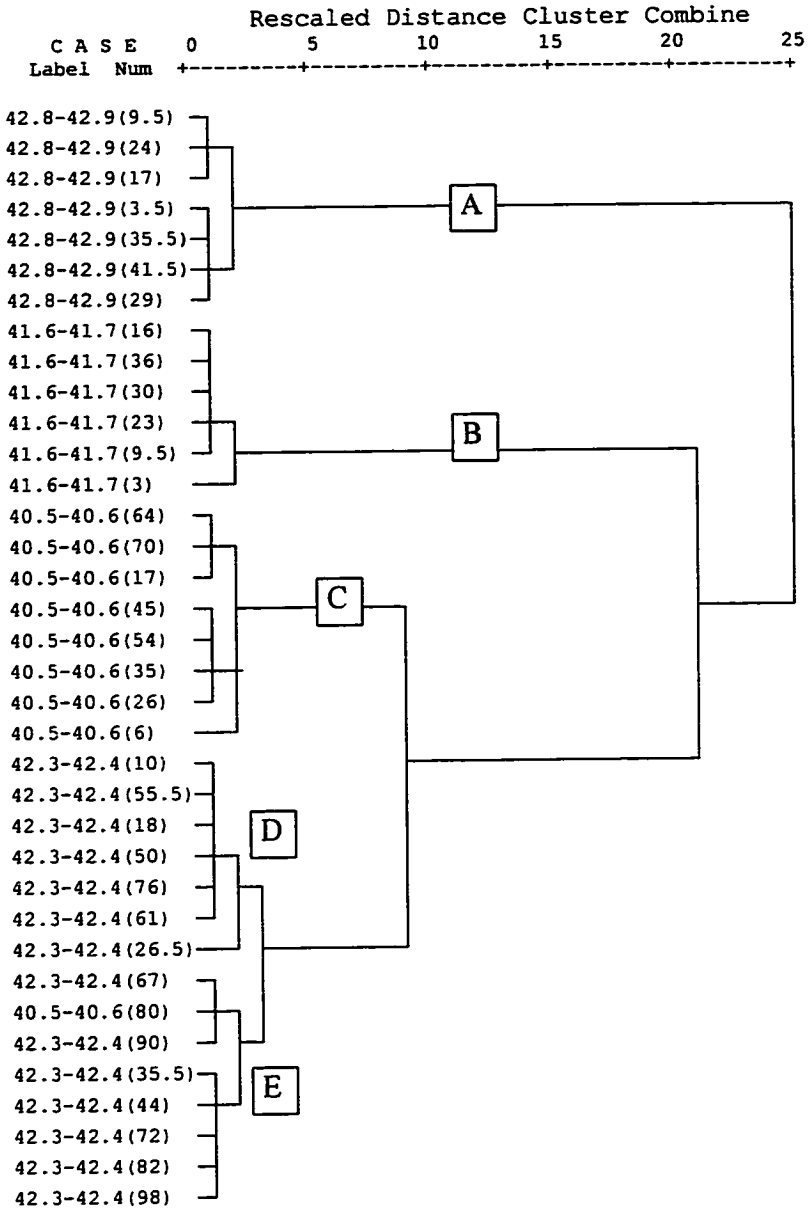

Figure 8.1. Hierarchical R-mode cluster analysis of four concretions from the *C. cyphus* Zone displayed as a dendrogram using Ward's method (error sum of squares). The values identifying the samples are composed of a concretion stratigraphic marker (e.g., 42.8-42.9) and in brackets the label of the residue (e.g., 9.5) that is the millimeter measure taken at mid-level from the layer dissolved.

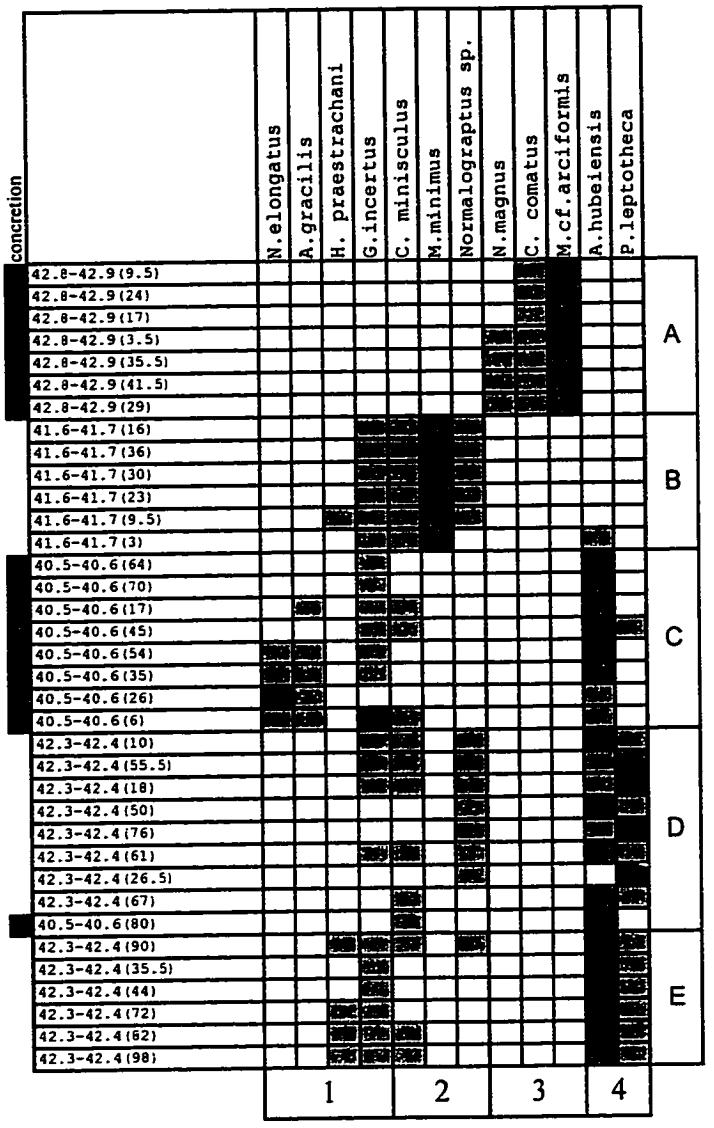

Table 8.3. Crossplot of residues from the *C. cyphus* Zone (ordering in dendogram Figure 8.1) versus species (ordering based on dendrogram in Figure 9.1). Dark shading indicates that the species is the most common element of the graptolite fauna in a residue while the light shading indicates which species are present. The clusters are defined A-E.

42.3-42.4 than to the species assemblage from the other residues of CM 40.4-40.5. The concretions CM 42.8-42.9 and CM 41.65-41.75 are observed to show greater internal similarity and less similarity with the other concretions in the biozone. The species assemblage of CM 42.8-42.9 is most dissimilar to the others. In Table 8.3, the crossplot of Q-mode vs. R-mode distribution and species presence and absence, it is clear that the species assemblage of CM 42.8-42.9 is distinct from the concretions below. This is not a zonal boundary effect, because some of the species present in the basal concretions of the *C. cyphus* Zone that are absent in CM 42.8-42.9, reappear in the *M. pectinatus* Zone. This change in species is interpreted in Chapter Nine to be recording a change in the graptoloid paleocommunity resulting from a shift in basin dynamics.

Monograptus pectinatus Zone (Figure 8.2; Table 8.4)

The graptoloid assemblages from all concretions examined from the *M. pectinatus* Zone cluster separately. The within concretion similarity between residues is greater than the between concretion residues. The species assemblages of concretions CM 46.35-46.5 and CM 48.5 are distinct from each other and form separate clusters, but these two concretions also have a rescaled distance of similarity that is less than five. The species distribution in concretions CM 46.35 and CM 48.5 are more similar to each other than to the other two concretions in this analysis (CM 45.3-45.4 and CM 47.4-47.5). The species assemblage of CM 47.4-47.5 is most dissimilar from the other concretion residues.

Within the larger clusters that define the individual concretions are smaller clusters of samples that are defined by the variable abundance of the three major species *Pribylograptus leptotheca*, *Monograptus* n. sp. B Melchin, and *Comograptus comatus*. The basal residues of CM 45.3-45.4 that were interpreted to be a basal lag in a transport event cluster separately from the rest of the residues of the concretion. The basal and top residues from CM 46.35-46.5 separate with the basal residues dominated by *C. comatus*, and the top residues dominated by *Monograptus* n. sp. B Melchin and *P. leptotheca*. Within the cluster of CM 48.5, two residues (3.5, 12.5) form a distinct group based on the similar abundance of *C. comatus* and the absence or rarity of species present in the upper residues of CM 48.5 (Figure 8.2). Within CM 47.4-47.5, the basal residues (3, 9.5, 14.5, 20.5, 27.5) form a cluster within the concretion (cluster D2, Table 8.4). The graptoloid

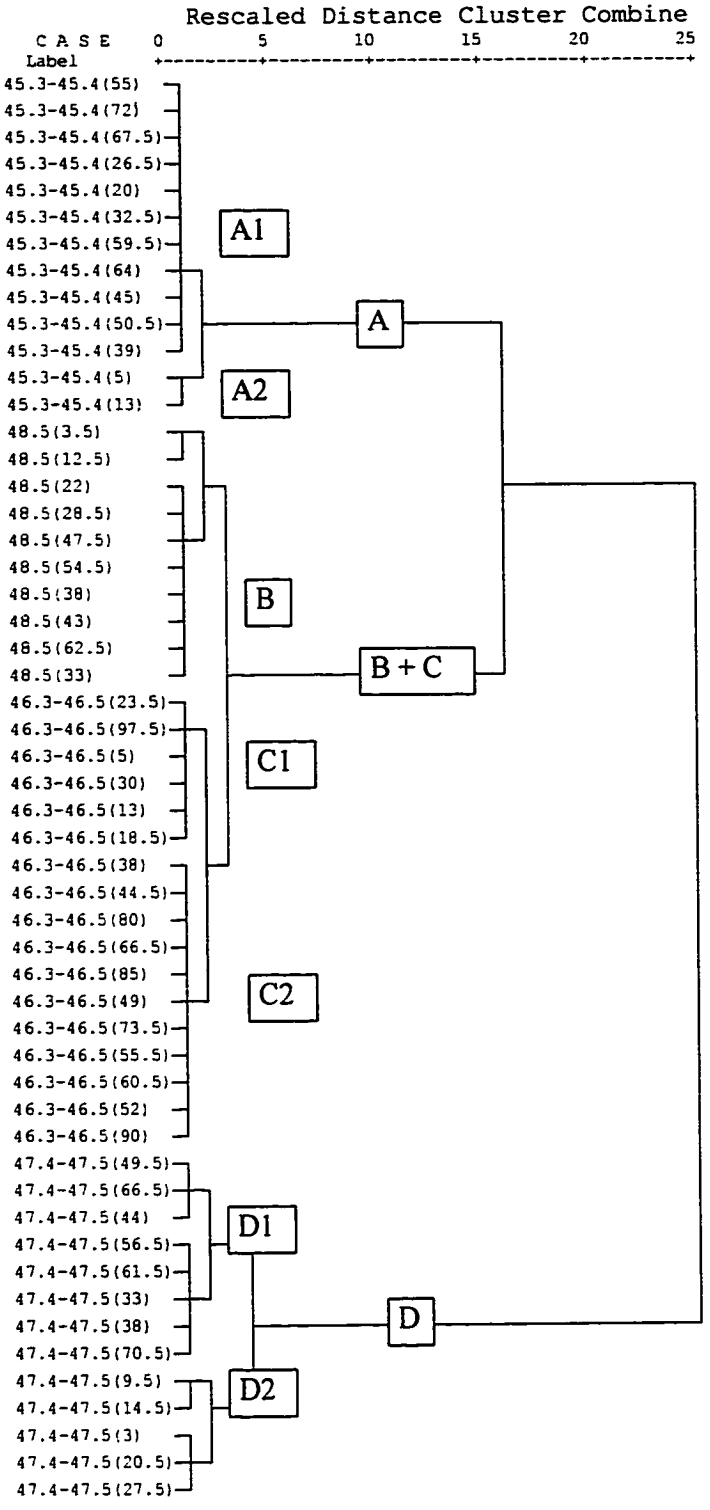

Figure 8.2. Hierarchical R-mode cluster analysis of four concretions from the *M. pectinatus* Zone displayed as a dendrogram using Ward's method (error sum of squares). The values identifying the samples are composed of a concretion stratigraphic marker (e.g., 45.3-45.4) and in brackets the label of the residue (e.g., 55) that is the millimeter measure taken at mid-level from the layer dissolved.

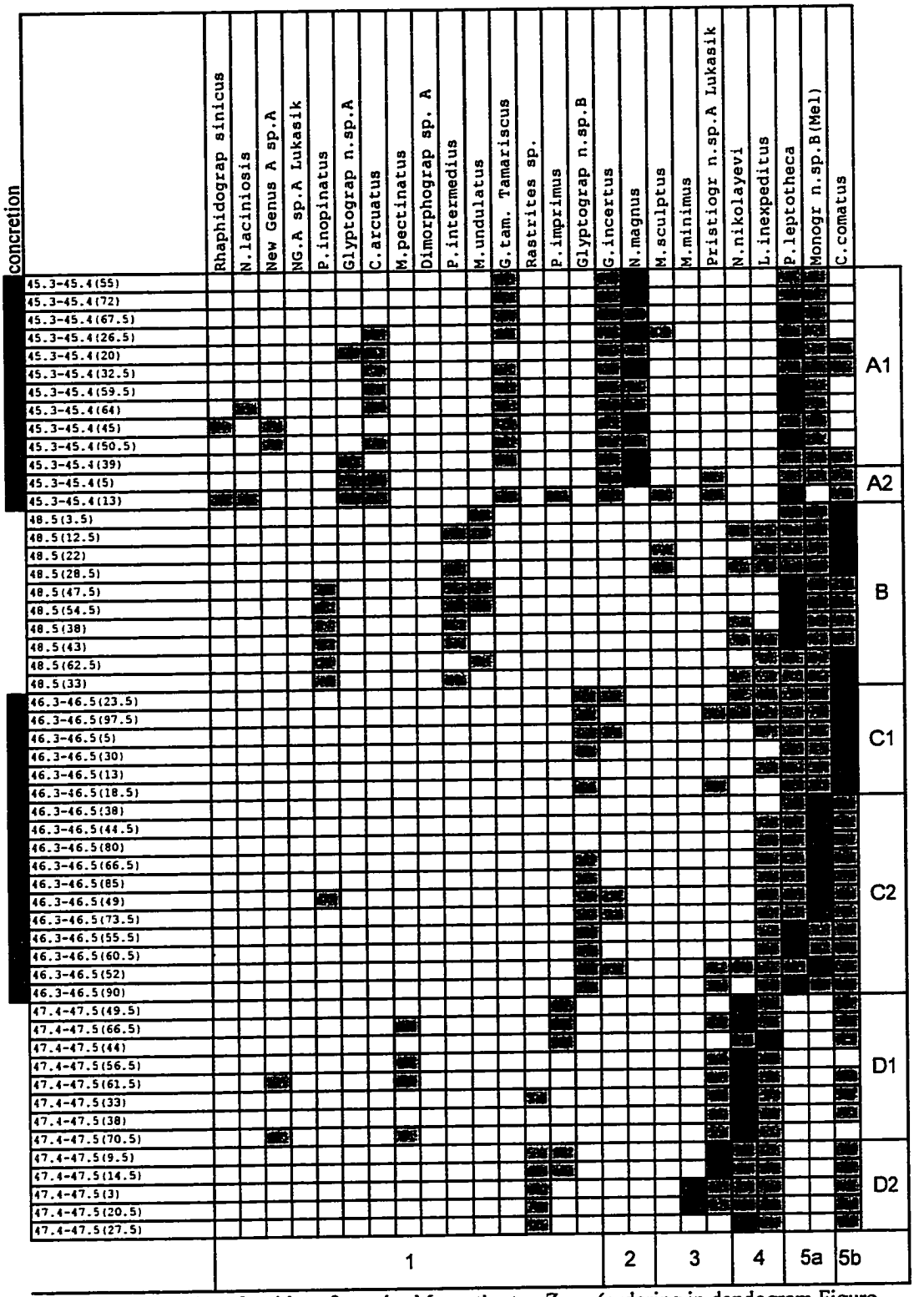

Table 8.4. Crossplot of residues from the *M. pectinatus* Zone (ordering in dendogram Figure 8.2) versus species (ordering based on dendrogram in Figure 9.2). Dark shading indicates that the species is the most common element of the graptolite fauna in a residue while the light shading indicates which species are present. The clusters are defined A-D.

assemblages of the basal residues are more similar to each other and dissimilar from the other residues of CM 47.4-47.5. In the thecal counts this was observed as a basal abundance of three species, *Pristiograptus* n. sp. A, *Metaclimacograptus minimus*, and *C. comatus* (Figure 4.25). The stratigraphic difference in graptoloid assemblages was paired with the lithologic observation of an overall grading of colour from a lighter base to a darker top; this was interpreted in Chapter Four to be the record of an intergrading of two populations of graptoloids and sediment from two different sources.

Each of the concretions selected for this analysis display some degree of biostratinomic alteration that resulted from an interpreted reworking of the sediments. This altered the vertical distribution of species. Species assemblages with in the stratigraphically separated concretions are still distinct, but within each concretion is a great deal more variability in species distribution. This is the result of an inconsistent graptolite source with ecologically (and perhaps temporally) distinct faunas being preserved in discrete strata. In all of the concretions this resulted in distinct assemblages within the concretions.

Rastrites orbitus Zone (Figure 8.3; Table 8.5)

The five concretions used in this study display an interesting clustering pattern and give insight to the degree of ecological stability during this time The between-concretion difference is greater than the within-concretion difference, except for concretions CM 51.2-51.3a and CM 51.2-51.3b collected from the same stratigraphic interval 1.2 meters apart. These two concretions are grouped together in this statistical analysis, based upon a similar graptoloid assemblage that is different from the other concretions in the subzone. The species assemblage of CM 49.8-49.9 form one cluster that differs significantly from the graptolite assemblage of the other concretions in this biozone. This concretion records the highest diversity of all of the concretions examined and is thought to also record a time of low sedimentation rates. CM 50.4-50.5 and CM 50.4 are a concretion and a limestone bed respectively, which are stratigraphically very closely related. The graptoloids from the residues of these concretions, however, are still distinct. The two units form separate clusters. The assemblages of the two clusters CM 50.4 and CM 50.4-50.5 are more similar to each other than to the other concretion

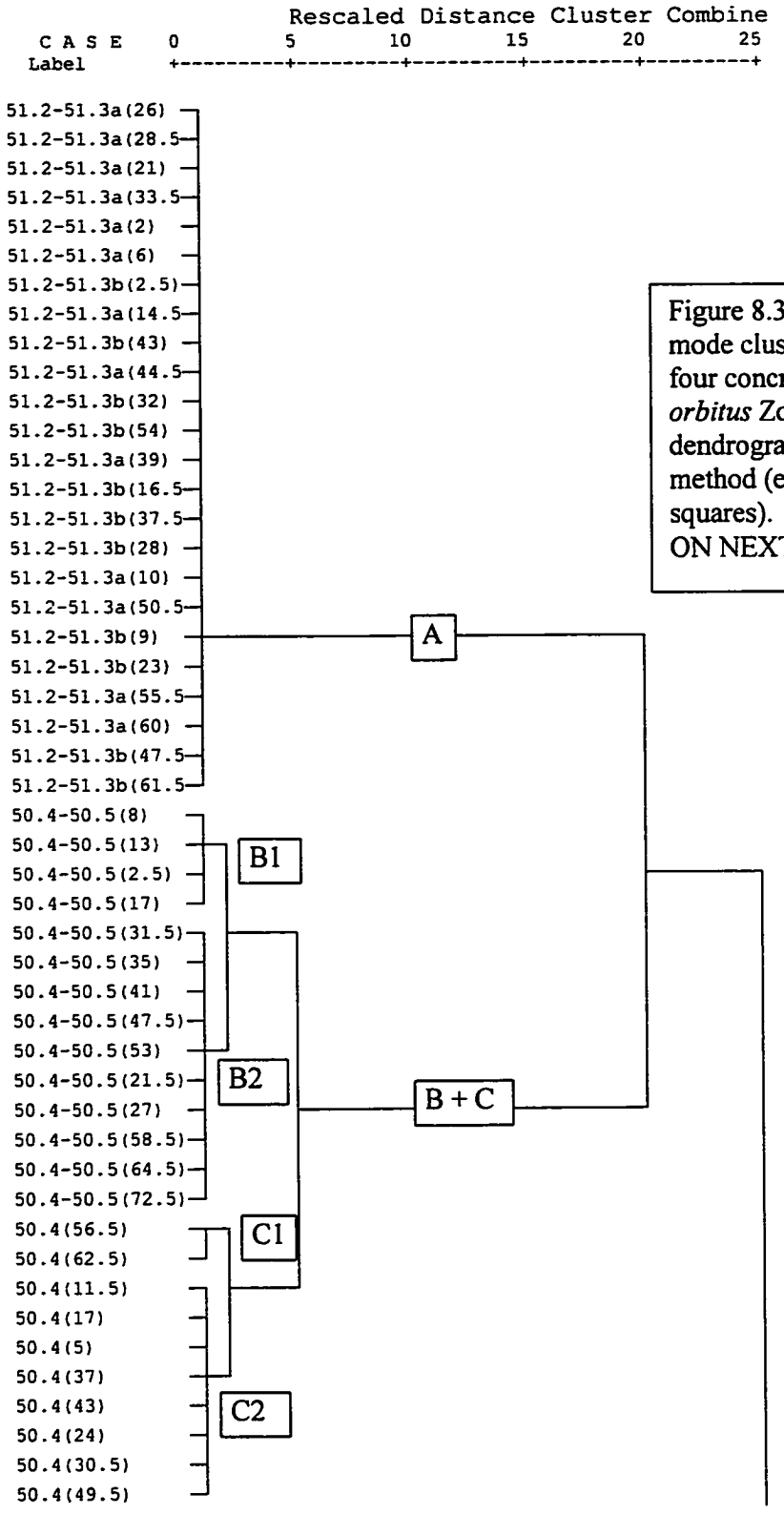

Figure 8.3. Hierarchical R-mode cluster analysis of four concretions from the *R. orbitus* Zone displayed as a dendrogram using Ward's method (error sum of squares). CONTINUED ON NEXT PAGE.

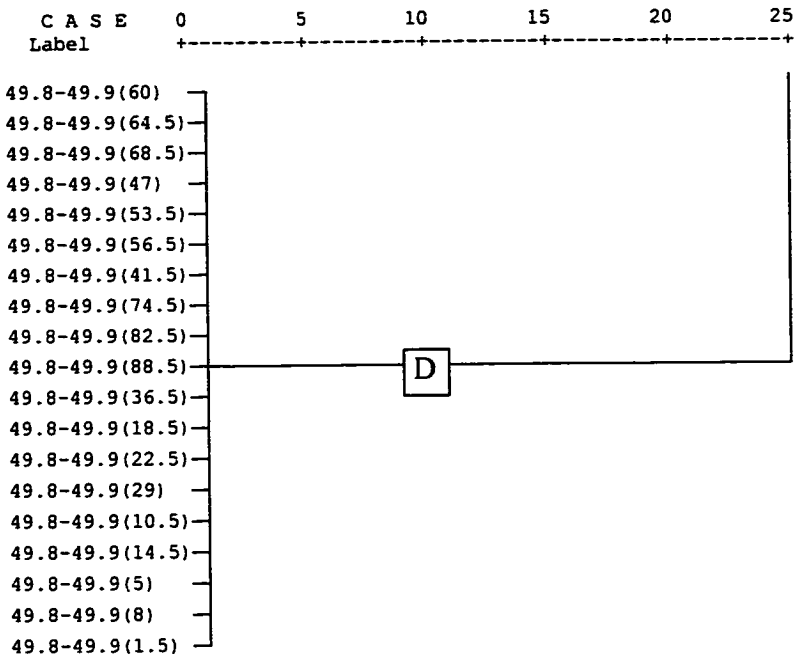

Figure 8.3. (Continued from previous page). Hierarchical R-mode cluster analysis of four concretions from the *R. orbitus* Zone displayed as a dendrogram using Ward's method (error sum of squares). The values identifying the samples are composed of a concretion stratigraphic marker (e.g., 51.2-51.3a (26) and in brackets the label of the residue (e.g., 26) that is the millimeter measure taken at mid-level from the layer dissolved.

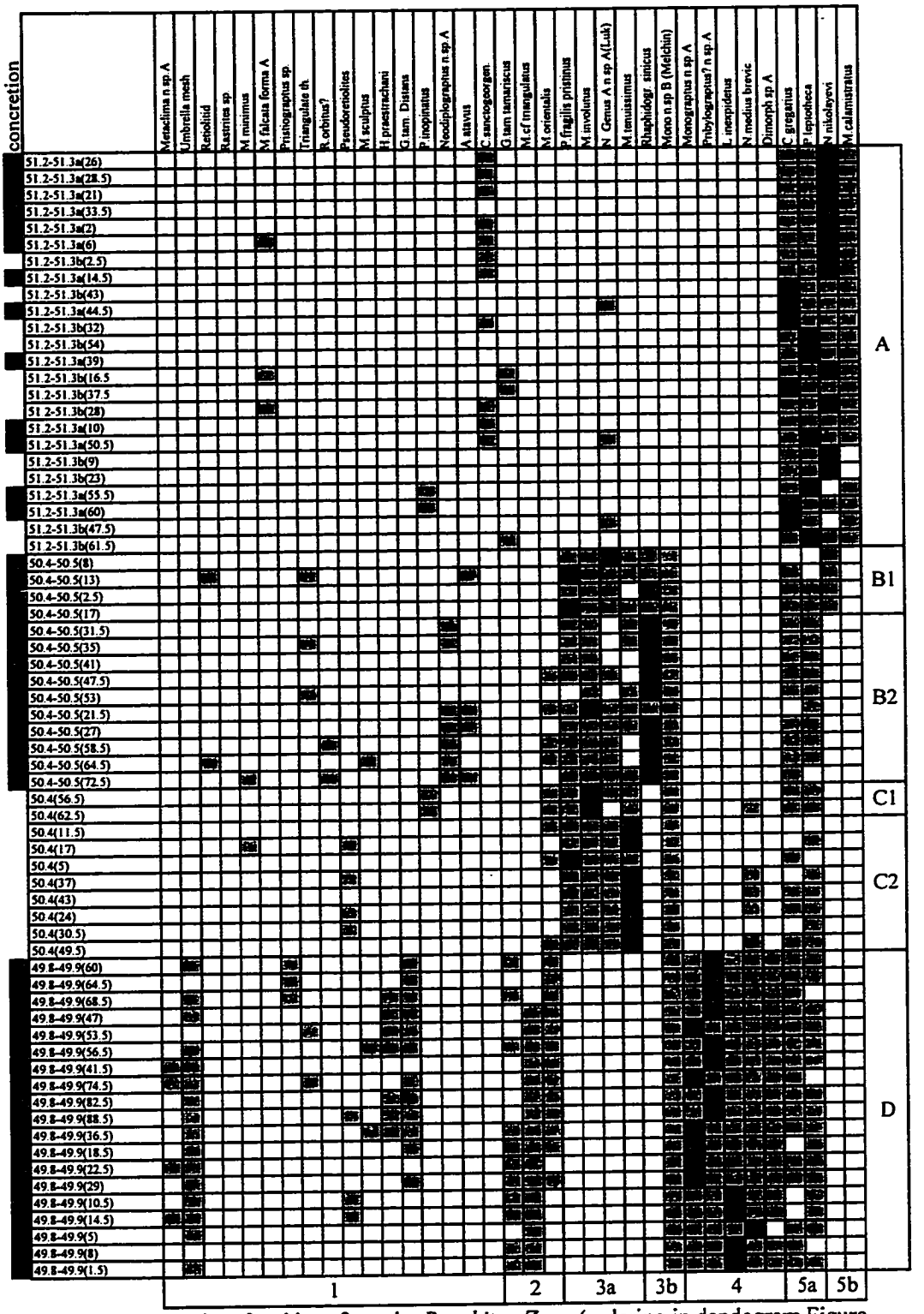

Table 8.5. Crossplot of residues from the *R. orbitus* Zone (ordering in dendogram Figure 8.3) versus species (ordering based on dendrogram in Figure 9.3). Dark shading indicates that the species is the most common element of the graptolite fauna in a residue while the light shading indicates which species are present.

clusters CM 51.2-51.3 a and b, and CM 49.8-49.9. This enables an estimate of the extent of the ecological stability during the *R. orbitus* Zone. CM 50.4 –50.5 is placed in the random flux of graptoloids and sediment taphofacies, whereas CM 50.4 is thought to be a rapidly deposited resedimented limestone bed. Although many species occur in both concretions, there are enough differences in some of the major fauna that result in the cluster analysis identifying the two assemblages as being distinct. For example, *Rhaphidograptus sinicus*, the most abundant species in CM 50.4- 50.5 is absent in the residues of CM 50.4. The graptoloid assemblages within the average thickness of the concretion (approximately 10 cm) record times of relative ecological stability, and do not record significant faunal turnovers. This is laterally extended to at least 1.2 meters (distance between CM 51.2-51.3a and CM 51.2-51.3b). Concretions sampled from stratigraphic intervals separated by 5 cm could reveal a different graptoloid assemblage (e.g., CM 50.4-50.5 and CM 50.4).

Lituigraptus convolutus Zone (Figure 8.4; Table 8.6)

The clustering pattern displayed in the dendrogram of the residues of five concretions from the *L. convolutus* biozone shows that the within concretion similarity is often greater than the between concretion similarity. The exception to this is the top-concretion residues from CM 59.1-59.2. These residues are more similar to residues from CM 58a than to other residues from CM 59.1-59.2. The rescaled difference between the two main clusters within CM 59.1-59.2 is just above 10. The top laminae of this concretion are interpreted to be the product of a transport event, and the change in graptolite assemblage results from the physical addition of graptolites from a slightly different source (Chapter Four). The residues from concretion CM 57.4-57.5 are more similar to residues from within the concretion and less similar to the residues from CM 57. The species assemblages from these two concretions (CM 57.4-57.5 and CM 57) are more similar to each other than to any of the residues from the other concretions examined in this biozone. Residues from CM 56.4-56.5 cluster into four groups based on the similarity of the graptoloid assemblages. In the species distribution profiles (Figure 4.50), I identified three assemblages that had their boundaries roughly at 21, and 53. In the cluster analysis, the basal group was separated into two clusters and included residue

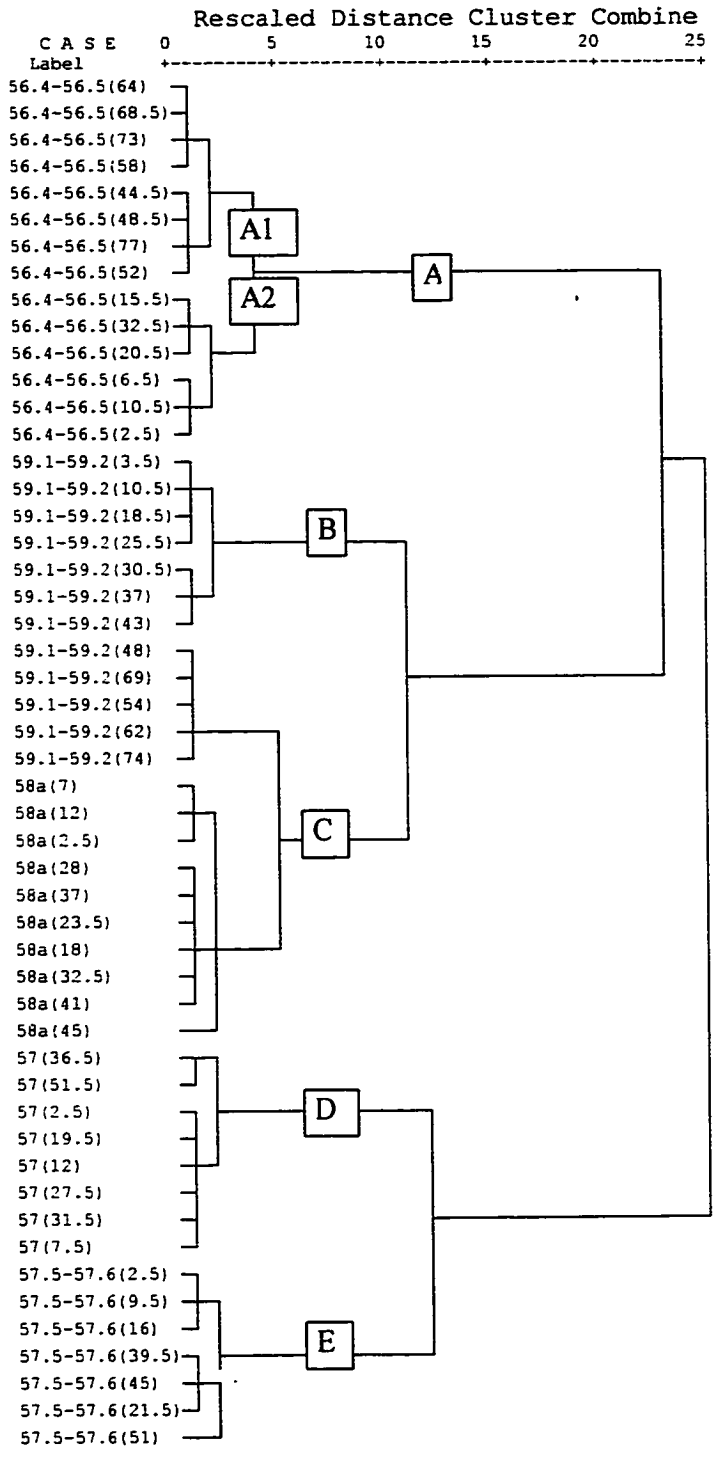

Figure 8.4. Hierarchical R-mode cluster analysis of five concretions from the *L. convolutus* Zone displayed as a dendrogram using Ward's method (error sum of squares). The values identifying the samples are composed of a concretion stratigraphic marker (e.g., 56.4-56.5) and in brackets the label of the residue (e.g., 64) that is the millimeter measure taken at mid-level from the layer dissolved.

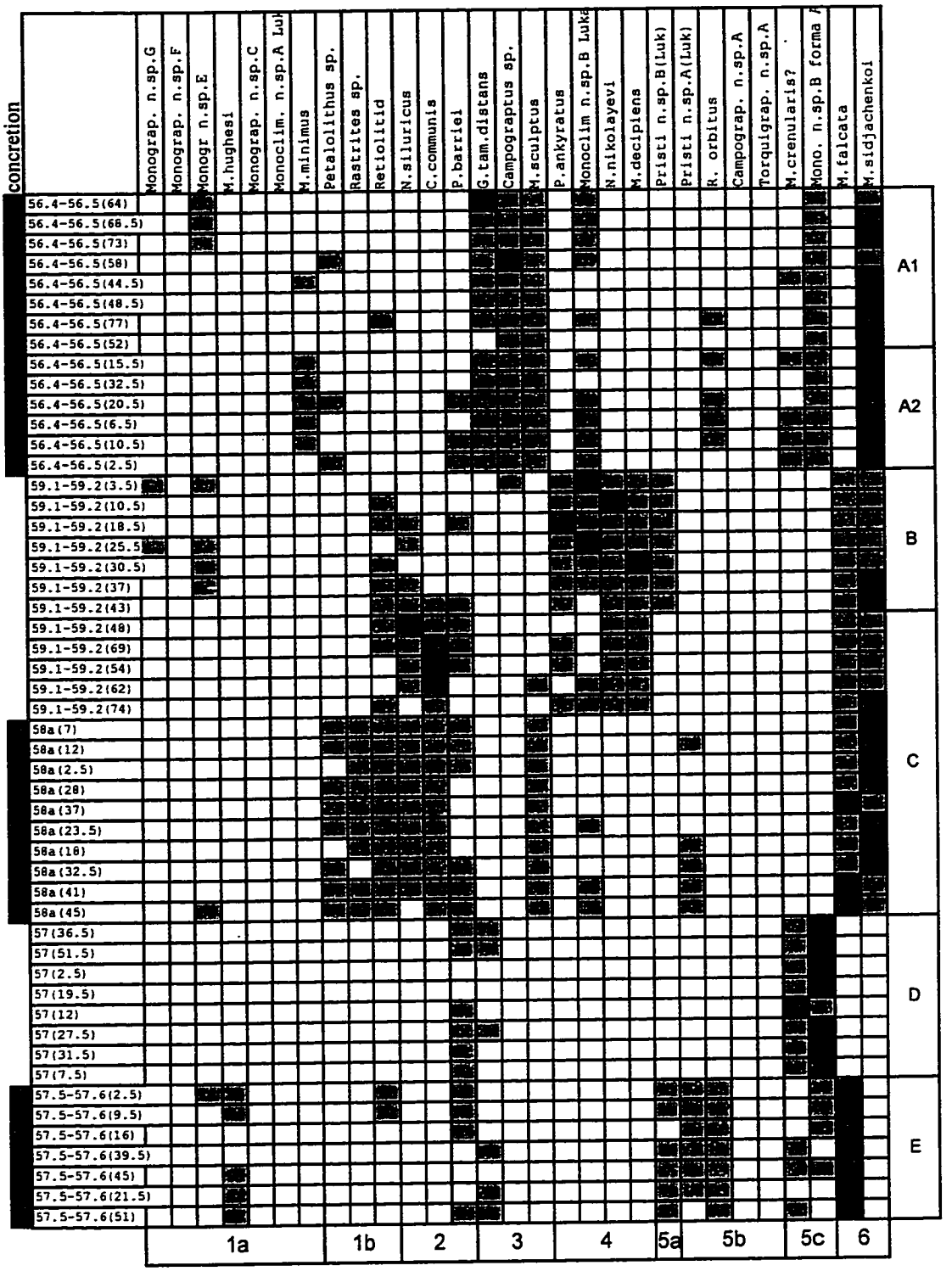

Table 8.6. Crossplot of residues from the *L. convolutus* Zone (ordering in dendogram Figure 8.4) versus species (ordering based on dendrogram in Figure 9.4). Dark shading indicates that the species is the most common element of the graptolite fauna in a residue while the light shading indicates which species are present. Clusters are defined A-E.

32.5. The mid-concretion assemblage remained as one group in the cluster analysis but also included residue 77. The top-concretion assemblage (minus residue 77) was also identified by cluster analysis. In Chapter Four and Chapter Nine I interpret this to be the intergrading of graptoloid communities.

Spirograptus guerichi Zone (Figure 8.5, Figure 8.6; Table 8.7, 8.8)

The species assemblages from the four different concretions of this biozone all form separate clusters of similarity. This indicates that the graptolite assemblages are more similar within the concretions than between. Two concretions are more similar than others, CM 72.6, and CM 74.9a. These have a rescaled distance of similarity of less than five. Together with CM 73.8 the three concretions have a rescaled distance of similarity of five. This on the same order of dissimilarity that is seen within the concretion CM 75.5. The residues from CM 75.5 cluster into two groups based upon the similarity of their graptoloid assemblages (Figure 7.5 and 4.71). The mid-concretion residues (26, 32.5, 19, 62.5, 66.5, 43, 56.5, 37.5, and 49.5) are dominated by *Pristiograptus regularis regularis* (residues 49.5-62.5), *S. guerichi* (19, 26, 32.5) or both (66.5). This cluster is characterised by the absence or rarity of *Monograptus halli*. The basal and top residues (84, 88.5, 78.5, 93, 102.5, 97.5, 13, 73.5, 7.5, 70, and 2.5) are dominated by *Monograptus halli*. Removing the other concretions from the analysis and just examining the trends of similarity within CM 75.5 elucidates these associations (Figure 8.6). This pattern of distribution is ecological in nature and will be more fully analysed in Chapter Nine. Even though there are distinct graptolite assemblages within this concretion, their dissimilarity can be as great as the dissimilarity between concretions (e.g., CM 73.8, 74.9a, and 72.6) of the same biozone.

Discussion: time-averaging, ecological stability and temporal resolution.

In part one of this chapter, I estimated the time that a 5 mm sample of shale may represent and introduced the thought that these samples are time-averaged, meaning that the time required to deposit a single lamination is greater than the life span of a graptoloid colony. In part two, I show that in most instances the between-concretion

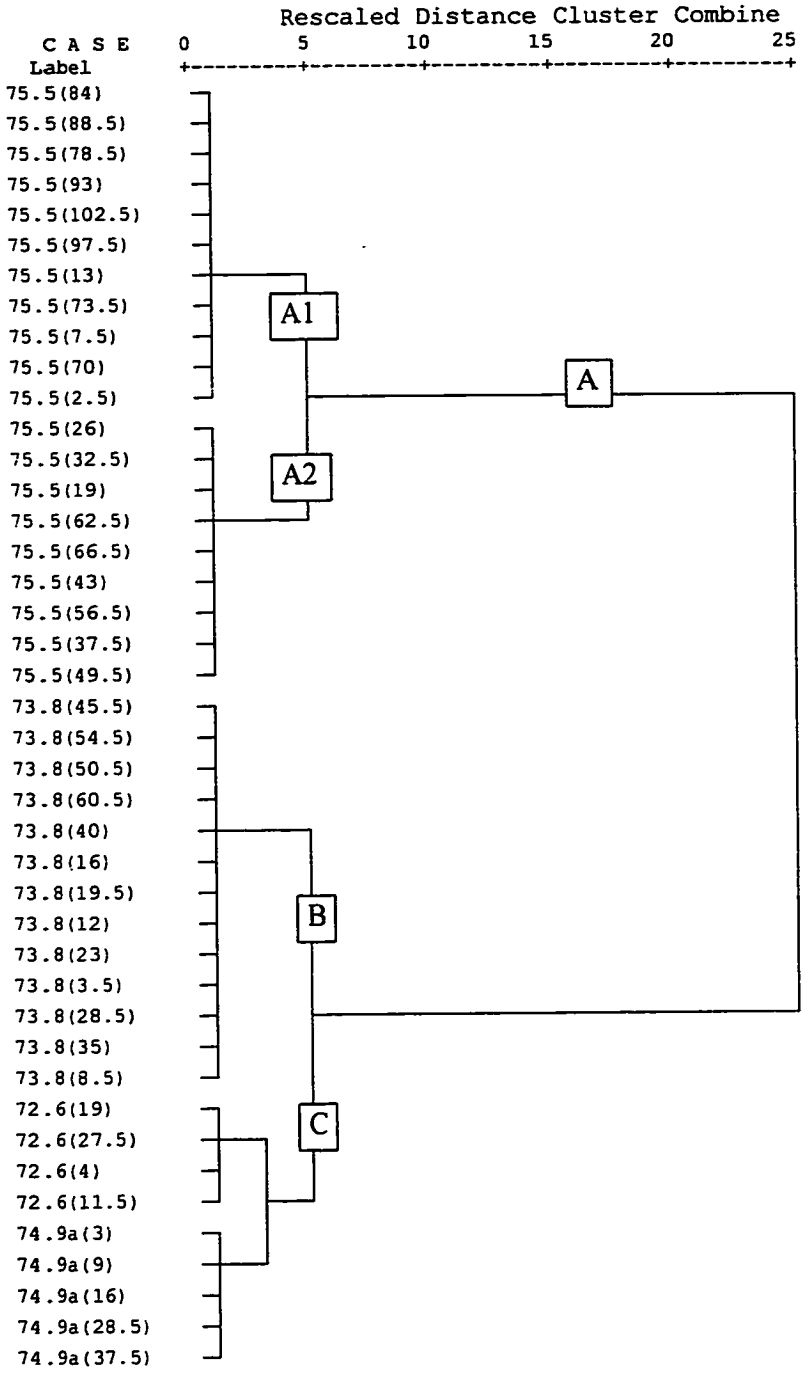

Figure 8.5. Hierarchical R-mode cluster analysis of four concretions from the *S. guerichi* Zone displayed as a dendrogram using Ward's method (error sum of squares). The values identifying the samples are composed of a concretion stratigraphic marker (e.g., 75.5) and in brackets the label of the residue (e.g., 84) that is the millimeter measure taken at mid-level from the layer dissolved.

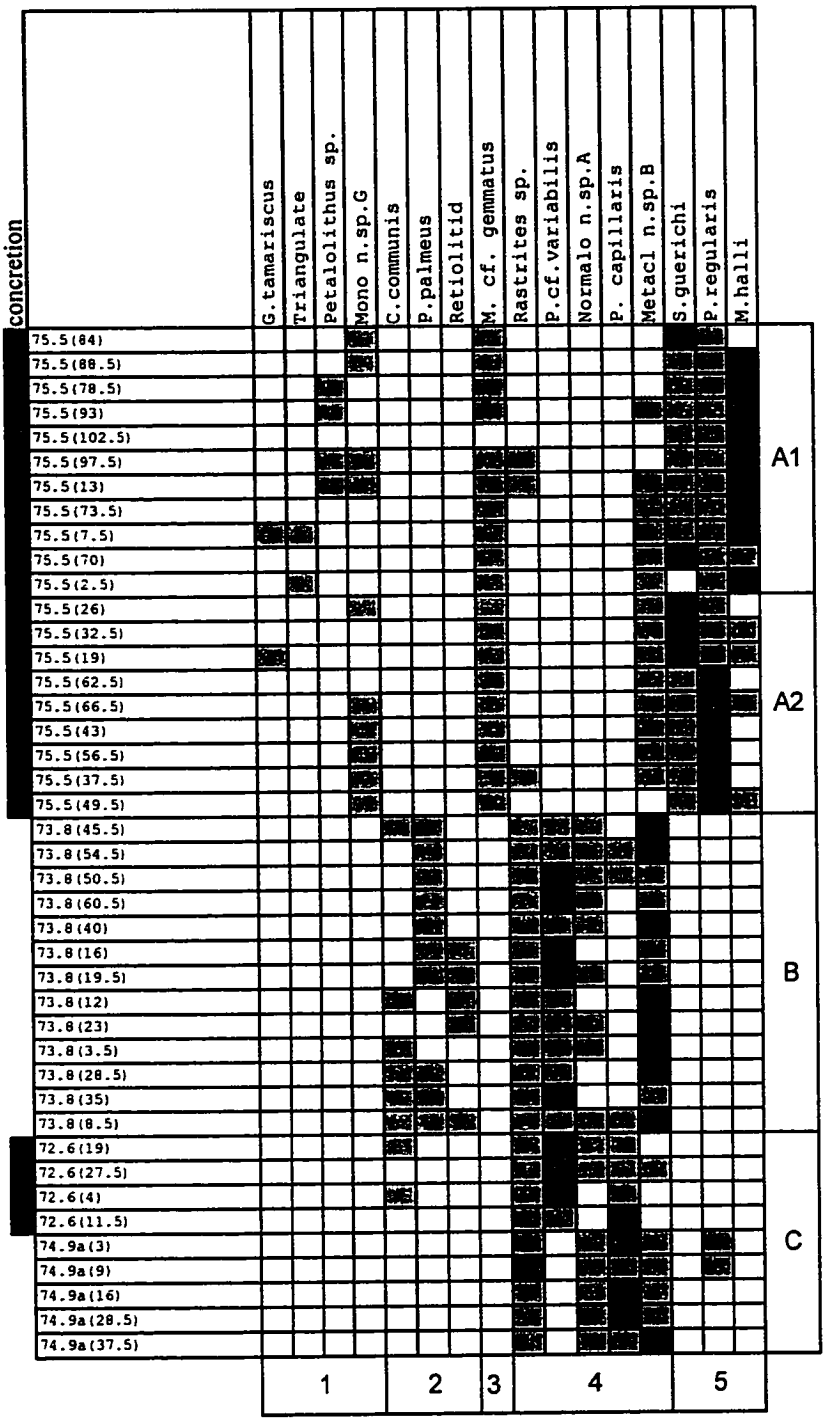

Table 8.7. Crossplot of residues from the *S. guerichi* Zone (ordering in dendogram Figure 8.5) versus species (ordering based on dendrogram in Figure 9.5). Dark shading indicates that the species is the most common element of the graptolite fauna in a residue while the light shading indicates which species are present. The clusters are defined A-D.

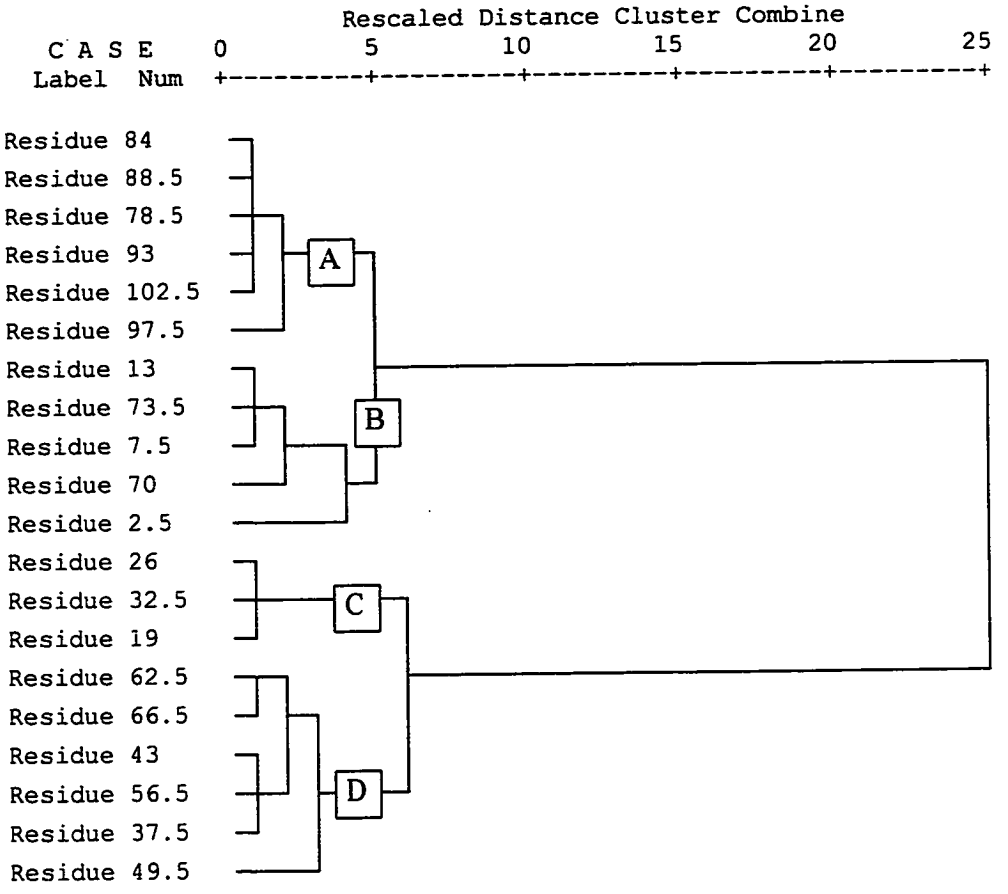

Figure 8.6. Hierarchical cluster analysis of concretion CM 75.5 from the *S. guerichi* Zone displayed as a dendrogram using Ward's method (error sum of squares).

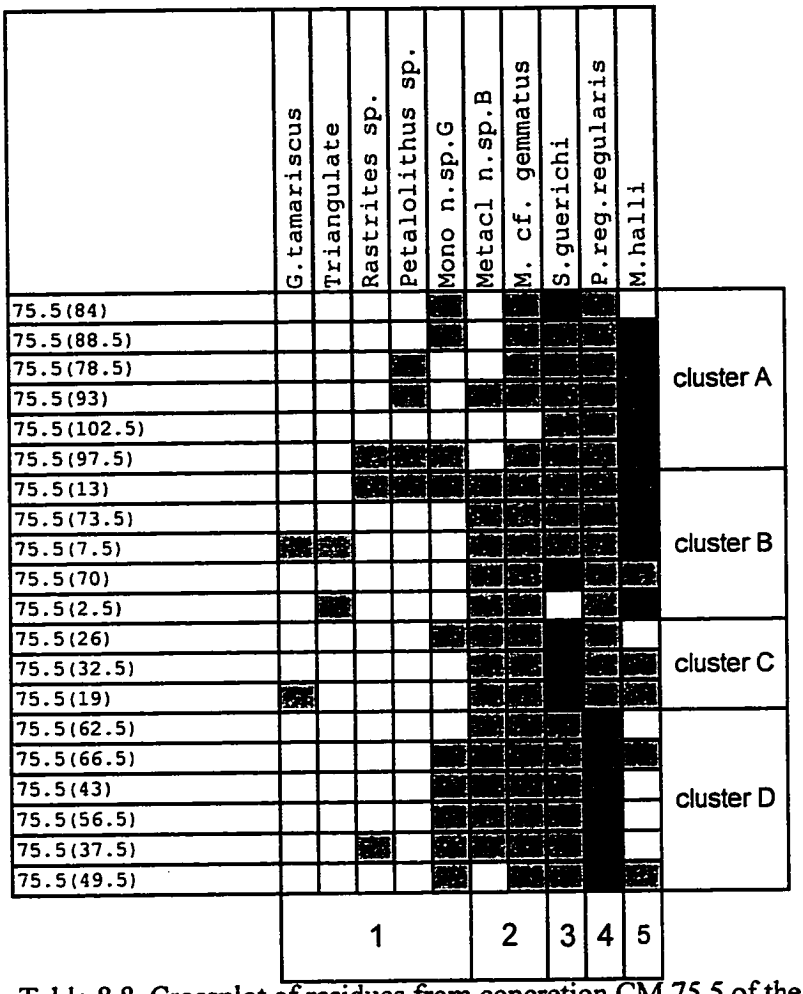

Table 8.8. Crossplot of residues from concretion CM 75.5 of the *S. guerichi* Zone versus species ordered based on cluster anaylses (Figures 8.6, 9.6). Dark shading indicates that the species is the most common element of the graptolite fauna in a residue while the light shading indicates which species are present. The clusters are

difference in graptoloid assemblages was greater than the within concretion difference. This is laterally extended to at least 1.2 meters (distance between CM 51.2-51.3a and CM 51.2-51.3b). Concretions sampled from stratigraphic intervals separated by 5 cm (compressed) can reveal a slightly different graptoloid assemblage (e.g., CM 50.4-50.5 and CM 50.4).

There are exceptions to the stratigraphic continuity of graptolite assemblages on the scale of a concretion thickness. Concretions CM 45.3-45.4, CM 46.35-46.5, CM 47.4-47.5, CM 48.5, and CM 59.1-59.2 display distinct clustering patterns within the concretion clusters that can be related to transport events and physical reworking. Concretion CM 56.4-56.5 records a change in the graptolite assemblage that is interpreted to be the result of three communities intergrading in time or space or both. Concretion CM 75.5 records an ecological event that creates two or three graptoloid assemblages within the 105 cm of concretion thickness. Even though these concretions contain events that create distinct graptoloid assemblages within the concretions, the within-concretion similarity is greater in all cases but one (CM 59.1-59.2) to the between-concretion similarity.

It generally applies that the greater the stratigraphic distance between two concretions, the greater the dissimilarity between the graptoloid assemblages. However, some assemblages show a greater affinity to those of a concretion sampled further away then to one stratigraphically adjacent (e.g., CM 40.5-40.6 is more similar to CM 42.3-42.4 then to CM 41.65-41.75). This is perhaps identifying recurrent species associations. In the case of CM 40.5-40.6 and CM 42.3-42.4, they have a similar species composition that is absent from CM 41.65-41.75 (Table 8.1). It should be noted that in most cases the residue stratigraphic order is not maintained in the Q-mode cluster order. The assemblage of graptolites within a 5 mm thick residue sample is not more similar to the residues stratigraphically above and below this than to residues within the same concretion but a few centimeters above or below. Concretion CM 49.8-49.9 does show some degree of correlation between stratigraphic position and relative similarity. This concretion contains the most diverse graptolite fauna of the concretions examined for this thesis and it is placed in the sediment-starved taphofacies. A slow sedimentation rate

with negligible benthic mixing and physical reworking would create such a clustering pattern.

The *C. cyphus R. orbitus*, and *S. guerichi* zones appear as intervals of relatively stable ecological communities and less destructive taphonomic processes. In these times, the concretion sediments record subtle changes in the taphocoenosis and a 6.5 cm thick section from a concretion is usually a good record of the assemblage of graptolites from any one residue. (The thickness of 6.5 cm was obtained by averaging the thickness of the concretion dissolved for the 13 concretions used in the cluster analysis from these three biozones.) The *M. pectinatus* Zone is an interval of instability when physical reworking was altering the sediment and graptolite distribution within the sediment. In the concretions from this interval, two or more distinct graptoloid assemblages are found in each concretion. The *L. convolutus* Zone is a time of variable graptolite distribution that results from physical reworking and transport or ecological shifts. The average concretion thickness for these distinct assemblages is 2.0 cm in the *L. convolutus* Zone and 2.9 cm in the *M. pectinatus* Zone.

Discussion: sample size in compressed and uncompressed graptolite samples.

In the ecologically and taphonomically "stable" time periods (*C. cyphus* Zone, *R. orbitus* Zone, and *S. guerichi* Zone) of the Cape Manning section of the Cape Phillips Formation, a 6.5 cm thick sample was observed to be generally a good record of the graptolite assemblage from any one lamina of that 6.5 cm interval. The range of sample thickness for a graptolite assemblage that clusters as a similar group at the rescaled distance of less than 3 is 3.6 – 9.8 cm (average, 6.5 cm). The 6.5 cm measure is a minimum value, given that this is an average sample thickness and the actual faunas could have been stable over intervals thicker than this. This is useful information for ecological and evolutionary studies that base their trends on evidence from bulk dissolution of these carbonate concretions. In these stratigraphic intervals, bulk dissolution of concretions that are 6.5 cm in thickness will yield ecologically relevant samples, which usually have not been additionally time-averaged as a result of sampling interval. Concretions thicker than this or multiple concretions taken from close

stratigraphic proximity (e.g., 50.4 and 50.4-50.5) should not be analysed as one sample. This mixes stratigraphically distinct assemblages, increases the degree of time-averaging and decreases temporal resolution.

The shales of this section are compacted by a ratio of 5:1 (73 to 84% compaction Coniglio and Melchin, 1995). If I assume the concretions are uncompacted, I can estimate the ideal sample size in the shales based on our knowledge of the temporal resolution of the concretions. A 6.5 cm sample interval in the concretions is equal to approximately 1.3 cm of adjacent shale. A sample size greater than this will likely mix temporally separated taphocoenoses. These are estimates for the three intervals identified as being relatively stable. How do these estimates vary for environments of greater ecological or taphonomic variation in graptolite distribution?

The average concretion thickness for distinct assemblages identified by cluster analysis is 2.0 cm (range 0.4 – 2.6 cm) in the *L. convolutus* Zone and 2.9 cm (range, 1.25 – 6.75 cm) in the *M. pectinatus* Zone. To obtain a sample size that reflects one assemblage, one must create a sampling interval that is muchless than approximately 2.45 cm (the average of the two). To be certain to sample one taphocoenosis, the sampling interval must be very thin (thinnest interval permissable by the methods) to avoid sampling a boundary between two distinct taphocoenoses. To increase the sample interval will be to increase the probability that the sample includes two or more distinct graptoloid assemblages. For these intervals of greater taphonomic reworking or increased rates of faunal turnover, I suggest breaking the concretions into three or four pieces along bedding and treating each as a separate sample during bulk dissolution.

These sampling intervals are difficult to apply to studies of the graptolites compressed in shale. The concretionary thickness of 2.45 cm is reduced to approximately 0.5 cm in shale. To accurately record small-scale fluctuations in graptolite distribution a 0.5 cm sampling interval less than would be necessary. A single bedding plane is the only reliable way to be sure you have captured a single taphocoenosis. The common graptolite sampling procedure of collecting specimens from multiple bedding planes over an interval of strata 5 or 10 cm in thickness will mix distinct taphocoenosis.

A highly resolved sampling interval is difficult to a achieve when working in shales; however, as I have shown, even the taphonomically altered samples, or those that

record major faunal shifts, display a greater internal similarity than similarity to concretions stratigraphically above or below. By increasing the sample thickness one will lose the finely resolved fluctuations in species abundance or assemblage composition, but one can still consider a 1.3 cm thick sample of shale to be a good representation of the total taphocoenosis.

9 GRAPTOLOID PALEOECOLOGY: A COMMUNITY ANALYSIS

Of prime importance to graptolite biostratigraphy is an understanding of graptoloid distribution and occurrence in the ancient waters and in the preserved Paleozoic rocks. Can we recognize graptoloid "communities" in the taphocoenosis (death assemblage) and can we relate these to the biocoenosis (life assemblage)?

This is a pilot study of graptolite community ecology, in which I examinespecies co-occurrence on a temporal scale. The finely resolved and exceptionally preserved graptoloids are used to study the ecology of ancient graptoloid communities (graptoloid paleosynecology). A fine-resolution sampling of the graptoloid species distribution vertically through a concretion is a quantitative record of the taphocoenosis (death assemblage). Small shifts in species composition and dominance are used to understand larger-scale basin dynamics by examining several stratigraphically consecutive concretions. Twenty-eight concretions spanned almost 20 meters of continuous strata from the lower to mid-Aeronian portion of the Cape Manning section. To avoid problems of major faunal changeovers that accompany some zonal boundaries, the analyses were conducted within concretions all from the same biozone. Five biozones were examined: *Coronograptus cyphus*, *Monograptus pectinatus*, *Rastrites orbitus*, *Lituigraptus convolutus*, and *Spirograptus guerichi* zones (statistical method described in Chapter Three). The recognition of recurrent species associations was performed using cluster analysis with the counts of thecae from the layer-by-layer dissolution residues. The identification of species that consistently co-occur and also have similar abundance profiles allows the reconstruction of graptoloid paleocommunities. Although based on thecal counts (quantitative data), the analysis of the dendograms is somewhat qualitative. With further research, it should be possible to use these data to quantitatively define communities by computing species richness or eveness indices. However, that work was beyond the scope of this thesis. Finally, I present evidence from thecal and sicular counts to refute the hypothesis that siculae (the earliest growth stage of the graptolite colony) had a benthic mode of life (Kirk, 1969, 1990a, b), and support the previously argued concept that the siculae were planktonic (e.g., Fortey, 1982; and Erdtmann, 1982).

Recurrent graptoloid species associations

The results of the Q-mode cluster analyses from each of the five biozones examined in the Cape Manning section are displayed as dendrograms (Figures 9.1-9.6). Crossplots of residues from the concretions studied within each biozone, compare the ordering of samples from the R-mode analysis with the ordering of species from the Q-mode analysis (Tables 8.3 to 8.8). In these diagrams, the abundant species of the residues are identified with dark shaded squares and the light grey squares identify the presence of a species in the residue. The crossplots and the dendrograms are both used to define recurrent species associations. For each of the five biozones, I present all of the species associations identified by the cluster analysis and then discuss their significance.

Coronograptus cyphus Zone (Figure 9.1; Table 8.3)

Neodiplograptus elongatus and *Atavograptus gracilis* have a close similarity in distribution and are a part of cluster 1 that also incorporates *Huttagraptus praestrachani* and *Glyptograptus incertus*. This group is most similar in distribution to cluster 2 that comprises *Coronograptus minisculus*, *Metaclimacograptus minimus*, and *Normalograptus* sp.; with *C. minisculus* and *M. minimus* most similar within the cluster. Cluster 1 and two have a rescaled similarity with cluster 3 that is greater than 15. Cluster 3 includes *Normalograptus magnus*, *Comograptus comatus*, and *Monograptus* cf. *arciformis*. *Normalograptus magnus* and *C. comatus* are more similar in their occurrence than *M.* cf. *arciformis*. Cluster 4 is most dissimilar in the occurrence of the species through the residues. The two species of this cluster, *Agetograptus hubeiensis* and *Pribylograptus leptotheca,* have distributions that are more similar to each other than any other species in the residues.

Cluster 1 defines the distinct appearance of *Neodiplograptus elongatus* and *Pribylograptus pleganopsis* in the lower-to mid-level residues of CM 40.5-0.5. In one residue, *N. elongatus* is the most abundant species. These two species are found together with *G. incertus*, but not the fourth species of the cluster, *H. praestrachani*. However, *G. incertus* and *H. praestrachani* are found together in some residues from CM 42.3-42.4

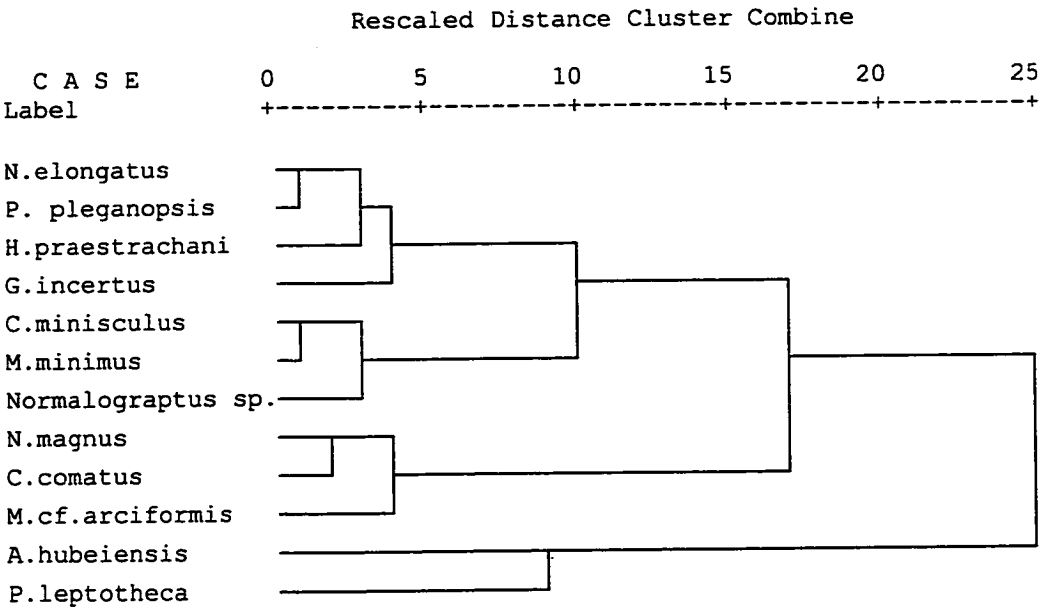

Figure 9.1. Hierarchical cluster analysis of graptoloid species from the *C. cyphus* Zone displayed as a dendrogram using Ward's method (error sum of squares).

and one residue from CM 41.65-41.75. *Huttagraptus praestrachani* is a less abundant in these residues than the other graptoloids in this cluster.

Cluster 2 contains the three species that are most abundant in CM 41.65-41.75: *C. minisculus*, *M. minimus*, and *Normalograptus* sp. In this biozone, the species *M. minimus* is only present in the residues of this concretion. In residues of CM 42.3-42.4, *C. minisculus* and *Normalograptus* sp. are found together and in CM 40.5-40.6 *C. minisculus* is found without the others. This does not seem to be a persistent species association.

Cluster 4 delineates the species association of *P. leptotheca* and *A. hubeiensis*. These two species occur together in two of the four concretions of this biozone. Cluster 3 comprises the three taxon found in CM 42.8-42.9; *N. magnus*, *C. comatus*, and *M.* cf. *arciformis*. These taxon are not found in any other dissolution residues from this biozone. Their abundance in these residues is clearly distinct from their absence from the residues of the other concretions. The three taxon are common in the some of samples above this (CM 44.0-44.1, CM 44.1, CM 45.3-45.4). In the residues from the concretion stratigraphically above this (CM 44.0-44.1), *H. praestrachani*, *M. minimus*, and *G. incertus* are abundant. These three species were common in the lower *C. cyphus* Zone concretion residues. Their appearance above CM 42.8-42.9 is evidence that these graptoloids did not permanently dissapear from the Cape Phillips Embayment either throughemigration or extinction. The species composition of CM 42.8-42.9 can be considered unique and may represent an incursion of immigrants and a temporary shift in the plankton community. Interestingly, the sediments and taphonomic character of the graptoloids of this concretion showed signs of sediment starvation. A change in the rate of sediment supply would likely be associated with a change in the paleocurrents of the Cape Phillips Embayment. It is possible that this shift in sediment and current dynamics altered the established community dominated by *P. leptotheca* and *A. hubeiensis*, and replaced it with a new community of graptoloids not previously present in these waters. When sediment supply rates returned to levels similar to those previous to CM 42.8-42.9, the graptoloids *H. praestrachani*, *M. minimus*, and *G. incertus* return to the waters above this sediment.

Monograptus pectinatus Zone (Figure 9.2; Table 8.4)

Cluster 1 of *Rhaphidograptus sinicus*, *Normalograptus laciniosis*, *Metaclimacograptus*? n. sp., New Genus A sp. A Lukasik, *Pseudorthograptus inopinatus*, *Glyptograptus* cf. *incertus*, *Coronograptus arcuatus*, *Monograptus pectinatus*, *Agetograptus secundus*, *Petalolithus intermedius*, *Metaclimacograptus undulatus*, *Glyptograptus tamariscus tamariscus*, *Rastrites* sp., and *Pribylograptus imprimus* is a grouping of species that are rare or absent in most of the residues (Table 8.4). All but *P. inopinatus* are absent from CM 46.35-46.5 (*P. inopinatus* is only found in one residue of CM 46.35-46.5). *Glyptograptus* n. sp. is a species of minor abundance, it is found in CM 46.35-46.5, but not in the other concretions, and therefore forms a single species cluster within cluster 1. *Glyptograptus incertus* and *N. magnus* cluster together as the second cluster of this analysis, based upon their co-occurrence in the residues of CM 45.3-45.4 and their relative rarity (*G. incertus*) or absence (*N. magnus*) from other concretions of the biozone. *Metaclimacograptus rigidus* and *Metaclimacograptus minimus* are rare species in the residues, although in the two residues in which *M. minimus* occurs (CM 47.4-47.5 residues 3, and 20.5) it is the most abundant species. These two taxon are clustered together with *Pristiograptus* n. sp. A Lukasik in the third cluster, even though these three species rarely co-occur. *Lagarograptus inexpeditus* and *Normalograptus nikolayevi* are two species that show a similarity in distribution and form cluster 4. In all but one residue (CM 48.5 residue 38) *N. nikolayevi* is found with *L. inexpeditus*; however, *L. inexpeditus* is found in 12 residues without *N. nikolayevi*. Cluster 5 of *Pribylograptus leptotheca*, *Monograptus* n. sp. B Melchin and *Comograptus comatus* is the species association with the largest stratigraphic range in this biozone. The two species *P. leptotheca* and *Monograptus* n. sp. B Melchin are found in relatively equal abundances in residues from all concretions except CM 47.4-47.5. These abundant species are absent from this concretion. *Comograptus comatus* differs in its presence in this concretion and occasional absence from residues from the other concretions. The association of *P. leptotheca* and *Monograptus* n. sp. B Melchin is the only species association of this biozone with good evidence for co-habitation in the water-column.

It is important to first exclude the possibility that I have misidentified the specimens and that *P. leptotheca* and *Monograptus* n. sp. B Melchin are the same species. Both are

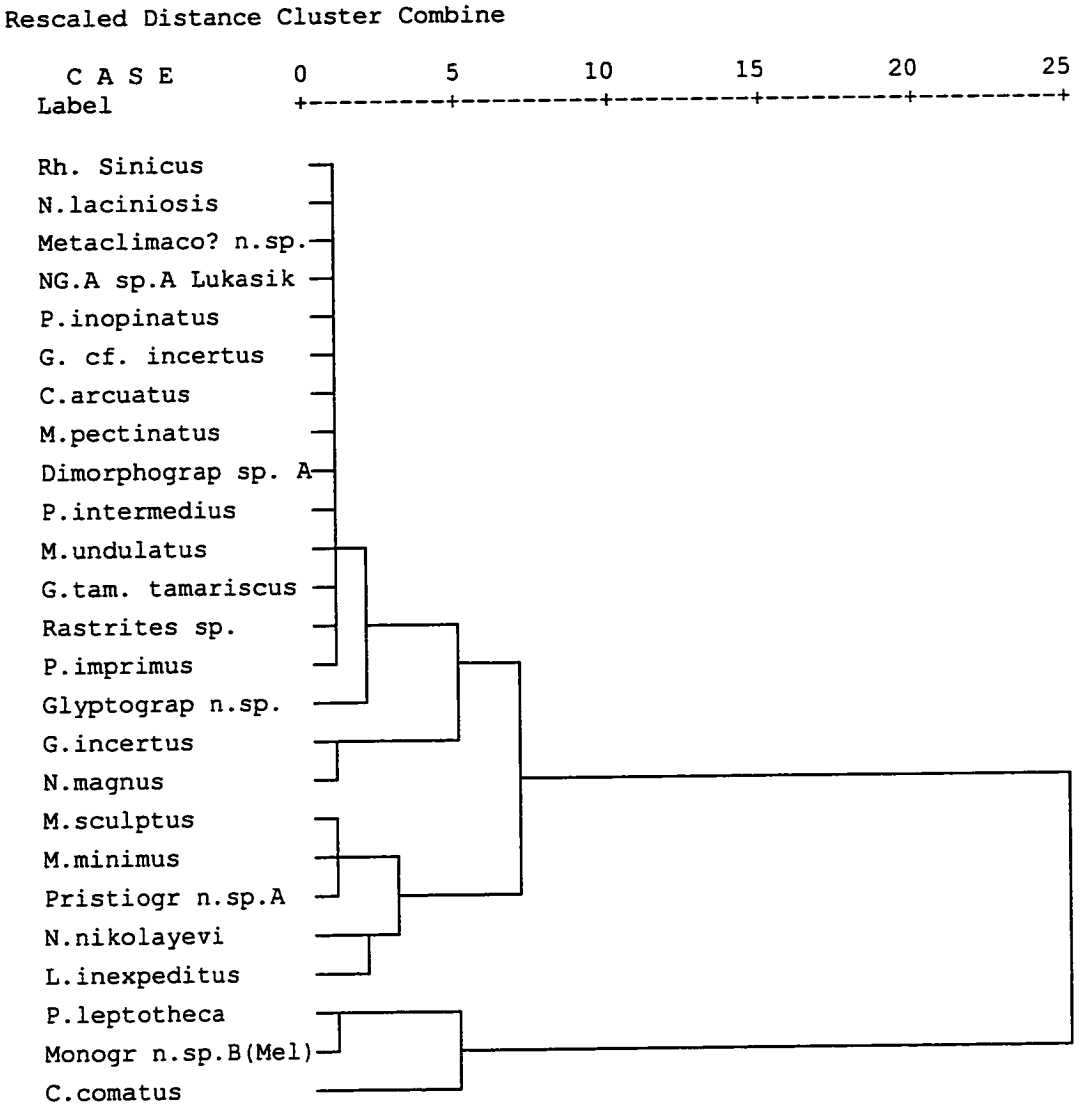

Figure 9.2. Hierarchical cluster analysis of graptoloid species from the *M. pectinatus* Zone displayed as a dendrogram using average linkage (between groups).

large "monograptids", but they differ greatly in the thecal aperture characteristics and biometrics along the length of the rhabdosome (Plate 3 i, n; Plate 5; Chapter Ten). It would not have been possible to interchange the two. As I have shown in previous chapters, there is evidence for physical reworking and transport of graptolite rhabdosomes in each of the concretions selected from this biozone (CM 45.3-45.4; CM 46.35-6.5; CM 47.4-47.5; and CM 48.5). Could the association of *P. leptotheca* and *Monograptus* n. sp. B Melchin be recording a biostratinomic association based upon their similar size? The graptoloid concentration beds of CM 45.3-45.4, CM 46.35-46.5, and CM 48.5 show a slight increase in these two species but they are also present through the non-event laminae, suggesting that this is not just a taphonomic association based on size. The co-occurrence of *P. leptotheca* and *Monograptus* n. sp. B Melchin appears to be a true species association and represents a graptoloid community. To explain this association is purely speculative, but the similarity in size and strong thecal change along the rhabdosome of the two "monograptids" may be indicative of their occupation of a similar niche.

Rastrites orbitus (Figure 9.3; Table 8.5)

The species association of *Prybilograptus leptotheca* and *Monograptus* n. sp. B Melchin identified in the *M. pectinatus* Zone does not extend into the *R. orbitus* Zone. The two species are separated by the maximum dissimilarity distance in the cluster analysis (Figure 9.3).

The first cluster is composed of species that are rare or in low abundance in the residues. *Glyptograptus tamariscus tamariscus* and *Monograptus* cf. *triangulatus* both are found in CM 49.8-49.8 and rare (*G. tamariscus tamariscus*) or absent (*M. cf. triangulatus*) in the residues from the other concretions in the analysis. For this reason they form cluster 2 that is close in distance in the similarity matrix. *Metaclimacograptus orientalis* is also a component of the assemblage from CM 49.8-49.9 and so it forms a third member of the cluster. The species *M. orientalis* is less similar in distribution because it also appears in residues of CM 50.4 and CM 50.4-50.5. Four thin "monograptids" form cluster 3a; *Pristiograptus fragilis pristinus*, *Monograptus involutus*, New Genus A sp. A Lukasik, and *Monograptus tenussimus*. These "monograptids" are

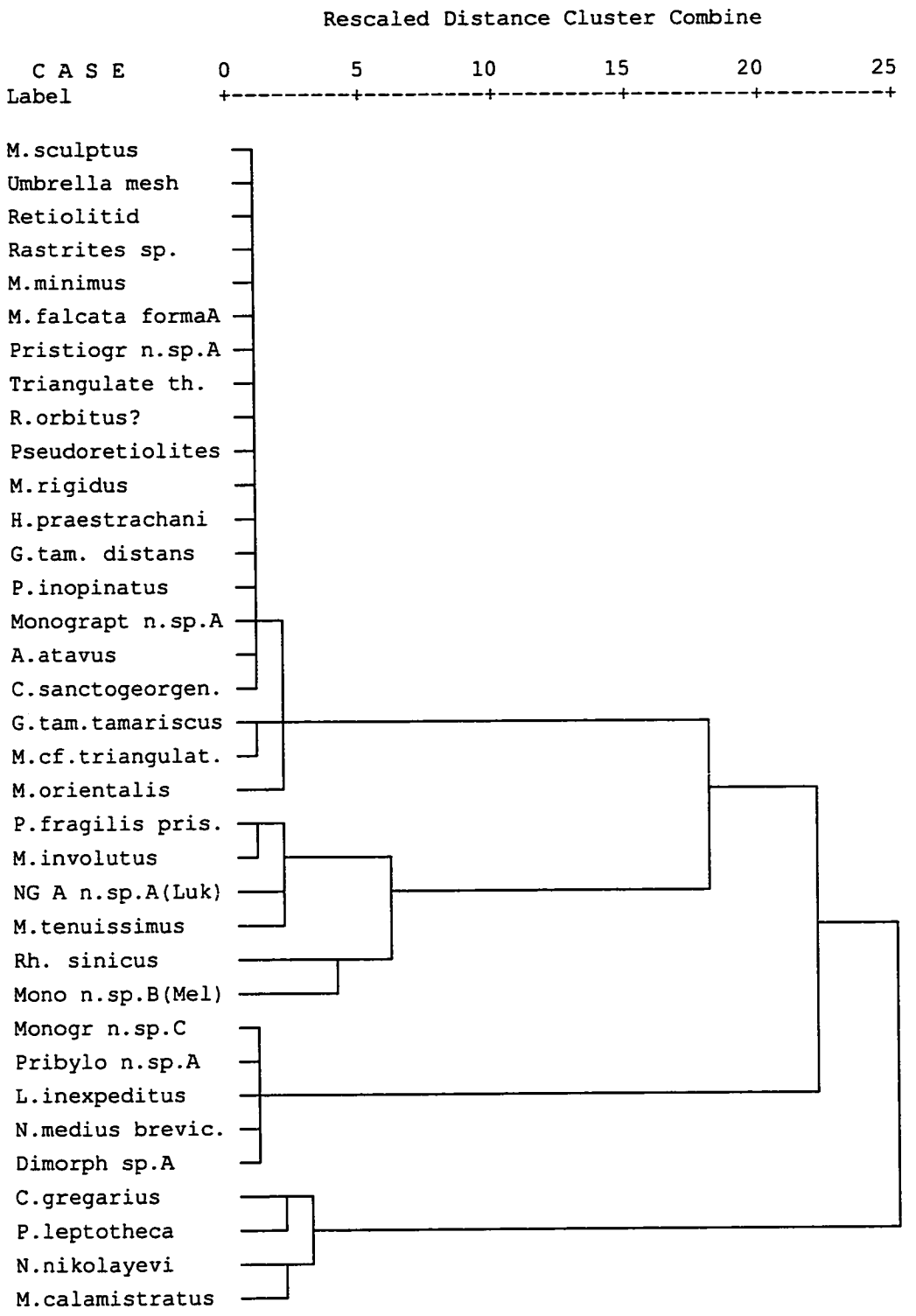

Figure 9.3. Hierarchical cluster analysis of graptoloid species from the *R. orbitus* Zone displayed as a dendrogram using Ward's method (error sum of squares).

most common in the concretion CM 50.4-50.5 and the limestone bed CM 50.4 and rare to absent in the other concretions. Because of the close stratigraphic proximity, this is not considered to be a long-lasting species association. Cluster 3b comprises *Rhaphidograptus sinicus* and *Monograptus* n.sp. B Melchin and shares this co-occurrence in CM 50.4 and CM 50.4-50.5. *Monograptus* n. sp. B Melchin has a greater stratigraphic distribution also being a component of the assemblage of CM 49.8-49.9. Cluster 4 includes five graptoloids that are all found in every residue from CM 49.8-49.9 and are rare or absent in the other residues in the biozone. Cluster 5 is divided into two groups: 5a comprises *Coronograptus gregarius* and *Pribylograptus leptotheca*; and 5b comprises *Normalograptus nikolayevi* and *Monograptus calamistratus*. The species association of *N. nikolayevi* and *M. calamistratus* is only found in the residues of the two stratigraphically equivalent concretions CM 51.2-51.3a and CM 51.2-51.3b. This association was relatively short in duration. The species association of *C. gregarius* and *P. leptotheca* is found in every concretion chosen from this biozone. This species association was of relatively long duration. The relative abundance of each species is similar through the section with a peak relative abundance for both in the residues of CM 51.2-51.3a and CM 51.2-51.3b.

One long-lasting species association is that of *C. gregarius* and *P. leptotheca*, which were found in similar abundances in most of the residues through the R. orbitus Zone. In the basal concretions and limestone bed the abundances of both species are low. In the previous biozone (*M. pectinatus* Zone), *P. leptotheca* was associated with *Monograptus* n. sp. B and *C. gregarius* was absent from the residues. *Coronograptus gregarius* is recorded from the *C. cyphus* Zones and *M. pectinatus* Zones of the Cape Phillips Formation (Melchin, 1987b). I record rare *Coronograptus arcuatus* from the *M. pectinatus* Zone and *Coronograptus minisculus* from the *C. cyphus* Zone, but I did not find *C. gregarius*. I can speculate the migration of *C. gregarius* into this part of the Cape Phillips Embayment was a cause for the disassociation of *Monograptus* n. sp. B and *P. leptotheca* as a result of direct or indirect competition with *Monograptus* n. sp. B. However, *Monograptus* n. sp. B Melchin and *C. gregarius* are found together in CM 50.4, CM 50.4-50.5 and CM 49.8-49.9, a time scale of tens of thousands of years and a

competitive exclusion hypothesis does not work on such long time scales (Prothero, 1998).

Lituigraptus convolutus Zone (Figure 9.4, Table 8.6)

Cluster 1 comprises ten graptoloids that are low in abundance and commonly absent through the biozone. *Neodicellograptus siluricus*, *Campograptus communis* and *Pseudoglyptograptus barriei* are the three species that comprise cluster 2. This species association is found in residues of CM 58A and the top residues of CM 59.1-59.2. Cluster 3 is an association of graptoloids that is found in CM 56.4-56.5. The species of this cluster include: *Glyptograptus tamariscus distans*, *Campograptus* sp., and *Metaclimacograptus rigidus*. Cluster 4 comprises *Petalolithus ankyratus*, *Monoclimacis* n. sp. B Lukasik, *Normalograptus nikolayevi*, and *Monograptus decipiens*. These are found together in CM 59.1-59.2. Cluster 5 is divided into three "subclusters": 5a, *Pristiograptus* n. sp. B (Lukasik); 5b, *Pristiograptus* n. sp. B (Lukasik), Rastrites *orbitus*, *Campograptus n. sp.*, and *Torquigraptus* n. sp. A; 5c, *Monograptus crenularis*?, and *Monograptus* n. sp. B. Species associations identified by cluster 5a and 5b are short in duration. *Monograptus crenularis*? and *Monograptus* n. sp. B are found together in the residues of one concretions (CM 57) and rarely together in two other concretions (CM 56.4-56.5 and CM 57.5-57.6). This is not strong evidence for a long-lasting paleoecological species association. Cluster 6 is distinct from the other clusters. The two taxon in this cluster, *Monograptus falcata* and *Monograptus sidjachenkoi*, were common in the residues of CM 58a and CM 59.1-59.2. These two species are "paramonoclimacids", graptoloids with proximal hooked thecae and distal monoclimacid type thecae. I was able to distinguish the two based on details of the thecal aperture and the curvature of the rhabdosome, and I am confident that they are distinct. This association did not extend to CM 57.5, in which the residues contain abundant *M. falcata* and no *M. sidjachenkoi*; or to CM 56.4-56.5, in which the residues contain abundant *M. sidjachenkoi* and barren of *M. falcata*.

In the *L. convolutus* Zone, the species associations identified in the cluster analysis are relatively short in duration. No one species was able to maintain abundance, and a species association between two or three graptolites never persisted for more than

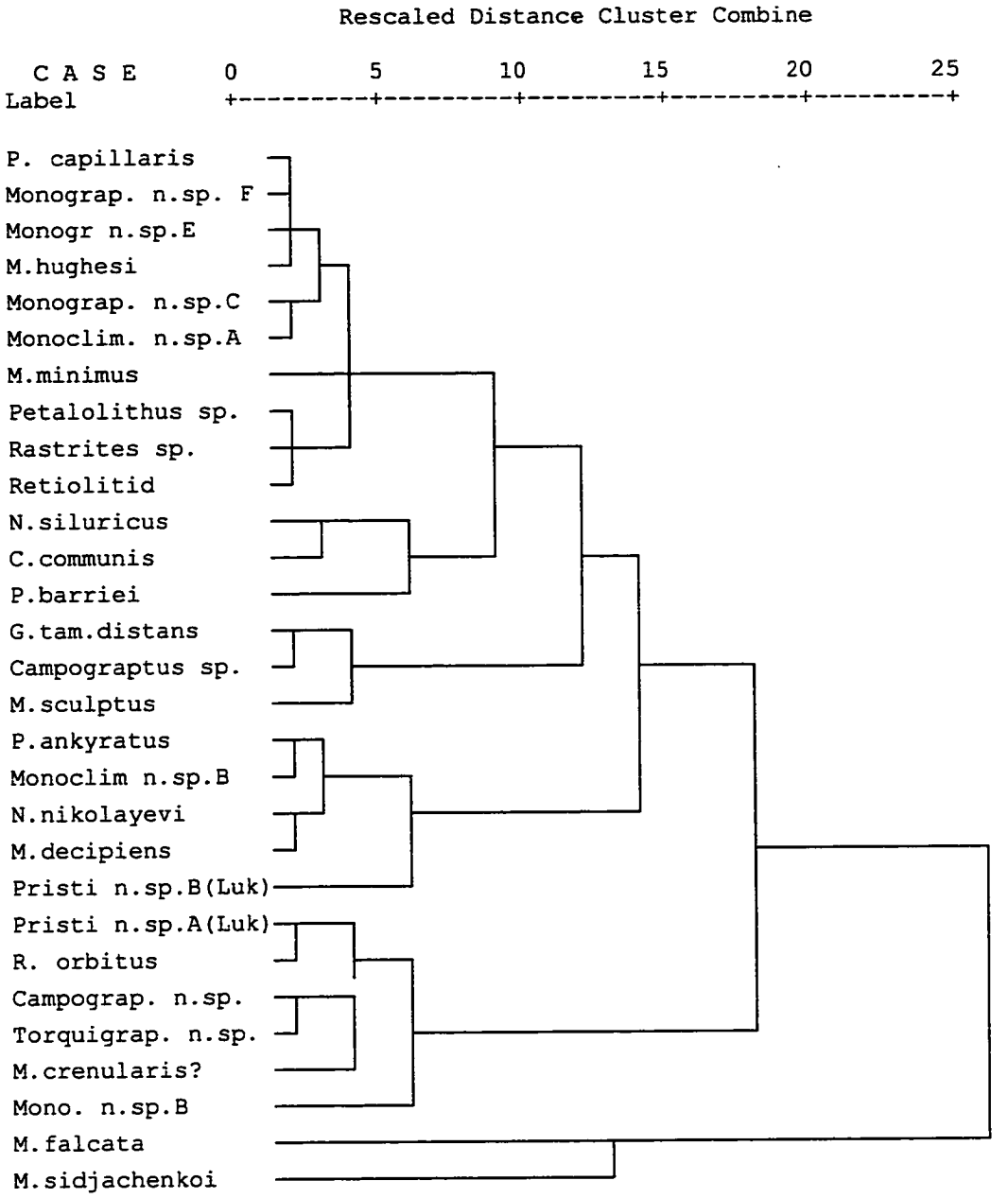

Figure 9.4. Hierarchical cluster analysis of graptoloid species from the *L. convolutus* Zone displayed as a dendrogram using average linkage (between groups).

approximately one meter of stratigraphic thickness. This is equivalent to approximately 25,000 to 120,000 years (Chapter Eight), which is considerable on an ecological time scale but the purpose of this chapter is to identify recurrent-species associations that were significant for longer periods of time.

Spirograptus guerichi Zone (Figure 9.5, Figure 9.6; Table 8.7, 8.8)

The distinction of clusters within the species distribution is controlled by the difference between CM 75.5 and the other concretions examined in this biozone. Clusters one and three comprise the rare species of CM 75.5. Cluster 2 comprises the rare species of CM 72.6 and CM 73.8. Cluster 4 comprises the more abundant species in the residues of CM 72.6, CM 73.8, and CM 74.9a. Species associations within this group of five graptoloid species are difficult to identify. Cluster 5 comprises the abundant species of CM 75.5. Because of the disparity between the two groups of concretions and the interesting distribution of graptoloids through the laminae of CM 75.5, I thought it appropriate to concentrate on this concretion in a detailed cluster analysis. This is not an examination of recurrent species associations but an examination of the species distribution through a small interval of strata that has been identified as not being taphonomically altered.

In the previous chapters, CM 75.5 was identified as a concretion that was not taphonomically altered and one that recorded a bloom in *Pristiograptus regularis regularis*. Three clusters were identified from the R-mode cluster analysis: Cluster A, dominated by *Monograptus halli*; Cluster B, dominated by *Spirograptus guerichi*; and Cluster C, dominated by *Pristiograptus regularis regularis*. Cluster C is the one that has in previous chapters been identified as the "bloom". *Pristiograptus regularis regularis* is a taxa present throughout the concretion but only displays peak abundance in the mid–concretion residues. Note how *M. halli* is scarce to absent in these same mid-concretion residues (Table 8.5), although it is the most dominant species in the residues from the base and top of the concretion (Cluster A). *Spirograptus guerichi* is abudant in the residues at the transition between *M. halli* and *P. regularis* and then again from *P. regularis* to *M. halli* (Cluster B). *Spirograptus guerichi* can be interpreted as a

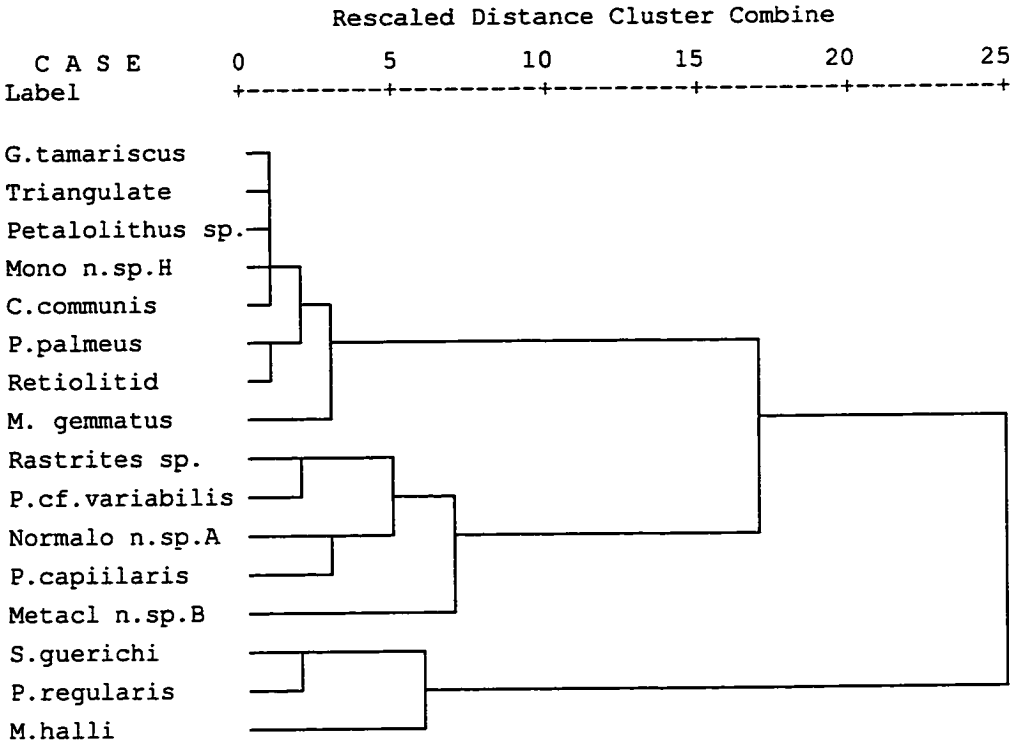

Figure 9.5. Hierarchical cluster analysis of graptoloid species from the *S. guerichi* Zone displayed as a dendrogram using average linkage (between groups).

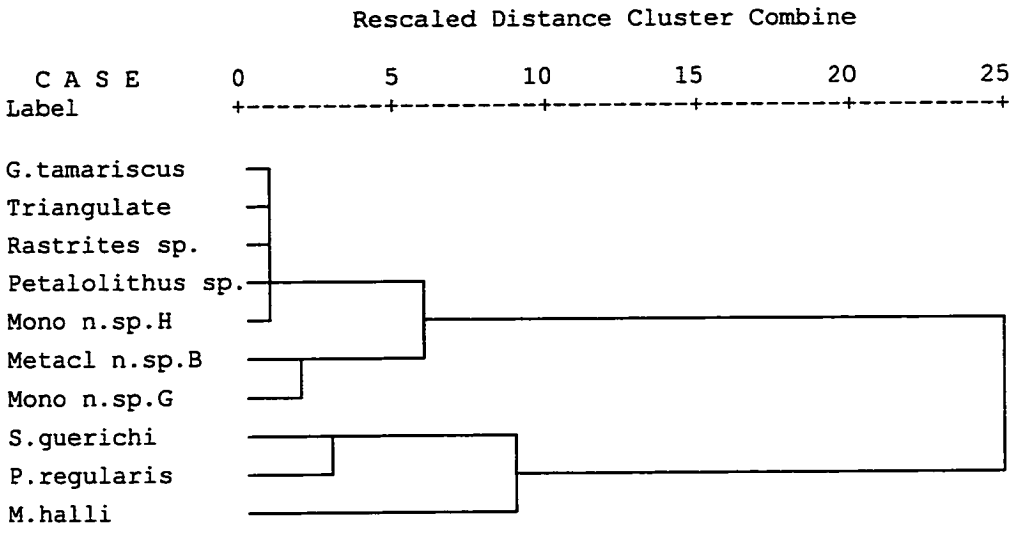

Figure 9.6. Hierarchical cluster analysis of graptoloid species from the *S. guerichi* Zone displayed as a dendrogram using average linkage (between groups).

transitional species bloom. This pattern of community replacement was occurring on the scale of thousands of years (Chapter Eight).

Summary: graptoloid communities

A species association of *Pribylograptus leptotheca* and *Agetograptus hubeiensis* through the lower strata of the *C. cyphus* Zone is most likely a record of a graptoloid community. This association and the assemblage of graptoloids that were found with the dominant species was not found in concretion CM 42.8-42.9, 0.5 m above the last concretion that records that community. This concretion also records a sediment-starved taphofacies. It was suggested earlier in this chapter that this interval might represent a shift in sedimentary dynamics, that reduced the sediment supply, and may have also altered the established community

The co-occurrence of *Pribylograptus leptotheca* and *Monograptus* n. sp. B Melchin in the *M. pectinatus* Zone appears to be another example of a species association and likely represents a graptoloid community. The similarity in rhabdosome size and structure of the two "monograptids" may be indicative of their occupation of a similar niche. This association was established in concretions that were identified to be taphonomically altered and of the taphofacies physical addition of graptoloids. It is possible that this community is being brought in from shallower water. The large, durable size of the distal fragments suggests they may have been resistant to physical damage inherent in shallow-water habitats, but this is purely speculative.

The species association of *Pribylograptus leptotheca* and *Monograptus* n. sp. B Melchin does not persist into the interval of the *R. orbitus* Zone. Instead, *Coronograptus gregarius* and *P. leptotheca* were found in similar abundances in most of the residues through this biozone. I suggested above that this may be a type of competitive exclusion. Species associations of the *L. convolutus* Zone were short in duration and this interval represents a time of ecologic or taphonomic instability.

It is unusual to find graptoloid associations that persist through a biozone. This suggests that most graptoloid species were not directly or indirectly linked to other species. The distribution of graptolites through CM 75.5 supports the idea that at least some species were free from the constraints of ecological relationships and could bloom

and die as individual populations. Rickards (1991) identified a type of graptolite occurrence in which diversity is low and age variation great on single bedding planes, and suggested this might be the result of mass-mortality of monospecific plankton clouds from a particular niche. In the waters of the Cape Phillips Embayment, most often graptoloids appear to have been living in diverse communities perhaps dominated by one or more taxa. Species associations identified herein do not support the hypothesis of monospecific life assemblages. However, in times of lower graptoloid diversity, in the Wenlock of the Cape Phillips Formation, the community structure may have been different. In the mass-transport events preserved in the concretion CP 214.5, I identified two taphocoenosis, each relatively monospecific in character. This seems to support Rickards' (1991) concept of mass-mortality from mono-specific plankton niches.

Age segregation in the graptoloid community

Controversy exists in the question of how the embryo or zygote metamorphs to the larva and early sicular stage of development. Two hypotheses exist. The first is that the mobile zygote matures to a mobile larva which, upon attaining a certain weight or size, settles to the sea floor and the secreted prosicula becomes attached to the substrate, later rising into the water column as the rhabdosome matures (Kirk, 1969, 1990a, b). This hypothesis is based upon the development of sessile dendroid graptoloids from which planktonic graptoloids are believed to have evolved. The second hypothesis does not involve the settling of the larva but instead describes all developmental stages as having occurred in the planktonic environment (e.g., Fortey, 1982; and Erdtmann, 1982). These hypotheses can be tested using the observations of sicular and thecal distribution through the samples examined for this thesis

The concomitant thecal and sicular distributions through most of the concretions examined layer-by-layer in this thesis is contrary to the predictions of the hypothesis of a benthic mode of life for graptoloid siculae. If graptoloid colonies began as benthic siculae and later in astogeny through the co-coordinated effort of the zooids achieved a planktonic mode of life, as suggested by Kirk (1969, 1990a, b), then we would not see the correlated thecae and sicular distributions (e.g., CM 55, and CM 56.4-56.5). The similar

distribution profiles of total thecae and siculae through the residues (Figure 4.48, 4.50) suggest that both the mature colony and the juvenile colony were planktonic and settling from the water column at a similar rate in geologic time scales. In addition, Kirk (1990a) proposed that the sicula was oriented with the sicular aperture up with the apex anchored in the sediment. The siculae observed on the dissolution surfaces during the layer-by-layer dissolution were most commonly found parallel to bedding (Appendix D) and did not show the *in situ* orientation proposed by Kirk (1990a).

10 INFORMAL GRAPTOLOID SPECIES DESCRIPTIONS

Included in this chapter are informal descriptions of 24 graptoloid species that have not been previously described. Three previously identified graptoloids are re-described in light of their excellent preservation in this material (*Comograptus comatus*, *Pribylograptus leptotheca*, *Monograptus falcata*). The other previously described graptoloid species are illustrated, but not described. Images were obtained using infrared video microscopy (IVM) and image capture with a scanning electron microscope (SEM). Species illustrations on the plates are grouped by zonal co-occurrence.

Family NORMALOGRAPTIDAE (Storch and Serpagli, 1993).

Comograptus comatus (Obut and Sobolevskaya, 1968)

Plate 2 a-k

Previously, this genus was split into two species; *Comograptus gorbiachinensis* Obut and Sennikov, 1980, a graptolite with three sicular spines; and *Comograptus comatus* Obut and Sobolevskaya, 1968, a graptolite with multiple sicular spines and thecal aperture spines. In our residues the two types, along with a spineless variant were commonly found in the same residues and are not considered to be separate populations. After careful investigation of isolated specimens in SEM, IVM, and transmitted light the two species are considered to be conspecific. The production of spines both sicular and thecal is thought to be a function of maturity. Specimens from the same residue show a relationship between rhabdosome maturity (length and thickness of cortical material) and quantity of sicular spines. Apertural spines on the thecae are only seen on very long or thick-walled rhabdosomes. Even then the apertural spines are limited to the proximal thecae and are rarely seen past the third thecal pair. The biometrics between the two groups (three spines and many spines) are identical and the early astogenetic development of the rhabdosome are both Pattern I. The width at th1 is 0.6-0.7 mm, and at th 3 is 0.8-0.9 mm. A maximum width of 1.1 to 1.3 mm is attained after the 6th thecal pair. Sicular length is 1.2 to 1.3 mm. Proximal 2TRD is 1.1 to 1.3 mm and the distal 2TRD is 1.6 to 1.8 mm.

Metaclimacograptus sculptus Chen and Lin, 1978

Plate 8 s.

Metaclimacograptus sculptus Chen and Lin, 1978 was correctly identified in the flattened material presented in Melchin (1989), and incorrectly identified in the isolated material presented in Melchin (1998). The specimen Melchin (1998) illustrated as *M. sculptus* is *Metaclimacograptus rigidus* (Chen and Lin, 1978). Melchin (pers. comm., 2001) assumed that the disparity between the thecal form was a difference between compressed and uncompressed specimens. Isolated specimens of *M. sculptus* and *M. rigidus* preserved in the residues examined for this thesis clarify the distinction between the two species. *Metaclimacograptus sculptus* is synonymous with *Metaclimacograptus khvorovi* (Koren and Rickards, 1996) that is described as having widely spaced thecae and strongly inward-sloping supragenicular walls.

The first few thecae of *M. sculptus* have a rounded geniculum. Thecae after the second thecal pair have a sharp geniculum that may be the product of a subtle ventral hood or flange. In this respect it resembles *Metaclimacograptus orientalis* (Obut and Sobolevskaya, 1968); however, the thecal spacing of this species is greater than that of the more compact *M. orientalis*. Inclined supragenicular walls differentiate this graptolite from *Pseudoclimacograptus rigidus* (Chen and Lin, 1978) and *M. orientalis* that have rounded supragenicular walls that are approximately parallel to the rhabdosomal axis. The width is 0.5 to 0.7 mm at the first thecal pair, and reaches a maximum width of 0.7-0.9 mm at the second. This is a rare species in the residues examined from the Cape Manning section, and the largest specimen (illustrated in Plate 8q) is fragmented after the fourth thecal pair. The proximal 2TRD (th2-th4) is 1.4 – 1.6 mm. Genicular hoods extend approximately 0.1 mm above the open, everted apertures.

Metaclimacograptus rigidus (Chen and Lin, 1978)

Plate 7 a.

This rare species that is found throughout most of Aeronian samples is not observed complete beyond the third thecal pair. Stratigraphic variation in the proximal 2TRD was found; the 2TRD was between 1.3 and 1.4 mm in the *R. orbitus* Zone and a 2TRD of 1.5 to 1.6mm in the *L. convolutus* Zone. The shorter 2TRD matches the holotype of

Metaclimacograptus rigidus Chen and Lin, 1978. Width of the rhabdosome at th1 is 0.65 to 0.7 and the width at th3 is 0.75 – this is the maximum width. As discussed above, Melchin (1989) grouped this species with *Metaclimacograptus sculptus* Chen and Lin, 1978. It differs from *M. sculptus* in the rounded supragenicular walls that are more nearly parallel to the rhabdosomal axis.

Metaclimacograptus n. sp.

Plate 13 a.

This species has a narrow rhabdosome with hooded, metaclimacograptid thecae and a wide thecal spacing, and could not be ascribed to any previously identified metaclimacograptids. It is most similar to specimens of *Metaclimacograptus undulatus* (Kurck, 1882) (Plate 8 e, f), but differs from *M. undulatus* in having a longer 2TRD, both proximally and distally, and a more slender rhabdosome. The width at theca 1 is 0.4 to 0.5 mm and shows little distally expansion with a maximum width at th5 of 0.55 to 0.65 mm. Proximal 2TRD is 1.4 to 1.6 mm and distal 2TRD is 1.6 to 1.9 mm.

Metaclimacograptus? n. sp.

Plate 7 f.

Only three specimens of this new species were found in the isolated material. This is a small graptoloid with metaclimacograptid-type thecae htat have metaclimacograptid-type hoods. What makes this graptoloid unique are the spines that project out from the lateral wall of the thecae and are not related to the aperture. Paired spines extend 0.1-0.3 mm from the lateral surface of the thecae in obverse and reverse directions. These spines begin on the first thecae and continue distally. An early growth stage specimen with just theca 1 shows two short spines extending in obverse and reverse directions from the theca 1 lateral walls. The sicula length is 0.9 mm. The width of the rhabdosome at th1 (minus spines) is 0.7 mm, and 0.75 mm at th4. Proximal 2TRD is approximately 0.9 mm. The largest specimen was four thecal pairs in length.

Normalograptus? n. sp.

Plate 13 f.

The proximal thecal apertures bear dorsal hoods that are less pronounced to absent distally. Distal thecae are climacograptid in shape. Hood development increases with maturity. Immature specimens with similar dimensions in the same residues have no hoods proximally and are classified in the same species. These immature specimens are similar in appearance to *Normalograptus nikolayevi*. The sicula is exposed to a height of 0.4 to 0.5 mm. The width at the first thecal pair is 0.5 to 0.6 mm and increases to a maximum width of 1.1 to 1.3 mm at the sixth thecal pair. The 2TRD is 1.4 to 1.6 mm proximally, and 1.7 to 2.0 mm distally.

Family PETALOLITHIDAE Bulman, 1955

Glyptograptus n. sp.

Plate 6 i.

A long rhabdosome with gently sigmoidal to straight thecae proximally that become more sharply geniculate distally. Many mature specimens show extra cortical thickening of the virgella and the proximal end. The width is 0.75 to 0.85 mm at the first thecal pair, 0.9 to 1.0 mm at the second, 1.0 to 1.2 mm at the fifth, and maximum width is 1.4 mm. The 2TRD proximally is 1.2 to 1.3 mm and distally is 1.5 to 1.7 mm. The length of the sicula is 1.5 mm. The virgella is not imbedded in the obverse wall and, therefore, it is dissimilar to *Glyptograptus tamariscus*. This species has a partial medium septum at the sixth thecal pair and is similar in this way to *Glyptograptus incertus* and to normalograptids such as *Normalograptus nikolayevi*. *Glyptograptus* n. sp. differs from *N. nikolayevi* in having a closer thecal spacing and a constant distal width that is obtained at the fifth thecal pair. Although the proximal end was not observed in IVM to asses the astogenetic pattern, the slightly sinusoidal glyptograptid-type thecae are suggestive of the genus *Glyptograptus*. This graptoloid is considered a new species, because it is too narrow for *Glyptograptus incertus,* and not assignable to other graptoloids with glyptograptid-type thecae..

Family MONOGRAPTIDAE Lapworth, 1873

Campograptus n. sp.

Plate 11 e.

This species is placed in the genus *Campograptus* because of the wide proximal end that is strongly curved in a dorsal direction. This species differs in the hoop-shaped apertural hoods that, when broken, appear as paired horns. *Campograptus* n. sp. differs from *Campograptus communis* in the less pronounced metatheca, greater width overall and a more elongate sicula and theca one. The sicula is 1.25 mm long and theca one begins approximately 0.2 mm above the sicular aperture. Theca one is 1.15 mm long. The width expands at a constant rate; at theca one the width is 0.4 mm, at theca two is 0.5 mm and at theca three is 0.6 mm. The 2TRD from the proximal thecae is 1.8 mm.

Monograptus cf. *arciformis* Chen and Lin, 1978 sensu Melchin, 1987

Plate 3 f, g, o, p

A long rhabdosome with weak dorsal curvature widens gradually from a proximal width of 0.3 to 0.4 mm to a maximum width of 0.8 to 1.0 mm. The proximal 2TRD is 1.8 to 2.0 mm and distally the 2TRD is 2.0 to 2.2 mm. Proximal thecae are axially elongate with slender prothecae and hooked metathecae that occupy approximately ½ of the width. Distally the prothecae are shorter and broader, the ventral wall is slightly inclined and the hooked metatheca occupies less than half of the width of the rhabdosome. The sicula is 0.6 to 0.7 mm long. Theca one originates approximately 0.3 mm above the sicular aperture and is approximately 1.1 mm in length and 0.2 mm in width. This could not be directly related to the holotype of *Monograptus arciformis* Chen and Lin, 1978, which has a wider distal end.

Monograptus falcata Chen and Lin, 1978; forma A

Plate 9 a-f.

Three different forms of *M. falcata* are found in the Cape Phillips Formation. Each is like *Monograptus falcata* Chen and Lin, 1978, in having streptograptid-type thecae with strongly coiled thecal apertures proximally and, after rapid increase in width, displaying a simplification of the thecal aperture to hooded, then to unornamented.

Forma A has a sicula 0.7 mm in length with theca 1 beginning 0.1-0.2 mm above the sicular aperture. Theca 1 is 0.8 – 0.9 mm in length. The hooked theca curves down onto the ventral wall and a flared aperture wraps around the lateral sides of the rhabdosome. The proximal width including the hooked thecae averages 0.2 mm. In flattened material (MCM 88-9 6.5 m) the proximal portion of the rhabdosome is gently dorsally curved. The proximal 2TRD is 2.4 mm. Rapid mesial expansion is matched with an increase in the rate of curvature and a retraction of the hooked thecae to dorsal hoods. The rhabdosome widens from the proximal width to the distal width (0.7mm) over approximately 3 thecae. Distal theca show further retraction of the hoods to dorsal flanges or hoops. Distal 2TRD is 2.7 mm and the distal rhabdosomes are straight to gently curved in the dorsal direction.

In the biostratigraphy of Cape Manning section (Chapter Three; Appendix B) no distinction between the three different forms of *M. falcata* was made in the flattened material. All specimens of *M. falcata* observed in shale were recorded as M. falcata forma A.

Monograptus falcata Chen and Lin, 1978; forma B

Plate 9 g-i.

The first theca of forma B is longer (1.2 mm) than that of forma A. Hooked proximal thecae display a slight lateral expansion not seen in the other forms of *M. falcata*. Also unique is the rapid expansion of the rhabdosome that appears to occur over one or two theca. The rhabdosome widens from 0.1-0.2 mm to 0.5 mm over the length of one theca. The maximum width is 0.9 to 1.0 mm. The thin proximal thecae are very fragmented and no true transition piece connecting the thin hooked thecae and the large, wide distal fragments was found. The assumed relationship is based on the similarity in hooked thecal aperture shape and the narrowness of the very proximal fragmented ends of distal pieces. In addition, this rhabdosome displays the characteristic retraction of the hooked theca distally.

Monograptus falcata Chen and Lin, 1978; forma C

Plate 9 j-k.

Forma C is a straight rhabdosome with minor to negligible dorsal curvature. Forma C is similar to forma A in many respects, including the biometrics of the sicula and the first thecae. Proximal thecae display a bulge in the metathecae. Expansion from the proximal width of 0.15 mm to distal width of 0.9 mm is more gradual and is estimated from measurement of width of mesial fragments to occur over 5 to 8 thecae. The hood retraction and distal hoop-shaped flanges are similar to forma A.

Monograptus n. sp. A

Plate 8 p, q.

This species is similar to the previously described *Monograptus* sp. 1 of Hutt, 1975. They cannot be definitely regarded as synonymous because of the uncertainties of relating the fragmented isolated specimens of the Cape Phillips to the single specimen preserved in relief that Hutt suspected had been tectonically distorted. *Monograptus* sp. 1 Hutt, 1975 is similar to *Monograptus* n.sp. A in that the thin protheca develops into a strongly lobate metatheca that recurves so that the ventral wall is adpressed to the early part of the metatheca and the metatheca is expanded laterally. The typical theaca of specimens of *Monograptus* n.sp. A has a protheca that expands from 0.05 mm at the base to 0.175 mm just before the metatheca. The dorso-ventral width of the rhabdosome at the metatheca is 0.4 mm. Biometrically, this is similar to *Monograptus* sp. 1 Hutt, 1975; however, the protheca of in *Monograptus* sp. 1 Hutt, 1975 are parallel-sided throughout its length. The 2TRD of *Monograptus* sp. 1 Hutt, 1975 is 2.0 mm. The isolated specimens of *Monograptus* n. sp. A were fragmented into single theca pieces so 2TRD could not be accurately measured; however, the fracture occurred preferentially at the thinnest portion of the rhabdosome, the base of the protheca. The longest fragment approached 1.0 mm and may match Hutt's 2TRD for *Monograptus* sp. 1. Proximal fragments and siculae attributed to *Monograptus* n.sp. A have a thecal hood that extends out from the rhabdosome at a right angle for approximately 0.15 mm and then hooks slightly in a proximal direction.

This specimen of *Monograptus* sp. 1. (Hutt, 1975) was found in the *Neodiplograptus magnus* Zone of Skelgil, stratigraphically slightly lower than the single appearance of *Monograptus* n.sp. A in the *R. orbitus* Zone. *Monograptus* n.sp. A is very similar to *Monograptus* n.sp. C found in the *L. convolutus* Zone. *Monograptus* n.sp. C has a more pronounced lateral expansion of the metatheca and the metatheca recurves very sharply.

Monograptus n. sp. B

Plate 11 i, j

Two forms, forma A and forma B, of this new species were identified in the isolated material from Cape Manning. Both forms of *Monograptus* n. sp. B are thin graptoloids with widely spaced thecae that have dorsally hooded apertures. These fragment very easily when isolated from the rock matrix and estimates of 2TRD for proximal vs. distal fragments are difficult to estimate. No clear example of a sicula with theca one of *Monograptus* n.sp. B type thecal appearance was found. The 2TRD varies from 2.0-3.0 mm. The dorso-ventral width is 0.15 to 0.2 mm at the aperture and including the hood. The lateral width of the hood is 0.2 mm. *Monograptus* n.sp. B forma A differs from *Monograptus* n.sp. B forma B in having a hood that is semicircular in shape when viewed from the ventral direction, as opposed to the crescent shape seen in forma B. Both forms are found in the *L. convolutus* biozone with no overlap in their stratigraphic ranges; forma A is stratigraphically lower than forma B.

Monograptus n.sp. C

Plate 8 m-o.

As noted above, this species is very similar to *Monograptus* n.sp. A, and in turn, is comparable to the previously described *Monograptus* sp. 1 of Hutt (1975). The protheca widens from 0.05 mm at the base to 0.1 mm at the base of the metatheca. The metatheca extends 0.1-0.2 mm from the rhabdosome at a right angle and then recurves sharply so that the ventral wall is adpressed to the early part of the metatheca. The aperture faces distally. The metathecae display a wide, lateral expansion at the point of recurvature. In

this way they differ from the more gently recurved metathecae with less pronounced metathecal expansion of *Monograptus* n.sp. A.

Proximal fragments and siculae attributed to *Monograptus* n.sp. C have a thecal hood that extends from the rhabdosome at a right angle for approximately 0.15 mm and then hooks slightly in a proximal direction. Theca one is 1.1 to 1.2 mm in length and begins approximately 0.1 mm above the sicular aperture. The sicula is 0.6 to 0.7 in length.

Monograptus n.sp. D

Plate 11 l, m.

This is a gently dorsally curving rhabdosome with simple hooked thecae. The metathecae are wide compared to the thin prothecae. The sicula is 0.75 mm long and theca 1 begins approximately 0.2 mm above the sicular aperture. Theca 1 is 0.9 mm long. The thecae are widely spaced (distal 2TRD is 3.5 to 3.9 mm). The proximal width of the rhabdosome is 0.2 to 0.3 mm and this increases continuously to distal widths that are 0.3-0.5 mm.

Monograptus n. sp. E

Plate 11 n, s.

The thecal character of this species is unique and cannot be attributed to previously described species. The ventral wall of the metatheca flares out from the rhabdosome and supports two short spines. Between the two spines the ventral wall is slightly thickened into an arch. The dorsal "hood" of the rhabdosome is consistently fragmented in the mesial to distal thecae giving the appearance of a distally facing aperture. If this was a full dorsal hood then the fusellar and cortical tissue was much reduced. With a dorsal hood, the actual aperture would be between the paired ventral spines. The dorso-ventral width at the thecal apertures is 0.3 to 0.35 mm. The distal 2TRD is 2.2 mm distally and 1.6mm proximally. The rhabdosome is slightly curved in a ventral direction. A sicular fragment assumed to be of this species has the following measurements; sicula length is 0.85 mm, th1 length is 0.75, th1 width (excluding spines) is 0.4 mm. This fragment displays a full dorsal hood on theca one along with the paired, ventral, aperture spines.

Monograptus n.sp. F

Plate 11k.

This very small rhabdosome is thin-walled and almost transparent pale brown in normal transimitted light. Never greater than one thecae in length, the rhabdosome was easily fragmented either during processing or biostratinomically prior to burial. The thecal apertures are proximally directed as a result of the ventral and dorsal hooked metatheca. The width of the metatheca averages 0.15 mm; the longest fragment is 0.35 mm long. No proximal end was found.

Monograptus n. sp. G

Plate 13 g, j.

The proximal end of this graptoloid is slightly dorsally curved but distally the rhabdosome is curved slightly in a ventral direction. The thecae are biform; proximally the thecae are hooded with paired aperture spines and between the third and fifth thecae the hoods are less pronounced and spineless. The distal thecal apertures are exposed and not covered by a hood. The sicula is 1.7 to 1.8 mm long and theca one begins approximately 0.5 mm above the sicular aperture. Theca one is 1.5 to 1.6 mm long and 0.7 to 0.8 mm wide. Distal rhabdosome widths are similar. The proximal 2TRD is approximately 1.5 mm and the distal 2TRD is approximately 2.5 mm. No "monograptid" previously described could be related to this graptolite. *Monograptus halli* (Barrande, 1850) shows evidence of hood retreat, but in the distal regions of the rhabdosome.

Pribylograptus leptotheca (Lapworth, 1876)

Plate 5 a-i.

The observed characters of this species are largely dependent upon preservational style and the section (proximal, mesial, or distal) of the often-fragmented rhabdosome that is sampled. Flattened rhabdosomes do not preserve the complicated thecal apparatus that adorns the mesial thecae. Differentiation of hoods, spines, and flanges are difficult in the flattened specimens (e.g., Loydell, 1991). Three-dimensional internal molds provide more accurate information about the pre-compacted rhabdosome but external

features created with cortical tissue are absent (e.g., Rickards and Rushton, 1968; Hutt, 1974-75). Rickards and Rushton (1968) described apertural structures that involve a "genicular" hood and paired horns that expand transversely (laterally). These apertural structures were not observed on more distal fragments of the rhabdosome and Rickards and Rushton (1968) assumed that the graptoloid must be biform. Previous descriptions of *P. leptotheca* do not include proximal fragments. The graptoloids identified in this thesis as *P. leptotheca* are preserved in full relief and preserve a complicated thecal apparatus that changes in form along the length of the rhabdosome. This long, multiform rhabdosome can be fragmented and the individual pieces are difficult to ascribe to the same species. Key transformation fragments that show two or more thecal styles are indispensable in the reconstruction of the complete rhabdosome.

Isolated specimens from this study are found in the *C. cyphus* Zone, *M. pectinatus*, and *R. orbitus* zones and correlate well with the temporal distributions of *P. leptotheca* from Bornholm and the British Isles. The *P. leptotheca* Zone of the British Isles is not named for the first appearance of *P. leptotheca* but for the dominance of this species within the strata (Rickards, 1976). The British *P. leptotheca* Zone correlates to the *R. orbitus* Zone of the Canadian Arctic.

The proximal thecae of *P. leptotheca* are hooded. Dorsal hoods extend over the thecal apertures and bend approximately 15° proximally in obverse, reverse and ventral directions. The ventral wall of the proximal theca flares slightly at the aperture. The first theca begins 0.1 to 0.2 mm above the aperture of the 0.6 to 0.7 mm long sicula. Theca 1 averages 1.25 mm in length and is 0.25 mm in width including the hood. The hood is reduced to a flange that extends over the thecal aperture in the proximal-mesial thecae. The rhabdosome is 0.3 – 0.4 mm wide (including the flange) and the 2TRD is 2.7 mm long in this proximal-mesial region. The flange appears to be an extension of the dorsal wall. Mesially, the flange takes the form of a spine with a wide base that grows from the dorsal wall. Paired lateral lappets extend distally towards the base of the spine. Lateral spines (extensions of the lappets) that protrude in an obverse and reverse direction are variable in the mesial theca of *P. leptotheca.* The three spine apparatus of mesial thecae of *P. leptotheca* appears in rhabdosomes from CM 46.35-46.5 in the *M. pectinatus* Zone and CM 48.5 and CM 49.8-49.9 of the *R. orbitus* Zone. Mesial thecae of *P. leptotheca*

that lack the lateral spines but show well-developed lateral lappets and a dorsal spine in the mesial thecae are found in CM 42.3-42.4 and CM 45.3-45.4 and of the *C. cyphus* Zone and *M. pectinatus* Zone, respectively. The difference in mesial apertural processes seems to be segregated stratigraphically. The mesial width (not including spines) ranges from 0.35 to 0.5

Lateral spines are absent from the mesial to distal thecae. Lateral lappets and the dorsal spine ornament the aperture. The mesial to distal thecae are between 0.5 and 0.8 mm in width. Distally, the dorsal spine is absent and only lateral lappets characterize the thecae with the lappets rarely reduced so that the thecae are simple and straight. The distal width average is 1 mm.

Pribylograptus? n. sp.

Plate 10 o-r.

Paired lateral lappets that are better developed distally, characterize the thecal aperture. Proximally, the thecae are simple and straight with everted apertures. When flattened, this species could be easily confused for *Pristiograptus fragilis pristinus*. The proximal width is 0.175 mm with a 2TRD of 2.3 mm. Distally, the width is approximately 0.2 mm and the 2TRD is 2.75 mm. In some respects, this species is similar to *Monograptus jonesi* Rickards 1970 that has similar biometrics. *Monograptus jonesi* is wider (0.25-0.30) than *Pribylograptus*? n. sp.Cape Phillips species, but this could be explained by diagenetic flattening. The two species are also from a similar zone interval; *M. jonesi* from the *M. argenteus* Zone, and *Pristiograptus* sp. A from the *R. orbitus* Zone. (correlated to the *M. argenteus* Zone). Rickards (1970) was unable to observe the details of the aperture, but reported that they appeared to be of the *Pribylograptus argutus* type.

Torquigraptus n.sp.

Plate 12d-g.

This species has been placed in the genus *Torquigraptus* Loydell (1993) because of the characteristic lateral torsion of the hooked thecae. Proximally, the rhabdosome curves gently in the dorsal direction and is nearly straight dorsally. The thin prothecae of

the proximal thecae are nearly parallel-sided with an average width of 0.15 mm. The height of the metathecae of these proximal thecae averages 0.3 mm as measured from the dorsal wall. In distal thecae, the prothecae expand towards the metathecae. Distal metathecae reach a maximum height of 0.675 mm. The 2TRD remains fairly constant throughout the length of the rhabdosome at 2.75 mm. This is considered a new species because it has a short metathecal height and a constant 2TRD proximally to distally that is not observed in other species with laterally twisted thecal apertures such as *Torquigraptus denticulatus* (Törnquist, 1899) and *Torquigraptus decipiens* (Törnquist, 1899).

11 CONCLUSIONS

1. Graptoloid-bearing carbonate concretions within shales and calcareous shales deposited in a slope-apron facies, below wave-base in the Lower Silurian Cape Phillips Embayment can be grouped into eleven microlithofacies based upon carbonate crystal size, colour, and lamination style.
2. A graptoloid taphofacies model consisting of seven graptoloid taphofacies was erected that describes particular taphonomic conditions or paleoecological events based upon the observed distribution of graptoloid rhabdosomes, and taphonomic characters.
3. Four taphofacies describe graptoloid concentration beds that were the product of increased input of graptoloid rhabdosomes or the removal or non-deposition of sediment. Increased input of graptoloid rhabdosomes was the result of taphonomic or paleoecological processes and defines the two taphofacies **physical addition of graptoloids** and **graptoloid bloom**, respectively. Cessation or reduction of sediment supply concentrated graptoloids and defines the taphofacies **sediment-starved**. The physical winnowing of sediment produced the taphofacies **sediment removal**, a sediment lag accumulation that is biased towards larger more mature rhabdosomes.
4. Three taphofacies describe statistically random (non-concentrated) graptoloid vertical distribution: **random flux of graptoloids and sediment, sediment event – low graptoloid abundance**, and **bioturbation**.
5. All taphofacies with the exception of the bioturbation taphofacies were recorded from the concretionary material collected from the Cape Phillips Formation. The distribution of microlithofacies and taphofacies through the two sections were used to asses the basin dynamics and sea-level history of the Lower Silurian Cape Phillips Embayment. This suggests:
    - a Rhuddanian to lower mid-Aeronian sediment bypass environment;
    - a mid-Aeronian change in basin dynamics followed by a deepening;

- a shallowing in the upper Aeronian and a change in basin morphology from inclined ramp to rimmed shelf (Melchin, 1989; de Freitas, 1999; and this thesis);
- a deepening in the lower Telychian; and
- a shallowing in the upper Telychian.

6. Background taphonomic processes and the resultant background sediments account for approximately 80% of the laminae examined from the concretions of the Aeronian Cape Manning . Episodic, short-duration event beds comprise the other 20 % of the laminae examined. Laminae identified as sediment-starved represent approximately 15% of the laminae examined and are considered to be a part of the background sediments. These beds can represent 2 to 4 times the amount of time recorded in non-event, non-hiatus horizons.
7. Time resolution of a 5 mm lamina of concretion material (the average sample size of this thesis) can be estimated to represent 25 to 114 years of accumulation based upon an estimated stratigraphic completeness at the 1,000 year scale of 21 to 95%. This is necessarily time-averaged because the accumulation time is longer than the assumed life span of a graptoloid colony.
8. Cluster analysis shows that graptoloid assemblages are relatively stable and have an average stratigraphic thickness of 6.5 cm. To accurately record small-scale stratigraphic fluctuations in the graptoloid taphocoenosis, a sampling interval of 6.5 cm of concretionary material or 1.3 cm of shale (corrected for compression) is required. In the *R. orbitus* and *L. convolutus* zones, graptolite assemblages were changing more rapidly (or sedimentation rates were lower) and the thickness of uniform graptolite assemblages was reduced to 2.0 and 2.9 cm, respectively. However, these samples still display greater internal similarity than similarity to concretions stratigraphically above or below. One will lose the finely resolved fluctuations in species abundance or assemblage composition in these samples by applying the sampling method described above, but one can still consider a 6.5 cm thick sample of concretionary material (1.3 cm sample of shale) to be a good representation of the total taphocoenosis.

9. Recurrent graptoloid species associations, identified by cluster analysis, are considered to represent graptoloid communities. *Agetograptus hubeiensis - Pribylograptus leptotheca* association in the *C. cyphus* Zone bypass environment was followed by the *Pribylograptus leptotheca – Monograptus* n. sp. B Melchin association of the *M. pectinatus* Zone resedimented carbonates and may represent a shallow-water community. In the *R. orbitus* Zone, *Pribylograptus leptotheca* was more closely associated with *Coronograptus gregarius* to the (competitive?) exclusion of *Monograptus* n. sp. B Melchin.
10. A cluster analysis was also used to deconstruct the species associations in an example of a graptoloid concentration bed described as representing a paleoecological bloom. Three communities could be described: a background community dominated by *Monograptus halli*, a transitional community dominated by *Spirograptus turriculatus*; and a bloom species of *Pristiograptus regularis regularis*.
11. The commonly concomitant distributions of mature rhabdosomes and siculae through the concretions were used as evidence to support the hypothesis that the mode of life of siculae was planktonic, like the mature rhabdosomes.
12. Thirteen new graptoloid species are informally described in this thesis; *Metaclimacograptus* n. sp., Metaclimacograptus? n. sp., *Glyptograptus* n. sp., *Campograptus* n. sp., *Monograptus* n. sp. A, *Monograptus* n. sp. B, *Monograptus* n. sp. C, *Monograptus* n. sp. D, *Monograptus* n. sp. E, *Monograptus* n. sp. F, *Monograptus* n. sp. G, *Monograptus* n. sp. H, *Pribylograptus*? n. sp., and *Torquigraptus* n. sp..
13. Three previously identified graptoloids are re-described in light of their excellent preservation in this material (*Comograptus comatus*, *Pribylograptus leptotheca*, *Monograptus falcata*).

Future work

1. Taphofacies analysis applied to the shales in detailed sampling intervals at Cape Manning.
2. Taphofacies analysis at lower sampling resolutions but with more spatial variability (more field sites) within the Aeronian strata of the Cape Phillips Embayment.
3. Taphofacies analysis of a different basin of the same time period using the method of layer-by-layer dissolution. The objective of this research would be to refine the taphofacies model and understand the variability in graptolite taphonomy. A possible comparative sample set are the graptolite-bearing limestones from the Sakmara Formation of The Orenburg District of the Southern Urals (Kazakhstan), or the calcareous nodules from Laggan Burn near Moffat in Southern Scotland. The graptolites of Laggan Burn are easily fragmented as a result of the coarse carbonate texture of the nodules that has weakened the graptolite periderm (Chapman, 1991). The limestones of the Sakmara Formation contain beautifully preserved graptolites (e.g., Russel et al. 2000) but they are stratigraphically isolated from each other and continuous successions of uncompressed graptolites have not been found. I know of no location other than the Cape Phillips Formation that contains such an abundance of graptoloid-bearing concretions or limestones over such a great stratigraphic interval.
4. Cluster analysis with the sample units as concretions not as residues.
5. Cluster analysis with presence/absence data, not relative abundances.
6. Calculation of error bars around thecal counts (Bennington and Rutherford, 1999).
7. Trials of alternative data normalization and other cluster methods
8. Development of a more process-based or theoretical model of community based upon quantitative calculations of species richness (S), evenness (E), and a correlation coeffient (H) (Buzas and Hayek, 1998).

GRAPTOLOID SEM AND IVM ILLUSTRATIONS

13 plates organizied by graptolite zonation

Plate 1

Graptoloids of the *C. cyphus* Zone

All magnification x 25 unless otherwise noted

a. *Agetograptus hubeiensis* (Ni, 1978); CM 40.5-40.6

b. *Atavograptus atavus* (Jones, 1909); CM 50.4-50.5

e, f. *Pribylograptus pleganopsis* (Lukasik and Melchin, 1997); CM 40.5-40.6; f, x 35

c, d, g, h. *Coronograptus minisculus* (Obut and Sobolevskaya, 1968); g, h, CM 41.65-41.75; d, i, CM 42.3-42.4, x 35

i, j. *Coronograptus gregarius* (Lapworth, 1876); CM 49.8-49.9

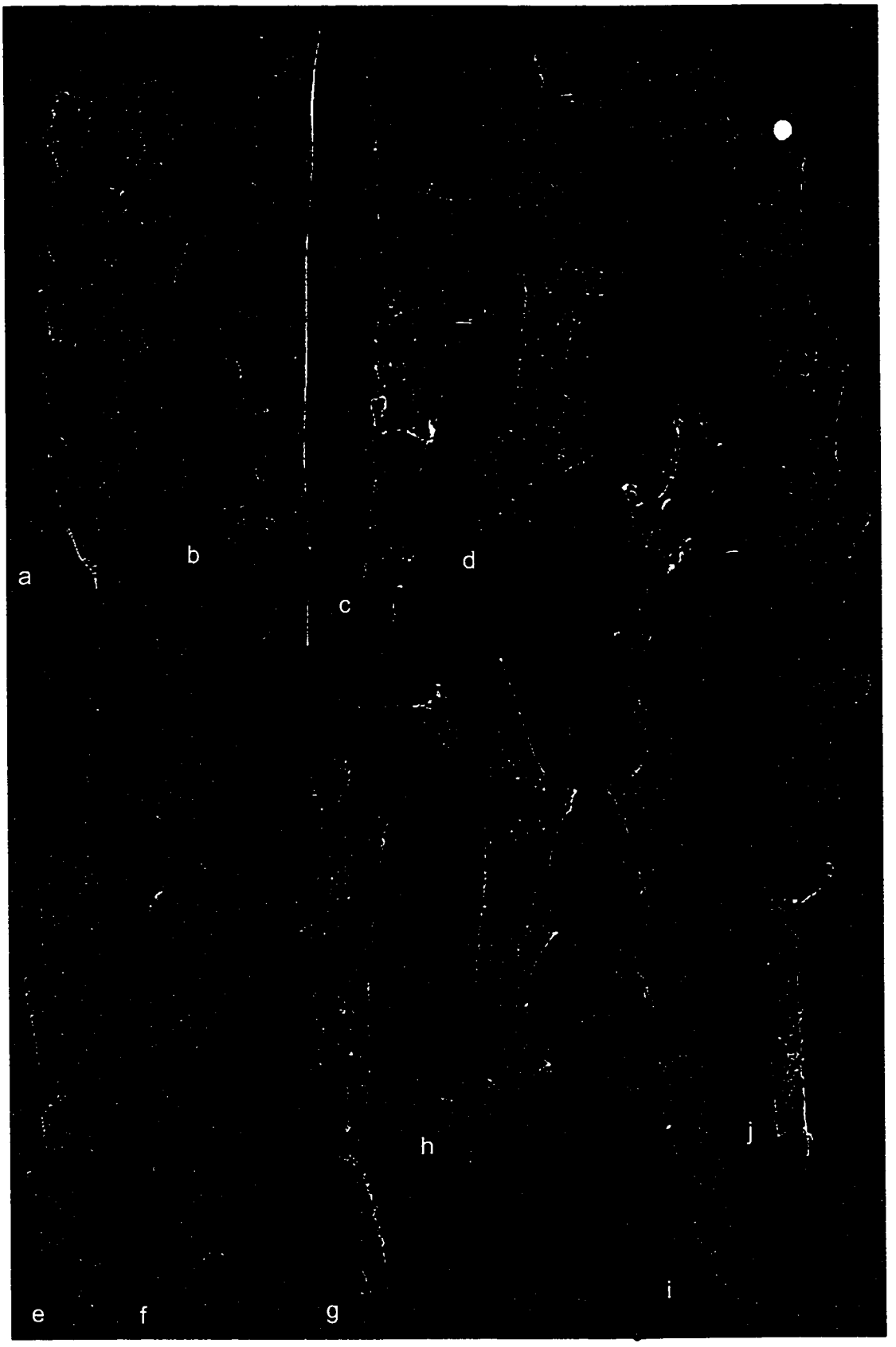
a
b
c
d
e
f
g
h
i
j

Plate 2

Graptoloid of the species *Comograptus comatus* (Obut and Sobolevskaya, 1968)

a-h. SEM images of *Comograptus comatus* (Obut and Sobolevskaya, 1968); a, three sicular spines, x 35; b, the sicular aperture, x 75; c, spineless variant, x 35; d, sicular aperture shows no signs of spines or fragmented spines, x 125; g, thecal aperture from graptoloid in image f, x 75; a-d, CM 42.8-42.9; e, CM 48.5, x 35; f-h, CM 46.35-46.5; f, x 35, h, x 25

i-k. IVM images of *Comograptus comatus* (Obut and Sobolevskaya, 1968); i) the same specimen shown in image c. i, spineless variant, x 25; j spine variant, x 25. Both sineless and spine variant have a pattern I astogeny; k, proximal end of graptolite illustrated in j, the single foramen on the downward growing portion of theca 1 is characteristic of Pattern I, x 150.

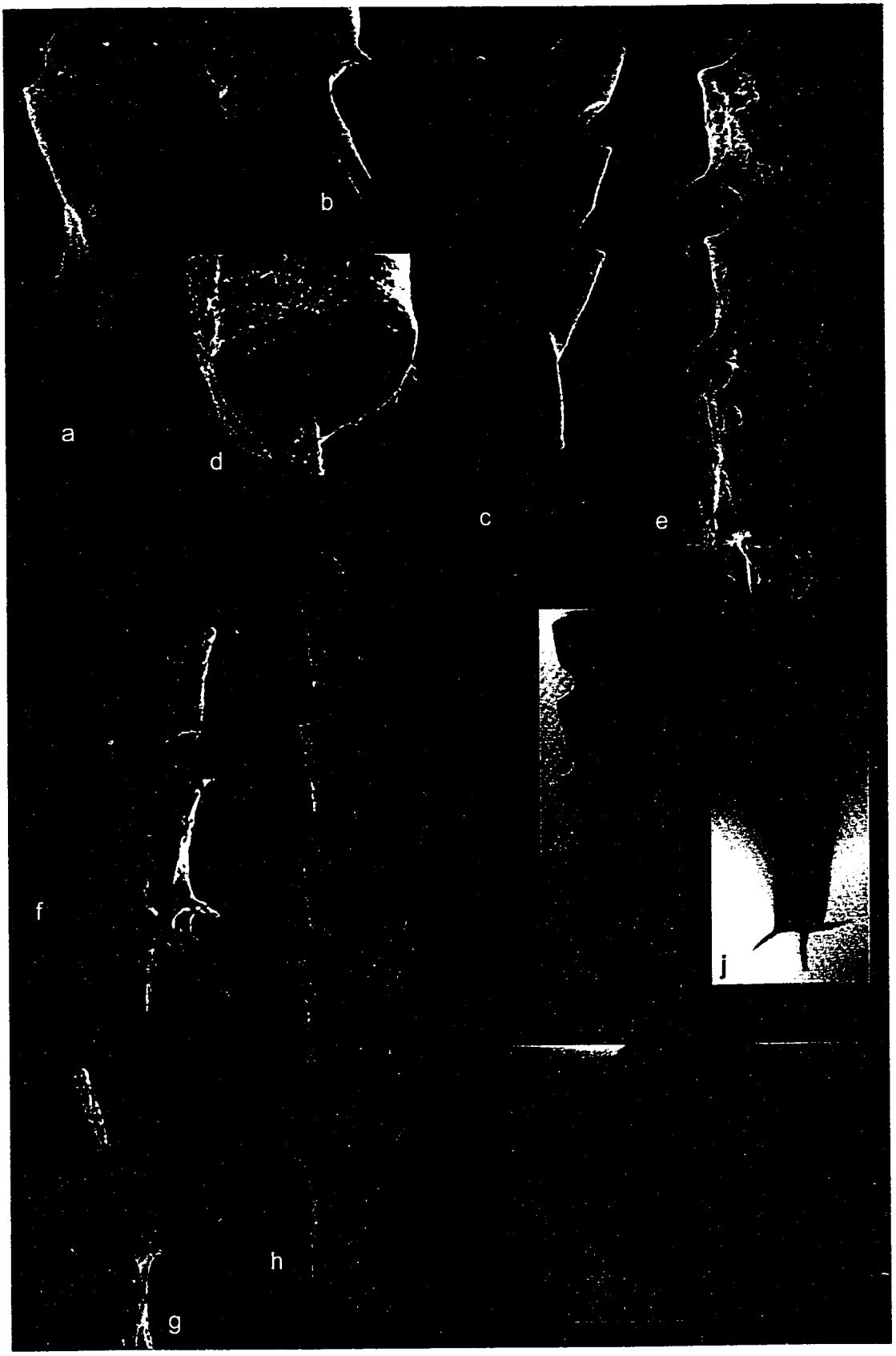
a
b
c
d
e
f
g
h
j

Plate 3

Graptoloids of the *C. cyphus* Zone

All magnification is x 25 unless otherwise noted.

a. *Glyptograptus incertus* (Elles and Wood, 1907); CM 46.35-46.5, x 16. .

b. *Huttagraptus praestrachani* (Rickards *et al.*, 1977); CM 42.3-42.4 mesio-proximal fragment, x 35.

c-e. *Lagarograptus inexpeditus* (Obut and Sobolevskaya, 1968); CM 49.8-49.9; c, proximal end, x 35; d, curved mesio-distal fragment; e. straight distal fragment with exaggerated ventral "lips".

f, g, o, p. *Monograptus* cf. *arciformis* Chen and Lin, 1978; CM 42.8-42.9. Proximally, the thecae display a hook that involves ventral and dorsal walls. Distally, the ventral wall of the hook is reduced; p, x 35.

h. *Metaclimacograptus minimus* (Paškevičius, 1976); CM 41.65-41.75,

i-n. *Monograptus* n. sp. B Melchin, 1987b; i, k , CM 46.35-46.5; j, l-n , CM 45.3-45.4. i, proximal end, with dorsal hood of second theca showing the thin rhabdosome that distally forms hoops. j, n. transition fragments that show hoop-shaped hoods retreat to form simple thecae over one transitional theca. l, mesial fragment with hooped or horned thecae (broken hoops) and a slight dorsal curvature. m. distal fragment with straight simple thecae; j-n, x 12

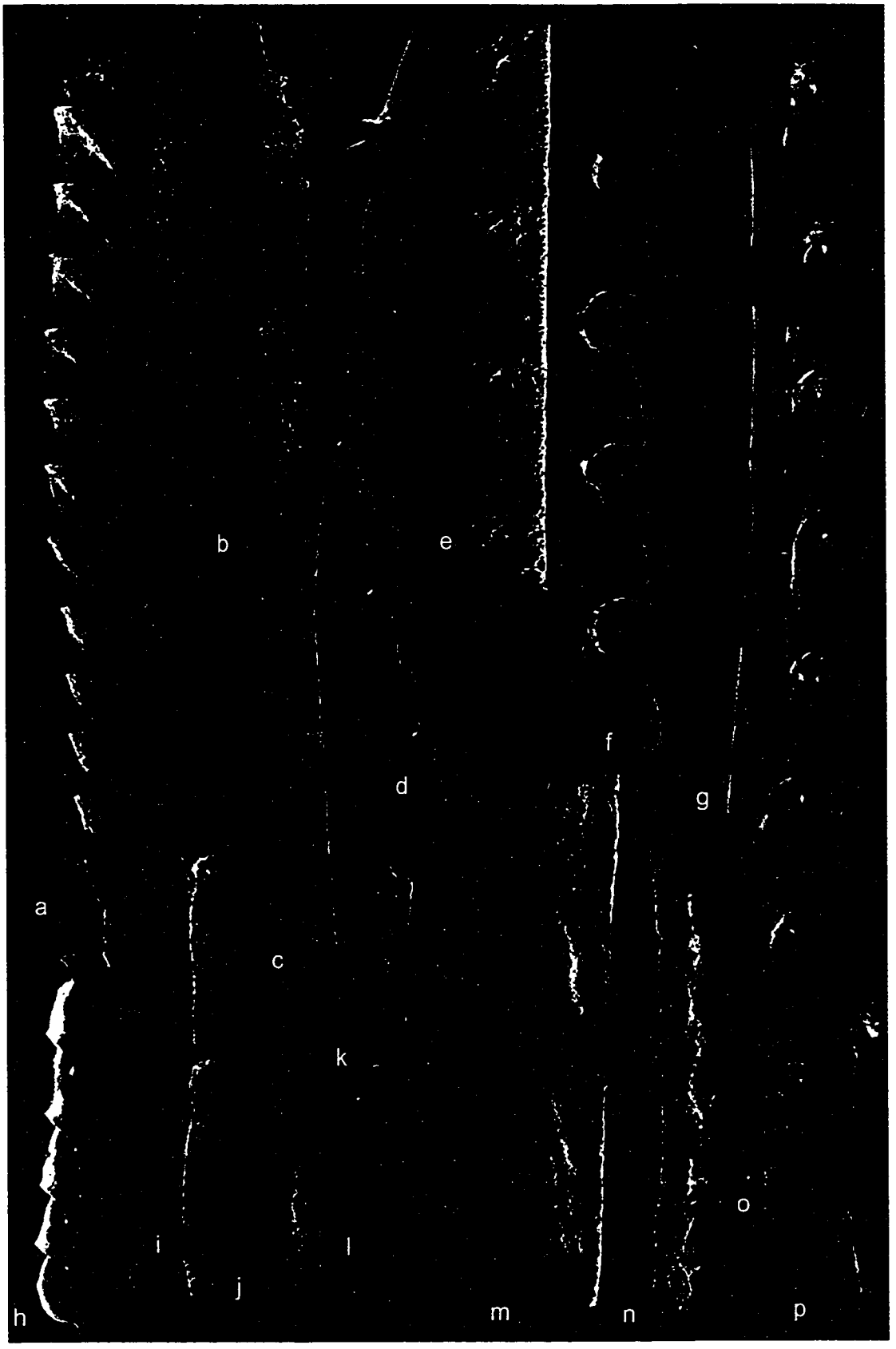
a
b
c
d
e
f
g
h
i
j
k
l
m
n
o
p

Plate 4

Graptoloids of the *C. cyphus* Zone

a., b. *Neodiplograptus elongatus* (Churkin and Carter, 1970); CM 40.5-40.6, x16.

c., d. *Neodiplograptus magnus* (Churkin and Carter, 1970); CM 45.3-45.4; c, x 16; d x 13.

e. *Normalograptus medius brevicaudatus* (Churkin and Carter, 1970); CM 49.8-49.9, x 16

f, j. *Normalograptus nikolayevi* (Obut, 1965); f, note the cyst-like structure just above the first thecal pair that may be evidence of paratism, CM 59.1-59.2, x 16; j, CM 50.4-50.5, x 25

g-i. *Pristiograptus biformis* (Mu *et al.*, 1974); biform thecae, CM 45.3-45.4, x 25

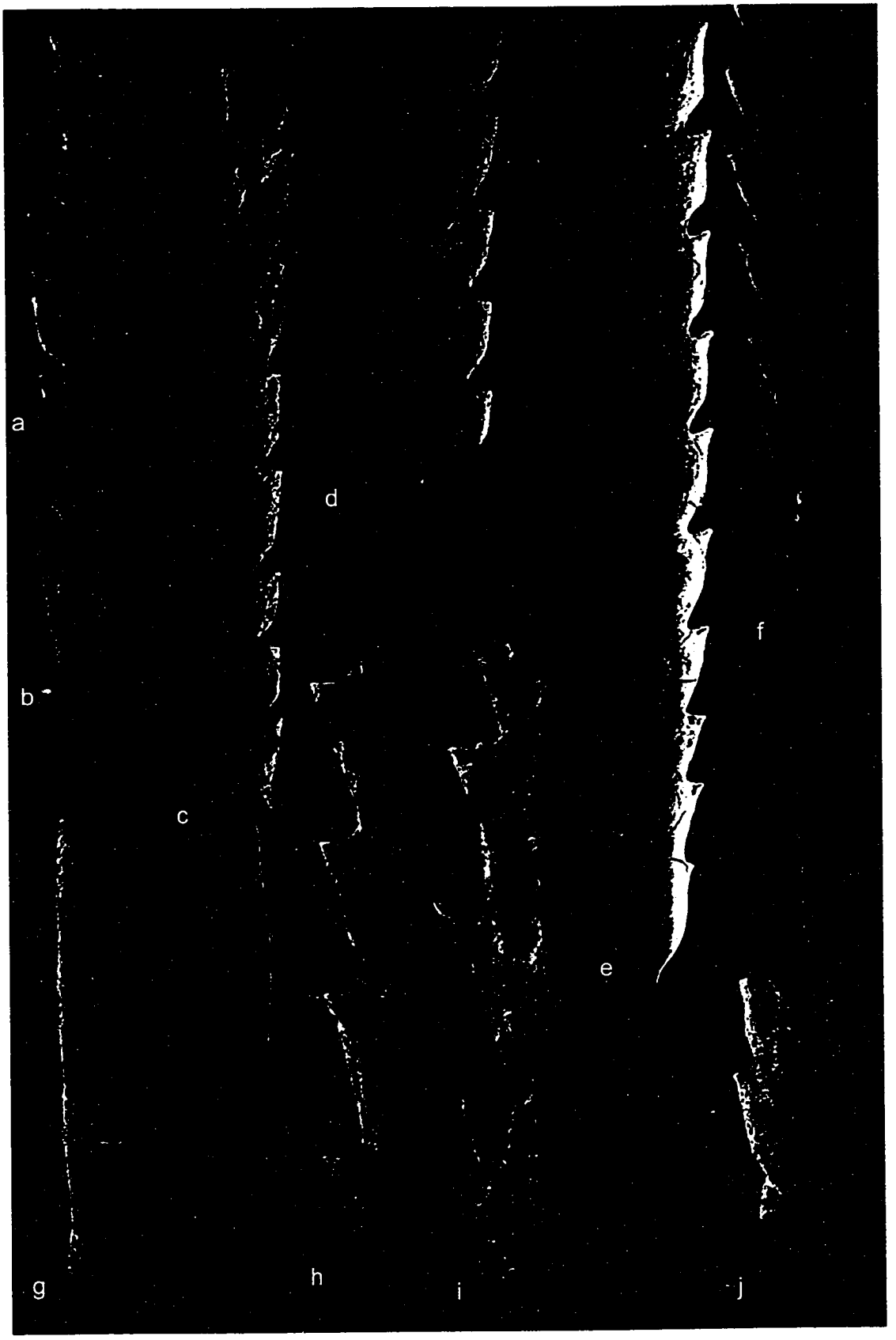
a
b
c
d
e
f
g
h
i
j

Plate 5

All magnification is x 25 unless otherwise noted.

Pribylograptus leptotheca (Lapworth, 1876) of the *M. pectinatus* Zone

a- i. *Pribylograptus leptotheca* (Lapworth, 1876); a, near-proximal fragment with dorsal hoods; b, proxi-mesial fragment with hoods reduced to dorsal "spikes"; c, mesial fragment with dorsal spikes and lateral lappets; d, mesial fragment, x 80; e, proximal end; f, far distal fragment with lappets; g, h, mesio-distal fragment with lappets developing into lateral spines; i, distal fragment with lateral spines reduced to lappets and dorsal spike present. a, c, d, f-i , CM 46.35-46.5; e, b , CM 51.2-51.3;

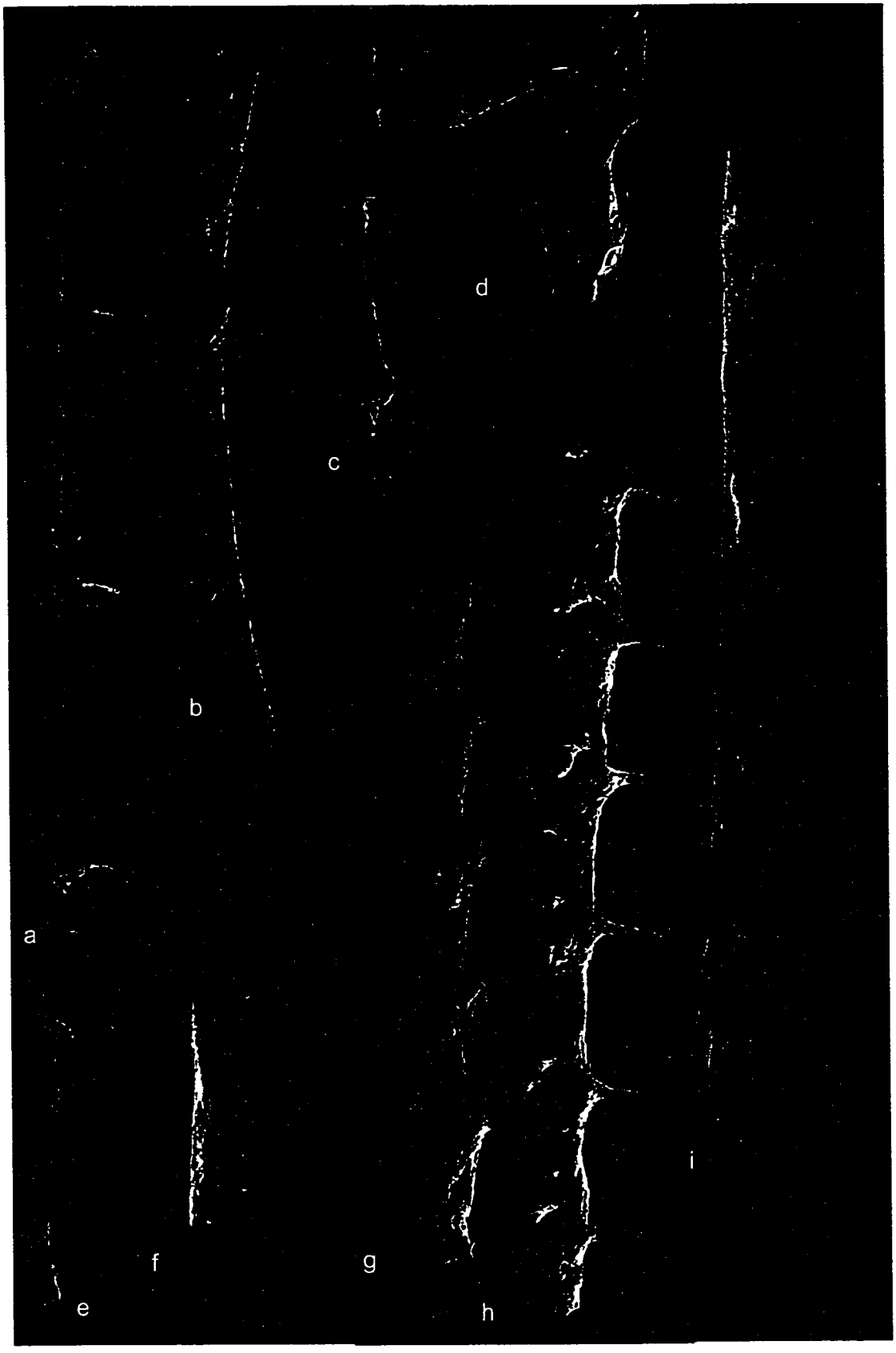
a
b
c
d
e
f
g
h
i

Plate 6

Graptoloids of the *M. pectinatus* Zone

All magnification is x 25 unless otherwise noted.

a-d. *Campograptus communis* (Lapworth, 1876); a-c, CM 53.2-53.3; a, b, x 32; c, x 50; d, CM 54.0-54.15

e. *Agetograptus secundus* Obut and Sobolevskaya, 1968; CM 48.5

f., g. *Coronograptus arcuatus* Obut and Sobolevskaya, 1968; CM 44.0-44.1

h. *Metaclimacograptus orientalis* (Obut and Sobolevskaya, 1968); CM 52.1-52.2

i. *Glyptograptus* n. sp.; CM 46.35-46.5

j. *Glyptograptus tamariscus tamariscus* (Nicholson, 1868); CM 54.0-54.15

k. *Glyptograptus* cf. *incertus* (Elles and Wood, 1907); CM 45.3-45.4

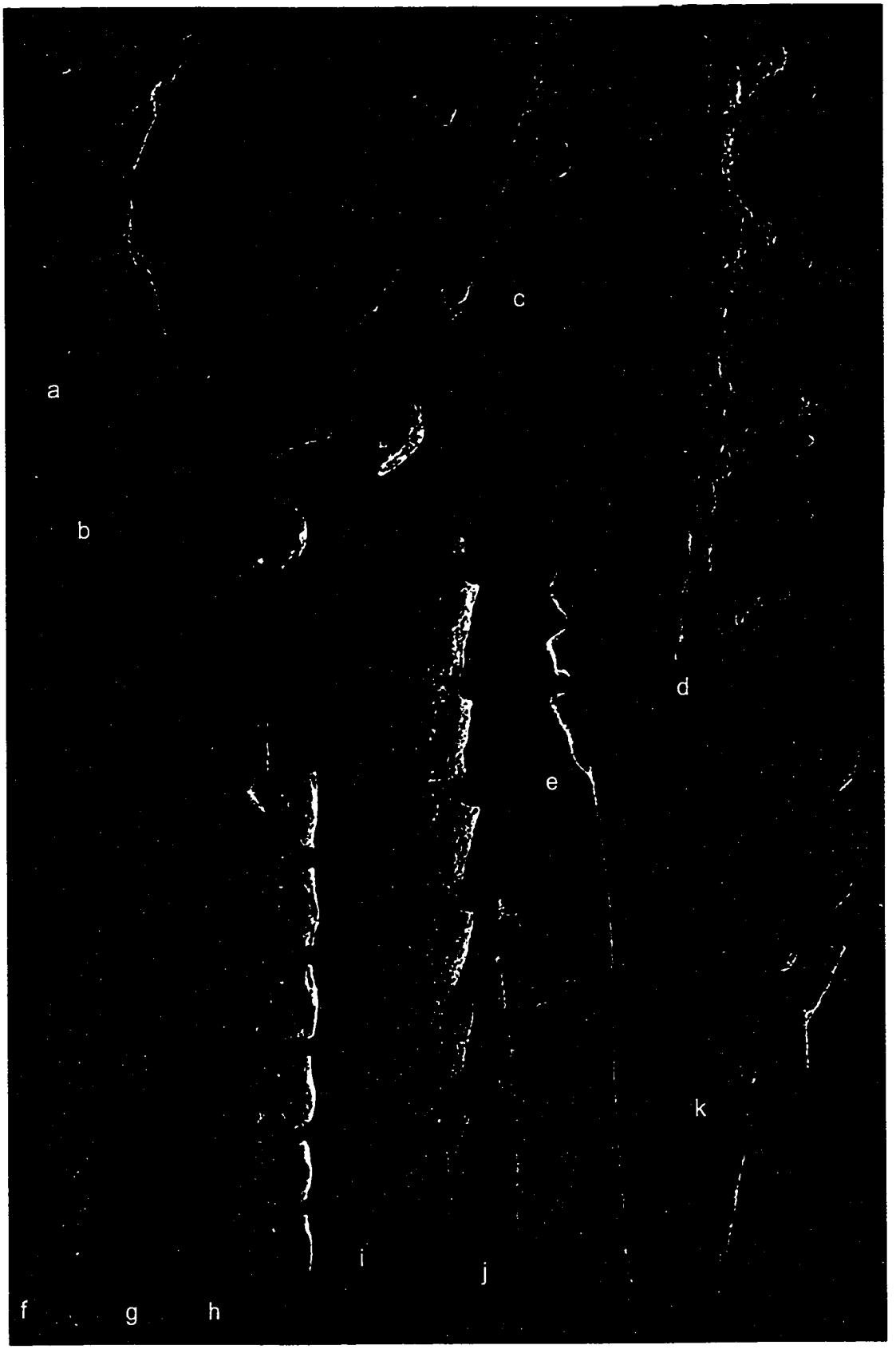
a
b
c
d
e
f
g
h
i
j
k

Plate 7

Graptoloids of the *M. pectinatus* Zone

All magnification is x 20 unless otherwise noted.

a. *Metaclimacograptus rigidus* (Chen and Lin, 1978); CM 55,

b, c. *Monograptus pectinatus pectinatus* Richter, 1853; CM 47.4-47.5; b, x 45; c, x 60.

d, e. New Genus A n.sp. A Lukasik, 1994; CM 50.4-50.5; d, x 30; e, x 140.

f. *Metaclimacograptus*? n. sp.; CM 45.3-45.4; x 30

g, h. *Rhaphidograptus sinicus* (Mu et al., 1974) ; CM 50.4-50.5

i. *Pribylograptus* cf. *imprimus* (Lukasik and Melchin, 1997); CM 47.4-47.5

j. *Pseudoglyptograptus barriei* Zalasiewicz and Tunnicliff, 1994; CM 59.1-59.2

k. *Normalograptus laciniosis* (Churkin and Carter, 1970); CM 45.3-45.4

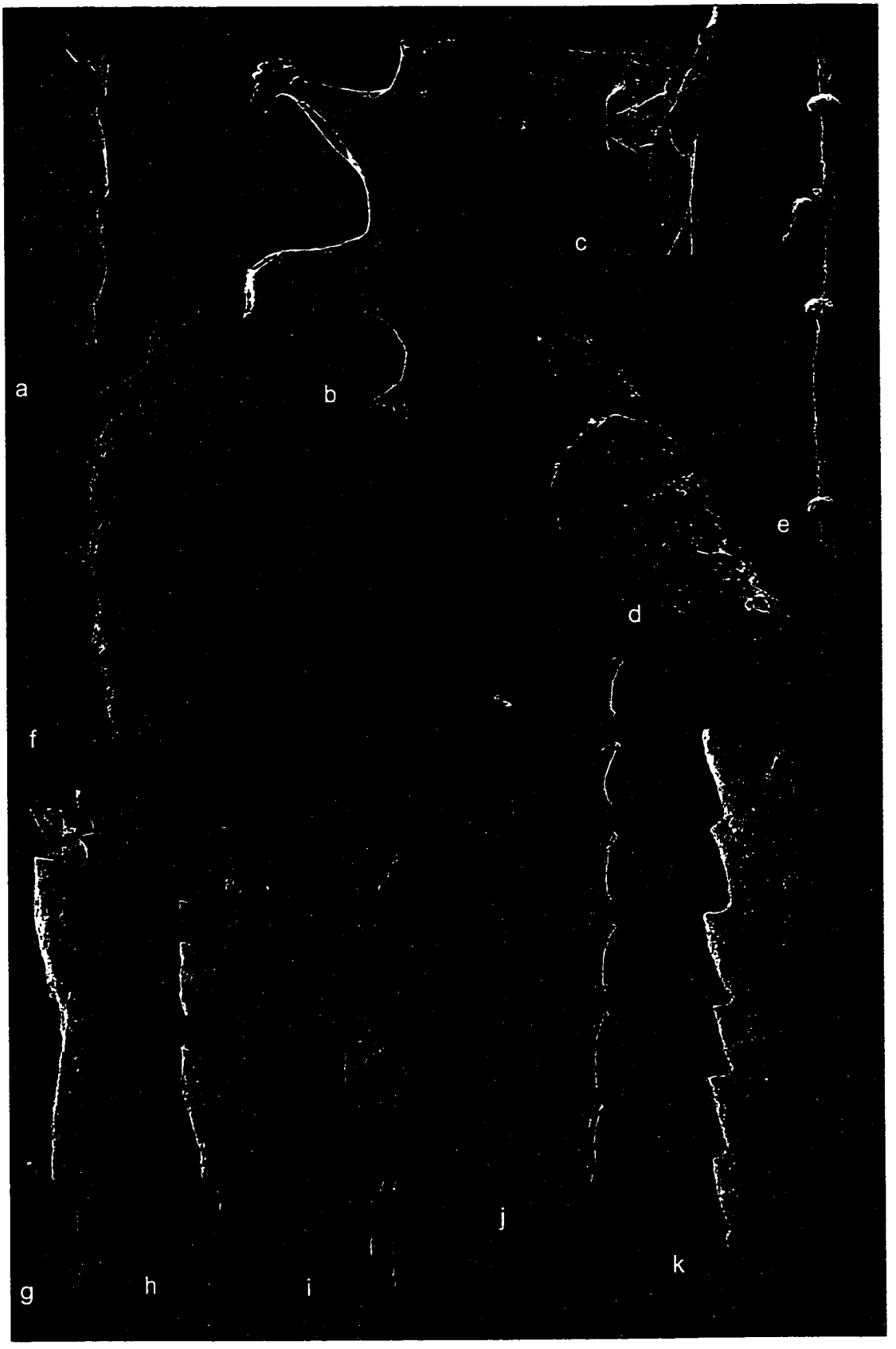
a
b
c
d
e
f
g
h
i
j
k

Plate 8

Graptoloids of the *R. orbitus* Zone.

All magnification is x 20 unless otherwise noted.

a.-c. *Campograptus sanctogeorgensis* Štorch, 1998; CM 51.2-51.3a

d. *Glyptograptus tamariscus distans* Packham, 1962; CM 56

e., f. *Metaclimacograptus undulatus* (Kurck, 1882); CM 48.5; f, x 40

g.-j. *Monograptus tenuissimus* (Obut and Sobolevskaya, 1968); g, i , CM 50.4-50.5; g, x 60; i, x 30; h, j, CM 50.4, x 45.

k, l. *Monograptus calamistratus* (Churkin and Carter, 1970); CM 51.2-51.3a; k., proximal, x 30; l, distal fragment, x 45

m–o. *Monograptus* n.sp. C; CM 53.2-53.3; m, x 60; n, x 100; o, x 120

p, q. *Monograptus* n.sp. A; CM 49.8-49.9; p, x 70; q, x 120

r. *Campograptus lobiferus lobiferus* (M'Coy, 1850); CM 55

s. *Metaclimacograptus sculptus* (Chen and Lin, 1978); CM 49.8-49.9

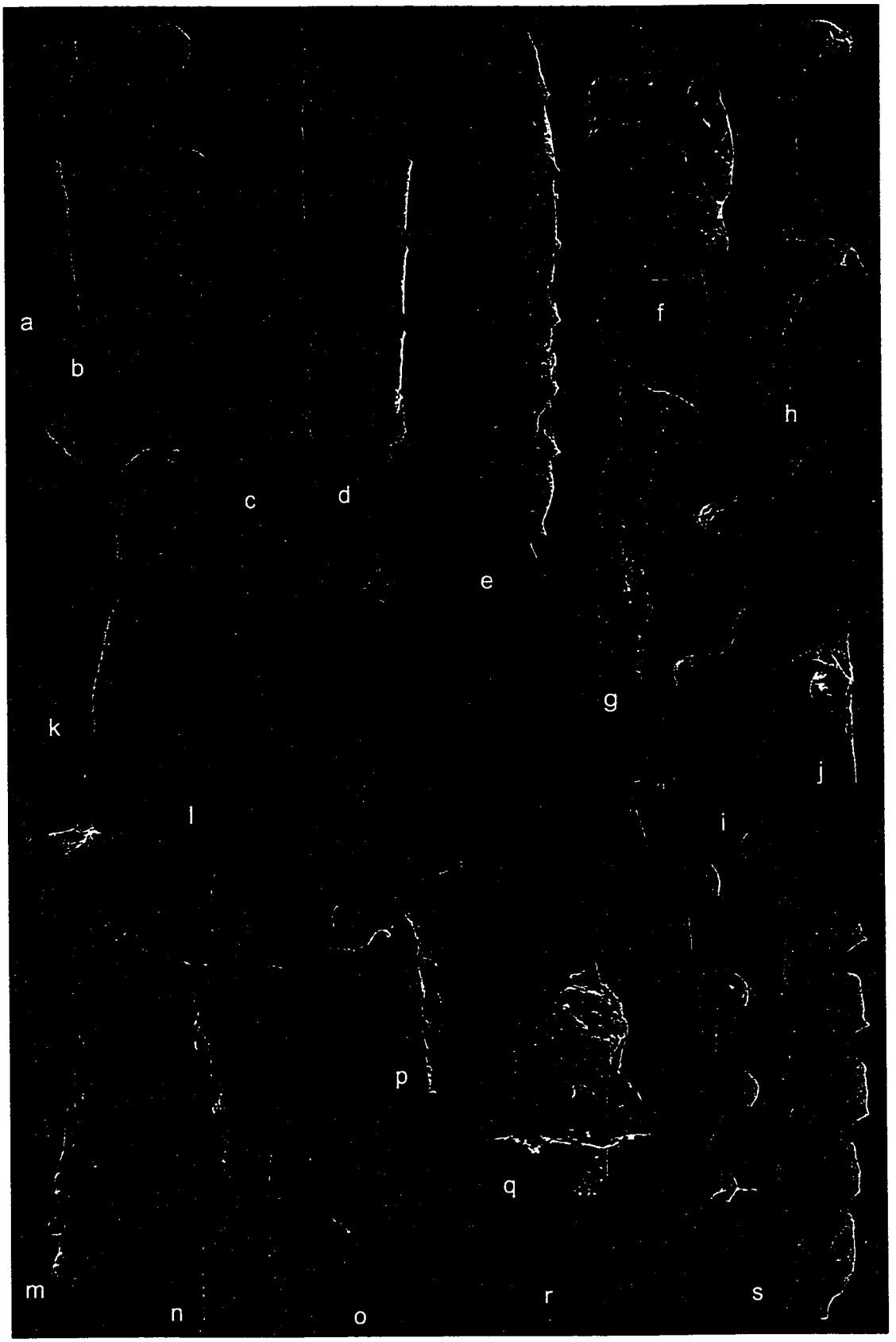
a
b
c
d
e
f
g
h
i
j
k
l
m
n
o
p
q
r
s

Plate 9

Forms of *Monograptus falcata* Chen and Lin, 1978; *R. orbitus* Zone, *C. convolutus* Zone.

All magnification is x 20 unless otherwise noted.

a-f. *Monograptus falcata* forma A; a, b, d, f , CM 50.4-50.5. a, mesial fragment, x 30; b, d, transitional fragments showing hood retreat; f, far distal fragment; c, e. proximal fragments, CM 53.2-53.3; c, x 30; e, x 45.

g-i. *Monograptus falcata* forma B; CM 56; g, rapidly widenling transitional fragment; h, proxio-mesial fragment, x 30; i, proximal end, x 45.

j, k. *Monograptus falcata* forma C; CM 56; j, mesial fragment; i, proximal fragment, x 45.

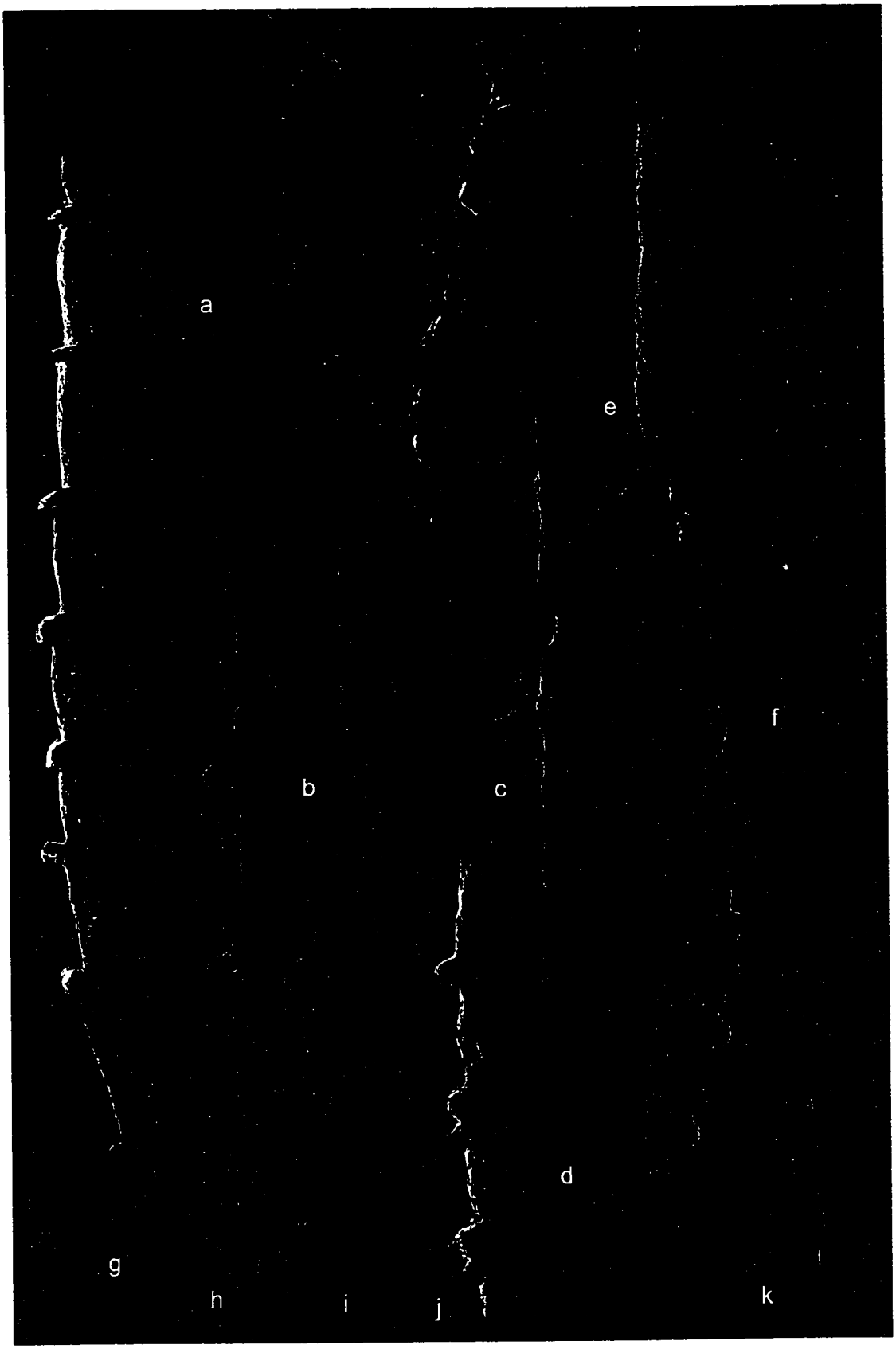
a
e
f
b
c
d
g
h
i
j
k

Plate 10

Graptoloids of the *R. orbitus* Zone.

All magnification is x 20 unless otherwise noted.

a-c. *Monograptus* cf. *triangulatus* (Harkness, 1851); CM 49.8-49.9; a, proximal end, x 45; b, distal fragment; c, mesial fragment.

d, e. *Monograptus involutus* (Lapworth, 1876); CM 50.4. d. proximal end, x 45; e, distal fragment, x 45.

f. *Rastrites spina*? (Richter, 1853); CM 56.4-56.5; x 45

g, j. *Petalolithus intermedius* (Bjerreskov, 1981); CM 48.5

h, i. *Rastrites orbitus* (Churkin and Carter, 1970); CM 55; x 30

k. *Neodiplograptus tcherskyi* (Obut and Sobolevskaya, 1967); CM 54.0-54.15

l. *Neodiplograptus* n. sp. A Melchin, 1987b; CM 44.0-44.1

m, n. *Pristiograptus fragilis pristinus* Hutt, 1974-75; CM 50.4-50.5; x 45

o-r *Pribylograptus?* n. sp. ; CM 49.8-49.9; o, x 200; p-r, x 45.

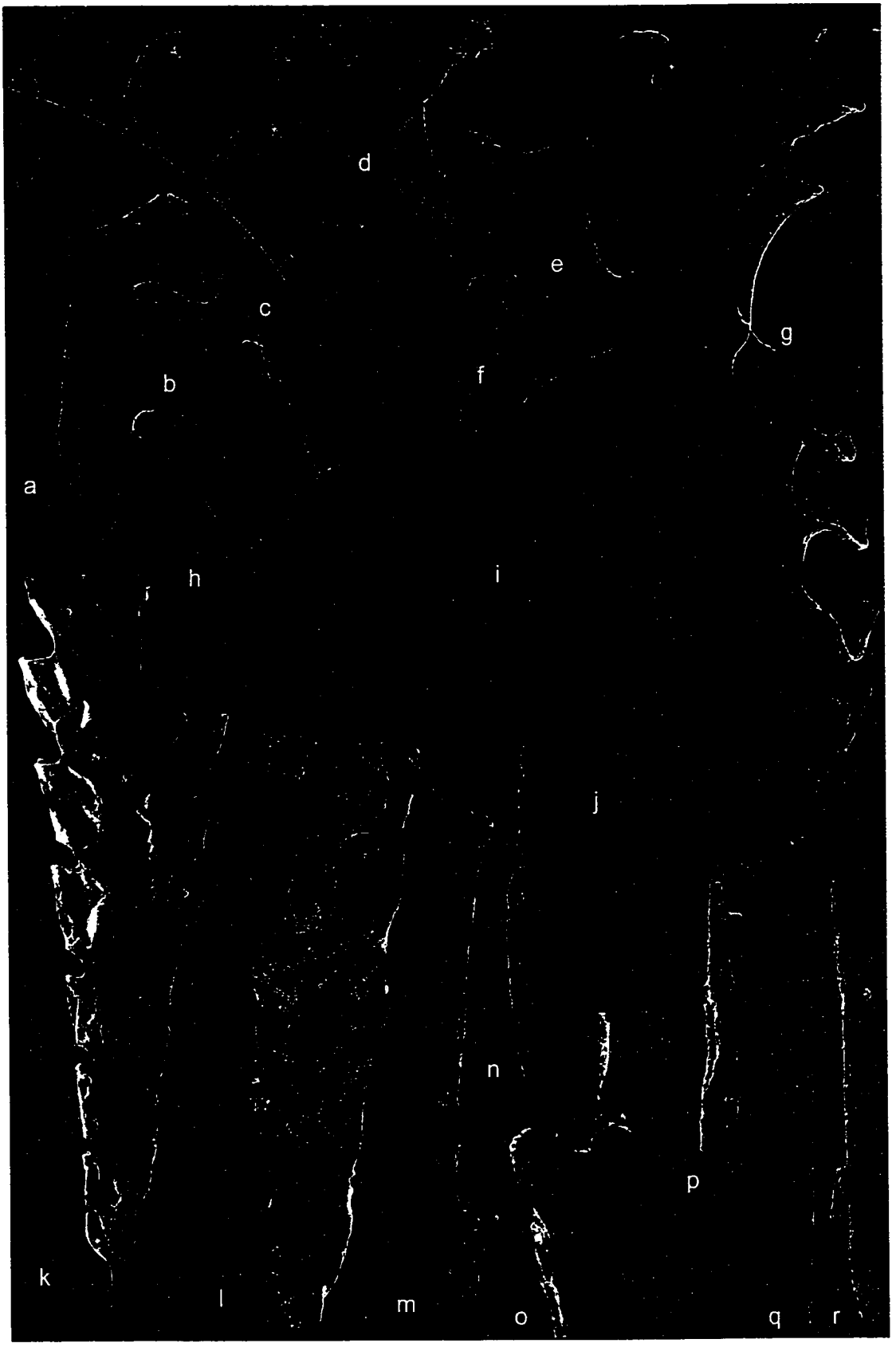
a
b
c
d
e
f
g
h
i
j
k
l
m
n
o
p
q
r

Plate 11

Graptoloids of the *L. convolutus* Zone.

a, b. *Campograptus lobiferus lobiferus* (M'Coy, 1850); CM 55, x 20

c,d. *Monoclimacis* n. sp. A Lukasik, 1994; CM 53.2-53.3; c, x45; d x 60.

e. *Campograptus* n. sp.; CM 55, x 20

f. *Monograptus dracocephalus* Štorch, 1998; CM 53.2-53.3; x 45

g, h. *Monoclimacis* n. sp. B Lukasik 1994; CM 58a; h, x 20; g, x 30.

i. *Monograptus* n. sp. B forma A; CM 53.2-53.3; x 85.

j. *Monograptus* n. sp. B forma B; CM 57; x 45.

k. *Monograptus* n. sp. F; CM 57; x 115.

l, m. *Monograptus* n. sp. D; CM 55; l, distal fragment, x 30; m, proximal end, x 60.

n, s. *Monograptus* n. sp. E; CM 55; n, x 200; s, x 30.

o-r. *Monograptus sidjachenkoi* Obut and Sobolevskaya, 1968; CM 56.4-56.5. o, mesial fragment; p, distal fragment; q, proximal fragment; r, theacal apertures from distal fragment shown in image p, x 45.

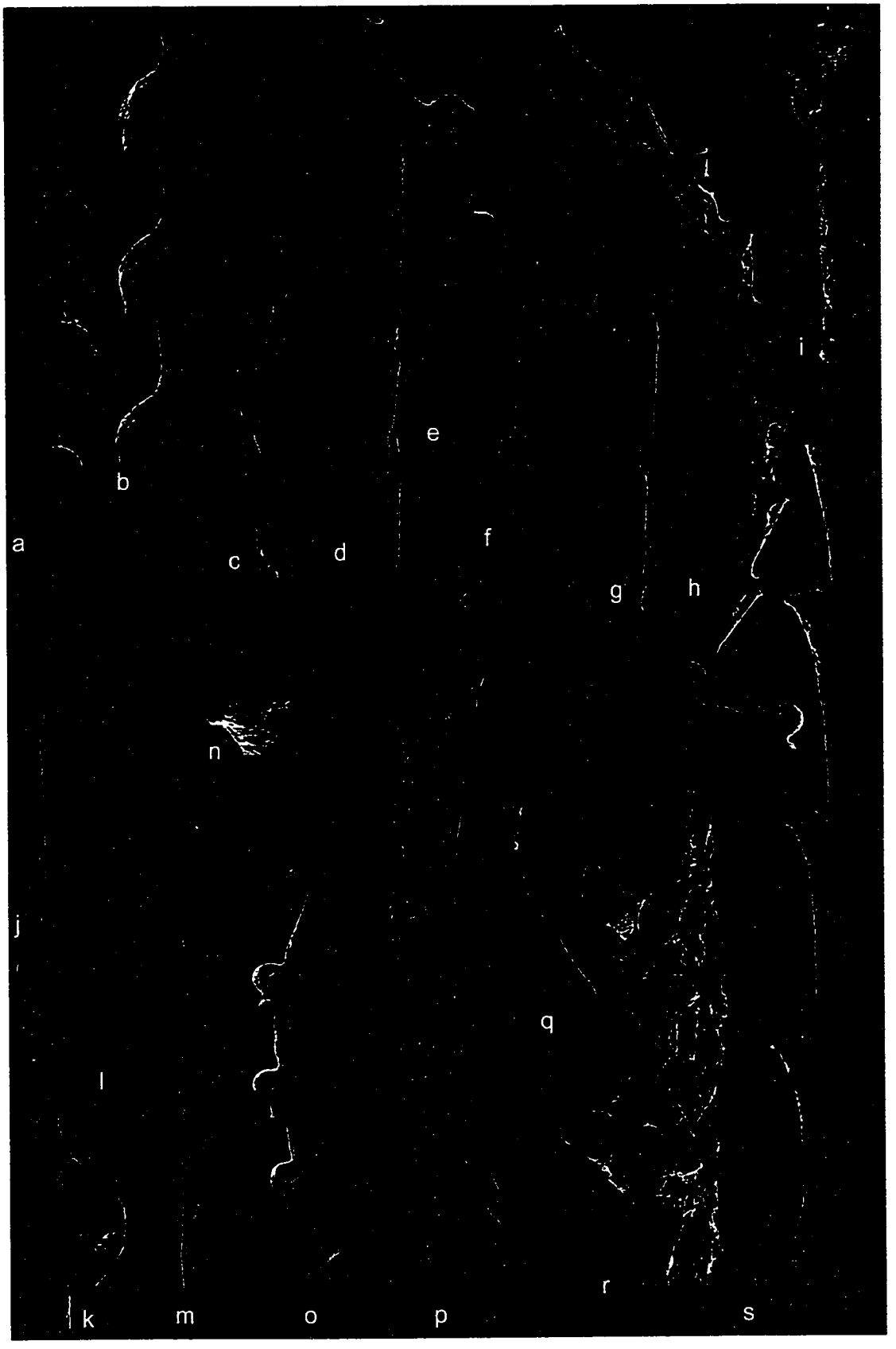
a
b
c
d
e
f
g
h
i
j
k
l
m
n
o
p
q
r
s

Plate 12

Graptoloids of the *L. convolutus* Zone.

All magnification is x 20 unless otherwise noted.

a. *Lituigraptus convolutus* (Hisinger, 1837); CM 55; x 30

b. *Petalolithus ankyratus* (Mu *et al.*, 1974); CM 59.1-59.2

c. *Pristiograptus* n. sp. A Lukasik 1994; CM 57.5-57.6; x 30

d-g. *Torquigraptus* n. sp. A; CM 57; d, x 30; g, x 45

h, i, m. *Pristiograptus* n. sp. B Lukasik, 1994; CM 55; i, x 30

j. *Neodicellograptus siluricus* (Mu et al., 1974); CM 59.1-59.2 note fragmentation of right stipe.

k. *Rivagraptus bellulus* (Törnquist, 1890); CM 56

l. *Rivagraptus kayi* (Churkin and Carter, 1970); CM 55

n, o. *Monoclimacis* n. sp. C Lukasik, 1994; n, CM 55, x 30; o, CM 54.0-54.15, x 30.

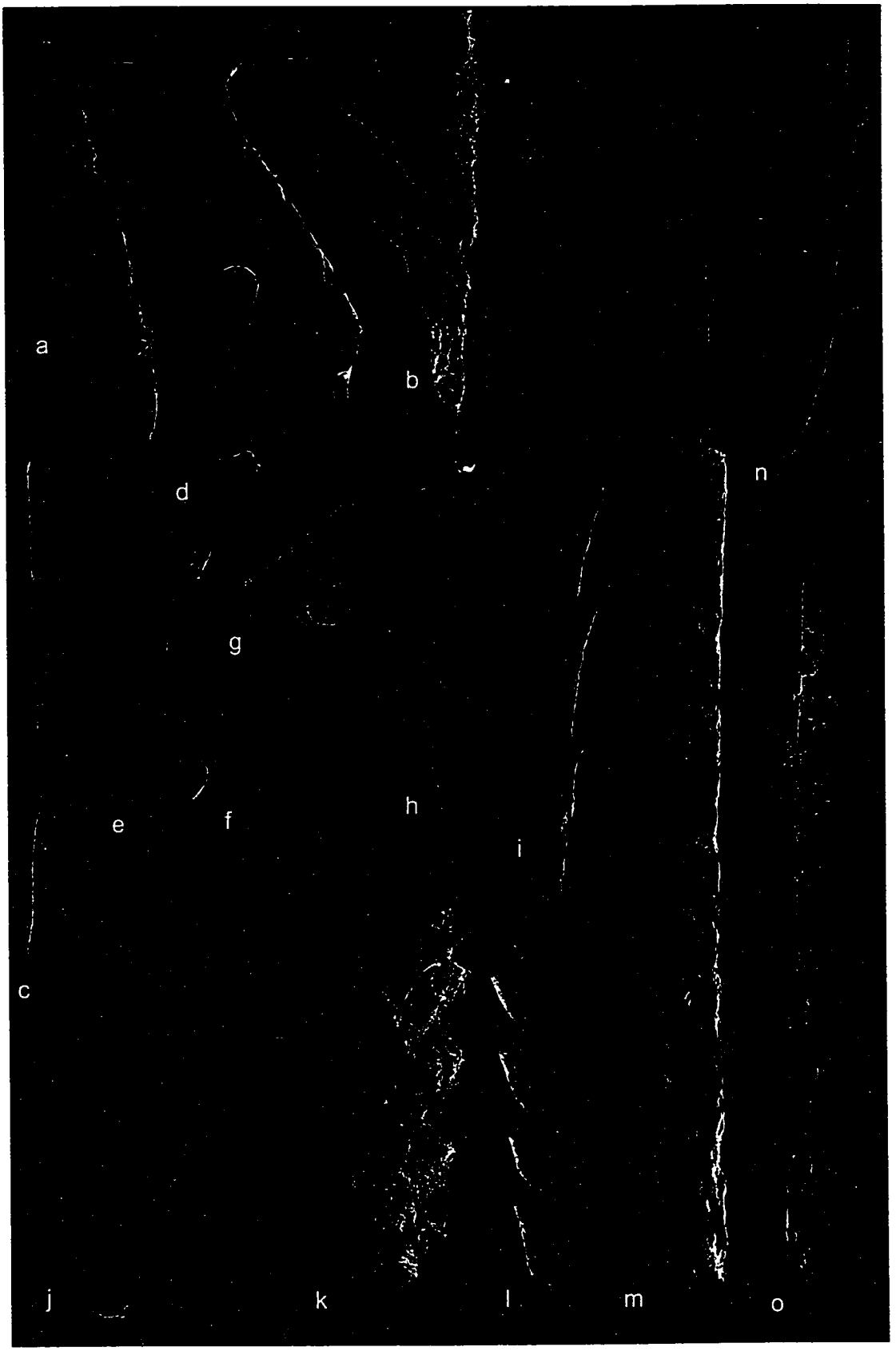
a
b
c
d
e
f
g
h
i
j
k
l
m
n
o

Plate 13

Graptoloids of the *S. guerichi* Zone

All magnification is x 20 unless otherwise noted.

a. *Metaclimacograptus* n. sp.; CM 73.8

b, *Monograptus crenularis*?; b, CM 59.1-59.2;

c, d. *Monograptus* cf. *gemmatus* (Barrande, 1850); CM 75.5; c, x 45.

e. *Pristiograptus regularis regularis* (Törnquist, 1899); CM 75.5

f. *Normalograptus* n. sp.; CM 74.9

g, j. *Monograptus* n. sp. G; CM 75.5

h, i, k. *Stimulograptus halli* (Barrande, 1850); CM 75.5

l. *Paradiversograptus capillaris* (Carruthers, 1867); CM 72.6

m, n. *Spirograptus guerichi* (Loydell, *et al.*, 1993); CM 75.5

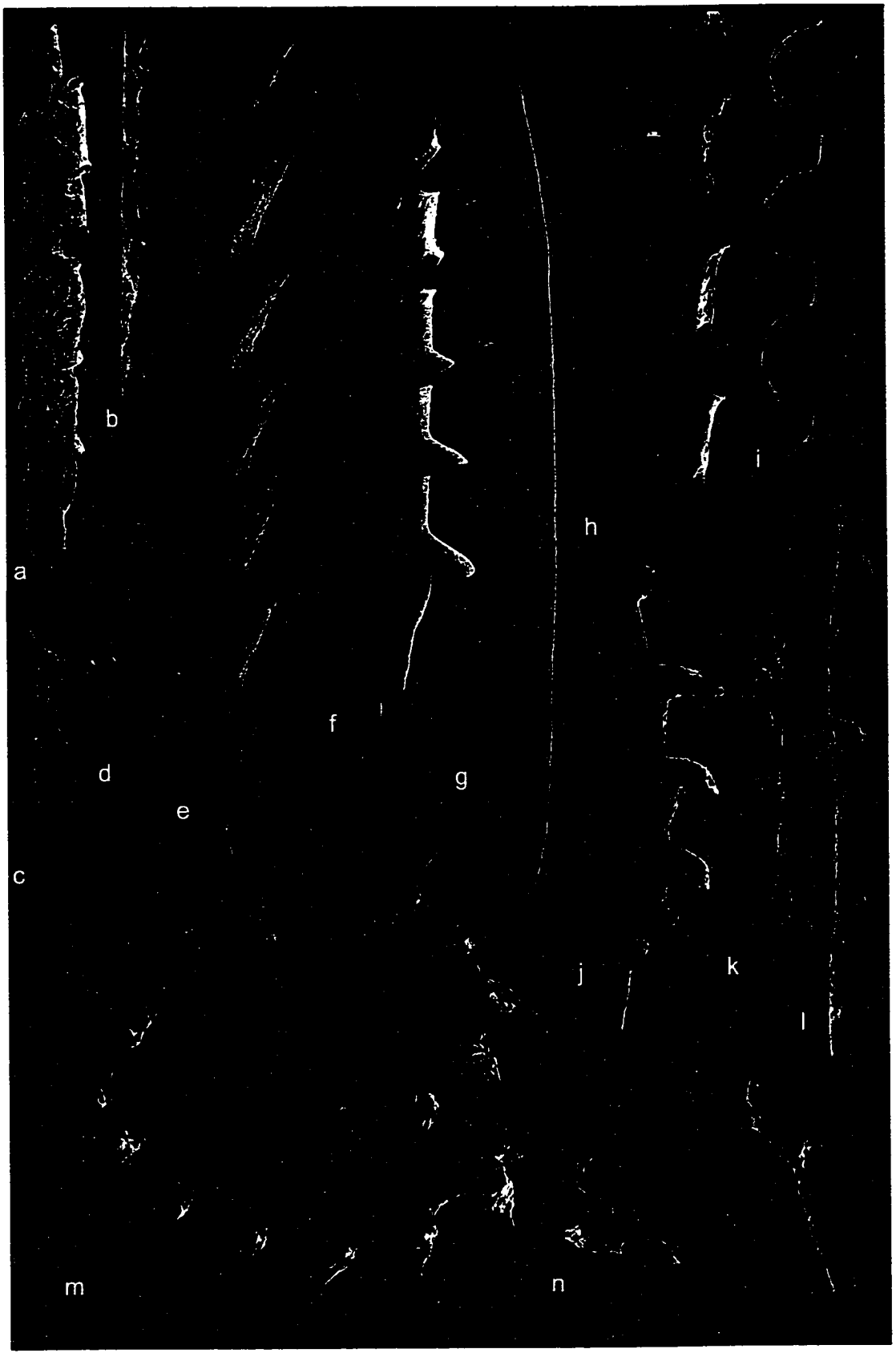
a
b
c
d
e
f
g
h
i
j
k
l
m
n

APPENDICES

Appendix A

1996 Field notes of Cape Phillips and Cape Manning section.

Appendix A. Field Notes, Cape Phillips (MCP 96), J. Russel, July 13, 14, 1996

Collection of concretions

4.7 m.	- from a nodular limestone bed, 15 cm thick
	- no graptoloids in surrounding limestone
	- Base of sequence – greistoniensis Zone
26.8 m.	- fine mudstones, thinly laminated
	- graptoloids in surrounding shale (sampled, marked as "26.8 tapho")
	- two concretions collected 50 cm apart
30.8 m.	- square cut from center of a large concretion – oblong approx. 30 cm.
	- Surrounding bedding similar to 26.8
46.9 m.	- many concretions in this layer
	- nodular – laminated mudstone
	- graptoloids in surrounding shale
83.5 m.	- very few large concretions in this bed
	- only few small concretions between 46.9 and 83.5
	- thinly bedded mudstone
	- rare "monograptids"
93.5 m.	- many concretions in this bed
	- all oblong in shape (slightly flattened)
	- bed approx. 30 cm thick
	- light buff alternates with grey
	- few graptoloids
108 m.	- a limestone strata 5-6 cm thick with uncompressed graptoloids
108.2 m.	- compressed graptoloids collected from surrounding shale to compare
132 m.	- shales with many graptoloids
	- beginning of sakmaricus Zone
137.8 m.	- concretion-rich
	- nodular bed with shale between concretions
	- shale collected marked "137.8 tapho"
139 m.	- larger concretion than in 137.8 – more shale between
	- shale collected marked "139 tapho"
149.8 m.	- graptoloid-rich strata
	- extremely weathered therefore no sample taken of surrounding shale
~150 m.	- lithology changes from flaggy to platy lime-mudstones, lime silts, mostly laminated
152.5-156.0 m.	- fish quarries
160-165 m.	- gradually changes to shaly-platy
180.0-182.8 m.	- a very rich concretion layer
	- buff and grey concretions
	- large, some complete beds (i.e. continuous concretions)
188.6-189.8 m.	- same zone as 180-182.8 repeated
	- graptoloid-rich.

Appendix A (continued). Field Notes, Cape Phillips (stream section – MCP 96a), J. Russel, July 15, 1996

Collection of concretions – biozone? – high Llandovery/Wenlock

0 m. - from a nodular limestone bed, 15 cm thick
- no graptoloids in surrounding limestone

1.6 m. - first concretion horizon.

6.0 m. - most eroded, no exposure

7.5 m. - concretion sampled

9.0 m. - concretion sampled

Appendix A (continued). Field Notes, Cape Manning (MCM 96), J. Russel, July 27, 1996

Reference of MCM96-9 = turbidite bed

0.1-0.2 m. below ref. - two collected 1.3 m apart

Reference of MCM 96-10, top of thickly bedded massive carbonate = 4.0 m.

Reference of MCM 96-11, 50 paces (JCR), 46 paces (MJM) from 10 last exposure

Appendix B

Graptolite species distribution through the Cape Manning section - biostratigraphy

Appendix B Table B1. Biostratigraphy of the Cape Manning Section. "o" isolated from 1996, 1998 samples, "●" isolated from 1988 samples, "x" flattened samples from 1988, 1996, 1998

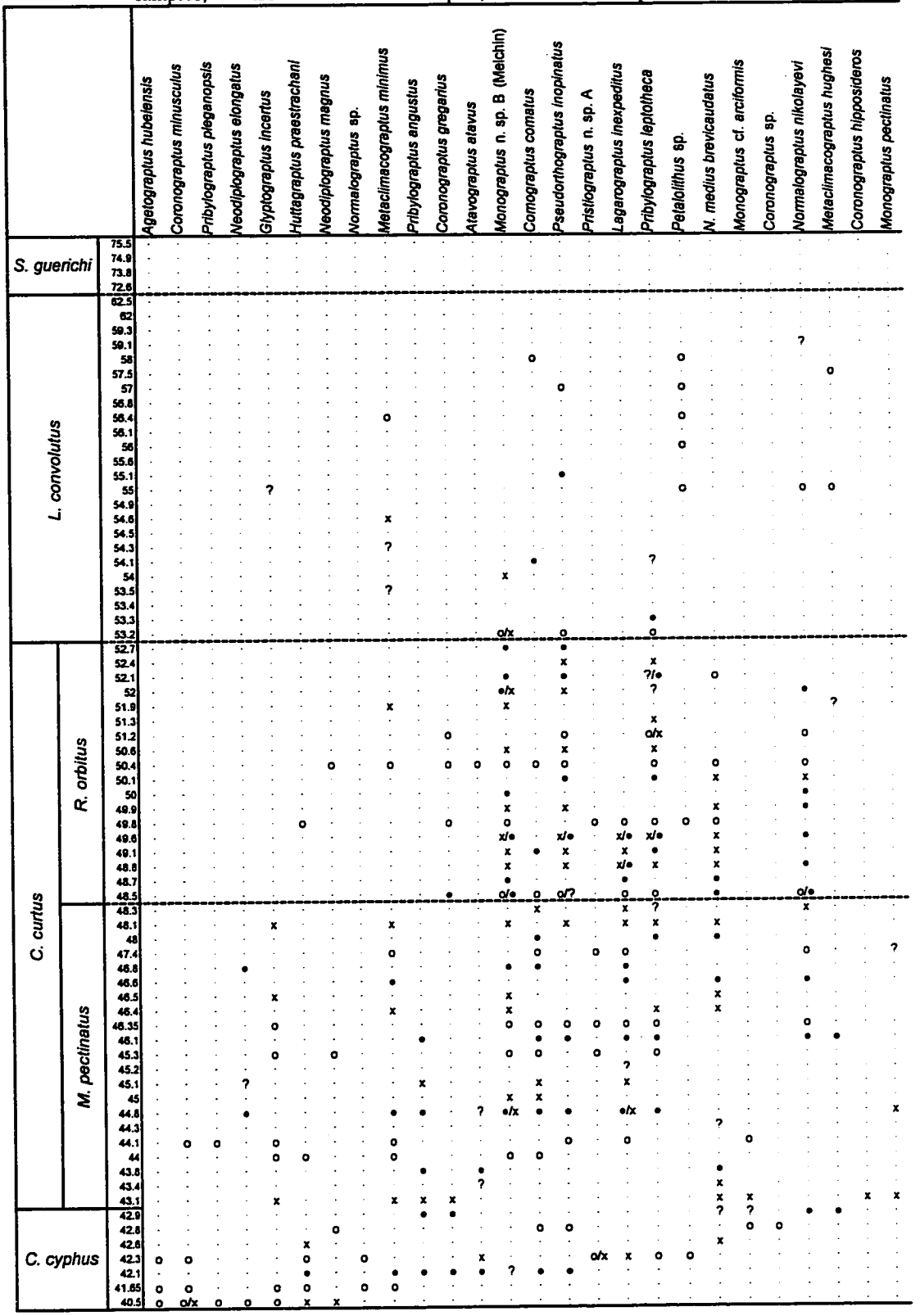

Appendix B

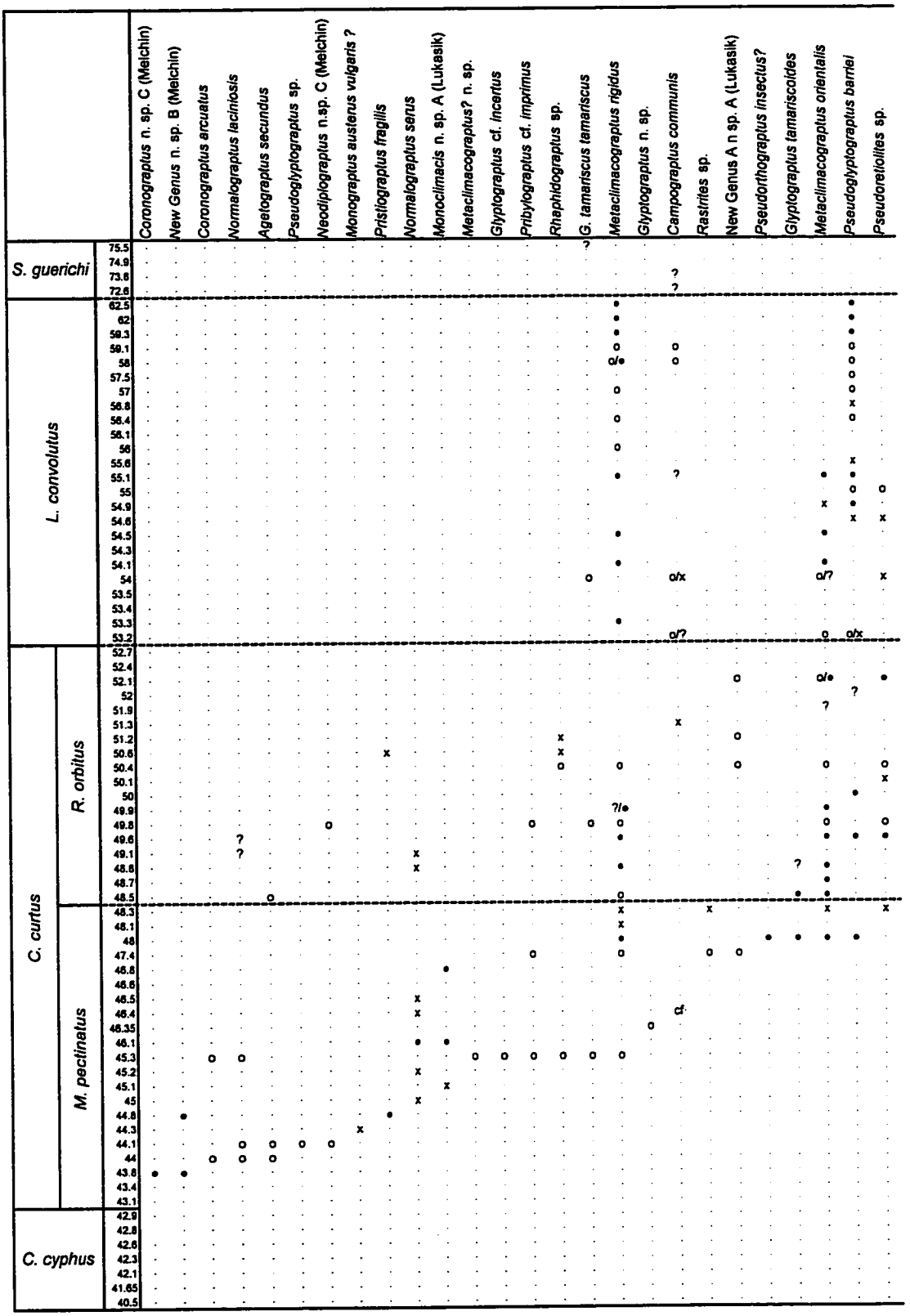
Coronograptus n. sp. C (Melchin)
New Genus n. sp. B (Melchin)
Coronograptus arcuatus
Normalograptus laciniosis
Agetograptus secundus
Pseudoglyptograptus sp.
Neodiplograptus n.sp. C (Melchin)
Monograptus austerus vulgaris ?
Pristiograptus fragilis
Normalograptus serus
Monoclimacis n. sp. A (Lukasik)
Metaclimacograptus? n. sp.
Glyptograptus cf. incertus
Pribylograptus cf. imprimus
Rhaphidograptus sp.
G. tamariscus tamariscus
Metaclimacograptus rigidus
Glyptograptus n. sp.
Campograptus communis
Rastrites sp.
New Genus A n sp. A (Lukasik)
Pseudorthograptus insectus?
Glyptograptus tamariscoides
Metaclimacograptus orientalis
Pseudoglyptograptus barrei
Pseudorelioliites sp.
S. guerichi
L. convolutus
C. curtus
R. orbitus
M. pectinatus
C. cyphus
75.5
74.9
73.8
72.6
62.5
62
59.3
59.1
58
57.5
57
56.8
56.4
56.1
56
55.6
55.1
55
54.9
54.6
54.5
54.3
54.1
54
53.5
53.4
53.3
53.2
52.7
52.4
52.1
52
51.9
51.3
51.2
50.6
50.4
50.1
50
49.9
49.8
49.6
49.1
48.8
48.7
48.5
48.3
48.1
48
47.4
46.8
46.6
46.5
46.4
46.35
46.1
45.3
45.2
45.1
45
44.8
44.3
44.1
44
43.6
43.4
43.1
42.9
42.8
42.6
42.3
42.1
41.65
40.5

Appendix B

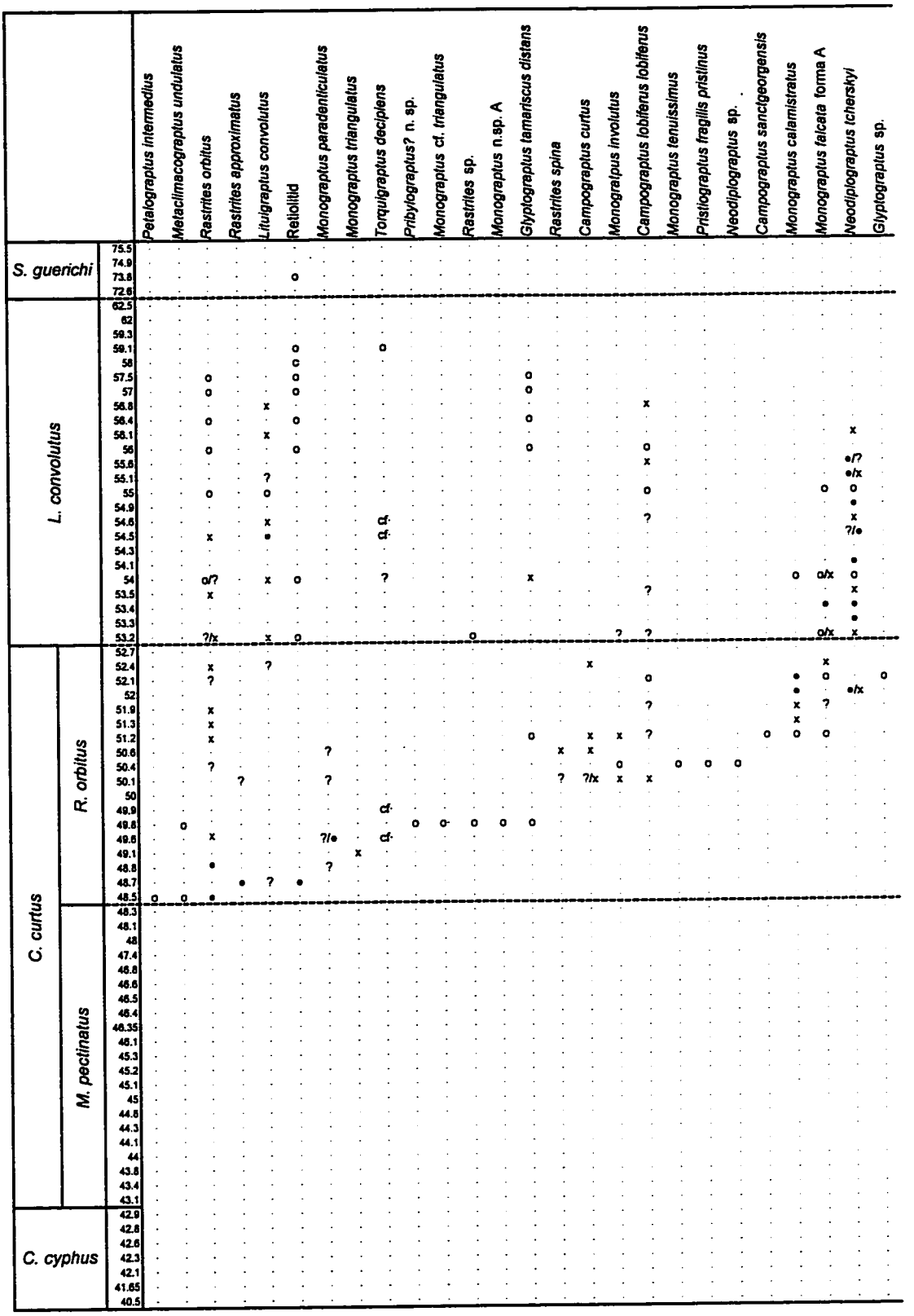
Petalograptus intermedius
Metaclimacograptus undulatus
Rastrites orbitus
Rastrites approximatus
Lituigraptus convolutus
Retiolitid
Monograptus paradenticulatus
Monograptus triangulatus
Torquigraptus deciplens
Pribylograptus? n. sp.
Monograptus cf. triangulatus
Rastrites sp.
Monograptus n.sp. A
Glyptograptus tamariscus distans
Rastrites spina
Campograptus curtus
Monograptus involutus
Campograptus lobiferus lobiferus
Monograptus tenuissimus
Pristiograptus fragilis pristinus
Neodiplograptus sp.
Campograptus sanctgeorgensis
Monograptus calamistratus
Monograptus falcata forma A
Neodiplograptus icherskyi
Glyptograptus sp.
S. guerichi
L. convolutus
C. curtus
R. orbitus
M. pectinatus
C. cyphus

Appendix B

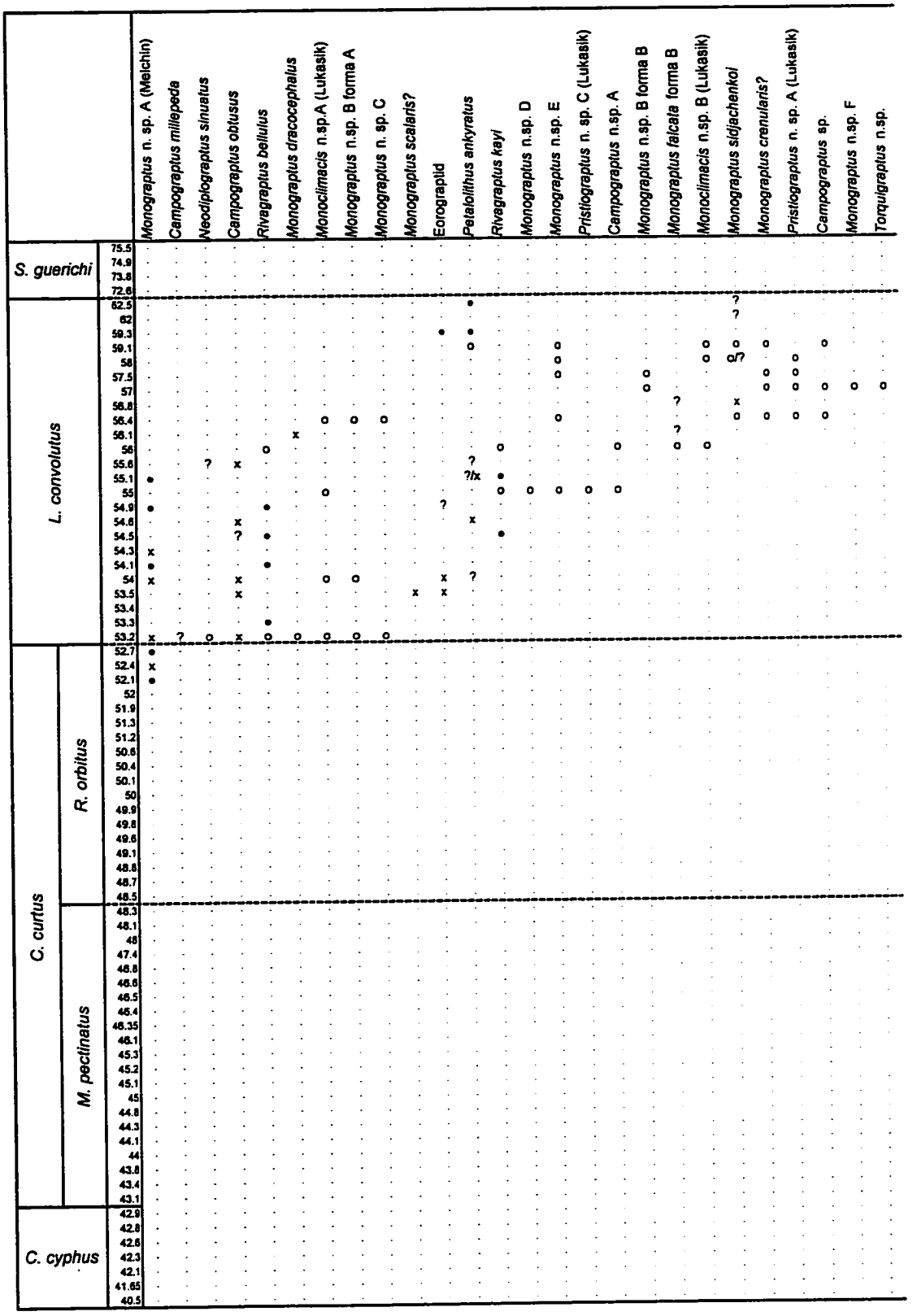
Monograptus n. sp. A (Melchin)
Campograptus millepeda
Neodiplograptus sinuatus
Campograptus obtusus
Rivagraptus bellulus
Monograptus dracocephalus
Monoclimacis n.sp.A (Lukasik)
Monograptus n.sp. B forma A
Monograptus n. sp. C
Monograptus scalaris?
Eorograptid
Petalolithus ankyratus
Rivagraptus kayi
Monograptus n.sp. D
Monograptus n.sp. E
Pristiograptus n. sp. C (Lukasik)
Campograptus n.sp. A
Monograptus n.sp. B forma B
Monograptus falcata forma B
Monoclimacis n.sp. B (Lukasik)
Monograptus sidjachenkoi
Monograptus cranularis?
Pristiograptus n. sp. A (Lukasik)
Campograptus sp.
Monograptus n.sp. F
Torquigraptus n.sp.
S. guerichi
L. convolutus
C. curtus
R. orbitus
M. pectinatus
C. cyphus

Appendix B

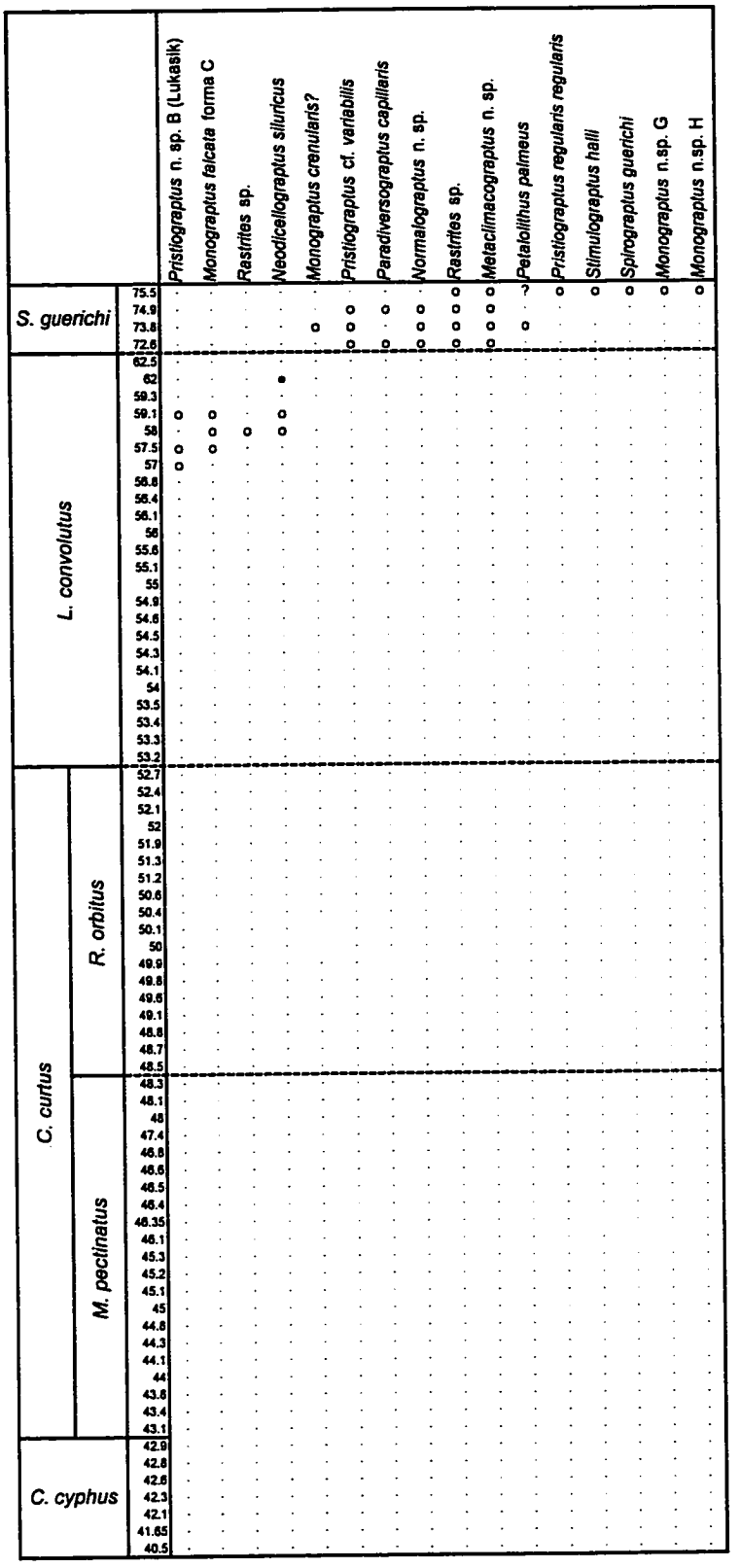
Pristiograptus n. sp. B (Lukasik)
Monograptus falcata forma C
Rastrites sp.
Neodicellograptus siluricus
Monograptus crenularis?
Pristiograptus cf. variabilis
Paradiversograptus capillaris
Normalograptus n. sp.
Rastrites sp.
Metaclimacograptus n. sp.
Petalolithus palmeus
Pristiograptus regularis regularis
Stimulograptus halli
Spirograptus guerichi
Monograptus n.sp. G
Monograptus n.sp. H
S. guerichi
L. convolutus
C. curtus
R. orbitus
M. pectinatus
C. cyphus
75.5
74.9
73.8
72.6
62.5
62
59.3
59.1
58
57.5
57
56.8
56.4
56.1
56
55.6
55.1
55
54.9
54.6
54.5
54.3
54.1
54
53.5
53.4
53.3
53.2
52.7
52.4
52.1
52
51.9
51.3
51.2
50.6
50.4
50.1
50
49.9
49.8
49.6
49.1
48.8
48.7
48.5
48.3
48.1
48
47.4
46.8
46.6
46.5
46.4
46.35
46.1
45.3
45.2
45.1
45
44.6
44.3
44.1
44
43.6
43.4
43.1
42.9
42.8
42.6
42.3
42.1
41.65
40.5

Appendix C

Correlation of measurements from 1998, 1996 and 1988 for the Cape Manning and Cape Phillips sections

Appendix C. Cape Manning samples from 1988 and 1996 corealated to 1998 meterages.

Table C1. Sample names and meterages from 1996 and 1998 field seasons correlated to the 1998 meterages. For the purpose of this thesis all concretions were refered to in the same stratigraphic scale (that of 1998). For example, concretion "MCM 96-10 5.9 above base" was renamed "CM 75.5". This is important to note if access to concretion stubs or residues is required.

1998 meterage	1988 Sample meterages and names	1996 Sample meterages and names
75.5		MCM 96-10 5.9 above base
74.9		MCM 96-10 5.3a above base
73.8		MCM 96-10 4.2 above base
72.6		MCM 96-10 3.0 above base
69.4	Top of dolomite marker	
65.0	Base of dolomite marker	
62.5	MCM 88-10 6.5	
62.0	MCM 88-10 6.0	
59.8	Base of shaley dolomite	
59.3	MCM 88-10 3.3	
58.0	MCM 88-10 2.0	MCM 96-10 2.5a below ref. (buff marker bed)
57.0		MCM 96-9 5.6 above
56.4-56.5		MCM 96-9 5.0-5.1 above
56.1	MCM 2-98 56.1	
56.0		MCM 96-9 4.6 above
55.6-57.0	MCM 88-9 8.5 (top - flattened)	
55.1- 56.5	MCM 88-9 8.0	
55.0		MCM 96-9 3.6 above
54.9-56.3	MCM 88-9 7.8	
54.6 - ?	MCM 88-9 7.5	
54.5 - ?	MCM 88-9 7.4	
54.5	MCM 88-9 7.4	
54.3	MCM 88-9 7.2	
54.1	MCM 88-9 7.0	
53.4	MCM 88-9 6.3	
53.3	MCM 88-9 6.2	
53.2-53.3		MCM 96-9 1.8-1.9 above
52.7	MCM 88-8 52.7	
52.1-52.2		MCM 96-9 0.7-0.8 above ref.
52.1	MCM 88-9 5.0	
52.0-52.2	MCM 88-9 4.9-5.1	
52.0	MCM 88-9 4.9	
51.4	Reference bed	
51.3	MCM 88-9 4.2	

Table C1. (continued). Cape Manning samples

1998 meterage	1988 Sample meterages and names	1996 Sample meterages and names
51.2-51.3		MCM 96-9 0.1-0.2a +b below ref
50.4-50.5		MCM 96-9 0.9-1.0 below ref
50.4		MCM 96-9 1.0 below ref
50.1	MCM 88-9 3.0	
50.0	MCM 88-8 12.0	
49.9	MCM 88-8 2.8	
49.8-49.9		MCM 96-9 1.6-1.7 below ref.
49.6	MCM 88-8 2.5	
49.1	MCM 88-9 2.0	
48.8	MCM 88-9 1.7	
48.5	MCM 88-8 9.5	MCM 96-9 2.9 below ref
48.3	MCM 88-9 1.2	
48.0	MCM 88-8 8.5	
46.8	MCM 88-8 6.2	
46.6	MCM 88-8 5.8	
46.1	MCM 88-8 4.8	
45.1	MCM 88-8 3.0	
44.8	MCM 88-8 2.7	
44.1		MCM 96-8 2.0
43.8	MCM 88-8 1.7	
43.1	MCM 88-8 1.0	
42.9	MCM 88-8 0.8	
42.6	MCM 88-8 0.5	
42.3-42.4		MCM 96-8 0.3-0.5
42.1	MCM 88-8 base	

Table C2. Cape Phillips section samples from 1996 correlated to 1998 meterages

98 meterage	1996 sample meterages and names
163.1	MCP96 149.8
163	MCP96 149.7a
163	MCP96 149.7b
162.8	MCP96 149.5
152	MCP96 139a
152	MCP96 139b
150.6	MCP96 137.8
148.1	MCP96 134.6
146.5 a	MCP96 133.2a
146.5 b	MCP96 133.2b
145.2	MCP96 132
96	MCP96 83.5
56.9	MCP96 46.9
38.4	MCP96 30.8
32	MCP96 26.8

Appendix D

Dissolution summaries for all concretions

Table D1. Dissolution summary of concretion CM 40.5 - 40.6

	parallel	subparallel, prox. down	subparallel, prox. up	near vertica prox. down	near vertical prox. up	TOTAL	
siculae	2					2	
monograptid 1-2 thecae						0	
monograptid 3-4 thecae						0	
monograptid mature	3					3	3
diplograptid 1-2 thecae	5					5	
diplograptid 3-4 thecae	1					1	
diplograptid mature	6		1			7	13
total	17	0	1	0	0	18	

LAYERS	7 (first layer was all core and not measurements were taken)
PHOTOS	none
FAUNA	3 monograptids, 10 diplograptids
OTHER FAUNA	none
RIMS/CORES	insoluble core at first layer covers 100% of surface - this was cut away.
COLOUR	grey
BARREN LAYERS	68, 72
FRAGMENTED GRAPS	layer 22; fragmented mono mature: layer 30; fragmented diplo mature.
PRESERVATION	all graptolites flattened: layer 59; black, insoluble
BARREN LAYERS	layer, less than 1mm at layer 58

layer	number	chi 2
72	0	2.2857143
68	0	2.2857143
59	3	0.2232143
49	1	0.7232143
40	5	3.2232143
30	3	0.2232143
22	4	1.2857143

number of layers	7
total number of graps.	16
ave. graps per layer	2.28571
total CHI2	10.25
plot on model	1.46429

v = 6, at 99.9% significance the null hypothesis of random distribution is accepted

Table D2. Dissolution summary of concretion CM 41.65-41.75

	parallel	subparallel, prox. down	subparallel, prox. up	near vertica prox. down	near vertical prox. up	TOTAL	
siculae	20					20	
monograptid 1-2 thecae	4	1				5	
monograptid 3-4 thecae	6					6	
monograptid mature	4					4	15
diplograptid 1-2 thecae	10					10	
diplograptid 3-4 thecae	2					2	
diplograptid mature	5					5	17
total	51	1	0	0	0	52	

LAYERS	6
PHOTOS	none
FAUNA	15 monos; 17 diplos
OTHER FAUNA	none
RIMS/CORES	none
COLOUR	
BARREN LAYERS	none
FRAGMENTED GRAPS	many mono fragments on layer 19
PRESERVATION	all graps are compressed

BARREN LAYERS

layer	number	chi 2
39	4	2.5128205
33	9	0.0128205
27	9	0.0128205
19	12	1.2820513
13	6	0.8205128
6	12	1.2820513

number of layers	6
total number of graps.	52
ave. graps per layer	8.66667
total CHI2	4.64103
plot on model	0.7735

v = 5, at 99.9% significance the null hypothesis of random distribution is accepted

Table D3. Dissolution summary of concretion CM 42.3-42.4

	parallel	subparallel, prox. down	subparallel, prox. up	near vertica prox. down	near vertical prox. up	TOTAL	
siculae	4					4	
monograptid 1-2 thecae	4					4	
monograptid 3-4 thecae	2					2	
monograptid mature	5		1			6	12
diplograptid 1-2 thecae	7					7	
diplograptid 3-4 thecae	1	1				2	
diplograptid mature	6					6	15
total	29	1	1	0	0	31	

LAYERS	14
PHOTOS	none
FAUNA	12 monograptids; 15 diplograptids
OTHER FAUNA	layer 41; large bivalve or brachiopod on preserved as calcite.
RIMS/CORES	none
COLOUR	brown
BARREN LAYERS	layer 13
FRAGMENTED GRAPS	fragmented in residue - no notes made from surface.
PRESERVATION	all graptolites flattened; very muddy

BARREN LAYERS

layers	number	chi 2
100	4	1.2857143
94	3	0.2232143
86	2	0.0357143
78	4	1.2857143
74	1	0.7232143
70	1	0.7232143
64	2	0.0357143
58	2	0.0357143
53	4	1.2857143
47	2	0.0357143
41	4	1.2857143
30	1	0.7232143
23	2	0.0357143
13	0	2.2857143

number of layers	14
total number of graps.	32
ave. graps per layer	2.28571
total CHI2	10
plot on model	0.71429

v = 13, at 99.9% significance the null hypothesis of random distribution is accepted

Table D4. Dissolution summary of concretion CM 42.8 - 42.9

	parallel	subparallel prox. down	subparallel prox. up	near vertic prox. down	near vertical prox. up	TOTAL	
siculae	63	3	1	1		68	
monograptid 1-2 thecae	16	1				17	
monograptid 3-4 thecae	5					5	
monograptid mature	2	1				3	25
diplograptid 1-2 thecae	9	1				10	
diplograptid 3-4 thecae						0	
diplograptid mature						0	10
total	95	6	1	1	0	103	

LAYERS	7
DISSOLUTION DATES	
PHOTOS	none
FAUNA	25 monos; 10 diplos
OTHER FAUNA	radiolarian internal molds present on every layer (including layer 44)
RIMS/CORES	layer 7; rim covers 25% of surface
COLOUR	
BARREN LAYERS	layer 44
FRAGMENTED GRAPS	none reported
BARREN LAYERS	

layer	number	chi 2	
44	0	15	
39	7	4.266667	
32	18	0.6	
26	42	48.6	** almost 1/2 of all graptolites in concretion are on this layer (30 sicula)
22	20	1.666667	
12	9	2.4	
7	9	2.4	corrected for rim (original count =7)

number of layers	7
total number of graps.	105
ave. graps per layer	15
total CHI2	74.933
plot on model	10.705

v = 6, at 99.9% significance the null hypothesis of random distribution is rejected

Table D5. Dissolution sumr Concretion:

	parallel	subparallel, prox. down	subparallel, prox. up	near vertica prox. down	near vertical prox. up	TOTAL	
siculae	194					194	
monograptid 1-2 thecae	18					18	
monograptid 3-4 thecae	4					4	
monograptid mature	6					6	28
diplograptid 1-2 thecae	37					37	
diplograptid 3-4 thecae	15	1				16	
diplograptid mature	34					34	87
total	308	1				309	

LAYERS	14
PHOTOS	none
FAUNA	28 monos; 87diplos
OTHER FAUNA	none reported
RIMS/CORES	rim on first 3 layers (still visible at layer 22)
COLOUR	
BARREN LAYERS	none
FRAGMENTED GRAPS	none reported
PRESERVATION	most graptolites flattened; pyritized mono on layer 45.
BARREN LAYERS	

layer	number	CHI2	
75	14	2.9516875	
70	24	0.168516	
64	13	3.7283865	
60	42	17.993759	*
56	32	4.4662506	
50	40	14.563338	*
45	43	19.844891	*
40	19	0.4274156	corealates to dark laminations and dark parts of
36	26	0.6992603	graded beds. Poss. interpretation =
32	9	7.7413315	graps are suspended (resuspended)
27	23	0.0390661	by a current/flow and then in the ebb are depsoited
22	13	3.7283865	with the finer clays that are also kicked
17	6	11.702497	up into suspension. Note that large increase in
10	5	13.204115	graps is a result of a large increase in sicula...

number of layers	14
total number of graps.	309
ave. graps per layer	22.071
total CHI2	101.26
plot on model	7.2328

v = 13, at 99.9% significance the null hypothesis of random distribution is rejected

Table D6. Dissolution sumr Concretion:

	parallel	subparallel, prox. down	subparallel, prox. up	near vertica prox. down	near vertical prox. up	TOTAL	
siculae	103	2	2			107	
monograptid 1-2 thecae	7					7	
monograptid 3-4 thecae	1					1	
monograptid mature	31	2	1			34	42
diplograptid 1-2 thecae	32		2			34	
diplograptid 3-4 thecae	10					10	
diplograptid mature	18					18	62
total	202	4	5	0	0	211	

LAYERS	6
DISSOLUTION DATES	May-98
PHOTOS	all layers
FAUNA	8 monos; 12 diplos
OTHER FAUNA	layer 29; cross-section through bivavle or brachiopod with carbonate shell - sketched.
RIMS/CORES	all graptolites are flattened except for where thecal thickenings prevented compaction: layer 14; insoluble core of lighter material
COLOUR	
BARREN LAYERS	none
FRAGMENTED GRAPS	lay 14; fragmented mono and diplo mature: layer 18; 2 fragmented mono matures: layer 25; mono 1-2 th.: layer 28; fragmented mono mat.
PRESERVATION	lay 8; graps are encrusted: lay 14; graps are flattened and encrusted

layers	number	chi 2	
72	13	0.0278784	
69	15	0.5397268	
64	13	0.0278784	
60	25	12.767215	**
55	30	24.923613	**
52	15	0.5397268	
48	12	0.0136604	
46	15	0.5397268	
44	13	0.0278784	
42	13	0.0278784	
35	8	1.5681628	
29	7	2.359632	
28	6	3.3122386	
25	13	0.0278784	
18	6	3.3122386	
14	3	7.1368832	
8	4	5.7008642	

number of layers	17	
total number of graps.	211	
ave. graps per layer	12.4118	v = 5, at 99.9% significance the null
total CHI2	62.8531	hypothesis of random distribution is rejected
plot on model	3.69724	

Table D7. Dissolution summary of concretion CM 45.3 - 45.4

	parallel	subparallel, prox. down	subparallel, prox. up	near vertica prox. down	near vertical prox. up	TOTAL	
siculae	28		1			29	
monograptid 1-2 thecae	1					1	
monograptid 3-4 thecae	2					2	
monograptid mature	13	8	7			28	31
diplograptid 1-2 thecae	10					10	
diplograptid 3-4 thecae	7					7	
diplograptid mature	28	11	4			43	60
total	89	19	12	0	0	120	

LAYERS	12
DISSOLUTION DATES	Jan-99
PHOTOS	layer 10; 16; 66
FAUNA	31 monos, 60 diplos
OTHER FAUNA	layer 24; two sponge spicules with length 1.5 and 2.0 cm.
	layer 36; orthocone in same orientation as non-parallel grap,
RIMS/CORES	none
COLOUR	
BARREN LAYERS	none; graptolite on layer 16 might have been recorded
BARREN LAYERS	on layer 10 (16 could be barren).
FRAGMENTED GRAPS	
PRESERVATION	layer 57; covered with brown "dust" - 2 or 3 graps are encrusted
	(lack of small rhabdosomes might be non-observation)

layer	number	chi 2	
75	19	9.0114943	**
69	11	0.183908	
66	11	0.183908	
62	7	0.7356322	
57	3	4.5977011	
48	7	0.7356322	
42	3	4.5977011	
36	3	4.5977011	
29	5	2.2528736	
24	4	3.3218391	
16	1	7.7701149	
10	42	108.14943	**

distributed on one half of concretion, many non-parallel to bedding.

number of layers	12
total number of graps.	116
ave. graps per layer	9.66667
total CHI2	146.138
plot on model	12.1782

v = 11, at 99.9% significance the null hypothesis of random distribution is rejected

Table D8. Dissolution summary of concretion CM 46.35 - 46.5

	parallel	subparallel, prox. down	subparallel, prox. up	near vertica prox. down	near vertical prox. up	TOTAL	
siculae	154	7	5	1	2	169	
monograptid 1-2 thecae	22	1	1			24	
monograptid 3-4 thecae	5					5	
monograptid mature	245	2	2			249	278
diplograptid 1-2 thecae	27	2	2	2		33	
diplograptid 3-4 thecae	11	3	1			15	
diplograptid mature	29	8	2	1		40	88
total	493	23	13	4	2	535	

LAYERS	17
PHOTOS	layer 53; 58; 63
FAUNA	278 monos; 88 diplos
OTHER FAUNA	none reported
RIMS/CORES	none
COLOUR	
BARREN LAYERS	none
FRAGMENTED GRAPS	none reported
PRESERVATION	not flattened.

BARREN LAYERS

layer	number	chi 2	
102	13	10.840682	
94	22	2.8500275	
87	23	2.279934	
83	58	22.364046	**
77	19	4.9416163	
70	27	0.6350742	
63	21	3.4836723	
58	112	206.06498	**
53	121	254.69863	**
51	33	0.0743266	
47	22	2.8500275	
42	6	20.614513	
34	10	14.648158	
26	5	22.264981	
21	8	17.504233	
16	26	0.9509621	
10	9	16.04442	

number of layers	17
total number of graps.	535
ave. graps per layer	31.4706
total CHI2	568.611
plot on model	33.4477

v = 16 , at 99.9% significance the null hypothesis of random distribution is rejected

Table D9. Dissolution summary of concretion CM 47.4 - 47.5

	parallel	subparallel, prox. down	subparallel, prox. up	near vertica prox. down	near vertical prox. up	TOTAL	
siculae	45	2	1		1	49	
monograptid 1-2 thecae	2					2	
monograptid 3-4 thecae	1					1	
monograptid mature	7		1			8	11
diplograptid 1-2 thecae	19			1	1	21	
diplograptid 3-4 thecae	4					4	
diplograptid mature	4					4	29
total						89	

LAYERS	13
DISSOLUTION DATES	
PHOTOS	none
FAUNA	11 monos; 29 diplos
OTHER FAUNA	layer 25, 30; x-section through bivalve (?) - sketched in lab book, bivalve is central location in concretion and may have been the locale for precipitation.
RIMS/CORES	rim at layer 65; rim is 50% of layer at layer 73.
COLOUR	
BARREN LAYERS	barren layers (65,48) correspond exactly to a thin dark irregular band parallel to bedding in polished slab... could this be a stylolite? pressure solution has obliterated graps.
FRAGMENTED GRAPS	none reported
PRESERVATION	not flattened.

layer	number	chi 2
73	2	3.4304235
68	3	2.1607606
65	1	4.9922213
58	3	2.1607606
55	11	2.5203111
48	0	6.8461538
40	10	1.4528954
36	5	0.4978392
30	12	3.8798617
25	7	0.0034572
16	17	15.059637
13	13	5.5315471
6	5	0.4978392

number of layers	13
total number of graps.	89
ave. graps per layer	6.84615
total CHI2	49.0337
plot on model	3.77182

minus barren layers

layer	number	chi 2
73	2	4.5
68	3	3.125
58	3	3.125
55	11	1.125
40	10	0.5
36	5	1.125
30	12	2
25	7	0.125
16	17	10.125
13	13	3.125
6	5	1.125

number of la	11
total numbe	88
ave. graps p	8
total CHI2	30
plot on mod	2.7272727

v = 12, at 99.9% significance the null hypothesis of random distribution is rejected

Table D10. Dissolution summary of concretion CM 48.5

	parallel	subparallel, prox. down	subparallel, prox. up	near vertica prox. down	near vertical prox. up	TOTAL	
siculae	26				1	27	
monograptid 1-2 thecae						0	
monograptid 3-4 thecae	1					1	
monograptid mature	25	23	13			61	62
diplograptid 1-2 thecae	8	1	2			11	
diplograptid 3-4 thecae	1	1	1		2	5	
diplograptid mature	11	10	4		1	26	42
total	72	35	20	0	4	131	

LAYERS	10
PHOTOS	layer 35, 45, 50
FAUNA	62 monos; 42 diplos
OTHER FAUNA	spar filled object on layer 35, 41, 45, 50 may be of organic origin orthocone on layer 45
RIMS/CORES	none (unless the spar cavity)
COLOUR	
BARREN LAYERS	none
FRAGMENTED GRAPS	many fragmented graps on layer 41 (difficult to id.)
BARREN LAYERS	layer 41; graps along bedding are compressed.

layer	number	chi 2	
66	12	0.0923664	
59	14	0.0618321	
50	26	12.703053	**
45	11	0.3366412	
41	17	1.1610687	
35	23	7.4816794	**
31	5	5.0083969	
26	5	5.0083969	
18	6	3.8480916	
7	12	0.0923664	

number of layers	10
total number of graps.	131
ave. graps per layer	13.1
total CHI2	35.794
plot on model	3.5794

v = 9 , at 99.9% significance the null hypothesis of random distribution is rejected

Table D11. Dissolution summary of concretion CM 49.8-49.9

	parallel	subparallel, prox. down	subparallel, prox. up	near vertica prox. down	near vertical prox. up	TOTAL	
siculae	216	6	8	6	8	244	
monograptid 1-2 thecae	46	1				47	
monograptid 3-4 thecae	29	1	4			34	
monograptid mature	52	4	7	1	1	65	146
diplograptid 1-2 thecae	81	3	5			89	
diplograptid 3-4 thecae	23	5	1	1		30	
diplograptid mature	41	7	4			52	171
total	488	27	29	8	9	561	

LAYERS	19
PHOTOS	none
FAUNA	146 monos; 171 diplos
OTHER FAUNA	2 encrusted orthocones on layer 43; 2 orthocones on layer 40, one encrusted; 2 orthocones layer 33;
RIMS/CORES	none
COLOUR	grey brown
BARREN LAYERS	none
FRAGMENTED GRAPS	none reported but graps in residue are very fragmented.
BARREN LAYERS	layer 43, 51, 71, 78; encrusted graptolites

layer	number	chi 2	
90	41	4.4585796	
87	35	1.0147293	
78	17	5.3141946	
71	38	2.4318416	
66	23	1.4425368	
63	18	4.4995778	
57	42	5.2696313	
56	35	1.0147293	
51	35	1.0147293	
43	38	2.4318416	
40	40	3.7152641	
33	34	0.6778309	
25	18	4.4995778	
20	45	8.1092035	**
17	39	3.0396848	
12	21	2.4621447	
9	19	3.7526973	
7	6	18.745567	**
3	17	5.3141946	

number of layers	19
total number of graps.	561
ave. graps per layer	29.5263
total CHI2	45.8943
plot on model	2.41549

v = 18, at 99.9% significance the null hypothesis of random distribution is rejected

Table D12. Dissolution summary of concretion CM 50.4

	parallel	subparallel, prox. down	subparallel, prox. up	near vertica prox. down	near vertical prox. up	TOTAL	
siculae	8					8	
monograptid 1-2 thecae	1					1	
monograptid 3-4 thecae	1					1	
monograptid mature	10					10	12
diplograptid 1-2 thecae	4					4	
diplograptid 3-4 thecae						0	
diplograptid mature	3		1			4	8
total	27	0	1	0	0	28	

LAYERS	10
PHOTOS	layer 10
FAUNA	12 monos; 8 diplos
OTHER FAUNA	none reported
RIMS/CORES	none
COLOUR	
BARREN LAYERS	65, 60
FRAGMENTED GRAPS	1 mono on layer 21
PRESERVATION	layer 21, brown opaque "dust" makes observation of graps difficult.

BARREN LAYERS

layer	number	chi 2	
65	0	2.8	
60	0	2.8	
53	1	1.1571429	
46	7	6.3	**
40	3	0.0142857	
34	1	1.1571429	
27	2	0.2285714	
21	1	1.1571429	
13	9	13.728571	**
10	4	0.5142857	

number of layers	10
total number of graps.	28
ave. graps per layer	2.8
total CHI2	29.8571
plot on model	2.98571

v = 9 , at 99.9% significance the null hypothesis of random distribution is rejected

Table D13. Dissolution summary of concretion CM 50.4-50.5

	parallel	subparallel, prox. down	subparallel, prox. up	near vertica prox. down	near vertical prox. up	TOTAL	
siculae	39					39	
monograptid 1-2 thecae	6					6	
monograptid 3-4 thecae	2					2	
monograptid mature	9	2				11	19
diplograptid 1-2 thecae	14	2		1		17	
diplograptid 3-4 thecae	8	2	1			11	
diplograptid mature	8	1	1			10	38
total	86	7	2	1	0	96	

LAYERS	14
PHOTOS	none
FAUNA	19 monos; 38 diplos
OTHER FAUNA	layer 11; 2 orthocones (2 cm long): layer 5; 2 orthocones (one 4 cm long)
RIMS/CORES	none
COLOUR	
BARREN LAYERS	none
FRAGMENTED GRAPS	layer 45; one mature mono is fragmented
PRESERVATION	

BARREN LAYERS

layers	number	chi 2
79	6	0.0909774
68	5	0.4699248
61	10	1.5225564
56	13	5.6909774
50	5	0.4699248
45	6	0.0909774
37	9	0.7225564
33	8	0.2172932
30	6	0.0909774
24	9	0.7225564
19	4	1.143609
15	6	0.0909774
11	5	0.4699248
5	3	2.1120301

number of layers	14
total number of graps.	95
ave. graps per layer	6.78571
total CHI2	13.9053
plot on model	0.99323

v = 13, at 99.9% significance the null hypothesis of random distribution is accepted

Table D14. Dissolution summary of concretion CM 51.2-51.3a

	parallel	subparallel, prox. down	subparallel, prox. up	near vertica prox. down	near vertical prox. up	TOTAL	
siculae	144	15	22	12	17	210	
monograptid 1-2 thecae	37	7	6		2	52	
monograptid 3-4 thecae	14	2				16	
monograptid mature	5	3			3	11	79
diplograptid 1-2 thecae	26	1	2	1	2	32	
diplograptid 3-4 thecae	8		1			9	
diplograptid mature	8	5	1			14	55
total	242	33	32	13	24	344	

LAYERS	12 plus..
PHOTOS	all layers
FAUNA	79 monos; 55 diplos
OTHER FAUNA	layer 12-17; gathering of graps (mostly siculae) perpendicular to surface in one section near an accumulation of sponge spicules in life orientation: layer 17; gastropod impression (5whirls, some infilling) sketched in lab book: layer48; small gastropods, bivalves, orthocones and a hemisph. bryozoan(??), pile of sponge spicules 1cm diameter is encusted with white material: layer 53; braciopod 5 x 2mm, sponge spicule pile from 48, orthocone, numerous small brachiopods: layer 58; sponge spicule pile
BARREN LAYERS	layer 48 - rim of brown coarser material; layer 53-58 - undissolvable of brown to buff material at center of concretion. Layer 25; vugs of CaC03.
COLOUR	lt. to dk. brown with buff undissovables and uneven planes of black org.
BARREN LAYERS	none
FRAGMENTED GRAPS	lay 4; mono mat.para fragment 3 th. long: lay 17; mono-mat.para fragment, 2 diplo-mat.para fragment: lay 53; mono-mat.frag 2th. long: layer 58; diplo-mat sub-para prox down 2 th. long, mono 1-2 th. sub para prox up.
PRESERVATION	lay 8; graps covered with brown silt which covers whole layer: layer 27; large diplos are encrusted with a brown substance: layer 30; many of the graps are encrusted witha dusty brown substance: lay 37; encrusted mono-mat: lay 41; graptolites are pitted with holes and encrusted with brown fine-grained substance

layer	number	chi 2	
58	28	1.5516779	
53	14	8.3771812	**
48	35	0.9073826	
41	20	3.2228188	
37	18	4.6724832	
30	36	1.2899329	
27	25	0.7731544	
25	32	0.1624161	
17	43	5.8469799	**
12	47	9.9275168	**
8	25	0.7731544	
4	23	1.5516779	
number of layers	10		
total number of graps.	298		
ave. graps per layer	29.8		
total CHI2	36.7315		
plot on model	3.67315		

v = 9, at 99.9% significance the null hypothesis of random distribution is rejected

Table D15. Dissolution summary of concretion CM 51.2-51.3b
(same strata as MCM 96-9 MCM 96-9 0.1-0.2a)

	parallel	subparallel, prox. down	subparallel, prox. up	near vertica prox. down	near vertical prox. up	TOTAL	
siculae	71	5	8		1	85	
monograptid 1-2 thecae	8	3	3			14	
monograptid 3-4 thecae	1	1				2	
monograptid mature	7					7	23
diplograptid 1-2 thecae	15					15	
diplograptid 3-4 thecae	2		1			3	
diplograptid mature	1	3				4	22
total	105	12	12	0	1	130	

LAYERS	10
PHOTOS	none
FAUNA	23 monos; 22 diplos
OTHER FAUNA	layer 5; orthocone 5 x 0.8 cm
RIMS/CORES	none
COLOUR	
BARREN LAYERS	none
FRAGMENTED GRAPS	none
PRESERVATION	

BARREN LAYERS

layer	number	chi 2
65	7	2.7692308
58	7	2.7692308
50	12	0.0769231
41	13	0
34	21	4.9230769
30	16	0.6923077
26	10	0.6923077
20	14	0.0769231
13	12	0.0769231
5	18	1.9230769

number of layers	10
total number of graps.	130
ave. graps per layer	13
total CHI2	14
plot on model	1.4

v = 9, at 99.9% significance the null hypothesis of random distribution is accepted

Table D16. Dissolution summary of concretion CM 52.1-52.2

	parallel	subparallel, prox. down	subparallel, prox. up	near vertica prox. down	near vertical prox. up	TOTAL	
siculae	7			1		8	
monograptid 1-2 thecae						0	
monograptid 3-4 thecae	1					1	
monograptid mature	2					2	3
diplograptid 1-2 thecae	6					6	
diplograptid 3-4 thecae	5					5	
diplograptid mature	30	5	3			38	49
total	51	5	3	1	0	60	

LAYERS	19 (data summarized from only 12 layers; layers 2, 5, 8, 11, 14, 31, 35, 39, 42, 55, 58, 62, 64
DISSOLUTION DATES	18/06/97-23/07/97
PHOTOS	all digital saved in "SNAPPY"
FAUNA	49 diplos, 3 Monos
OTHER FAUNA	layer 2-6; orthocone: lay 11, 12; orthocone with calcite infill with pieces of
RIMS/CORES	carbon/bitumen: lay 31; brachiopod(?): lay 35; brachiopod imprint: lay 62; mid-conispiral gastropod preserved as opaque org., orthocone as white calcite with inner black carbon: lay 64; orthocone, sponge spiclue mass black carbon/birumen core 5.5 x 4.5 cm at layer 35
BARREN LAYERS	grey with black core
BARREN LAYERS	none
FRAGMENTED GRAPS	lay 32; one d-frag sub-para-prox-up buried to 3rd theca - few observations may be the result of not looking/reporting the evidence for fragmentation.
PRESERVATION	not flattened, slightly pyritized - no pits.

dissolved top down.

layers	number	chi 2
2	9	4.1653846
5	8	2.4820513
8	2	1.4820513
11	5	0.0320513
14	4	0.0820513
31	3	0.5653846
35	9	4.1653846
39	9	4.1653846
42	2	1.4820513
55	3	0.5653846
58	2	1.4820513
62	2	1.4820513
64	2	1.4820513
number of layers	13	
total number of graps.	60	
ave. graps per layer	4.61538	
total CHI2	23.6333	
plot on model	1.81795	

corrected for core

layers	number	chi 2	
2	9	2.04	
5	8	1.0126	
8	2	2.3277	
11	5	0.0674	
14	4	0.4647	
31	5	0.0674	x 1.5
35	14	12.519	x 1.5
39	14	12.519	x 1.5
42	3	1.2181	x 1.5
55	3	1.2181	
58	2	2.3277	
62	2	2.3277	
64	2	2.3277	
number of layers	13		
total number of graps.	73		
ave. graps per layer	5.6154		
total CHI2	40.438		
plot on model	3.1106		

v = 12, at 99.9% significance the null hypothesis of random distribution is rejected

Table D17. Dissolution summary of concretion CM 53.2-53.3

	parallel	subparallel, prox. down	subparallel, prox. up	near vertica prox. down	near vertical prox. up	TOTAL	
siculae	79	8	3	1		91	
monograptid 1-2 thecae	6	2				8	
monograptid 3-4 thecae	1					1	
monograptid mature	14	1	1			16	25
diplograptid 1-2 thecae	17	1				18	
diplograptid 3-4 thecae	1	1	1			3	
diplograptid mature	7		1			8	29
total	125	13	6	1	0	145	

LAYERS	14
PHOTOS	none
FAUNA	25 monos; 29 diplos
OTHER FAUNA	layer 55, orthocone: layer 43, 47, sponge spicule mass 2 x 3 cm.
	layer 24; bivalve (0.4 x 0.8 cm; both valves present) in core
	layer 18; sponge spicule mass with spicules in lattice
RIMS/CORES	buff core at layers 5 - 31(5.5 x 3 cm at max diameter at layer 13 and 18)
COLOUR	
BARREN LAYERS	none
BARREN LAYERS	1 broken mature diplo on layer 43
PRESERVATION	

layers	number	chi 2
67	8	0.5364532
65	9	0.1778325
63	12	0.2605911
55	9	0.1778325
53	14	1.2812808
49	18	5.6399015
47	20	8.9778325
43	6	1.8330049
31	5	2.770936
24	6	1.8330049
18	15	2.0812808
13	7	1.0881773
8	5	2.770936
5	11	0.0399015

number of layers	14
total number of graps.	145
ave. graps per layer	10.3571
total CHI2	29.469
plot on model	2.10493

corrected for core

layers	number	chi 2	
67	8	1.578	
65	9	0.9458	
63	12	0.0148	
55	9	0.9458	
53	14	0.1987	
49	18	2.4975	
47	20	4.6125	
43	6	3.3251	added
31	8	1.578	3
24	11	0.1642	5
18	22	7.3711	7
13	14	0.1987	7
8	9	0.9458	5
5	14	0.1987	3

number of layers	14
total number of graps.	174
ave. graps per layer	12.429
total CHI2	24.575
plot on model	1.7553

v = 13, at 99.9% significance the null hypothesis of random distribution is rejected

Table D18. Dissolution summary of concretion CM 54.0 - 54.15

	parallel	subparallel, prox. down	subparallel, prox. up	near vertica prox. down	near vertical prox. up	TOTAL	
siculae	44	1				45	
monograptid 1-2 thecae	13		1			14	
monograptid 3-4 thecae	3					3	
monograptid mature	8		2			10	27
diplograptid 1-2 thecae	18	2				20	
diplograptid 3-4 thecae	8					8	
diplograptid mature	4					4	32
total	98	3	3	0	0	104	

LAYERS	15
PHOTOS	layer 85
FAUNA	27 monos; 32 diplos
OTHER FAUNA	layer 92; orthocone 4 cm long parallel to surface
	layer 59; 4.5 cm long orthocone with calcite and bitumen infill
	layer 37, 44, 52; large sponge spicule mass covers 1/5 of surface.
	layer 34; two spongle spicule masses
RIMS/CORES	none
COLOUR	
BARREN LAYERS	none
FRAGMENTED GRAPS	layer 85 mature diplo is fragmented.
PRESERVATION	

layer	number	chi 2
92	5	0.5391026
85	13	5.3083333
82	11	2.3852564
74	7	0.000641
67	5	0.5391026
59	7	0.000641
52	6	0.125641
44	5	0.5391026
37	4	1.2410256
34	3	2.2314103
30	9	0.6160256
23	5	0.5391026
17	1	5.0775641
12	13	5.3083333
6	10	1.3564103
number of layers	15	
total number of graps.	104	
ave. graps per layer	6.9333	
total CHI2	24.451	
plot on model	1.6301	

corrected for sponge layer

layer	number	chi 2	
92	5	0.638	
85	13	4.8249	
82	11	2.096	
74	7	0.0025	
67	5	0.638	
59	7	0.0025	added
52	7	0.0025	1
44	6	0.1801	1
37	5	0.638	1
34	3	2.395	
30	9	0.4885	
23	5	0.638	
17	1	5.2735	
12	13	4.8249	
6	10	1.152	
	15		
	107		
	7.1333333		
	22.642368		
	1.5094912		

v = 14, at 99.9% significance the null hypothesis of random distribution is accepted

Table D19. Dissolution summary of concretion CM 55

	parallel	subparallel, prox. down	subparallel, prox. up	near vertica prox. down	near vertical prox. up	TOTAL	
siculae	113	4	1	2		120	
monograptid 1-2 thecae	7					7	
monograptid 3-4 thecae	6		2			8	
monograptid mature	19	1	2			22	37
diplograptid 1-2 thecae	44	1	1			46	
diplograptid 3-4 thecae	7	2		1		10	
diplograptid mature	15	1	1			17	73
total	211	9	7	3	0	230	

LAYERS	10
DISSOLUTION DATES	
PHOTOS	none
FAUNA	37 monos; 73 diplos
OTHER FAUNA	layer 59; 4 orthocones (no apparent orientation): layer 47; sm. Orthocone layer 30: orthocone in core; layer 24; 2 orthocones in core: layer 5; 2 sm. white orthocones and a mass of the same material (3mm diameter) many small spheres of white material (internal molds of radiolarian?)
RIMS/CORES	layer 24, 30; small black (bitumen) core at layer 24, 30 (1 x 2 cm)
BARREN LAYERS	
BARREN LAYERS	none
FRAGMENTED GRAPS	none reported
PRESERVATION	

layer	number	chi 2		
59	27	0.6956522		19 sicula
51	16	2.1304348		
47	37	8.5217391	**	24 sicula
40	42	15.695652	**	19 sicula
37	29	1.5652174		
30	8	9.7826087		
24	8	9.7826087		
17	10	7.3478261		
13	25	0.173913		
5	28	1.0869565		

number of layers	10
total number of graps.	230
ave. graps per layer	23
total CHI2	56.7826
plot on model	5.67826

corrected for core

layer	number	chi 2
59	27	0.5538
51	16	2.3402
47	37	7.9043
40	42	14.785
37	29	1.3402
30	10	7.6735
24	10	7.6735
17	10	7.6735
13	25	0.1094
5	28	0.9043

number of layers	10
total number of graps	234
ave. graps per layer	23.4
total CHI2	50.957
plot on model	5.0957

v = 9, at 99.9% significance the null hypothesis of random distribution is rejected

Table D20. Dissolution summary of concretion CM 56

	parallel	subparallel, prox. down	subparallel, prox. up	near vertica prox. down	near vertical prox. up	TOTAL	
siculae	45	6	5	1		57	
monograptid 1-2 thecae	9	1	1			11	
monograptid 3-4 thecae	2		1			3	
monograptid mature	6	2				8	22
diplograptid 1-2 thecae						0	
diplograptid 3-4 thecae						0	
diplograptid mature	1		1			2	2
total	63	9	8	1	0	81	

LAYERS	10
PHOTOS	photos of all layers
FAUNA	22 monos; 2 diplos.
OTHER FAUNA	layer 27; encrusted orthocone
RIMS/CORES	from layer 33 - 53; layer 40; inner core 5x4cm, outer core 8x6.5 cm
COLOUR	
BARREN LAYERS	none
FRAGMENTED GRAPS	fragmented mat.mono on lay.33; fragmented diplo and 2 monos on lay.16
PRESERVATION	lay.13; rhabdosomes are not well preserved with holes and broken
BARREN LAYERS	fragments removed... some are possibly graptolites but unidentifiable.

layer	number	chi 2
49	11	1.4142857
45	18	13.777922
40	7	0.0636364
33	2	4.2194805
27	6	0.3753247
23	8	0.0116883
16	4	1.7779221
13	5	0.9467532
12	5	0.9467532
4	11	1.4142857
number of layers	10	
total number of graps.	77	
ave. graps per layer	7.7	
total CHI2	24.9481	
plot on model	2.49481	

corrected for core

layer	number	chi 2	
49	22	9.58696	x 2
45	36	52.1957	x 2
40	14	0.54348	x 2
33	4	4.8913	x 2
27	6	2.63043	
23	8	1.06522	
16	4	4.8913	
13	5	3.67391	
12	5	3.67391	
4	11	0.02174	
number of la	10		
total numbe	115		
ave. graps p	11.5		
total CHI2	83.173913		
plot on mod	8.3173913		

v = 9, at 99.9% significance the null hypothesis of random distribution is rejected

Table D21. Dissolution summary of concretion CM 56.4-56.5

	parallel	subparallel, prox. down	subparallel, prox. up	near vertica prox. down	near vertical prox. up	TOTAL	
siculae	187	6	4		1	198	
monograptid 1-2 thecae						0	
monograptid 3-4 thecae	7	1				8	
monograptid mature	17	7	3	1		28	36
diplograptid 1-2 thecae	16					16	
diplograptid 3-4 thecae	5					5	
diplograptid mature	8	1				9	30
total	240	15	7	1	1	264	

LAYERS	31(excluded many layers from survey too avoid recounting graps.) included: layers 2, 5, 8, 13, 16, 21, 42, 47, 50, 54, 62, 69, 73, 77.=14 layers.
DISSOLUTION DATES	25/06/97-19/11/97
PHOTOS	all layers (3 photos, 28 digital images)
FAUNA	36 mono; 30 diplo
OTHER FAUNA	none
RIMS/CORES	lay.49 to top, organic carbon rim is visible; sometimes two rims present
COLOUR	fine dusting of dark brown sediment covers layers making id of sicula difficult. - rims black
BARREN LAYERS	lay.54 and 55 are covered by insoluble organics, few graps are observed.
FRAGMENTED GRAPS	lay 3; 2monos: lay 14; 2sub-para prox.down, 2 sub-para. Prox.up and 5
BARREN LAYERS	parallel, all are monos 1-3 thecae in length with no view of proximal ends: lay. 23; 2 mono frags perpendicular to surface with only 3 thecae revealed: lay. 44; 2 mono frags. Sub-para. prox.up: lay 52 diplo broken: lay 66; 2 mono frags, one sub-para. prox.up, one par.: lay 71; mono frag sub-para. prox.up with 3 th. visible, diplo frag sub-para.prox.down with 2 th. showing: lay 75; mono mat. fragmented: lay 77; 2 graps too frgmented to id.
PRESERVATION	lay 48 graps encrusted with a brown/tan. graptolites not well preserved. Other layers = ok. Graptolites commony robust and well preserved.

dissolution from bottom to top.

layer	number	chi 2	
2	20	0.0692641	
5	20	0.0692641	rims
8	25	2.0010823	19 sicula
13	18	0.038961	
16	27	3.5162338	40% cover
21	22	0.5238095	
42	25	2.0010823	
47	17	0.1829004	
50	12	2.4935065	
54	4	11.705628	
62	11	3.2738095	
69	23	0.9101732	
73	4	11.705628	
77	36	15.584416	
number of layers	14		
total number of graps.	264		
ave. graps per layer	18.8571		
total CHI2	26.7857		
plot on model	1.91327		

corrected for rims

layer	number	chi 2
2	20	0.0003
5	20	0.0003
8	25	1.2102
13	18	0.2138
16	27	2.3917
21	22	0.1853
42	25	1.2102
47	17	0.47
50	12	3.2458
54	8	7.26
62	22	0.1853
69	25	1.2102
73	4	12.869
77	36	12.641
	14	
	281	
	20.071429	
	17.583122	
	1.2559373	

v = 13, at 99.9% significance the null hypothesis of random distribution is accepted

Table D22. Dissolution summary of concretion CM 57

	parallel	subparallel, prox. down	subparallel, prox. up	near vertica prox. down	near vertical prox. up	TOTAL	
siculae	31		1			32	
monograptid 1-2 thecae	3		1			4	
monograptid 3-4 thecae	5		2			7	
monograptid mature	5	2	1			8	19
diplograptid 1-2 thecae	8		1			9	
diplograptid 3-4 thecae	3		1			4	
diplograptid mature	1			1		2	15
total	56	2	7	1	0	66	

LAYERS	8
PHOTOS	none
FAUNA	19 monos; 15 diplos
OTHER FAUNA	layer 5; orthocone
RIMS/CORES	layer 5; white to buff core 1.5 x 2.0 cm.
COLOUR	
BARREN LAYERS	none
FRAGMENTED GRAPS	none reported
PRESERVATION	layer 14; insolube layer 30% black organic, 50% white to buff
BARREN LAYERS	this layer remains attached for counts at 25 and 30.
	lay.10; 3 graps. encrusted, guessed identity to be mature monos.

layer	number	chi 2
53	10	0.3712121
50	16	7.280303
33	15	5.5227273
30	6	0.6136364
25	2	4.7348485
14	5	1.280303
10	6	0.6136364
5	6	0.6136364

corrected for core/insoluble mass

layer	number	chi 2
53	10	0.0015
50	16	3.409
33	15	2.3472
30	8	0.446
25	8	0.446
14	10	0.0015
10	8	0.446
5	6	1.6806

number of layers	8	number of la	8
total number of graps.	66	total numbe	81
ave. graps per layer	8.25	ave. graps p	10.125
total CHI2	21.0303	total CHI2	8.7777778
plot on model	2.62879	plot on mod	1.0972222

v = 8, at 99.9% significance the null hypothesis of random distribution is accepted

Table D23. Dissolution summary of concretion CM 57.5 - 57.6

	parallel	subparallel, prox. down	subparallel, prox. up	near vertica prox. down	near vertical prox. up	TOTAL	
siculae	4					4	
monograptid 1-2 thecae	3	2				5	
monograptid 3-4 thecae		2				2	
monograptid mature						0	7
diplograptid 1-2 thecae	2					2	
diplograptid 3-4 thecae	2					2	
diplograptid mature						0	4
total	11	4	0	0	0	15	

LAYERS	9
PHOTOS	none
FAUNA	7 monos; 4 diplos
OTHER FAUNA	none
RIMS/CORES	none
COLOUR	
BARREN LAYERS	layers 46, 48
FRAGMENTED GRAPS	none
PRESERVATION	increased amount of sand/silt increased topography of each layer

BARREN LAYERS

layer	number	chi 2
54	3	1.0666667
48	0	1.6666667
46	0	1.6666667
44	2	0.0666667
42	1	0.2666667
25	2	0.0666667
18	1	0.2666667
14	4	3.2666667
5	2	0.0666667

number of layers	9
total number of graps.	15
ave. graps per layer	1.66667
total CHI2	8.4
plot on model	0.93333

v = 8 , at 99.9% significance the null hypothesis of random distribution is accepted

Table D24. Dissolution summary of concretion CM 58a

	parallel	subparallel, prox. down	subparallel, prox. up	near vertica prox. down	near vertical prox. up	TOTAL	
siculae	117	22	18	5	6	168	
monograptid 1-2 thecae	24	10	4		2	40	
monograptid 3-4 thecae	6	2	1			9	
monograptid mature	30	17	6	3	1	57	106
diplograptid 1-2 thecae	25		1			26	
diplograptid 3-4 thecae	8		1			9	
diplograptid mature	9	6	3			18	53
total	219	57	34	8	9	327	

LAYERS	10
PHOTOS	none
FAUNA	106 monos; 53 diplos
OTHER FAUNA	none reported
RIMS/CORES	layer 21; rim of core
COLOUR	
BARREN LAYERS	none
FRAGMENTED GRAPS	layer 30; evidence for fragmentation prior to final burial: layer 35; thin monos fragmented
PRESERVATION	

BARREN LAYERS

layer	number	chi 2
47	16	8.5287462
43	44	3.904893
39	41	2.1067278
35	28	0.6755352
30	35	0.1617737
26	32	0.0149847
21	37	0.5654434
15	22	3.5012232
9	43	3.2443425
5	29	0.4186544

number of layers	10	
total number of graps.	327	
ave. graps per layer	32.7	v = 9, at 99.9% significance the null
total CHI2	23.1223	hypothesis of random distribution is accepted
plot on model	2.31223	

Table D25. Dissolution summary of concretion CM 58b

	parallel	subparallel, prox. down	subparallel, prox. up	near vertica prox. down	near vertical prox. up	TOTAL	
siculae	34	6	5	1		46	
monograptid 1-2 thecae	1		1			2	
monograptid 3-4 thecae	1					1	
monograptid mature	5	1				6	9
diplograptid 1-2 thecae	10	1	1			12	
diplograptid 3-4 thecae	3		1			4	
diplograptid mature	2					2	18
total	56	8	8	1	0	73	

LAYERS	7
PHOTOS	none
FAUNA	9 monos; 18 diplos
OTHER FAUNA	none reported
RIMS/CORES	lay.37; core covers 95% of surface (7.5 cm diameter): lay.27; core 90% (6.5 cm): lay.20; core 60% (4.5 cm): lay.15 core of dark brown (3 cm diam.)
COLOUR	
BARREN LAYERS	none
FRAGMENTED GRAPS	layer 12; mature monos are fragmented, one mono is bent.
BARREN LAYERS	layer 8; mature mono and diplo are fragmented
PRESERVATION	

layers	number	chi 2
37	1	8.5244618
27	2	6.8121331
20	4	3.962818
15	21	10.716243
12	13	0.6340509
8	20	8.7847358
5	12	0.2367906

layers	number	chi 2
37	19	0.50569
27	18	0.21365
20	10	2.33755
15	21	1.46144
12	13	0.61188
8	20	0.92162
5	12	1.06321

number of layers	7	7
total number of graps.	73	113
ave. graps per layer	10.4286	16.142857
total CHI2	39.6712	7.1150442
plot on model	5.66732	1.0164349

v = 6, at 99.9% significance the null hypothesis of random distribution is accepted

Table D26. Dissolution summary of concretion CM 59.1-59.2

	parallel	subparallel, prox. down	subparallel, prox. up	near vertica prox. down	near vertical prox. up	TOTAL	
siculae	60	5	2	1		68	
monograptid 1-2 thecae	6					6	
monograptid 3-4 thecae	3					3	
monograptid mature	22				1	23	32
diplograptid 1-2 thecae	25	2	1	2		30	
diplograptid 3-4 thecae	5					5	
diplograptid mature			1			1	36
total	121	7	4			136	

LAYERS	12
PHOTOS	layer 57
FAUNA	32 monos; 36 diplos
OTHER FAUNA	none reported
RIMS/CORES	layer 33; sandy buff-coloured core
COLOUR	
BARREN LAYERS	none reported
FRAGMENTED GRAPS	none reported
PRESERVATION	layer 57; orientation in horizontal plane is weakly present
BARREN LAYERS	

layer	number	CHI2	
77	6	3.2522523	
71	18	2.6036036	
67	5	4.3603604	
57	32	31.36036	**
51	12	0.009009	
45	7	2.3063063	
41	10	0.4414414	
33	5	4.3603604	
28	8	1.5225225	
23	13	0.036036	
14	11	0.1441441	
7	9	0.9009009	

number of layers	12	
total number of graps.	148	
ave. graps per layer	12.3333	v = 11 at 99.9% significance the null
total CHI2	51.2973	hypothesis of random distribution is rejected
plot on model	4.27477	

Table D27. Dissolution summary of concretion CM 72.6

	parallel	subparallel, prox. down	subparallel, prox. up	near vertica prox. down	near vertical prox. up	TOTAL	
siculae	4	1	1			6	
monograptid 1-2 thecae	2					2	
monograptid 3-4 thecae						0	
monograptid mature	1					1	3
diplograptid 1-2 thecae						0	
diplograptid 3-4 thecae	1					1	
diplograptid mature						0	1
total	8	1	1	0	0	10	

LAYERS	4
DISSOLUTION DATES	20/03/98-26/03/98
PHOTOS	all
FAUNA	3 mono, 1 diplo
OTHER FAUNA	layer 32; retiolitid piece
RIMS/CORES	core of light brown to buff, 3 x 9cm (largest size at layer 23) composed of sand-sized particles. Almost takes up entire squared up concretion.
COLOUR	grey to black with a buff core
BARREN LAYERS	layer 32
BARREN LAYERS	none
PRESERVATION	good

layers	number	chi 2
32	0	2.5
23	4	0.9
15	2	0.1
8	4	0.9

number of layers	4
total number of graps.	10
ave. graps per layer	2.5
total CHI2	4.4
plot on model	1.1

corrected for core

layers	number	chi 2
32	2	1
23	6	1
15	4	0
8	4	0

number of la	4
total numbe	16
ave. graps p	4
total CHI2	2
plot on mod	0.5

v = 3, at 99.9% significance the null hypothesis of random distribution is accepted

Table D28. Dissolution summary of concretion CM 73.8

	parallel	subparallel, prox. down	subparallel, prox. up	near vertica prox. down	near vertical prox. up	TOTAL	
siculae	42	4	1			47	
monograptid 1-2 thecae	4					4	
monograptid 3-4 thecae	2					2	
monograptid mature	2		1			3	9
diplograptid 1-2 thecae	8					8	
diplograptid 3-4 thecae	2					2	
diplograptid mature	3					3	13
total	63	4	2	0	0	69	

LAYERS	13
DISSOLUTION DATES	08/10/97-02/12/1997
PHOTOS	layer 2-23 digital, layer 25-52 photo, no image for 57,64.
FAUNA	9 monos, 13 diplos,
OTHER FAUNA	none
RIMS/CORES	layer 18, 21, 23,25, ; silica nodules 2-5mm diameter: layer 25-64 (end); large insoluble core occupies 80% of surface at layers 45-49.
COLOUR	greyish brown with white/buff core.
BARREN LAYERS	layer 23
BARREN LAYERS	layer 10; mature diplo-para is fragmented
PRESERVATION	lay.2; graps are slightly pyritized: lay.32; some siculae are pyritized, all well preserved: layer 14; graps well preserved just not abundant.

layer	number	chi 2		
64	2	2.2606838	x3	
57	6	0.0384615	x3	
52	2	2.2606838	x3	
49	5	0.0523504	x4	
42	2	2.2606838	x4	
32	9	2.1634615	x3	
25	15	16.163462	x3	
23	0	5.5384615		3
21	5	0.0523504	x2	
18	2	2.2606838	x2	
14	7	0.3856838		
10	10	3.5940171		
2	7	0.3856838		

corrected for core

layer	number	chi 2
64	8	1.2908
57	18	3.0973
52	6	2.9424
49	20	5.4715
42	8	1.2908
32	9	0.7166
25	45	91.762
23	3	6.6779
21	10	0.3102
18	4	5.265
14	7	2.0328
10	10	0.3102
2	7	2.0328

number of layers	13	13
total number of graps.	72	155
ave. graps per layer	5.53846	11.923077
total CHI2	37.4167	123.2
plot on model	2.87821	9.4769231

v = 13 , at 99.9% significance the null hypothesis of random distribution is rejected

Table D29. Dissolution summary of concretion CM 74.9a

	parallel	subparallel, prox. down	subparallel, prox. up	near vertica prox. down	near vertical prox. up	TOTAL	
siculae	39	4	5			48	
monograptid 1-2 thecae	2					2	
monograptid 3-4 thecae						0	
monograptid mature	1	1				2	4
diplograptid 1-2 thecae	6	2	1			9	
diplograptid 3-4 thecae	1					1	
diplograptid mature	2	1				3	13
total	51	8	6	0	0	65	

LAYERS	4
PHOTOS	none
FAUNA	4 monos; 13 diplos
OTHER FAUNA	none
RIMS/CORES	layer 12; large core of white/buff material (7 x 4 cm)
COLOUR	
BARREN LAYERS	none
FRAGMENTED GRAPS	layer 6; one mature mono and one mature diplo fragmented:
PRESERVATION	

BARREN LAYERS

layer	number	chi 2
33	13	0.65
24	12	1.1115385
12	2	12.496154
6	38	29.111538

corrected for core

layer	number	chi 2
33	13	2.59568
24	12	3.36111
12	18	0.25
6	38	15.5586

number of layers	4	4
total number of graps.	65	81
ave. graps per layer	16.25	20.25
total CHI2	43.3692	21.765432
plot on model	10.8423	5.441358

v = 3, at 99.9% significance the null hypothesis of random distribution is rejected

Table D30. Dissolution summary of concretion CM 74.9b

	parallel	subparallel, prox. down	subparallel, prox. up	near vertica prox. down	near vertical prox. up	TOTAL	
siculae	125	10	26	4	4	169	
monograptid 1-2 thecae	12	1	3	1		17	
monograptid 3-4 thecae	2					2	
monograptid mature	5					5	24
diplograptid 1-2 thecae	16	2	2			20	
diplograptid 3-4 thecae	2			2		4	
diplograptid mature	8		2			10	34
total	170	13	33	7	4	227	

LAYERS	6
PHOTOS	
FAUNA	24 monos; 34 diplos
OTHER FAUNA	none reported
RIMS/CORES	layer 16; white/buff core (5.5 x 3 cm)
COLOUR	
BARREN LAYERS	none
FRAGMENTED GRAPS	lay.24; all mature diplos have distal ends that are fragmented but complete proximal ends. layer 5; one diplo is fragmented
BARREN LAYERS	from dissolution; another is clearly fragmented pre-diagenesis.
PRESERVATION	

layer	number	chi 2
38	47	2.1315789
32	16	12.736842
24	14	15.157895
16	13	16.447368
11	47	2.1315789
5	91	73.921053
number of layers	6	
total number of graps.	228	
ave. graps per layer	38	
total CHI2	122.526	
plot on model	20.4211	

corrected for core

layer	number	chi 2	
38	47	0.54352	
32	48	0.35881	x 3
24	42	2.04034	x 3
16	39	3.39703	x 3
11	47	0.54352	
5	91	28.569	**
	6		
	314		
	52.333333		
	35.452229		
	5.9087049		

v = 5, at 99.9% significance the null hypothesis of random distribution is rejected

Table D31. Dissolution summary of concretion CM 75.5

	parallel	subparallel, prox. down	subparallel, prox. up	near vertica prox. down	near vertical prox. up	TOTAL	
siculae	390	26	25	4	12	457	
monograptid 1-2 thecae	95	8	10	1	5	119	
monograptid 3-4 thecae	33	1	2			36	
monograptid mature	222	25	17	4	3	271	426
diplograptid 1-2 thecae	9	1	2			12	
diplograptid 3-4 thecae	2	1		1		4	
diplograptid mature	1	1				2	18
total	752	63	56	10	20	901	

LAYERS	20
PHOTOS	none
FAUNA	426 monos; 18 diplos
OTHER FAUNA	none reported
RIMS/CORES	dark brown core at layers 65, 68
COLOUR	med. Brown
BARREN LAYERS	none
FRAGMENTED GRAPS	layer 72, 91; all mature monos are fragmented: layer 86, evidence of fragmentation prior to burial
PRESERVATION	layer 95, patch of lighter material 4 x 1.1 cm with rounded end and sharp contact with other concretion material (possibly a burrow) - light patch is
BARREN LAYERS	relatively barren of graps. -only one sicula.

layers	number	chi 2		adjustment for core layers	number	chi 2	
105	79	25.584961	**	105	79	23.7715	**
100	52	1.0721976		100	52	0.79657	
95	59	4.3197003		95	59	3.70626	
91	48	0.1931743		91	48	0.09146	
86	61	5.6471143		86	61	4.92933	
82	37	1.4384573		82	37	1.74325	
75	27	7.23202		75	27	7.81507	
72	32	3.7802997		72	32	4.23509	
68	30	5.0278024	core	68	36	2.15457	* 1.20
65	59	4.3197003	core	65	71	13.6562	* 1.20
60	39	0.8124861		60	39	1.0512	
53	113	102.49062	**	53	113	97.839	**
46	71	14.947891	**	46	71	13.6562	**
40	39	0.8124861		40	39	1.0512	
35	25	8.9234739		35	25	9.55174	
30	28	6.4528857		30	28	7.01202	
22	21	12.839123		22	21	13.5474	
16	20	13.929023	**	16	20	14.6551	**
10	26	8.0555494		10	26	8.66164	
5	35	2.2420089		5	35	2.60941	

number of layers	20	20
total number of graps.	901	919
ave. graps per layer	45.05	45.95
total CHI2	177.679	176.49695
plot on model	8.88395	8.8248477

v = 19, at 99.9% significance the null hypothesis of random distribution is rejected

Table D32. Dissolution summary of concretion CM 84.5

	parallel	subparallel, prox. down	subparallel, prox. up	near vertica prox. down	near vertical prox. up	total
siculae	8					8
monograptid 1-2 thecae	4					4
monograptid 3-4 thecae	2					2
monograptid mature	1					1
diplograptid 1-2 thecae						
diplograptid 3-4 thecae						
diplograptid mature						
total	15					15

LAYERS	7
DISSOLUTION DATES	02/02/98-18/02/98
PHOTOS	all 7 good
FAUNA	all monos
OTHER FAUNA	none
RIMS/CORES	core of brown/tan insolubles, greatest at layer 30 (2.5 x 6.5 cm)
COLOUR	dark brown/black
BARREN LAYERS	13, 38
FRAGMENTED GRAPS	lay 7 (1 mono 3th long)

BARREN LAYERS

layer	number	chi 2
50	5	3.8095238
44	3	0.3428571
38	0	2.1428571
30	1	0.6095238
18	5	3.8095238
13	0	2.1428571
7	1	0.6095238

number of layers	7
total number of graps.	15
ave. graps per layer	2.14286
total CHI2	13.4667
plot on model	1.92381

v = 6, at 99.9% significance the null hypothesis of random distribution is rejected

barren layer removed

layer	number	chi 2
50	5	1.3333
44	3	0
30	1	1.3333
18	5	1.3333
7	1	1.3333

number of la	5
total numbe	15
ave. graps p	3
total CHI2	5.3333333
plot on mod	1.0666667

corrected for core

layer	number	chi 2
50	5	1.9248
44	3	0.0301
38	0	2.7143
30	4	0.609
18	6	3.9774
13	0	2.7143
7	1	1.0827

number of layers	7
total number of graps.	19
ave. graps per layer	2.7143
total CHI2	13.053
plot on model	1.8647

Table D33. Dissolution summary of concretion CM 114.4a

	parallel	subparallel, prox. down	subparallel, prox. up	near vertica prox. down	near vertical prox. up	TOTAL	
siculae	8	1	1	1		11	
monograptid 1-2 thecae	2					2	
monograptid 3-4 thecae						0	
monograptid mature	2	1				3	5
diplograptid 1-2 thecae						0	
diplograptid 3-4 thecae						0	
diplograptid mature						0	0
total	12	2	1	1	0	16	

LAYERS	6
PHOTOS	
FAUNA	5 monos, 0 diplos
OTHER FAUNA	none reported
RIMS/CORES	lay. 37; dark brown core 3.5 x 2 cm: lay. 31; 4 x 2.5 cm: lay. 23; 4.5 x 3 cm
COLOUR	grey
BARREN LAYERS	47, 23, 16
FRAGMENTED GRAPS	none reported
PRESERVATION	

BARREN LAYERS

layer	number	chi 2	
60	4	2.3594771	
53	7	13.830065	**
47	0	1.8888889	
43	2	0.0065359	
37	2	0.0065359	
31	1	0.4183007	
23	0	1.8888889	
16	0	1.8888889	
7	1	0.4183007	

corrected for core

layer	number	chi 2
60	4	0.5378
53	7	6.4178
47	0	2.7778
43	2	0.2178
37	4	0.5378
31	4	0.5378
23	3	0.0178
16	0	2.7778
7	1	1.1378

number of layers	9	9
total number of graps.	17	25
ave. graps per layer	1.88889	2.7777778
total CHI2	22.7059	14.96
plot on model	2.52288	1.6622222

v = 8, at 99.9% significance the null hypothesis of random distribution is accepted

Table D34. Dissolution summary of concretion CM 114.4 b

	parallel	subparallel, prox. down	subparallel, prox. up	near vertica prox. down	near vertical prox. up	TOTAL	
siculae	10	1	1			12	
monograptid 1-2 thecae	10	1	1		1	13	
monograptid 3-4 thecae	4	1				5	
monograptid mature	5	2				7	25
diplograptid 1-2 thecae	1					1	
diplograptid 3-4 thecae						0	
diplograptid mature	2					2	3
total	32	5	2	0	1	40	

LAYERS	19
PHOTOS	none
FAUNA	25 monos; 3 diplos
OTHER FAUNA	layer 77, 73; minor rads
	layer 67, 70 many rads, small gastropods and bivalves
RIMS/CORES	layer 46; core is 4 x 6 cm (irregular/kidney bean, not oval);
	layer 37; buff coloured insoluble core 5 x 3 cm.
COLOUR	
BARREN LAYERS	57, 40, 23
FRAGMENTED GRAPS	layer 61; 2 fragments of thin mature mono (one theca and 2 thecae long)
PRESERVATION	layer 46, 52; insoluble buff/brown material covers 1/4 of surface.

BARREN LAYERS

layer	number	chi 2
77	4	1.4486216
73	4	1.4486216
70	3	0.2819549
67	1	0.6629073
61	4	1.4486216
57	0	2.2105263
54	0	2.2105263
52	1	0.6629073
46	1	0.6629073
40	0	2.2105263
37	2	0.0200501
33	1	0.6629073
28	3	0.2819549
23	0	2.2105263
20	3	0.2819549
18	3	0.2819549
15	4	1.4486216
10	5	3.5200501
5	3	0.2819549
number of layers	19	
total number of graps.	42	
ave. graps per layer	2.21053	
total CHI2	16.4236	
plot on model	0.8644	

corrected for core

layer	number	chi 2
77	4	0.94177
73	4	0.94177
70	3	0.11198
67	1	0.87794
61	4	0.94177
57	0	2.47368
54	0	2.47368
52	1	0.87794
46	3	0.11198
40	2	0.09071
37	3	0.11198
33	1	0.87794
28	3	0.11198
23	0	2.47368
20	3	0.11198
18	3	0.11198
15	4	0.94177
10	5	2.58007
5	3	0.11198
	19	
	47	
	2.4736842	
	13.418813	
	0.7062533	

v = 18, at 99.9% significance the null hypothesis of random distribution is accepted

Table D35. Dissolution summary of concretion CM 96-6 loose

	parallel	subparallel, prox. down	subparallel, prox. up	near vertica prox. down	near vertical prox. up	TOTAL	
siculae	8	1				9	
monograptid 1-2 thecae	5	2				7	
monograptid 3-4 thecae	2		1			3	
monograptid mature	2					2	12
diplograptid 1-2 thecae			1			1	
diplograptid 3-4 thecae						0	
diplograptid mature						0	1
total	17	3	2	0	0	22	

LAYERS	14
DISSOLUTION DATES	18/02/98-26/03/98
PHOTOS	all layers
FAUNA	11monos, 1diplo, many retiolitids;
OTHER FAUNA	lay.22; small brachiopod 3mm in length in undissolvable material suspended 1mm above layer: lay 45; 2 small orthocones (7mm length)
RIMS/CORES	layer 40, 45, 53; core of bitumen 35mm diameter at layer 45: layer 64; rimming of undissovable material
COLOUR	dark brown concretion with black core of more granular material and with clumps of white to buff to brown undissovable material
BARREN LAYERS	layer 12, 27
FRAGMENTED GRAPS	layer 17; 3 fragments of mat-monos all 2 thecae long: layer 22; broken siculae: layer 32; one cyrtograptid fragment 3 thecae long: layer 53; graptolite periderm broken/fragmented
PRESERVATION	layer 53; graptolite periderm broken/fragmented, encrusted and flattened: layer 75; graptolite is pocketed with holes

layers	number	chi 2	
75	4	3.047619	**
68	2	0.047619	
64	4	3.047619	**
60	1	0.297619	
53	2	0.047619	
45	0	1.7142857	
40	1	0.297619	
32	1	0.297619	
27	0	1.7142857	
22	1	0.297619	
17	1	0.297619	
12	0	1.7142857	
10	3	0.9642857	
6	4	3.047619	**

number of layers	14
total number of graps.	24
ave. graps per layer	1.71429
total CHI2	16.8333
plot on model	1.20238

core correction

layers	number	chi 2
75	4	1.6095
68	2	0.0095
64	4	1.6095
60	1	0.6095
53	4	1.6095
45	2	0.0095
40	3	0.3429
32	1	0.6095
27	0	2.1429
22	1	0.6095
17	1	0.6095
12	0	2.1429
10	3	0.3429
6	4	1.6095

number of layers	14
total number of graps.	30
ave. graps per layer	2.1429
total CHI2	13.867
plot on model	0.9905

v = 13, at 99.9% significance the null hypothesis of random distribution is accepted

Table D36. Dissolution summary of concretion CP 32

	parallel	subparallel, prox. down	subparallel, prox. up	near vertica prox. down	near vertical prox. up	total
siculae	7		1			8
monograptid 1-2 thecae	1					1
monograptid 3-4 thecae	1	1				2
monograptid mature	7	4				11
diplograptid 1-2 thecae			1			1
diplograptid 3-4 thecae						
diplograptid mature						
total	16	5	2			23

LAYERS	13
DISSOLUTION DATES	16/12/98-29/01/98
PHOTOS	9/13 (7,22,33,36,40,43,47,50,53)
FAUNA	all monos except one diplo on layer 5; questionable mature mono on layer 22 because of fragmentation
OTHER FAUNA	lay 12, 17; cylindrical objects (possibly encrusted graps): lay 33; possibl orhtocone: lay 40; large coarse-grained object at center of core
RIMS/CORES	black core (3cm daimeter) of fine grained mudstone surrounded by a white/buff material with an internal object of the same white/buff
BARREN LAYERS	material (possibly organic in origin)
COLOUR	brown to tan with a black core
BARREN LAYERS	lay 43
FRAGMENTED GRAPS	lay 5; diplo 1-2: lay 7; mat. Mono plus 2 unidenifiable grap fragments: lay 28; fragment of unidentifiable grap: lay 36; 2 fragments of mature monos: lay 50; 3 fragments of mat. Mono
PRESERVATION:	many graps are crushed, broken and flattened, graps inside of core are preserved sub-parallel

layer	number	chi 2
53	3	0.8561873
50	3	0.8561873
47	3	0.8561873
43	0	1.7692308
40	1	0.3344482
36	1	0.3344482
33	1	0.3344482
28	1	0.3344482
22	1	0.3344482
17	2	0.0301003
12	3	0.8561873
7	2	0.0301003
5	2	0.0301003

number of layers	13
total number of graps.	23
ave. graps per layer	1.76923
total CHI2	6.92642
plot on model	0.5328

v = 12, at 99.9% significance the null hypothesis of random distribution is accepted

Table D37. Dissolution summary of concretion CP 38.4

	parallel	subparallel, prox. down	subparallel, prox. up	near vertica prox. down	near vertical prox. up	TOTAL	
siculae	2		2			4	
monograptid 1-2 thecae	7					7	
monograptid 3-4 thecae	1					1	
monograptid mature	4		1			5	13
diplograptid 1-2 thecae						0	
diplograptid 3-4 thecae	1?					0	
diplograptid mature						0	0
total	14	0	3	0	0	17	

LAYERS	14
DISSOLUTION DATES	03/02/98-19/03/98
PHOTOS	all layers
FAUNA	all monos - one possible diplo layer43 but crushed and broken beyond recognition: lay 71; one retiolitid
OTHER FAUNA	none.
RIMS/CORES	none.
COLOUR	light brown
BARREN LAYERS	layers 7, 14, 20, 28, 36, 50
BARREN LAYERS	lay.41; large mono is terribly fragmented (related to processing methods or preservation?): lay 43; possible diplo is crshed and broken beyond recognition: lay 50; one fragment of a possible graptolite: lay
PRESERVATION	lay.26; graps are flattened: lay 56 both graps are slightly pyritized and the sicula is flattened: lay 64; monos are flattened in ceratin parts of the rhabdosome - parts not flattened include the thecal apertures which seem to be thickened with thecal apparatus (spines): lay 71; monos are flattened: lay 77; monos are collapsed "flattened".

layer	number	chi 2
77	5	10.730159
71	2	0.3968254
64	2	0.3968254
56	2	0.3968254
50	0	1.2857143
43	1	0.0634921
41	1	0.0634921
36	0	1.2857143
32	2	0.3968254
28	0	1.2857143
26	3	2.2857143
20	0	1.2857143
14	0	1.2857143
7	0	1.2857143

number of layers	14
total number of graps.	18
ave. graps per layer	1.28571
total CHI2	19.873
plot on model	1.4195

v = 13, at 99.9% significance the null hypothesis of random distribution is accepted

Table D38. Dissolution summary of concretion CP 56.9

	parallel	subparallel, prox. down	subparallel, prox. up	near vertica prox. down	near vertical prox. up	TOTAL	
siculae	9					9	
monograptid 1-2 thecae	2					2	
monograptid 3-4 thecae	3					3	
monograptid mature						0	5
diplograptid 1-2 thecae	1					1	
diplograptid 3-4 thecae						0	
diplograptid mature	1					1	2
total	16	0	0	0	0	16	

LAYERS	12
PHOTOS	none
FAUNA	5 monos; 2 diplos
OTHER FAUNA	layer 58; rare rads and sponge spicules: layer 44; mass of white spheres (1mm diameter each with total mass aobut 3 cm): layer 36; rare rads: layers 10, 19, 25; abundant rads: layer 7 common rads
RIMS/CORES	none
COLOUR	
BARREN LAYERS	layers 66, 36, 30, 7
BARREN LAYERS	none reported
PRESERVATION	layer 7; possibly encrusted graps.

layer	number	chi 2
83	2	0.4807692
78	1	0.0432692
72	4	6.2307692
66	0	1.2307692
58	1	0.0432692
53	2	0.4807692
44	1	0.0432692
36	0	1.2307692
30	0	1.2307692
25	1	0.0432692
19	2	0.4807692
10	2	0.4807692
7	0	1.2307692

number of layers	13
total number of graps.	16
ave. graps per layer	1.23077
total CHI2	13.25
plot on model	1.01923

v = 12, at 99.9% significance the null hypothesis of random distribution is accepted

Table D39. Dissolution summary of concretion CP 96

	parallel	subparallel, prox. down	subparallel, prox. up	near vertica prox. down	near vertical prox. up	TOTAL	
siculae	5					5	
monograptid 1-2 thecae						0	
monograptid 3-4 thecae						0	
monograptid mature	1					1	1
diplograptid 1-2 thecae						0	
diplograptid 3-4 thecae						0	
diplograptid mature						0	0
total	6	0	0	0	0	6	

LAYERS	12
DISSOLUTION DATES	03/12/97-07/01/98
PHOTOS	missing 9/12 (have layers 18, 31,40)
FAUNA	1 mono, no diplos
OTHER FAUNA	3-5mm long encrusted cylindrical shaped objects; many radiolarians; layer 14; two orthocones; layer21; brachiopod (2.5width x 2mm height); layer 24; one orthocone: layer 31; parabola-shaped sponge spicule mass with spicules in lattice (hectinae spicules):
RIMS/CORES	none
BARREN LAYERS	light to med. Brown
BARREN LAYERS	8/12 barren (layers 6, 8, 14, 24, 31, 35, 51, 45)
FRAGMENTED GRAPS	none
PRESERVATION	layer 40; mature mono is pyritized - rhabdosome appears compacted.

layer	number	chi 2
51	0	0.5
45	0	0.5
40	3	12.5
35	0	0.5
31	0	0.5
24	0	0.5
21	1	0.5
18	1	0.5
14	0	0.5
8	0	0.5
6	0	0.5
4	1	0.5

number of layers	12
total number of graps.	6
ave. graps per layer	0.5
total CHI2	18
plot on model	1.5

v = 11, at 99.9% significance the null hypothesis of random distribution is accepted

Table D40. Dissolution summary of concretion CP 145.2

	parallel	subparallel, prox. down	subparallel, prox. up	near vertica prox. down	near vertical prox. up	TOTAL	
siculae						0	
monograptid 1-2 thecae						0	
monograptid 3-4 thecae						0	
monograptid mature	3					3	3
diplograptid 1-2 thecae						0	
diplograptid 3-4 thecae						0	
diplograptid mature						0	0
total	3	0	0	0	0	3	

LAYERS	4
PHOTOS	none
FAUNA	3 monos
OTHER FAUNA	none reported
RIMS/CORES	none
COLOUR	
BARREN LAYERS	layers 19, 11
FRAGMENTED GRAPS	layer 6; mono is fragmented
PRESERVATION	layer 19; very muddy.

BARREN LAYERS

layer	number	chi 2
19	0	0.75
13	2	2.0833333
11	0	0.75
6	1	0.0833333

number of layers	4
total number of graps.	3
ave. graps per layer	0.75
total CHI2	3.66667
plot on model	0.91667

v = 3, at 99.9% significance the null hypothesis of random distribution is accepted

Table D41. Dissolution summary of concretion CP 146.5 a

	parallel	subparallel, prox. down	subparallel, prox. up	near vertica prox. down	near vertical prox. up	TOTAL	
siculae	1					1	
monograptid 1-2 thecae	1	1	1			3	
monograptid 3-4 thecae						0	
monograptid mature						0	3
diplograptid 1-2 thecae						0	
diplograptid 3-4 thecae						0	
diplograptid mature						0	0
total	2	1	1	0	0	4	

LAYERS	5
DISSOLUTION DATES	
PHOTOS	none
FAUNA	3 monos
OTHER FAUNA	layer 12; encrusted rads.
RIMS/CORES	none
COLOUR	
BARREN LAYERS	layers 7, 27
FRAGMENTED GRAPS	none reported
BARREN LAYERS	

layer	number	chi 2
37	1	0.05
27	0	0.8
20	2	1.8
12	1	0.05
7	0	0.8

number of layers	5
total number of graps.	4
ave. graps per layer	0.8
total CHI2	3.5
plot on model	0.7

v = 4 , at 99.9% significance the null hypothesis of random distribution is accepted

Table D42. Dissolution summary of concretion CP 146.5 b

	parallel	subparallel, prox. down	subparallel, prox. up	near vertica prox. down	near vertical prox. up	TOTAL	
siculae						0	
monograptid 1-2 thecae			1			1	
monograptid 3-4 thecae						0	
monograptid mature						0	1
diplograptid 1-2 thecae				1		1	
diplograptid 3-4 thecae						0	
diplograptid mature						0	1
total	0	0	1	1	0	2	

LAYERS	5
PHOTOS	none
FAUNA	1 mono; 1 diplo
OTHER FAUNA	layer 37; crinoid ossicles: layer 27; orthocone 1cm long
	layer 10, 22; rare rads
RIMS/CORES	none
COLOUR	
BARREN LAYERS	layers 22, 27, 37
FRAGMENTED GRAPS	none reported
BARREN LAYERS	lay.10, 16, 22; clusters of silica nodules, + insoluble buff/brown material

layer	number	chi 2
37	0	0.4
27	0	0.4
22	0	0.4
16	1	0.9
10	1	0.9

number of layers	5
total number of graps.	2
ave. graps per layer	0.4
total CHI2	3
plot on model	0.6

v = 4, at 99.9% significance the null hypothesis of random distribution is accepted

Table D43. Dissolution summary of concretion CP 148.1

	parallel	subparallel, prox. down	subparallel, prox. up	near vertica prox. down	near vertical prox. up	TOTAL	
siculae	113		3		1	117	
monograptid 1-2 thecae	9					9	
monograptid 3-4 thecae	5					5	
monograptid mature	8		2			10	24
diplograptid 1-2 thecae						0	
diplograptid 3-4 thecae						0	
diplograptid mature						0	0
total	135	0	5	0	1	141	

LAYERS	9
DISSOLUTION DATES	
PHOTOS	none
FAUNA	24 monos, 0 diplos
OTHER FAUNA	layer 51; two orthocones (1.5 and 2.5 cm long): layer 22; two orthocones, minor rads: layer 13; orthocone (2 cm long)
RIMS/CORES	none
COLOUR	
BARREN LAYERS	none
BARREN LAYERS	layer 33; mono is fragmented; layer 8: mature monos are fragmented
PRESERVATION	

layer	number	chi 2		
41	12	0.858156		
37	8	3.751773		
33	55	98.751773	**	51 sicula
27	22	2.5602837		
22	5	7.2624113		
17	13	0.4539007		
13	6	5.964539		
11	11	1.3900709		
8	9	2.8368794		

number of layers	9
total number of graps.	141
ave. graps per layer	15.6667
total CHI2	123.83
plot on model	13.7589

v = 8, at 99.9% significance the null hypothesis of random distribution is rejected

Table D44. Dissolution summary of concretion CP 150.6

	parallel	subparallel, prox. down	subparallel, prox. up	near vertica prox. down	near vertical prox. up	TOTAL
siculae	6					6
monograptid 1-2 thecae	4					4
monograptid 3-4 thecae						0
monograptid mature	10	1				11
diplograptid 1-2 thecae						
diplograptid 3-4 thecae						
diplograptid mature	1					
total	21	1	22			44

LAYERS	9 (remove 49, 50 from survey)
DISSOLUTION DATES	15/01/98-17/02/98
PHOTOS	all layers
FAUNA	all monos
OTHER FAUNA	abundant orthocones, slightly pyritized: lay 5; 8 orthocones, two largest 0.7cm diameter: lay 14; retiolitid 15mm in length, 9 orthocones: lay 19; are 15 orthocones: lay 23; large orthocone still present plus 4 small ones: lay 27; 4 orhtocones: lay 39; 7 orthocones: lay 41; 5 orthocones: lay 47; 9orthocones: lay 48; 2 orthocones (many fragments of graps): lay 50;
BARREN LAYERS	49 orthocones: lay 50; brachiopod imprint,retiolitid, 2 orthocones
RIMS/CORES	none
COLOUR/LITHOLOGY	brown; very "muddy", many fine grained undissovables
BARREN LAYERS	2/11(5,14)
FRAGMENTED GRAPS	lay 27; fragment 2 thecae long: lay 39; 2 mat.mono fragments 2-3 th in length: lay48; 4 fragments of mat.monos 1 to 4 thecae in length, 2 fragments of unidentifiable graps.: lay 49; two mono fragments (<2th)

layer	number	chi 2
49	4	0.8164251
47	1	0.9468599
41	1	0.9468599
39	3	0.0772947
27	8	11.599034
23	3	0.0772947
19	1	0.9468599
14	2	0.1207729
5	0	2.5555556

number of layers	9
total number of graps.	23
ave. graps per layer	2.55556
total CHI2	15.5314
plot on model	1.72571

v = 8, at 99.9% significance the null hypothesis of random distribution is accepted

Table D45. Dissolution summary of concretion CP 152 a

	parallel	subparallel, prox. down	subparallel, prox. up	near vertica prox. down	near vertical prox. up	TOTAL	
siculae	38	4	5			47	
monograptid 1-2 thecae	5	1	1			7	
monograptid 3-4 thecae						0	
monograptid mature	8					8	15
diplograptid 1-2 thecae						0	
diplograptid 3-4 thecae						0	
diplograptid mature						0	0
total	51	5	6	0	0	62	

LAYERS	8
PHOTOS	none
FAUNA	15 monos; 0 diplos
OTHER FAUNA	layer 13, 17; common rads
	layer 6, 24; sponge spicule mass covers 1/3 of surface.
	layer 10, 13, 17; insoluble material (spicules) covers 1/2 of surface
	lay.6; solitary coral (4 x 1 cm), tabulate - silica preserves striated walls
RIMS/CORES	none
COLOUR	
BARREN LAYERS	none
FRAGMENTED GRAPS	none
PRESERVATION	

layer	number	chi 2
43	22	34.453704
34	15	10.083333
31	2	3.3425926
24	4	1.1203704
17	3	2.0833333
13	1	4.8981481
10	5	0.4537037
6	2	3.3425926

number of layers	8
total number of graps.	54
ave. graps per layer	6.75
total CHI2	59.7778
plot on model	7.47222

corrected for spicule mass

layer	number	chi 2
43	22	22.9167
34	15	5.52273
31	2	4.73485
24	6	0.61364
17	6	0.61364
13	2	4.73485
10	10	0.37121
6	3	3.34091

number of l	8
total numbe	66
ave. graps p	8.25
total CHI2	42.848485
plot on mod	5.3560606

v = 7, at 99.9% significance the null hypothesis of random distribution is rejected

Table D46. Dissolution summary of concretion CP 152 b

	parallel	subparallel, prox. down	subparallel, prox. up	near vertica prox. down	near vertical prox. up	TOTAL	
siculae	16	2	1			19	
monograptid 1-2 thecae	1					1	
monograptid 3-4 thecae	1					1	
monograptid mature	8		1			9	11
diplograptid 1-2 thecae						0	
diplograptid 3-4 thecae						0	
diplograptid mature						0	0
total	26	2	2	0	0	30	

LAYERS	8
PHOTOS	none
FAUNA	11 monos
OTHER FAUNA	none reported
RIMS/CORES	none
COLOUR	
BARREN LAYERS	layer 5
FRAGMENTED GRAPS	layer 40; evidence of fragmentation of mature mono
PRESERVATION	layer 26; 3 of 4 mature monos are aligned.

BARREN LAYERS

layer	number	chi 2
40	5	0.1773399
26	5	0.1773399
22	4	0.0049261
19	5	0.1773399
17	3	0.3152709
11	7	1.9704433
5	0	4.1428571

number of layers	7
total number of graps.	29
ave. graps per layer	4.14286
total CHI2	6.96552
plot on model	0.99507

v = 7, at 99.9% significance the null hypothesis of random distribution is accepted

Table D47. Dissolution summary of concretion CP 162.8

	parallel	subparallel, prox. down	subparallel, prox. up	near vertica prox. down	near vertical prox. up	TOTAL	
siculae	2					2	
monograptid 1-2 thecae	4					4	
monograptid 3-4 thecae						0	
monograptid mature	3				1	4	8
diplograptid 1-2 thecae						0	
diplograptid 3-4 thecae						0	
diplograptid mature	2					2	2
total	11	0	0	0	1	12	

LAYERS	6
PHOTOS	none
FAUNA	8 monos; 2 diplos (all retiolitids)
OTHER FAUNA	lay.33 many small white nodules, some elongate and irregular (burrows?). layer 33; rare radiolarians
RIMS/CORES	none
COLOUR	
BARREN LAYERS	5, 33
FRAGMENTED GRAPS	none reported
BARREN LAYERS	nodules on layer 33

layer	number	chi 2
33	0	2
25	4	2
19	3	0.5
13	2	0
9	3	0.5
5	0	2

number of layers	6
total number of graps.	12
ave. graps per layer	2
total CHI2	7
plot on model	1.16667

v = 5, at 99.9% significance the null hypothesis of random distribution is accepted

Table D48. Dissolution summary of concretion CP 163a

	parallel	subparallel, prox. down	subparallel, prox. up	near vertica prox. down	near vertical prox. up	TOTAL	
siculae	15	1				16	
monograptid 1-2 thecae	4	2				6	
monograptid 3-4 thecae	2					2	
monograptid mature	5	1				6	14
diplograptid 1-2 thecae	2					2	
diplograptid 3-4 thecae						0	
diplograptid mature						0	2
total	28	4	0	0	0	32	

LAYERS	9
DISSOLUTION DATES	24/11/97-10/12/1997
PHOTOS	missing 6/9 (have layers 3, 9, 43)
FAUNA	14 monos, 2 diplos
OTHER FAUNA	sponge spicules and radiolaria; layer 17, 30; unidentified white cylindrical forms (encrusted graps? Orthocones?):
RIMS/CORES	core: layer 30, 36, 43
COLOUR	dark brown
BARREN LAYERS	layer 12
BARREN LAYERS	none
PRESERVATION	no obs.

layer	number	chi 2
43	1	1.8368056
36	4	0.0555556
30	3	0.0868056
26	6	1.6805556
21	5	0.5868056
17	3	0.0868056
12	0	3.5555556
9	9	8.3368056
3	1	1.8368056

layer	number	chi 2
43	4	0.0117
36	6	0.7485
30	4	0.0117
26	6	0.7485
21	5	0.1433
17	3	0.3538
12	0	4.2222
9	9	5.4064
3	1	2.4591

number of layers	9	number of l	9
total number of graps.	32	total numbe	38
ave. graps per layer	3.55556	ave. graps p	4.2222222
total CHI2	18.0625	total CHI2	14.105263
plot on model	2.00694	plot on mod	1.5672515

v = 8, at 99.9% significance the null hypothesis of random distribution is accepted

Table D49. Dissolution summary of concretion CP 163b

	parallel	subparallel, prox. down	subparallel, prox. up	near vertica prox. down	near vertical prox. up
siculae	6				
monograptid 1-2 thecae	2				
monograptid 3-4 thecae	1				
monograptid mature					
diplograptid 1-2 thecae					
diplograptid 3-4 thecae					
diplograptid mature					
total	9				

LAYERS	5
DISSOLUTION DATES	23/11/97-03/12/97
PHOTOS	2/5 (6,12)
FAUNA	all monos
OTHER FAUNA	lay 6; orthocone, hemispherical bryozoan(?): lay 12; bryozoan(same) lay25; unidentified cylindrical encrusted object.
RIMS/CORES	layer 17 insoluble material covers 30%
COLOUR	brown to light tan
BARREN LAYERS	layer 32
FRAGMENTED GRAPS	none

BARREN LAYERS

layer	number	chi 2
32	0	1.8
25	2	0.0222222
17	2	0.0222222
12	3	0.8
6	2	0.0222222

number of layers	5
total number of graps.	9
ave. graps per layer	1.8
total CHI2	2.666667
plot on model	0.533333

corrected for core

layer	number	chi 2
32	0	2
25	2	0
17	3	0.5
12	3	0.5
6	2	0

number of la	5
total numbe	10
ave. graps p	2
total CHI2	3
plot on mod	0.6

v = 4, at 99.9% significance the null hypothesis of random distribution is accepted

Table D50. Dissolution summary of concretion CP 163.1

	parallel	subparallel, prox. down	subparallel, prox. up	near vertica prox. down	near vertical prox. up	TOTAL	
siculae	11		1			12	
monograptid 1-2 thecae	9	1	2			12	
monograptid 3-4 thecae	3	1				4	
monograptid mature	5		1	1		7	23
diplograptid 1-2 thecae						0	
diplograptid 3-4 thecae						0	
diplograptid mature						0	0
total	28	2	4	1	0	35	

LAYERS	10
PHOTOS	none
FAUNA	23 monos
OTHER FAUNA	layers 19 - 38 (less common on 41, 47); white/buff irregular tubes, approx. 1mm long and diameter of 10um. - possibly burrows or diagenetic nodules: layers 19 - 38 (less common on 41, 47); radiolarian.
RIMS/CORES	none
COLOUR	
BARREN LAYERS	none
FRAGMENTED GRAPS	none reported
BARREN LAYERS	irregular tubes on layers 19-47 could be remobilized silica from the rads.

layer	number	chi 2
47	3	0.1
41	4	0.0444444
38	1	1.8777778
34	7	3.2111111
28	2	0.7111111
23	3	0.1
19	1	1.8777778
16	3	0.1
12	5	0.5444444
6	7	3.2111111

number of layers	10
total number of graps.	36
ave. graps per layer	3.6
total CHI2	11.7778
plot on model	1.17778

v = 9, at 99.9% significance the null hypothesis of random distribution is accepted

Table D51. Dissolution summary of concretion CP 214.5

	parallel	subparallel, prox. down	subparallel, prox. up	near vertica prox. down	near vertical prox. up	TOTAL	
siculae	29	4	3		1	37	
monograptid 1-2 thecae	28			1	2	31	
monograptid 3-4 thecae	7					7	
monograptid mature	2615	42	35	5	3	2700	2738
diplograptid 1-2 thecae						0	
diplograptid 3-4 thecae						0	
diplograptid mature	4					4	4
total	2683	46	38	6	6	2779	

LAYERS	21
PHOTOS	lay27-66
FAUNA	2738 monos; 4 diplos
OTHER FAUNA	lay.44; orthocones; gastropod; bivalves; sponge spicules: lay12: orthocone lay40; 2 orthocones: rads abundant on all layers but lay.61-72 lay48; spnoge spicule mass
RIMS/CORES	none
COLOUR	
BARREN LAYERS	ncne
BARREN LAYERS	lay 36; fragmented mat. Mono: lay40, fragmentation prior to burial lay53: fragmentation of M. priodons lay57-66: fragmentation
PRESERVATION	lay36;SE corner a cluster of M.priodon shows a NW-SE orientation; lay44; SE corner is all aligned (NW-SE) M.priodon, NW corner is all a type of Pribylograptus (aligned N-S, not parallel to bedding) lay53: North side, many graps exposed,NE is more flat-lying aligned (NE-SW) branching Pribylograptids, NW is more chaotic (some oriented NE-SW) Pribylograptids and some priodons, many are flattened, many of the pribylograptids here are bent. SE corner M. priodon and minor Pribylograptids are aligned NE-SW, evidence of fragmentation of the priodon and bending of the pribylograptids. lay57; majority of graptolites are oriented NE-SW; some on the West side are oriented E-W. Distribution of two species is more random than in previous layers lay61: bent pribylograptids and curved priodons, many flattened pribylodgraptids (in SW corner and middle to west half of concretion surface. Priodons are not flattened. More priodons to the NW. Most grapps are aligned NE-SW but some in center and to the North are chaoticly oriented. lay66: less strongly oriented than previous layers.-Graps bent and fragmented lay76: very little azimuthal orientation; not all of surface is covered with graps. lay82: no alignment, lay 95: matures are aligned NW-SE, lay102: aligned lay95; matures are aligned NW-SE

Dissolution summary (continued) Concretion: CP 214.5

layer	number	chi 2	
102	17	100.51721	
95	6	120.60537	
87	2	128.36356	
82	60	39.537364	**
76	355	374.66331	
72	519	1129.8069	
66	478	902.91268	
61	422	634.05626	**
57	375	444.99076	**
53	266	135.01343	
48	109	4.1141898	
44	49	52.47691	
40	49	52.47691	
36	32	76.071369	
32	9	114.94542	
27	7	118.70361	
23	1	130.34089	
16	4	124.45424	
12	3	126.40134	
9	5	122.52225	
4	11	111.24769	

number of layers	21
total number of graps.	2779
ave. graps per layer	132.333
total CHI2	4195.61
plot on model	199.791

v = 20 , at 99.9% significance the null hypothesis of random distribution is rejected

Table D52. Dissolution summary of concretion CP 96a 6.0

	parallel	subparallel, prox. down	subparallel, prox. up	near vertica prox. down	near vertical prox. up	TOTAL	
siculae	10	2				12	
monograptid 1-2 thecae	6					6	
monograptid 3-4 thecae						0	
monograptid mature	4					4	10
diplograptid 1-2 thecae						0	
diplograptid 3-4 thecae						0	
diplograptid mature	3					3	3
total	23	2	0	0	0	25	

LAYERS	8 (layer 56 not included)
DISSOLUTION DATES	April 28, 98 - May 6, 98
PHOTOS	none
FAUNA	10 monos; 3 diplos
OTHER FAUNA	layer 8; spar filled cavity (organic origin?, possibly orthocone).
RIMS/CORES	
COLOUR	
BARREN LAYERS	49
FRAGMENTED GRAPS	layer 20; one very large mon is broken in two with
BARREN LAYERS	two pieces ~45 degrees apart.
PRESERVATION	layer 56; not dissolving - comes into the sieve as mud chunks (flocs?)
	many pyrtized graptolites from different layers

layer	number	chi 2
55	3	0.005
49	0	3.125
44	2	0.405
38	3	0.005
27	4	0.245
20	4	0.245
8	7	4.805
4	2	0.405

number of layers	8
total number of graps.	25
ave. graps per layer	3.125
total CHI2	9.24
plot on model	1.155

v = 7, at 99.9% significance the null hypothesis of random distribution is accepted

Table D53. Dissolution summary of concretion CP 96a 7.5

	parallel	subparallel, prox. down	subparallel, prox. up	near vertica prox. down	near vertical prox. up	TOTAL
siculae	37		2			39
monograptid 1-2 thecae	6		2			8
monograptid 3-4 thecae	8	1	2		1	12
monograptid mature	26	5	1			32
diplograptid 1-2 thecae						
diplograptid 3-4 thecae						
diplograptid mature						
total	77	6	83		1	91

LAYERS	10 but only 9 used in study... layer 55 was unreliable.
DISSOLUTION DATES	16/12/97-21/01/98
PHOTOS	3/10 (14, 40, 55)
FAUNA	all monos (many mature), some retiolitids
OTHER FAUNA	lay 14: 2 unidentified objects, organic black possibly trilobite
RIMS/CORES	rim of compositional difference which dissolves more slowly (dolomite?) but is not blackened
COLOUR	light brown
BARREN LAYERS	none
BARREN LAYERS	lay 51; frag. mat mono.

layer	number	chi 2
51	7	0.9
44	12	0.4
40	5	2.5
34	10	0
28	13	0.9
21	12	0.4
14	12	0.4
8	8	0.4
6	11	0.1

number of layers	9
total number of graps.	90
ave. graps per layer	10
total CHI2	6
plot on model	0.66667

v = 10, at 99.9% significance the null hypothesis of random distribution is accepted

Appendix E

Species distribution: thecal count raw data.

Table E1. Thecal counts from dissolution residues of CM 40.5-40.6.

CM 40.5 - 40.6 thecae count	0-12	12-22	22-30	30-40	40-49	49-59	59-68	68-72	72-88	22-30
Glyptograptus incertus	20	72	0	23	8	12	10	10	0	0
distal		12		4						
theca 3-1 or 4-2										
theca 1-1 to 2-2	14	43		14	5	8	6	7		
sicula	6	17		5	3	4	4	3		
Agetograptus hubeiensis	12	127	22	89	37	212	157	53	39	16
distal		39				39	30	5	9	
theca 3-1 or 4-2		20		2	2	36	27	9	4	
theca 1-1 to 2-2	9	50	15	61	25	102	74	29	20	11
sicula	3	18	7	26	10	35	26	10	6	5
Neodiplograptus elongatus	8	0	36	36	4	22	0	0	0	27
distal			36	28		8				27
theca 3-1 or 4-2				3		4				
theca 1-1 to 2-2	6			4	3	8				
sicula	2			1	1	2				
Diplograptid	59	141	88	197	99	130	107	44	48	66
distal		25		19	22	45	35	16	18	
theca 1-1 to 2-2	30	58	44	89	39	43	36	14	15	33
sicula	29	58	44	89	38	42	36	14	15	33
Coronograptus minisculus	14	2	0	0	0	0	0	0	3	0
distal	14	2							3	
theca 1-2										
sicula										
Pribylograptus pleganopsis	2	2	13	29	3	1	0	0	0	10
distal	2		13	24	1					10
proximal		2		5	2	1				
theca 1-2										
sicula										

		note: layer 22-30 was spilled
		sample has been multiplied by 1.33
number of diplograptid species	3	to account for the third that was spilled
number of monograptid species	2	
number of species	7	
total diplograptid theca	2031	
total monograptid theca	79	
total graptolite theca	2110	all specimens are flattened.

Table E2. Thecal counts from dissolution residues of CM 41.65-41.75

CM 41.65 - 41.75 thecae count	0-6	6-13	13-19	19-27	27-33	33-39
Metaclimacograptus minimus	67	72	87	63	81	229
distal	12	3	14	17	14	34
theca 3-1 or 4-2	7		7	8	8	31
theca 1-1 to 2-2	31	47	42	25	36	115
sicula	17	22	24	13	23	49
Glyptograptus incertus	33	12	8	17	3	13
distal						
theca 3-1 or 4-2	1					
theca 1-1 to 2-2	21	7	5	10	2	7
sicula	11	5	3	7	1	6
Agetograptus hubeiensis	4					
distal						
theca 3-1 or 4-2						
theca 1-1 to 2-2	3					
sicula	1					
***Normalograptus* sp.**	0	22	34	49	37	54
distal						
theca 3-1 or 4-2			6	1		
theca 1-1 to 2-2		14	19	33	22	34
sicula		8	9	15	15	20
Diplograptid	76	90	57	66	50	89
distal					2	11
theca 1-1 to 2-2	40	46	31	34	25	42
sicula	36	44	26	32	23	36
Coronograptus minisculus	40	59	55	19	17	91
distal	21	29	29	10	10	35
theca 1-2	11	16	14	5	4	31
sicula	8	14	12	4	3	25
Huttagraptus praestrachani	0	18	0	0	0	1
distal		6				
mesial		5				
proximal		7				1
sicula						
Monograptid	0	0	0	0	2	0
distal						
mesial						
proximal					2	
sicula						

number of diplograptid species	3
number of monograptid species	2
number of species	5
total diplograptid theca	1309
total monograptid theca	302
total graptolite theca	1611

Table E3. Thecal counts from dissolution residues of CM 42.3-42.3

CM 42.3-42.4 thecae count	7-13	13-23	23-30	30-41	41-47	47-53	53-58	58-64	64-70	70-74	74-78	78-86	86-94	94-102
Glyptograptus incertus	18	5	0	9	12	0	3	3	0	9	0	17	9	58
distal														
theca 3-1 or 4-2	2													3
theca 1-1 to 2-2	11	4		6	9		2	2		6		12	6	42
sicula	5	1		3	3		1	1		3		5	3	13
***Petalolithus* sp.**	0	0	0	0	0	0	0	0	0	0	0	0	0	4
distal														
theca 3-1 or 4-2														
theca 1-1 to 2-2														3
sicula														1
Agetograptus hubeiensis	35	42	0	90	132	69	54	64	36	22	14	48	40	114
distal		6		8	3	9	8				1			20
theca 3-1 or 4-2	6	6		13	20	11	11	6	4	6	4	8	1	16
theca 1-1 to 2-2	23	23		51	83	37	27	44	24	12	7	30	29	60
sicula	6	7		18	26	12	8	14	8	4	2	10	10	18
***Normalograptus* sp.**	7	6	4	0	0	13	11	28	0	0	7	0	3	0
distal														
theca 3-1 or 4-2	2	1				2					2			
theca 1-1 to 2-2	4	4	3			8	8	20			4		2	
sicula	1	1	1			3	3	8			1		1	
Diplograptid	55	97	63	173	193	58	138	170	109	94	95	103	153	119
distal	4	16	10	9	23		11	9		15	8	11	15	23
theca 1-1 to 2-2	26	43	27	84	87	30	65	82	55	40	44	47	70	49
sicula	25	38	26	80	83	28	62	79	54	39	43	45	68	47
Coronograptus minusculus	3	1	0	0	5	0	4	6	2	0	0	3	2	2
distal		1			3		4	6				1		
theca 1-2	2				1				1			1	1	1
sicula	1				1				1			1	1	1
Pribylograptus leptotheca	25	73	28	88	83	58	64	21	3	6	17	20	1	62
distal	7	54	0	88	32	14	61	15			5	3		35
mesial - distal	18	9	0		38	10			2	1		7	1	10
mesial		10	0		13	34	3	6	1	5	12	10		17
proximal	21	14	26	96	109	71	26	67	73	51	49	79	84	178
theca 1			1	2	2	2		4	15	4	1	12	15	34
sicula			1	2	2	2		4	15	4	1	12	15	34
Huttagraptus praestrachani	0	0		0	0	0	0	0	0	4	0	6	9	45
distal										4		6	9	45
theca one														
sicula														
Pristiograptus biformis	0	0	0	0	0	0	0	0	0	0	0	0	0	13
distal														6
theca one														7
sicula														
Monograptid	2	2	4	4	4	0	2	10	2	0	0	0	0	0
distal														
proximal	1	1	2	2	2		1	5	1					
sicula	1	1	2	2	2		1	5	1					

number of diplograptid species	4
number of monograptid species	4
number of species	8
total diplograptid theca	2606
total monograptid theca	656
total graptolite theca	3262

Table E4. Thecal counts from dissolution residues of CM 42.8-42.9

CM 42.8-42.9 thecae count	0-7	7-12	12-22	22-26	26-32	32-39	39-44
Pseudorthograptus inopinatus	0	0	0	0	1	0	0
distal							
theca 3-1 or 4-2							
theca 1-1 to 2-2							
sicula					1		
Normalograptus magnus	24	0	0	0	24	62	40
distal					10	15	
theca 3-1 or 4-2					4	8	8
theca 1-1 to 2-2	3				8	29	25
sicula	1				2	10	7
Comograptus comatus	10	34	127	80	138	26	37
distal		4	31	17	86	1	7
theca 3-1 or 4-2	4	4	17	11	24	5	10
theca 1-1 to 2-2	4	19	60	39	23	16	16
sicula	2	7	19	13	5	4	4
Diplograptid	36	42	154	92	91	205	164
distal							
theca 1-1 to 2-2	18	22	78	46	46	106	84
sicula	18	20	76	46	45	99	80
***Coronograptus* sp.**	0	0	0	2	0	0	0
distal							
mesial				2			
theca one							
sicula							
Monograptus* cf. *arciformis	270	338	383	656	334	305	172
distal		17			2		
mesial	18	91	74	81	31	19	8
proximal	248	227	306	568	297	281	164
sicula	4	3	3	7	4	5	
Monograptid	14	3	5	11	6	8	5
distal							
proximal							
sicula with theca one	14	3	5	11	6	8	5
Dendroid fragments					1		

	conodont
number of diplograptid species	3
number of monograptid species	2
number of species	5
total diplograptid theca	935
total monograptid theca	2512
total graptolite theca	3447

Table E5. Thecal counts from dissolution residues of CM 44.0-44.1

CM 44.0-44.1 thecae count	0-10	10-17	17-22	22-27	27-32	32-36	36-40	40-45	45-50	50-56	56-60	60-64	64-70	70-76
Metaclimacograptus minimus	33	10	72	17	4	8	0	6	6	2	2	0	0	0
			11	5				6						
theca 3-1 or 4-2			6	4				1						
theca 1-1 to 2-2	24	7	47	10	3	6		4	4	1	1			
sicula	9	3	19	3	1	2		1	2	1	1			
Glyptograptus incertus	7	0	12	55	44	76	118	76	38	73	77	62	33	31
distal					13	8		2		6	20	10		
theca 3-1 or 4-2				5	6	9	6	5	5	15	14	6	4	8
theca 1-1 to 2-2	5		9	37	20	43	84	55	26	41	34	36	21	18
sicula	2		3	13	5	16	28	14	7	11	9	10	8	5
Normalograptus laciniosus		0	0	0	0	9	0	0	0	0	0	6	0	20
distal														7
theca 3-1 or 4-2						4						1		4
theca 1-1 to 2-2						4						4		7
sicula						1						1		2
Comograptus comatus	29	13	38	52	55	137	148	59	41	69	104	103	63	95
distal					8		2		3	9		12		6
theca 3-1 or 4-2	2		3	3	6	4	10				3	10	8	10
theca 1-1 to 2-2	13	8	21	29	28	84	87	36	27	35	67	51	34	48
sicula	14	5	14	20	13	49	49	23	11	25	34	30	21	31
Agetograptus secundus		0	4	6	0	0	0	0	0	0	0	0	0	0
theca 1-1 to 2-2			3	4										
sicula			1	2										
Diplograptid	12	50	115	190	171	363	534	476	254	255	373	364	203	182
distal			45	56	65	105	192	161	38	141	245	173	57	76
theca 1-1 to 2-2	6	25	35	68	55	134	180	162	114	59	66	102	75	55
sicula	6	25	35	66	51	124	162	153	102	55	62	89	71	51
Coronograptus* cf. *cirrus	2	0	17	86	41	98	122	165	86	43	25	75	110	39
distal	2		9	41	16	33	49	58	38	11	9	32	33	25
theca 1-2			4	24	13	33	38	55	24	16	8	22	39	7
sicula			4	21	12	32	35	52	24	16	8	21	38	7
Huttagraptus praestrachani	46	3	63	111	51	65	116	206	98	101	143	58	22	0
distal - no hoods	44	3	18	23	9	3	3	15	30		36	7		
mesio-distal - shortened dorsal hooks	2							53		9	21			
mesial - dorsal hooks			20	33	1	2	10	37		10	18	6		
proximal - dorsal hoods			17	35	33	42	67	65	54	52	56	29	10	
theca one			4	10	4	9	18	18	7	15	6	8	6	
sicula			4	10	4	9	18	18	7	15	6	8	6	
***Monograptus* n. sp. B Melchin**	9	1	0	2	2	32	2	9	1	0	3	0	6	9
distal						2								
mesial	9			2	2	23		9	1		2		4	6
proximal		1				7	2				1		2	2
sicula														1
Monograptid	1	1	3	0	10	10	17	24	16	11	3	12	3	0
sicula with theca one	1	1	3		10	10	17	24	16	11	3	12	3	
Dendroid fragments		7												
			conodont			conoc	conodont							

number of diplograptid species	7
number of monograptid species	4
number of species	11
total diplograptid theca	5455
total monograptid theca	2179
total graptolite theca	7634

Table E6. Thecal counts from dissolution residues of CM 44.1

CM 44.1 thecae count	0-8	8-14	14-18	18-25	25-28	28-29	29-35	35-42	42-48	48-52	52-55	55-60	60-64	64-69	69-72	72-82
Glyptograptus incertus	0	21	51	10	14	7	10	32	43	36	9	0	7	0	30	0
distal		8	29	10	5		1	19	16	8						
theca 3-1 or 4-2			8		4		4	8	4	7	1		2		7	
theca 1-1 to 2-2		10	11		4	5	4	4	16	16	7		4		18	
sicula		3	3		1	2	1	1	7	5	1		1		5	
Metaclimacograptus minimus	26	20	0	0	0	0	0	0	0	0	0	0	0	0	0	0
distal		2														
theca 3-1 or 4-2		2														
theca 1-1 to 2-2	16	11														
sicula	10	5														
***Neodiplograptus* n. sp. C Melchin**	33	56	12	0	24	10	21	83	9	30	45	24	40	12	30	5
distal		8			2		1	40					3		7	
theca 3-1 or 4-2	7	8			5		4	12			6	2	4	2	5	
theca 1-1 to 2-2	20	30	9		13	7	11	23	6	21	29	16	25	8	14	4
sicula	6	10	3		4	3	5	8	3	9	10	6	8	2	4	1
Normalograptus lacinosis	7	32	24	18	44	7	8	31	77	13	29	4	62	10	27	11
distal					2			3	11							
theca 3-1 or 4-2					6			10	17		3		4	1	3	3
theca 1-1 to 2-2	5	23	17	13	26	5	6	14	39	10	20	3	44	7	19	6
sicula	2	9	7	5	10	2	2	4	10	3	6	1	14	2	5	2
***Pseudoglyptograptus* sp.**	0	0	0	0	0	0	0	25	26	0	0	0	0	0	0	0
distal								16	8							
theca 3-1 or 4-2								4	8							
theca 1-1 to 2-2								4	8							
sicula								1	2							
Pseudorthograptus inopinatus	0	0	0	0	0	0	0	0	0	4	0	0	0	0	0	0
theca 1-1 to 2-2										3						
sicula										1						
Agetograptus secundus	0	0	0	0	0	0	0	0	0	0	0	0	0	0	5	8
theca 3-1 or 4-2																3
theca 1-1 to 2-2															4	4
sicula															1	1
Diplograptid	122	214	145	165	158	198	119	198	354	355	355	216	297	126	264	149
distal	17	16	18	4	34	11	26	23	84	90	35	26	9		22	44
theca 1-1 to 2-2	54	104	66	83	66	101	52	93	142	138	167	99	152	66	126	54
sicula	51	94	61	78	58	86	41	82	128	127	153	91	136	60	116	51
Lagarograptus inexpeditus	2	2	0	0	0	0	0	2	2	0	0	0	0	0	0	0
distal	2	2							2							
theca 1-2								1								
sicula								1								
Monograptus* cf. *arciformis	28	97	52	26	58	164	66	212	251	214	349	198	190	145	334	90
distal	6	12	12	3	3	39	6	69	57	4	16	15	24	78	247	37
proximal	22	83	40	23	55	121	60	139	192	208	309	183	164	65	85	51
theca one		1				2		2	1	1	12		1	1	1	1
sicula		1				2		2	1	1	12		1	1	1	1
Coronograptus minisculus	0	0	0	0	0	0	0	1	0	2	1	0	0	0	0	0
distal								1		2	1					
Pribylograptus pleganopsis	0	3	0	0	0	0	0	0	0	1	0	0	0	0	0	0
distal		3								1						
Monograptid	6	0	0	0	2	0	0	0	0	0	1	0	0	0	0	0
distal	6															
theca one																
sicula with theca one					2						1					

number of diplograptid species	7
number of monograptid species	4
number of species	11
total diplograptid theca	4657
total monograptid theca	2499
total graptolite theca	7156

Table E7. Thecal counts from dissolution residues of CM 45.3-45.4

CM 45.3 - 45.4 thecae count	0-10	10-16	16-24	24-29	29-36	36-42	42-48	48-53	53-57	57-62	62-66	66-69	69-76
Rhaphidograptus sinicus	0	8	0	0	0	0	4	0	0	0	0	0	0
theca 1-1 to 2-2		6					3						
sicula		2					1						
Metaclimacograptus rigidus	0	4	0	3	0	0	0	0	0	0	0	0	0
theca 1-1 to 2-2		3		2									
sicula		1		1									
Glyptograptus incertus	388	350	25	17	29	19	5	9	50	40	10	112	67
distal	208	125	16	8	20	10	5	9	29	31		65	12
theca 3-1 or 4-2	61	94	4	4	4	4			4	4	1	13	20
theca 1-1 to 2-2	94	104	4	4	4	4			13	4	7	27	27
sicula	25	27	1	1	1	1			4	1	2	7	8
Comograptus comatus	2	22	7	0	5	36	0	0	0	0	0	0	0
distal		18				23							
theca 3-1 or 4-2						4							
theca 1-1 to 2-2	1	3	4		3	7							
sicula	1	1	3		2	2							
Glyptograptus* cf. *incertus	18	16	4	0	0	23	0	0	0	0	0	0	0
distal	8					5							
theca 3-1 or 4-2	3	4				8							
theca 1-1 to 2-2	6	9	3			8							
sicula	1	3	1			2							
Normalograptus laciniosis	0	19	0	0	0	0	0	0	0	0	7	0	0
distal		4											
theca 3-1 or 4-2		5									2		
theca 1-1 to 2-2		8									4		
sicula		2	0								1		
***Metaclimacograptus?* n. sp.**	0	0	0	0	0	0	4	10	0	0	0	0	0
distal								1					
theca 3-1 or 4-2								4					
theca 1-1 to 2-2							3	4					
sicula							1	1					
Glyptograptus tamariscus tamariscus	0	9	0	4	15	4	15	22	14	44	16	13	30
distal													
theca 3-1 or 4-2							2	4	4	2	1		
theca 1-1 to 2-2		7		3	11	3	10	15	7	31	11	10	23
sicula		2		1	4	1	3	3	3	11	4	3	7
Normalograptus magnus	489	587	50	83	137	149	107	64	102	89	58	139	210
distal	251	359		5	22	25	11		9	30	2	23	51
theca 3-1 or 4-2	79	71	2	9	22	19	16	1	5	5	7	24	31
theca 1-1 to 2-2	126	123	36	49	69	78	61	47	64	40	39	70	100
sicula	33	34	12	20	24	27	19	16	24	14	10	22	28
Diplograptid	134	167	221	177	134	200	264	210	233	215	211	435	544
distal		17	3			5						4	
theca 1-1 to 2-2	70	77	112	90	68	101	135	108	119	112	109	223	287
sicula	64	73	106	87	66	94	129	102	114	103	102	208	257
***Pribylograptus leptotheca* forma A**	305	685	74	66	58	53	79	78	56	172	131	194	94
distal 2 - simple theca - horizontal ap.	8	38		5		3				11		4	
distal - lappets, no spines	91	156	2		4	11		12	21	28	39	68	48
mesiodistal - inc. width no lappet spines	18	27	1	5						3	5	16	3
mesioproximal - spine and lappets	112	177	10	19	4	4	8	33	10	41	31	56	3
proximal - dorsal hoods	76	287	61	37	50	35	61	23	11	67	26	22	14
theca one							5	5	7	11	15	14	13
sicula							5	5	7	11	15	14	13
Pristiograptus biformis	120	214	0	0	0	0	0	0	0	0	0	0	0
distal	101	161											
mesial (pristio like)	10												
mesial (atavus like)	5	33											
proximal	4	19											
sicula		1											
Coronograptus arcuatus	2	4	7	1	12	0	0	5	0	8	10	0	0

Table E7. Thecal counts from dissolution residues of CM 45.3-45.4

CM 45.3 - 45.4 thecae count	0-10	10-16	16-24	24-29	29-36	36-42	42-48	48-53	53-57	57-62	62-66	66-69	69-75
distal	2	4	2		8			3		4	10		
proximal			1	1						4			
theca one			2		2			1					
sicula			2		2			1					
***Monograptus* n sp. B Melchin**	236	387	20	20	66	38	34	6	23	17	23	53	40
distal - simple theca - everted ap.	168	307		13	28	17						6	9
mesial - horns or loops	65	68	11	5	28	12	9				3	14	13
proximal - dosal and ventral hook	3	12	9	2	10	9	25	6	22	17	20	33	16
theca one													1
sicula									1				1
Pribylograptus* cf. *imprimus	0	11	0	0	0	0	0	0	0	0	0	0	0
distal		11											
theca one													
sicula													
Monograptid thecae	2	9	10	9	7	14	17	16	26	54	37	26	27
distal													
proximal													
sicula with theca one	2	9	10	9	7	14	17	16	26	54	37	26	27

number of diplograptid species	9
number of monograptid species	5
number of species	14
total diplograptid theca	6908
total monograptid theca	3656
total graptolite theca	10564

Table E8. Thecal counts from dissolution residues of CM 46.35-46.5

CM 46.35 - 46.5	0-10	10-16	16-21	21-26	26-34	34-42	42-47	47-51	51-53	53-58	58-63	63-70	70-77	77-83	83-87	87-93	93-102
Comograptus comatus	181	132	149	127	77	47	53	68	188	45	54	46	70	82	150	79	188
distal	49	57	38	13	6			4	13				4	34	31	3	38
theca 3-1 or 4-2	10		3	4		2	4	3	7	9	3	2	1		8	8	10
theca 1-1 to 2-2	80	42	64	62	45	26	29	36	114	24	33	28	37	25	73	39	85
sicula	42	33	44	48	26	19	20	25	54	12	18	16	28	23	38	29	55
***Glyptograptus* n. sp.**	23	0	4	11	15	0	0	3	270	117	46	3	3	0	13	28	24
distal				1	4				111	60	9						
theca 3-1 or 4-2				7	4				40	20	4				4		4
theca 1-1 to 2-2	15		3	2	5			2	87	28	24	2	2		7	20	15
sicula	8		1	1	2			1	32	9	9	1	1		2	8	5
Normalograptus nikolayei	0	0	0	10	0	0	0	0	40	0	0	0	0	0	0	0	33
distal																	4
theca 3-1 or 4-2				1					4								4
theca 1-1 to 2-2				7					25								19
sicula				2					11								6
Glyptograptus incertus	3	0	0	3	0	0	0	3	21	0	0	0	3	0	0	0	0
theca 1-1 to 2-2	2			2				2	14				2				
sicula	1			1				1	7				1				
Pseudorthograptus inopinatus	0	0	0	0	0	0	0	6	0	0	0	0	0	0	0	0	0
theca 1-1 to 2-2								4									
sicula								2									
Diplograptid	12	2	4	20	8	2	14	22	229	16	17	4	23	5	9	29	33
distal									6						5		6
theca 1-1 to 2-2	6	1	2	10	4	1	7	11	115	9	9	2	12	3	2	15	14
sicula	6	1	2	10	4	1	7	11	108	7	8	2	11	2	2	14	13
Pribylograptus leptotheca	35	7	5	21	25	36	88	85	614	739	1065	72	60	37	92	203	30
distal 2 -simple straight																	
distal - lappets, no spine		2		10					365	413	680	5	2		3	9	
mesiodistal - lappets, spine, thick	2	4	1		8	2	5	9	127	205	205	4	6	8	23	75	
mesial - 3 spines	6			2	5	3		3	10	15	60			1	20	38	
mesioproximal - spine and lappets	8	1	4	7	5	16	18	12	28	46	76	4	5	3	24	60	13
proximal - hood (some with lappets)	19		7	2	7	15	65	61	84	60	40	59	47	25	22	21	17
theca 1											2						
sicula											2						
***Monograptus* n. sp. B Melchin**	122	88	41	19	39	58	104	203	949	708	359	168	104	196	428	203	93
distal - straight, simple (none)	3	2							2								
mesial - hood, loop, horns, thick	11	9		5				7	170	183	118	4	2	10	32	39	6
proximal - hood, loop	106	77	41	14	39	58	104	190	773	515	235	162	102	186	392	158	87
theca 1	1							3	2	5	3	1			2	3	
sicula	1							3	2	5	3	1			2	3	
Lagarograptus inexpeditus	4	2	0	4	0	0	1	3	11	7	1	3	1	2	12	18	17
distal	1			4			1	3	8	7	1	3	1	2	10	9	7
thecae 1, 2	2	1							2						1	5	6
sicula	1	1							1						1	4	4
***Pristiograptus* n. sp. A Lukasik**	0	0	2	0	0	0	0	0	2	0	0	0	0	0	0	7	5
proximal			2													7	5
theca 1									1								
sicula									1								
Monograptid	48	21	22	8	24	28	22	70	144	87	34	31	26	31	80	49	34
distal																	
theca 1																	
sicula (with theca one fragment)	48	21	22	8	24	28	22	70	144	87	34	31	26	31	80	49	34

number of diplograptid speci	5
number of monograptid spec	4
number of species	9
total diplograptid theca	2867
total monograptid theca	7957
total graptolite theca	10824

Table E9. Thecal counts from dissolution residues of CM 47.4.47.5

CM 47.4 - 47.5 thecae count	0-6	6-13	13-16	16-25	25-30	30-36	36-40	40-48	48-55	55-58	58-65	65-68	68-73
Metaclimacograptus minimus	112	67	32	71	7	0	0	0	0	0	0	0	0
distal	2												
theca 3-1 or 4-2	2												
theca 1-1 to 2-2	77	42	20	46	4								
sicula	31	25	12	25	3								
Metaclimacograptus rigidus	10	16	25	20	6	2	10	0	0	12	9	0	0
distal													
theca 3-1 or 4-2													
theca 1-1 to 2-2	5	8	14	10	3	1	5			7	5		
sicula	5	8	11	10	3	1	5			5	4		
Normalograptus nikolayei	36	34	10	51	33	20	25	19	60	127	116	76	28
distal							8			8	16	31	
theca 3-1 or 4-2		2							6	5	5	11	4
theca 1-1 to 2-2	23	20	7	34	20	12	12	13	35	80	61	23	15
sicula	13	12	3	17	13	8	5	6	19	34	34	11	9
Comograptus comatus	58	31	17	54	20	8	2	6	0	0	5	4	2
distal													
theca 3-1 or 4-2	2				4	4							
theca 1-1 to 2-2	34	19	11	27	8	2	1	4			4	2	1
sicula	22	12	6	27	8	2	1	2			1	2	1
Diplograptid	47	27	6	24	48	16	12	10	38	14	19	0	2
distal	6	9		4	22	10	2	2	16	2			
theca 1-1 to 2-2	21	13	3	10	13	3	5	4	11	6	10		1
sicula	20	5	3	10	13	3	5	4	11	6	9		1
Lagarograptus inexpeditus	9	1	1	6	3	2	2	20	8	4	14	5	2
distal	9	1	1	6	1	2	2	12	3		12	5	2
theca 1					1			4	3	2	1		
sicula					1			4	2	2	1		
***Pristiograptus* n. sp. A Lukasik**	12	159	92	2	0	3	9	0	0	2	6	3	2
distal	2	138	54	1			2				3		
mesial	2	16	16	1		2	2				2		
proximal	6	4	15			1	3			2	1	2	2
sicula	2	1	7				2					1	
***Rastrites* sp.**	7	14	24	1	3	2	0	0	0	0	0	0	0
distal	3	14	20	1									
proximal	4		4		3	1							
sicula						1							
Monograptus pectinatus ?	0	0	0	0	0	0	0	0	0	3	4	1	9
distal										3	3	1	9
proximal											1		
sicula													
New Genus A n. sp.A Lukasik	0	0	0	0	0	0	0	0	0	0	1	0	1
distal													
proximal											1		1
sicula													
Pribylograptus* cf. *imprimus	0	11	19	0	0	0	0	1	1	0	0	5	0
distal								1	1			5	
proximal		11	19										
sicula													

increased mud flakes

number of diplograptid species	4
number of monograptid species	7
number of species	11
total diplograptid theca	1504
total monograptid theca	474
total graptolite theca	1978

Table E10. Thecal counts from dissolution residues of CM 48.5

CM 48.5 thecal count	0-7	7-18	18-26	26-31	31-36	36-41	41-46	46-50	50-59	59-66
Metaclimacograptus rigidus	0	0	17	12	0	0	0	0	0	0
distal				6						
theca 3-1 or 4-2			2	1						
theca 1-1 to 2-2			12	4						
sicula			3	1						
Metaclimacograptus undulatus	35	62	0	0	0	0	0	0	0	5
distal		6								
theca 3-1 or 4-2	4	8								
theca 1-1 to 2-2	20	35								4
sicula	11	13								1
Agetograptus secundus	0	0	0	0	7	0	0	26	7	4
distal								4		
theca 3-1 or 4-2								8		
theca 1-1 to 2-2					5			11	5	3
sicula					2			3	2	1
Petalolithus intermedius	0	2	0	10	26	1	28	35	12	0
distal					12		19	16	3	
theca 3-1 or 4-2				4	4			1		
theca 1-1 to 2-2				4	7		2	9	6	
sicula		2		2	3	1	7	9	3	
Normalograptus nikolayei	0	9	0	6	19	6	18	0	0	0
theca 3-1 or 4-2					4					
theca 1-1 to 2-2		6		4	11	4	13			
sicula		3		2	4	2	5			
Pseudorthograptus inopinatus	0	0	0	0	3	3	10	1	2	3
theca 1-1 to 2-2					2		6			
sicula					1	3	4	1	2	3
Comograptus comatus	142	274	195	196	190	150	190	170	135	235
distal		2	2	32	39	5	46	24	17	13
theca 3-1 or 4-2	5	9	9	10	6	3	17	13	5	9
theca 1-1 to 2-2	76	161	110	90	88	80	78	79	69	127
sicula	61	102	74	64	57	62	49	54	44	86
Diplograptid	36	111	42	55	64	67	95	70	29	55
distal				7	3		2			
theca 1-1 to 2-2	18	56	21	24	32	34	47	35	15	28
sicula	18	55	21	24	29	33	46	35	14	27
Lagarograptus inexpeditus	0	15	9	2	9	0	3	0	0	3
distal		11	7	2	3		3			1
theca 1		2	1		3					1
sicula		2	1		3					1
***Pribylograptus leptotheca* forma B**	24	42	41	44	125	328	326	264	196	111
distal 2 -simple straight	6									
distal - lappets, no spine		14	12	3	40	124	94	96	64	36
mesiodistal - lappets, spine, thick	1	1	3	8	72	169	155	128	119	52
mesial - 3 spines		1	4	2	5	13	6	2	1	
mesioproximal - spine and lappets		7	3	10	4	6	33	9	3	7
proximal - hood (reduced to spine short hood then spine)	15	19	19	19	4	16	38	29	7	14
theca 1	1			1					1	1
sicula	1			1					1	1
***Monograptus* n. sp.B Melchin**	5	17	11	17	12	45	100	67	47	32
distal (straight or monoclimacid)						33	80	57	43	23
mesial (hoops, thick metatheca)					2	2		1		
proximal	5	17	11	17	10	10	20	9	4	9
Monograptid	11	22	11	22	19	17	27	17	14	14
distal	1	2			8					
proximal										
sicula with theca one	10	20	11	22	11	17	27	17	14	14

number of diplograptid species	7
number of monograptid species	3
number of species	10
total diplograptid theca	2870
total monograptid theca	2069
total graptolite theca	4939

Table E11. Thecal counts from dissolution residues of CM 49.8-49.9

CM 49.8-49.9	0-3	3-7	7-9	9-12	12-17	17-20	20-25	25-33	33-40	40-43	43-51	51-56
Agetograptus secundus	0	28	21	33	74	28	93	218	145	52	74	42
distal								13	28			
theca 2-2 to 4-2				2			5		2			
theca 1-1 to 3-1		20	14	23	51	18	57	130	74	34	44	25
sicula		8	7	8	23	10	31	75	41	18	30	17
Glyptograptus tamariscus tamariscus	0	17	3	24	25	0	10	31	8	0	0	0
distal								6				
theca 3-1 or 4-2				2				4				
theca 1-1 to 2-2		13	2	16	15		7	17	6			
sicula		4	1	6	10		3	4	2			
Glyptograptus tamariscus distans	0	0	0	0	0	0	0	30	10	0	23	14
distal												
theca 3-1 or 4-2												
theca 1-1 to 2-2								21	7		18	9
sicula								9	3		5	5
Normalograptus medius brevicaudatus	53	175	30	61	119	78	115	228	118	100	112	46
distal		55	4	4	31	24	22	87	26	49	36	14
theca 3-1 or 4-2		12	4	3		8	11	10	4	6	5	4
theca 1-1 to 2-2	34	72	16	38	59	33	59	96	64	31	49	19
sicula	19	36	6	16	29	13	23	35	24	14	22	9
Metaclimacograptus sculptus	0	0	0	0	10	0	4	0		5	0	0
distal					1							
theca 3-1 or 4-2					4							
theca 1-1 to 2-2					4		3			4		
sicula					1		1			1		
Umbrella (short sicula) meshwork	2	2	0	1	5	1	1	2	1	2	5	0
sicula	2	2	0	1	5	1	1	2	1	2	5	
Umbrella (long sicula) meshwork	0	0	0	0	0	0	0	0	0	0	0	0
theca 1-1 to 2-2												
sicula												
***Pseudoretiolites* sp.**	0	0	0	4	2	0	0	0	0	0	0	0
theca				4	2							
sicula												
Metaclimacograptus orientalis	0	0	0	0	0	0	0	61	14	3	47	18
distal								18			8	2
theca 3-1 or 4-2								8	3		9	4
theca 1-1 to 2-2								25	8	2	22	8
sicula								10	3	1	8	4
Metaclimacograptus rigidus	0	0	0	0	0	0	0	0	19	0	0	0
distal												
theca 3-1 or 4-2									4			
theca 1-1 to 2-2									12			
sicula									3			
Petalolithus sp.	0	0	0	0	0	0	6	0	0	0	0	0
theca 1-1 to 2-2							4					
sicula							2					
Diplograptid	26	129	132	137	174	108	141	320	190	101	150	132
distal		3										
theca 1-1 to 2-2	13	64	67	69	87	55	71	162	97	51	75	66
sicula	13	62	65	68	87	53	70	158	93	50	75	66
Lagarograptus inexpidetus	122	158	160	193	276	128	139	325	94	89	212	125
distal	102	116	120	139	204	108	111	239	78	67	178	101
theca 1	10	21	20	27	36	10	14	43	8	11	17	12
sicula	10	21	20	27	36	10	14	43	8	11	17	12
Monograptus* cf. *triangulatus	22	30	16	47	53	31	57	68	37	6	1	2
distal	13	15		23	24	13	18	30	9		1	
proximal - **rastritid th.1**	8	13	14	21	25	18	38	34	24	6		2
sicula	1	2	2	3	4		1	4	4			
***Rastrites* sp.**	0	0	0	0	0	0	2	0	0	0	0	0

Table E11. Thecal counts from dissolution residues of CM 49.8-49.9

CM 49.8-49.9	0-3	3-7	7-9	9-12	12-17	17-20	20-25	26-33	33-40	40-43	43-51	51-56
distal							2					
proximal												
sicula												
***Monograptus* n. sp. A**	46	84	102	95	195	138	186	380	202	116	273	179
non-sicula	46	84	102	95	195	138	186	380	202	116	273	179
sicula												
***Pribylograptus?* n. sp.**	103	166	112	97	242	103	152	326	175	127	284	126
distal	97	161	109	90	233	103	150	318	168	121	284	123
proximal	6	4	3	7	9		2	8	6	6		3
sicula		1							1			
***Monograptus* n. sp.B Melchin**	27	86	52	76	85	61	96	186	130	70	110	75
distal	5	10	1	8	15	11	15	19	14	10	7	24
proximal	22	75	49	66	67	50	76	157	111	58	98	51
sicula		1	2	2	3		5	10	5	2	5	
Coronograptus gregarius	2	5	2	0	0	0	13	49	43	28	67	28
distal		5	2				6	31	29	18	53	12
theca 1	1						6	9	7	5	7	8
sicula	1						1	9	7	5	7	8
Pribylograptus leptotheca	2	11	0	3	27	46	75	167	10	7	15	13
distal	2				17	19	26	52	2	5	6	13
mesiodistal						1	2	7			3	
mesial					1	8	15	14:				
mesioproximal								26				
proximal		7		1	9	18	22	52	4	2	6	
theca 1		2		1			5	8	2			
sicula		2		1			5	8	2			
Pribylograptus* cf. *imprimus	0	0	0	0	2	0	0	0	0	0	0	0
no sicula attached					2							
sicula												
***Pristiograptus* sp.**	0	0	0	0	0	0	0	0	0	0	0	0
distal												
proximal												
Huttagraptus praestrachani	0	0	0	0	0	0	0	0	26	0	11	2
distal									11		7	2
mesial									13		2	
theca 1									1		1	
sicula									1		1	
triangulate thecae	0	0	0	0	0	0	0	0	0	0	0	1
non-sicula												1
sicua												
Monograptid	0	0	5	7	6	4	2	8	10	1	5	6
distal												
proximal												
sicula with theca one			5	7	6	4	2	8	10	1	5	6

number of diplograptid species	11
number of monograptid species	14
number of species	25
total diplograptid theca	7175
total monograptid theca	15866
total graptolite theca	23041

Table E11. Thecal counts from dissolution

CM 49.8-49.9	56-57	57-63	63-66	66-71	71-78	78-87	87-90
Agetograptus secundus	109	158	99	102	47	104	117
distal	6		8	11	24	4	56
theca 2-2 to 4-2	4	1	1			5	5
theca 1-1 to 3-1	66	97	56	56	13	55	34
sicula	33	60	34	35	10	40	22
Glyptograptus tamariscus tamariscus	23	4	0	7	0	0	0
distal	1	4					
theca 3-1 or 4-2	5			2			
theca 1-1 to 2-2	13			4			
sicula	4			1			
Glyptograptus tamariscus distans	33	43	15	10	5	11	12
distal		7					
theca 3-1 or 4-2	2						
theca 1-1 to 2-2	23	25	11	7	4	7	7
sicula	8	11	4	3	1	4	5
Normalograptus medius brevicaudatus	80	95	81	105	192	165	85
distal	15	18	39	25	71	58	19
theca 3-1 or 4-2	7		2	7	10	5	9
theca 1-1 to 2-2	42	53	29	50	78	70	41
sicula	16	24	11	23	33	32	16
Metaclimacograptus sculptus	0	0	0	0	9	0	0
distal							
theca 3-1 or 4-2					4		
theca 1-1 to 2-2					4		
sicula					1		
Umbrella (short sicula) meshwork	3	4	0	3	5	5	1
sicula	3	4		3	5	5	1
Umbrella (long sicula) meshwork	5	0	0	0	0	0	0
theca 1-1 to 2-2	3						
sicula	2						
***Pseudoretiolites* sp.**	0	0	0	0	0	0	0
theca							frag.
sicula							
Metaclimacograptus orientalis	16	29	22	13	39	29	11
distal		5			6		2
theca 3-1 or 4-2	1	4	4	4	6	5	4
theca 1-1 to 2-2	11	13	13	6	19	18	4
sicula	4	7	5	3	8	6	1
Metaclimacograptus rigidus	15	0	0	0	0	0	0
distal							
theca 3-1 or 4-2							
theca 1-1 to 2-2	11						
sicula	4						
Petalolithus sp.	0	0	0	0	0	0	0
theca 1-1 to 2-2							
sicula							
Diplograptid	198	156	120	168	129	223	77
distal							
theca 1-1 to 2-2	100	78	60	84	67	112	39
sicula	98	78	60	84	62	111	38
Lagarograptus inexpidetus	161	150	112	162	126	137	42
distal	119	104	104	142	110	115	32
theca 1	21	23	4	10	8	11	5
sicula	21	23	4	10	8	11	5
Monograptus* cf. *triangulatus	5	0	0	0	11	75	29
distal	1				7	53	14
proximal - **rastritid th.1**	3				4	20	14
sicula	1					2	1
***Rastrites* sp.**	0	0	0	0	0	27	0

Table E11. Thecal counts from dissolution

CM 49.8-49.9	56-57	57-63	63-66	66-71	71-78	78-87	87-90
distal							
proximal						27	
sicula							
***Monograptus* n. sp. A**	268	309	253	330	228	565	243
non-sicula	268	309	253	330	228	565	243
sicula							
***Pribylograptus?* n. sp.**	356	492	403	514	224	1038	352
distal	356	492	403	514	224	1032	351
proximal						6	1
sicula							
***Monograptus* n. sp.B Melchin**	104	102	75	102	83	146	74
distal	19	7	5	9	25	36	14
proximal	82	92	67	91	57	110	59
sicula	3	3	3	2	1		1
Coronograptus gregarius	63	48	40	37	11	54	26
distal	31	26	24	23	5	40	10
theca 1	16	11	8	7	3	7	8
sicula	16	11	8	7	3	7	8
Pribylograptus leptotheca	9	2	4	0	0	5	1
distal	7	2				5	
mesiodistal							
mesial							
mesioproximal							
proximal	2		4				1
theca 1							
sicula							
Pribylograptus* cf. *imprimus	0	0	0	0	0	0	0
no sicula attached							
sicula							
***Pristiograptus* sp.**	0	9	5	26	0	0	0
distal		9	5	26			
proximal							
Huttagraptus praestrachani	10	0	0	8	0	2	1
distal	5			8		2	1
mesial	5						
theca 1							
sicula							
triangulate thecae	0	0	0	0	7	0	0
non-sicula					7		
sicua							
Monograptid	6	5	2	10	1	7	4
distal							
proximal							
sicula with theca one	6	5	2	10	1	7	4

Table E12. Thecal counts from dissolution residues of CM 50.4

CM 50.4	0-10	10-13	13-21	21-27	27-34	34-40	40-46	46-53	53-60	60-65
Comograptus comatus		1	0	0	0	0	0	0	0	0
theca 1-1 to 2-2		1								
Pseudorthograptus inopinatus		0	0	0	0	0	0	0	11	1
theca 3-1 or 4-2									3	
theca 1-1 to 2-2									6	
sicula									2	1
Normalograptus medius brevicaudatus		0	0	12	0	3	6	51	0	3
distal								44		
theca 1-1 to 2-2				9		3	4	5		2
sicula				3			2	2		1
Metaclimacograptus minimus		0	3	0	0	0	0	0	0	0
theca 1-1 to 2-2			2							
sicula			1							
Metaclimacograptus orientalis	52	3	0	0	0	0	0	11	6	13
theca 3-1 or 4-2	8							1		
theca 1-1 to 2-2	32	2						7	4	7
sicula	12	1						3	2	6
Pseudoretiolites sp.		0	7	4	10	3	0	0	0	0
theca 3-1 or 4-2					3					
theca 1-1 to 2-2			5	3	5	2				
sicula			2	1	2	1				
Diplograptid	45	21	23	13	14	8	27	16	16	20
distal		10								
theca 1-1 to 2-2	23	6	12	7	7	4	14	8	8	10
sicula	22	5	11	6	7	4	13	8	8	10
Monograptus n. sp. B Melchin	12	17	42	45	30	20	17	10	20	8
distal		1	11	15	17	8	1	2	4	
proximal	11	14	29	28	13	12	14	8	15	7
sicula		2	2	2			2		1	1
Coronograptus gregarius	1	0	0	4	0	0	2	4	6	10
distal	1							2	2	6
theca 1				2			1	1	2	2
sicula				2			1	1	2	2
Pristiograptus fragilis pristinus	504	166	261	67	25	39	86	43	21	17
distal	464	148	243	67	25	39	86	43	21	17
theca 1	20	9	9							
sicula	20	9	9							
Monograptus tenuissimus	145	308	597	228	221	295	317	152	6	0
distal	111	206	401	166	161	205	197	106	6	
thecae one	17	51	98	31	30	45	60	23		
sicula	17	51	98	31	30	45	60	23		
New Genus A sp. A Lukasik	31	22	62	59	42	13	17	15	9	0
distal	31	22	60	59	42	13	17	15	9	
thecae one			1							
sicula			1							
Monograptus involutus	26	34	56	109	68	77	119	73	89	31
distal	26	22	34	87	54	67	79	59	65	25
theca one		6	11	11	7	5	20	7	12	3
sicula		6	11	11	7	5	20	7	12	3
Pribylograptus leptotheca forma B		0	14	16	11	7	16	11	5	11
distal					1	1				
mesiodistal						4				
mesial			3	1		1	1	3		3
mesioproximal			1	4	2		5			1
proximal			10	11	8	1	8	8	5	7
theca 1							1			
sicula							1			
Monograptid	40	3	0	1	0	1	1	1	2	0
distal	8									
sicula with theca one	32	3		1		1	1	1	2	

number of diplograptid species	6
number of monograptid species	8
number of species	14
total diplograptid theca	403
total monograptid theca	4838
total graptolite theca	5241

Table E13. Thecal counts from dissolution residues of CM 50.4-50.5

CM 50.4-50.5	0-5	5-11	11-15	15-19	19-24	24-30	30-33	33-37	37-45	45-50	50-56	56-61	61-68	68-79
Rhaphidograptus sinicus	142	103	72	28	35	41	70	77	79	43	48	191	241	157
distal	12	5			4			9				41	53	11
theca 3-1 or 4-2	12		2			1	4		2	6		21	15	8
theca 1-1 to 2-2	81	66	47	17	22	27	45	45	51	26	29	93	123	89
sicula	37	32	23	11	9	13	21	23	26	11	19	36	50	49
Normalograptus magnus	0	15	0	0	0	0	0	0	0	0	0	0	0	0
theca 1-1 to 2-2		10												
sicula		5												
Metaclimacograptus orientalis	0	0	0	0	11	0	0	0	0	3	0	25	13	0
distal					2							2		
theca 3-1 or 4-2					4							5	2	
theca 1-1 to 2-2					4					2		14	8	
sicula					1					1		4	3	
Metaclimacograptus minimus	0	0	0	0	0	0	0	0	0	0	0	0	0	6
distal														
theca 3-1 or 4-2														1
theca 1-1 to 2-2														4
sicula														1
Neodiplograptus? sp.	0	0	0	0	23	12	5	3	0	0	0	26	27	7
distal					15							4	14	
theca 3-1 or 4-2						4						4		
theca 1-1 to 2-2					6	6	4	2				14	10	5
sicula					2	2	1	1				4	3	2
Normalograptus nikolayei	35	24	5	17	0	0	0	0	0	0	0	0	0	0
distal				5										
theca 3-1 or 4-2		2		4										
theca 1-1 to 2-2	25	16	4	6										
sicula	10	6	1	2										
Retiolitid	0	0	2	0	0	0	0	0	0	0	0	0	3	0
theca 1-1 to 2-2			1											
sicula			1										3	
Metaclimacograptus sculptus	0	0	0	0	0	0	0	0	0	0	0	0	3	0
theca 1-1 to 2-2													2	
sicula													1	
Diplograptid	162	176	85	84	100	60	74	72	76	64	80	156	180	129
distal					14									
theca 1-1 to 2-2	81	88	43	42	43	30	37	36	38	32	40	78	91	65
sicula	81	88	42	42	43	30	37	36	38	32	40	78	89	64
Atavagraptus atavus	0	0	6	0	5	4	0	0	0	0	0	0	0	33
distal			1		5	4								33
proximal			5											
sicula														
***Monograptus* n. sp. B Melcin**	49	43	26	15	30	32	20	28	18	3	11	57	64	61
distal			7	3		3	3		1			9		3
proximal	29	25	9	6	18	17	7	20	11	3	9	32	40	42
theca one	10	9	5	3	6	6	5	4	3		1	8	12	8
sicula	10	9	5	3	6	6	5	4	3		1	8	12	8
Coronograptus gregarius	15	0	4	3	0	2	4	5	1	2	3	35	21	25
distal	11		2					3	1		1	13	6	8
theca 1 and 2	2		1	2		1	2	1		1	1	11	8	9
sicula	2		1	1		1	2	1		1	1	11	7	8
Pristiograptus fragilis pristinus	25	72	102	40	20	11	15	11	26	4	0	16	181	64
distal	11	54	74	30	18	9	11	9	26	4		16	167	46
theca 1	7	9	14	5	1	1	2	1					7	9
sicula	7	9	14	5	1	1	2	1					7	9
Monograptus involutus	18	1	6	38	37	26	8	8	6	10	12	36	23	24
distal	4	1	6	34	35	22	4	8	6	6	12	16	15	16
thecae one	7			2	1	2	2			2		10	4	4
sicula	7			2	1	2	2			2		10	4	4

Table E13. Thecal counts from dissolution residues of CM 50.4-50.5

CM 50.4-50.5	0-5	5-11	11-16	16-19	19-24	24-30	30-33	33-37	37-45	45-50	50-56	56-61	61-68	68-79
Rastrites orbitus ?	0	0	0	0	0	0	0	0	0	0	0	13	0	2
distal												13		2
proximal														
thecae one														
sicula														
triangulate theca	0	0	3	0	0	0	0	3	0	0	1	0	0	0
distal			1					3			1			
thecae one			1											
sicula			1											
New Genus A sp. A Lukasik	58	122	38	18	22	21	0	0	0	2	0	3	2	8
distal	58	119	38	18	22	21				2		3	2	8
proximal		3												
thecae one														
sicula														
Monograptus tenuissimus	0	13	18	15	2	3	2	2	0	0	2	0	0	6
distal		7	18	13		3								6
theca one		3		1	1		1	1			1			
sicula		3		1	1		1	1			1			
Pribylograptus leptotheca	1	0	0	5	3	8	37	9	12	2	4	8	6	0
distal 2 -simple straight									10					
distal - lappets, no spine														
mesiodistal - lappets, spine, thick				1					1					
mesial - 3 spines														
mesioproximal - spine and lappets				2		3	13			2	1	8	4	
reduced to spine short hood then spine)	1			2	1	3	22	9	1		3			
theca 1					1	1	1						1	
sicula					1	1	1						1	
Monograptid	29	27	36	19	11	9	14	12	17	4	7	26	15	33
distal														
proximal										4	7	26		
sicula with theca one	29	27	36	19	11	9	14	12	17				15	33
triangulate theca			1											

number of diplograptid species	8
number of monograptid species	10
number of species	18
total diplograptid theca	3090
total monograptid theca	2198
total graptolite theca	5288

Table E14. Thecal counts from dissolution residues of CM 51.2-51.3a

CM 51.2-51.3a	0-4	4-8	8-12	12-17	17-25	26-27	27-30	30-37	37-41	41-48	48-53	53-58	58-62
Normalograptus nikolayei	153	88	88	122	150	44	100	37	11	22	21	0	5
distal	48	18		29	25	4	21	17					
theca 3-1 or 4-2	24		14	15	32	8	15	6		4	2		
theca 1-1 to 2-2	62	54	57	60	71	24	49	11	8	14	14		4
sicula	19	16	17	18	22	8	15	3	3	4	5		1
Pseudorthograptus inopinatus	0	0	0	0	0	0	0	0	0	0	0	8	4
distal													
theca 3-1 or 4-2													
theca 1-1 to 2-2												6	3
sicula												2	1
Diplograptid	234	207	130	119	159	89	126	32	61	139	52	71	70
distal													
theca 1-1 to 2-2	120	107	66	60	80	45	63	16	31	70	26	36	36
sicula	114	100	64	59	79	44	63	16	30	69	26	35	34
Coronograptus gregarius	115	79	41	33	53	35	58	21	44	81	18	43	43
distal	33	38	13	5	28	4	15	1	1	17		13	10
theca 1, 2	46	24	14	15	13	18	26	11	22	36	9	18	19
sicula	36	17	14	13	12	13	17	9	21	28	9	12	14
Campograptus sanctgeorgensis	9	6	21	2	2	1	1	0	0	0	17	0	0
distal	9	6	13	2	2	1	1				17		
thecae one			4										
sicula			4										
New Genus A sp. A Lukasik	0	0	0	0	0	0	0	0	0	5	1	0	0
distal										5	1		
thecae one													
sicula													
Monograptus calamistratus	32	27	17	12	62	25	42	11	20	45	7	27	20
distal	16	15	15	4	42	17	16	5	4	9	1	11	12
thecae one	8	6	1	4	10	4	13	3	8	18	3	8	4
sicula	8	6	1	4	10	4	13	3	8	18	3	8	4
***Monograptus falcata* forma A**	0	2	0	0	0	0	0	0	0	0	0	0	0
distal													
thecae one		1											
sicula		1											
Pribylograptus leptotheca	27	20	21	22	44	32	47	27	57	27	69	48	40
distal													
mesiodistal	3	3	1				11	5	9	17	31		
mesial	1	6	7	9	7	5	10	9	19	3	8	4	8
mesioproximal	9	5	5	3	11	2	5	3	6	1	6	8	10
proximal	10	4	6	10	18	17	17	10	21	6	16	22	14
theca 1	2	1	1		4	4	2		1		4	7	4
sicula	2	1	1		4	4	2		1		4	7	4
Monograptid	1	1	1	1	0	1	3	0	4	2	1	0	1
distal							2						
proximal													
sicula with theca one	1	1	1	1		1	1		4	2	1		1

many sponge spicules

number of diplograptid species	2
number of monograptid species	6
number of species	8
total diplograptid theca	2342
total monograptid theca	1575
total graptolite theca	3917

many gastropods, bivavles, sponge spicules, ostracods?

Table E15. Thecal counts from dissolution residues of CM 51.2-51.3b

CM 51.2-51.3b	0-5	5-13	13-20	20-26	26-30	30-34	34-41	41-45	45-50	50-58	58-65
Glyptograptus tamariscus tamariscus	0	0	8	0	0	0	9	0	0	0	4
distal											
theca 3-1 or 4-2											
theca 1-1 to 2-2			6				7				3
sicula			2				2				1
Normalograptus nikolayei	50	34	56	45	17	12	18	3	0	18	4
distal	7		42	1			4			4	
theca 3-1 or 4-2	5			9			1			4	
theca 1-1 to 2-2	28	24	10	27	12	8	10	2		8	3
sicula	10	10	4	8	5	4	3	1		2	1
Diplograptid	74	44	52	21	50	54	96	16	46	68	58
distal											
theca 1-1 to 2-2	37	22	26	11	25	27	48	8	23	34	29
sicula	37	22	26	10	25	27	48	8	23	34	29
Coronograptus gregarius	35	25	29	14	6	25	27	12	31	19	36
distal	15	7	8	6		11	10	7	6	7	16
theca 1, 2	11	9	11	4	3	7	10	3	13	7	10
sicula	9	9	10	4	3	7	7	2	12	5	10
Campograptus sanctgeorgensis	3	0	0	0	6	1	0	0	0	0	0
distal	1				2	1					
thecae one	1				2						
sicula	1				2						
New Genus A sp. A Lukasik	0	0	0	0	0	0	0	0	1	0	0
distal									1		
thecae one											
sicula											
Monograptus calamistratus	13	0	13	0	8	7	16	12	9	5	26
distal	9		3		6	3	6	6	3	3	20
thecae one	2		5		1	2	5	3	3	1	3
sicula	2		5		1	2	5	3	3	1	3
***Monograptus falcata* forma A**	0	0	1	0	1	0	0	0	0	0	0
distal			1		1						
thecae one											
sicula											
Pribylograptus leptotheca	27	25	6	12	9	23	19	2	9	26	36
distal 2 -simple straight											
distal - lappets, no spine										2	
mesiodistal - lappets, spine, thick	4						1				
mesial - 3 spines											
mesioproximal - spine and lappets	17	9	2			5	6		3	12	14
proximal - short hood then spine	6	14	4	10	7	12	10		2	10	18
theca 1		1		1	1	3	1	1	2	1	2
sicula		1		1	1	3	1	1	2	1	2
Monograptid	10	4	1	1	1	5	10	8	4	9	8
distal											
proximal											
sicula with theca one	10	4	1	1	1	5	10	8	4	9	8

number of diplograptid species	2	many other fauna - bivalves
number of monograptid species	6	
number of species	8	
total diplograptid theca	857	
total monograptid theca	636	
total graptolite theca	1493	

Table E16. Thecal counts from dissolution residues of CM 52.1-52.2

CM 52.1-52.2	0-8	8-12	12-27	27-32	32-35	35-39	39-42	42-52	52-55	55-58	58-62	62-64
***Glyptograptus* sp.**	0	0	0	4	0	0	0	0	0	0	0	0
distal												
theca 3-1 or 4-2												
theca 1-1 to 2-2				2								
sicula				2								
Normalograptus medius brevicaudatus	0	0	0	21	4	15	12	0	0	0	0	0
distal				17		15	3					
theca 3-1 or 4-2							4					
theca 1-1 to 2-2				3	3		4					
sicula				1	1		1					
Metaclimacograptus orientalis	986	314	1164	236	323	292	512	346	78	88	199	156
distal	220	70	288	51	74	81	137	72	17	22	56	59
theca 3-1 or 4-2	118	51	163	27	38	41	59	32		4	20	14
theca 1-1 to 2-2	449	140	504	114	146	120	223	162	38	39	82	52
sicula	199	53	209	44	65	50	93	80	23	23	41	31
Campograptus communis	82	50	89	17	0	0	0	0	0	0	8	9
distal	40	20	63	11							6	9
thecae one	21	15	13	3							1	
sicula	21	15	13	3							1	
New Genus A sp. A Lukasik	0	0	1	4	0	0	0	0	1	0	0	0
distal			1	4					1			
thecae one												
sicula												
Rastrites orbitus ?	0	0	2	0	0	0	0	0	0	0	0	0
distal			2									
thecae one												
sicula												
Pribylograptus leptotheca	4	0	0	0	0	0	0	0	0	0	0	0
distal 2 -simple straight												
distal - lappets, no spine	4											
Monograptid	4	0	3	0	0	0	0	0	0	0	0	0
distal												
proximal												
sicula with theca one	4		3									

number of diplograptid species	3
number of monograptid species	4
number of species	7
total diplograptid theca	4750
total monograptid theca	274
total graptolite theca	5024

Table E17. Thecal counts from dissolution residues of CM 53.2-53.3

CM 53.2-53.3	0-5	5-8	8-13	13-18	18-24	24-31	31-43	43-47	47-53	53-56	56-63	63-65	65-67
Glyptograptus sinuatus sinuatus	0	0	14	0	35	0	66	0	0	0	4	8	0
distal			5		26		48						
theca 3-1 or 4-2			4		4		8						
theca 1-1 to 2-2			4		4		8				3	6	
sicula			1		1		2				1	2	
Metaclimacograptus orientalis	0	0	0	0	0	0	16	8	3	7	16	3	21
distal							2						2
theca 3-1 or 4-2							4	1		2	1		4
theca 1-1 to 2-2							8	5	2	4	11	2	11
sicula							2	2	1	1	4	1	4
Pseudoglytopgraptus barriei	12	0	11	0	0	0	0	0	0	0	0	0	0
distal	3												
theca 3-1 or 4-2	4												
theca 1-1 to 2-2	4		8										
sicula	1		3										
Pseudorthograptus inopinatus	5	14	0	4	1	2	1	0	7	0	3	4	3
distal													
theca 3-1 or 4-2													
theca 1-1 to 2-2	3								4		1	3	2
sicula	2	14		4	1	2	1		3		2	1	1
Rivagraptus bellulus	0	11	5	0	1	1	9	0	25	8	6	16	31
distal		6			1	1						3	6
theca 3-1 or 4-2												5	4
theca 1-1 to 2-2		4	4				6		18	6	4	6	16
sicula		1	1				3		7	2	2	2	5
Retiolitid	0	3	0	0	0	0	8	0	0	0	1	0	0
distal		3					2						
theca 1-1 to 2-2							4						
sicula							2				1		
Diplograptid	54	39	94	56	38	24	73	40	61	32	40	42	46
distal		6											
theca 1-1 to 2-2	28	18	47	28	19	13	37	20	31	16	20	21	23
sicula	26	15	47	28	19	11	36	20	30	16	20	21	23
***Monograptus* n. sp. C**	1	0	3	8	22	15	113	116	135	56	59	5	11
distal	1		3	8	22	13	107	112	135	56	59	5	11
thecae one						1	3	4					
sicula						1	3						
***Monoclimacis* n. sp. A Lukasik**	2	0	24	10	12	18	43	19	10	10	5	4	1
distal			2			9	2	7		1	2	3	
mesial			1		3	2	7	5	1		1		
proximal	2		19	8	9	7	28	5	9	7	2	1	1
thecae one			1	1			3	1		1			
sicula			1	1			3	1		1			
***Monograptus falcata* forma A**	98	70	202	66	114	44	28	16	40	25	50	19	25
distal		5	4	2	2	4				7	10		
proximal	82	61	162	58	102	40	22	14	38	18	36	19	25
thecae one	8	2	18	3	5		3	1	1		2		
sicula	8	2	18	3	5		3	1	1		2		
***Pribylograptus leptotheca* forma A**	1	6	10	2	0	22	24	6	34	42	11	3	6
distal		6	10			5	14		26	36	11		
mesiodistal				2		7	2						
mesial						3	3			3			4
mesioproximal						7	4	1	3	2			
proximal	1						1	5	5	1		3	2
theca 1													
sicula													
Rastrites orbitus ?	0	0	3	0	5	5	19	4	0	0	0	2	1
distal			3		5	5	15	4				2	1
proximal							2						

Table E17. Thecal counts from dissolution residues of CM 53.2-53.3

CM 53.2-53.3	0-5	5-8	8-13	13-18	18-24	24-31	31-43	43-47	47-53	53-55	55-63	63-65	65-67
thecae one							1						
sicula							1						
***Monograptus* n. sp. B Melchin**	0	0	0	0	0	7	46	42	29	19	18	13	10
distal						2	2			7	3	3	1
proximal						3	30	22	25	6	9	10	7
theca 1						1	7	10	2	3	3		1
sicula						1	7	10	2	3	3		1
Campograptus communis	0	0	0	0	0	6	75	13	11	3	3	9	0
distal						6	63	7	5	1	1	9	
theca one							6	3	3	1	1		
sicula							6	3	3	1	1		
Monograptus dracocephalus	0	0	0	0	1	3	16	0	8	2	1	0	0
mesial (spines, dorsal curvature)					1	1	10		8		1		
theca one						1	3			1			
sicula						1	3			1			
***Monograptus* n. sp. B forma A**	3	2	6	0	3	2	66	13	4	9	2	0	4
distal	3	2	6		3	2	66	13	4	9	2		4
theca one													
sicula													
Monograptid	13	2	22	21	25	16	44	26	27	13	23	13	18
distal													
proximal													
sicula with theca one	13	2	22	21	25	16	44	26	27	13	23	13	18

2 con 3 conodonts many chitinozoans
these P. leptotheca have the lappets
extending into spines in the "mesiodistal" section

number of diplograptid species	7
number of monograptid species	10
number of species	17
total diplograptid theca	1032
total monograptid theca	2417
total graptolite theca	3449

Table E18. Thecal counts from dissolution residues of CM 54.0-54.15

CM 54.0-54.15	0-6	6-12	12-17	17-23	23-30	30-34	34-37	37-44	44-52	52-59	59-67	67-74	74-82	82-86	86-92
Neodiplograptus tcherskyi	40	10	7	10	33	73	22	4	17	39	0	3	57	0	78
distal	24	5			17	18							19		46
theca 3-1 or 4-2	4		2	2	4	8	3		2	4			6		8
theca 1-1 to 2-2	9	4	4	6	9	35	15	3	11	27		2	24		18
sicula	3	1	1	2	3	12	4	1	4	8		1	8		6
Glyptograptus tamariscus	0	12	0	11	0	0	0	0	0	0	13	9	0	0	7
distal															
theca 3-1 or 4-2		1									1				
theca 1-1 to 2-2		8		8							9	6			5
sicula		3		3							3	3			2
Metaclimacograptus orientalis	116	42	33	121	105	79	57	98	98	159	159	114	308	109	322
distal			4										4	10	20
theca 3-1 or 4-2	9	3	4	6	7	4	5	3	7	15	9	3	22	6	16
theca 1-1 to 2-2	74	26	17	83	70	52	35	65	61	100	101	74	184	63	186
sicula	33	13	8	32	28	23	17	30	30	44	49	37	98	30	100
Retiolitid	0	0	3	0	5	0	0	0	0	0	1	3	4	0	0
theca 1-1 to 2-2			2		5						1	2	4		
sicula			1									1			
Diplograptid	42	103	14	56	61	76	32	40	50	71	32	43	111	49	83
distal														3	
theca 1-1 to 2-2	21	53	7	28	31	38	16	20	25	36	16	22	56	23	42
sicula	21	50	7	28	30	38	16	20	25	35	16	21	55	23	41
***Monograptus* n. sp. B forma A**	136	489	108	409	214	122	65	134	383	494	345	203	114	42	32
distal	136	489	108	409	214	122	65	134	383	494	345	203	114	42	32
theca 1															
sicula															
Campograptus communis	33	60	3	19	7	23	37	53	34	148	65	77	122	24	31
distal	25	44	3	9	7	19	29	37	20	104	43	51	88	16	23
theca 1	4	8		5		2	4	8	7	22	11	13	17	4	4
sicula	4	8		5		2	4	8	7	22	11	13	17	4	4
***Monograptus falcata* forma A**	9	107	24	148	35	35	51	81	84	76	31	88	137	108	85
distal		14	16	99	19	9	13	49	55	38	10	50	10	10	10
proximal	5	59	6	23	6	12	14	12	23	16	11	20	91	60	55
thecae one	2	17	1	13	5	7	12	10	3	11	5	9	18	19	10
sicula	2	17	1	13	5	7	12	10	3	11	5	9	18	19	10
Rastrites orbitus	34	179	12	42	10	22	9	15	27	25	12	4	1	0	0
distal	34	179	12	42	10	22	9	15	27	25	12	4	1		
thecae one															
sicula															
***Monoclimacis* n. sp. C Lukasik**	0	47	1	31	9	0	2	0	1	0	0	2	17	0	0
distal		47	1	24	9		2		1			2	6		
proximal				7									11		
thecae one															
sicula															
Monograptus calamistratus	0	0	0	0	3	0	0	0	0	0	0	0	0	0	0
distal					3										
thecae one															
sicula															
Monograptid	14	59	10	16	13	14	19	21	18	30	26	35	57	21	52
sicula with theca one	14	59	10	16	13	14	19	21	18	30	26	35	57	21	52
						inc. other fauna					dec. in other fauna				

number of diplograptid species	4
number of monograptid species	8
number of species	13
total diplograptid theca	3244
total monograptid theca	6035
total graptolite theca	9279

Table E19. Thecal counts from dissolution residues of CM 55

CM 55	0-5	5-13	13-17	17-24	24-30	30-37	37-40	40-47	47-51	51-59
Glyptograptus incertus ?	0	0	0	0	0	0	0	9	0	0
distal										
theca 3-1 or 4-2								4		
theca 1-1 to 2-2								4		
sicula								1		
Normalograptus nikolayvei	0	0	0	0	0	0	4	12	38	0
distal									21	
theca 3-1 or 4-2								4	4	
theca 1-1 to 2-2							3	6	10	
sicula							1	2	3	
Pseudoglyptograptus barriei	0	0	0	0	0	0	135	55	58	115
distal							64	21	27	60
theca 3-1 or 4-2							16	9	8	11
theca 1-1 to 2-2							43	20	18	34
sicula							12	5	5	10
Neodiplograptus tcherskyi tcherskyi	34	74	19	0	4	14	43	68	0	43
distal	12	25				2	12	32		5
theca 3-1 or 4-2	8	9	1			4	5			6
theca 1-1 to 2-2	10	29	12		3	6	20	27		25
sicula	4	11	6		1	2	6	9		7
Rivagraptus kayi	0	0	4	15	3	40	64	118	47	61
distal				2		9	15	34	13	30
theca 3-1 or 4-2				4		12	16	24	9	8
theca 1-1 to 2-2			3	7	2	16	27	47	20	18
sicula			1	2	1	3	6	13	5	5
Metaclimacograptus hughesi	20	26	6	27	0	0	16	7	0	0
distal		6		4						
theca 3-1 or 4-2	6		1	4				2		
theca 1-1 to 2-2	11	14	4	14			10	4		
sicula	3	6	1	5			6	1		
***Petalolithus* sp.**	0	0	0	0	0	0	0	0	0	9
distal										1
theca 1-1 to 2-2										6
sicula										2
Pseudoretiolities	1	0	0	2	0	0	0	11	4	7
distal								2		
theca 1-1 to 2-2								6		
sicula	1			2				3	4	7
Diplograptid	145	239	118	138	32	65	178	120	113	227
distal		3								
theca 1-1 to 2-2	73	119	59	69	16	33	90	61	57	115
sicula	72	117	59	69	16	32	88	59	56	112
***Monograptus falcata* forma A**	31	25	9	12	16	2	0	4	0	5
mesial	2	2	1		13	2				3
proximal	19	15	7	12	16	2		4		5
theca 1	6	5	1							
sicula	6	5	1							
Campograptus lobiferus lobiferus	11	46	9	20	4	0	21	37	1	22
distal	3	38	7	14	2		21	31	1	16
theca 1	4	4	1	3	1			3		3
sicula	4	4	1	3	1			3		3
***Monograptus* n. sp. E**	0	2	0	3	19	0	8	0	2	10
distal		2		1	19		6		2	10
theca 1				1			1			
sicula				1			1			
***Monograptus falcata* forma B**	332	241	97	466	250	216	457	385	360	880
distal		17	10	46	24		60	73	31	116
mesial	2	2	1		13	2				3
proximal	296	203	88	402	191	186	389	343	338	841

Table E19. Thecal counts from dissolution residues of CM 55

CM 55	0-5	5-13	13-17	17-24	24-30	30-37	37-40	40-47	47-51	51-59
thecae one	17	18	4	32	23	14	34	21	11	18
sicula	17	18	4	32	23	14	34	21	11	18
Rastrites orbitus	42	39	53	53	25	7	114	8	18	59
distal	32	25	41	41	15	3	70	8	16	47
thecae one	5	7	6	6	5	2	22		1	6
sicula	5	7	6	6	5	2	22		1	6
Lituigraptus convolutus	5	0	40	7	0	0	3	8	0	0
distal	5		40	7			3	8		
thecae one										
sicula										
Pristiograptus **n. sp. B Lukasik**	2	16	2	22	0	0	0	11	0	22
distal	2	14	2	22				11		22
thecae one		1								
sicula		1								
Monoclimacis **n. sp. C Lukasik**	19	38	18	69	22	24	46	65	24	25
far distal (no hood, atavus like)			4				17			
distal	15	20	8	49	14	8	13	37	20	17
thecae one	2	9	3	10	4	8	8	14	2	4
sicula	2	9	3	10	4	8	8	14	2	4
Monograptus **n. sp. D**	6	28	38	7	0	0	0	0	0	0
distal	2	22	22	3						
thecae one	2	3	8	2						
sicula	2	3	8	2						
Campograptus **n. sp.**	0	0	0	4	0	0	0	0	2	0
distal				2						
thecae one				1					1	
sicula				1					1	
Monograptid	54	33	28	48	31	28	40	87	112	241
distal										
proximal										
sicula with theca one	54	33	28	48	31	28	40	87	112	241

number of diplograptid species	8
number of monograptid species	10
number of species	18
total diplograptid theca	2588
total monograptid theca	5696
total graptolite theca	8284

Table E20. Thecal counts from dissolution residues of CM 56

CM 56	0-4	4-12	12-16	16-23	23-27	27-33	33-40	40-46	46-49	49-53
Rivagraptus kayi	4	7	4	0	0	0	0	0	0	0
theca 1-1 to 2-2	3	5	3							
sicula	1	2	1							
Rivagraptus bellulus	0	0	0	0	12	0	0	0	0	0
distal					3					
theca 3-1 or 4-2					4					
theca 1-1 to 2-2					4					
sicula					1					
Glyptograptus tamariscus distans	0	0	13	22	10	38	4	19	17	4
distal				2						
theca 3-1 or 4-2			2	4	2	6		6	1	1
theca 1-1 to 2-2			8	12	6	24	3	11	12	3
sicula			3	4	2	8	1	2	4	
Metaclimacograptus rigidus	0	0	8	0	0	5	0	3	5	6
theca 3-1 or 4-2										
theca 1-1 to 2-2			6			4		2	3	4
sicula			2			1		1	2	2
***Petalolithus* sp.**	12	35	27	20	11	0	0	0	0	0
distal			3							
theca 1-1 to 2-2	7	22	16	12	7					
sicula	5	13	8	8	4					
Retiolitid	7	2	0	0	2	0	0	0	0	0
distal	6									
theca 1-1 to 2-2										
sicula	1	2			2					
Diplograptid	10	8	94	70	40	34	18	18	14	20
distal										
theca 1-1 to 2-2	5	4	47	35	20	17	9	9	7	10
sicula	5	4	47	35	20	17	9	9	7	10
***Monograptus falcata* forma B**	90	172	202	148	38	3	4	0	8	2
distal	12	30	18	10	8					
proximal	64	108	144	114	24	1	4		4	2
theca 1	7	17	20	12	3	1			2	
sicula	7	17	20	12	3	1			2	
Campograptus lobiferus lobiferus	16	26	60	70	22	41	40	29	59	21
distal	6	6	26	36	12	21	20	13	41	13
theca 1	5	10	17	17	5	10	10	8	9	4
sicula	5	10	17	17	5	10	10	8	9	4
***Campograptus* n. sp.**	5	22	17	28	31	21	10	9	24	21
distal	1	6	3	6	3	3	2	1	4	5
thecae one	2	8	7	11	14	9	4	4	10	8
sicula	2	8	7	11	14	9	4	4	10	8
***triangulate theca* (with hoops)**	2	1	0	1	1	0	0	0	0	0
distal (narrower protheca)	2			1	1					
mesial		1								
Rastrites orbitus	1	4	2	21	30	10	1	2	2	4
distal	1	4	2	13	8	4	1	2		
thecae one				4	11	3			1	2
sicula				4	11	3			1	2
***Monoclimacis* n. sp. B Lukasik**	19	61	21	22	50	16	5	10	16	31
distal (no hood)	5	23	3	1				3	3	13
proximal	2	12	4	9	18	4	3	3	9	8
thecae one	6	13	7	6	16	6	1	2	2	5
sicula	6	13	7	6	16	6	1	2	2	5
Monograptid	47	64	145	136	63	53	49	59	73	45
sicula with theca one	47	64	145	136	63	53	49	59	73	45

number of diplograptid species	6
number of monograptid species	6
number of species	12
total diplograptid theca	623
total monograptid theca	2306
total graptolite theca	2929

Table E21. Thecal counts from dissolution residues of CM 56.4-56.5

CM 56.4-56.5	0-5	5-8	8-13	13-18	18-23	23-42	42-47	47-50	50-54	54-62	62-66	66-71	71-75	75-79
Glyptograptus tamariscus distans	41	19	54	24	21	33	8	13	0	15	45	30	21	25
distal						3					9			3
theca 3-1 or 4-2	2		6	3		6				3	3	2		8
theca 1-1 to 2-2	30	14	36	16	15	18	6	9		9	22	20	15	10
sicula	9	5	12	5	6	6	2	4		3	11	8	6	4
Pseudoglyptograptus barriei	24	0	21	0	19	0	0	0	0	0	0	0	0	0
distal	10		12		10									
theca 3-1 or 4-2	2		4		4									
theca 1-1 to 2-2	9		4		4									
sicula	3		1		1									
Metaclimacograptus minimus	0	5	56	111	67	159	5	0	0	0	0	0	0	0
distal					2	5								
theca 3-1 or 4-2			14	17	14	23								
theca 1-1 to 2-2		4	32	72	37	96	4							
sicula		1	10	22	14	35	1							
Metaclimacograptus rigidus	65	70	116	59	30	87	6	20	10	12	26	14	6	16
distal	2	11				2		9			2			
theca 3-1 or 4-2	11	5		1	1	12		4	2		4			
theca 1-1 to 2-2	37	38	77	39	20	51	4	5	5	7	13	10	3	10
sicula	15	16	39	19	9	22	2	2	3	5	7	4	3	6
Petalolithus sp.	3	0	0	0	5	0	0	0	0	4	0	0	0	0
theca 1-1 to 2-2	2				3					3				
sicula	1				2					1				
Retiolitid	0	0	0	0	0	0	0	0	0	0	0	0	0	1
sicula														1
Diplograptid	121	74	152	84	54	90	56	38	18	56	68	50	68	106
theca 1-1 to 2-2	61	37	76	42	27	45	28	19	9	28	34	25	34	53
sicula	60	37	76	42	27	45	28	19	9	28	34	25	34	53
Monograptus n. sp. B forma A	15	2	2	3	2	10	5	12	18	10	22	21	10	39
distal	15	2	2	3	2	10	5	12	18	10	22	21	10	39
Campograptus sp.	27	58	46	45	34	31	9	9	3	26	18	8	5	8
distal	21	42	20	29	30	11	3	3	1	14	16	8	1	4
theca 1	3	8	13	8	2	10	3	3	1	6	1		2	2
sicula	3	8	13	8	2	10	3	3	1	6	1		2	2
Monoclimacis crenularis?	16	1	4	3	0	0	3	0	0	0	0	0	0	0
distal	12	1	2	3			1							
theca 1	2		1				1							
sicula	2		1				1							
Monograptus n. sp. E	0	0	0	0	0	0	0	0	0	1	1	1	0	0
distal										1	7	5		
proximal-mesial											1	1		
Rastrites spina?	11	16	5	6	0	8	0	1	0	13	12	6	4	3
distal (narrower protheca)	4									2			1	
mesial	7	16	5	6		8		1		11	12	6	3	3
Monograptus sidjachenkoi	182	139	291	213	239	494	139	139	14	20	27	33	26	82
distal	53	33	38	41	29	55	7	13					4	3
proximal	63	50	129	92	128	215	64	74	4	8	13	17	12	41
thecae one	33	28	62	40	41	112	34	26	5	6	7	8	5	19
sicula	33	28	62	40	41	112	34	26	5	6	7	8	5	19
Rastrites orbitus	0	7	46	5	1	0	0	0	0	0	0	0	0	10
distal		5	38	5	1									8
thecae one		1	4											1
sicula		1	4											1
Monoclimacis n. sp. B Lukasik	0	0	0	0	0	0	0	0	0	8	18	8	6	2
distal (no hood)	49	49	36	13	4						11			
proximal	16	13	17	8						4	3	2	4	
thecae one	7	12	13	3						2	2	3	1	1
sicula	7	12	13	3						2	2	3	1	1
Monograptid	39	30	53	38	13	66	28	18	3	10	11	14	7	19
distal										5				
sicula with theca one	39	30	53	38	13	66	28	18	3	5	11	14	7	19

number of diplograptid species	6	other fauna; gastropods, ostracods
number of monograptid species	9	
number of species	15	
total diplograptid theca	2401	
total monograptid theca	3111	
total graptolite theca	5512	

Table E22. Thecal counts from dissolution residues of CM 57.

CM 57	0-5	5-10	10-14	14-25	25-30	30-33	33-50	50-53
Pseudorthograptus inopinatus	0	0	0	0	0	3	0	1
theca 1-1 to 2-2						2		
sicula						1		1
Pseudoglyptograptus barriei	0	23	12	0	33	76	140	20
distal		14	12		8	14	18	4
theca 3-1 or 4-2		4			6	17	35	6
theca 1-1 to 2-2		4			15	34	71	8
sicula		1			4	11	16	2
Glyptograptus tamariscus distans	0	0	0	0	3	0	15	23
theca 3-1 or 4-2								3
theca 1-1 to 2-2					2		11	16
sicula					1		4	4
Metaclimacograptus sculptus	6	2	9	2	14	4	0	3
theca 1-1 to 2-2	4	1	6	1	9	2		2
sicula	2	1	3	1	5	2		1
Petalolithus	2	0	0	0	0	0	0	0
sicula	2							
retiolitid	0	0	1	0	0	0	0	1
sicula			1					1
diplograptid	16	22	34	34	54	56	82	58
distal								
theca 1-1 to 2-2	8	11	17	17	27	28	41	29
sicula	8	11	17	17	27	28	41	29
***Monograptus* n. sp. B forma B**	83	141	94	115	164	256	196	69
distal	83	141	94	115	164	256	196	67
theca 1								1
sicula								1
***Campograptus* n. sp.**	14	44	10	9	14	14	20	0
distal	8	28	6	5	6	6	12	
theca 1	3	8	2	2	4	4	4	
sicula	3	8	2	2	4	4	4	
***Monograptus* n. sp. F**	2	3	1	0	0	9	3	2
distal	2	3	1			9	3	2
Monoclimacis crenularis?	39	84	106	115	55	127	157	17
distal (retracted hoods, thicker width)		11	22	13		2	72	
prox-mesial (simple hooked thecae)	25	55	32	56	25	61	43	11
theca 1	7	9	26	23	15	32	21	3
sicula	7	9	26	23	15	32	21	3
***Torquigraptus* n. sp.**	40	44	32	56	50	144	273	34
distal (narrower protheca)	40	44	32	56	50	144	271	34
theca 1							1	
sicula							1	
Rastrites orbitus	2	9	9	14	15	29	3	4
distal	2	7	3	10	11	21	1	2
thecae one		1	3	2	2	4	1	1
sicula		1	3	2	2	4	1	1
***Pristiograptus* n. sp. B Lukasik**	0	6	0	0	0	0	0	0
proximal		4						
thecae one		1						
sicula		1						
***Pristiograptus* n. sp. A Lukasik**	36	38	37	24	24	57	16	0
distal (no hood)	12	11	13					
proximal	10	7	10	12	14	31	10	
thecae one	7	10	7	6	5	13	3	
sicula	7	10	7	6	5	13	3	
Monograptid	42	31	39	58	35	53	38	1
distal	2							
sicula wtth theca one	40	31	39	58	35	53	38	1

number of diplograptid species	6
number of monograptid species	8
number of species	14
total diplograptid theca	749
total monograptid theca	3256
total graptolite theca	3324

Table E23. Thecal counts from dissolution residues of CM 57.5-57.6

CM 57.5-57.6	0-5	5-14	14-18	18-25	37-42	42-48	48-54
Pseudoglyptograptus barriei	16	19	16	0	0	0	16
distal	2	10	3				
theca 3-1 or 4-2	4		4				3
theca 1-1 to 2-2	8	7	7				10
sicula	2	2	2				3
Glyptograptus tamariscus distans	0	0	0	10	5	0	4
distal							
theca 3-1 or 4-2				3			
theca 1-1 to 2-2				6	4		3
sicula				1	1		1
Metaclimacograptus hughesi	5	8	0	12	0	4	17
distal				3			
theca 3-1 or 4-2				4			4
theca 1-1 to 2-2	4	6		4		3	10
sicula	1	2		1		1	3
Retiolitid	5	1	0	0	0	0	0
distal	5						
theca 1-1 to 2-2							
sicula		1					
Diplograptid	8	16	14	16	12	16	12
distal							
theca 1-1 to 2-2	4	8	7	8	6	8	6
sicula	4	8	7	8	6	8	6
Monograptus n. sp. B. forma B	2	3	3	0	0	2	0
distal	2	3	3			2	
theca 1							
sicula							
Montograptus falcata forma C	126	101	23	26	37	85	24
distal	4	3			2	2	
mesial	112	88	19	22	27	81	22
theca 1	5	5	2	2	4	1	1
sicula	5	5	2	2	4	1	1
Monoclimacis crenularis?	0	0	0	0	26	39	32
distal					3		1
proximal-mesial					7	17	17
theca one					8	11	7
sicula					8	11	7
Monograptus n. sp. E	15	0	0	0	0	0	0
distal	15						
Rastrites orbitus	23	18	1	17	13	16	2
distal	23	18	1	13	7	8	2
thecae one				2	3	4	
sicula				2	3	4	
Pristiograptus n. sp. B Lukasik	10	10	0	22	14	7	4
distal (no hood)	6	1		8	11	2	1
proximal	2	7		6	3	3	3
theca one	1	1		4		1	
sicula	1	1		4		1	
Pristiograptus n. sp. A Lukasik	5	13	5	15	9	16	0
distal	3	3	1	9	3	6	
thecae one	1	5	2	3	3	5	
sicula	1	5	2	3	3	5	
Monograptid	18	26	22	25	10	17	18
distal	1	2	5				
proximal							
sicula with theca one	17	24	17	25	10	17	18

number of diplograptid species	4	bivavles and gastropods
number of monograptid species	7	
number of species	11	
total diplograptid theca	232	
total monograptid theca	900	
total graptolite theca	1132	

Table E24. Thecal counts from dissolution residues of CM 58a

CM 58a	0-6	5-9	9-15	16-21	21-26	26-30	30-35	35-39	39-43	43-47
Metaclimacograptus rigidus	36	3	3	38	11	16	15	34	57	38
distal				10			3			
theca 3-1 or 4-2	6			2				7	5	2
theca 1-1 to 2-2	23	2	2	19	8	10	8	20	35	25
sicula	7	1	1	7	3	6	4	7	17	11
Pseudoglyptograptus barrei	137	62	38	0	0	0	50	0	19	40
distal	24	2	8				24			
theca 3-1 or 4-2	23	14	8				8		1	3
theca 1-1 to 2-2	69	36	17				14		14	28
sicula	21	10	5				4		4	9
Neodicellograptus siluricus	130	44	33	10	54	8	13	14	34	0
arms	33	6	6	7	15		2	4	10	
theca 1-1 to 2-2	72	29	20	2	30	6	8	8	18	
sicula	25	9	7	1	9	2	3	2	6	
***Petalolithus* sp.**	0	8	8	0	8	13	3	18	13	9
distal		2								
theca 1-1 to 2-2		4	6		6	9	2	12	9	6
sicula		2	2		2	4	1	6	4	3
Retiolitid	4	8	29	37	34	21	9	18	8	16
distal		2	3	4	9			3	2	2
theca 1-1 to 2-2		4	18	16	16	11	2	6	2	4
sicula	4	2	8	17	9	10	7	9	4	10
Diplograptid	152	68	36	48	25	29	18	20	20	52
distal										
theca 1-1 to 2-2	78	34	18	24	13	15	9	10	10	26
sicula	74	34	18	24	12	14	9	10	10	26
***Monograptus falcata* forma C**	121	51	95	261	102	172	116	203	165	177
proximal	121	49	93	243	98	168	116	195	127	151
theca 1		1	1	9	2	2		4	19	13
sicula		1	1	9	2	2		4	19	13
Monograptus sidjackenkoi	672	436	464	509	151	186	123	193	55	2
distal	160	133	163	214	26	18	14	23	15	
mesial	282	195	165	163	59	66	61	78	22	
theca 1	115	54	68	66	33	51	24	46	9	1
sicula	115	54	68	66	33	51	24	46	9	1
Campograptus communis	59	8	5	25	11	17	4	19	61	134
distal	15			9	3	1	1	2	17	49
mesial	12	4	1	6	2	4	1	11	16	43
theca 1	16	2	2	5	3	6	1	3	14	21
sicula	16	2	2	5	3	6	1	3	14	21
***Rastrites* sp.**	93	45	51	51	11	7	0	1	11	4
distal	87	39	47	47	11	7		1	5	2
thecae one	3	3	2	2					3	1
sicula	3	3	2	2					3	1
***Monoclimacis* n. sp. B Lukasik**	0	0	0	0	10	0	0	0	5	8
proximal-distal					10				1	8
theca one									2	
sicula									2	
***Monograptus* n. sp. E**	0	0	0	0	0	0	0	0	0	3
distal										3
***Pristiograptus* n. sp. A Lukasik**	0	0	5	7	0	0	3	0	2	2
distal			3	5			1		2	
theca one			1	1			1			1
sicula			1	1			1			1
Monograptid	92	52	53	44	34	28	40	35	50	30
distal									4	
sicula with theca one	92	52	53	44	34	28	40	35	46	30

number of diplograptid species	5	some spec. encrusted
number of monograptid species	7	
number of species	12	
total diplograptid theca	1669	
total monograptid theca	5374	
total graptolite theca	7043	

Table E25. Thecal counts from dissolution residues of CM 59.1-59.2

CM 59.1-59.2	0-7	7-14	14-23	23-28	28-33	33-41	41-46	46-51	51-57	57-67	67-71	71-77
Metaclimacograptus rigidus	0	0	0	0	0	0	0	0	0	8	0	0
distal												
theca 3-1 or 4-2												
theca 1-1 to 2-2										6		
sicula										2		
Pseudoglyptograptus barriei	0	0	17	0	0	0	5	5	49	0	7	0
distal			8						25			
theca 3-1 or 4-2			4						12		2	
theca 1-1 to 2-2			4				4	4	10		4	
sicula			1				1	1	2		1	
Neodicellograptus siluricus	0	0	10	6	0	3	34	142	92	21	47	0
arms			2	3		3	9	38	41	6	7	
theca 1-1 to 2-2			6	2			18	75	38	11	29	
sicula			2	1			7	29	13	4	11	
Normalograptus nikolayevi ??	16	59	33	35	14	27	12	33	50	104	32	32
distal		24								25		
theca 3-1 or 4-2	1	8		4	2			4	2	17		1
theca 1-1 to 2-2	11	21	23	22	9	20	9	21	35	49	22	24
sicula	4	6	10	9	3	7	3	8	13	13	10	7
Petalograptus ankyratus	31	23	60	39	20	45	13	0	2	0	6	5
distal			5	9								
theca 1-1 to 2-2	15	11	31	16	9	25	8		1		4	4
sicula	16	12	24	14	11	20	5		1		2	1
Retiolitid	0	2	2	0	1	12	10	8	0	0	11	33
distal								2				12
theca 1-1 to 2-2						7	7	4			5	12
sicula		2	2		1	5	3	2			6	9
Diplograptid	30	70	108	46	34	40	60	128	102	92	162	125
distal												
theca 1-1 to 2-2	15	35	39	23	17	20	30	64	51	46	81	63
sicula	15	35	39	23	17	20	30	64	51	46	81	62
***Monograptus falcata* forma C**	15	15	13	45	9	27	61	42	145	109	51	43
mesial	15	15	13	43	9	15	53	34	143	105	47	41
theca 1				1		6	4	4	1	2	2	1
sicula				1		6	4	4	1	2	2	1
Monograptus sidjachenkoi	1	1	4	45	20	81	68	62	53	53	41	57
distal				1	2	12	11	19	15	11	11	13
mesial	1	1	2	42	14	45	33	31	26	36	26	36
theca 1			1	1	2	12	12	6	6	3	2	4
sicula			1	1	2	12	12	6	6	3	2	4
Campograptus communis	0	0	0	0	0	0	16	42	209	339	78	29
distal							2	3	160	253	37	3
mesial							2	17	23	42	9	8
theca 1							6	11	13	22	16	9
sicula							6	11	13	22	16	9
***Campograptus* sp.**	6	0	0	0	0	0	0	0	0	0	0	0
distal												
mesial												
theca 1	3											
sicula	3											
Monograptus crenularis?	6	0	0	3	0	0	0	0	0	0	0	0
distal	5											
proximal-mesial	1			3								
theca one												
sicula												
***Monograptus* n. sp. E**	4	0	0	2	3	2	0	0	0	0	0	0
distal	4			2	3	2						
thecae one												
sicula												

Table E25. Thecal counts from dissolution residues of CM 59.1-59.2

CM 59.1-59.2	0-7	7-14	14-23	23-28	28-33	33-41	41-46	46-51	51-57	57-67	67-71	71-77
Monograptus decipiens	14	17	34	55	47	56	65	78	90	55	47	5
distal	14	17	34	53	43	52	61	72	88	51	39	5
thecae one				1	2	2	2	3	1	2	4	
sicula				1	2	2	2	3	1	2	4	
Monoclimacus n.sp. B Lukasik	33	25	33	59	12	7	0	0	0	4	0	8
proximal-distal	15	19	11	51	6	1						4
theca one	9	3	11	4	3	3				2		2
sicula	9	3	11	4	3	3				2		2
Pristiograptus n. sp. B Lukasik	23	10	6	5	30	31	52	0	0	0	0	0
distal	19	5	2	3	12	13	30					
proximal	2	3	2	2	12	14	14					
theca one	1	1	1		3	2	4					
sicula	1	1	1		3	2	4					
Monograptid	47	33	15	28	14	25	34	34	22	21	21	15
distal									12			
proximal												
sicula with theca one	47	33	15	28	14	25	34	34	10	21	21	15

number of diplograptid species	6
number of monograptid species	9
number of species	15
total diplograptid theca	2213
total monograptid theca	3010
total graptolite theca	5223

Table E26. Thecal counts from dissolution residues of CM 72.6

CM 72.6	0-8	8-16	16-23	23-32
***Metaclimacograptus* n. sp.**	0	0	0	5
distal				
theca 3-1 or 4-2				
theca 1-1 to 2-2				4
sicula				1
***Normalograptus* n. sp.**	0	0	13	5
distal			9	
theca 3-1 or 4-2			2	
theca 1-1 to 2-2			2	4
sicula				1
Diplograptid	6	20	0	8
distal				
theca 1-1 to 2-2	3	11		4
sicula	3	9		4
***Campograptus* sp.**	5	0	2	0
distal				
mesial	3			
theca 1	1		1	
sicula	1		1	
***Rastrites* sp.**	8	2	8	13
distal	8	2	8	13
thecae one				
sicula				
Paradiversograptus capillaris	17	19	20	24
distal	9	7	14	16
theca one	4	6	3	4
sicula	4	6	3	4
Pristiograptus* cf. *variabilis	23	12	60	96
distal	9	2	14	42
theca one	7	5	7	27
sicula	7	5	7	27
Monograptid	8	19	16	33
distal				
proximal				
sicula with theca one	8	19	16	33

number of diplograptid species	2
number of monograptid species	4
number of species	6
total diplograptid theca	57
total monograptid theca	385
total graptolite theca	442

Table E27. Thecal counts from dissolution residues of CM 73.8

CM 73.8	0-7	7-10	10-14	14-18	18-21	21-25	25-32	32-38	38-42	42-49	49-52	52-57	57-64
***Metaclimacograptus* n. sp.**	47	50	37	8	8	74	29	33	44	19	9	45	8
distal	5	9	1				3		1			4	
theca 3-1 or 4-2	4		4			7	8		9	2		11	
theca 1-1 to 2-2	27	31	24	6	6	51	14	24	26	13	7	23	6
sicula	11	10	8	2	2	16	4	9	8	4	2	7	2
***Normalograptus* n. sp.**	4	4	0	0	17	3	0	0	18	13	17	20	7
distal					5				4	9			
theca 3-1 or 4-2					4				4			2	
theca 1-1 to 2-2	3	3			6	2			8	3	12	13	5
sicula	1	1			2	1			2	1	5	5	2
Petalolgraptus palmeus	0	10	0	3	12	0	8	9	0	3	5	7	5
distal		1											
theca 3-1 or 4-2		4											
theca 1-1 to 2-2		4		2	10		6	7		2	4	5	4
sicula		1		1	2		2	2		1	1	2	1
Retiolitid	0	1	3	6	26	6	0	0	0	0	0	0	0
distal					12	3							
theca 1-1 to 2-2				4	10	3							
sicula		1	3	2	4								
Diplograptid	87	50	71	41	48	103	38	57	32	44	25	48	56
distal													
theca 1-1 to 2-2	44	25	36	21	25	52	19	29	16	22	13	24	28
sicula	43	25	35	20	23	51	19	28	16	22	12	24	28
***Campograptus* sp.**	4	4	2	0	0	0	2	2	0	2	0	0	0
distal													
mesial		2											
theca 1	2	1	1				1	1		1			
sicula	2	1	1				1	1		1			
***Rastrites* sp.**	5	10	20	13	16	6	8	15	6	13	13	24	6
distal	5	10	20	13	16	6	8	11	6	13	13	24	6
thecae one								2					
sicula								2					
Monoclimacis crenularis?	0	2	0	0	0	0	0	0	0	0	2	1	0
distal											2	1	
theca one		1											
sicula		1											
Pristiograptus* cf. *variabilis	21	12	25	33	58	60	14	37	6	15	32	36	32
far distal	5		2	1	53	19	3	7		5	8	6	
distal	6	4	9	16	5	17	7	16	2	2	6	16	14
theca one	5	4	7	8		12	2	7	2	4	9	7	9
sicula	5	4	7	8		12	2	7	2	4	9	7	9
Monograptid	19	23	22	11	7	26	9	15	2	14	7	19	17
distal													
proximal													
sicula with theca one	19	23	22	11	7	26	9	15	2	14	7	19	17

reprecipitated silca throughout concretion

number of diplograptid species	4	(cement within rhabdosomes and sometimes encrusting)
number of monograptid species	4	gastropods
number of species	8	
total diplograptid theca	1318	
total monograptid theca	748	
total graptolite theca	2066	

Table E28. Thecal counts from dissolution residues of CM 74.9a

CM 74.9a	0-6	6-12	12-24	24-33	33-42
***Metaclimacograptus* n. sp.**	44	5	25	32	73
distal					4
theca 3-1 or 4-2	5		1	4	9
theca 1-1 to 2-2	29	4	18	21	45
sicula	10	1	6	7	15
***Normalograptus* n. sp.**	34	19	9	46	34
distal				6	
theca 3-1 or 4-2	4	1		8	2
theca 1-1 to 2-2	23	14	6	23	23
sicula	7	4	3	9	9
Diplograptid	86	66	70	121	92
distal					
theca 1-1 to 2-2	43	33	35	61	46
sicula	43	33	35	60	46
***Monograptus* n. sp. G**	0	0	1	2	1
distal			1	2	1
theca 1					
sicula					
***Rastrites* sp.**	35	34	14	11	3
distal	35	34	14	11	3
thecae one					
sicula					
Paradiversograptus capillaris	59	25	61	82	55
distal	41	19	55	70	51
theca one	9	3	3	6	2
sicula	9	3	3	6	2
Pristiograptus regularis regularis	11	4	0	0	0
distal	7				
theca one	2	2			
sicula	2	2			
Monograptid	26	13	11	23	11
distal					
proximal					
sicula with theca one	26	13	11	23	11

number of diplograptid species	2
number of monograptid species	4
number of species	6
total diplograptid theca	756
total monograptid theca	482
total graptolite theca	1238

Table E29. Thecal counts from dissolution residues of CM 75.5

CM 75.5	0-5	5-10	10-16	16-22	22-30	30-35	35-40	40-46	46-53	53-60	60-65	65-68	68-72	72-75
***Metaclimacograptus* n. sp.**	11	23	67	28	26	16	16	10	0	36	60	141	48	24
distal			5									12		
theca 3-1 or 4-2		2	9		2							12		
theca 1-1 to 2-2	8	16	41	20	18	11	12	8		28	44	81	36	16
sicula	3	5	12	8	6	5	4	2		8	16	36	12	8
estimated rhabdosome count	3	5	12	8	6	5	4	2	0	8	16	36	12	8
***Petalolithus* sp.**	0	0	4	0	0	0	0	0	0	0	0	0	0	0
theca 3-1 or 4-2														
theca 1-1 to 2-2			3											
sicula			1											
estimated rhabdosome count	0	0	1	0	0	0	0	0	0	0	0	0	0	0
Glyptograptus tamariscus	0	4	0	4	0	0	0	0	0	0	0	0	0	0
theca 1-1 to 2-2		3		3										
sicula		1		1										
estimated rhabdosome count	0	1	0	1	0	0	0	0	0	0	0	0	0	0
diplograptid	34	50	36	46	6	16	0	8	0	0	0	0	0	0
distal														
theca 1-1 to 2-2	17	25	18	23	3	8		4						
sicula	17	25	18	23	3	8		4						
triangulate thecae	7	8	0	0	0	0	0	0	0	0	0	0	0	0
distal	3	2												
mesial	4	4												
theca 1		1												
sicula		1												
estimated rhabdosome count	1	1	0	0	0	0	0	0	0	0	0	0	0	0
***Monograptus* n. sp. G**	8	2	2	2	1	9	52	28	44	48	16	30	52	12
distal	8	2	2	2	1	9	52	28	44	48	16	30	44	12
theca 1													4	
sicula													4	
estimated rhabdosome count	1	1	1	1	1	1	3	2	3	3	1	2	4	1
Spirograptus guerichi	0	34	92	210	583	527	176	28	36	32	30	66	168	24
far distal														
distal		24	76	164	411	361	96	24	28	32	28	36	120	16
theca 1		5	8	23	86	83	40	2	4		1	15	24	4
sicula		5	8	23	86	83	40	2	4		1	15	24	4
estimated rhabdosome count	0	5	8	23	86	83	40	4	4	4	4	15	24	4
***Rastrites* sp.**	0	1	0	0	0	0	5	0	0	0	0	0	0	0
distal		1					5							
estimated rhabdosome count	0	1	0	0	0	0	1	0	0	0	0	0	0	0
Monograptus halli	423	113	100	2	0	2	0	0	3	0	0	4	56	124
distal (dorsal, ventral hoods)	411	103	98	2		2			1			4	56	92
theca one	6	5	1						1					16
sicula	6	5	1						1					16
estimated rhabdosome count	20	12	8	0	0	0	0	0	1	0	0	0	4	16
***Monograptus* n. sp. H**	0	0	1	0	3	0	2	4	140	16	0	6	0	0
far distal									2					
distal			1		3		2	4	132	16		6		
theca one									4					
sicula									4					
estimated rhabdosome count	0	0	1	0	1	0	1	1	8	2	0	1	0	0
Pristiograptus regularis regularis	80	59	45	79	97	202	428	628	798	456	256	159	112	36
distal	66	49	31	57	65	128	308	380	590	328	136	93	80	28
theca one	7	5	7	11	16	37	60	124	104	64	60	33	16	4
sicula	7	5	7	11	16	37	60	124	104	64	60	33	16	4
estimated rhabdosome count	7	5	7	11	16	37	60	124	104	64	60	33	16	4
Monograptid	124	57	85	104	95	122	88	32	52	24	28	6	16	16
sicula with theca one	124	57	85	104	95	122	88	32	52	24	28	6	16	16

pyritized gastropods

Table E29. Thecal counts from dis

CM 75.5	76-82	82-86	86-91	91-95	95-100	100-105	
***Metaclimacograptus* n. sp.**	0	0	0	3	0	0	
distal							
theca 3-1 or 4-2							
theca 1-1 to 2-2				2			
sicula				1			
estimated rhabdosome count	0	0	0	1	0	0	
***Petalolithus* sp.**	3	0	0	3	44	0	
theca 3-1 or 4-2					44		
theca 1-1 to 2-2	2			2			
sicula	1			1			
estimated rhabdosome count	1	0	0	1	1	0	
Glyptograptus tamariscus	0	0	0	0	0	0	
theca 1-1 to 2-2							
sicula							
estimated rhabdosome count	0	0	0	0	0	0	
diplograptid	8	0	0	8	8	8	
distal							
theca 1-1 to 2-2	4			4	4	4	
sicula	4			4	4	4	
triangulate thecae	0	0	0	0	0	0	
distal							
mesial							
theca 1							
sicula							
estimated rhabdosome count	0	0	0	0	0	0	
***Monograptus* n. sp. G**	20	12	9	4	4	0	
distal	12	12	7	4	4		
theca 1	4		1				
sicula	4		1				
estimated rhabdosome count	4	1	1	1	1	0	
Spirograptus guerichi	116	176	156	36	60	64	2614
far distal				6	44	12	
distal	60	120	132	22	16	52	
theca 1	28	28	12	4			
sicula	28	28	12	4			
estimated rhabdosome count	28	28	12	4	0	0	
***Rastrites* sp.**	0	0	0	0	4	0	
distal					4		
estimated rhabdosome count	0	0	0	0	1	0	
Monograptus halli	292	104	160	116	312	188	1999
distal (dorsal, ventral hoods)	276	96	136	92	296	180	
theca one	8	4	12	12	8	4	
sicula	8	4	12	12	8	4	
estimated rhabdosome count	20	8	12	12	12	8	
***Monograptus* n. sp. H**	0	0	0	0	0	0	
far distal		40	44		36		
distal							
theca one							
sicula							
estimated rhabdosome count	0	0	0	0	0	0	
Pristiograptus regularis regularis	44	28	56	40	32	52	3687
distal	36	12	40	32	32	52	
theca one	4	8	8	4			
sicula	4	8	8	4			
estimated rhabdosome count	4	8	8	4	0	0	
Monograptid	20	48	96	36	28	60	
sicula with theca one	20	48	96	36	28	60	

number of diplograptid species	4
number of monograptid species	7
number of species	11
total diplograptid theca	799
total monograptid theca	9989
total graptolite theca	10788

Appendix F

Additional concretion description figures.

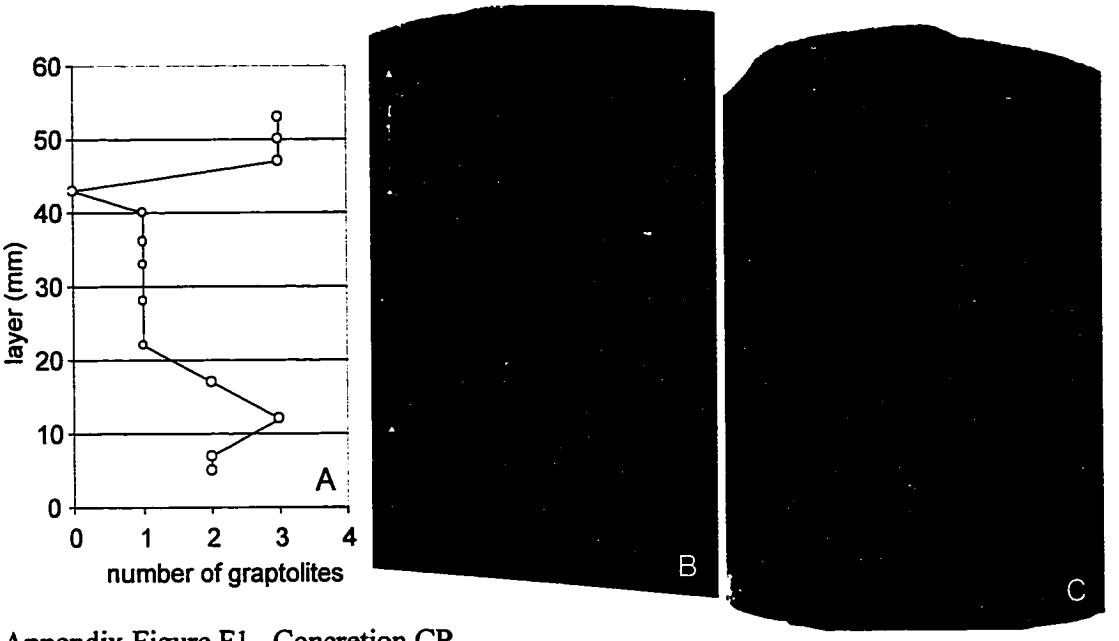

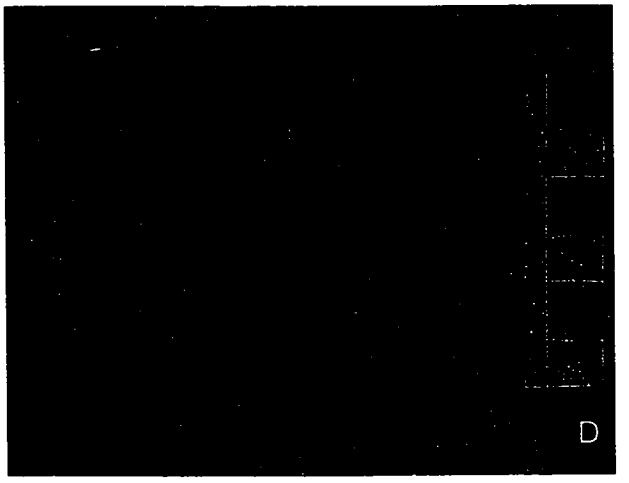

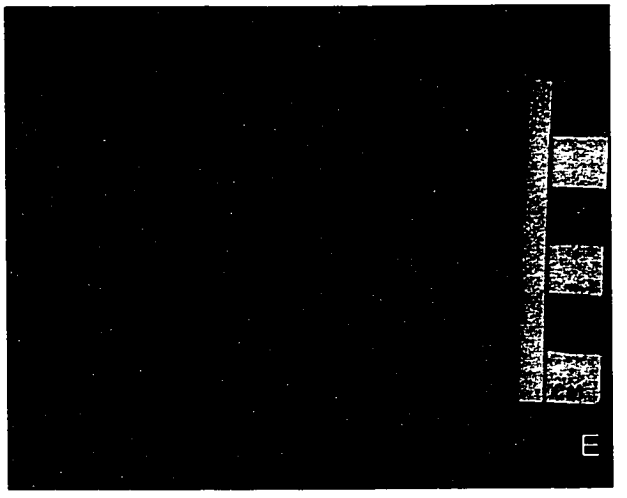

Appendix Figure F1. Concretion CP 32. A. Vertical distribution of graptolites through the strata. B, C. Digital scans of two polished slabs from off-cuts of the concretion. Relative heterogenity defines the laminae. Heterogeneous laminae are medium brown with dark brown and light brown flattened grains and light brown thin discontinuous internal laminae. Homogeneous beds are medium brown with rare visible grains and may represent an original texture that was finer than the heterogeneous layers. Layer 0-12, 35-43, and 43-60 each grade from a heterogeneous, medium brown base with many internal laminae to a homogeneous, greyish brown top. Actual size. D. Dissolution surface layer 36. The core contained graptolites within and therefore the graptolite distribution was not corrected. E. Dissolution surface layer 42. Large object within the center of the core that may by organic in origin.

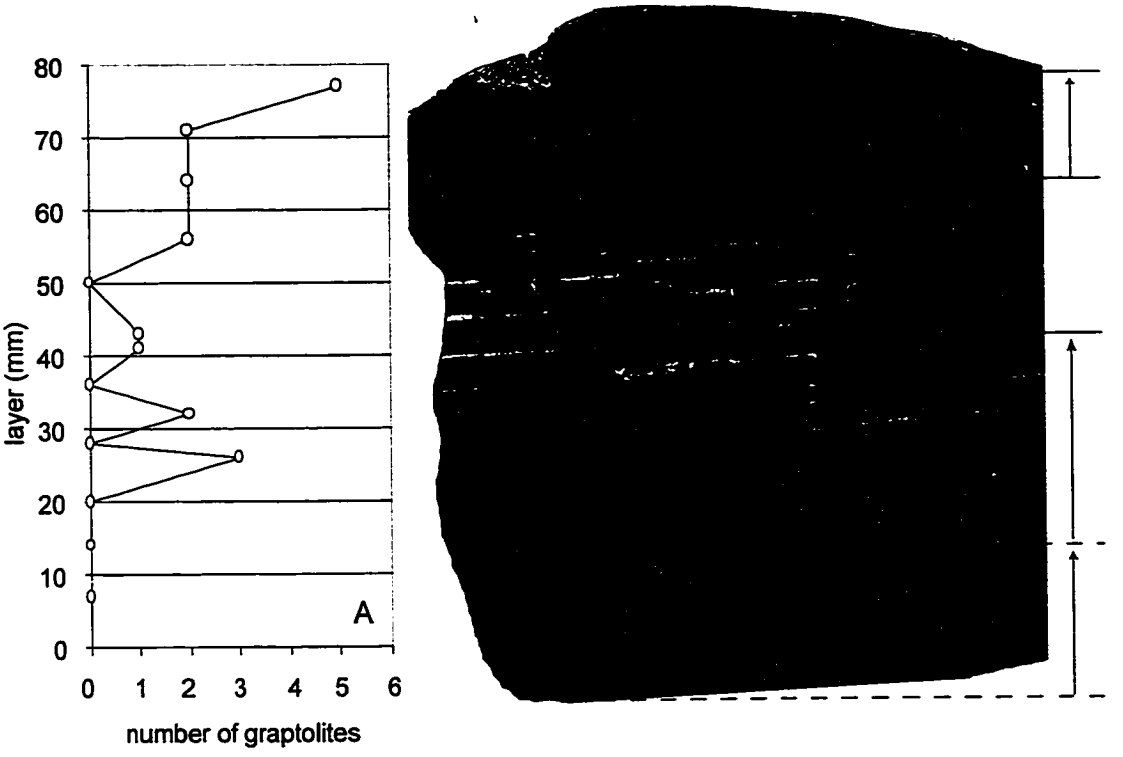

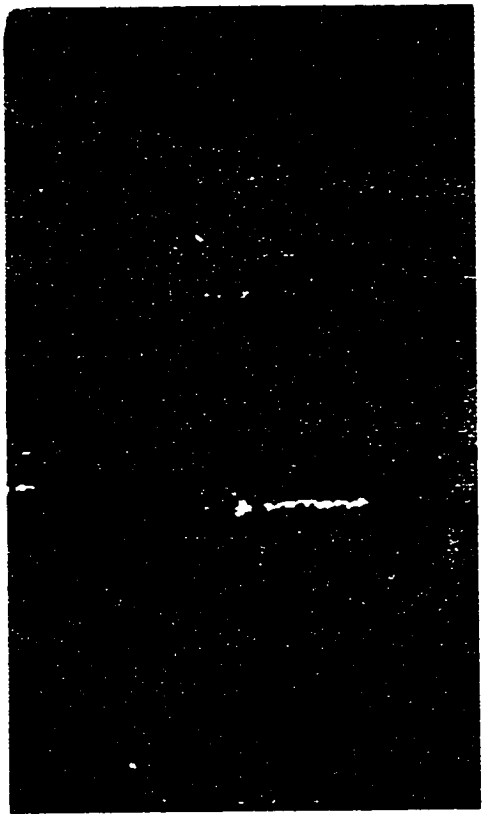

Appendix Figure F2. Concretion CP 38.4. A. Distribution of graptolites vertically through the concretion as revealed on the dissolution surfaces. B. Digital scan of polished slab. Bedding-parallel, calcite-filled veins are diagenetic in origin and possibly septarian cracks. Many of the laminae (0-13, 13-42, 62-70) show a grading of colour and relative heterogeneity. C. Digital scan of thin section. Carbonate crystals range 10-100 μm in diameter and average 30 μm. The grey-brown matrix has rare visible grains with poorly defined boundaries that average 10 μm in size. The veins are filled with carbonate crystals that are larger than 1 mm in dimension. The jagged edge to the veins is related to the euhedral growth of the carbonate crystals. Magnification x1.5.

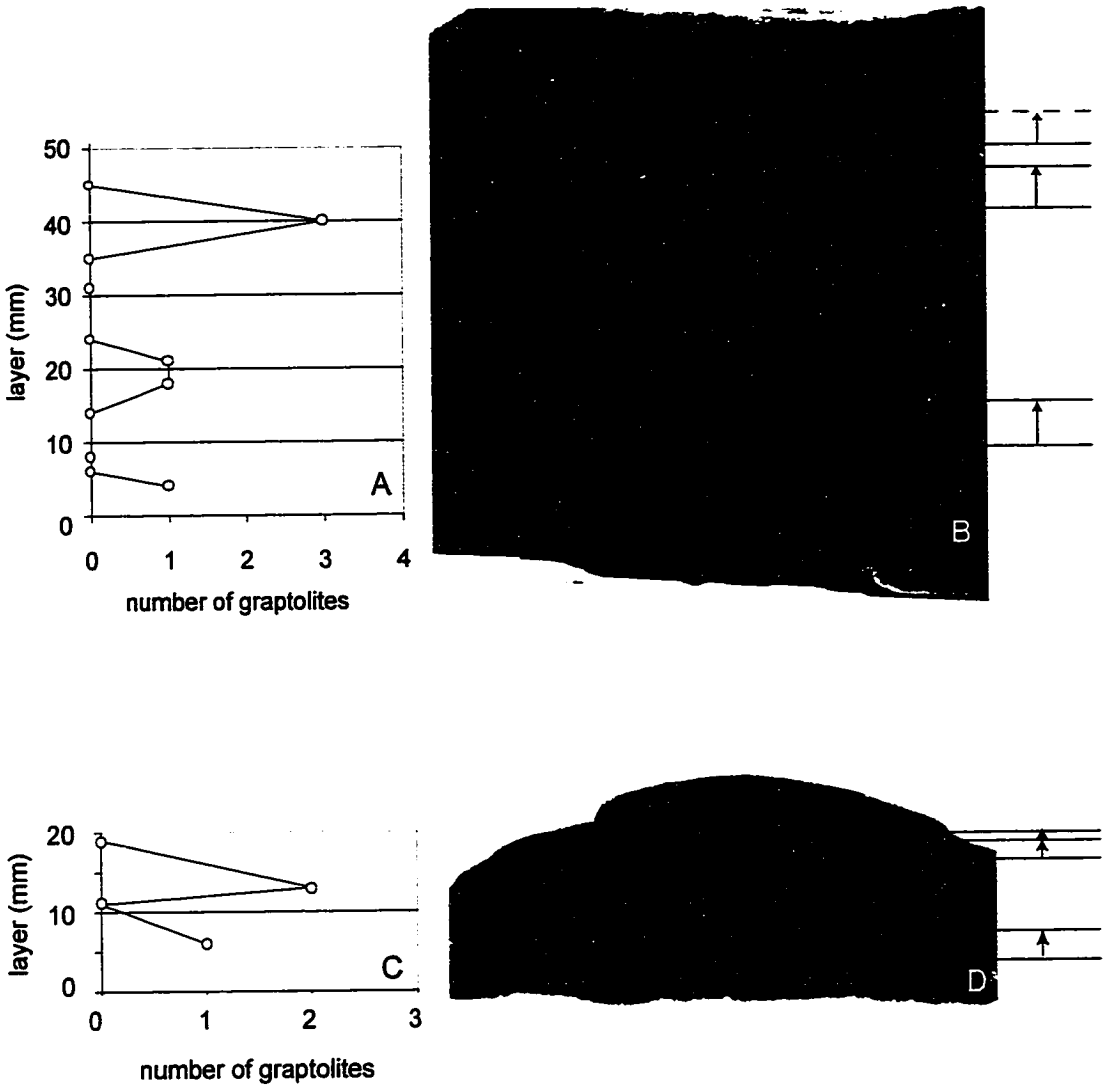

Appendix Figure F3. A, B. Concretion CP 96. C, D. Concretion CP145.2. A. Vertical distribution of graptolities through the concretion. Low total abundance although many radiolarians, three nautiloids, a brachiopod and sponge spicules in lattice were present. Increase in graptolites at layer 40 is statistically insignificant. B. Digtial scan of polished slab. Thin laminae are continuous and commonly display gradational boundaries. Three laminae grade from a light brown sharp base to a medium brown (identified with arrows). Actual size, aligned with dissolution layers in A. C. Graptolite distribution as recorded during the layer-by-layer dissolution. D. Digital scan of polished slab. Thin laminae are defined by colour variation and relative heterogeneity. Laminae are continuous but irregular. No clear biotubation evidence is observed although this could be disrupting the lamination. Three thin laminae grade from light brown homogeneous bases to medium-dark brown tops. Actual size, aligned with dissolution layers in C.

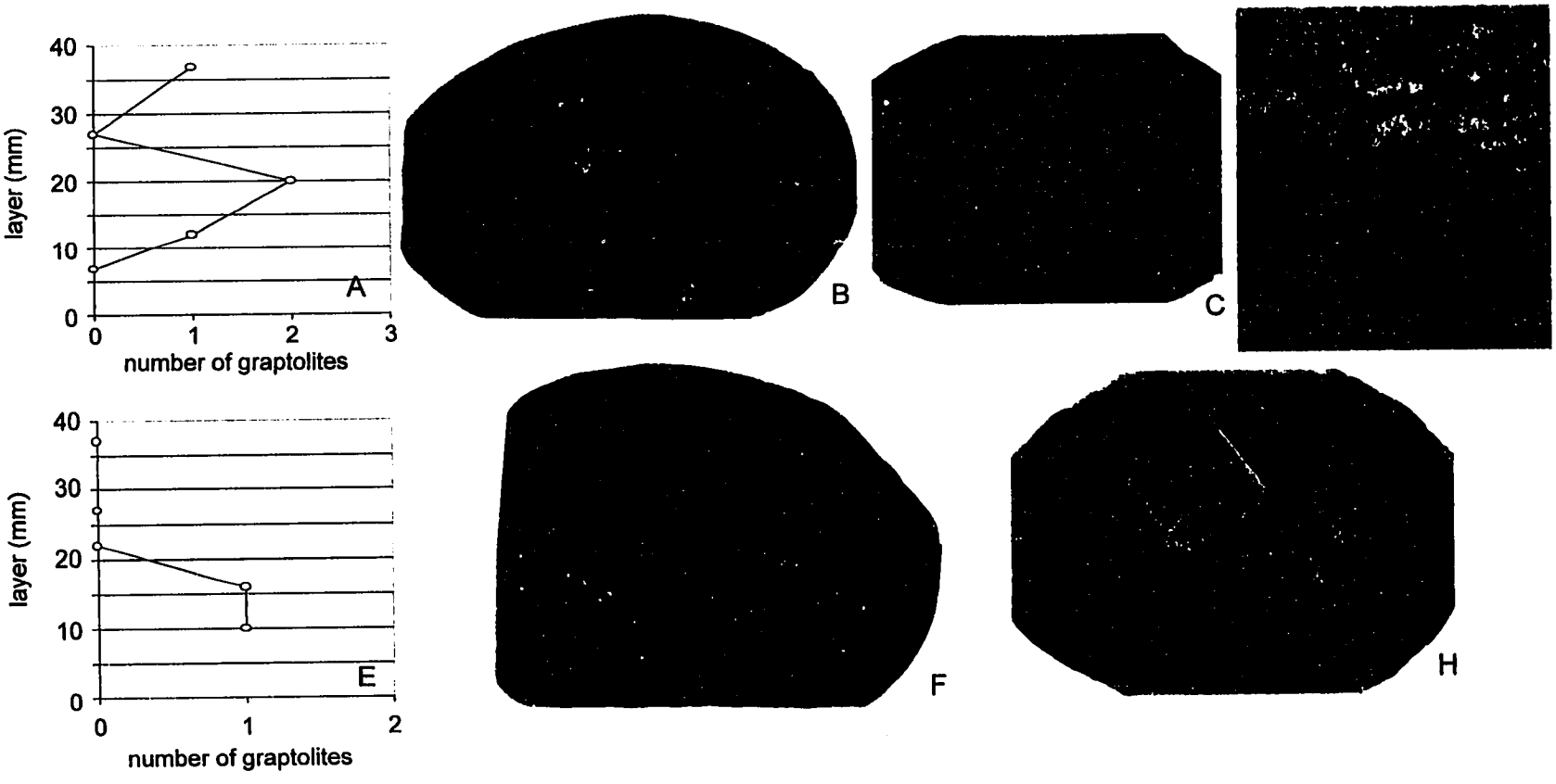

Appendix Figure F4. Two concretions collected from strata CP 146.5. A-D Concretion CP 146.5A. E-G. Concretion CP 146.5B. A, E. Vertical distribution of graptolites as observed during the layer-by-layer dissolution. B, F. Digital scans of polished slabs aligned with the dissolution layers. Actual size. C, H. Digital scans of thin sections (actual size). C. The dark lamina between 10 and 20 mm has a finer carbonate crystal size and more of the very fine grained matrix or micrite. D. The basal lamina is a more coarsely crystalline lamina with minor matrix. This is in sharp contact with the dark lamina above that has a finer texture and more of the micrite. Magnification x3. G. Similar to CM 146.5A the laminations are defined by the percentage of fine-grained matrix and the carbonate crystal size.

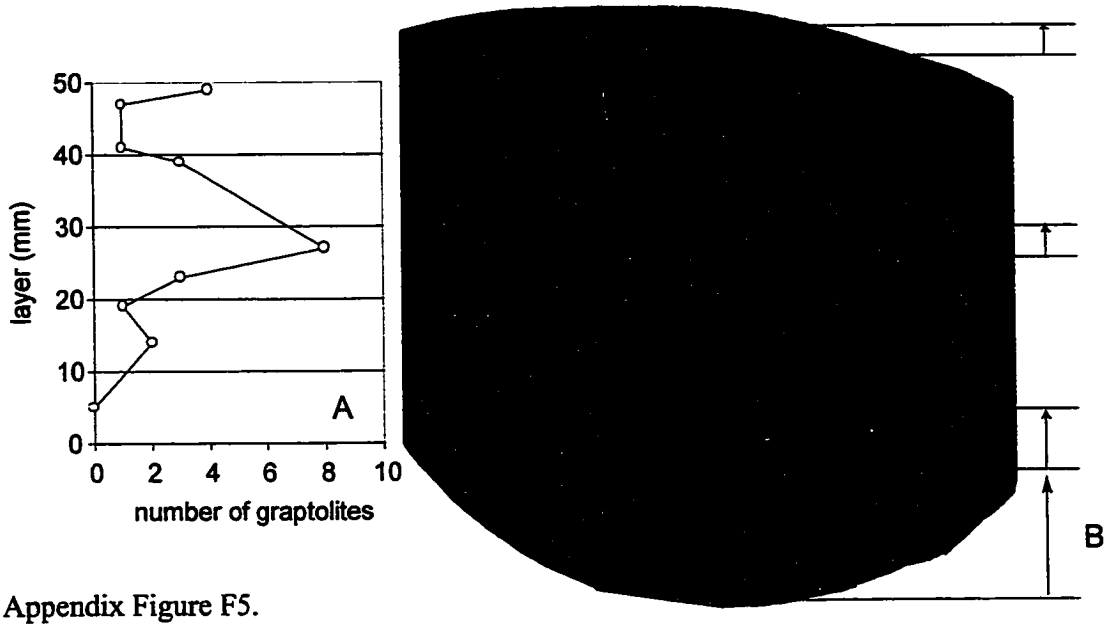

Appendix Figure F5. Concretion CM 150.6. A. Vertical distribution of graptolite rhabdosomes. B. Digital scan of polished slab. Laminae are defined by colour variation and relative heterogeneity. Four graded laminae can be identified. The four laminae grade from a medium brown, heterogeneous basal unit into a homogeneous medium brown top. C, D. Digital scan of thin sections. Dark brown grains range in size from 10-60 μm and have well-defined boundaries. Medium brown grains have poorly defined boundaries and are 30-80 μm. Light brown grains are very poorly defined and often elongate ranging 50-150 μm in length. The matrix is greyish-brown with an indistinguishable grain size. Nautiloids in cross-section. Magnification x1.5.

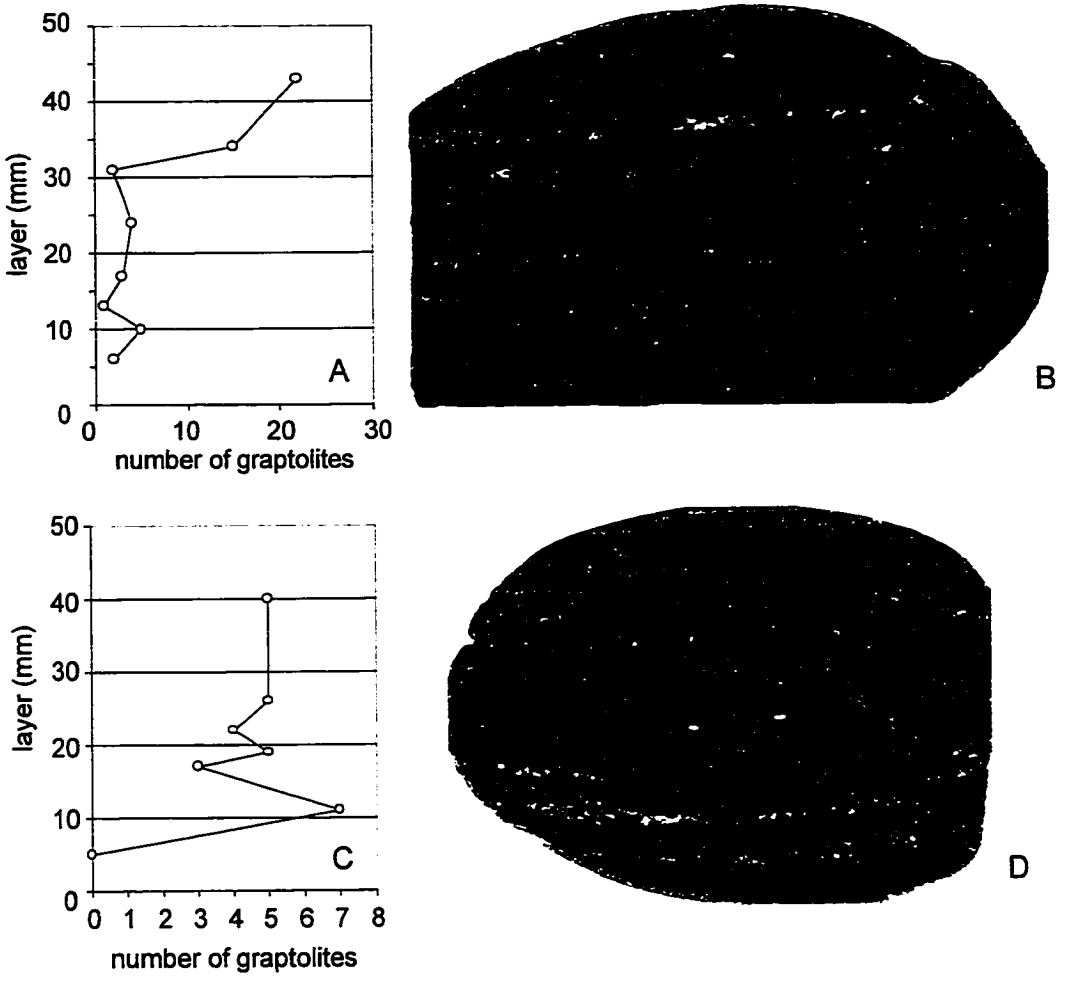

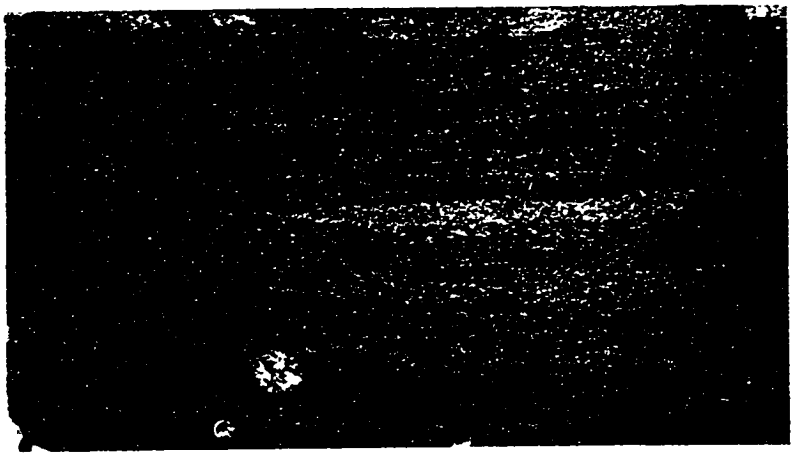

Appendix Figure F6. Two concretions from the same strata CP 152. A, B, E Concretion CP 152A. C, D. Concretion CP 152B. A, C. Graptolite distribution vertically through the concretions. B, D. Digital scan of polished slab showing fine laminae defined by colour variation. White silicate material of likely diagenetic origin preferentially occurs along some beds possibly indicating a higher original porosity/peremeability within these laminae. Graptolites and nautiloids visible in cross-section. E. Darker laminae have a finer concretionary carbonate size and contain more brown matrix. Silica precipitate visible. Magnification x1.5.

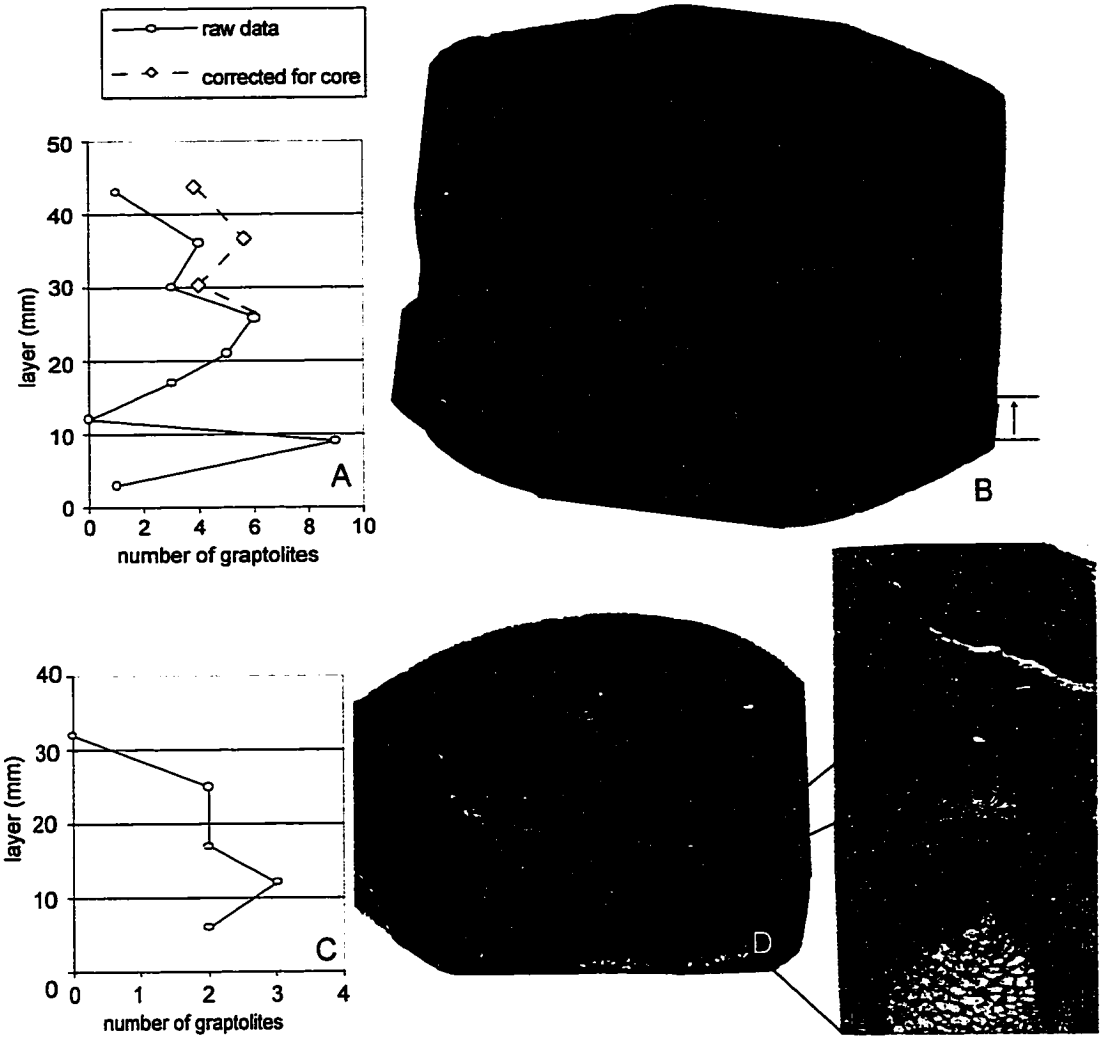

Appendix Figure F7. Two concretions from strata CP 163. A, B. Concretion CP 163A. C-E. Concretion CP 163B. A, C. Distribution of graptoltie rhabdosomes vertically through the concretions. B, D. Digital scan of polished slabs. Actual size. B. The matrix is medium brown with dark brown and light brown grains. Laminae are defined by the distribution of these grains. The core is a light brown that is more homogeneous in texture than the srrounding sediment. A graded lamina is seen at layer 10 -15 and thin discontinuous laminae of light brown are seen at layers 5 and 25 . D. The poorly defined laminae are identified by colour variation, relative heterogeneity and the distribution of diagenetic precipitates. Crinoid ossicles and a bioclastic layer are visible at 0-3 mm. A light brown, more homogeneous layer with irregular boundaries exists at 18-23 along with three irregular-shaped patches of a light material. E. Digital scan of thin section. Coarse crystals (50-300 μm.) of silica and calcite fill the voids within graptolites and the organic structure at the base of the thin-section. During dissolution this structure was seen to be hemispherical in shape and identified as coral or bryozoan. Crystal size throughout the rest of the concretion was indistinguishable. A graded bed is identified by the arrow. Magnification x1.5.

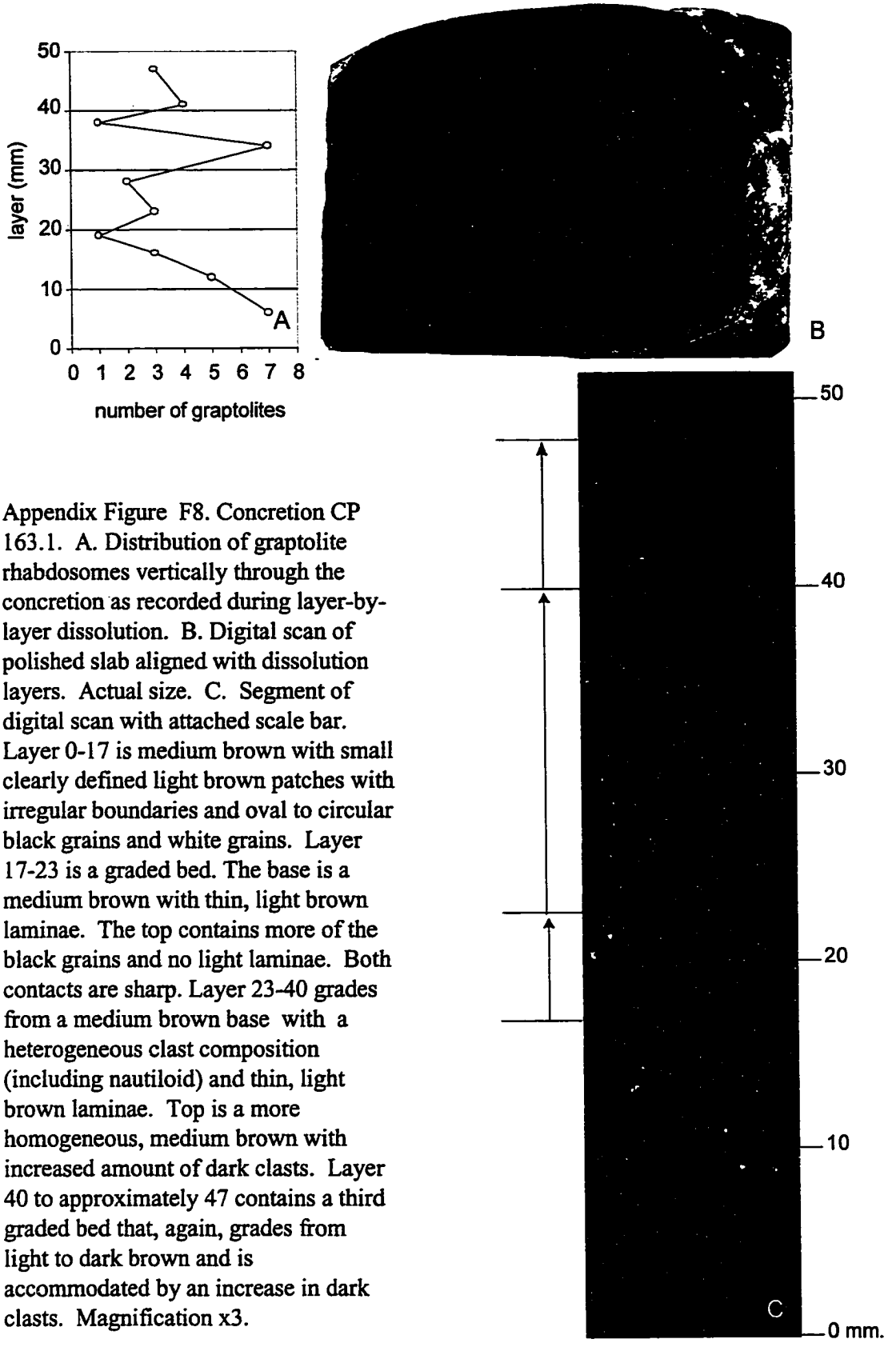

Appendix Figure F8. Concretion CP 163.1. A. Distribution of graptolite rhabdosomes vertically through the concretion as recorded during layer-by-layer dissolution. B. Digital scan of polished slab aligned with dissolution layers. Actual size. C. Segment of digital scan with attached scale bar. Layer 0-17 is medium brown with small clearly defined light brown patches with irregular boundaries and oval to circular black grains and white grains. Layer 17-23 is a graded bed. The base is a medium brown with thin, light brown laminae. The top contains more of the black grains and no light laminae. Both contacts are sharp. Layer 23-40 grades from a medium brown base with a heterogeneous clast composition (including nautiloid) and thin, light brown laminae. Top is a more homogeneous, medium brown with increased amount of dark clasts. Layer 40 to approximately 47 contains a third graded bed that, again, grades from light to dark brown and is accommodated by an increase in dark clasts. Magnification x3.

Appendix G

Chi-square (χ^2) distribution table

Appendix G. The χ^2 distribution

Table H1. The table gives the percentage points most frequently required for significance tests based on χ^2. Thus, the probility of observing a χ^2 with 5 degrees of freedom greater in value than 11.07 is 0.05 or 5 percent. Again the probability of observing a χ^2 with 5 degrees of freedom smaller in value than 0.554 is 1-0.99 = 0.01 or 1 percent (from Bailey, 1995, Appendix 3).

Degrees of freedom	Value of *P*					
	0.99	0.95	0.05	0.10	0.01	0.001
1	0.000157	0.00393	3.841	2.706	6.635	10.83
2	0.0201	0.103	5.991	4.605	9.210	13.82
3	0.115	0.352	7.815	6.251	11.34	16.27
4	0.297	0.711	9.488	7.779	13.28	18.47
5	0.554	1.145	11.07	9.236	15.09	20.51
6	0.872	1.635	12.59	10.64	16.81	22.46
7	1.239	2.167	14.07	12.02	18.48	24.32
8	1.646	2.733	15.51	13.36	20.09	26.13
9	2.088	3.325	16.92	14.68	21.67	27.88
10	2.558	3.940	18.31	15.99	23.21	29.59
11	3.053	4.575	19.68	17.27	24.72	31.26
12	3.571	5.226	21.03	18.55	26.22	32.91
13	4.107	5.892	22.36	19.81	27.69	34.53
14	4.660	6.571	23.68	21.06	29.14	36.12
15	5.229	7.261	25.00	22.31	30.58	37.70
16	5.812	7.962	26.30	23.54	32.00	39.25
17	6.408	8.672	27.59	24.77	33.41	40.79
18	7.015	9.390	28.87	25.99	34.81	42.31
19	7.633	10.12	30.14	27.20	36.19	43.82
20	8.260	10.85	31.41	28.41	37.57	45.31
21	8.897	11.59	32.67	29.62	38.93	46.80
22	9.542	12.34	33.92	30.81	40.29	48.27
23	10.20	13.09	35.17	32.01	41.64	49.73
24	10.86	13.85	36.42	33.20	42.98	51.18
25	11.52	14.61	37.65	34.38	44.31	52.62
26	12.20	15.38	38.89	35.56	45.64	54.05
27	12.88	16.15	40.11	36.74	46.96	55.48
28	13.56	16.93	41.34	37.92	48.28	56.89
29	14.26	17.71	42.56	39.09	49.59	58.30
30	14.95	18.49	43.77	40.26	50.89	59.70

REFERENCES

Aigner, T. 1982. Calcareous tempestites: storm-dominated stratification. Upper Muschelkalk limestones (Middle Trias, SW Germany). In Einsele, G. and Seilacher, A. (eds.) *Cyclic and Event Stratification*, Springer-Verlag, Berlin, pp, 180-198.

Allison, P. A. 1990. Carbonate nodules and plattenkalks. In Briggs, D. E. G. and Crowther, P. R. (eds.) *Paleobiology: A Synthesis*. Blackwell Scientific Publications, Oxford, pp. 250-253.

Allison, P. A. 1986. Soft-bodied animals in the fossil record: the role of decay in fragmentation during transport. *Geology*, 14: 979-981.

Allison, P. A. 1988. Soft-bodied squids from the Jurassic Oxford clay, *Lethaia*, 21: 403-410.

Allison, P.A. and Briggs, D.E.G. 1991. *Taphonomy: Releasing the Data Locked in the Fossil Record.* Plenium Press, New York, 560p.

Allison, P. A. and Pye, K. 1994. Early diagenetic mineralization and fossil preservation in modern carbonate concretions. *Palaios*, 9: 561-575.

Astin, T. R. 1987. Septarian crack formation in carbonate concretions from shales and mudstones. *Clay Minerals*, 21: 617-631.

Bailey, N. T. J. 1995. *Statistical Methods in Biology, thrid edition.* Cambridge University Press, Cambridge, 255p.

Barrande, J. 1850. *Graptoloids de Boheme*, VI. Prague, L'auteur, 74p.

Bates, D. E. B. 1989. The graptolites: strange plankton of the past. *Endeavour, New Series*, 13: 54-62.

Bates, D. E. B., and Kirk, N. H. 1985. Graptolites, a fossil case-history of evolution from sessile, colonial animals to automobile superindividuals. *Proceedings of the Royal Society of London*, B, 228: 207-224.

Bates, R. L. and Jackson, J. A. (eds). 1987. *Glossary of Geology, third edition.* Geological Institute, Alexandria, VA, 788p.

Bearman, G. 1989. *Ocean Circulation.* Pergamon Press, Oxford. 238p.

Behrensmeyer, A, K., and Hook, R. W. 1992. Paleoenvironmental contexts and taphonomic modes. In Behrensmeyer, A. K, Damuth, J. D., DiMichele, W. A.,

Potts, R., Sues, H. D., and Wing, S. L. (eds.) *Terrestial Ecosystems Through Time.* University of Chicago Press, Chicago, pp. 15-136.

Behrensmeyer, A, K. and Kidwell, S. M. 1985. Taphonomy's contributions to paleobiology. *Paleobiology*, 11: 105-119.

Behrensmeyer, A, K., Kidwell, S. M., and Gastaldo, R. A. 2000. Taphonomy and paleobiology. In Erwin, D. H. and Wing, S. L. (eds.) *Deep Time: paleobiology's perspective*, pp. 103-147.

Bennington, J. B. and Rutherford, S. D. 1999. Precision and reliability in paleocommunity comparisons based on cluster confidence intervals: how to get more statistical bang for your sampling buck. *Palios*, 14: 506-515.

Berry, W. B. N. 1962. Graptolite occurrence and ecology. *Journal of Paleontology*, 36: 285-293.

Berry, W. B. N. and Wilde, P. 1978. Progressive ventilation of the Oceans – An explanation for the distribution of the Lower Paleozoic black shales. *American Journal of Science*, 278: 257-275.

Berry, W. B. N., Wilde, P., and Quinby-Hunt, M. S. 1987. The oceanic nonsulphide oxygen minimum zone: a habitat for graptolites? *Bulletin of the Geological Society of Denmark*, 35: 103-114.

Best, M. M. R. and Kidwell, S. M. 2000. Bivalve taphonomy in tropical mixed siliclastic-carbonate settings. I. Environmental variation in shell condition. *Paleobiology*, 26: 80-102.

Bjerreskov, M. 1981. Silurian graptolites from Washington Land, western North Greenland. *Grønlands Geologiske Undersøgelse Bulletin*, 142: 1-58.

Bjerreskov, M. 1976. A new type of graptolite synrhabdosome. *Bulletin of the Geological Society of Denmark*, 25: 41-47.

Bjerreskov, M. 1991, Pyrite in Silurian graptolites from Bornholm, Denmark: *Lethaia*, v. 24, p. 351-361.

Bjerreskov, M. 1994. Pyrite diagnesis of graptolites from Bornholm. In Chen Xu, B. D. Erdtmann, and Ni Yunan (eds), *Graptolite Research Today*, Nanjing University Press, pp. 217-222.

Bouček, B. 1944. O nekterych ostnitych diplograptidech ceskeho a saského Siluru. *Rozpravy Česke Akademie Věd. Uměni. Tř. II*, 53(25): 1-6.

Bougis, P. 1976. *Marine Plankton Ecology*. North Holland Publishing Company, Amsterdam, 355p.

Bouma, A.H. 1962. *Sedimentology of Some Flysch Deposits*. Elsevier, Amsterdam, 168p.

Brandt Velbel, D. S. 1984. On defining limits to paleoecological interpretation in the fossil record. *Géobios Mémoire Spéciale*, 8: 415-418.

Brenchley, P. J., and Harper, D. A. T. 1998. *Paleoecology: Ecosystems, Environments and Evolution*. Chapman and Hall, London, 402p..

Brett, C. E. 1995. Sequence stratigraphy, biostratigraphy, and taphonomy in shallow marine environments. *Palaios*, 10: 597-616.

Brett, C. E. and Baird, G. C. 1986, Comparative taphonomy: a key to paleoenvironmental interpretation based on fossil preservation. *Palaios*, 1:207-227.

Brett, C. E. and Baird, G. C. 1993. Taphonomic approaches to temporal resolution in stratigraphy: examples from Paleozoic marine mudrocks. In Kidwell, S. M, and Behrensmeyer, A. K. (eds.). *Taphonomic Approaches to Time Resolution in Fossil Assemblages*. The Paleontological Society, Short Courses in Paleontology, 6: 188-209.

Brett, C.E., Dick, V. B, and Baird, G. C. 1991. Comparative taphonomy and paleoecology of Middle Devonian dark gray and black shales facies from western New York. In Landing, E. and Brett, C.E. (eds.). *Dynamic Stratigraphy and Depositional Environments of the Hamilton Group (Middle Devonian) in New York State, Part II* New York State Museum Bulletin, 469: 5-36.

Briggs, D. E. G. 1990. Flattening. In Briggs, D. E. G. and Crowther, P. R. (eds.) *Paleobiology: A Synthesis*. Blackwell Scientific Publications, Oxford, pp. 244-247.

Briggs, D. E. G., Kear, A. J., Baas, M., de Leeuw, J.W., and Rigby, S. 1995. Decay and composition of the hemichordate *Rhabdopleura*: implications for the taphonomy of graptolites. *Lethaia*, 28, 15-23.

Bulman. O. M. B. 1955. Part V: Graptolithina. In Moore, R. C. (ed.). *Treatise on Invertebrate Paleontology*, Geological Society of America, Inc. 101p.

Bulman, O.M.B. 1964. Lower Paleozoic Plankton. *Quarterly Journal Geological Society of London*, 120: 455-476.

Bulman, O. M. B. 1970. ,Part V: Graptolithina. In Bulman, O. M. B. (ed.). *Treatise on Invertebrate Paleontology*, Geological Society of America, Inc. 163p.

Buzas, M. A. and Culver, S. J. 1994. Species Pool and Dynamics of Marine Paleocommunites. *Science*, 264:1439-1441.

Buzas, M. A. and Hayek, L. C. 1998. Biodiversity resolution: an integrated approach. *Biodiversity Letters*, 3: 40-43.

Buzas, M. A. and Hayek, L. C. 1998. SHE analysis for biofacies identification. *Journal of Foraminiferal Research*, 28(3): 233-239.

Cadée, G. C. 1991. The history of taphonomy. In Donovan, S. K. (ed.). *The Process of Fossilization.* Colombia University Press, New York, pp. 3-22.

Chapman, A. 1991. How are they preserved? In Palmer, D. and Rickards, R.B. (eds.). *Graptolites: Writing in the Rocks.* Boydell Press, pp. 6-11.

Carruthers, W. 1867. Graptolites: their structure and position. *Intelligent Observer*, 11: 283-292, 365-374.

Chave, K. E. 1964. Skeletal durability and preservation. In Imbrie, J. and Newell, N. D. (eds.) *Approaches to Paleoecology.* Wiley, New York. pp. 377-387.

Chen, Xu and Lin, Yao-kun. 1978. Lower Silurian graptolites from Tongzi, northern Guizhou. *Memoirs of the Nanjing Institiute of Geology and Palaeontology, Academia Sinica*, 12: 1-76.

Churkin, M. and Carter, C. 1970. Early Silurian graptolites from southeastern Alaska and their correlation with graptolite sequences in North America and the Arctic. *Professional Papers of the U.S. Geological Survey*, 653: 1-51.

Coniglio, M., and Melchin, M.J., 1995, Petrography and isotope geochemistry of diagenetic carbonates in the lower Cape Phillips Formation, Cornwallis Island, Arctic Archipelago, Canada. *Bulletin of Canadian Petroleum Geology*, 43: 251-266.

Cooper, R. A. 1998. Towards a general model for depth ecology of graptolites. In Gutiérrez-Marco, J-C. and Rábano I. (eds.). *Proceedings of the 6th International Graptolite Conference (GWG-IPA) and 1998 Field Meeting, IUGS Subcommision on Silurian Stratigraphy.* Temas Geológico-Mineros ITGE, 23, 161-163.

Cooper, R. A. 1999a. Ecostratigraphy, zonation and global correlation of earliest Ordovician planktic graptolites. *Lethaia*, 32: 1-16.

Cooper, R. A. 1999b. The Ordovician time scale – calibration of graptolite and conodont zones. *Acta Universitatis Carolinae – Geologica*, 43: 1 – 4.

Cooper, R. A, Fortey, R. A., and Lindholm, K. 1991. Latitudinal and depth zonation of Early Ordovician graptolites. *Lethaia*, 24: 199-218.

Crowther, P. R. 1981. The fine-structure of graptolite periderm. *Special Papers in Palaeontology*, 26: 1-119.

Cummins, H., Powell, E. N., and Stanton Jr., R. J. 1986. The rate of taphonomic loss in modern benthic habitats: how much of the potentially preservable community is preserved? *Palaeogeography, Palaeoclimatology, Palaeoecology*, 52: 291-320.

Cutler, A. H. 1993. Mathematical models of temporal mixing in the fossil record. In Kidwell, S. M, and Behrensmeyer, A. K. (eds.). *Taphonomic Approaches to Time Resolution in Fossil Assemblages*. The Paleontological Society, Short Courses in Paleonology, 6: 169-187.

Davies, D. J., Powell, E. N., and Stanton Jr., R. J. 1989. Relative rates of shell dissolution and net sediment accumulation – a commentary: aan shell beds form by the gradual accumulation of biogenic debris on the sea floor? *Lethaia*, 22: 207-212.

de Freitas, T.A., Trettin, H. P., Dixon, O. A., and Mallamo, M. 1999. Silurian System of the Canadian Arctic Archipleago. *Bulletin of Canadian Petroleum Geology*, 47: 136-193.

Dilly, P. N. 1986. Modern pterobranchs: observations on their behaviour and tube building. In Hughes, C. P., Rickards, R. B., and Chapman, A. J. (eds.) *Palaeoecology and Biostratigraphy of Graptolites*. Geololgical Society of London, Special Publication, 20: 261-269

Dilly, P. N. 1993. *Cephalodiscus graptolitoides* sp. nov.: a probable extant graptolite. *Journal of the Zoological Society of London*, 229: 69-78.

Dodd, J. R. and Stanton, R. J. 1981. *Paleoecology, Concepts and Applications*. John Wiley and Sons, 382p.

Donovan, S. K. (ed.). 1991. *The Process of Fossilization*. Colombia University Press, New York, 303p..

Durham, J. W. 1967. The incompleteness of our knowledge of the fossil. *Journal of Paleontology*, 41: 559-565.

Duxbury, A. C, and Duxbury, A. B. 1994. *An Introduction to the World's Oceans (Third Edition)*. Dubuque, Iowa, Wm. C. Brown Publishers, 446 p.

Elles, G. L. andWood, E. M. R. 1901-1918. *A Monograph of British graptolites*. Palaeontographical Society Monograph, 539 p.

Edwards, L. 1989. *Organic Petrographic and Rock-eval Analysis of the Cape Phillps Formation on Cornwallis Island Canadian Arctic Archipelago*. B.Sc. thesis, University of Waterloo, Waterloo, ON, 38 p.

Efremov, J. A. 1940. Taphonomy: new branch of paleontology. *Pan-American Geologist*, 74: 81-93.

Erdtmann, B. D. 1973. Life forms and feeding habits of graptolites. In Boardman, R. S., Cheetham, A. H., and Oliver, W. A. (eds.) *Animal Colonies, Development and Function Through Time*. Downden, Hutchinson and Ross, Strousberg, Pennsylvania, pp. 523-532.

Erdtmann, B. D. 1976. Ecostratigraphy of Ordovician graptolites. In Bassett, M. B. (ed.) *The Ordovician System*. Cardiff, University Wales Press and National Museum of Wales, pp. 621-643.

Erdtmann, B. D. 1982. Palaeobiogeography and environments of plaktic dictyonemid graptolites during the earliest Ordovician. In M. G. Bassett and W. T. Dean (eds.) *The Cambrian- Ordovician Boundary*, Univeristy of Wales Press, Cardiff. pp. 9-27.

Etter, W. 1999. Community analysis. In Harper, D. A. T. (ed.) *Numerical Paleobiology: Computer-based Modelling and Analysis of Fossils and their Distributions*. John Wiley and Sons Ltd., Chichester, pp. 285-360

Fagerstrom, 1964. J. A. 1964. Fossil communities in paleoecology: their recognition and significance. *Geological Society of America Bulletin*, 75(12):1197-1216

Finney, S. C. 1979. Mode of life of planktonic graptolites: flotation structure in Ordovician *Decellograptus* sp. *Paleobiology*, 5: 31-39.

Finney, S. C. 1984. Biogeography of Ordovician graptolites in southern Appalachians. In Bruton. D. L. (ed.) *Aspects of the Ordovician System*. Palaeontological Contributions from the University of Oslo, Norsk Universitersforlaget, pp. 161-170.

Finney, S. C. 1986. Graptolite biofacies and correlation of eustatic subsidence and tectonic events in the Middle and Upper Ordovician of North America. *Palaios*, 6: 435-461.

Finney, S. C, and Berry, W.B.N. 1997. New Perspectives on graptolite distribution and their use as indicators of platform margin dynamics. *Geology*, 25: 919-922.

Finney, S.C. and Jacobson, S.R. 1985. Floatation devices in plankic graptolites. *Lethaia*, 18: 349-359.

Flessa, K. W. 1993. Time-averaging and temporal resolution in Recent marine shelly faunas. In Kidwell, S.M. and A.K. Behrensmeyer (eds.). *Taphonomic Approaches*

to Time Resolution in Fossil Assemblages. Short Couses in Paleontology, Publication of the Paleontological Society, 6: 9-33.

Flessa, K. W. 1998. Well-traveled cockles: shell transport during the Holocene transgression of the southern North Sea. *Geology*, 26: 187-190.

Flessa, K. W. and Kowalewski, M. 1994. Shell survival and time-averaging in nearshore and shelf environments: estimates from the radiocarbon literature. *Lethaia*, 27: 153-165.

Flessa, K. W., Cutler, A. H., and Meldahl, K. H. 1993. Time and taphonomy: quantitative estimates of time-averaging and stratigraphic disorder in a shallow marine habitat. *Paleobiology*, 19:266-286.

Fortey, R.A. 1982. In Fortey, R.A., Landing, E. and Skevington, D. 1982. Cambrian-Ordovician Boundary Sections in the Cow Head Group, western Newfoundland. In Basset, M.G. and Dean, W.T. (ed.), *The Cambrian-Ordovician Boundary.* University of Wales Press, Cardiff, pp. 95-129.

Fortey, R.A. and Bell, A.D. 1987. Branching geometry and function of multiramous graptolites. *Paleobiology*, 13: 1-19.

Fürsich, F. T. 1978. The influence of faunal condensation and mixing on the preservation of fossil benthic communities. *Lethaia*, 11: 243-250.

Fürsich, F. T. and Aberhan, M. 1990. Significance of time-averaging for paleocommunity analysis. *Lethaia*, 23: 143-152.

Fürsich, F.T. and W. Oschmann. 1993. Shell beds as tools in basin analysis: the Jurassic Kachchh, western India. *Journal of the Geological Society of London*, 150: 169-185.

Goldman, D. and Mitchell, C. E. 1994. Three-dimensional graptolites from the upper Middle Ordovician Neuville Formation, Quebec. *New York State Museum, Bulletin,* 481: 87-100.

Goldman, D., Bergstrom, S. M., and Mitchell, C. E. 1995. Revision of the Zone 13 graptolite biostratigraphy in the Marathon, Texas, standard succession and its bearing on Upper Ordovician graptolite biostratigraphy. *Lethaia*, 28:1 15-128.

Gutiérrez –Marco, J. C. and Lenz, A. C. 1998. Graptolite synrhabdosomes: biological or taphonomic entities? *Paleobiology*, 24: 37-48.

Harkness, R. 1851. Description of the graptolites found in the Black Shales of Dumfriesshire. *Quarterly Journal of the Geological Society of London*, 7:58-65.

Heath, R. J. 1998. *Palaeoceanographic and Faunal Changes in the Early Silurian.* Unpublished PhD thesis, Univeristy of Liverpool, 239p.

Hisinger, W. 1837. *Lethaea Suecica, seu Petrificata Sueciae. Supplementum* I. Stockholm, 124 pp.

Holland, S. M. 2000. The quality of the fossil record: a sequence stratigraphic perspective. In Erwin, D. H. and Wing, S. L. (eds.) *Deep Time: Paleobiology's Perspective*, p. 148-168.

Howe, M. P. A. 1982. The Lower Silurian graptolites of the Oslo Region. *Palaeontological Contributions from the Univeristy of Oslo*, 278: 21-32.

Hundt, R. 1938. [Describes a slab containing graptolites showing by their position the direction of contemporary currents]. *Zentralblatt für Mineralogie Abtelin* B, 7: 269-271. [In Bulman, 1955]

Hutt, J. E. 1974-1975. The Llandovery graptolites of the English Lake District. *Palaeontolographical Society Monograph: (I)*, 1974, 1-56; (II), 1975, 57-137

Hutt, J. E. 1991. What was their sex life like? In Palmer, D. and Rickards, R. B. (eds.). *Graptolite: Writing In the Rocks.* Boydell Press. pp 50-52.

Jackson, D.E. 1971. Development of *Glyptograptus hudsoni* sp. nov. from Southampton Island, North West Territories, Canada. *Palaeontology*, 14: 478-486.

Jaeger, H. 1970. Remarks on the stratigraphy and morphology of Pragian and probably younger monograptids. *Lethaia*, 3: 273-292.

Johnson, R. G. 1960. Models and methods for analysis of the mode of formation of fossil assemblages. *Geological Society of America Bulletin*, 71: 1075-86.

Johnson, R. G. 1964. The community approach to paleoecology. In Imbrie, J. and Newell, N. D. *Approaches to paleoecology.* John Wiley and Sons, New York, pp. 107-134.

Johnson, M. E. 1996. Stable cratonic sequences and a standard for Silurian eustacy. In Witzke, G., Ludvigson, A., and Day, J. (eds.) *Paleozoic Sequence Stratigraphy: Views from the North American Craton.* Geological Society Paper, no. 306, pp. 203-211.

Jones, O. T. 1909. The Hartfell-Valentian succession in the district around Plynlimon and Pont Erwyd (North Cardiganshire). *Quarterly Journal of the Geological Society of London*, 65: 463-537.

Jones, B. 1999. Biostatistics in paleontology. In Nowlan, G. S. (ed.) *PaleoScene: A Series of Papers on Paleontology Reprinted from Geosciene Canada*, Reprint Series 7, Geological Association of Canada, Paleontology Division, pp. 113-132.

Keary, P. 1996. *Dictionary of Geology*. Penguin Books, London, 365 p.

Kemp, A.E.S. 1991. Mid Silurian pelagic and hemipelagic sedimentation and palaeoceanography. *Special Papers in Palaeontology*, 44, pp. 261-299.

Kidwell, S. M. 1991. The stratigraphy of shell concentrations. In Allison, P. A. and Briggs, D. E. G. 1991. *Releasing the Data Locked in the Fossil Record*, Volume 9 of Topics in Geobiology, Plenum Press, New York, pp. 211-290.

Kidwell, S. M. 1993. Taphonomic expressions of sedimentary hiatus: field observations on bioclastic concentrations and sequence anatomy in low, moderate, and high subsidence settings. *Geologische Rundschau*, 82: 189-202.

Kidwell, S. M. 1998. Time-averaging in the marine fossil record: overview of strategies and uncertainties. *Geobios*, 30: 977-995.

Kidwell, S. M. and Bosence, D. W.J. 1991. Taphonomy and time-averaging of marine shelly faunas. In Allison, P. A. and Briggs, D. E. G. (eds.) 1991. *Taphonomy: Releasing the Data Locked in the Fossil Record.* Plenum Press, New York, pp.115-209.

Kidwell, S. M. and Brenchley, P. J. 1996. Evolution of the fossil record: thickness trends in marine skeletal accumulations and their implications. In Jablonski, D., Erwin, D. H., and Lipps, J. H. (eds.). *Evolutionary Paleobiology*. University of Chicago Press, Chicago, pp. 290-336.

Kidwell, S. M. and Flessa, K. W. 1995. The quality of the fossil record: populations, species, and communities. *Annual Review of Ecology and Systematics*, 26: 269-299.

Kirk, N. H. 1969. Some thoughts on the ecology, mode of life and evolution of the Graptolithinia. *Proceedings of the Geological Society of London*, 1659: 273-292.

Kirk, N. H. 1972. More thoughts on the automobility of the graptolites. *Journal of the Geological Society of London,* 128: 127-133.

Kirk, N. H. 1978. Mode of life of graptolites. *Acta Paleontologica Polonica*, 23: 427-448.

Kirk, N. H. 1990a. Juvenile sessility, vertical automobility, and passive lateral transport as factors in graptolite evolution. *Modern Geology*, 14: 153-187.

Kirk, N. H. 1990b. Construction, form and function in the Graptolithina: a review. *Modern Geology*, 15: 287-311.

Koren, T. N. and Rickards, R. B. 1996. Taxonomy and evolution of Llandovery biserial graptoloids from the Southern Urals, Western Kazakhstan. *Special Papers in Palaeontology*, 54, 49 p.

Kozlowski, R. 1948. Les Graptoliths et quelques nouveaux groupes d'animaux du Tremadoc de la Pologne. *Palaeontologica Polonica*. 3: 1-235.

Kowalewski, M. 1997. The reciprocal taphonomic model. *Lethaia*, 30: 86-88.

Kowalewski, M., Goodfriend, G. A., and Flessa, K. W. 1998. High-resolution estimates of temporal mixing with shell beds: the evils and virtues of time-averaging. *Paleobiology*, 24: 287-304.

Krebs, C. J. 1989. *Ecological Methodology*. Harper and Row, New York.

Kurck, C. 1882. Några nya graptolitarter från Skåne. *Geologiska Föreningens Stockholm Förhandlingar*, 6: 294-304.

Lapworth, C. 1876. On Scottish Monograptidae. *Geological Magazine*, 3: 308-321, 350-36-, 499-507, 544-552.

Lapworth, C. 1897. Die Lebensweise der Graptolithen. In Walther, J. Lebensweise fossiler Meeresthiere, *Deutschen Geologischen Gesellschaft, Zeitschr*. 49: 238-258.

Lenz, A.C. 1995. Upper Homerian (Wenlock, Silurian) graptolites and graptolite biostratigraphy, Arctic Archipelago, Canada. *Canadian Journal of Earth Sciences*, 32: 1378-1392.

Lenz, A. C. and Chen, Xu. 1985. Graptolite distribution and lithofacies: some case histories. *Journal of Paleontology*, 59: 636-642.

Lenz, A.C. and Melchin, M.J. 1991. Wenlock (Silurian) graptolite biostratigraphy of the Cape Phillips Formation, Canadian Arctic Islands. *Canadian Journal of Earth Sciences*, 27: 1-13.

Lenz, A. C., Jin, J., McCracken, A. D., Utting, J., and Westrop, S. R. 1993. Paleoscene 15. Paleozoic biostratigraphy: *Geoscience Canada*, 20: 41-73.

Loydell, D. K. 1991. Isolated graptolites from the Llandovery of Kallholen, Sweden. *Palaeontology*. 34: 653-671.

Loydell, D. K. 1998. Early Silurian sea level changes. *Geological Magazine*, 135: 447-471.

Loydell, D. K., Štorch, P., and Melchin, M. J. 1993. *Spirograptus turriculatus* and related Llandovery graptolites. *Palaeontology*, 36: 909-926.

Loydell, D. K., Zalasiewicz, J. A., and Cave, R. 1998. Predation on graptoloids: new evidence from the Silurian of Wales. *Palaeontology*, 41: 423-427.

Lukasik, 1994. *Morphology, Taxonomy and Phylogeny of Some Early to Middle Llandovery (Lower Silurian) "Monograptids", Cape Phillips Formation, Canadian Arctic Islands.* Unpublished Masters thesis, Dalhousie University, Halifax, Nova Scotia, 210 p.

Lukasik J. J. and Melchin, M. J. 1997. Morphology and classification of some Early Silurian "monograptids" (Graptoloidea) from the Cape Phillips Formation, Canadian Arctic Islands. *Canadian Journal of Earth Science*, 34: 1128-1149.

Lyman, R. L. 1994. *Vertebrate taphonomy.* Cambridge Manuals in Archaeology, Cambridge University Press, Cambridge, 550p.

Madin, L. P. 1990. Aspects of jet propulsion in salps. *Canadian Journal of Zoology*, 68: 765-777.

Martin, R. E. 1993. Time and taphonomy: actualistic evidence for time-averaging of benthic foraminiferal assemblages. In Kidwell, S. M, and Behrensmeyer, A. K. (eds.) 1993. *Taphonomic Approaches to Time Resolution in Fossil Assemblages.* The Paleontological Society, Short Courses in Paleontology, 6, pp. 35-56.

Martin, R. E., Wehmiller, J. F., Harris, M. S., and Liddell, W. D. 1996. Comparative taphonomy of bivalves and foraminfera from Holocene tidal flat sediments, Bahia la Choya, Sonora, Mexico (northern Gulf of California): taphonomic grades and temporal resolution. *Paleobiology*, 22: 80-90.

Marshall, N.B. 1979. *Developments in Deep Sea Biology.* Blandford Press, Dorset, 566 p.

M'Coy, F. 1850. On some new genera and species of Silurian Radiata in the collection of the Univeristy of Cambridge. *Annals and Magazine of Natural History, Series 2*, 6: 270-290.

McCave, I. N. 1984. Erosion, transport and deposition of fine-grained marine sediments. In Stow, D. A. V. and Piper, D, J. W. (eds), Fine-grained Sediments: Deep-water Processes and Facies, Geolological Society of London Special Publication, 15. Oxford, Blackwell Scientific, pp. 35-69.

Melchin, M. J. 1987a. Upper Ordovician and Early Silurian graptolites from the Cape Phillips Formation, Canadian Arctic Islands. *Bulletin of the Geological Society of Denmark*, 35: 191–202.

Melchin, M. J. 1987b. Late Ordovician and Early Silurian graptolites, Cape Phillips Formation, Canadian Arctic Archipelago. Ph.D. thesis, The University of Western Ontaio, London, ON, 760 p.

Melchin, M. J. 1989. Llandovery graptolite biostratigraphy and paleobiogeography, Cape Phillips Formation, Canadian Arctic Islands. *Canadian Journal of Earth Sciences*, 26: 1726-1746.

Melchin, M. J. 1998. Morphology and phylogeny of some early Silurian "diplograptid" genera from Cornwallis Island, Arctic Canada. *Palaeontology*, 41:263-315.

Melchin, M. J. and A. J. Anderson. 1998. Infrared video microscopy for the study of graptolites and other organic-walled fossils. *Journal of Paleontology*, 72(2):397-400.

Melchin, M. J. and Cooper, R. A. in prep. The Silurian System. In Gradstein, F. M., Ogg, J. G., and Smith, A. G. (eds.) *A Geologic Time Scale*. Cambridge University Press.

Melchin, M. J. and Demont, M. E. 1995. Possible propulsion modes in Graptoidea: a new model for graptolite locomotion. *Paleobiology*, 21: 110-120.

Melchin, M. J. and Lenz, A. C. 1986. Uncompressed specimens of *Monograptus turriculatus* (Barrande, 1850) from Cornwallis Island, Arctic Canada. *Canadian Journal of Earth Sciences*, 23: 579-582.

Melchin, M. J., Beson, M., and Lukasik, J. J., 1994. A new technique for taphonomic study of graptolites in concretionary or bedded limestones. *Graptolite News* 8, pp. 50-51.

Melchin, M. J., Koren, T. N., and Storch, P. 1998. Global diversity and survivorship of Silurian graptolites. In Landing, E. and Johnson, M. E. (eds.) *Silurian Cycles*, New York State Museum Bulletin, 491, pp. 165-182.

Melchin, M. J., McCracken, A. D., and Oliff, F. J. 1991. The Ordovician-Silurian boundary on Cornwallis and Truro islands, Arctic Canada: preliminary data. *Canadian Journal of Earth Sciences*, 28: 1854-1862.

Meldahl, K. H., Flessa, K. W., and Cutler, A. H. 1997. Time–averaging and postmortem skeletal survival in benthic fossil assemblages: quantitative comparisions among Holocene environments. *Paleobiology*, 23: 207-229.

Meyer, D. L., Ausich, W. I., and Terry, R. E. 1989. Comparative taphonomy of echinoderms in carbonate facies: Fort Payne Formation (lower Mississippian) of Kentucky and Tennessee. *Palaios*, 4: 533-552.

Mitchell, C. E. 1987. The evolution and phylogenetic classification of the Diplograptacea. *Palaeontology*, 30: 353-405.

Mu En-Zhi, Li Ji-Jin, Ge Mei-yu, Chen xu, Ni yu-nan, Lin Yao-kun, and Mu, H. –N. 1974. [Silurian Graptoloidea.] In Nanjing Institue of Geology and Paleontology, Academia Sinica (ed.). *A Handbook of the Stratigraphy and Paleontology in Southwest China*, Science Press, Nanjing. [In Chinese]

Mullins, H. T. and Cook, H. E. 1986. Carbonate apron models: alternatives to the submarine fan model for paleoenvironmental analysis and hydrocarbon exploration. *Sedimentary Geology*, 48: 37-79.

Mutti, E. and Ricci Lucchi, F. 1975. Turbidite facies and facies associations. In Mutti, E. *et al.* (eds.), *Examples of Turbidite Facies and Associations from Selected Formations of the Northern Apennies, Field Trip Guidebook A-11*, 9th International Association of Sedimentologists Congress, Nice. pp. 21-36.

Mutti, E. and Normack, W. R. 1987. Comparing Examples of Modern and Ancient Turbidite Systems: Problems and Concepts. In Leggett, J.K. and Zuffa, G.G. *Marine Clastic Sedimentology: Concepts and Case Studies*. Graham and Trotman. pp. 1-38.

Ni, Y. –N. 1978. [Lower Silurian graptolites from Yichang, western Hubei]. *Acta Palaeontologica Sinica*, 17: 387-416 [In Chinese].

Nicholson, H. A. 1868. On the graptolites of the Coniston Flags; with notes on the British species of the genus *Graptolites*. *Quarterly Journal of the Geological Society of London*, 24: 521-545.

Obut, A. M. 1965. Silurian graptolites from the Chukotskiy Peninsula. In *Ordovician and Silurian Stratigraphy and Faunas of the Chukotskiy Peninsula.* Obut, A. M. (ed.). Izdatel'stvo Nauka, Sibirskoe Otdelenie, pp. 103-221. [In Russian].

Obut, A. M. and Sennikov, N. V. 1980. Silurian graptolites from the Siberian Platform. In Sokolov, B. S., Obut, A. M., Tesakov, Yu. I., and, Predtechenskiy, N. N. (eds.) *Silurian of the Siberian Platform.* Izdatel'stvo Nauka, Sibirskoe otdelenie, pp. 1-51.

Obut, A. M. and Sobolevskaya, R. F. 1965. Opisanie Graptolitoc. In Obut, A. M. and Sobolevskaya, R. F, and Bondarev, V. I. (eds.) *Graptolity Silura Taimyra.* Akademiya Nauk SSR. Sibirskoe Otdelenie Institut Geologii I Geofiziki, pp. 1-120.

Obut, A. M. and Sobolevskaya, R. F. 1967. [Graptolite description] In Obut, A. M., Sobolevskaya, R. F., and Nikolyaev, A. A. (eds.) [*Lower Silurian Graptolites and Stratigraphy of the Uplifted Marigin of the Kolyma Massif* (northeastern USSR).] Akademiya Nauk SSSR, Moscow, pp. 45-136. [In Russian].

Obut, A. M. 1968. [Graptolite description] In Obut, A. M., Sobolevskaya, R. F., and Merkur'eva, A. P. (eds.) [*Llandovery Graptolites from a Borehole Core in the Noril'sk Region.*] Akademiya Nauk SSSR, Moscow, pp. 57-118. [in Russian].

Olszewski, T. 1999. Taking advantage of time-averaging. *Paleobiology*, 25: 226-238.

Packham, G. H. 1962. Some diplograptids from the British Lower Silurian. *Palaeontology*, 5: 498-526.

Palmer, D. 1991. What other organisms did they live with? In Palmer, D. and Rickards, R.B. (eds.) *Graptolites: Writing in the Rocks.* Boydell Press. pp. 41-49.

Palmer, D. C. 1986. The monotypic 'population' accompanying the lectotype of *Saetograptus varians* (Wood 1890). In Hughes, C. P., Rickards, R. B., and Chapman, A. J. (eds.) *Palaeoecology and Biostratigraphy of Graptolites.* Geololgical Society of London, Special Publication, 20: 249-260.

Palmer, D. C. and Rickards, R. B. (eds.) 1991. *Graptolites: Writing in the Rocks.* The Boydell Press, Woodridge, 182 pp.

Parsons, K. M. and Brett, C. E. 1991. Taphonomic processes and biases in modern marine environments: an actualistic persepctive of fossil assemblage preservation. In Donovan, S. K.(ed.). *The Processes of Fossilization.* Columbia University Press, New York, pp. 22-65.

Paškevičius, J. 1976. On some new Llandoverian "diplograptids" of the eastern Baltic. In Kaljo, D. and Kore, T. N. (eds.) *Graptolites and Stratigraphy.* Academy of Sciences of Estonian SSR, Institute of Geology, pp. 140-151.

Peterson, C. H. 1977. The paleoecological significance of undetected short-term temporal variability. *Journal of Paleontology*, 51: 976-981.

Peterson, W. T., Miller, C. B., and Hutchinson, A. 1979. Zonation and maintenance of copepod population in the Oregon upwelling zone. *Deep-Sea Research*, 26: 467-494.

Pickard, G. L. and Emery, W. J. 1990. *Descriptive Phyiscal Oceanography: an Introduction.* Butterworth-Heinemann, Oxford, 320 p.

Pickering, K. T. and Hiscott, R. N. 1985. Contained (reflected) turbidity currents from the Middle Ordovician Cloridorme Formation, Quebec, Canada: an alternative to the antidune hypothesis. *Sedimentology*, 32: 373-94.

Pickering, K. T., Stow, D. A. V., Watson, M. and Hiscott, R. N. 1986. Deep-water facies, processes and models: a review and classification scheme for modern and ancient sediments. *Earth Science Reviews*, 22: 75-174.

Pickering, K. T., Hiscott, R. N. and Hein, F. J. 1989. *Deep Marine Environments: Clastic Sedimentation and Tectonics*. Unwin Hyman, London, pp. 416.

Piper, D. J. W. 1972a. Turbidite origin of some laminated mudstones. *Geological Magazine*. 109: 115-126.

Piper, D. J. W. 1972b. Sediments of the Middle Cambrian Burgess Shale, Canada. *Lethaia*. 5: 169-175.

Piper, D. J. W. 1978. Turbidites, muds and silts on deep-sea fans and abyssal plains. In Stanley, D.J. and Kelling, G. (eds.) *Sedimentation in Submarine Canyons, Fans and Trenches*. Dowden, Hutchinson and Ross, Stroudsburg, pp.163-176.

Piper, D. J. W. and Deptuck M. 1997. Fine-grained turbidites of the Amazon fan: facies characterization and interpretation. In Flood, R. D., Piper, D. J. W., Klaus, A., and Peterson, L. C. (eds.) *Proceedings of the Ocean Drilling Program, Scientific Results*, 155: 79-107.

Piper, D. J. and Stow, D. A. V. 1991. Fine-Grained Turbidites. In Einsele *et al.* (eds.) *Cycles and Events in Stratigraphy*. Springer-Verlag, Berlin, pp. 361-376.

Potter, P. E., Maynard, J. B., and Pryor, W. A. 1980. *Sedimentology of Shale*. Springer-Verlag, New York, 306p.

Prothero, D. R. 1998. *Bringing Fossils to Life: an Introduction to Paleontology*. McGraw-Hill, Boston, 457p.

Prothero, D. R. and Schwab, F. 1996. *Sedimentary Geology: an Introduction to Sedimtary Rocks and Stratigraphy*. W.H. Freeman and Company, New York, 575p.

Příbyl. A. 1948. Bibliographic index of Bohemian Silurian graptolites. *Knihovna Státního Geologického ústavu Republiky Československe*, 22: 1-97.

Raiswell, R. 1976. The microbial formation of carbonate concretions in the Upper Lias of N.E. England. *Chemical Geology*, 18: 227-244.

Raymont, J. E. G. 1983. *Plankton and productivity in the oceans, Volume 2 - Zooplankton (Second Edition)*. United Kingdom, Pergammon Press, Oxford, 824p.

Raup, D. M. 1976. Species richness in the Panerozoic: a tabulation. *Paleobiology*, 2: 289-297.

Rice, W. R. 1988. Analyzing tables of statistical tests. *Evolution.* 43 (1): 223-225.

Richter, R. 1853. Thuringische Graptolischen. *Deutschlandische Geologische Gesellschaft Zeitschrift*, 5: 439-464.

Rickards, R. B. 1970. The Llandovery (Silurian) graptolites of the Howgill Fells, northern England. *Palaeontographical Society Monograph*, 108p.

Rickards, R. B. 1975. Palaeoecology of the Graptolithina, an extinct class of the phylum hemichordata. *Biological Review*, 50: 397-436.

Rickards, R. B. 1976. The sequence of Silurian graptolite zones in the British Isles. *Geological Journal*, 11: 153-188.

Rickards, R. B., 1991, How common were they? In Palmer D. C. and Rickards, R. B. (eds.) *Graptolites: Writing in the Rocks*, The Boydell Press, Woodridge, pp. 38-40.

Rickards, R. B. and Crowther, P. R. 1979. New observations on the mode of life, evolution and ultrastructure of graptolites. In Larwood, G, and Rosen, B. R. (eds.) *Biology and Systematics of Colonial Organisms*, Systematics Association Special Volume, 11: 397-410.

Rickards, R. B., and Palmer, D. 1991. What are they? What do they look like? In Palmer, D. C. and Rickards, R. B. (eds.) *Graptolites: Writing in the Rocks*, The Boydell Press, Woodridge, pp.1-6.

Rickards, R. B. and Rushton, W. A. 1968. The thecal form of some slender Llandovery *Monograptus*. *Geological Magazine*, 105: 264-274.

Rickards, R. B., Rigby, S., and Harris, J. H. 1990. Graptolite biogeography: recent progress, future hopes. In McKerrow, W. S. and Scotese, C. R. (eds.) *Palaeozoic palaeogeography and biogeography*. Memoir, Geological Society of London , 12, pp. 139-145.

Rickards, R. B., Hutt, J. E. and Berry, W. B. N. 1977. Evolution of Silurian and Devonian graptolites. *Bulletin of the British Museum (Natural History), Geology*, 28, 120p.

Rigby, S. 1991. Feeding strategies of graptolites. *Palaeontology*, 34: 797-815.

Rigby, S. 1992. Graptolite feeding efficiency, rotation and astogeny. *Lethaia*, 25: 51-68.

Rigby, S.. 1993. Population analysis and orientation studies of graptolites from the Middle Ordovician Utica Shale, Quebec. *Palaeontology*, 36: 267-282.

Rigby, S. and Dilly, P.N. 1993. Growth rates of pterobranchs and the lifespan of graptolites. *Palaeobiology*, 19: 459-475.

Rigby, S. and Rickards, R.B. 1989. New evidence for the life habit of graptolites from physical modeling. *Paleobiology*, 15: 402-413.

Rigby, S. and Rushton, A. 1991. Where and when did they live? In Palmer, D. and Rickards, R.B. (eds). *Graptolites: Writing in the Rocks.* Boydell Press, pp 33-37.

Rigby, S. and Sudbury, M. 1995. Graptolite ontogeny and the size of the graptolite zooid. *Geological Magazine*, 132: 427-433.

Ruedman, R. 1897. Evidence of current action in the Ordovician of New York. *American Geologist*, 19: 367-391

Ruedman, R. 1947. *Graptolites of North America.* Geological Society of America Memoir,19, 652p..

Russel, J. C., Melchin, M. J. and Koren, T. N. 2000. Development, taxonomy, and phylogenetic relationships of species of Paraclimacograptus (Graptoloidea) from the Canadian Arctic and the Southern Urals of Russia. *Journal of Paleontology*, 74: 84-91.

Sadler, P. M. 1981. Sediment accumulation rates and the completeness of stratigraphic sections. *Journal of Geology*, 89: 569-584.

Sadler, P. M. 1993. Models of time-averaging as a maturation process: how soon do sedimentary sections escape reworking? *In* Kidwell, S. M, and Behrensmeyer, A. K. (eds.) *Taphonomic Approaches to Time Resolution in Fossil Assemblages.* The Paleontological Society, Short Courses in Paleonology, 6, pp. 188-209.

Sadler, P. M. and Strauss, D. J. 1990. Estimation of completeness of stratigraphical sections using empirical data and theoretical models. *Journal of the Geological Society of London*, 147: 471-485.

Schäfer, W. 1972. . In Craig, G. Y. (ed.), Oertel, I (translator). *Ecology and Palaeoecology of Marine Environments* Oliver and Boyd, Edinburgh, 568p.

Schindel, D. E. 1982. Resolution analysis: a new approach to the gaps in the fossil record. *Paleobiology*, 6: 340-353.

Schopf, T. J. M. 1978. Fossilization potential of an intertidal fauna: Friday Harbor, Washington. *Paleobiology*, 4: 261-270.

Scotese, C. R. and McKerrow, W. S. 1990. Revised world maps and introduction. *In* Scotese, C. R., and McKerrow, W. S. (eds) *Paleozoic Palaeogeography and Biogeography*, Geological Society Memoir, 12: 1-21.

Skevington, D. W. 1974. Controls influencing the composition and distribution of Ordovician graptolite faunal provinces. In Rickards, R. B., Jackson, D. E., and Hughes, C. P. (eds.). *Graptolite Studies in Honour of O.M.B. Bulman. Palaeontological Association Special Papers in Palaeontology*, 13: 59-73.

Sodero, D. E. and Hobson, J. P. Jr. 1979. Depositional facies of lower Paleozoic Allen Bay carbonate rocks and contiguous shelf and basin strata, Cornwallis and Griffith Islands, Northwest Territories, Canada. *American Association of Petroleum Geologist, Bulletin*, 63: 1059-1091.

Southwood, T. R. E. 1987. The concept and nature of the community. In Gee, J. H. R. and Giller, P. S. (eds.), *Organization of Communities: Past and Present*. Blackwell Science, Oxford, pp. 3-27.

Speyer, S. E. 1991. Taphofacies controls: background and episodic processes in fossil assemblage preservation. In Allison, P.A. and Briggs, D.E.G. (eds.) *Taphonomy: Releasing the Data Locked in the Fossil Record.* Volume 9 of Topics in Geobiology Plenium Press, New York pp, pp. 501-545.

Speyer, S. E., and Brett, C. E. 1986. Trilobite taphonomy and Middle Devonian taphofacies. *Palaios*, 1: 312-327.

Speyer, S.E., and Brett, C.E., 1991. Taphofacies controls: background and episodic processes in fossil assemblage preservation. In Allison, P. A. and Briggs, D. E. G. (eds.) *Taphonomy: Releasing the Data Locked in the Fossil Record*, Volume 9 of Topics in Geobiology, Plenum Press, New York, pp. 501-541.

Stanton, R. J., Jr. 1976. The relationship of fossil communities to the original communities of living organisms. In Scott, R. W. and West, R. R. (eds.) *Structure and Classification of Paleocommunities*. Dowden, Hutchinson, and Ross, Stoudsburg, Pennsylvania, pp. 107-142.

Strachan, I. 1971. *A Synoptic Supplement to "A Monograph of British Graptolites by Miss G. L. Elles and Miss E. M. R. Wood.* Palaeontographical Society Monograph, 130p.

Strachan, I. 1974. Further isolated graptolites from the Ordovician of Girvan. *Special Papers in Palaentology*, 13: 99-105.

Štorch, P. 1998. Graptolites of the *Pribylograptus leptotheca* and *Lituigraptus convolutus* biozones of Tmaň (Silurian, Czech Republic). *Journal of the Czech Geological Society*, 43: 209-272.

Štorch, P. and E. Serpagli. 1993. Lower Silurian graptolites from the southwestern Sardinia. *Bollettino della Societa Paleontologica Italiana*, 32: 3-57.

Stow, D. A. V. 1979. Distinguishing between fine-grained turbidites and contourites on the Nova Scotian deep water margin. *Sedimentology*, 26: 371-387.

Stow, D. A. V. and Lovell, J.P.B. 1979. Contourites: their recognition in modern and ancient sediments. *Earth Science Reviews*, 14: 251-291.

Stow, D. A. V. and Piper, D.J.W. 1984. Deep-water fine-grained sediments: facies models. In Stow, D. A. V. and Piper, D. J. W. (eds.) *Fine-grained Sediments: Deep-water Processes and Facies.* Geologic Society (London) Special Publication 15. Blackwell Scientific, Oxford, pp. 611-646.

Thorsteinsson, R. 1958. *Cornwallis and Little Cornwallis Islands, Distric of Franklin, Northwest Territories.* Geological Survey of Canada, Memoir 294, 134 p.

Törnquist, S. 1890. Undersökningar öfver Siljansområdets graptoliter, I. *Acta Universitets Lunds*, 26: 1-33.

Törnquist , S. 1899. Researches into the Monograptidae of the Scanian Rastrites Veds. *Acta Universitets Lunds*, 35: 1-25.

Trettin, H. P., Mayr, U., Long, G. D. F., and Packard, J. J. 1991. Cambrian to Early Devonian Basin development, sedimentation, and volcanism, Arctic Islands. In Trettin, H. P. (ed.) *Geology of the Innuitian Orogen and Arctic Platform of Canada and Greenland.* Geological Survey of Canada, Geology of Canada, no. 3: 165-238.

Tucker, M. E. and Wright, V. P. 1990. *Carbonate Sedimentology.* Blackwell Scientific, Oxford, pp. 482.

Underwood, C. J. 1992. Graptolite preservation and deformation. *Palaios*, 7: 178-186.

Underwood, C. J. 1993a. The position of graptolites within Lower Palaeozoic planktic ecosystems. *Lethaia*, 26: 189-202.

Underwood, C. J. 1993b. *The Taphonomy of Graptolites*, Unpublished Ph.D. Thesis, University of Bristol, 228p.

Underwood, C. J. 1994, Faunal transport within event horizons in the British Upper Silurian. *Geological Magazine*, 131: 485-498.

Underwood, C. J. 1998. Population structure of graptolite assemblages. *Lethaia*, 31: 33-41.

Underwood, C. J. and Bottrell, S. H. 1994. Diagenetic controls on multiphase pyritization of graptolites. *Geological Magazine*, 131: 315-327.

Urbanek, A. 1990. Reproductive strategy and the life cycle in graptolite colonies. *Lethaia*, 23: 33-340.

Valentine, J. W. 1970. How many marine invertebrate species? A new approximation. *Journal of Paleontology*, 44: 410-415.

Van Valen, L. 1973. A new evolutionary law. *Evolutionary Theory*, 1: 1-30.

Walker K. R. and Bambach R. K. 1971. The significance of fossil assemblages from fine-grained sedimentas: time-averaged comminites. *Geological Society of America Abstrats with Programs*, 3: 783-384.

Walker, R. G. 1978. Deep-water sandstone facies and ancient sub-marine fans: models for exploration for stratigraphic traps. *Bulletin of the American Association of Petroleum Geologists*, 62: 932-966.

Watkins, R. and Berry, W. B. N. 1977. Ecology of a Late Silurian fauna of graptolites and associated organisms. *Lethaia*, 10: 267-286.

Wehmiller, J. F., York, L. L., and Bart, M. L. 1995. Amino acid racemization geochronology of reworked Quaternary mollusks on US Atlantic coast beaches: implications for chronostratigraphy, taphonomy, and coastal sediment transport. *Marine Geology*, 124: 303-337.

Wilde, P. and Berry, W. B. N. 1984. Destabilisation of the oceanic density structure and its significance to marine "extinction" events. *Palaeogeography, Palaeoclimatology, Palaeoecology*, 48: 143-162.

Williams, S. H. and Stevens, R. K. 1988. Early Ordovician (Arenig) graptolites of the Cow Head Group, western Newfoundland. *Palaeontographica Canadiana*, 5: 1-167.

Williams, S. H., Bashforth, A. R., and Dilly, N. P. 1997. Growth rates and skeletal secretion of siculae in Early Ordovician (Arenig) graptolites from Western Newfoundland: implications for development and paleoecology of graptolites. *Palaios*, 12: 591-597.

Williams, S. H., Ingham, J. K., McManus, K., and Murray, I. 1982. The use of experimental palaeontology in reproducing the effects of diagenetic flattening on graptolites. *Lethaia*, 15: 365-372.

Wilson, M. V. H. 1988. Taphonomic processes: information loss and information gain. *Geoscience Canada*, 15: 131-148.

Zalasiewicz, J. A. 1984. Dichograptid synrhabdosomes from Arenig of Britian. *Palaeontology*, 27: 425-429.

Zalasiewicz, J. A. 1996. Aeronian (Silurian: Llandovery) graptolites from central Wales. *Geologica et Palaeontologica*, 30: 1-14.

Zalasiewicz, J. A. and Tuncliff, S. 1994. Uppermost Ordovician to Lower Silurian graptolite biostratigraphy of the Wye Valley, Central Wales. *Palaeontology*, 37: 695-720